SESSION

VISUALIZATION + TOOLS AND TECHNIQUES

Chair(s)

TBA

Visualising Multi-Phase Lattice Gas Fluid Layering Simulations

K.A. Hawick
Computer Science, Institute for Information and Mathematical Sciences,
Massey University, North Shore 102-904, Auckland, New Zealand
email: k.a.hawick@massey.ac.nz
Tel: +64 9 414 0800 Fax: +64 9 441 8181

ABSTRACT
Complex fluids that exhibit phenomena such as layering and separation of multiple phases are computationally expensive to model using conventional numerical integration of partial differential equations. Lattice gas approaches are significantly cheaper to simulate and can still reveal good insights into the essential behaviours. We describe simulations of multi-phase layering in a lattice gas based on the Kawasaki exchange model and introduce a gravitational potential parameter to complement the temperature coupling. We identify the existence of some phase transitional behaviours in the number of phases as well as shifts in the critical temperature arising from the gravitational layering. We illustrate the model with graphical renderings in both two and three dimensions.

KEY WORDS
multi-phase fluid; Kawasaki model; lattice gas; gravitational bias; diffusion.

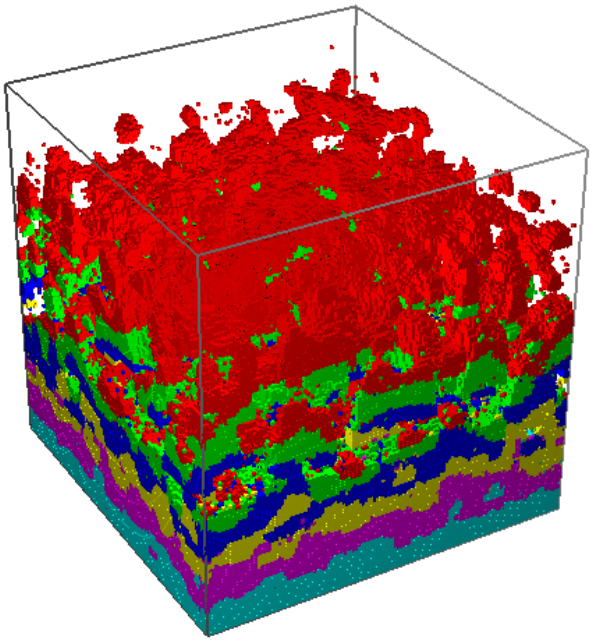

Figure 1: A $Q = 7$ species system run for 16384 steps on a 128^3 model with $p_v = 0.5$.

1 Introduction

Complex fluids such as multi-phase systems of sand, mud, oil and so forth[1] have attracted considerable recent interest in the literature due to recent oil industry events. Simulating and visualising such systems is attractive – particularly on a semi-interactive manner so that the effect of thermal and other parameters can be experienced.

Simulating a lattice gas mode[2] is considerably cheaper computationally than simulating a full numerical time integration of the corresponding partial differential equations. Full symmetry lattice gas models[3] are based on a correct momentum and energy treatment of microscopic particle constituents. These models have been shown to handle the microscopic details of single phase fluids well, but it is non trivial to add multiple particle species.

Complex fluid model such as invasion percolation[4] can be based on straightforward assumptions about fluid flow in porous media [5] – essentially basing the flow model on a definite substrate model. Work has been reported in the literature[6] on the effect of destabilizing gravitational gradients[7] and viscous gravitational forces[8].

Other important effects occurring in complex systems include phase separation due to Ostwald ripening[9] as well as surface-tension driven effects at species interfaces[10] particularly when the system is biased to favour some species, such as when an external magnetic or gravitational field is applied[11]. A variation of the simpler Monte-Carlo based model known as the Kawasaki model is used in this present work to investigate both multi-species effects but also gravitational perturbations that can cause layering.

Figure 1 shows a graphical rendering of a $Q = 7$ state

multi phase system after 16,384 time steps following a random initialisation and temperature quench. A unit gravitational field is applied and the species have separated out from the initial random mix into ordered layers with some surface roughening still persisting due to thermal inter-diffusion.

The Kawasaki spin-exchange model[12] has been used successfully to simulate diffusional behaviour, nucleation and growth, and spinodal decomposition in binary and ternary alloys. The model is based on nearest neighbour coupling terms in much the same manner as the Ising model, but whereas the Ising model uses "spins" that can flip amongst states, the Kawasaki model starts with a fixed fraction of different atomic species on a lattice, and allows them to diffuse around using an exchange mechanism which conserves species populations. In effect the Kawasaki model is a simplified lattice gas[13] although it has been show that it does not attain the correct symmetries for full Navier-Stoke regime fluid flow, it does give a good computational approximation and as seen in the work reported here, provides a flexible and extensible model to experiment with additional parameters such as gravity and it also supports arbitrary numbers of species states - or phases.

We report on some simulation experiments and graphical renderings of the Kawasaki model in both two and three dimensional systems, with a simple gravitational field mechanisms added into the Monte-Carlo model mechanisms. We also look at how the model scales with up to nine constituent species present in a system.

The paper is structured as follows: In Section 2 we describe the essentials of the Kawasaki model and how a Monte-Carlo dynamics gives a =good computational approximation to a real physical dynamics of multiphase separation in a complex fluid. In Section 3 we show how a gravitational force can be added in as a perturbative effect. We give some graphical results and some measurements of simulated systems in Section 4 alongwith some discussion of their implications in Section 5. Finally we offer some conclusions and areas for further model development in Section 6.

2 Kawasaki Exchange Model

Consider initially a two component substitutional alloy consisting of a single crystallite of material. There are only two chemical species present and they occupy the sites of a regular lattice. They may be imagined as oscillating about some mean positions, but the bulk material retains its structure and the mean positions do not change, and there are no interstitial atoms permitted in the structure. Suppose that there are some N atoms on the lattice and they are subdivided by chemical species into N_A of species A and N_B of species B so that $N = N_A + N_B$. Consider the possible arrangements of the two species of atoms on the lattice. Focusing attention on species A the number of possible arrangements W of the N_A atoms of species A is simply given by:

$$W = \frac{N!}{N_A!(N - N_A)!} = \frac{N!}{N_A!(N_B)!} \tag{1}$$

given that the A-species atoms are indistinguishable. The micro-structure produced by the set of atomic arrangements constitutes a microstate of the model alloy and to make the model able to simulate the dynamics of an alloy, it is necessary to impose a dynamical scheme whereby the system can explore its microstates.

It is first necessary to consider the interactions between the species on the lattice. The simplest model Hamiltonian ($\mathcal{H}$) consists of an assignment of pair-wise interactions or bonds between neighbouring atoms. Consider a local concentration variable c_i for each lattice site which has the value 1 for A-sites and value 0 for B-sites. The Hamiltonian may then be written in terms of coupling constants $V_{ij}^{c_i - c_j}$ between sites i and j.

The Kawasaki model Hamiltonian (or energy functional) for a binary alloy of the two species "A" and "B" is written:

$$\begin{aligned} \mathcal{H}_{\text{Alloy}} = \mathcal{H}^0 + \quad \sum_{i \neq j} \quad & V_{ij}^{\mathbf{A-A}} c_i c_j + \\ & V_{ij}^{\mathbf{A-B}} c_i (1 - c_j) + \\ & V_{ij}^{\mathbf{B-A}} (1 - c_i) c_j + \\ & V_{ij}^{\mathbf{B-B}} (1 - c_i)(1 - c_j) \end{aligned} \tag{2}$$

in terms of the potential terms V, and where any chemical potential term has been omitted, as we wish to operate at a *fixed* value of the global concentration $< c >$. All the parameters used in this Hamiltonian can be specified explicitly, or we can limit the model to nearest neighbour isotropic interactions, so that only one parameter V^{A-A} is not redundant. By expressing this one parameter in Boltzmann units of $k_b T$, we are actually specifying the temperature T of the system, and a quench experiment is possible. This Hamiltonian has no explicit dynamical scheme associated with it, and so one must be imposed artificially using Monte Carlo techniques to make the model system evolve between different microstate configurations "X" along a trajectory in state space that is physically realistic.

This gives the pair-wise interactions and the relative chemical potential of the A-B mixture, it being more energetically favourable for the alloy to have more or less A-atom constituents. In practice, the interaction

sum would not be over all pairs but over a restricted number of distance shells around individual atomic sites. The assumption is that long range electrostatic atomic interactions are screened in consequence of the overall neutral charge of the material and so the interactions are relatively short range.

This form of Hamiltonian can be shown to be isomorphic to that of the Ising model for a spin-$\frac{1}{2}$ magnet in a magnetic field [14] and was first employed by Bragg and Williams to study order-disorder processes in alloys [15], and by Cernuschi and Eyring as a model for lattice gases [16]. The chemical potential is directly related to the Ising model magnetic field and providing the interactions $V_{ij}^{c_i - c_j}$ are chosen so that the A-species and B-species are treated on an equal footing then the Hamiltonian can be written in the form:

$$\mathcal{H}_{Ising} = -\sum_{i \neq j} \mathcal{J}_{ij} s_i s_j + H \sum_i s_i \tag{3}$$

where the Ising spins s_i take the values $s_i = \pm 1$ and are given by the transformation:

$$s_i = 2c_i - 1 \tag{4}$$

$$c_i = \frac{s_i + 1}{2} \tag{5}$$

It is useful to consider the simplest case of this, where the interactions are very short range, isotropic, and are restricted to nearest neighbouring sites on the lattice. For this purpose, the Ising coupling parameter $\mathcal{J}_{ij}$ can be written as a single value $\mathcal{J}$ and taken outside of the summation. This allows the Ising coupling $\mathcal{J}$ and magnetic field strength H to be written as:

$$\mathcal{J}_{ij} = \frac{1}{4}\{(V^{\mathbf{A}-\mathbf{A}} + V^{\mathbf{B}-\mathbf{B}}) - (V^{\mathbf{A}-\mathbf{B}} + V^{\mathbf{B}-\mathbf{A}})\} \tag{6}$$

$$H = -\frac{1}{2} \triangle \mu^{\mathbf{A}-\mathbf{B}} \tag{7}$$

Since this only leaves two free parameters, the alloy Hamiltonian can be expressed in terms of just $V^{\mathbf{A}-\mathbf{A}}$ and $\triangle \mu^{\mathbf{A}-\mathbf{B}}$, giving a form where it is easier to generalise to a ternary alloy with less parameter redundancy. The binary alloy can be thought of as just the A-species in a background of B. The lattice gas picture merely involves treating the B sites as "vacancies". It is possible to reduce the parameters involved to one, by operating with zero chemical potential, as described in the dynamical scheme below.

Both the alloy and Ising Hamiltonians as expressed above do not give rise to a dynamical equation so it is necessary to introduce a stochastic mechanism whereby the system can explore its microstates. Focusing attention on the A-particles, there are two dynamical processes that need to be considered. Firstly, a mechanism for the particles to change position and explore the lattice but keeping the number of particles present (N_A) constant. Secondly, a means of operating with constant chemical potential $\mu^{\mathbf{A}-\mathbf{B}}$ and increasing or decreasing the particle population. The first mechanism is know as 'spin-exchange' or Kawasaki dynamics [12] and is used for a canonical thermodynamical simulation of the alloy model where neighbouring site variables c_i and $c_{i\pm1}$ are exchanged. The second is the conventional 'spin-flip' dynamics where the site variable is inverted. In fact the exchanges or flips must be performed with a carefully specified probability if the system is to have valid thermodynamic properties.

One normally proceeds by recognizing that for a Boltzmann statistical weighting of the microstates, the probabilities $P(\mathbf{X}$ can be expressed in terms of the Hamiltonians $\mathcal{H}(\mathbf{X})$.

$$P(\mathbf{X}) = A e^{-\frac{\mathcal{H}(\mathbf{X})}{k_b T}} \tag{8}$$

Where A is a normalising constant, k_b is Boltzmann's constant and T the temperature. This gives:

$$\frac{W_{\mathbf{X}' \to \mathbf{X}}}{W_{\mathbf{X} \to \mathbf{X}'}} = e^{-\frac{\{\mathcal{H}(\mathbf{X}) - \mathcal{H}(\mathbf{X}')\}}{k_b T}} \tag{9}$$

This does not have a unique solution. The two most commonly used are [17, 18] and for the purposes of the work reported here we use the conventional Metropolis solution:

$$W_{\mathbf{X} \to \mathbf{X}'} = \begin{array}{ll} \frac{1}{\tau} e^{-\frac{\triangle \mathcal{H}}{k_b T}}, & \triangle \mathcal{H} > 0 \\ \frac{1}{\tau}, & \triangle \mathcal{H} \leq 0 \end{array} \tag{10}$$

The simulation time can then be defined in units of 'an average of one Metropolis update attempt per site'. It is important to include every site in this definition of the time-step. Without such a universal definition, it becomes impossible to compare other works in the literature and on slightly different models, in terms of their dynamical properties. The problem remains that this is only an artificially constructed time. It is also noticeable that for deep quench experiments, there is little thermal activity below the phase transition temperature and the system evolves very slowly. This effect is known as hydro-dynamic slowing down.

The subject of whether the stochastic time variable in a Monte-Carlo simulation bears any resemblance to a *real* time is still controversial [19, 20]. In general it does not, but it is thought that for certain models it can be scaled to a real time, at least in the long-time limit. There is strong evidence that the Monte-Carlo time *is* scalable to real aging time.

We can generalise the above model to an arbitrary number of Q states, using just the like-like potential coupling terms. This is analogous to the Potts extension of the Ising model to arbitrary spin sates, whereas

here for the multi-phase Kawasaki gas we conserve the number of species present.

3 Introducing Gravity

It is convenient to identify one of the species as "vacancies" that do not directly interact with one another. The way we formulate our model nomenclature and interactions is therefore to specify a temperature which in the absence of gravity is just the reciprocal of the nearest neighbour coupling energy between like-like species which attract one another. We simplify matters for the work reported here and do not specify any direct interaction – attractive or repulsive – between non-like species.

We generalise the species names so that vacancies do not interact and are termed "V' or state-0 and have zero mass. The remaining $Q-1$ species can be introduced with integer unit-incremented masses – so they are progressively heavier, and so that each species attracts others of its own species, but does not otherwise interact or couple to other species.

We can further modify the energy interactions so that a (weak) gravitational field is applied and so that heavier species preferentially fall towards the bottom of the simulated containment vessel. This is controlled by a gravitational weighting g – which for the work reported here is either zero or unity. The simulation algorithm we employ is shown in algorithm 1.

Algorithm 1 Monte-Carlo Model Algorithm.

```
N = L^2 or N = L^3 sites on square or cubic lattice
for all runs do
  initialise sites with p_v = 0.5 vacancies
  choose non-vacant Q−1 species with equal probability
  for all time-steps do
    for all sites i in random order do
      choose a random neighbour site j
      compute energy change if i, j exchanged
      if energy falls then
        accept change and do exchange
      else
        compute Metropolis probability p
        generate random probability r
        accept change conditionally on r < p
      end if
    end for
  end for
  average results over runs
end for
```

If the exchange does not take place the energy of the system remains the same[21]. The energy calculation favours like-like nearest neighbour bonds but also favours heavier species moving downwards. The probabilities are based on integer counts so are completely discrete and countable. The Boltzmann factors are of the form $\exp -(\Delta E/k_B T)$ and even on modern processors, the *exp* function usually costs several tens of clock cycles to compute. It is therefore useful to pre-compute the Boltzmann exponential values in a look-up table at the beginning of the program rather than re-compute then inside the inner loops of the algorithm, since this vastly speeds up the computation.

The measurements we report for this present paper include the height population profiles $P(y)$ of the vacancies (species 0) and an exemplar non-vacant species (1). This is defined simply as the fractional population of each species at a height y within the simulated containment vessel. Another useful metric is to study the fractional number of Like-like energy bonds N_{L-L} that we count in the model system as it evolves in simulation time.

4 Results

We present some results for simulated systems in two and three dimensions. Throughout we use a vacancy fraction of 0.5 with the remaining $Q-1$ states all given equal fractional probability when the system is initialised. Results are all based on averages over at least ten independent runs and for the system sizes stated.

We establish the model system so that the boundary conditions are completely periodic in the horizontal directions but are fixed in the vertical direction. The practical upshot of this is that species wrap around horizontally but hit the roof or floor of the simulated vessel. We define N sites where $N = L_x \times L_y \times L_z$ in three dimensions. We can work with a thin two dimensional vessel by making the z dimension unity. This yields a system not-unlike the popular sand pictures where various coloured sands in an oil suspension are held between two sheets of glass and shaking and inverting the system initially randomises the grains which then separate out in a manner shown in our simulation.

Figure 2 shows some graphically rendered systems of a sand picture style system with $Q = 4$ different species. On the left there is no gravity applied, and the three non vacant species do attract one another and the system is essentially quenched so that domains nucleate and grow. The vacancies allow a lot of surface effects and this effectively raises the temperature over that would arise in the exchange dynamical scheme without vacancies. The times shown are $2^9 = 512$ up to $2^{14} = 8192$ time steps. This power-of two time-scale is typical of models of this sort. The formation of nucleation clusters happens early on but it takes longer

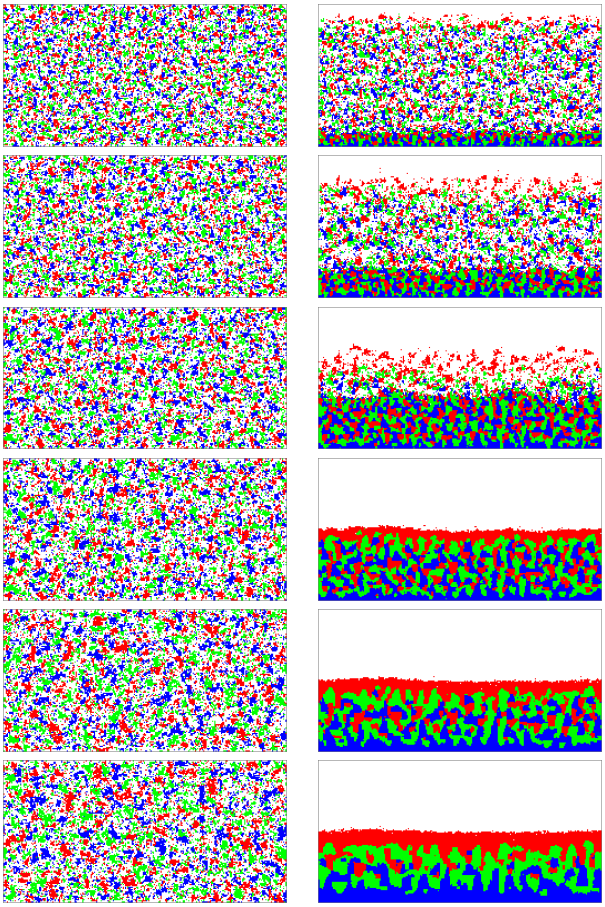

Figure 2: Configuration snapshots at power-of-two time steps $2^9 ... 2^{14}$ for a two dimensional (256×128) model system of $Q = 4$ species, coloured red, green and blue with vacancies not shown, and where the quench temperature was $T = 1.25$. On the left there is no gravity, and on the right unit gravity.

and longer time for surface tension effects to drive the clusters to merge and join into larger structures that span the system.

The images on the right of figure 2 is quite different and represents the situation when unit gravity has been applied. Again like-like species rapidly nucleate but the gravitational force encourages a much more rapid and complete separation of the different species into layers, ranked in height according to the relative masses. This is a two-dimensional analogy to the effect rendered in Figure 1. A certain amount of surface roughening is still present due to thermal diffusion effects and although after 8192 time steps the layers have become very pronounced and in correct order, there is still some inter penetration of the species into alternating layers.

It is instructive to study the species population profiles in more detail. Our simulated systems are large enough

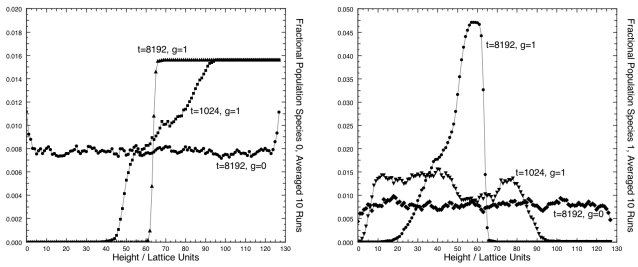

Figure 3: The fractional population profile for species 0 (vacancies) and species 1 averaged over 10 runs on a model system of 128^2 at quench temperature $T = 1.25$, and with $Q = 4$, run for 2^{12} time-steps.

to show layering behaviour but not large enough to balance out the fluctuations that manifest themselves in noise from measurement on a single run. It is therefore useful to average height profiles for the different species over several separate runs – comparing snapshots at the same time-step from the initial quench.

Figure 3 shows the fractional populations of both the vacancies and the lightest species in a 128^2 system that has evolved to long times. The upper figure shows the fractional population of vacancies. The middle curve is for an experiment (over ten runs) with no gravity and shows that the population profile is almost flat (subject to fluctuational thermal noise) apart from the top and bottom of the box. There is an interesting meniscus formed since vacancies do not directly interact with one another (or the walls) they are preferentially encouraged to occupy space at the top and bottom of the box in the absence of gravity. The lower figure shows the opposite effect for (representative) species number 1 - the 1-1 interactions encourage species one to preferentially avoid the floor and top of the box.

The top part of the figure shows two times of the population profile of vacancies when gravity is applied. The long term behaviour is for the vacancies to form a vapour with quite a sharp surface region between the vapour and the other species' "liquid" layered phases. There are transitional regions that form as the layers condense with the application of gravity. The lower part of figure 3 shows similar effects for species 1 when gravity is applied. The long term behaviour is for each non-vacant species to become very much confined to its own layer and to squeeze out both vacancies and other species from that volume layer. The intermediate time shows that this is a non trivial process as species 1 is gradually concentrating above and below the middle of the box, and is in fact initially depleted near its final mean layer position. This is a competing effect due to the other species but is representative of them all – albeit for different accretion/depletion positions.

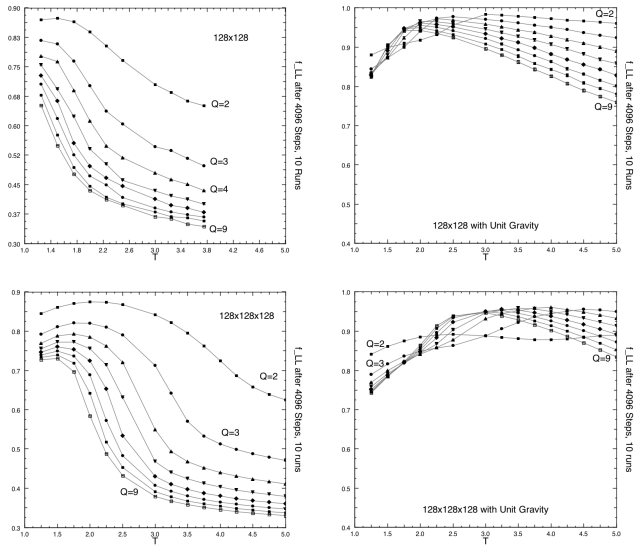

Figure 4: The fraction of Like-Like nearest-neighbour links in 2d (top) and 3d (bottom) systems with zero gravity (left) and unit gravity applied (right). Lattice length is 128, run for 4096 steps, averaged over 10 independently started configurations. Different curves are for each number of Q states in the system.

Figure 4 shows the fraction of Like-Like bonds, and thus a measure of total energy of the system when two and three dimensional systems are quenched to a particular temperature and annealed at that temperature for 4096 time steps. The different curves are for the number of Q states present in the system. The two dimensional case is shown on the top, and the three dimensional below, with the zero gravity case shown on the left and unit gravity applied on the right. The same temperature scale is used for all cases but a slid-fractional scale is used for with/without gravity.

In two dimensions the curves are well separated out without gravity and (apart from a high-Q effect probably due to noise from insufficiently large simulation size), they vary smoothly with increasing numbers of states. The critical temperature for the Q=2 Ising case is approximately $T_c = 2.269$ and this appears to map to the inflection point of the curve. Similarly for three dimensions the Ising $Q = 2$ critical temperature is around $T_c \approx 4.511$. It is known that for increased numbers of Q states the Potts spin-flip model[22] the critical temperature shifts and our simulation confirms this in both two and three dimensions.

The behaviour when gravity is added however is less easily predicted. In two dimensions there is an obvious difference between the $Q = 2$ case and the higher-Q cases at low temperatures. This is likely due to the special role the vacancies play – having no vacancy-vacancy coupling – when there are no other competing non vacant species present. Otherwise the $Q = 3, 4, ..., 9$ curves are relatively smooth for two dimensions.

In the case of a three dimensional system however both the $Q = 2, 3$ cases are different from the rest and we speculate this is a dimensional crossover effect. The number of sites in a 128^2 layer of a 128^3 system is large enough that the three dimensional curves are a lot smoother, although as figure 1 shows there are still marked individual fluctuations occurring in the surfaces between layers.

5 Discussion

The curves with gravity show that the volume compression effect as species are encouraged into their own layers means there are a lot more like-like bonds and overall the system energy has lowered a lot compared to the gaseous morphous mixture exhibited for zero gravity. The crossover effect shown at around 1.75 when gravity is applied appears to be due to a freezing out effect. Below this temperature domains of individual species form due to their mutual attraction and once formed are unable to fall under the influence of gravity. This is an artifact of the way mobility is included in the model.

Individual particles can move by exchanging with their neighbour in what is essentially a monomer based diffusion process. Individual particles are thus susceptible to gravity. However, once tightly bonded, even a dimer is impervious to gravity. A dimer of a heavy species pair will sit bonded together essentially floating ins sea of lighter particles when it should not. This suggests that to more accurately model gravity effects some sort of cluster-cluster diffusion is necessary. Some mechanism for dimers and other tightly bonded clusters to be able to fall with a whole sea or layer of lighter species is needed. The monomer-activated dynamics may be insufficient to capture key behaviours. It should be noted however that the whole model is very much lattice oriented and might not truly be expected to model true fluid flow, but rather to be indicative of pseudo-fluid in complex multi-phase systems.

The layering due to ranked mass species is quite clear cut and monotonic. It may be possible to simulate more complex inversion layers by using less trivial coupling interactions. There is also scope for using non-equal proportions of the non vacant species and thus deliberately creating thin layers that will be much more pervious to cross diffusion of species.

6 Conclusions

We have shown how a lattice gas model based on Kawasaki exchange dynamics is capable of supporting multiple species and therefore representing some of the multi-phase behaviours present in complex fluids. We have added a gravitational field mechanism and shown that the Monte-Carlo updating mechanism successfully uses this to drive a quenched mixture of species states into discernible fluid layers ranked by mass.

The overall model works well and we have rendered and measured systems in both two and three dimensions, scaling up to $Q = 9$ species states. We have identified one weakness of the model in that it is based entirely on monomer activated dynamical exchanges and therefore cannot model the effect of whole frozen clusters of one species falling in a sea of background layer of another. There is therefore scope for experimenting with a cluster-cluster diffusional dynamics in this sort of model

We have experimented with equal fractions of integer massed particles and a binary gravitational field. There is scope for simulating very thin films that would allow other species to inter-penetrate them but also to search the gravitational field parameter space to determine if there is a gradual or more phase transitional change when gravity is applied. Our work has demonstrated the continuing value of building a simulation capable of semi interactive graphical rendering alongside detailed statistical measurements so that human interaction with the former leads to better identification of the phenomena and behaviours pinpointed in the latter.

References

[1] Arratia, P.E.: Complex fluids at work. Physics **4** (2011) 1–3

[2] Johnson, M., Playne, D., Hawick, K.: Data-parallelism and gpus for lattice gas fluid simulations. In: Proc. International Conference on Parallel and Distributed Processing Techniques and Applications (PDPTA'10). Number CSTN-109, Las Vegas, USA (2010) PDP4521.

[3] Rivet, J.P., Boon, J.P.: Lattice Gas Hydrodynamics. Number ISBN 0-521-019710. Cambridge (2001)

[4] Ebrahimi, F.: The shape of invasion percolation clusters in random and correlated media. J. Stat. Mech: Theory and Experiment **P04005** (2008) 1–8

[5] Lenormand, R.: Liquids in porous media. J. Phys.: Condens. Matter **2** (1990) SA79–SA88

[6] Ma'soum, S., Masihi, M.: Invasion percolation in presence of gravity. Iran J. Chem. Chem. Eng. **29** (2010) 71–82

[7] Meakin, P., Feder, J., Frette, V., Jossang, T.: Invasion percolation in a destabilizing gradient. Phys. Rev. A **46** (1992) 3357–3368

[8] Glass, R.J., Conrad, S.H., Yarrington, L.: Gravity-destabilized nonwetting phase invasion in macro-heterogeneousp orous media: Near-pore-scale macro modified invasion percolation simulation of experiments. Water Resources Research **37** (2001) 1197–1207

[9] Tokuyama, M., Enomoto, Y., Kawasaki, K.: Dynamics of fluctuations in Ostwald Ripening. Physica A **143** (1987) 183–209

[10] R.Harris, Jorgenson, L., Grant, M.: Monte carlo lattice-gas simulations of stable and unstable interfaces. Phys.Rev.A **45** (1992) 1024–1034

[11] G.D.Mahon, F.H.Claro: Ising Model with Magnetic Field and the Lattice Gas. Phys.Rev.B **16** (1977) 1168–1176

[12] Kawasaki, K.: Diffusion constants near the critical point for time dependent Ising model I. Phys. Rev. **145** (1966) 224–230

[13] O.Penrose, A.Buhagiar: Kinetics of nucleation in a lattice gas model: Microscopic theory and simulation compared. J.Stat.Phys **30** (1983) 219–241

[14] Lee, T.D., Yang, C.N.: Statistical theory of equations of state and phase transitions. II Lattice Gas and Ising model. Phys. Rev. **87** (1952) 410–419

[15] Bragg, W.L., Williams, E.J.: The effect of thermal agitation on atomic arrangement in alloys I. Proc. Roy. Soc. A **145** (1934) 699–730 Bakerian lecture 1934.

[16] Cernuschi, F., Eyring, H.: An elementary theory of condensation. J. Chem. Phys. **7** (1939) 547–551

[17] Metropolis, N., Rosenbluth, A.W., Rosenbluth, M.N., Teller, A.H., Teller, E.: Equation of state calculations by fast computing machines. J. Chem. Phys. **21** (1953) 1087–1092

[18] Glauber, R.: Time dependent statistics of the Ising Model. J. Math. Phys. **4** (1963) 294–307

[19] Binder, K., ed.: Monte Carlo Methods in Statistical Physics. 2 edn. Topics in Current Physics. Springer-Verlag (1986) Number 7.

[20] Muller-Krumbhaar, H., Binder, K.: Dynamic properties of the Monte Carlo Method in Statistical Physics. J. Stat. Phys. **8** (1973) 1–24

[21] Binder, K., ed.: Applications of the Monte Carlo Method in Statistical Physics. Topics in Current Physics. Springer-Verlag (1987)

[22] Wu, F.Y.: The Potts model. Rev. Mod. Phys. **54** (1982) 235–268

3DCIS: A Real-time Browser-rendered 3D Campus Information System Based On WebGL

Nils Hering[1], **Martin Rünz**[1], **Lubosz Sarnecki**[1] **and Lutz Priese**[1]
[1]Institute of Computational Visualistics, University of Koblenz-Landau, Koblenz, Germany

Abstract— *Most of the current real-time 3D web applications are only available with plug-ins as Flash or additional software as Java. Avoiding this drawback, the new WebGL technology provides hardware accelerated computer graphics for web browsers without requiring plug-ins. Using Blender, WebGL, the WebGL-expanding framework GLGE, and an in-house developed exporter B2G from Blender to GLGE we have realized the cutting-edge web application 3DCIS based on a complex 3D model of our campus. With 3DCIS one is able to explore the campus interactively and to become acquainted with local persons and institutions. Textual information about buildings, rooms and persons is linked with 3D model information to enhance the intuitive experience of 3DCIS.*

Keywords: Web 3D, WebGL, GLGE, export, information system

1. Introduction

It is state of the art to use plug-in based systems to create 3D web applications. Well-known and widely spread examples are Adobe Flash, Unity3D or Microsoft Silverlight. Their main handicap is the user's obligation to install the corresponding plug-in. Another common software system to provide 3D applications in the web browser is the Java applet concept. Java applets do not require an explicit plug-in but an installed Java virtual machine.

The relatively new 3D web technology WebGL [9] avoids those drawbacks. A user may navigate in a 3D environment solely in a WebGL compatible web browser. This comfort is payed by the developer of a WebGL application as WebGL provides only a rudimentary application programming interface (API). On the other hand, development of 3D models is rather simple in Blender. Therefore, we had to build an exporter from Blender to WebGL that we will introduce in this paper. We have released the exporter under the GNU GLPv3 free software license to the community. As an application of B2G we present the campus information system **3DCIS** of our university. An interested visitor may navigate in 3DCIS through a 3D model of our campus and interactively gather further information about persons, rooms, facilities, etc. from the application. 3DCIS uses the probably largest online WebGL model in a real-time application world-wide at present (May 2011). The latest version of 3DCIS is currently available at `http://explore.uni-koblenz.de`.

2. Related work

The WebGL API provides capabilities in developing 3D web content which were previously the exclusive domain of the desktop environment. Leung and Salga deal in [10] with the question how mid level APIs can help the developer to create unique 3D web content. They emphasize the fact that WebGL gives the chance to not just replicate desktop 3D content and applications, but rather to exploit other web features to develop richer content and applications.

DeLillo presents in [5] the WebGLU development library for WebGL. WebGLU provides an API which allows the developer to implement WebGL based content easier and more clearly than with the WebGL API only.

In [6] Di Benedetto et al. introduce SpiderGL, a JavaScript library for developing 3D web applications. The aim of SpiderGL is to simplify the use of WebGL and to provide some extra features like e.g. the handling of asynchronous data loading. SpiderGL is used in [4] where Callieri et al. present a WebGL and SpiderGL based method for the building of interactive 3D visualization schemes for scientific data produced by molecular and cellular biology research.

In [11] Niebling and Becker deal with a web extension of the COVISE visualization environment [13]. To reach this goal they deploy WebGL to provide a web rendering component which allows to explore e.g. post-processed simulation results in a web browser.

Esnault et al. present a flexible framework for the 3D visualization of data in the web in [8]. They mention WebGL as one of the technologies to present the Web 3D result scene to the user.

In [2] Behr et al. introduce a scaleable architecture that implements the HTML5/X3D integration model X3DOM [1]. This architecture offers a single declarative interface to application developers while it provides several render backends. One of those backends is WebGL supplemented by a scenegraph.

Di Cerbo et al. deal with the extension of their e-learning platform DIEL in [7]. By using X3D and X3DOM in combination with WebGL to create a Web 3D interface they achieved to render 3D content on the web without requiring additional software.

In [12] Sons et al. present XML3D, a new technology for the support of interactive 3D content in mixed 2D/3D documents. A portable implementation of XML3D is based on JavaScript and WebGL.

3. WebGL and GLGE

WebGL is a platform independent API used to create 3D content for web browsers. It utilizes the HTML5 *canvas* element and therefore requires a web browser capable of processing both HTML5 and WebGL. WebGL and HTML5 are still in further development by different consortia. WebGL is based on OpenGL ES 2.0, a popular 3D API designed for embedded devices. WebGL simply enables users to draw 3D primitives on a 2D canvas. But it has no scene graph and is not able to load and instantiate textured meshes. WebGL is already supported by a variety of browsers. The future of WebGL is promising, especially as it is a standard since March 2011.

A lot of WebGL frameworks are currently in development. 3DCIS uses GLGE [3]. GLGE is a programming library based on WebGL, providing more comfortable handling of WebGL features. The main benefit of such a library is that much of the low-level operations of WebGL are wrapped by higher-level functionality. This means easier access to WebGL's scope and more comfort in developing usable 3D web applications.

GLGE provides text rendering and offers fast picking of objects. It is open source and written in JavaScript. GLGE is able to load Collada scenes (widely used Khronos standard) as well as scenes stored in it's own XML structure.

4. Blender-to-GLGE exporter

The desired workflow is to maintain 3D models in Blender and to export them to GLGE in such a smooth way that changes in the model can be studied in WebGL immediately, without manual modifications. Blender is free software, productive and available for all major operating systems. It possesses a powerful Python API.

4.1 Blender export situation

Since Blender 2.5 was still in it's beta stages during the beginnings of our work, there was, and in places still is, a lack of community supplied plug-ins like exporters. Fortunately, Blender 2.4 and Blender 2.5 file formats are cross compatible in both directions. This means that a workflow using Blender 2.5 for content creation and 2.4 for export is possible. However, this would result in using two different program instances simultaneously.

Another possibility to export Blender 2.5 data is Collada. Both, Blender 2.5 and GLGE support this XML based format, but lack feature completeness. The Collada export in Blender is implemented with OpenCOLLADA in C++, an MIT licensed Collada API, also available for Maya and 3DStudio. At the start of our work Blender and OpenCOLLADA had to be compiled from source in order to export Collada which is harder to deploy on an artist's system than a plain Python script.

We thus decided to write a new exporter from Blender to the GLGE XML format to have more control over the final result and appearance of the scene. Therefore, two exporters have been implemented. An early one running in Blender 2.49 and our advanced **B2G** (Blender-to-GLGE) running in Blender 2.5x. Both are written in Python and produce GLGE-readable data.

4.2 Early exporter

The early exporter allows to either export the complete Blender project, the complete scene, or the current selection such as separate buildings or objects. It was written for Blender 2.49b in Python 2.6. Mesh objects with position, normal and UV (texture mapping) information are exported. Also camera objects are exported correctly. The material information only holds the texture name but no additional shading information, so only flat shading is possible.

4.3 GLGE scene format and B2G

The new Blender 2.5 Python API uses Python 3.1 and can access the whole range of scene data available in Blender. The aim has been that the resulting GLGE export looks like the Blender 2.5 scene (see the comparison in figure 1). It should be easily modifiable by an artist without editing the exported markup.

The following listing describes a basic GLGE scene XML structure.

```
<glge>
  <material/>
  <mesh/>
  <scene>
    <object/>
    <light/>
    <camera/>
  </scene>
</glge>
```

The root element of the GLGE document format is *glge*. Inside the root element meshes and materials are defined with *mesh* and *material* tags. The mesh to material relation and the instancing of the meshes is defined inside the *scene* tag. A scene can contain 3 different types of children with transformation information. An *object* tag, which is a mesh linked with a material definition, and also *camera* and *light* tags which define the scene's cameras and lights. Furthermore, there is a possibility to group objects which is currently unused by B2G.

The scene tag itself contains an ambient color, a background color and fog settings as attributes. All this information can be found in the world settings in Blender and is exported.

B2G is able to export mesh objects with mixed triangle and quad faces. Beside the vertex position, also the UV coordinates for texture mapping and face normals are exported. The artist can decide if he uses smooth, interpolated normals or solid normals per face in Blender. The normal information is required by the renderer for advanced shading techniques with a Phong model and normal mapping.

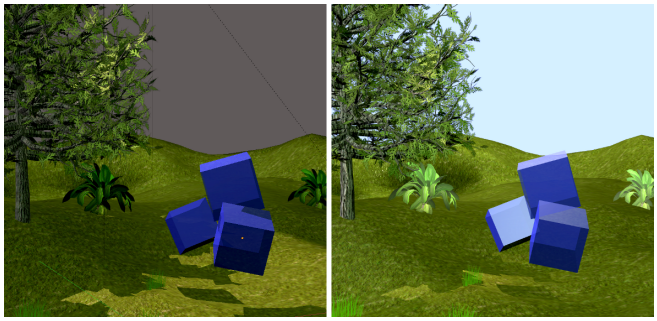

Fig. 1: Comparison between the scene in the Blender 2.55 editor (left) and the exported GLGE scene in the Chromium 9 web browser (right). The sky color is not rendered in Blender's GLSL view. Differences in the specular highlight are also noticeable, since GLGE and Blender use different shading algorithms.

A common technique is the multiresolution modifier where a tessellation can be applied to the mesh data. Blender's mesh modifiers are also supported by B2G.

There are three different types of light objects in GLGE. Point lights, spot lights, and directional lights. Each of these lights can have a different attenuation and color. Constant, linear and quadratic attenuation is implemented in GLGE. For spot lights GLGE renders shadows using shadow mapping. This requires a direction and some extra options. Spotlights are exported, thus shadow mapping in a scene is possible. This slows down performance since the scene has to be rendered one more time for each spot light. Also a shadow map texture has to be stored for each spotlight.

The GLGE material holds the information relevant for the object's shading. Common shading values like specular, shininess and emit are possible. Those options are exported from the Blender material. A material can have a uniform color or can take the information from a color texture map. Additionally normal maps can be set in Blender to gain bump mapping in GLGE. All textures have to have a width and height which is power of two as specified in the OpenGL ES Specification. To render plants B2G handles transparent textures. It is also possible to set the transparency of whole objects which is used to visualize rooms in the campus application. The GLGE scene graph takes care of sorting the transparent objects for every frame.

The GLGE scene file can include further XML files. B2G utilizes that feature and writes the scene, materials and meshes into separate files to maintain readability in a text editor. Opening the big mesh files in an editor is slow and unstable and may result in editor crashes. The exporting of readable XML files is optional, so B2G strips newlines and indentations if desired.

5. 3DCIS

The goal of 3DCIS (3D campus information system of our campus) is to provide a virtual web-based access to the campus and consequently the possibility to explore the campus online. Besides the model-provided local architectural information 3DCIS also visualizes information about the university's departments, employees, facilities and institutions. This information is valuable for students and employees, but 3DCIS shall also attract interested scholars. For the 3DCIS' realization the open source web application framework Django was used with a MySQL database. It is running on an Apache server on Ubuntu Server 10.04 LTS.

The GUI of 3DCIS in the browser consists of three areas: a left vertical navigation bar, an upper horizontal information bar and the central 3D application (see figure 2).

Fig. 2: The GUI of the German 3DCIS version without the browser parts.

5.1 Basic 3D model

Originally, we had created a model of our campus in SketchUp in a previous project and exported it to Blender. So the starting point was a highly detailed 3D model **HPCM** (High-poly campus model) with more than 1 470 000 polygons.

Since in WebGL the model has to be transferred to the client on each page view, a much smaller number of polygons is required. For this reason, we had to downscale HPCM into **LPCM** (Low-poly campus model) in Blender. LPCM uses only 5590 polygons. Figure 3 shows a snapshot of HPCM in Blender, while figure 4 gives a snapshot from LPCM in the web browser.

LPCM simply has flat surfaces where HPCM uses geometry for doors and windows (see figure 5). Consequently, the textures used in LPCM have to contain more information than those in HPCM. On that account a technique called texture baking has been used. Texture baking allows one to render lighting data and geometry data to a texture. As a result, flat surfaces in LPCM reproduce the shape of HPCM

Fig. 3: The HPCM rendered with the Blender 2.5 internal renderer using ambient occlusion and ray tracing.

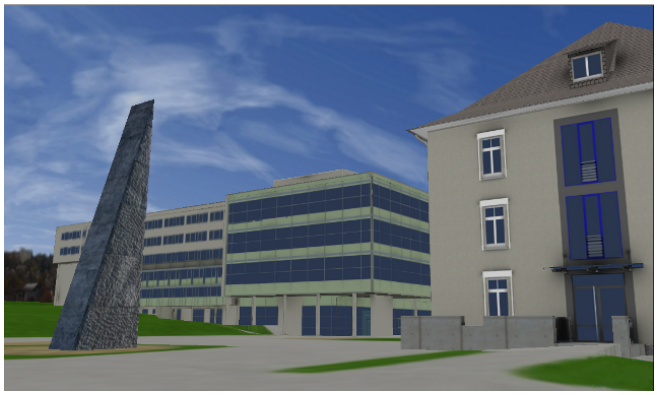

Fig. 4: The LPCM used in 3DCIS.

and contain fixed lightning information. By UV mapping the web application is aware of how to apply textures to objects.

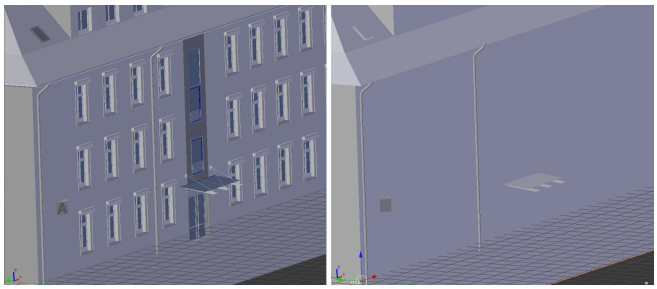

Fig. 5: Comparison of high-poly geometry in HPCM (left) and low-poly geometry in LPCM (right).

To increase the usability of 3DCIS, annotations have been added to LPCM. These annotations imply the locations of rooms, stairways, and elevators which are stored as an instance of a cube mesh as depicted in figure 6. These annotations are used to join the 3D model information with additional information of persons in 3DCIS.

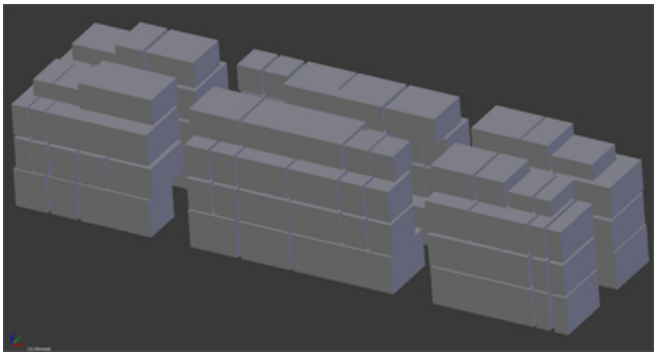

Fig. 6: Annotated rooms (as cubes) in the LPCM Blender model.

5.2 3D user interaction

The handling of 3DCIS is oriented towards 3D computer games to get students interested in our application. The entire campus is presented in WebGL and explorable in a way known from computer games with first-person view.

As usual in 3D applications the view of the user is represented by a camera. This camera indicates e.g. the user's position and view directions. By pressing an arrow key the camera position moves on the ground plane. Shifting the mouse cursor on the 3D application changes the view direction of the camera. A camera-synchronized mini map adapts all the user's movements and alleviates orientation in 3DCIS. The motion speed can be modulated via an options menu. This menu also allows the activation and deactivation of simple billboard texture vegetation.

As there are differences in altitude in the campus model the camera's height has to be set correctly. Using the arrow keys just affects the camera's x- and y-position but not the camera's height. In order to receive height information of the modeled area, a height-map was generated. Our height-map is a simple grayscale image where dark pixels (0 means black) represent lower altitudes and lighter pixels (255 means white) represent higher altitudes (see figure 7).

To move the camera correctly the z-value of its current and aimed position is queried from the height-map. A high gap between those two values indicates that the user is passing an incline. If the gap is too high the terrain is not passable and further movement is prevented. 3DCIS contains a collision detection that prohibits movements into solid objects using the same height map.

There are many possibilities to get information within 3DCIS. The easiest way to receive information is to click on buildings. When a click on a building occurs the building gets highlighted in blue and additional information about this building is displayed. Buildings are also accessible via the navigation bar or via search requests as we will explain in the next subsection.

Rooms can only be addressed via the information or navigation bar. Selected rooms are highlighted in blue and

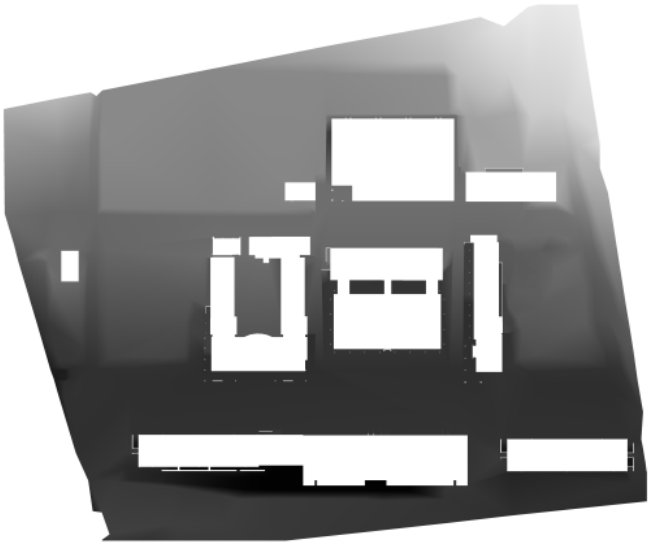

Fig. 7: Height and collision map in which the gray value of a location represents its height in the application.

Fig. 8: A model-annotated room visualized in 3DCIS by a blue cuboid.

their 3D position can be seen in the now transparent building, see figure 8. Rooms are represented by cuboids as described in section 5.1. In order to achieve these different graphic representations (ordinary, highlighted and transparent objects), different materials are in use.

A further interesting feature is the flight option. In addition to the room's visualization the user will experience an automatic flight to the building which contains the requested room. To generate these flights instantly, the 3D environment is divided in 1 216 nodes. Each node is either passable or not passable. The distribution of the nodes is stored in a bitmap which is working as the height-map.

The A* graph search algorithm is used to find the shortest way from the user's position to the room's position. At the end of the flight the camera pans to the room's position in the building.

5.3 Informational features

3DCIS combines the experience of moving through the 3D campus model with useful search features. It is possible to search for buildings, departments, institutions, persons, rooms etc. The search results provide as many information as possible of the linked data, see subsection 5.4. The search result of a person e.g. is visualized in an information window which shows the name and title, an image, telephone number, e-mail address, homepage url and room number. The information window is realized as an overlay over the WebGL content (see figure 2). By clicking the room number, the accordant room gets visualized as described in section 5.2. A click on the flight button next to the room number initiates a flight to the person's room as described in 5.2.

The provided information is accessible by search queries via a search bar on the larger information bar. The automatic search for matching search terms is extended by keyword mapping. The keyword mapping maps syntactical different search terms on semantically similar ones. Alternatively, most information is also available via accordion tabs on the navigation bar. Highest level entries divide the information in "persons", "rooms" and "for persons interested in studies".

5.4 Data mining

To provide the informational features 3DCIS has to have access to data that is contained in three main data sources. The first source is the university's content management system (CMS). Nearly all the university's employees, namely professors, scientific assistants, public employees or student assistants, are documented in the CMS's database. The CMS data is obtained by polling a current XML file regularly using a Python script. This script uses a XML Python module and is called up by a cronjob. The CMS person entries contain data such as name, title, picture, room, telephone number, e-mail address, homepage url etc.

Besides the university's CMS data its LDAP address book is also accessed. For the LDAP access an accordant Python LDAP module is used. The LDAP address book's person entries contain a unique ID, the person's name, room number, phone number and e-mail address. The third main data source consists of manual data. Information about e.g. whole buildings are not available in easy-accessible manner and had to be added manually.

The data is checked having regard to data privacy. E.g. names or e-mail addresses of students from the LDAP which are not published in the CMS, are not published or searchable in 3DCIS.

The collected data is combined using Django data-models. A Django data-model is a python class which automatically sets the data base schema. By using these models one is able to describe and organize a data structure in Python

code. Such models have been designed for *Person, Group, Room* and *Building* for example. The Room data-model, respectively the Room class, looks like this e.g.:

```
class Room(WCObject):
    name = models.CharField(...)
    room_type = models.CharField(...)
    telephones = models.ManyToManyField(...)
    building = models.ForeignKey(...)
    tags = models.ManyToManyField(...)
```

The above code listing is not valid Python code. The dots in brackets are place holders for further descriptions.

6. Conclusion

We use Blender to develop and maintain 3D models. With our in-house developed Blender-to-GLGE exporter B2G we can export our Blender models to WebGL. B2G accomplishes that the GLGE export almost looks like the original Blender scene by exporting all relevant artefacts like e.g. light sources or object's shading information. The user may use WebGL models in the internet browser without any plug-in.

Our 3D campus information system 3DCIS is based on such a WebGL model. 3DCIS provides for example

- interactive navigation in our 3D campus model,
- a camera-synchronized mini map,
- different search options,
- visualization of the search results via
  - automatic flights,
  - correct display of 3D room locations.

Considering nowadays Web 3D conditions 3DCIS uses a rather large model (although we broke down the HPCM to the LPCM). Nevertheless, 3DCIS performs real-time rendering of the campus scene.

3DCIS can be used as an information system for university's employees. It is composed like a common 3D game to attract potential students.

This work is not completed yet. In the future we want to add several more features to 3DCIS. Besides a nicer campus scene, with plants and changing light conditions, we want to increase the number of user adaptable "gameplay" options, e.g. the model's level of detail. Additionally, an English version of 3DCIS is currently under construction. According to this step the data management parts of 3DCIS will be re-engineered and a change from Django to a PHP based system is likely.

Acknowledgments

We would like to thank everybody involved in this work for their commitment. Special thanks go to the student project "Interaktiver Campuswegweiser", Christian Fuchs, Markus Lohoff and Christian Schneider.

References

[1] J. Behr, P. Eschler, Y. Jung, and M. Zöllner. X3dom: a dom-based html5/x3d integration model. In *Proceedings of the 14th International Conference on 3D Web Technology*, Web3D '09, pages 127–135, New York, NY, USA, 2009. ACM.

[2] J. Behr, Y. Jung, J. Keil, T. Drevensek, M. Zoellner, P. Eschler, and D. Fellner. A scalable architecture for the html5/x3d integration model x3dom. In *Proceedings of the 15th International Conference on Web 3D Technology*, Web3D '10, pages 185–194, New York, NY, USA, 2010. ACM.

[3] P. Brunt. Glge api documentation, December 2010. http://www.glge.org/api-docs/.

[4] M. Callieri, R. M. Andrei, M. Di Benedetto, M. Zoppè, and R. Scopigno. Visualization methods for molecular studies on the web platform. In *Proceedings of the 15th International Conference on Web 3D Technology*, Web3D '10, pages 117–126, New York, NY, USA, 2010. ACM.

[5] B. P. DeLillo. Webglu development library for webgl. In *ACM SIGGRAPH 2010 Posters*, SIGGRAPH '10, pages 135:1–135:1, New York, NY, USA, 2010. ACM.

[6] M. Di Benedetto, F. Ponchio, F. Ganovelli, and R. Scopigno. Spidergl: a javascript 3d graphics library for next-generation www. In *Proceedings of the 15th International Conference on Web 3D Technology*, Web3D '10, pages 165–174, New York, NY, USA, 2010. ACM.

[7] F. Di Cerbo, G. Dodero, and L. Papaleo. Integrating a web3d interface into an e-learning platform. In *Proceedings of the 15th International Conference on Web 3D Technology*, Web3D '10, pages 83–92, New York, NY, USA, 2010. ACM.

[8] N. Esnault, J. Royan, R. Cozot, and C. Bouville. A flexible framework to personalize 3d web users experience. In *Proceedings of the 15th International Conference on Web 3D Technology*, Web3D '10, pages 35–44, New York, NY, USA, 2010. ACM.

[9] KHRONOS. Webgl specification, December 2010. https://cvs.khronos.org/svn/repos/registry/trunk/public/webgl/doc/spec/WebGL-spec.html.

[10] C. Leung and A. Salga. Enabling webgl. In *Proceedings of the 19th international conference on World wide web*, WWW '10, pages 1369–1370, New York, NY, USA, 2010. ACM.

[11] F. Niebling, A. Kopecki, and M. Becker. Collaborative steering and post-processing of simulations on hpc resources: everyone, anytime anywhere. In *Proceedings of the 15th International Conference on Web 3D Technology*, Web3D '10, pages 101–108, New York, NY, USA, 2010. ACM.

[12] K. Sons, F. Klein, D. Rubinstein, S. Byelozyorov, and P. Slusallek. Xml3d: interactive 3d graphics for the web. In *Proceedings of the 15th International Conference on Web 3D Technology*, Web3D '10, pages 175–184, New York, NY, USA, 2010. ACM.

[13] A. Wierse, U. Lang, and R. Rühle. A system architecture for data-oriented visualization. In J. Lee and G. Grinstein, editors, *Database Issues for Data Visualization*, volume 871 of *Lecture Notes in Computer Science*, pages 148–159. Springer Berlin / Heidelberg, 1994.

Multilevel Display for Aggregated Document Networks

Richard H. Fowler, Wendy A. L. Fowler, Raul A. Huerta, and Rahul Varshney
Department of Computer Science, University of Texas – Pan American, Edinburg, TX, USA

Abstract *– The challenge of finding documents relevant to a task is pervasive in today's information rich society. Current methods for finding documents focus on keyword search using resources such as Internet search engines or digital libraries provided by professional organizations. Visual representations can augment the search for information, yet the vastness of sources must be dealt with in a way that makes these large bodies of documents comprehensible and individual documents identifiable. The current work describes a system that provides a means to organize documents through graph based clustering and allows the user to display and interact with an abstracted multilevel visual display of information. The clustering techniques used by the system to provide abstracted views exploit the organizational characteristics of document collections and web based sources to supply users a seamless representation useful for overview, document identification, and document retrieval.*

Keywords: visualization, information visualization, information search, multilevel display, network display

1 Introduction

The challenge of finding documents relevant to a task is pervasive in today's information rich society. The tasks range from the consumer's need to gather information to make informed decisions to the scientist's need to remain abreast of new knowledge in his or her field. Current methods focus on keyword search, whether through widely available Internet search engines or digital libraries provided by professional organizations. Visual representations can augment the search for information, yet the vastness of sources must be dealt with in a way that makes these large bodies of documents comprehensible and relevant individual items identifiable.

Grouping, or clustering, of documents such that documents within a cluster are related in some way is one mechanism to provide orderings that can facilitate search. Nonetheless, depending on the nature of the clustering organization imposed on the documents, the user can still be presented with an overwhelming number of possibilities. Multilevel orderings provide one approach that can supply an organization natural and useful for information display.

The current work describes a system that provides a means to organize documents through graph based clustering and allows the user to display and interact with an abstracted multilevel display of information. This multilevel view provides a mechanism for document abstraction and aggregation that makes the visual representation of large data sets tractable in an interactive system. Though the principles applied in the system are domain independent, the system's techniques are particularly appropriate for data organizations commonly found for document collections and web information structures.

2 Related work

Among the earliest characterizations of the information visualization process is that of Shneiderman [28] in which he suggests that systems should provide "overview first, zoom and filter, then details-on-demand." To facilitate this approach most information visualization systems display structure at several different scales or levels of abstraction. In such multilevel systems overview of the information's structure is provided by high level views, the user navigates to lower levels of abstraction to filter information through identification of relevant parts of the structure, and finally is able to access individual items at the lowest level view.

2.1 Multilevel display and aggregation for visualization

Techniques for data reduction used in information visualization center on providing representations that allow the user to explore and make sense of a data set by means of data abstractions. Among the most useful are techniques for aggregation, such as clustering in which individual items are successively grouped to form subsets of related data items. For visualization, the aggregation in *data space* is coupled with a visual representation in the *display space* [11] that can convey information about the underlying data elements.

2.1.1 Multilevel display

Multilevel visualization is an effective technique for facilitating the processes of overview and data exploration because it changes the visual representation to present the data at different levels of abstraction or detail as the user pans and zooms [13, 29]. With a high level view, because a large amount of data must be displayed, data elements are highly abstracted. As the user zooms in, the data density decreases,

and more detailed representations of individual data elements are shown.

Two types of abstraction are performed in multilevel visualizations, *data abstraction* and *visual abstraction* [29]. Data abstraction, such as the aggregation of individual elements, changes the underlying data before the abstracted elements are mapped to visual representations. Visual abstractions change the visual representation of data elements to provide more information as the user changes level of abstraction or view. In multilevel systems, the user determines which parts of the whole structure or which objects are displayed and the scale at which the substructure or object is displayed.

Interaction techniques may change structure scale uniformly in the user's display, such as with zooming, or structure may be varied within a single display, such as with distortion techniques, e.g., fisheye views [12], which have non-uniform display scales within a single user display. In both approaches the goal is that the user will attain an integrated understanding of a very large structure and its contents by moving through the space. As examples, geographic display typically holds scale constant within the user display and provides different scales as the user zooms in and out. Panning holds scale constant, but displays a different part of the geographic structure at the same scale. Cities might be represented as labeled, colored regions when the display is zoomed out, but add increasing level of detail, as the user zooms in changing scale, e.g., first by showing streets, then ultimately a satellite photograph. In systems for visualizing semantic domains, for which there is no physical representation, high level views are often characterizations of the domain, e.g., for a document collection high level views might present topics and the user might navigate through successively more detailed subtopics, until the document itself is displayed.

2.1.2 Aggregation

Aggregation of data elements is at the core of techniques to form multilevel displays. For physically based systems, such as zoomable geographic maps, the aggregates are necessarily hierarchical, due to the direct mapping of physical spaces. When the data elements are not physical, the choice of aggregate is less straightforward [10], and the relations of aggregates need not be hierarchical. This is noteworthy because the mapping of data space to visual space and derivation of multilevel display is more challenging with non-hierarchical aggregations. Typically, the data organization can be manipulated as a multilevel structure for selecting the current level of detail displayed. Depending on the visualization technique, the visual aggregate can also convey information about the underlying data items.

A fundamental distinction in deriving data organizations is whether the procedure is top-down, forming the organization by successively dividing the set of data elements, or bottom up, forming the organization by successively combining elements of the data set. Both approaches use similarity measures defined using a data-specific distance function. Bottom-up, or agglomerative, aggregation proceeds by considering each data item as an aggregate, then iteratively combines similar aggregates into a single aggregate. Top-down, or divisive, aggregation begins with one aggregate containing all the items and repeatedly divides aggregates until a particular number of aggregates has been reached. At completion of the process, a set of aggregates has been created that provides an abstraction of the data space. In hierarchical organization each aggregate item consists of one or more children, while in non-hierarchical organizations relations among aggregates is more general. The most common aggregation techniques are clustering approaches, such as graph-based (discussed below) or k-means clustering [20, 21]. Others include quadtree and octree-based methods [10], as well as data cube aggregation [29].

2.1.3 Graph-theoretic clustering

Graph-theoretic clustering techniques operate on data elements considered as a graph, often with data elements as nodes in the graph and similarity measures as edge weights. Graph-theoretic clustering can often support a straightforward mapping of data space to visual space, and it has found wide application in information visualization.

Among the most widely used graph-theoretic divisive clustering algorithms is Zahn's [31], based on a minimal spanning tree (MST) derived from data element distances [20]. The algorithm to form MST based clusters in its simplest form proceeds by successively deleting MST edges with the largest lengths to generate clusters. For example, Figure 1 shows the MST obtained from nine points. By deleting the link labeled CD, the edge with the maximum length, two clusters are obtained. The second cluster might be further divided into two clusters by deleting the edge EF, which has the maximum length after CD is deleted.

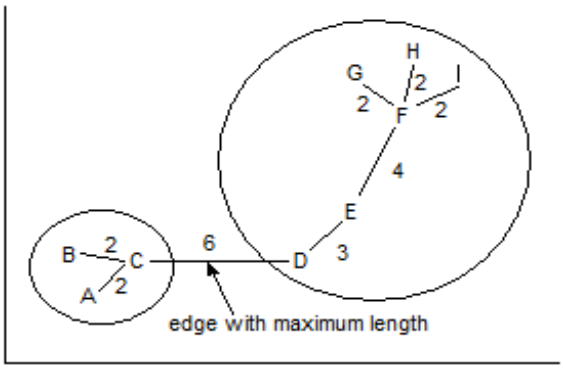

Figure 1. Graph-theoretic clustering using MST. Clusters of items are formed by successively deleting high distance edges in the MST. After Jain [20].

Jain [20] points out that many hierarchical clustering algorithms are also related to graph-theoretic clustering. For example, single-link clusters are subgraphs of the minimum spanning tree of the data [15] that are also the connected components [14], and complete-link clusters are maximal complete subgraphs. Maximal complete subgraphs have been proposed as the strictest definition of a cluster [2, 26]. Ozawa [25] provides a graph-oriented approach for non-hierarchical structures and overlapping clusters, and many other approaches have been described [1, 11, 20].

2.2 Multilevel graph and cluster display for visualization

The utility of aggregation for visualization is well-known, and a number of systems incorporate various schemes for the derivation of aggregated data spaces and display [1, 31]. Elmvquist and Fekete [11] provide a broad-based review and suggest guidelines for design.

Among the earliest descriptions of three dimensional visual representations of clustered graphs for multilevel display is that of Eades and Feng [9]. The authors provide techniques for drawing clustered graphs, which they define as graphs with recursive clustering structures over the vertices. The techniques are relevant to the aggregate organizations discussed earlier, as well as a wide range of other techniques. In one of their techniques using plane drawing, each level in a tree is represented by a line drawing in a single plane, as shown in Figure 2. This provides a sequence of plane drawings, one for each level in the hierarchy, and a three dimensional drawing of the tree displays the planes of each level together with edges of the tree between the planes.

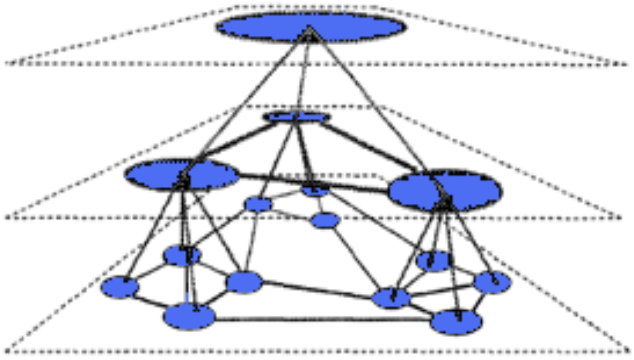

Figure 2. Multilevel graph display. Each level in a recursively formed clustering is displayed on a plane and a three dimensional drawing is used to show connections between levels.

Even with the general schema for display given by Eades and Feng for multilevel display, the question of node placement within a level remains. Force-directed node positioning is extensively used to create aesthetically pleasing results and satisfy a number of criteria for effective graph layout, e.g., number of edge crossings [4, 6, 7, 17, 24]. Force-directed node placement algorithms treat a graph as a physical system in which nodes are connected by springs that model edges. Springs pull connected vertices together when stretched and push vertices apart when compressed. Starting with an arbitrary placement of vertices, the algorithm iteratively calculates the force in the system of springs and moves nodes to minimize force in the system.

Force-directed layout has been used in visualizing clustered graphs [18], including navigation within the drawing [8]. The general approach has been to provide techniques for interaction and navigation based on expanding and collapsing clusters in which each time a cluster is expanded in navigation, the lower level is drawn using force-directed layout [1, 16, 23].

3 Display of document network aggregates

The current work addresses the need to display the large information spaces common to document collections by providing a browsable interface that utilizes aggregation of documents to provide both orientation within large collections and navigation mechanisms facilitating user search. The system utilizes a variant of MST based clustering for the data abstractions upon which display and interaction mechanisms are based. This approach has the advantage of providing computationally efficient derivations of both data space and visualization space. Additionally, the system provides mechanisms for text based user search to initiate placement within the visualization and aid efficient user directed search.

3.1 Document collection clustering – data space

The system's data organization for a document collection is formed by using clustering techniques to divide the collection into subsets of documents that are related by their semantic content. The graph based clustering technique utilizes a distance matrix reflecting similarity of document pairs formed by measuring term co-occurrence for each document with every other document. Document pair distance used in deriving the data organization is calculated using the vector space model [27]. In this technique documents are represented as vectors of terms, and document similarity reflects the number of terms common to a document pair.

Distances among documents are used to form a MST that serves as the basis for the system's graph based clustering algorithm. Figure 3 shows the complete MST arranged using force directed layout in three dimensions to position nodes that represent individual documents in the collection. Clearly, such a display is far too dense for users to effectively utilize

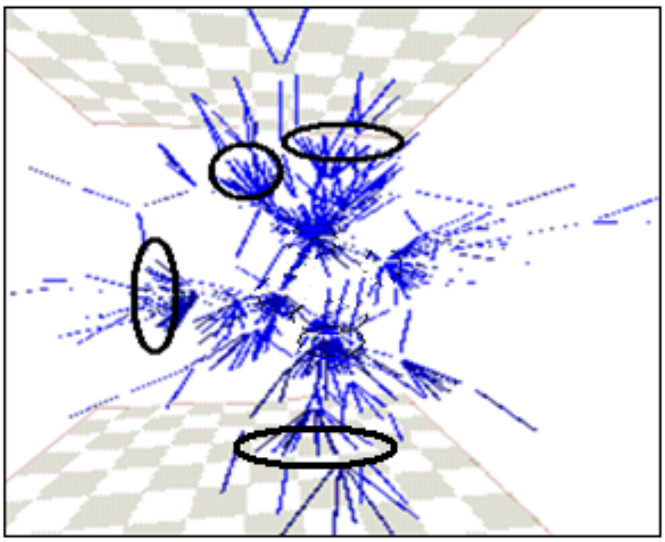

Figure 3. MST of documents positioned in three dimensions using force directed layout. Using such a display would at best be of limited utility to users. Leaf nodes of high degree parents are circled.

in search and navigation. Graph based clustering is used for data abstraction to reduce complexity and serve as the basis for display in visualization space.

The basic approach of Zahn's original description of MST based graph theoretic clustering [31] has seen many refinements and variations [21]. The approach used here provides a variant that has proved effective for forming useful groupings of elements with organizations characteristic of a number of domains for which visualization is useful, such as document collections and web based information sources. Such data sets often have many individual elements connected to a single element. As examples, the characteristic "star" organization evident in web sites, in which many documents are pointed to by a single page, or the hubs and authority description of the web [22], in which hub documents have many links out and authority pages have many links in. Similarly in document citation graphs, often cited documents have high in degree and review articles have high out degree. The MST representation of Figure 3 exhibits this sort of organization. There are many cases in which a large number of documents are connected to a single document. The circled documents in the figure highlight examples.

The system's data organization centers on graph-based clusters formed in a multi-step process using the MST formed from document similarities. Initially, a first level aggregate node set is formed. The set consists of those nodes that have number of leaf nodes above some threshold, and the aggregate is that node together with its children. These first level, or leaf, aggregate nodes are used both in formation of clusters and in display to the user during navigation. In general they capture and abstract much of the "star-like" link quality of the MST.

The second step follows the general MST based cluster formation approach in which clusters are formed successively by removing high distance links to form an arbitrary number of clusters. Varying the number of clusters provides a mechanism to vary the level of abstraction and detail to be used by the system in its display and retrieval capabilities. These clusters contain sets of documents and aggregates with high content similarity, as reflected in the link structure of the original MST. For display and navigation, clusters are connected using minimum distance among cluster centroids.

3.2 Creating views effective for user navigation and search – visualization space

The system's visualization facilities create a display space with which the user can interact to facilitate information search and understanding, as shown in Figure 4. The system makes use of aggregate nodes representing clusters to provide multilevel views. Pan and zoom facilities are provided for this space of aggregates. The upper left window shows the current view and navigational position in the multilevel cluster space, and so provides an abstracted view of the document collection. The size of the ellipse enclosing the cluster's topic label reflects number of documents in the cluster.

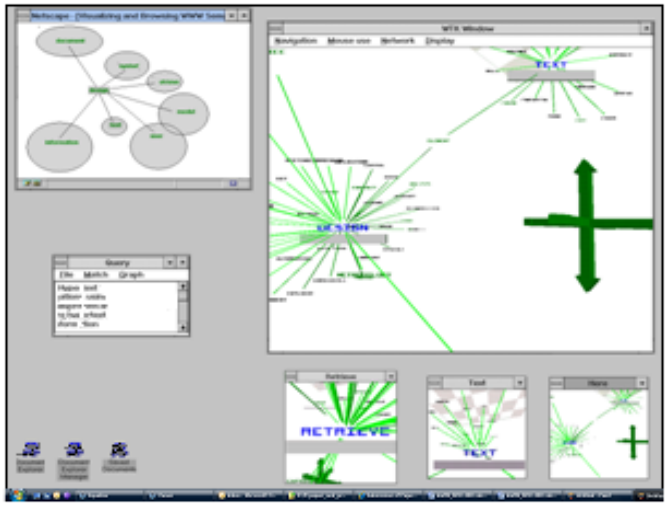

Figure 4. The system's visual displays. The upper left window displays aggregate node clusters at the user's current level within the document structure. The window to right is a linked display of lowest multilevel views showing cluster labels and individual documents. Below the detail view window are "visual bookmarks" used for navigation. A keyword query used to initiate search is shown below the multilevel window.

A second display window, shown to the right of the multilevel window, shows the user a detailed view of clusters, including individual documents. Upon selection of a particular aggregate node in the multilevel view window, the view in the detail window is centered on the aggregate node with individual child documents of the aggregate node displayed, as well as any other aggregate node directly connected to the selected node. The user can navigate in the document space, and the two windows are linked so that a change of position in one is reflected in the other. The user can select an individual document to view its contents.

The aggregate node window serves to provide orientation within the document collection, both by displaying the abstraction of the document space created by the clustering scheme and by focusing the user's view on a particular level of the multilevel document organization. This abstracted view can be contrasted with the detailed view provided by the linked window for individual document viewing, the most fine grained of the views. Here, documents are displayed in a three dimensional space with elements positioned by force directed layout. As a three dimensional space, it presents the user with well known display and navigation challenges. The system provides "visual bookmark" navigation facilities to assist in navigation and search, as shown in the bottom right of Figure 4. At any point in browsing the user can create a visual bookmark to which the user can later return that records the user's position and view direction together with a snapshot of the viewing window.

3.3 Assisting user-directed search

A principle of information search is to provide users' multiple paths of access to information [3]. The capabilities of the system center on cluster based document collection organization and its use in visual user directed search. Keyword search for individual documents can provide a useful complement to group based search as provided by clusters [5, 19]. The system provides such a combination through guidance in directing users to clusters that contain documents likely to be relevant to the user's information needs. In addition to browsing and display functions, the system also provides conventional vector-space keyword query match to individual documents. Using keywords, Figure 5 shows the location of the documents that best match the query. The cluster of best match is provided to the user as a point to initiate search, and the user can select to have matched documents highlighted in the detailed view window during visual search.

4 Conclusions

The present work explores the utility of graph theoretic cluster mechanisms based on MSTs for deriving structures useful in visualization of document structures. The formation of two types of aggregate nodes and their use as part of both cluster formation and visual display provides a mechanism for multilevel display that can serve to augment other techniques.

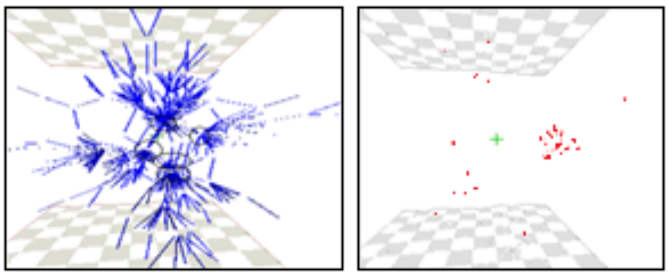

Figure 5. Location of best matches to keyword query used to provide information to assist in user directed search.

5 Acknowledgements

This work was supported by Department of Education grant P116Z0202159 and the University of Texas – Pan American Computing and Information Technology Center.

6 References

[1] F. Abello and N. Krishnan, Ask-graphview A large graph visualisation system," *IEEE Trans. on Visualization and Computer Graphics*, vol. 12, no. 5, pp. 669–676, 2006.

[2] J. G. Auguston and J. Minker, "An analysis of some graph theoretical clustering techniques," *J. of the ACM*, vol. 17, no. 4, pp. 571–588, 1970.

[3] M. J. Bates, "Subject access in online catalogs: A design model," *J. of the American Society for Information Science*, vol. 37, no. 6, pp. 357-386, 1986.

[4] J. Barnes and P. Hut, "A hierarchical $O(n \log n)$ force calculation algorithm," *Nature*, vol. 324, no. 4, pp. 444–449, 1986.

[5] D. B. Crouch, C. J. Crouch, and G. Andreas, "The use of cluster hierarchies in hypertext information retrieval," in *Proc. Hypertext '89*, pp. 225- 237, 1989.

[6] T. Dwyer, K. Marriott, and M. Wybrow, "Integrating edge routing into force-directed layout," in *Proc. 14th Int. Symp. on Graph Drawing (GD'06)*, pp. 8-19, 2007.

[7] P. Eades, "A Heuristic for graph drawing," *Congressus Numerantium*, vol.42, pp. 149-160, 1984.

[8] P. Eades, "Navigating clustered graphs using force-directed methods," *J. of Graph Algorithms and Applications*, vol. 4, pp. 157–181, 2000.

[9] P. Eades and Q.W. Feng, "Multilevel visualization of clustered graphs," in *GD '96: Proc. 4th Int. Symp. on Graph Drawing*, pp. 101–112, 1996.

[10] N. Elmqvist, T. N. Do, H. Goodell, N. Henry, and J. D. Fekete, "ZAME: Interactive large-Scale graph visualization," in *Proc. IEEE Pacific Visualization Symp.*, pp. 215-222, 2008.

[11] N. Elmqvist and J. Fekete, "Hierarchical aggregation for information visualization: Overview, techniques, and design guidelines," *IEEE Trans. on Visualization and Computer Graphics*, vol. 16, no. 3, pp. 439-454, 2010.

[12] G. W. Furnas, "Generalized fisheye views," in *Proc. Human Factors in Computing Systems CHI '86*, pp. 16-23, 1986.

[13] G. W. Furnas and B. B. Bederson, "Space-scale diagrams: Understanding multiscale interfaces," in *Proc. Human Factors in Computing Systems CHI '95*, pp. 234-241, 1995.

[14] G. C. Gotlieb and S. Kumar, "Semantic clustering of index terms," *J. of the ACM*, vol. 15, pp. 493–513, 1968.

[15] J. C. Gower and G. J. S. Ross, "Minimum spanning trees and single-linkage cluster analysis," *Applied Statistics*, vol. 18, pp. 54–64, 1969.

[16] M. Granitzer, W. Kienreich, V. Sabol, K. Andrews, and W. Klieber, "Evaluating a system for interactive exploration of large, hierarchically structured document repositories," in *Proc. IEEE Symp. on Information Visualization (INFOVIS'04)*, pp. 127–134, 2004.

[17] W. Huang, P. Eades, S. Hong, and C. Linz, "Improving force-directed graph drawings by making compromises between aesthetics," in *IEEE Symp. on Visual Languages and Human-Centric Computing*, pp. 176-183, 2010.

[18] M. Huang and P. Eades, "A fully animated interactive system for clustering and navigating huge graphs," in *GD '98: Proc. 6th Int. Symp. on Graph Drawing*, pp. 374–383, 1998.

[19] N. Jardine and C.J. van Rijsbergen, "The use of hierarchical clustering in information retrieval," *Information Storage and Retrieval*, vol. 7, pp. 217–240, 1971.

[20] A.K. Jain, M.N. Murty, and P.J. Flynn, "Data clustering: A review," *ACM Computing Surveys*, vol. 31, no. 3, pp. 264-323, 1999.

[21] L. Kaufman and P.J. Rousseeuw, "*Finding Groups in Data: An Introduction to Cluster Analysis,"* John Wiley and Sons, 1990.

[22] J. M. Kleinberg, "Hubs, authorities, and communities," *ACM Computing Surveys*, vol. 31, no. 4. 1999.

[23] G. Kumar and M. Garland, "Visual exploration of complex time-varying graphs," *IEEE Trans. on Visualization and Computer Graphics*, vol. 12, no. 5, pp. 805–812, 2006.

[24] P. Kumar and K. Zhang, "Visualization of clustered directed acyclic graphs with node interleaving," in *Proc. ACM Symp. on Applied Computing (SAC'09)*, pp. 1800-1805, 2009.

[25] K. Ozawa, "A stratificational overlapping cluster scheme," *Pattern Recogn.*, vol.18, pp. 279–286, 1985.

[26] V. V. Raghavan and C. T. Yu, "A comparison of the stability characteristics of some graph theoretic clustering methods," *IEEE Trans. Pattern Anal. Mach. Intell*, vol. 3, pp. 393–402, 1981.

[27] G. Salton, C. Yang, and A. Wong, "A vector space model for automatic indexing," *Communications of the ACM*, vol. 18, no. 11, pp. 613-620, 1975.

[28] B. Shneiderman, "The eyes have it: A task by data type taxonomy for information visualizations," in *Proc. IEEE Symp. Visual Languages*, pp. 336-343, 1996.

[29] C. Stolte, D. Tang, D., and P. Hanrahan, "Multiscale visualization using data cubes," *IEEE Trans. Visualization and Computer Graphics*, vol. 9, no. 2, pp. 176-187, 2003.

[30] R. Bourqui, D. Auber, and P. Mary, "How to draw clustered weighted graphs using a multilevel force-directed graph drawing algorithm," in *Proc. 11th Int. Conference Information Visualization*, pp. 757-764, 2007.

[31] C. T. Zahn, "Graph-theoretical methods for detecting and describing gestalt clusters," *IEEE Trans. Computing*, vol. 20, pp. 68–86, 1971.

3D Visualization of High-Dimensional Discrete Data

SeungJin Lim
Integrated Science and Technology, Marshall University, Huntington, WV, U.S.A.

Abstract— *The need for effective visualization of high-dimensional data is still in demand in the field of scientific data analysis. In this paper, we present interactive 3D hyperedges as a 3D metaphor for visualizing high-dimensional discrete datasets with an emphasis of enhancing the separation of data instances in a dataset by means of statistical significance. The effectiveness of the proposed visual metaphor is demonstrated by examples throughout the paper.*

Keywords: 3D visualization, high-dimensional data, 3D metaphor, frequent itemset mining

1. Introduction

High-dimensional data is prevailing in the world of scientific data analysis. Examples include spatial co-located feature analysis in spatial databases [8], biomedical analysis of cellular proteins for early cancer detection using mass spectroscopy [4], [12], [5], and social network analysis on the Web [9], [3], to name a few. Visualization techniques and tools of such high-dimensional data are necessity rather than convinience in modern data analysis due to the high complexity and volume of data.

Visualization of high-dimensional data can be achieved by a series of two-dimensional visualization for every distinct pair of dimensions. This technique has been widely used because it is easy to understand and implement. An example is found in Weka [1] as shown in Figure 1 in which $25(= 5 \times 5)$ 2D scatter plots are created from the UCI Iris dataset. This dataset has four independent variables (`petalwidth`, `petallength`, `sepallength` and `sepalwidth`) and three class labels (*Iris-setosa*, *Iris-versicolor* and *Iris-virginica*), and is frequently used to benchmark classification algorithms. In the figure, it is easy to see that even without running a classification algorithm, the `petalwidth` and `petallength` attributes together are capable of separating one class from another whereas `sepallength` and `sepalwidth` are not as good as the previous two. Scatter plots, however, do not generalize or scale up well with high-dimensional data as it would require to generate up to n^2 plots from an n dimensional dataset.

Two alternative, more sophisticated visualization techniques are noticeable for their capability of handling high-dimensional data: Parallel coordinates [10], [13] and Circle segmentation techniques [6]. In Parallel coordinates, each dimension is represented as a line parallel to each other. The values of each dimension are drawn on the respective

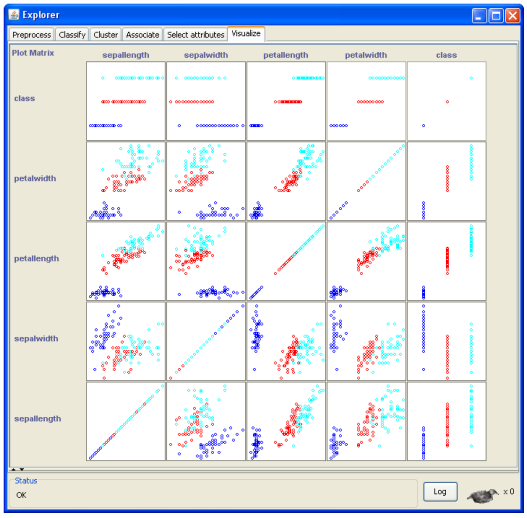

Fig. 1: Scatter plots for UCI Iris dataset in Weka. The visual feedback from the plots indicates that `petalwidth` and `petallength` are good to separate the data into classes.

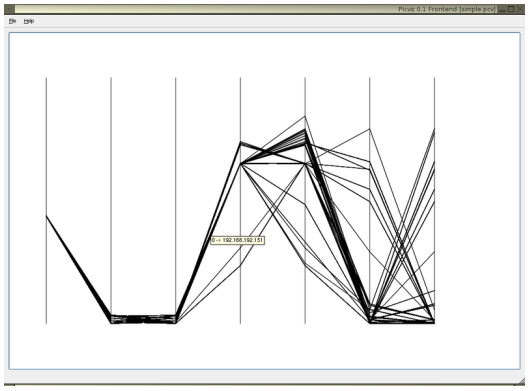

Fig. 2: Parallel coordinates for a 7-dimensional dataset. Image source: Wikipedia

line as points. Hence, the universe of the n-dimensional data is represented as n parallel axes. A data instance in the dataset is an n-dimensional vector $(p_1, p_2, \ldots, p_n)$ forming a polyline with p_i as a vertex on the i-th axis. As illustrated in Figure 2, Parallel coordinates generalize well for high-dimensional datasets by means of adding more axes. It is also clear in the figure that the first three axes do not separate the data well.

The primary concern of Parallel coordinates, however, is the potential misinterpretation of the dataset D when

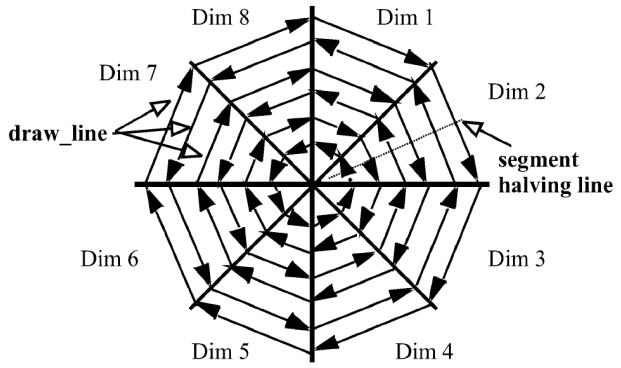

Fig. 3: Circle segmentation technique [6] for high dimensional data

D is rendered in different axis ordering. It is because the technique typically divides the screen left to right and vertical axes are evenly spaced horizontally. Hence, the technique unexpectedly creates a distinct notion of left (or first) and right (or last) axes, as in traditional histograms and scatter plots. In most scientific domains, however, the axes in fact form a *named tuple*, i.e., a unordered data entity, like a set of attributes in relational databases. Putting unordered data into a traditionally ordered visualization framework may cause biased visual feedback. (We call this positional or orientational visual bias without a formal definition.) Due to this inherent positional or orientational visual bias, Parallel coordinates support manual reordering, rotation and scaling of the axes.

In the circle segmentation techniques [6], axes are originated from the midpoint of the screen as radial lines, as illustrated in Figure 3. The figure shows an example of circle segmentation for a 8-dimensional data. Each data instance is represented as a concentric polygon in the techniques. The lengths or vertices of the data instance correspond to the numeric magnitude of the data values. The techniques are less prone to biased visual feedback since the divided areas are circular and do not have a distinct notion of the first and last axes.

These two techniques are mainly adopted in 2D visualization [7], [14], [11]. 3D visualization of high-dimensional data is still in its infancy stages. A major difficulty of 2D visualization techniques such as Parallel coordinates and Circle segmentation techniques is that visual cues can quickly become cluttered as the amount of visual information increases. It is generally accepted that 3D can provide a better visualization platform than 2D mainly because 3D is more natural to human cognitive processing for high dimensional data. In addition, visual cues in 3D are far less cluttered than in 2D for the same amount of visual information.

We present a 3D visualization metaphor for high-dimensional discrete data in this paper. The universe of the n-dimensional dataset is mapped onto a circle of n dimensions, rather than a rectangular parallel axes, represented by 3D objects in our work to minimize bias in visual feedback. Each data instance is modeled as a k-ary tuple, $k \leq n$, where k is the number of values present in the instance, which is in turn modeled as a k-ary hyperedge in our work. We also present a prototype of the proposed 3D metaphor. The key highlights of our work include

1) Each k-ary tuple being modeled as a 3D k-hyperedge whose vertical height along the y-axis represents the statistical significance of the data instance within the dataset while the constituent dimensions (i.e., axes) are arranged on the circumference of a circle as 3D objects on the x-z plane. This layout guarantees not only to minimize positional or orientational visual bias but also to maximize the amount of visual information displayed on the screen.
2) Each hyperedge being equipped with multiple visual cues, i.e., color, brightness, thickness and height, for highly effective visual feedback to capture the statistical significance of each data instance.
3) The 3D metaphor being general enough and suitable for visualizing any undirected, quantifiable many-to-many relationships among data instances.
4) The visual model being highly interactive in our implementation for effective user-driven exploration of the embedded information. The user can start with a global summary of the input dataset and drill down the detailed local information by zoom-in, and catch different useful global synopses of the dataset by rotation and navigation through the underlying relationship network. All the 3D visual objects are clickable for this purpose.

The rest of this paper is organized as follows: the proposed 3D visual metaphor is presented in Sec. 2 with examples. A brief summary of our experimentation on the proposed metaphor is presented in Sec. 3. Finally, concluding remarks are presented in Sec. 4.

2. The 3D Visual Metaphor

The purpose of the proposed 3D visual metaphor is enabling the user to visually and interactively explore the given high dimensional discrete dataset in search of any patterns of high statistical significance. In the end, the user would appreciate the old axiom “a picture is worth a thousand words." We begin with a discussion on the visual representation of a high-dimensional space in the proposed metaphor.

2.1 High-Dimensional Space

Since we focus on the visualization of discrete datasets, a nominal representation of dimensions is sufficient. We do not

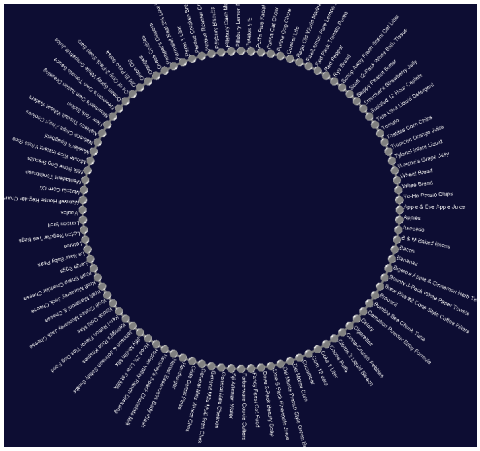

Fig. 4: Objects of uniform shape and size that are arranged along the circumference of the circle, and viewed from $+y$-axis.

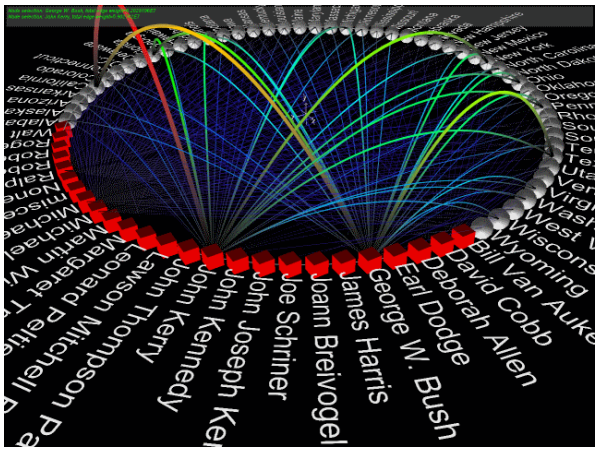

Fig. 6: Objects of different shapes. 25 Presidential candidates are represented by red boxes and the 50 states by gray spheres.

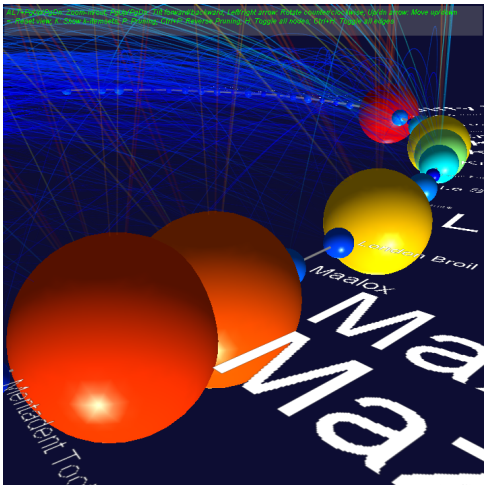

Fig. 5: Objects of different radii signifying different statistical importance.

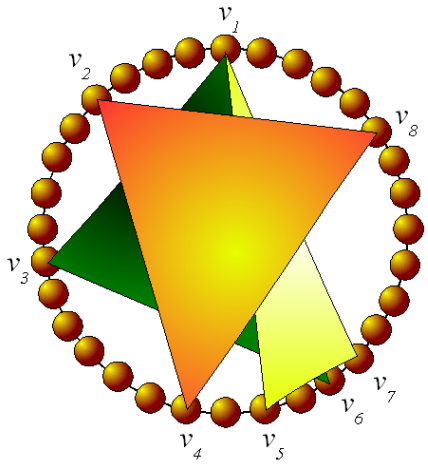

Fig. 7: 3-ary hyperedges as simple triangles

need an ordinal representation because there is no implicit ordering in the dimensions. Should the dataset represent continuous data, an interval or ratio representation would be necessary. For this reason, a dimension is represented using a point geometry such as a sphere with a minimal radius rather than a line or an area.

For the layout of the 3D objects representing dimensions, the circular layout (as presented in the circle segmentation techniques) is preferred over rectangular layouts (as seen in Parallel coordinates) for mainly two reasons: first, to minimize the positional or orientational visual bias that has been discussed earlier, and second to maximize the information density given a number of pixels on the screen. For the second point, consider a circle of radius r and a square of side $2r$. The number of dimensions that can be represented on the square is proportional to the side length, i.e., $2r$, whereas that of the circle is proportional to the circumference of the circle which is $2\pi r$. That is, a circle of radius r will have π times more visual capacity than a square of side length $2r$.

a) Object shape, color and size: In our model, objects representing dimensions primarily have the same shape and size when there is no important semantic division in them, as shown in Figure 4. At times, however, dimensions may have different meanings in the dataset. One typical example can be found in frequent itemset mining or information retrieval in which some items or words may have different statistical significance. Different object sizes can be employed in such a case, as illustrated in Figure 5. Also, we may consider a situation where dimensions are conveniently divided into different semantic groups. Different object shapes can be used to accommodate this need. For example, objects in

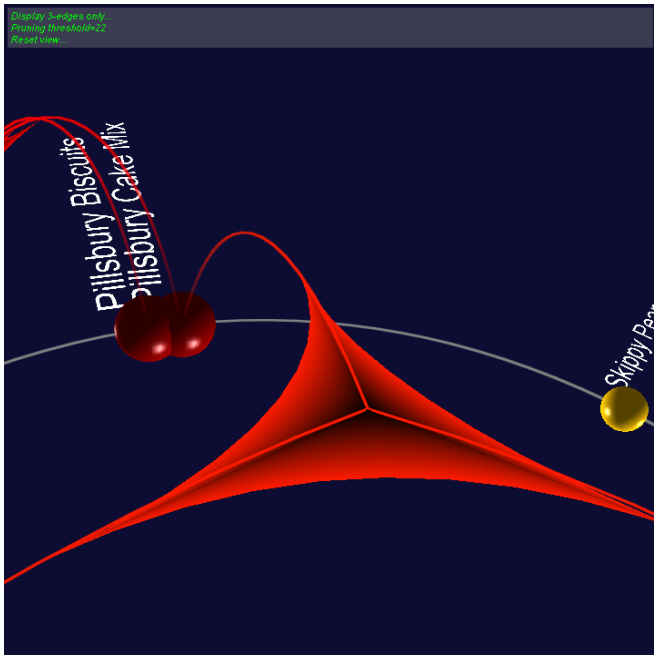

Fig. 8: A 3-tuple with constituent dimensions in background represented as a hyperedge of degree 3 whose red color signifies its high statistical significance.

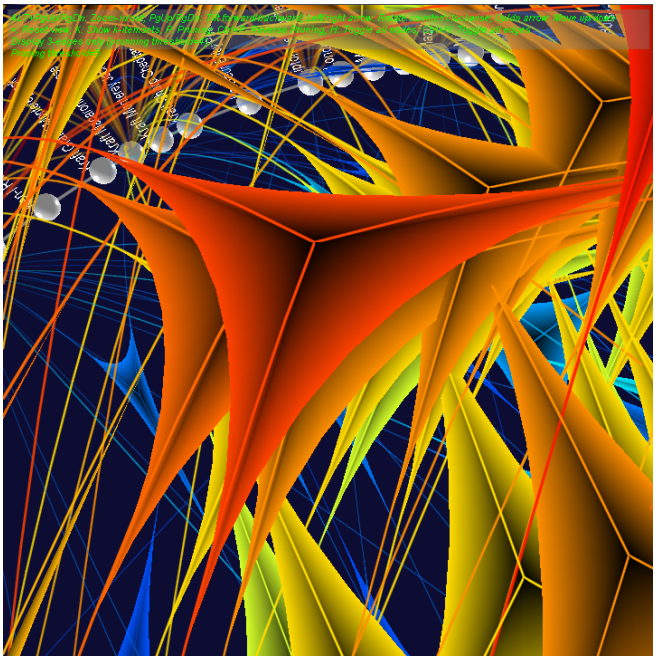

Fig. 9: 3-tuples with peer 3-tuples of different statistical significance represented in different colors and heights

Figure 6 represent two distinct groups: US presidential candidates and states. The candidates are represented by red cubes and states by gray spheres to reinforce visual feedback.

2.2 High-Dimensional Data as Hyperedges

Our main focus in this work is to develop an effective 3D metaphor for n-dimensional data instances where n is a reasonably large integer value. We investigated several geometric shapes as option. One naive option would be a simple 3D polygon which has k edges for k-ary tuples, as illustrated in Figure 7. The advantage of this option is the easiness of implementation. However, it has a significant drawback: when a data instance d whose arity is close to n exists, it is possible that the hyperedge of d would block other hyperedges of lower arities from the user's view.

A remedy to the problem is to use spherical edges for the polygon. One such an example for 3-ary hyperedge can be found in hyperbolic geometry, namely hyperbolic triangle. The characteristics of hyperbolic triangle are well studied in a 2D space. However, extending the theory of hyperbolic triangle to a higher dimensional geometric shape in a 3D space for the purpose of implementation requires substantially more effort.

An alternative approach employed in our work is to use Bezier curve for edge shape as discussed below.

b) Geometry of hyperedges: A 3D hyperedge has two parts in our metaphor: legs and a cover. A k-ary hyperedge has k legs plus a 3D surface covering the midpoint of the legs to augment the 3D look of the hyperedge. In designing and implementing such hyperedges, we are ought to maximize the separation of hyperedges from each other for effective data analysis. We begin with the construction of legs.

Each k-ary tuple is first mapped to a k-ary hyperedge of k legs, each of which is a quadratic half Bezier curve standing vertically. A quadratic Bezier curve requires three control points to define: given three control points p_0, p_1 and p_2, the quadratic Bezier curve is defined as a function of $t\in$ [0,1]

$$B(t) = (1-t)^2 \cdot p_0 + 2t(1-t) \cdot p_1 + t^2 \cdot p_2$$

where t denotes a curve segment.

Let I be a k-tuple whose constituent k dimensions i_1, ..., i_k are located on the circumference of the circle, and p_m be the middle point of the k objects representing the k dimensions on the x-z plane. Then, we can construct the hyperedge for the k-tuple as follows: first, take i_1 as p_0 of the corresponding quadratic Bezier curve. We can compute the location of p_2 such that p_2 is the opposite point of p_0 on the circle about p_m. Furthermore, set the y-axis value of p_m to the statistical significance value of I. Now we can create a quadratic Bezier curve using the three control points p_0, p_m and p_2. Take the half of the curve on the p_0 side as the component curve for i_1. Repeat the steps to construct component half Bezier curves for the other dimensions. The resulting k half Bezier curves are joined at the peak point to yield a parabolic-shaped hyperedge whose height is scaled

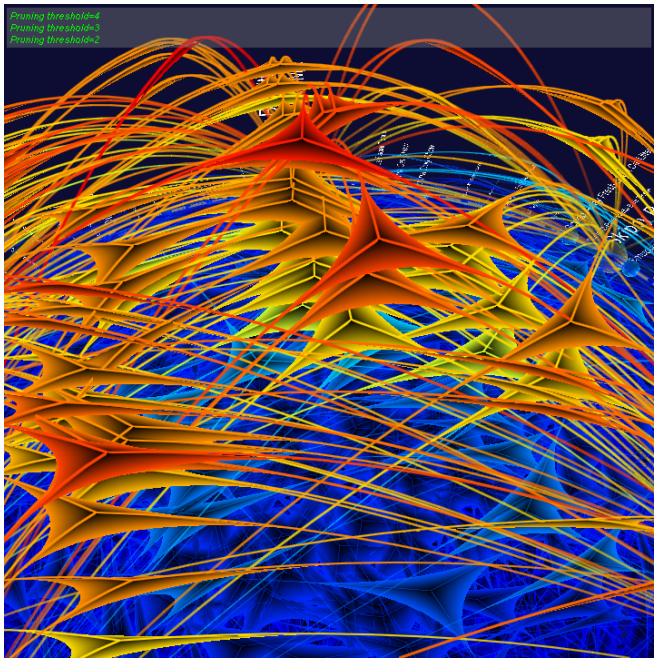

Fig. 10: 3-tuples with peers at a different view angle

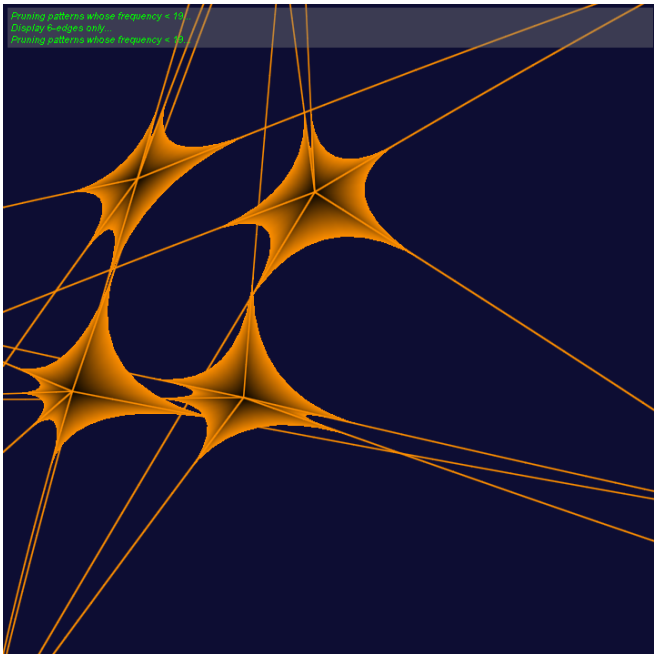

Fig. 11: A group of 6-tuples in dark orange color. Their close proximity indicates a high level of constituent item sharing.

by the statistical significance of the corresponding k-tuple automatically. The hyperedge is further decorated with a polygon cover over the peak point for visual clarity.

Figures 8 through 13 show examples of 3-tuples, 6-tuples and 10-tuples. Hyperedges for 3-tuples are constructed from three half Bezier curves with a cover at the joining point of each hyperedge as shown in Figures 8, 9 and 10. Figures 11, 12 and 13 illustrate that tuples of higher arity can also be constructed seamlessly using the same algorithm. Notice that each edge of the polygon cover of a hyperedge is also a Bezier curve.

The length of a hyperedge cover from the peak along a leg is about 80% of the leg length. We found that this percentile yields a good visual feedback while not dominantly cover other hyperedges. Once the location of each vertex of the hyperedge cover is determined, every pair of adjacent vertices serve as quadratic Bezier control points to generate the final hyperegde cover.

c) Visual cues: Visualization of tuples of arbitrary arities would be challenging mainly due to that fact that tuples can be very long and the number of tuples that are embedded in a dense database can be very large. Also, users may respond to the visual stimuli coming from a large number of tuples differently. For example, one user may be sensitive to variations in color but not in length, and vice versa. For these reasons, in designing a 3D metaphor for tuples we need to use more visual cues to reinforce the meaning of each tuple in the context and to minimize any user-level distortion of the visual information. Visualization of tuples using multiple visual cues is generally more effective than using a single visual cue as long as they are used with consistency. In the proposed 3D metaphor for k-tuples, multiple visual cues are used to maximize the discriminative power of the metaphor: shape, color, illumination, height, and thickness. These visual cues are demonstrated in the figures throughout this paper.

d) Relative location: Since the peak point of each component Bezier curve of a hyperedge is a function of its associated control points (i.e., item objects), hyperedges tend to be spatially cohesive when hyperedges share dimensions. For example, the four 6-tuples in Figure 11 form a clump. The relatively close proximity between them indicates that the level of dimension sharing is high among them.

e) Color: The hue of an edge e representing a k-tuple is determined by the statistical significance of the tuple using the following formula:

$$hue(e) = \frac{\max - weight(e)}{\max}$$

where $\max$ is the maximum significance in the dataset and $weight(e)$ is the statistical significance of the corresponding tuple. With this color scheme, the most significant edges are rendered in red, least significant ones in blue with yellow and green edges in between. Figures 9 and 10 show that highly significant 2-tuples are red and tall whereas less significant tuples are blue and short. Note in the figure that there are

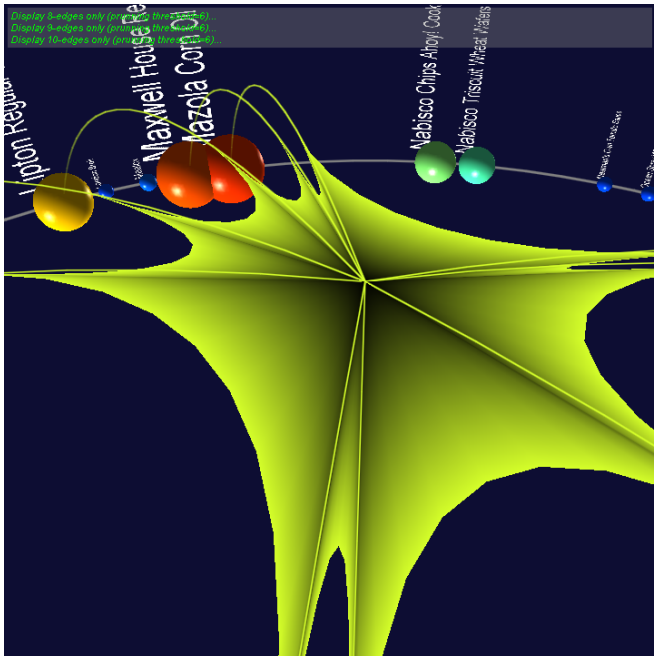

Fig. 12: A 10-tuple in green color with three constituent items in background

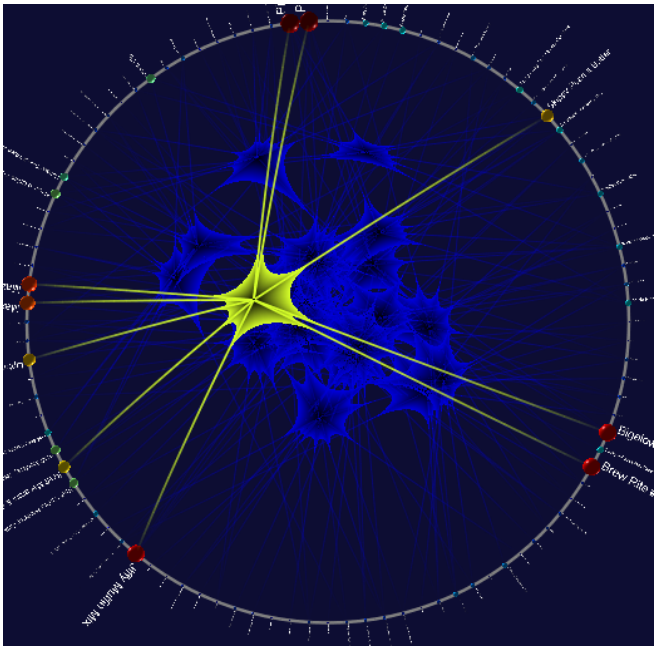

Fig. 13: The green 10-tuple is outstanding among other less significant, blue 10-tuples in background.

generally much fewer red, tall edges than blue, short edges in background. Also note that the 3-tuple in Figure 8 is red while the 10-tuple in Figure 12 is green because tuples of larger arity generally occur less frequently than those of smaller arity in a database.

f) Illumination: Shading is natural to real 3D objects under illumination. We add a pseudo-shading effect to edges to augment their 3D look by applying varying illumination rather than uniform illumination.

The edge illumination is defined as a function of $t \in [0,1]$

$$illumination(t) = -\frac{(t-0.5)^2}{0.5^2} + 1$$

where t denotes a curve segment.

The above formula guarantees an edge to be the brightest at the vertex point and gradually darker toward the both end points, as illustrated in Figures 8 through 13.

g) Thickness: The thickness of an edge is proportional to the statistical significance of the corresponding tuple.

2.3 User interaction

As discussed above, the circular layout is preferred for its superior visual capacity and intuitive visual feedback that it offers. However, its effectiveness is ultimately challenged when the number of visual objects becomes large. The objects will be cluttered, and subsequently feedback from the visualization will be compromised. A natural remedy to this problem is an integration of user interaction that lets the user navigate through multiresolutional views. We follow the Visual Information-Seeking Mantra in this regard: overview first, zoom and filter, then details on demand, as suggested in [2], through the following user interaction functions:

h) Rotation: The user can change his/her view direction to any direction in the 3D space. This offers the effect of rotation of the entire grid. In addition, the entire grid can rotate around x-, y-, or z-axis incrementally or automatically at the user's discretion, as shown in the figures. The consistent, automatic rotation around a particular axis is useful to inspect a global summary of the entire data from a particular perspective.

i) Zoom: The zoom function allows the user to zoom into any visual components such as nodes, node labels, hyperedges, as well as the entire grid. Examples of zoomed views are also shown in Figures 5 and 8 through 13 at various level of magnification. Note that when the dataset size is relatively large, node labels may be too small to read at a low magnification level. By zooming the view in, we can inspect all the node labels clearly without losing any information.

j) Filter: The user is able to filter nodes and hyperedges by their statistical significance. This function helps the user focus on significant patterns without being distracted by minor details by having to filter out less significant objects.

This filter function provides run-time pruning of tuples.

Examples of filtered views are shown in Figures 8, 11, and 12. In the figures, hyperedges are pruned interactively using different minimum statistical significance through which prominent 3-, 6- or 10-tuples are easily discovered. A pruning action can also be instantly revoked in our prototype.

k) Query interface: Our model also provides a query interface. As the user clicks a node n, n's appearance changes to a wire framed shape in a different color and the detailed information of n is displayed on top of the screen. The information includes the name of n, and the support count of n in the given dataset. As the user clicks a hyperedge e, the support count of the corresponding tuple and the names of the constituent dimensions are displayed. Examples are shown in Figures 8 through 13.

3. Experiment

The prototype of the proposed visual model was implemented using the Java 3D programming language, and experimented upon with a number of real world datasets as well as artificial datasets. Their sizes range up to ≈20,000 3D spheres/cubes and 10^4 hyperedges. The figures presented in this paper are taken from our experiments.

In particular, the figures shown in Figures 8 through 13 are generated from a market basket analysis dataset which comprises 100 dimensions, 1,126 2-arity hyperedges, and numerous k-hyperedges ($k > 2$). With this amount of visual information, exploration of the dataset for statistically significant patterns on a Pentium-based PC with 2GB main memory was smooth and pleasant.

4. Conclusion and Future Work

A 3D visual metaphor for high-dimensional datasets is presented in this paper. It resolves the potential positional and orientational visual bias inherent in a rectangular layout of dimensions by arranging dimensions as a circle. Each k-dimensional data instance is modeled as a k-arity hyperedge. The metaphor is implemented as visual objects of high quality and shows a good separation of data instances.

While the effectiveness of our model is generally demonstrated through a handful of experiments, we forewarn the reader that efficiency in terms of memory requirement could be a concern in comparison to 2D multivariate visualization techniques as we render information as high quality 3D objects.

In the future, the proposed metaphor will be investigated for its applicability to visual data mining.

References

[1] Weka: Data Mining Software in Java. `http://www.cs.waikato.ac.nz/ml/weka/`.

[2] J. Abello and J. Korn. MGV: A System for Visualizing Massive Multidigraphs . *IEEE TVCG*, 8(1):21–38, Jan-Mar 2002.

[3] S. Chakrabarti. *Mining the Web, Discovering Knowledge from Hypertext Data*. Elsevier Science, 2003.

[4] M. Cohenford, S. Lim, C. Brown, M. Chaudhry, S. Sigdel, and B. Rigas. FT-IR Analysis of Normal and Malignant Mouse Colorectal Tissues; A Study Employing Chemo- metric Analysis. In *Proc. of the Pittsburgh Conference on Analytical Chemistry and Applied Spectroscopy (PITTCON 2011)*, March 2011.

[5] M. A. Cohenford and B. Rigas. Cytologically normal cells from neoplastic cervical samples display extensive structural abnormalities on IR spectroscopy: Implications for tumor biology. *Proc. of the National Academy of Sciences of the United States of America (PNAS)*, 95(26):15327–15332, December 22 1998.

[6] D. A. Keim. Designing Pixel-Oriented Visualization Techniques: Theory and Applications. *IEEE TVCG*, 6(1):59–78, Jan-Mar 2000.

[7] C. K.-S. Leung, P. P. Irani, and C. L. Carmichael. Wifisviz: Effective visualization of frequent itemsets. *Data Mining, IEEE International Conference on*, 0:875–880, 2008.

[8] Z. Lin and S. Lim. Optimal Candidate Generation in Spatial Colocation Mining. In *Proc. of the 2009 ACM Symposium on Applied Computing*, 2009.

[9] B. Liu. *Web Data Mining, Exploring Hyperlinks, Contents, and Usage Data*. Springer, 2007.

[10] R. Moustafa and E. Wegman. Multivariate continuous data–parallel coordinates. In *Graphics of Large Datasets*, Statistics and Computing, pages 143–155. Springer, 2006.

[11] M. E. J. Newman. Coauthorship networks and patterns of scientific collaboration. *Proc. of the National Academy of Sciences of the United States of America*, 101(1):5200–5205, April 6 2004.

[12] P. R. Srinivasa, B. S. Kramerb, and S. Srivastava. Trends in biomarker research for cancer detection. *The Lancet Oncology*, 2(11):698–704, November 2001.

[13] E. J. Wegman. Hyperdimensional Data Analysis Using Parallel Coordinates. *Journal of the American Statistical Association*, 85(411):664–675, 1990.

[14] L. Yang. Visual data mining. chapter Visual Exploration of Frequent Itemsets and Association Rules, pages 60–75. Springer-Verlag, Berlin, Heidelberg, 2008.

QuestMonitor: A Visualization Platform for Declarative Network Protocols

Eric Bellemon[1], **Vincent Dubosclard**[1], **Stéphane Grumbach**[1] **and Kun Suo**[2]
[1]INRIA-LIAMA, Beijing, China
[2]CASIA-LIAMA, Beijing, China

Abstract— *We present the QuestMonitor system, which allows to visualize dynamic networks, and monitor the execution of protocols written in a data centric and declarative language: Netlog. This language allows to write protocols, which are two orders of magnitude shorter than imperative programs. Nevertheless, their behavior is sometimes tricky to understand in dynamic networks. QuestMonitor, allows to monitor all the communication between the nodes, the evolution of the data stores on each node, as well as the execution of the declarative code. It also allows to color the virtual data structures, such as routes, backbones, etc. It allowed us to identify flaws in programs. Together with the code editing facility, it constitutes a good tool for rapid prototyping.*

Keywords: distributed programming; data centric; declarative languages; network monitoring; visualization

1. Introduction

Distributed programming has tremendously gained in importance in recent years, with the wide development of networks, which now become ubiquitous and support applications in many domains; the emergence of large commodities for data storage and computation such as cloud computing; as well as, at the micro scale, the rise of multicore processors which, in an attempt to preserve Moore's law, palliate the bound on clock speed, by augmenting the number of cores on chips and parallelizing the computation.

Distributed programming though is still a very complex task, which requires high programming skills, and whose correction is very difficult to guarantee. The need for high level programming abstraction for distributed applications is striking in all the above mentioned areas. Their success will indeed strongly depend upon the ability to program them efficiently and in a reliable manner.

Data centric programming languages constitute a very promising model for distributed applications. They are more declarative, so facilitate programming, they parallelize well, so facilitate the execution, they manipulate explicitly data structures, so facilitate verification of their properties.

[0]This work has been supported by the French Agence Nationale de la Recherche, under grant ANR-09-BLAN-0131-01.

The use of rule-based languages, à la Datalog [1], [2], [3], [4], developeded in the field of databases in the 1980's, for distributed applications, was initially proposed in UC Berkeley [5], [6], under the name "declarative networking". It was shown that such languages augmented with communication primitives, allowed to express communication protocols or P2P systems with code about two orders of magnitude shorter than imperative programs, and with reasonable execution models.

The data centric approach offers great advantages. It is easier to program, results in code which is two orders of magnitude shorter, much more declarative, so relieve the programmer from the intricacy of distributed programming. Moreover, it parallelizes well in general, as database languages such as SQL. Nevertheless, the behavior of declarative programs over dynamic networks might be tricky to understand. The possibility to visualize their behavior in networks greatly help developing code, and might reveal flaws in programs.

We considered the rule-based language, Netlog [7], which extends Datalog with aggregation and non-deterministic constructs as well as communication primitives, in the spirit of the declarative networking approach. It has a sound distributed fixpoint semantics, which takes explicitly into account the in-node behavior as well as the communication between nodes.

Netlog runs on the *Netquest Virtual Machine*, which is coupled with an embedded Data Management System, DMS, which stores all the data as well as the bytecode of the Netlog programs. The bytecode is obtained by a compilation from Netlog into an SQL dialect. The Virtual machine makes calls to the DMS to evaluate the bytecode of the Netlog programs, which result in updates of the database, and production of messages. The machine has been shown to be portable over small devices, as long as they support an embedded DMS [8].

Several network simulators are accessible in open source, giving access to various grain of analysis of the activity of the network such as NS, OMNET, or WSNet to name a few, but to the best of our knowledge non that can monitor the distributed execution of declarative code. QuestMonitor allows to monitor the execution of declarative programs in a distributed environment, which can be either a simulated network or a monitored system such as a testbed. QuestMon-

itor also includes a simple network simulator. The exchanged messages and the content of the database of each node can be displayed as well.

Networking protocols have constituted our first experimental area, with declarative design of basic services, which construct and maintain distributed data structures, such as spanning trees, shortest paths, dominating sets, etc. Many networking protocols have been designed, including various routing protocols, such as DSDV [9], OLSR [10], AODV [11], and VRR [12], as well as self-configuration and self-organization protocols, such as ASCNET [13] or FISCO [14]. QuestMonitor has been essential to understand the behavior of declarative code. In some cases it has allowed us to find classical flaws, such as the route flapping problem, or dependency on the order of messages. But more generally, it has helped understanding what procedural behavior could be associated to the declarative code.

The paper is organized as follows. In the next section, we present the Netlog language through simple examples. In Section 3, we describe the virtual machine. The Netlog editor and compiler is briefly described in Section 4, while the visualization platform is presented in Section 5. We illustrate the use of QuestMonitor on concrete applications in Section 6.

2. The Netlog language

Netlog programs consist of sets of recursive rules of the form *head* :- *body*, where the *head* is derived when the *body* is satisfied. The programs are installed on each node of a network, where they run concurrently. The computation is distributed and the nodes exchange information. The facts deduced from the rules can be either stored on the node on which the rules run, or sent to other nodes.

We present the language through some fundamental examples of programs for network organization, routing, mobile servers and sensor network monitoring.

2.1 Network organization protocol

We consider the construction of a spanning tree. The results are distributed so that each node stores the knowledge of its parent in the tree.

Program Tree

$$\updownarrow onST(self) : -Root(self). \quad (1)$$
$$\updownarrow ST(@ \diamond y, self) : -Link(self, y); onST(y); \neg onST(self). \quad (2)$$
$$\updownarrow onST(self) : -Link(self, y); onST(y); \neg onST(self). \quad (3)$$

The variable $self$ is interpreted by the node address. The **store/push operator**, "$\updownarrow$", in front of rules, determines where the results are assigned. The effect of "$\downarrow$" is to **store** the results of the rule on the node where it runs; "$\uparrow$", to **push** them to its neighbors; and "$\updownarrow$", to both store and push them.

The location instruction "@" in the head of rules represents the destination. Rule (2) **unicasts** its results, using the **location instruction** "@", on the first variable of the head, instead of pushing them to all neighbors.

The negation is interpreted by local closed world assumption (a fact is not true on a node if it is not stored on that node). The **choice operator** $\diamond$ chooses non-deterministically a parent among the possible choices.

Assume that $Root(\rho)$ holds on a root node ρ exclusively. When a node α is on the spanning tree, it broadcasts $onST(\alpha)$ to its neighbors (rules 1 and 3). The fact $ST(\alpha, \beta)$ is stored exclusively on nodes α and β. It is deduced by node β and sent to node α, its parent, by rule (2).

2.2 Routing protocol

Program DSDV is a simplified version of the DSDV protocol [9] which constructs and maintains proactively all possible routes in adhoc networks. The routes are stored in relation $Route$ with attributes $destination$, $nextHop$, $nbHops$ and $destinationSN$, used for sequence numbers.

Each node creates a route to itself when the program starts with rule (4). Periodically, using the timer $hello$, each node broadcasts all its route information to its neighbors, rule (5), and increases the value of the $destinationSN$ of the route to itself, using rule (6). The symbol "!" denotes the deletion of the facts used in the evaluation of the rules.

The route informations are sent using facts of the form $RtInfo$. A node updates its route table according to the route information received from its neighbors as follows.

(i) A new route is stored if there is no route to the same destination in the local route table, rule (7). The expression $\neg Route(x, \_, \_, \_)$ in the body of rule (7) means that there is no fact $Route(x, a, b, c)$ for any value a, b, c.

(ii) The old route is deleted and replaced with a new one if the new route has a larger destination sequence number, rule (8), or the new route has the same sequence number as the old one but has a smaller number of hops, rule (9).

Program DSDV

$$\downarrow Route(self, self, 0, 1) : -TimeEvent('ini'). \quad (4)$$
$$\uparrow RtInfo(self, x, n, s) : -TimeEvent('hello'); \quad (5)$$
$$Route(x, y, n, s).$$
$$\downarrow Route(self, self, 0, s) : -TimeEvent('hello'); \quad (6)$$
$$!Route(self, y, z, s', 0); s := s' + 1.$$
$$\downarrow Route(x, \diamond y, n, s) : -RtInfo(y, x, n', s); \quad (7)$$
$$\neg Route(x, \_, \_, \_); n := n' + 1.$$
$$\downarrow Route(x, \diamond y, n, s) : -RtInfo(y, x, n', s); n := n' + 1; \quad (8)$$
$$!Route(x, y', n'', s'); s' < s.$$
$$\downarrow Route(x, \diamond y, n, s) : -RtInfo(y, x, n', s); n := n' + 1; \quad (9)$$
$$!Route(x, y', n'', s); n'' > n' + 1.$$

2.3 Mobile clients

The Mobile clients program allows a mobile client to always maintain a route to a server. This program is divided in three sub-programs: server, relay and client. Servers provide a service, relays maitain a route to the nearest server and clients need a route to a server. The route to the nearest server is stored in relation $Provider$ with attributes $server$, $nextHop$, $nbHops$ and $timeout$ used to delete expired entries.

Servers answer to a relay when receiving a request with rule (10). Each relay creates a route to the nearest server in the network with rule (11), (12) and (13). When the timer $relay$ is fired, relays broadcast a request to find a server.

In clients node, when the timer $route$ is fired, they broadcast a request for routes to all their neighbors with rule (15) if there is no existing route to a server. Answers are treated by rule (17). If the client knows a route to a server, it sends a request to the next hop to check the validity of the route (16). The reply of the next hop is treated by rule (18). The keyword $time$ is the system time of the node. In rule (17) and (18), the timeout of the route to the server is set to the current time system plus nine seconds.

Program Mobile Clients - Server

$$\uparrow RelayRep(self, @x, self, 1) : -!RelayReq(x). \quad (10)$$

Program Mobile Clients - Relay

$$\uparrow RelayReq(self) : -!TimeEvent('relay'); \quad (11)$$
$$\neg Provider(\_,\_,\_,\_).$$
$$\uparrow RelayRep(x, @y, self, n) : -!RelayReq(y); \quad (12)$$
$$Provider(x,\_,n',\_); n := n' + 1.$$
$$\downarrow Provider(x, y, n, t) : -RelayRep(x, self, y, n); \quad (13)$$
$$\neg Provider(\_,\_,\_,\_).$$
$$\uparrow ClientRep(x, self, @y, n) : -!ClientReq(y,\_); \quad (14)$$
$$Provider(x,\_,n',\_); n := n' + 1.$$

Program Mobile Clients - Client

$$\uparrow ClientReq(self, self) : -!TimeEvent('route'); \quad (15)$$
$$\neg Provider(\_,\_,\_,\_).$$
$$\uparrow ClientReq(self, @x) : -!TimeEvent('route'); \quad (16)$$
$$Provider(\_, x,\_,\_).$$
$$\downarrow Provider(x, y, n, t) : -!ClientRep(x, y, self, n); \quad (17)$$
$$\neg Provider(\_,\_,\_,\_); t := time + 9.$$
$$\downarrow Provider(x, y, n, t) : -!ClientRep(x, y, self, n); \quad (18)$$
$$!Provider(\_, x, n,\_); t := time + 9.$$

2.4 Sensor networks monitoring

The program is monitoring temperature on captors. Temperature of the nodes are stored in the relation $Temperature$ with attributes $nodeId$ and $temperature$. If the temperature of a device is higher than a threshold, it sends a request to all its neighbors to retrieve their temperatures (19). $meta\_threshold$ is a constant defined in the header of the program.

When a node receives a request, it sends its current temperature to the source of the request (20).

The node which receives the replies saves the temperature of its neighbor in $temperature$, rule (21). With the aggregation avg, it also computes the average of the temperature of all its neighbors with rule (22) and stores it in the relation $TpAvg$.

Program Sensor monitoring

$$\uparrow Req(self) : -Temperature(self, t); \quad (19)$$
$$t > meta\_threshold.$$
$$\uparrow Rep(self, @x, t) : -Req(x); Temperature(self, t). \quad (20)$$
$$\downarrow Temperature(x, t) : -Rep(x, self, t); \quad (21)$$
$$\neg Temperature(x,\_).$$
$$\downarrow TpAvg(x, avg[t]) : -Temperature(x, t). \quad (22)$$

3. Netquest Virtual Machine

The Netquest Virtual Machine executes the Netlog bytecode and manipulates data and messages. It is working as a daemon in the device, and applications can use it to communicate with other devices on the network. The virtual machine is portable and can be installed in small devices with embedded DMS. A previous implementation was done in iMote sensors [8].

The Netquest Virtual Machine is composed of six components (Fig. 1):

- Device Wrapper for QuestMonitor: provides an abstraction layer of the network. It does the address translation between Netlog internal addresses and the network addresses. It also receives and sends data over the network.
- Data Management System (DMS): provides an access to the data. This module evaluates the bytecode, manipulates data (insertion, update and deletion) and produces messages.
- Router: receives and sends Netquest messages through the device wrapper. It chooses the best route to reach a destination. The strategy to select the route can be easily defined in Netlog.
- Engine: executes Netlog programs. When the node receives a new message, the engine loads the rules matching the facts of the message and evaluates them through the DMS.
- Timer Manager (TM): manages time event of the system. Netlog programs can create and manipulate timers. These timers are managed and fired by this module.
- Application API: this module is an interface between the virtual machine and applications. An external application can use the Netlog Virtual Machine to send and receive messages over the network.

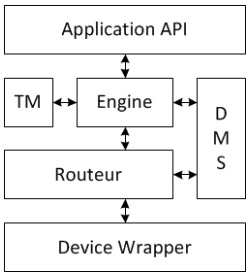

Fig. 1: Netquest Virtual Machine architecture

When a message is received by a device, the device wrapper transfers it to the router. The message is read by the router and the payload is sent to the engine if the device belongs to the destination. The engine loads rules from Netlog programs matching the facts contained in the payload and then evaluate these rules using the DMS. The DMS can update or delete data and create messages to be sent. These new messages are sent to the network through the device wrapper.

The Netlog Engine does not execute directly the bytecode. It orchestrates the tasks to be done to treat messages and facts. When receiving facts, a new round starts and a first stage is executed. In this stage, the engine loads and executes rules triggered by these facts. If there are derived facts produced by the engine, a new stage is executed recursively again with these new facts. A round is finished when there are no new derived facts. At the end of a round, produced messages are sent to other nodes in unicast or broadcast mode.

4. Netlog Editor and compiler

The code editor (Fig. 2) is an environment for helping developers to write Netlog programs, with standard functionalities such as syntax coloring and error detection, and which also ensures the compilation of Netlog.

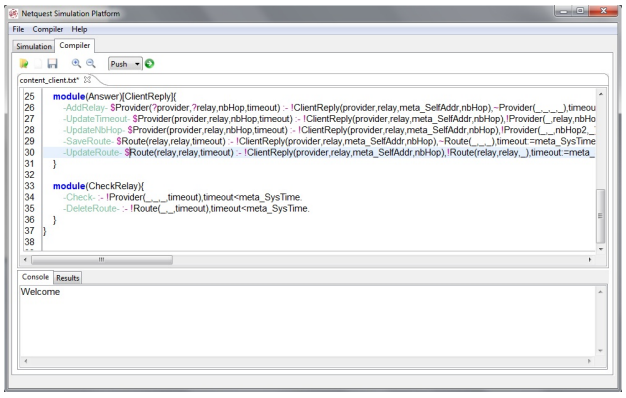

Fig. 2: Code editor interface

The Netlog compiler is a multi-pass compiler which compiles the Netlog code to an intermediate bytecode. This bytecode is then executed by the Netlog engine.

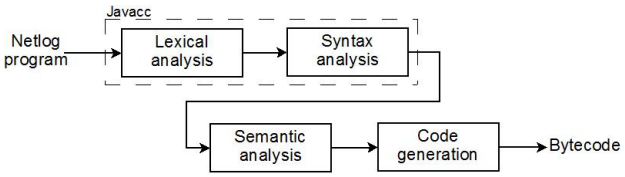

Fig. 3: Compiler architecture

The compilation is done in four steps (Fig. 3). First, the input program is parsed and transformed into an abstract syntax tree. Then the syntax tree is browsed by the semantic analysis module and an enhanced intermediate tree is built. After an intermediate code is generated and finally the output bytecode is generated depending upon the target engine.

The generated bytecode is a SQL dialect. A query is built for each operator (store, push and deletion) in a rule. Consider for instance the following rule which contains the three operators:

$$\updownarrow Link(a,b) : -!Hello(b,@a); \neg Link(a,b). \quad (23)$$

Rule 23 is evaluated when the engine receives a $Hello$ message. It is translated into three SQL queries corresponding to each operator:

```
SELECT Hello.a, Hello.b
  FROM Hello
  WHERE Hello.a='meta_selfAddr'
  AND NOT EXISTS (
    SELECT Link.a, Link.b
    FROM Link
    WHERE Link.a=Hello.a AND Link.b=Hello.b);

INSERT INTO Link
  SELECT Hello.a, Hello.b
  FROM Hello
  WHERE Hello.a='meta_selfAddr'
  AND NOT EXISTS (
    SELECT Link.a, Link.b
    FROM Link
    WHERE Link.a=Hello.a AND Link.b=Hello.b);

UPDATE Hello
  SET Hello.deleted=1
  WHERE Hello.a='meta_selfAddr'
  AND NOT EXISTS (
    SELECT Link.a, Link.b
    FROM Link
    WHERE Link.a=Hello.a AND Link.b=Hello.b);
```

The first query is the result for the operator push, the second for the operator store and the third for the deletion. All the keyword beginning by $meta\_$ are replaced by the engine during the evaluation of the rule. The negation of $Link$ is translated with the sub-query into the section $not\ exists$.

5. Visualization Platform

The visualization platform (Fig. 4) allows to interact with a network on a 2D graphical interface. The objective is to monitor the behavior of protocols which have been written in Netlog. This network might be a simulated one or a monitored testbed. Currently, we made experiments only on simulated networks.

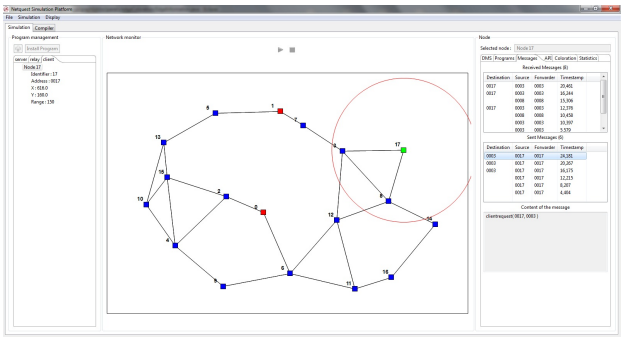

Fig. 4: QuestMonitor user interface

QuestMonitor has three main components:

- The Network Editor, which allows to simulate a network with various groups of nodes;
- The Network Monitor, which allows to visualize and interact with the network at run time; and
- The Node Monitor, which allows to monitor the activity of and interact with individual nodes.

The Network Editor allows to create groups of nodes, to display the status of the nodes in each group and to install Netlog programs on them. They can have different colors, radio range, and characteristics, such as mobile or fixed. The system creates the groups and display the nodes on the left part of the screen. Each node is listed and for each node one can see its identifier, address, position and radio range. In order to finalize the creation of a group, Netlog protocols have to be installed on the nodes. The system allows the possibility to install several protocols on a unique group of nodes.

The Network Monitor offers the view of the different groups of nodes represented by different shapes and different colors and the connections between them (if the nodes are located inside the radio range of another node). Each node is identified by a unique number. The Network Monitor also allows to interact with the network, and modify its configuration before starting the simulation, by moving nodes, changing their radio range, or deleting edges or nodes for instance. This part was implemented using Piccolo2d[1] which allows to create Zoomable User Interfaces (ZUIs). The user can smoothly zoom in or out in order to get more details or have a global overview of the network. Piccolo2d has also a hierarchical structure which permits to manipulate easily a group of identical objects: edges, messages, ranges, nodes identifiers and so on. The users can thus very easily display the layers they are interested in without being disturbed by too many information (especially for big networks).

The Node Monitor exhibits informations about the node selected by the user, displayed on the right part of the screen. It contains six tabs: Display itemSet, Programs, Messages, API, Coloration and Statistics. The "Display itemSet" tab allows the user to choose a table existing in the database of the node and to display the values of each attribute of this table. It is important to notice that the content is updated on the fly. For example, you can choose to display the content of the table "Route" to see all the routes contained on the selected node. The next tab simply displays which protocols are installed on the node with the possibility for the user to enable or disable them on this node. The tab "Messages" displays all the messages received or sent by the node. If you click on one message in particular, you can display its content. The tab "API" permits to modify the content of the database of the selected node by adding a tuple in one of the tables of the nodes, as an application would do, by updating some sensed data for instance. The last tab shows some basic statistics about the node such as the number of Select queries or Update queries done in the database of the node.

The "Coloration" is one of the fundamental functionalities of QuestMonitor. It allows the user to color nodes and edges according to different criteria and with four distinct levels: (i) local, (ii) recursive, (iii) path, or (iv) global. The user first selects a table and a least one of its attributes.

At the local level, the system checks in the selected table, if for one of the tuples, the selected attribute corresponds to one of the neighbors of the selected node and color the edge between the two.

At the recursive level, the user is asked to select two attributes. Then the system checks exactly as in the precedent case, if one of the neighbor satisfies the condition. If one neighbor satisfies the condition, then the link is colored. If this is not the case, it will check with the second selected attribute. If there is no result, then there will be no coloration. But if one neighbor matches the condition with the second attribute, then the system does the same operation again but this time starting from the matching neighbor of the selected node. This is repeated recursively until there is a match for the first attribute or there are no neighbors for the second attribute.

At the path level, the user is also required to select two attributes as well as a source and a destination nodes. The system tries to find a path from the source to the destination using the method described above.

At the global level, the algorithm is exactly the same as at the recursive level, except that the system performs the task not only for the selected node, but for all the nodes of the network.

[1] http://piccolo2d.org/

6. Experiments with network protocols

We present below some simple examples to illustrate the use of the QuestMonitor system, and show it helps in the design of programs, based on the samples of declarative programs presented in Section 2.

6.1 Tree construction

The tree protocol defined in Program Tree can be easily experimentally checked with QuestMonitor. The program is creating a tree with node 0 as root. It should built a loop-free subnetwork. In the coloration tab, the tool can be configured to display the global tree of the root node by selecting the type global and the relation ST. When the simulation starts, we can immediately visualize the different steps of the creation of the tree and if there is any error. The final state of the execution of this program is in the Fig. 5. The tree is colored in blue with node 0 as root.

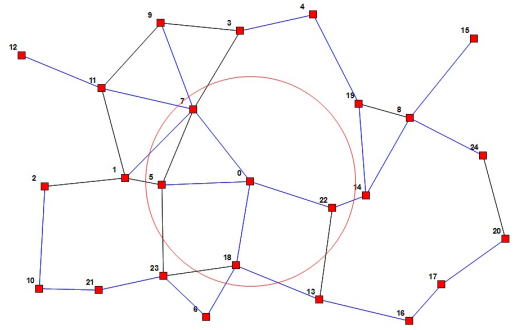

Fig. 5: Network with Tree protocol

6.2 DSDV Route

We can easily test and debug the implementation of the DSDV protocol defined in Program DSDV.

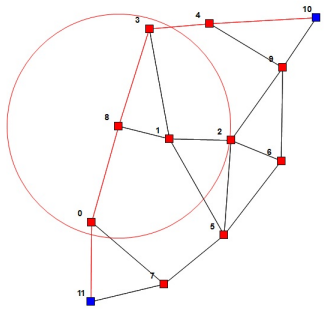

Fig. 6: Network with DSDV

In Fig. 6, there is a network running the DSDV protocol with 12 nodes. QuestMonitor is configured to color in red the route between node 10 and 11 with the path mode of the coloration tab and the relation $route$ selected. With this tool, we could detect that our first implementation of DSDV had a problem because the routes were not stable.

The route from node 10 to 11 is flapping because there are three different routes with the same number of hops. Rule (8) updates the relation $route$ when a new $route$ is received with a higher sequence number. The node 10 has two neighbors: node 4 and node 9. The "Display itemSet" tab of QuestMonitor shows that node 9 knows a route to node 11 through node 6 with a number of hops of 4, and node 4 also knows a route to node 11 through node 3 with the same number of hops. In the "Messages" tab, the list of received messages of node 10 is displayed and it received messages $RtInfo(4, 11, 4, 10)$ form node 4 then $RtInfo(9, 11, 4, 12)$ form node 9 and $RtInfo(4, 11, 4, 18)$ from node 4. Each time the node received a message $RtInfo$, rule 8 is applied and the route is updated because the sequence number is increasing.

Rule (8) can be fixed by adding the condition related to relation $Route$ that the route is updated if the sequence number is higher and if the next hop is the same:

$$\downarrow Route(x, \diamond y, n, s) : -RtInfo(y, x, n', s); n := n'+1; \quad (24)$$
$$!Route(x, y, n'', s'); s' < s.$$

6.3 Mobile Client

Protocol Mobile Client runs on the network of Fig. 7.

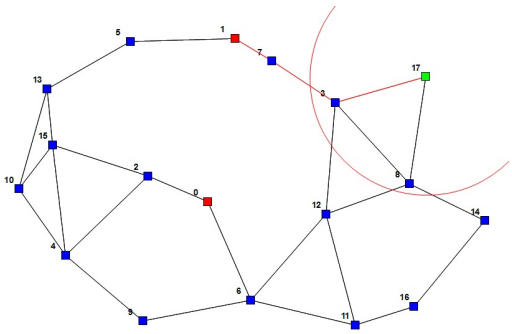

Fig. 7: Network with Mobile Client

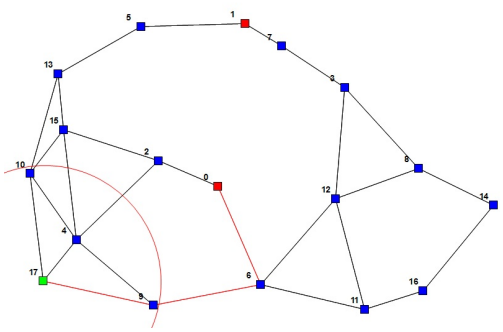

Fig. 8: Network with Mobile Client after the client moved

The simulated network is composed of 2 servers (nodes 0 and 1), 15 relays (nodes 2-16) and 1 moving client (node 17). With this program, the client always has a route to the nearest server through relays.

With the tab coloration, by selecting the type recursive and the relation $provider$, QuestMonitor displays the route from the client to the nearest server in red. When the client is moving the coloration is updated on the fly to reflect the new values of the data (Fig. 8).

6.4 Sensor network monitoring

In this experiment, 25 nodes are executing the program sensor network monitoring (Fig. 9). For the simulation, each node generates a temperature every 15 seconds to simulate a captor. If the temperature is above a threshold, the node broadcasts a request for retrieving the temperature of all its neighbors. If the average of the temperature of the neighbors is higher than the threshold, all the edges of the node are colored.

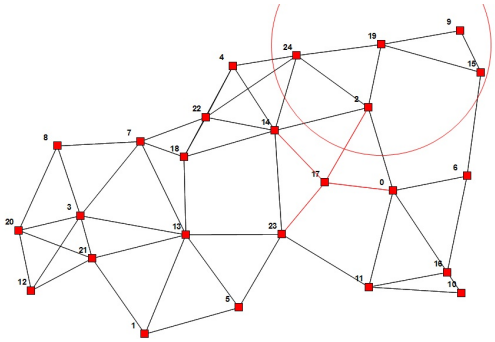

Fig. 9: Network with Temperature alert program

With QuestMonitor, the temperature and the average can be easily visualized. In the coloration tab, by selecting the type global, the edges of the nodes with an average higher than the threshold can be colored.

7. Conclusion

Data centric languages facilitate the writing of distributed programs, resulting in much shorter and more declarative code. Nevertheless, their behavior over dynamic networks is sometimes difficult to understand. The QuestMonitor system allows to visualize their execution over dynamic networks, and to monitor the communication as well as the evolution of the data stored on the nodes. It has helped prototyping protocols, and detect flaws in our programs. This was the case in particular for flapping routes in routing protocols, or errors due to protocols sensitive to the order of messages. It has been shown in addition, that the data centric approach facilitate as well the verification of the programs. Netlog protocols have been verified [15] using the Coq proof assistant. The next step will be to replace the homemade network simulator by a more powerful and efficient one (e.g. ns-3) while keeping the existing functionalities (as real-time dynamic network simulation).

Acknowledgment

The authors are greatly indebted to Michel Bauderon for his seminal influence on this development. They would like to thank as well Ahmad Ahmad-Kassem, Christophe Bobineau, Christine Collet, Fuda Ma, and Stéphane Ubéda, for their suggestions on a previous version of the software.

References

[1] F. Bancilhon, "Naive evaluation of recursively defined relations," pp. 165–178, 1986.

[2] F. Bancilhon, D. Maier, Y. Sagiv, and J. D. Ullman, "Magic sets and other strange ways to implement logic programs (extended abstract)," in *PODS '86: Proceedings of the fifth ACM SIGACT-SIGMOD symposium on Principles of database systems*. New York, NY, USA: ACM, 1986, pp. 1–15.

[3] L. Vieille, "Recursive axioms in deductive databases: The query/subquery approach," in *Expert Database Conf.*, 1986, pp. 253–267.

[4] R. Ramakrishnan and J. D. Ullman, "A survey of research on deductive database systems," *Journal of Logic Programming*, vol. 23, pp. 125–149, 1993.

[5] B. T. Loo, J. M. Hellerstein, I. Stoica, and R. Ramakrishnan, "Declarative routing: extensible routing with declarative queries." in *Proc. ACM SIGCOMM '05*, 2005.

[6] B. T. Loo, T. Condie, M. N. Garofalakis, D. E. Gay, J. M. Hellerstein, P. Maniatis, R. Ramakrishnan, T. Roscoe, and I. Stoica, "Declarative networking: language, execution and optimization." in *Proc. ACM SIGMOD'06*, 2006.

[7] S. Grumbach and F. Wang, "Netlog, a rule-based language for distributed programming," in *PADL'10, Twelfth International Symposium on Practical Aspects of Declarative Languages, Madrid, Spain, january*, 2010.

[8] M. Bauderon, S. Grumbach, D. Gu, X. Qi, W. Qu, K. Suo, and Y. Zhang, "Programming imote networks made easy," in *The Fourth International Conference on Sensor Technologies and Applications*. IEEE Computer Society, 2010, pp. 539–544.

[9] C. Perkins and P. Bhagwat, "Highly dynamic destination-sequenced distance-vector routing (dsdv) for mobile computers," in *ACM SIGCOMM'94 Conference on Communications Architectures, Protocols and Applications*, 1994, pp. 234–244.

[10] P. Jacquet, P. Muhlethaler, T. Clausen, A. Laouiti, A. Qayyum, and L. Viennot, "Optimized link state routing protocol for ad hoc networks," in *Multi Topic Conference, 2001. IEEE INMIC 2001. Technology for the 21st Century. Proceedings. IEEE International*, 2001, pp. 62–68.

[11] C. E. Perkins, "Ad-hoc on-demand distance vector routing," in *In Proceedings of the 2nd IEEE Workshop on Mobile Computing Systems and Applications*, 1999, pp. 90–100.

[12] M. Caesar, M. Castro, E. B. Nightingale, G. O'Shea, and A. Rowstron, "Virtual ring routing: network routing inspired by dhts," *SIGCOMM Comput. Commun. Rev.*, vol. 36, pp. 351–362, 2006.

[13] A. Cerpa and D. Estrin, "Ascent: Adaptive self-configuring sensor network topologies," *SIGCOMM Comput. Commun. Rev.*, vol. 32, pp. 62–62, 2002.

[14] J.-L. Lu, F. Valois, D. Barthel, and M. Dohler, "Fisco: A fully integrated scheme of self-configuration and self-organization for wsn." in *IEEE/WCNC*, 12007.

[15] Y. Deng, S. Grumbach, and J.-F. Monin, "A framework for verifying data-centric protocols," in *FORTE 2011: The 31th IFIP International Conference on FORmal TEchniques for Networked and Distributed Systems*, Reykjavik, Iceland, 2011.

VisSAT: Visualization of SAT Solver Internals for Computer Aided Hardware Verification

Robert Wille **André Sülflow** **Rolf Drechsler**

Institute of Computer Science
University of Bremen
29359 Bremen, Germany
{rwille,suelflow,drechsle}@informatik.uni-bremen.de

Abstract— *Today, many applications for formal circuit verification exist that rely on solvers for Boolean satisfiability (SAT). Usually, these applications use the SAT solver as a black-box. However, exploiting information on the internals of the solving process can speed-up the treatment of the verification task.*

In this paper, we present the tool VisSAT. VisSAT *provides insights into the internals of SAT solvers. Statistics of the internal solving process are collected and visualized on the circuit. By this, a verification engineer gets insight about potential bottlenecks for formal verification. This can be used to reconfigure the SAT solver or to improve the encoding.*

Keywords: Boolean satisfiability, hardware verification, visualization

1. Introduction

Verification gains an increasing amount of design costs in modern computer aided design. With increasing complexity and continuous demands for correctness, the application of formal methods in verification becomes indispensable [1], [2]. SAT solvers [3] are essential tools building the basis of many formal verification approaches like equivalence checking [4], [5], property checking [6], [7], [8], or automated debugging [9].

Typically, the following flow is thereby applied: The problem is encoded into an instance of Boolean satisfiability which is passed to the SAT solver. Then, the SAT solver returns either a satisfying assignment or proves that no such assignment exists. From this result, a solution of the verification problem is deduced. In this sense, the SAT solver is utilized as a black-box.

However, since the SAT problem is proven to be NP-complete [10], SAT solvers may need a significant amount of time to produce results for large instances. In contrast, advanced problem encodings [11], [12], [13], [14], adjusted decision heuristics [15], [3], or specialized propagation strategies [16] may accelerate the solving process significantly. But choosing the proper problem encoding or solver configuration, respectively, requires a deep technical understanding of how the SAT solver processes the instance. Internal data structures of a SAT solver give valuable information concerning the traversal as well as the structure of the search space. Unfortunately, such information is hard to extract.

In this work, we present *VisSAT*, a graphical interface which visualizes internals of SAT solvers applied to hardware verification tasks. *VisSAT* collects statistical information about the search process (e.g. the number of decisions on certain variables, the variables most frequently involved in conflicts, etc.). Afterwards, these statistics are evaluated and correlated to the overlying hardware verification problem. Therewith, *VisSAT* pinpoints the verification engineer to critical parts of the problem instance, e.g. hotspots with large occurrences of conflicts. This feedback helps to reconfigure the solver or alter the problem formulation accordingly. The explicit choice and the application of an optimization technique stays in the hands of the engineer.

While in previous work visualization of SAT instances already have been shown to be helpful [17], for the first time statistical information about the solving process itself is intuitively highlighted using *VisSAT*. Since additionally our approach gives insights on the circuit level (and not in terms of SAT variables and clauses) even verification engineers not familiar with SAT solvers are able to perform the respective heuristic and parameter tunings.

The remaining tool presentation is structured as follows: The next section briefly introduces Boolean satisfiability and provides a brief overview about the application of SAT in formal hardware verification. Afterwards, *VisSAT* is introduced in Section 3. By means of small examples, possible use cases are illustrated in Section 4. Finally the tool presentation is concluded in Section 5.

2. Formal Hardware Verification Using Boolean Satisfiability

In the recent years, Boolean satisfiability has become an established technique in many fields of formal hardware verification. Property checking, equivalence checking, as well as sophisticated techniques for automated debugging and for proving the fault tolerance of circuits are only some of the typical applications [6], [5], [9], [18]. The performance of the underlying SAT solver is crucial for all these applications.

In a typical flow, the application encodes the problem instance in *Conjunctive Normal Form* (CNF), i.e. a product-of-sum representation, and passes the CNF instance to a SAT solver. Then, the SAT solver returns either a satisfying solution (i.e. a consistent assignment of variables) or provides a proof of unsatisfiability for the CNF instance. Afterwards, the application maps the results of the SAT solver to the overlying verification problem.

For example, property checking proves the correctness of a property (e.g. given in some temporal logic like PSL [19]) on a design (e.g. given in a hardware description language like Verilog or VHDL). A property checker reads in the property and the design as input, translates the verification problem into an instance of Boolean satisfiability, and passes the instance to a SAT solver [6], [7], [8]. A property is either proven to be correct on the design (i.e. the instance is unsatisfiable) or a counterexample is returned (i.e. the instance is satisfiable).

Most SAT solvers accept a CNF as input. A CNF is a set of clauses where each clause is a set of literals and each literal is a propositional variable or its negation. While translating the hardware verification problem into a CNF, each n-bit signal is represented by a set of n SAT variables. The relation between the circuit signals and the SAT variables additionally is stored in internal data structures. For example, a 32-bit output signal of an adder corresponds to 32 propositional SAT variables. A satisfying model, i.e. a set of consistent assignments to the SAT variables in the SAT instance, can easily be mapped back to assignments on signals and by this to the original problem instance.

The underlying search process of the SAT solver remains thereby as a black-box process for the application and, by this, for the verification engineer. However, depending on the complexity of the verification problem, the run time of the SAT solver may range from a few seconds to up to several hours or even days. Having knowledge about the internal search procedure (e.g. about decisions or conflicts on variables) enables the verification engineer to adjust the parameters of the SAT solver or to improve the encoding of the problem instance in order to gain a speed-up. Moreover, the information is also worthwhile to analyze the progress of the verification.

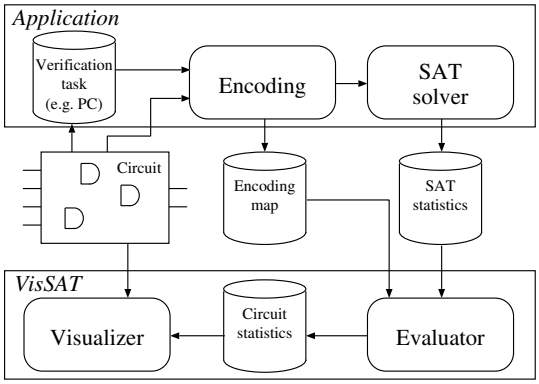

Fig. 1: Architecture of VisSAT

3. The VisSAT Tool

VisSAT collects statistical information about the solving process of a SAT solver and correlates this data to the overlying hardware verification problem. Accordingly, the tool is composed of two main components as illustrated in the lower part of Fig. 1[1].

The evaluator collects and processes statistical data of the solving process. The number of decisions on certain variables, the number of conflicts a SAT variable is involved, and further statistics provided by the SAT solver are thereby obtained[2]. Afterwards, these statistics are mapped to the respective hardware components of the circuit. Therefore, an encoding map is used to store which circuit signal is represented by which SAT variables. For example, if an one bit signal s is represented by a SAT variable x_{10} and, additionally, x_{10} was involved in four conflicts, then four conflicts are assigned to s. For signals representing multiple bits, the sum over all corresponding SAT variables is assigned to s. All these assignments are finally stored in a container.

The visualizer maps this data to a register transfer level or gate level schematic of the overlying circuit and, finally, visualizes both, the circuit and the obtained statistics. The visualization engine *RTLvision Pro* [20] is utilized which calculates a fitting layout that can be rendered. *RTLvision Pro* further allows cross-probing of the results to the source code of a design. The statistics are visualized by different color codes and, in order to obtain concrete values, tooltips. For example, if the conflict statistic is displayed, signals whose corresponding SAT variables were often involved in conflicts are highlighted in red, signals whose corresponding SAT variables were only occasionally involved in conflicts are highlighted in yellow, and signals whose corresponding SAT variables were never involved in a conflict are highlighted in green. Other statistics (e.g. the number of decisions) are displayed in a similar way.

[1]The upper part of Fig. 1 illustrates the SAT-based verification flow as described in Section 2.

[2]In this work, we extended MiniSat [3] to provide these statistics.

Using this visualization, the verification engineer is pinpointed to critical parts of the problem instance, e.g. hotspots with a large occurrence of conflicts. This feedback enables conclusions on why a verification tasks is hard to solve using SAT engines. The next section illustrates this by means of examples.

4. Use Cases

4.1 Using Information on Conflicts

Fig. 2 shows the distribution of conflicts occurred while solving a property checking instance. More precisely, the correct behavior of a multiplication in an ALU circuit was verified. The visualization shows the considered circuit highlighting the number of conflicts.

The coloring intuitively differentiates parts with a large number of conflicts (highlighted in red) from parts with a smaller number of conflicts (highlighted in yellow) or from parts without conflicts (highlighted in green), respectively. As indicated by the red signal, the multiplier module frequently causes conflicts. With this information, the designer can apply changes to the SAT solver parameters (e.g. preferring signals of the multiplier in order to address all these conflicts first during the solve process) or modify the design (e.g. replacing the multiplier by shifters), respectively.

4.2 Using Information on Decisions

Fig. 3 shows information on the number of decisions made for each signal while checking the correct behavior of the ADD instruction of another ALU. As expected, most decisions have been made for the output of an adder that was also involved in many conflicts, too. Thus, decisions on the output of the adder should have higher priority than on signals in the fan-in of the adder.

Moreover, decisions have been made for signals that do not influence the output of the property check, e.g. on the output of the subtraction module. In order to avoid this and, thus, to improve the solving process either, decisions on such signals can be deactivated or the verification model itself can be simplified.

5. Conclusions

In this paper, we presented *VisSAT*, a tool for the visualization of SAT solver internals within computer aided hardware verification. *VisSAT* collects statistics of the internal solving process and visualizes them on the considered circuit structure. By this, verification engineers are pinpointed to critical parts of the problem instance. This can be used to reconfigure the SAT solver or to improve the encoding. The application of VisSAT was illustrated by two use cases.

6. Acknowledgments

We thank Concept Engineering, in particular Gerhard Angst and Lothar Linhard, for providing us with the *RTLvision Pro* tool. This work was supported in part by the European Union (project DIAMOND, FP7-2009-IST-4-248613).

References

[1] R. Drechsler, *Formal Verification of Circuits*. Kluwer Academic Publishers, 2000.

[2] R. Drechsler, Ed., *Advanced Formal Verification*. Kluwer Academic Publishers, 2004.

[3] N. Eén and N. Sörensson, "An extensible SAT solver," in *SAT 2003*, ser. LNCS, vol. 2919, 2004, pp. 502–518.

[4] D. Brand, "Verification of large synthesized designs," in *Int'l Conf. on CAD*, 1993, pp. 534–537.

[5] S. Huang and K. Cheng, *Formal Equivalence Checking and Design Debugging*. Kluwer Academic Publisher, 1998.

[6] A. Biere, A. Cimatti, E. Clarke, and Y. Zhu, "Symbolic model checking without BDDs," in *Tools and Algorithms for the Construction and Analysis of Systems*, ser. LNCS, vol. 1579. Springer Verlag, 1999, pp. 193–207.

[7] K. Winkelmann, H.-J. Trylus, D. Stoffel, and G. Fey, "Cost-efficient block verification for a UMTS up-link chip-rate coprocessor," in *Design, Automation and Test in Europe*, vol. 1, 2004, pp. 162–167.

[8] M. Nguyen, M. Thalmaier, M. Wedler, J. Bormann, D. Stoffel, and W. Kunz, "Unbounded protocol compliance verification using interval property checking with invariants," *IEEE Trans. on CAD*, vol. 27, no. 11, pp. 2068–2082, 2008.

[9] A. Smith, A. Veneris, M. Fahim Ali, and A.Viglas, "Fault diagnosis and logic debugging using boolean satisfiability," *IEEE Trans. on CAD*, vol. 24, no. 10, pp. 1606–1621, 2005.

[10] S. Cook, "The complexity of theorem proving procedures," in *3. ACM Symposium on Theory of Computing*, 1971, pp. 151–158.

[11] O. Bailleux and Y. Boufkhad, "Efficient CNF encoding of boolean cardinality constraints," in *Principles and Practice of Constraint Programming*, ser. LNCS, no. 2833, 2003, pp. 108–122.

[12] C. Sinz, "Towards an optimal CNF encoding of boolean cardinality constraints," in *Principles and Practice of Constraint Programming*, ser. LNCS, no. 3709, 2005, pp. 827–831.

[13] O. Bailleux, Y. Boufkhad, and O. Roussel, "A translation of pseudo-boolean constraints to SAT," in *Journal on Satisfiability, Boolean Modeling and Computation*, vol. 2, 2006, pp. 191–200.

[14] J. Marques-Silva and I. Lynce, "Towards robust cnf encodings of cardinality constraints," in *Principles and Practice of Constraint Programming*, ser. LNCS, no. 4741, 2007, pp. 483–497.

[15] M. Moskewicz, C. Madigan, Y. Zhao, L. Zhang, and S. Malik, "Chaff: Engineering an efficient SAT solver," in *Design Automation Conf.*, 2001, pp. 530–535.

[16] R. Wille, G. Fey, D. Große, S. Eggersglüß, and R. Drechsler, "SWORD: A SAT like Prover Using Word Level Information," in *Int'l Conference on Very Large Scale Integration*, 2007, pp. 88–93.

[17] C. Sinz and E.-M. Dieringer, "DPvis - a tool to visualize structured SAT instances," in *Proc. of the 8th Intl. Conf. on Theory and Applications of Satisfiability Testing (SAT 2004)*. St. Andrews, Scotland: Springer-Verlag, June 2005, pp. 257–268.

[18] G. Fey, A. Sülflow, and R. Drechsler, "Computing bounds for fault tolerance using formal techniques," in *Design Automation Conf.*, 2009, pp. 190–195.

[19] Accellera, *Property Specification Language – Reference Manual*. Accellera Organization Inc., 2004, available at http://www.accellera.org/home.

[20] Concept Engineering GmbH, *RTLvision PRO*, http://www.concept.de, 2011.

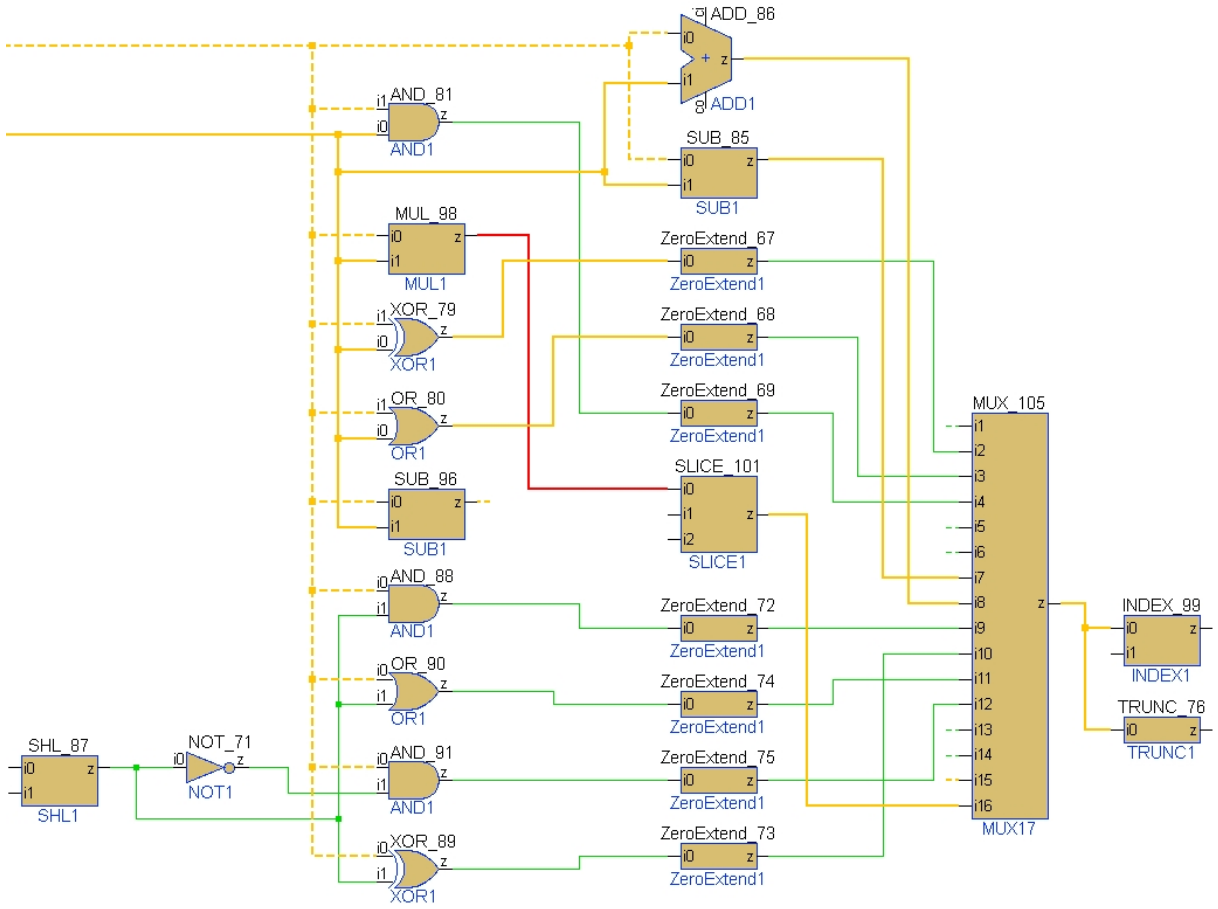

Fig. 2: Visualization of conflict statistics

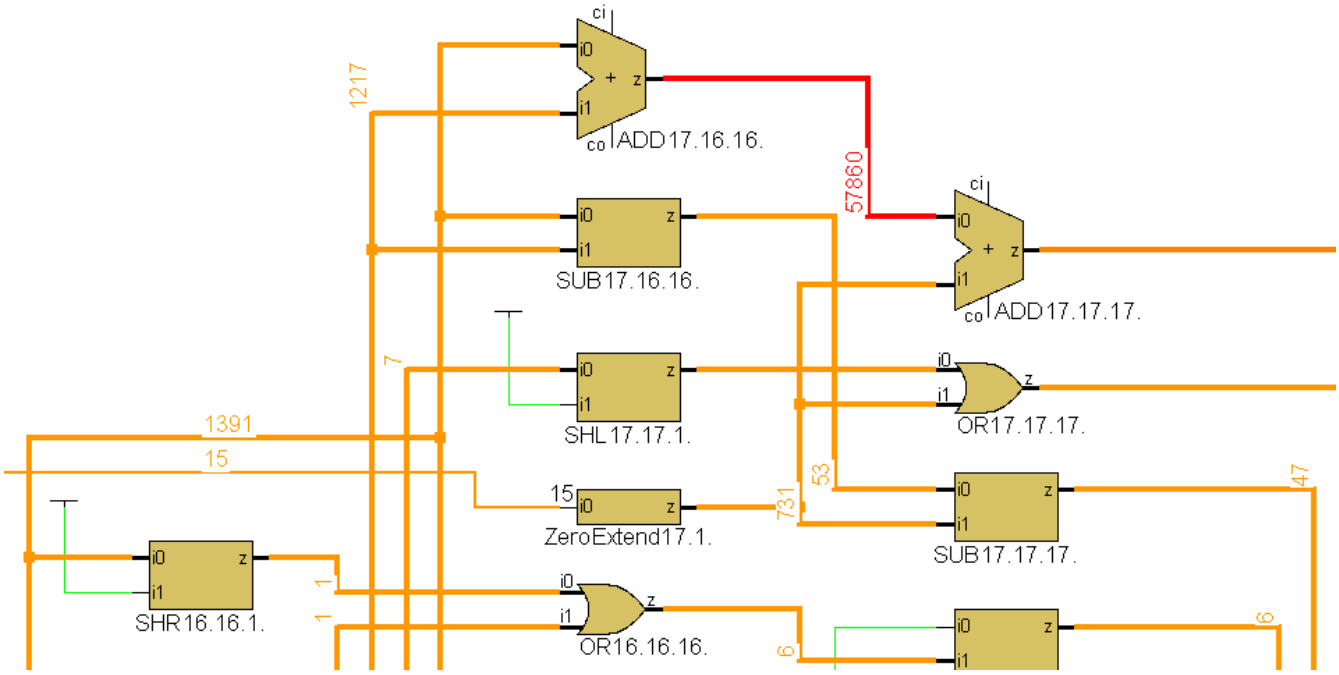

Fig. 3: Visualization of decision statistics

VR BioViewer: A new interactive-visual model to represent medical information

Antonio Gracia, Santiago González, Jorge Veiga and Víctor Robles

Abstract — **Virtual reality (VR) techniques to understand and obtain conclusions of data in an easy way are being used by the scientific community. However, these techniques are not used frequently for analyzing large amounts of data in life sciences, particularly in genomics, due to the high complexity of data (curse of dimensionality). Nevertheless, new approaches that allow to bring out the real important data characteristics, arise the possibility of constructing VR spaces to visually understand the intrinsic nature of data. It is well known the benefits of representing high dimensional data in tridimensional spaces by means of dimensionality reduction and transformation techniques, complemented with a strong component of interaction methods. Thus, a novel framework, designed for helping to visualize and interact with data about diseases, is presented. In this paper, the framework is applied to the Van't Veer breast cancer dataset is used, while oncologists from La Paz Hospital (Madrid) are interacting with the obtained results. That is to say a first attempt to generate a visually tangible model of breast cancer disease in order to support the experience of oncologists is presented.**

Keywords: dimensionality reduction, visualization, bio-informatics, manifold learning, virtual reality spaces, cancer classification, visual data mining, genetic algorithms, similarity structure preservation, genomics.

I. Introduction

Nowadays, around 60 people die of diseases such as cancer every minute. The value is even more concerning if instead of thinking in minutes, we do it in hours or days. It is, therefore, a problem of high social impact that must be solved as quickly as possible. Finding a cure for diseases such as cancer would translate into a much higher life expectancy. In the scientific field, expert biologists are devoted to the study of possible solutions to these kinds of diseases. Among the many approaches, the DNA microarray technology will be the application field of this research.

Medical and biologist experts have a lot of genomic (based on DNA microarray) and clinical information of patients with any disease. Even more, they have available different published gene profiles (*biomarkers*) for diseases as Breast Cancer. However, for them is very difficult to analyze all this information and obtain any conclusion in a short time. Visualization techniques have been of great assistance to experts in different fields of research. These techniques allow to bring out the real important data characteristics, arising the possibility of constructing VR spaces to visually understand the intrinsic nature of data in a very short time. Although some techniques as PCA (Principal Component Analysis) [1] have been used in genomic field to see relationship between genes, these are not frequently used to obtain patterns and conclusions of any gene in any disease. That is because the representation in 3D transforms gene features in 3 new values (x_i,y_i,z_i), but this with the transformation we have lost its scientific significance and there is not any possibility of reverse the transformation.

However, trying to obtain a representation that allows us to see the behavior of all gene features as well as the possibility of real interaction with experts. A novel framework, called VR BioViewer, is presented in this paper, applying it to Van't Veer breast cancer dataset. With this, medical experts from La Paz Hospital (Madrid) can visualize patients as points in a VR space, gene features as different axis represented in 3D, and can interact with the model: moving any gene axis (f. e. two genes are related, thus their axis have to be closed), seeing gene information of other past researches (using literature), or clinical information of patients by clicking in any point.

The structure of the paper is as follows: Next section presents DNA microarray technology. Section 3 analyzes briefly a state of art about Visualization and the use of optimization in visualization. Section 4 describes the VR BioViewer framework. Finally, conclusions, future lines and acknowledgments are presented in the last sections.

II. DNA Microarray

DNA microarrays [2,3,4,5] are a relatively new and complex technology used in molecular biology and medicine. Microarrays present unique opportunities in analyzing gene expression and regulation in an overall cellular context. This technology has been applied in diverse areas ranging from genetic and drug discovery to disciplines such as virology, microbiology, immunology, endocrinology

Antonio, Santiago, Jorge and Victor are from the Department of Computer Architecture, Universidad Politécnica de Madrid in Spain. (emails: {agracia,sgonzalez,jveiga,vrobles}@laurel.datsi.fi.upm.es).

and neurobiology. Microarray technology is the most widely used technology for the large-scale analysis of gene expression because it provides a simultaneous study of thousands of genes by single experiment.

A DNA microarray consists of an arrayed series of thousands of microscopic spots of DNA oligonucleotides (shorts molecules consisting of several linked nucleotides, between 10 and 60, chained together and attached by covalent bonds), called Expressed Sequence Tags (ESTs), each containing several molecules of a specific DNA sequence. This can be a short section of a gene or other DNA element.

There are several biological steps [6, 7] in the design and implementation of a DNA microarray experiment: Probe, Chip Manufacture, Sample preparation, Assay (*Hibridization* [6]), Readout and Informatics.

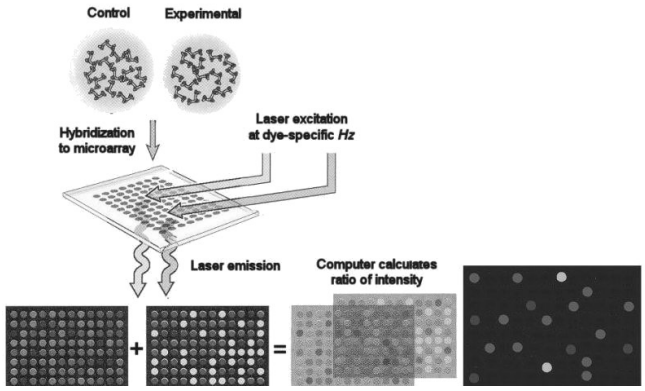

Fig. 1. Biological process of DNA Microarray analysis. Image from Gibson & Muse 2002

A. Breast Cancer dataset

The Van't Veer dataset [8] on Breast Cancer has been considered to use in this research. Van't Veer results have been approved by the FDA (Food and Drug Administration) and were applied in a genomic profiling test, called MammaPrint, that predicts whether patients will suffer breast cancer relapse or not. The data is divided into two groups, learning and validation instances. The training data consist of 78 patients, 34 of whom are patients that developed distance metastases within 5 years (poor prognosis). The rest of the dataset (44 patients) are the ones who remained healthy from the disease after their initial diagnosis for an interval of 5 years (good prognosis). The second group of patients (validation dataset) consists of 19 patients, 12 patients with poor prognosis and 7 with good prognosis. DNA microarray analysis was used to determine the mRNA expression levels of approximately 24,500 genes for each patient. All the tumors were hybridized against a reference pool made by pooling equal amounts of RNA from each patient.

- **Preprocessing:** Obviously real data have a lot of redundancy, as well as incorrect or missing values, depending on some factors. So, as first step, we carry out some pre-processing in order to clean up and prepare the data. We also discard variables with low internal variance or low Pearson correlation with outcome.

  Several pre-processing algorithms have been carried out through the training data. Firstly, we have discarded genes that are replicated. Next, we have discarded patients that had more than 80% of missing gene values. All data have been background corrected, normalized and log-transformed using Lowess Normalization [9]. Missing values were estimated using a 15-weighted nearest neighbor algorithm [10] (kNN Impute).

- **Biomarker selection:** The objective of this paper is not to obtain a feature selection of 24,500 genes expressions, but to create a model that represents this data efficiently. Thus, the microarray data is filtered to the 70 Van't Veer [8] selected genes (accepted by the FDA as breast cancer biomarkers), and these are the features we will use to represent the data in BioViewer.

III. Optimization and Visualization

The role of visualization techniques in the knowledge discovery process (KDD) [28] is well known. The increasing complexity of the data analysis procedures makes it more difficult for the user to extract useful information out of the results generated by the various techniques. So, a graphical representation is appealing from the point of view of the user. Besides, if this visualization is complemented with elements coming from a VR space, such as interaction or immersion in real time, we obtain a suitable framework for visualizing high dimensional data. The creation of VR spaces for visualizing high-dimensional dataset means a bigger insight of the underlying patterns or trends in data. To achieve that, we try to visually stimulate the human skills of understanding the intrinsic nature of data. The key is interaction. Interacting with 3D representations allow us to observe, for example, how clustered data is or the variation over time. These features make VR a much more intuitive environment than traditional ones for representing high dimensional data.

In many cases, the input data of these representations come directly from optimization techniques [27]. There are several examples that have been previously reported in [11,12,13]. Here, a multi-objective (MOO) optimization is used to the visualization of high dimensional datasets (i.e. leukemia or lung cancer). MOO optimization [26] studies

optimization problems involving more than one objective function and the goal is to find one or more optimal solutions. It is very common to use evolutionary algorithms for solving MOO problems (MOEA in general and MOGA if based on genetic algorithms). An evolutionary algorithm has four different steps: initialization, mutation, recombination and selection.

- **Initialization:** This initial phase focuses on select a population randomly.
- **Mutation:** the idea is to create a new individual v, for each one of the population x_i. To make it possible we need to select three different individuals of the population (r1, r2, r3). Where r_i has to be different and no one can be the parent. Consider that, F is a parameter in the interval [0, 2].
- **Recombination:** this operator generates the crossover between the element of the population x_i and the new individual generated, v. Implementation is made based on the exponential criteria.
- **Selection:** each element has a metric to evaluate how good or bad is the individual, this metric is called fitness. Comparing the new element generated v and the selected x_i, the algorithm select the one which has the best fitness.

Several multi-objective optimization algorithms inspired by this principles have been proposed. Among them, VEGA [14], HLGA [15], NSGA, NSGA-II [16,17,18], SPEA [19] and many others. In any case, a MOO optimization is out of scope in this study. Instead, an optimization technique involving two different available objective functions is carried out, particularly a differential evolution algorithm.

Handling large amounts of data arises a problem known as 'curse of dimensionality'. The high dimensional nature of genomic datasets makes difficult a straightforward analysis. So, it requires using several techniques for overcoming these problems. Dimensionality reduction is the transformation of high-dimensional data into a meaningful representation of reduced dimensionality. Ideally, the reduced representation has a dimensionality that corresponds to the intrinsic dimensionality of the data. The intrinsic dimensionality of data is the minimum number of parameters needed to account for the observed properties of the data. Dimensionality reduction is important in many fields, since it facilitates visualization, classification and compression of high-dimensional data, by mitigating the curse of dimensionality and other undesired properties of high-dimensional spaces [20]. Among this techniques, there are also another that accomplish a transformation of the involved features (transformation-based dimensionality reduction) i.e. 'Star Coordinates' algorithm [21]. It constructs a low dimensional space composed of a linear combination of the attributes.

IV. VR BioViewer

Here, VR BioViewer framework is presented. We divide it into two basic modules. The first one deals with the optimization part and the second one is for visualizing the results produced after the optimization. So, we are going to explain both methods in order to get a clear understanding of the pipeline of the process pipeline.

A. Optimization

Seeing the optimization module as a black box model (fig. 2), we can consider that the input is the n-dimensionality data and the output is the best distribution of the axes. That is, the distribution that better preserves the intrinsic geometry of n-dimensional data, after a representation using star coordinates algorithm.

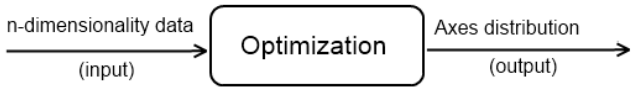

Fig.2. Optimization process of the axis

To set up the optimization module we implemented the differential evolution. The population of our model is the set of the different spatial distribution of the axes, and the initialization is done in a randomly way. So, the optimization tries to find the best configuration of the axis in order to preserve, as possible , the geometry of the n-dimensional data. Note that each axis corresponds to each one of the attributes in the input data, and has three components normalized in spherical coordinates (*t, p, r*) where *r* is the radius, *p* is the azimuthal angle in the interval [0, π] and *t* corresponds to the polar angle, interval [0, 2π]. In fact, we have to transform this problem to the cartesian coordinates to evaluate de distances. In the following formula, the transformation between spherical and cartesian coordinates is shown.

$$\begin{Bmatrix} x = r\sin(t)\cos(p) \\ y = r\sin(t)\sin(p) \\ z = r\cos(t) \end{Bmatrix}$$

At the beginning, the model has to calculate pair to pair distances of all the instances in the initial data. So this is stored in a matrix that is considered as the *target distance matrix*, and it is squared. In other words, it represents the distance between the instance *i-th* in the rows and the instance *j-th* in the columns.

In the study, the Manhattan distance metric ($L1$ norm) is considered because is consistently more preferable than the

Euclidean distance metric (*L*2 norm) for high dimensional data mining applications [22].

So, the aim is to preserve the distance of the data with high dimensionality and resemble the low dimensional data. As consequence of this, the model extracts the geometry of the initial data and this geometry is mapped into the low dimensionality data.

Before calculating the fitness, it is needed a representation of the data with the optimized axes, by means of the star coordinates algorithm. Then, the *generated distance matrix* is obtained and it represents the distances between all the instances of the data using these new optimizated axes. Needless to say, that this algorithm makes a linear combination of all the axes, or attributes, of the data.

Finally, the *generated matrix* and the *target matrix* are compared. To establish the comparison between two rows of those matrixes we implemented the *Pearson correlation*. To get a value of the fitness there are to methods: (1) based on the mean of the correlations and (2) based on a threshold. In the first option all the correlations between same rows in both matrixes are computed, and have a arithmetic mean of them. In the second one, however, all the correlations are obtained and for each one a threshold is evaluated to each of them, so then one vote is counted. Lastly, all the votes are added up and the result is divided between the number of instances.

B. Visualization

Once the optimization module has produced the results, the aim is just to obtain a 3D representation of the data in order to study in detail possible patterns, trends or outliers in the dataset as well as separation of classes, if it is possible. The input data of the visualization module consist of the set of optimized axes that will make possible a successful 3D embedding of the intrinsic geometric structure of the n-dimensional manifold. This results in a structure preservation with a minimum information loss, depending on the quality of the optimization process.

A visualization tool, 'Unity3D' [23], is used. Unity3D is a game engine designed for the creation of multiple 3D powerful interactive contents. The implemented visualization algorithm takes the output data of the optimization module as input data, and generates a 3D representation of the original n-dimensional dataset according to the optimized axes. The background of this dimensionality transformation is the star coordinates algorithm. The original algorithm works as follows. First, it considers the attributes of the dataset as coordinate axes. Then it arranges the coordinate axes onto a flat (two-dimensional) surface forming equidistant angles between axes. The mapping of an n-dimensional point to a two-dimensional cartesian coordinate is computed by means of the sum of all unit vectors of every coordinate, multiplied by the data value of that coordinate. In this framework a 3D mapping is used, so it can be described as the next formula:

$$P_j(x,y,z)=\begin{pmatrix} o_x+\sum_{i=1}^{n} u_{xi}(d_{ji}-min_i), \\ o_y+\sum_{i=1}^{n} u_{yi}(d_{ji}-min_i), \\ o_z+\sum_{i=1}^{n} u_{zi}(d_{ji}-min_i) \end{pmatrix}$$

Where d_{ji} is the *j-th* data with the *i-th* value, min_i is the minimum value of the scaled values in every coordinate, u_{xi} and u_{yi} are unit vectors in the direction of every coordinate, and o_x,o_y,o_z is the origin of the coordinate system. Figure 3 illustrates an example of the final position of a data point in a 8-dimensional dataset (the example is 2D but easily extensible to 3D by dimensional analogy).

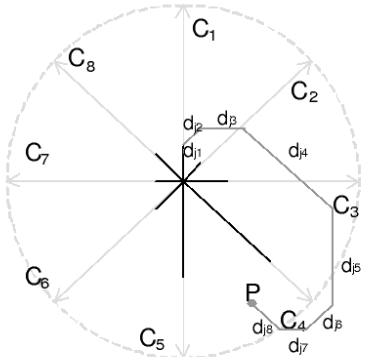

Fig. 3. Process of obtaining the final position of a data point for a 8-dimensional dataset (two-dimensional space).

Once the representation is done, the fundamental objective is that the expert oncologist classify, in a visually way, the breast dataset by a representation with colored spheres according to the class (black: relapse (R); gray: non-relapse (N.R) in breast cancer disease). It would be very useful if the oncologist could establish any kind of relations or connections between patients or genes, so a new mechanism of interaction based on the variation of the positions of the axes is provided. This variation will generate in real time a new spatial distribution of the spheres. Interacting with the coordinate axis could provide us valuable information. There might be many observations the expert might be interested in.

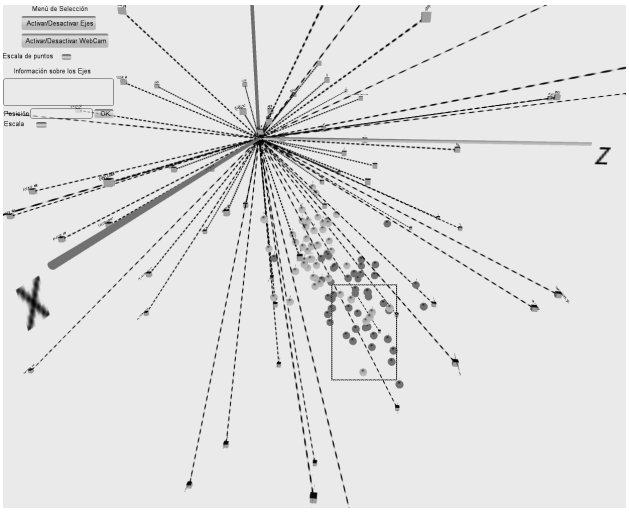

Fig. 4. Final visualization after the optimization process. Black spheres represent patients who suffered a relapse in breast cancer disease. Gray spheres represent healthy patients who do not relapse. Dotted lines represent coordinate axes (genes). A separation of classes is clearly visible. Last, the dotted square shows healthy patients in the relapse side.

The first one is related with clustering. Just looking at the distribution of data points. Playing with the coordinate axes, scaling or rotating. Finally one must see how spheres move in and out of clusters. The second one is correlation. The idea is the same, the oncologist could interact with the coordinate axes, multiple of them at the same time, scale a number of them at the same time, and observe how spheres move. He also has the possibility of turn on tracking so that consecutive movements of a data point are represented as lines so he can better observe where spheres go. Then he can examine, the direction points go, that tells you how the genes are correlated. It is important to mention that every operation above described must be supported by the expert's opinion in order to achieve valid and useful conclusions. Thus, a new tool that could make easier the acquisition of knowledge from medical data is provided.

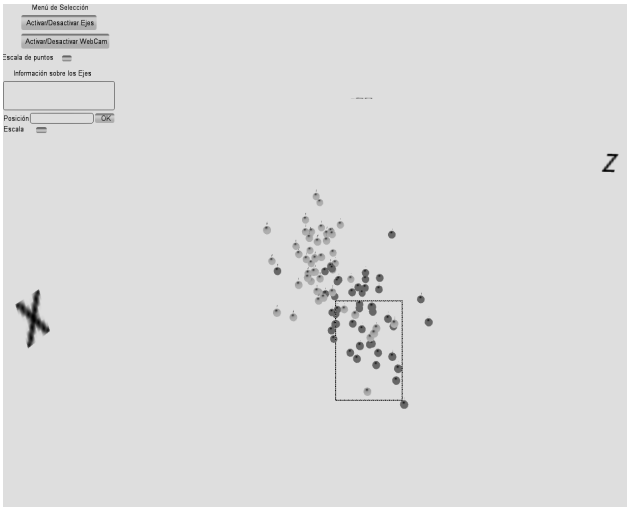

Fig. 5. Final visualization after the optimization process. No coordinate axes.

Fig. 4 and 5 shows a clear separation of the two classes. A possible interpretation is that in a n-dimensional space, the intrinsic nature of data makes evident a real division between patients who have relapsed and non-relapsed in breast cancer disease. After all, a three-dimensional embedding of the data's intrinsic geometric structure is mapped from the original n-dimensional space, what it means that the original geometry is being approximated.

If the results are analyzed with more detail, it is noticeable that several gray spheres lie on the black side. In fact, if the optimization process is continually repeated, in all cases the same representation is obtained. Moreover, always the same N.R patients lie on the black side. This fact could be exclusively seen from a medical point of view and it is possible that it has a major importance. For example, a priori patients with similar values for attributes must be grouped together but, why always the same N.R patients lie on the black side if the are supposed to be on the gray one? What does it means? Maybe, a valid interpretation could be that these patients consumed a certain kind of medicine during the chemotherapy process, so they didn't suffer a relapse. In this case, the next step could be to identify this medicine and the biomarkers, with the help of an expert.

Finally, the knowledge acquisition process is complemented with a strong interaction component. The expert also has the possibility of interacting with the application by means of rotating, scaling, or deleting axes in real time (fig.6). An optimal tradeoff between graphic quality and performance has been achieved. The expert can navigate and become absorbed into the environment thanks to the head tracking system. It works in the following way: just by using a standard webcam and FaceAPI software [24]. The visualization algorithm recognizes the data stream, previously filtered by FaceAPI software, and makes a mapping of the head movements to the main camera.

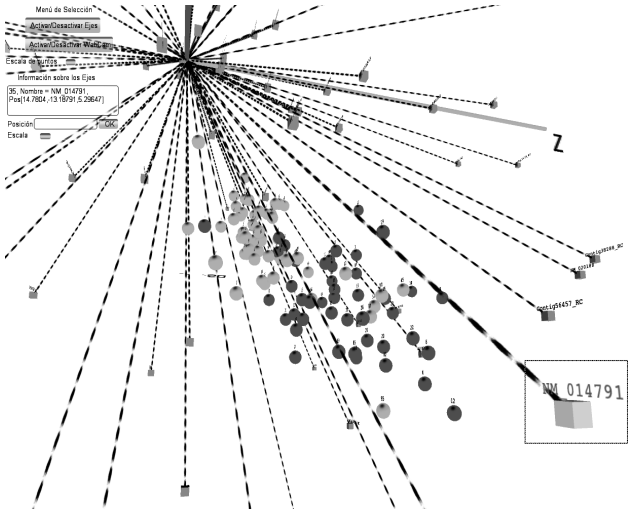

Fig. 6. Interacting with the coordinate axes. The dotted square shows a selected gen , 'NM_014791'.

C. Results

Here, final results have been separated into two categories depending on the objective function used in the optimization process. The first one represents the method based on the mean of the correlations, and the second one is based on the threshold method.

Table 1 shows the experimental settings in the optimization process.

Parameters	**Experimental values**
Number of generations	*15000*
Population size	*50*
Crossover probability	*0.7*
Mutation factor	*0.5*
Distance Metric	*Manhattan (L1 norm)*

Table 1. Experimental settings for computing the set of optimized axes.

Different parameters are shown. For example, the number of generations or the size of the initial population in differential evolution algorithm. We can also observe the crossover probability (C.P) and the mutation factor (M.F). Regarding to the distance metric, a Manhattan distance is used.

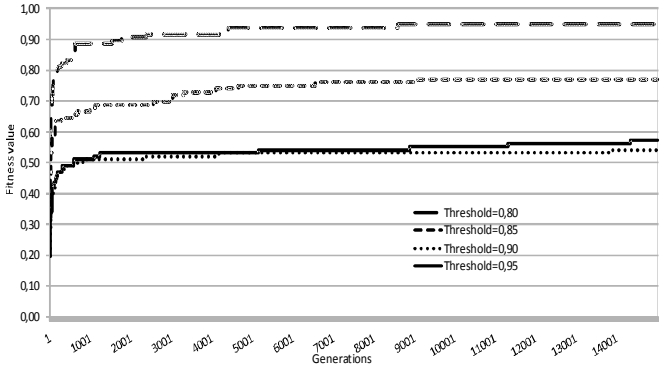

Fig. 7. Evolution of the fitness value using different threshold values. Threshold method.

Different fitness values are obtained according to the threshold value we use (fig. 7). For example, using a near 1 threshold will cause obtaining a small fitness value. For a 0.95 value, the explanation is that we are voting only if the correlation between the same row in *target matrix* and *generated matrix* is greater or equal than 0.95. The final fitness value for a 0.95 threshold is 0.572917, it means that the 57.2917% of individuals in the population (55 of 96 patients) are correlated each other with a threshold greater or equal than 0.95. Nevertheless, if a 0.80 threshold value is used, the 0.947917 fitness value is obtained, so 91 of 96 patients are correlated with a threshold greater or equal than 0.80. These high correlations between pair of distances in both matrixes (*target* and *generated* by optimization) show that it is necessary to find a tradeoff between the final fitness value and the geometry preservation in data visualization.

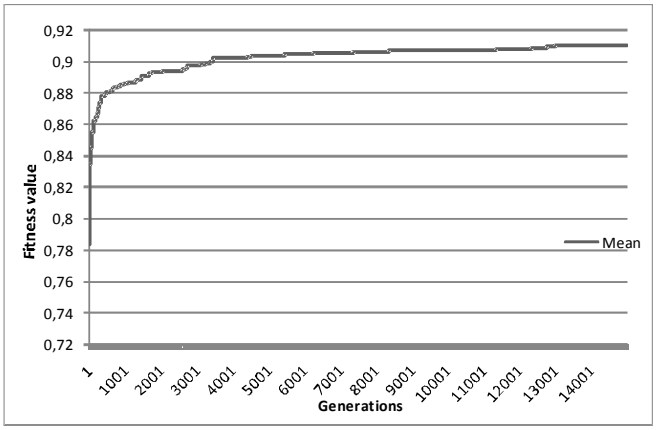

Fig. 8. Evolution of the fitness value for different threshold values. Method based on the mean of the correlations.

Figure 8 illustrates the method based on the mean of the correlations. It is simpler than the previous one. Here, the main benefit of this method is that a more uniform convergence is obtained. In consequence, the fitness value for every individual of the population is being fitted gradually. Instead, the drawback is that it penalizes high correlations and gives more importance to low correlations, because of the arithmetic mean.

V. Conclusions and Future Lines

This paper presented a new VR framework for visualizing and interacting with high dimensional DNA microarray datasets. The development is supported by an optimization process. It tries to find an optimal solution to preserving the intrinsic geometric structure of the n-dimensional manifold where the original dataset is embedded.

Taking into account the biological nature of data and the limitations for a computer engineer in terms of understanding and interpreting the data visualization, it is necessary to complement the final results with the experience of a specialist. For that reason, it is needed a close collaboration with the expert in order to validate appropriately the results.

Due to the medical nature of data and considering they are labeled, a direct approach based on supervised classification is carried out. The axes optimization process is done independently of the data class, so the same concept could be applied to different fields, for example in semi-supervised classification or unsupervised classification. In other words, the underlying idea is based on the possibility of extrapolating this development to any dataset that requires a visual and interactive representation.

It could be useful to use VR BioViewer to get better insight into prediction issues, particularly survival analysis in cancer. Using different data sources, for example the patient clinical information and the medicines used during the treatment, a complete visual study about who are alive for a given period could be done. Another possibility is to identify the biomarkers and add additional information about them, or giving them more intensity in the final representation.

Regarding to the distance metric used to get a suitable geometry preservation, it is considered that the use of geodesic distances over the neighborhood graph could improve the manifold learning [25]. It will be considered for next revisions.

These are preliminary results for which further experimentation would be required and they show a potential for advising and supporting the criterion of the oncologist expert.

Acknowledgements

The authors are grateful to the Blue Brain Project Team (http://cajalbbp.cesvima.upm.es/) and the La Paz Hospital, especially Cristobal Belda, for their assistance of medical knowledge. They also thankfully acknowledge the computer resources, technical expertise and assistance provided by the Centro de Supercomputación y Visualización de Madrid (CeSViMa) and the Spanish Supercomputing Network. It is also necessary to thank Ramón Toral from Operative Systems Laboratory, Universidad Politécnica de Madrid. This work is partially supported by the Madrid Regional Authority (Comunidad de Madrid) and the Universidad Rey Juan Carlos under the URJC-CM-2010-CET-5185 contract.

References

[1] Jolliffe, I. T. Principal Component Analysis. Springer-Verlag. pp. 487, 1986.

[2] S. Knudsen. A biologist's guide to Analysis of DNA microarray data. JohnWilley and Sons, 2002.

[3] J. Quackenbush. Computational analysis of microarray data. Nat Rev Genet, 6(2):418–427, June 2001.

[4] M. Schena, R. A. Heller, T.P. Theriault, K. Konrad, E. Lachenmeier, and R.W. Davis. Microarrays: biotechnology's discovery platform for functional genomics. Trends Biotechnol, 7(16):301–306, July 1998.

[5] Wolfgang Huber, Anja Von Heydebreck, and Martin Vingron. Analysis of microarray gene expression data. In in Handbook of Statistical Genetics, 2nd edn. Wiley, 2003.

[6] J. Quackenbush. Computational approaches to analysis of dna microarray data. Methods Inf Med, 45 Suppl 1:91–103, 2006.

[7] D. J. Lockhart and E. A. Winzeler. Genomics, gene expression and dna arrays. Nature, 405(6788):827–836, June 2000.

[8] L. J. van 't Veer, H. Dai, M. J. van de Vijver, Y. D. He, A. A. art, M. Mao, H. L. Peterse,K. van der Kooy, M. J. Marton, A. T. Witteveen, G. J. Schreiber, R. M. Kerkhoven, C. Roberts, P. S. Linsley, R. Bernards, and S. H. Friend. Gene expression profiling predicts clinical outcome of breast cancer. Nature, 415(6871):530–536, January 2002.

[9] J. Quackenbush. Microarray data normalization and transformation - nature genetics.

[10] O. Troyanskaya, M. Cantor, G. Sherlock, P. Brown, T. Hastie, R. Tibshirani, D. Botstein, and R. B. Altman. Missing value estimation methods for dna microarrays. Bioinformatics, 17(6):520–525, June 2001.

[11] J. J. Valdés and A. J. Barton, "Virtual reality spaces for visual data mining with multiobjective evolutionary optimization: Implicit and explicit function representations mixing unsupervised and supervised properties," in IEEE Congress of Evolutionary Computation (CEC 2006). Vancouver: IEEE, July 16-21 2006, pp. 5592–5598.

[12] J. J. Valdés, A.J. Barton: Visualizing High Dimensional Objective Spaces for Multi-objective Optimization: A Virtual Reality Approach. Submitted to CEC 2007. Congress on Evolutionary Computation. 2007.

[13] J. J. Valdés, Alan J. Barton: Multiobjective evolutionary optimization for visual data mining with virtual reality spaces: application to Alzheimer gene expressions. GECCO 2006: 723-730.

[14] R. Schaffer, "Multiple objective optimization with vector evaluated genetic algorithms," in Proc. First International Conference on Genetic Algorithms, 1985, pp. 93–100.

[15] P. Hajela and C. Lin, "Genetic search strategies in multicriterion optimal design," Structural Optimization, vol. 4, pp. 99–107, 1992.

[16] N. Srinivas and K. Deb, "Multiobjective optimization using nondominated sorting in genetic algorithms," Evol. Comput., vol. 2, no. 3, pp. 221–248, 1994.

[17] K. Deb, S. Agarwal, A. Pratap, and T. Meyarivan, "A fast elitist nondominated sorting genetic algorithm for multi-objective optimization: Nsga-ii," in Proceedings of the Parallel Problem Solving from Nature VI Conference, Paris, France, 16-20 September 2000, pp. 849–858.

[18] K. Deb, S. Agarwal, and T. Meyarivan, "A fast and elitist multiobjective genetic algorithm: Nsga-ii." in IEEE Transaction on Evolutionary Computation, vol. 6 (2), 2002, pp. 181–197.

[19] E. Zitzler and L. Thiele, "Multiobjective Evolutionary Algorithms: A Comparative Case Study and the Strength Pareto Approach," IEEE Transactions on Evolutionary Computation, vol. 3, no. 4, pp. 257– 271, 1999.

[20] L.O. Jimenez and D.A. Landgrebe. Supervised classification in high-dimensional space: geometrical,statistical, and asymptotical properties of multivariate data. IEEE Transactions on Systems, Man and Cybernetics, 28(1):39 – 54, 1997.

[21] E. Kandogan, Visualizing Multi-dimensional Clusters, Trends, and Outliers Using Star Coordinates, KDD 2001, pp. 107-116, 2001.

[22] Aggarwal C., Hinneburg A., Keim D.A.: On the Surprising Behavior of Distance Metrics in High Dimensional Space,in Proc. of 8th International Conference on Database Theory, ICDT 2001, London, pp. 420-434.

[23] Reference Manual, 2009. Unity3D. [online] Available at: <http://www.unity3d.com> [Accessed 05 January 2011].

[24] FaceAPI software, 2010. FaceAPI. [online] Available at: <http://www.seeingmachines.com/product/faceapi/> [Accessed 15 January 2011].

[25] J. B. Tenenbaum, V. de Silva, J. C. Langford, A Global Geometric Framework for Nonlinear Dimensionality Reduction, Science 290, (2000), 2319–2323.

[26] C.A. Coello, D.A. Van Veldhuizen, G.B. Lamont, Evolutionary Algorithms for Solving Multi-Objective Problems. Kluwer Academic Publishers, 2002.

[27] J.A. Foster. Computational genetics: Evolutionary computation. Nature Reviews Genetics, 2:428–436, June 2001.

[28] Jiawei Han and Micheline Kamber. Data Mining: Concepts and Techniques (The Morgan Kaufmann Series in Data Management Systems). Morgan Kaufmann, 1st edition, September 2000.

Empire 3D: A Collaborative Semantic Annotation Tool for Virtual Environments

D. Abbott[1], K. Bale[1], R. Gowigati[1], D. Pritchard[1], and P. Chapman.[1]
[1]Digital Design Studio, Glasgow School of Art, Glasgow, United Kingdom

Abstract – *Visualizations based on incomplete primary material lead to a recognised danger that 3D models can be misinterpreted as a totally accurate replica of reality. Good practice in creating reconstructions of non-extant architecture requires meticulous documentation of the process and its outputs. However, unless the research sources and methods are made explicit, the danger of mis-reading visualized data remains. This paper describes the development of software that allows research sources, methods, and interpretation to be added as multimedia annotations to a 3D scene. All real-world and digital objects are semantically described and spatially placed within the scene. The software is built on a CIDOC-CRM export-compatible data model and presents a novel collaborative interface for simultaneously creating annotations in an intuitive visualization environment using remote tablet PCs. The development of a life-size, stereo visualization of this lost architecture, with spatialised semantic annotations, will enhance understanding of this hugely significant event in history.*

Keywords: semantic annotation; information visualization; architecture; heritage; remote interaction

1 Introduction

The 1938 British Empire Exhibition was a stunning display of architectural achievement and a reflection of the life and culture of Glasgow, the UK and the Commonwealth. (Figure 1) As the last public showcase of the British Empire, the 1938 Exhibition was of huge international significance and continues to be a crucial event for the study of modernist architecture as well as British social and industrial history. Only one of over 100 innovative buildings remains on the site of the exhibition. Previous research was undertaken by the Digital Design Studio at Glasgow School of Art to digitally reconstruct the Empire Exhibition as a 3D scene using original sources (Figure 2). The main output was a robustly researched and constructed 3DSMax visualization mapping the buildings and structures of the Exhibition to the topography of the original site at Bellahouston Park, Glasgow [1]. To achieve this, a large collection of related cultural artefacts (architectural plans, photos, drawings, and ephemera) was assembled and digitised, and interpretation from people who had visited the Exhibition and architecture scholars was captured as video interviews[1].

[1]Low-resolution outputs of this research are available at the project website http://www.empireexhibition1938.co.uk

Figure 1 – A photo of the Empire Exhibition taken in 1938

Figure 2 - An example of the 3DSMax visualization produced at the Digital Design Studio

This paper presents research which builds on this remarkable digital resource by linking the 3D scene of the Exhibition directly with the evidence on which the model was based and providing a customisable toolkit for the spatialised, collaborative annotation of 3D scenes.

Due to the paucity of original information such as architectural plans, a collaborative research methodology was critical to the original project's aim of producing an accurate 3D reconstruction via robust interpretation of incomplete evidence and the combination of a variety of sources, including testimony from direct witnesses and architecture experts. This methodology is expanded in the development of a tool which allows users to semantically connect 3D

modelled data with its source(s) in an intuitive, discursive environment more appropriate for visualization of large scenes such as architecture. The cultural archive on which the reconstruction of the Empire Exhibition is based is visualised within the 3D scene, along with research notes on the digital reconstruction, to enrich the building models and allow further interpretation via annotations.

2 Research Background

Semantic annotation, and the ways in which it can enhance engagement with 3D visualizations, is an emerging research area. The EPOCH Research Agenda for the Applications of ICT to Cultural Heritage identifies it as a crucial issue for development [2] as does the 3D-COFORM Consortium which deals with 3D documentation of tangible cultural heritage and states that 3D artefact models should be handled together with their context and interpretation represented by metadata, the modelled real world objects, and documentary sources [3]. The London Charter for the Computer-based Visualization of Cultural Heritage [4] brings together the most contemporary research issues in heritage visualization. Particularly pertinent to this research are Principles 3 and 4 which emphasise the need for transparent identification and communication of research sources in order to allow a rigourous evaluation of the purpose, accuracy, and methodology of the visualization and of visualization practice more generally, particularly in datasets where there is by necessity a level of uncertainty. Access to research sources and transparent methodology is now seen as crucial for the development of the discipline:

"Whilst it is unlikely that perfect reconstruction accuracy relative to an ancient monument's original appearance can be achieved for complex models, offering complete transparency about the underlying source data and decision making process determines the scientific authenticity of the resulting models. […] One particularly interesting concern is methods for allowing interactive exploration of the relevant metadata displayed in corresponding locations in the 3D environment." [5, pp.10-11]

Previous research in this area has developed interfaces for adding textual semantic annotations to specific areas of visualizations, using an MPEG-7 framework [6], or for viewing information attached to specific parts of 3D models of individual sculptures, semantically described with the CIDOC Conceptual Reference Model [7,8,9]. Related disciplines have investigated immersive visualizations mapped onto CIDOC-CRM (for example the VENUS project's models of the archaeology of underwater sites [10]).

Despite a defined need for tools for semantic annotation of 3D data by existing research in the field, there are no publicly available tools that can be used to connect visualizations of 3D scenes with digital cultural heritage artefacts in a variety of formats. Early steps have been taken in the development of scientific archives of 3D models presented alongside their metadata, such as the Digital Roman Forum [11], however current examples make neither 3D models nor descriptive tools publicly accessible [5].

One reason for the slow development of modelling and visualization research specific to architecture is the scarcity of suitable visualization laboratories available to arts and humanities researchers. One innovation of this research is to enable novel immersive interaction with the Exhibition 3D scene via a large-scale (13m x 8m), high-definition stereo projection, and the ability to annotate using separate tablet computers, connected to the 3D environment in real-time. Simulation of real movement within the scene, visualised at life-size, allows users to inhabit the virtual space and interact with it as a group, in addition to the more typical single-user, desktop mode of interaction.

This paper discusses how previous research in the intellectual sustainability and transparency of 3D heritage visualizations has been extended by developing software to allow collaborators to add multimedia annotations to a 3D dataset and create both semantic and spatial relationships between the annotations themselves and the 3D models they document. The software is built on a CIDOC-CRM export-compatible data model and uses a variety of data relating to the 1938 British Empire Exhibition as a demonstrator. At the end of the project, the customisable annotation toolkit will be made freely available, as will a packaged visualization of the Exhibition and its related annotations.

3 Software Development

3.1 Optimisation of Data

One of the challenges of this research is the size and scale of the dataset. The original 3D scene was intended for offline rendering and contains over 100 high resolution buildings (each made up of between 10,000 and 60,000 polygons) and a vast number of auxiliary features such as statues, benches, fountains, and vegetation – in total around ten million polygons. These models were all placed in an accurate geographical context, a digital representation of 175-acre Bellahouston Park, Glasgow. It was necessary to facilitate interactivity via real-time presentation as both a desktop application and a stereo visualization with remote data input. In the taxonomy dimensions defined by [12] the new visualization grants interactivity with a negligible loss of precision and visual consistency, therefore a great deal of care was taken to optimise the scene whilst preserving as much detail as possible.

Data optimisation was performed in a number of stages and at each stage the performance was evaluated, using an PC equiped with an Intel i7 590, 6Gb of RAM and a QuadroFX 580 graphics card. Performance was deemed acceptable once the frame remained above a stable 60 frames per second. The

first pass removed redundant elements such as hidden surfaces and structures. The second stage separated out the high detail decorative features such as lights, statues and furniture and simplified them where possible. All of the high detail shrubbery and trees were removed in this stage and replaced with billboard variants. The third stage was to do an aggressive polygon reduction on the building models. The fourth and final stage was to generate alternative level of detail versions of each building model (Figure 3).

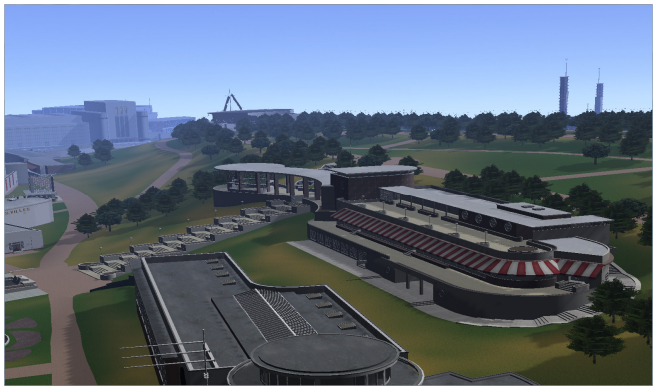

Figure 3 - An example of the real-time visualization of the Empire Exhibition

In the interest of preserving the models for future projects all of the processed models were exported and archived using the COLLADA, a freely available open standard digital asset schema [13].

3.2 Data Model

In order to ensure that the software would be usable by other researchers in the cultural heritage domain (and to increase the interoperability of existing research data on the Empire Exhibition) the CIDOC-CRM (official standard ISO 21127:2006) was chosen as the basis of the underlying data model for describing the 3D building models and scenery, the digitised archive of source material, and their inter-relationships. The CIDOC-CRM is a "a formal ontology intended to facilitate the integration, mediation and interchange of heterogeneous cultural heritage information" [14] which provides detailed definitions of Entities and Properties for describing the underlying semantics of cultural heritage information and objects. Previous research has focussed on Persistent Items as the basis for semantic tagging [8] in order to provide detailed descriptions for visualizations of real-world objects. The purpose of this research was not to implement a full CIDOC-CRM data structure for the Exhibition and all its related entities but to create explicit relationships between visualizations, the real objects they represent, and the evidence on which they were based. Therefore, a compact data model was designed which is export-compatible with the CIDOC-CRM, but condenses the core semantic concepts of the virtual reconstruction of a now-vanished architectural exhibition into a simpler structure. The naming conventions of CIDOC-CRM were maintained.

The two core concepts were that of **real objects** (modelled as E22 *Man-made object*) comprising the buildings of the Empire Exhibition and the real archive objects relating to them, and **digital objects** (annotations) which communicate information about the tangible objects via placement in the 3D scene (modelled as *E31 Document*, a specialisation of *E73 Information Object*). Relationships between real objects and digital surrogates or derivatives (for example a building and its corresponding digital model or a souvenir postcard and a scanned image) are represented through the *P70 Is documented by* property, demonstrating evidence for the visualization methodology, or the *P67 Refers to* property which allows the structured semantic modelling of non-documentary information such as multiple (potentially conflicting) interpretations of the architecture or the 3D scene itself. Both real and digital objects have associated information such as titles, creators (architects, photographers, 3D modellers etc.), and dates. This information was also semantically modelled to allow users to investigate implicit relationships, such as finding all the buildings designed by a particular architect. A list of types was also created using the *E55 Type* property to increase search and interpretation functionality for this particular dataset; this types list is customisable to enable other instantiations of the software to fit completely different datasets. In this way, the data model allowed a clear focus on the core research issue of linking up visualizations with their source evidence, whilst also allowing future customisation and interoperability.

3.3 System Architecture

The visualization system was developed using the OpenSceneGraph graphics library, an open source, high performance graphics toolkit [15]. The wide range of inbuilt functionality that OpenSceneGraph offers such as paged level of detail, occlusion culling and full shader support enabled the graphical element of the software to developed very rapidly. Below this graphical layer the system uses a locally stored Compact Edition of SQL Server to implement and manage the database. Interaction with the system is provided through two methods. The first is aimed at desktop PCs, comprising a point and click 3D viewer with webpages in a separate window for creating and editing annotations. The second is a novel wireless tablet approach. Remote control of the application is provided through an embedded web server and a series of interactive web pages. Consequently, bidirectional communication between the browser and the server is provided using an XMLHttpRequest system.

3.4 Interface, Navigation and Immersion

The Empire Exhibition viewer is aimed at two different user groups. The first is the general public: primarily non-expert content consumers with the principal interest of

navigating around the scene and reading/watching the various annotations. This group will typically be using the system from a desktop PC. The second group are researchers, or other cultural intermediaries such as architecture experts [12], who are interested in contributing further annotations to the scene. This group of users could work alone at a desktop PC or in groups using the large stereo display and require the means to add further annotations by uploading media or simply entering text.

As they can stimulate the perception of real depth and communicate a higher level of overall visual consistency, stereoscopic visualizations can be considered superior to non-stereo 3D scenes [12]. In the context of architectural research it is particularly important to present a realistic, full-scale view of buildings from ground level. By presenting the scene using the large scale stereo display available at the Digital Design Studio, it is possible to greatly increase a user's sense of immersion within the scene. The sheer size of the screen (13m x 8m) allows for the buildings to be rendered to scale, whilst the stereo projection enhances the perception of structure and depth. However, to use such large displays intuitively and effectively control methods that are not based around the classical keyboard and mouse paradigms must be considered.

Over the past year, there has been a rise in the availability of cheap, powerful and lightweight tablet PCs. This hardware presents many exciting possibilities in terms of interface development. By linking tablet PCs to host software it is possible to provide users with a customisable touchscreen interface whilst also providing the freedom to move around within a virtual space. Using this approach, a web server aimed at serving interactive web pages to the tablet PCs was embedded within the host application. Through the use of AJAX, these web pages are able to provide a wide range of functionality ranging from camera control and displaying annotations to more complex tasks such data input. The use of a web server also means that the system is highly scalable in terms of adding additional users. However, managing the flow of interaction of multiple users can be very challenging. In order to prevent confusion, only one user is granted control of the camera at any time. Each tablet interface is then given a mechanism which allows them to request control over the camera from the designated controller. Should the request be granted, control over the camera is passed to the next user. Whilst control of the camera is only accessible to a single user, the remaining tablet interfaces remains fully functional allowing other users to browse, search and input elements into the annotation database on their respective devices (Figure 4).

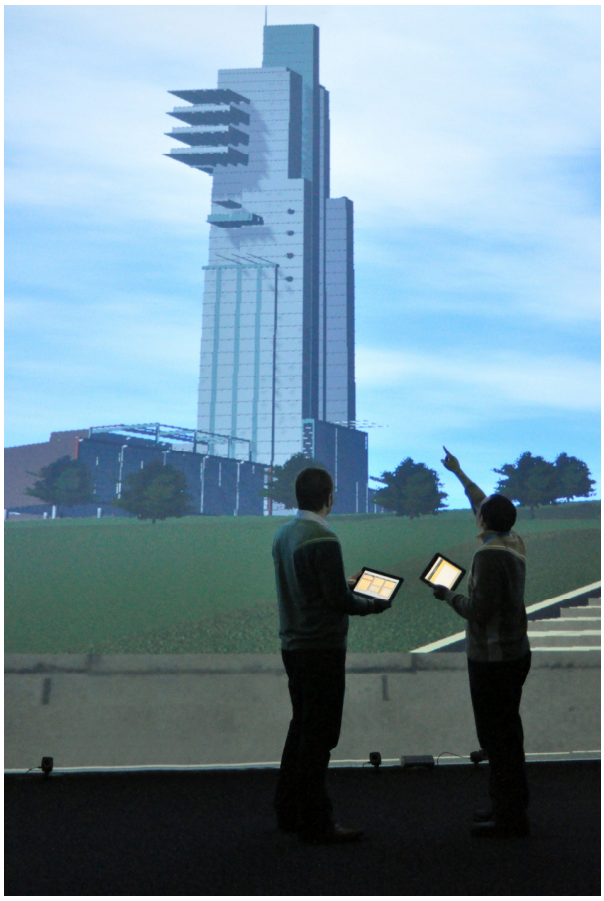

Figure 4 - Two researchers using the touchpad interface in front of the large stereo display at the Digital Design Studio.

Navigation and camera control methods were also used to increase immersion within the 3D scene. An extensive network of footpaths were designed as part of the original Exhibition and were modelled along with the buildings. These tracks are used to provide a realistic, ground-level navigation between buildings selected by users in both the desktop and stereo visualizations. A series of camera tracks were created (Figure 5), linking each building, its default camera view, and the pathways. To navigate the scene, users select their desired destination from an aerial map displayed in a floating pane either on the screen (desktop) or on the tablet PC. The camera then travels along the automatically calculated shortest route to the default camera view for the destination. Users can then use a mouse (desktop) or camera controls (tablet) to zoom and rotate around the focal point for closer inspection, without being restricted to pathways and ground level. This navigation method aims to convey a sense of physically inhabiting the space, and instead of 'teleporting' users to particular points, simulates real travel. This is not only highly intuitive but inherently communicates a sense of each building in the context of the whole Exhibition, and reduces the chance of users becoming lost or disoriented within the scene.

Figure 5 - An example of the camera tracks defined within the scene, shown as yellow lines.

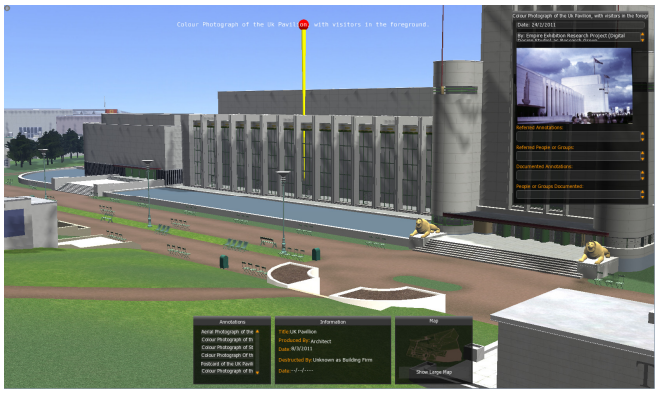

Figure 6 - An example of a marker showing the reference point for an image annotation.

Within this interface, annotations must be displayed in a way that is easily navigable and communicates each annotation clearly. The annotations associated with the Empire Exhibition cover a range of formats: short textual references, high resolution images and video, audio, and longer text. Some building models are documented by over 100 annotations and there are thousands in total. This number of annotations displayed within the scene by default would quickly cause symptoms of occlusion as the screen became more and more cluttered. Visual 'clutter' is a known user-interaction issue for visualization of annotations in 3D scenes [16] therefore in order to present the annotations in such a way that they can be viewed, browsed and searched for efficiently, a building-centric approach was adopted. At the point of being created, each annotation is assigned a default spatial placement based on its relationship to a modelled Exhibition building. By marking a point on the 3D model, it is possible to assign other co-ordinates to annotations if desired, for example if the annotation documents or refers to a specific architectural feature. Annotations with specific co-ordinates are shown as labelled, clickable pins in the 3D scene (Figure 6), however to avoid saturating the scene with thousands of annotations, those without specific co-ordinates are shown as a clickable list in a floating pane over the default building view. When clicked, another floating pane shows the full annotation (text, image, etc.) along with information about its relationships, creator and so on (Figure 6).

The tablet PCs implement annotation display through a series of web pages which allow users who are not currently in control of the main projected camera view to continue to add or view other annotations simultaneously.

4 Further work

In addition to widely disseminating the 3D models and related cultural artefacts relating to the 1938 British Empire Exhibition, the primary purpose of this research is to enable further investigation of the methodology of 3D architectural visualization by other researchers. After a period of user-testing by experts including architects, historians, and 3D modellers (during which they will have the opportunity to add further interpretive text annotations), the customizable software will be packaged in a form suitable for use by other content holders, i.e. with the option to create different *Types* and upload different data. The entire visualization with all annotations will also be packaged for download by content consumers with the annotation edit functionality removed.

In the future, there is the potential to continue with the approach used by the initial modelling project and encourage contributions from members of the public, both in terms of interpretation of the Exhibition and in providing additional sources of evidence for Exhibition structures. Assembling information from disparate sources was a crucial part of the creation of 3D representations of the buildings and further information would allow this research to progress with confirmations or contradictions of those aspects of the scene which were modelled with uncertainty. However, interaction of this level (for example, allowing members of the public to submit comments or images through a website, with the potential to make corrections to the 3D models) would require significant moderation and is therefore subject to further funding.

It is also hoped that the software is used by researchers on other similar projects and that in the future, the data can be integrated into a larger, interoperable collection of information on architectural history.

5 Conclusion

This paper has presented research to create an interactive, immersive visualization of the hugely significant 1938 British Empire Exhibition which took place in Bellahouston Park, Glasgow with the functionality to explicitly link the digital 3D models with their research sources and interpretation, in 3D space. This was achieved by optimising existing 3D data designed for offline rendering and incorporating the 175-acre scene into a real-time application. A lightweight data model based on CIDOC-CRM was designed and a multimedia collection of research sources and methodological notes were semantically described and uploaded as spatialised annotations to the application.

Two interfaces are provided by the software, one aimed at general content consumers (using a desktop PC) and one with stereo visualization of the data and a novel method of annotating in collaborative groups, using remote tablet PCs. Both simulate real-world navigation to increase immersion. Annotations are shown in a non-obstructive way within the 3D scene either as clickable map pins or as a clickable list relevant to the current building view. At the end of the project the scene, associated annotations, and software itself will be made freely available via the project website.

6 Acknowledgements

Both this research and the initial project to model the Empire Exhibition were funded by the Arts & Humanities Research Council (AHRC).

7 References

[1] Johnston, I. & Pritchard, D. 2007 "Recreating the 1938 British Empire Exhibition" in *8th International Symposium on Virtual Reality, Archaeology and Cultural Heritage* (VAST2007)

[2] Arnold D., & Geser, G. 2008 EPOCH research agenda for the applications of ICT to cultural heritage, EPOCH.

[3] 3D-COFORM, http://www.3d-coform.eu/ [accessed Mar 2011]

[4] The London Charter for the use of 3-dimensional visualisation in the research and communication of cultural heritage (Draft2.1, Feb 2009), www.londoncharter.org [accessed Mar 2011]

[5] Koller, D., Frischer, B., & Humphreys, G. 2009 "Research challenges for digital archives of 3D cultural heritage models" in *Journal on Computing and Cultural Heritage (JOCCH)* Vol. 2 No. 3, December 2009, ACM New York, USA, Article No. 7

[6] Bilasco, I.M., Gensel, J., Villanova-Oliver, M., & Martin, H. 2006 "An mpeg-7 framework enhancing the reuse of 3D models" in *Proceedings of the 11th International Conference on 3D Web Technology* ACM, New York, USA, pp. 65-74

[7] SCULPTEUR project, http://www.sculpteurweb.org/ [accessed Mar 2011]

[8] Rodriguez-Echavarria, K., Morris, D., & Arnold, D. 2009 "Web based presentation of semantically tagged 3d content for public sculptures and monuments in the UK" in *Proceedings of the 14th International Conference on 3D Web Technology* ACM, New York, USA, pp. 119–126

[9] Havemann, S., Settgast,V., Berndt, R., Eide, O. & Fellner, D.W. 2008 "The Arrigo Showcase Reloaded – towards a sustainable link between 3D and semantics" in *The 9th International Symposium on Virtual Reality, Archaeology and Cultural Heritage (VAST2008)* pp. 125-132

[10] Chapman, P., Bale, K. & Drap, P. 2010 "We All Live in a Virtual Submarine" in *IEEE Computer Graphics and Applications*, Vol. 30, No. 1, Jan/Feb 2010, pp. 85-89

[11] Digital Roman Forum, UCLA, http://dlib.etc.ucla.edu/projects/Forum [accessed Mar 2011]

[12] Foni, A.E., Papagiannakis, G., & Magnenat-Thalmann, N. 2010 "A taxonomy of visualization strategies for cultural heritage applications" in *Journal on Computing and Cultural Heritage (JOCCH)* Vol. 3 No. 1, June 2010, ACM New York, USA, Article No. 1

[13] COLLADA, http://www.collada.org/ [accessed Mar 2011]

[14] Crofts, N., Doerr, M., Gill, T., Stead, S., & Stiff, M. (ed.s), 2010 ***Definition of the CIDOC Conceptual Reference Model,*** ICOM/CIDOC Documentation Standards Group/CIDOC CRM Special Interest Group, http://www.cidoc-crm.org/.

[15] OpenSceneGraph, http://www.openscenegraph.org [accessed Mar 2011]

[16] Kadobayashi , R., Lombardi, J., McCahill, M.P., Stearns, H., Tanaka, K., & Kay, A. 2005 "Annotation authoring in collaborative 3D virtual environments" in *Proceedings of the 2005 international conference on Augmented tele-existence (ICAT2005)* ACM, New York, USA p. 256

SystemC Code Generation from UML for Wireless Sensor Networks Design

S. Villa, D. Serna, J. Aedo
ARTICA, Microelectronic and Control Research Group
Electronics Department, Universidad de Antioquia,
Medellín, Colombia

Abstract *- Due to increasing complexity in embedded systems, it became necessary to develop new design methodologies that will address the design from a high level of abstraction. In this context, our study suggests an approach for modeling wireless sensor networks (WSN) from system specification using the Unified Modeling Language (UML), describing both structure and functionality. Process for automatic code generation from UML models to SystemC executable models has been presented. It was found that transformation process will provide the exploration and system functional verification before being implemented.*

Keywords *- UML, MARTE, SystemC, Embedded System, Wireless Sensor Network.*

1. Introduction

In recent years, embedded systems have appeared in many applications which require that the system possesses certain quality factors such as: good performance, reliability, security, portability, interoperability, robustness, scalability, among others. These factors make the design of embedded systems become increasingly complex, particularly for wireless sensor networks (WSN), which also must meet low power consumption.

In order to make optimal design, embedded systems modeling and simulation are becoming an important area of research. Also, for greater productivity in the design process, the literature has proposed the System Level Design (SLD) methodology, which suggests that the initial design stages are made at high level of abstraction, omitting the implementation details [1][2][3]. This involves specifying the functionality of the system without having defined how it will implement.

This research supports the SLD methodology, proposing an approach for modeling a WSN from the system requirements. In this context, the Unified Modeling Language (UML) has been introduced to support the specification, design, and verification stages in the development process, describing both structure and functionality. A process for automatically generating code from UML models to SystemC executable models has been presented.

This paper is organized as follows: Section II presents the related work. Section III describes the transformation process. Section IV illustrates the process through a case study. Finally, Section V presents conclusions and future work.

2. Related work

In order to perform complex system designs, while maintaining high productivity, decreasing marketing time and low cost, literature has proposed to use UML as modeling tool. Moreover, system simulation is carried out by system description languages such as SystemC. Thus, a design trend is the integration of these two modeling languages, to obtain models based on HW / SW from high abstraction levels, appearing the automatic code generation between UML and SystemC.

In [4][5][6] a comparison between UML and SystemC is presented. The comparison purpose is to find and motivate the mapping rules for automatic code generation; this is one of main steps in this research. The focus is on concepts that are equivalent in both languages, as well as the concepts and constraints that are only present in each one. However, these articles do not present system behavior models at a high abstraction level or the corresponding transformation, focusing solely on the system structure.

Seeking to improve the model transformation, studies like [7] present a strategy to exploit the capabilities of both languages by creating a

UML/SystemC profile, performing the behavior modeling using state diagrams. However, this project only is possible to model the behavior of not very complex systems. Currently, this research seeks to describe the behavior of systems using various UML diagrams such as state diagrams and/or activity diagrams to allow for greater flexibility.

In [8] shows a way to convert the models developed in UML to SystemC simulation models. Initially, [8] developed a model with UML/SysML sub-profile, bringing them closer through a series of restrictions. They performed a transformation 1 to 1 (diagram/code) between the models. After completing the simulation, it is possible to pass SystemC to VHDL code for implementation on a FPGA (Field Programmable Gate Array). Although this research presents an interesting approach in the process of transformation, which leads directly to the implementation models, it does not focus on embedded systems.

Trying to correct this, in [9][10][11][12], authors perform real-time systems models using SysML and UML/MARTE profiles and employing Papyrus tool [13] (an open source tool based on Eclipse environment for modeling using UML2.0) and SC2 (based code generator models). This research develops an innovation over others, allowing the insertion of code using Scripts. But the use of two profiles for the description of real-time systems, mean that the model is somewhat complex.

In [14], a design environment called Gaspard2 was presented. The process starts from a model made in UML/MARTE, which represents a high-level model. This model is directly converted to a specific domain model (Gaspard). Then, this is transformed into a polyhedron model, in which the application is reconfigured and divided into different processing units. This derived model is transformed into a cycle model, where the application is represented according to a traditional pattern of nested loops. After these transformations, the simulation level is specified, such as SystemC TLM level. This environment focuses on MPSoC (Multiprocessor System-on-Chip), but not in WSN.

As illustrated by the literature, it is possible to adapt UML for modeling embedded systems. And although UML lacks real-time features, it has profiles that limit the domain of application according to the designers needs. Thus, in comparison with existing efforts, the approach this research approximates the modeling language (UML) to target language (SystemC) through the UML/SystemC profile; while real-time requirements are modeled through the UML/MARTE profile. In this way, models that approximate the real system and are easily adjustable to the SystemC code are obtained.

3. METHODOLOGY

As mentioned above, in the literature there are studies that seek to transform UML models to SystemC code. Many of these studies perform an incomplete system model; some of them focus on the system structure without addressing the behavior, while others only seek to represent the behavior regardless the system physical architecture; and those which try to cover both fronts are not able to model complex systems. In this research the solution to these problems by implementing the transformation process shown in Figure 1 was sought. It started with the system specification using the UML 2.0, then there were the automatic generation of SystemC code through a series of analysis. Finally a simulation and validation model was obtained.

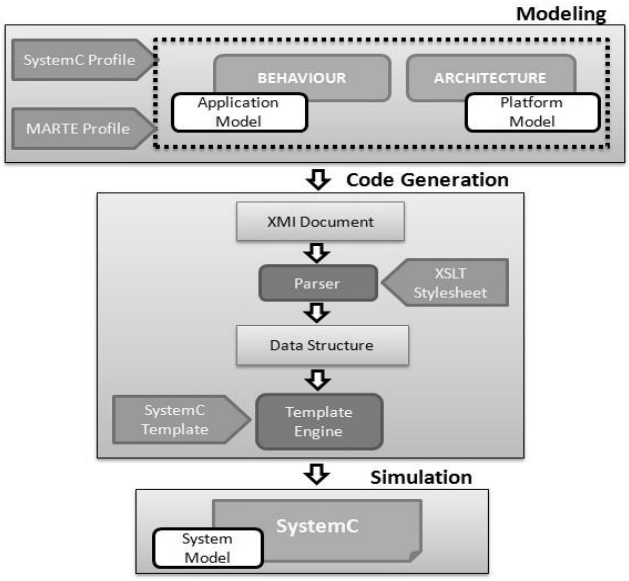

Figure 1. ***Transformation Process*****.**

3.1 Modeling System

The transformation process begins with a system description at a high level of abstraction. Functional model (application model) and physical structure (platform model) are separately described. Thus, it is possible to make a platform independent application, obtaining a greater flexibility in designs.

The physical structure describes platform execution including processing units (such as CPU), storage units (such memories), and communication modules. In the physical structure the platform is empty, since the CPU does not execute any instructions and components are not connected with logic yet.

The functionality describes the application with real-time constraints. The functions are synchronized through events, exchange of variables and message queues. The application model has two aspects: the structural aspect responsible for encapsulating the various functions which provides paths for exchanging data among them; the behavioral aspect provides flow used in data processing and sync functions.

Finally, a virtual system is the result of the mapping stage, which involves the functions allocation on the various modules of the platform; i.e. the application model is projected on the model platform to add physical constraints, such as scheduling, communication rate and memory size. The assignment can be deemed as a model itself.

3.1.1 UML diagrams selection

Due to UML is a really broad language, it is necessary to make a diagrams subset selection for the research domain. It was found that the diagrams that best fit the research objectives are: package diagram, class diagram, composite structure diagram, state diagram, activity diagrams.

3.1.1.1 Package Diagram

Package diagram is used to group elements, providing an order in the system modeling. This diagram reflects the separation between application models and platform. In addition, each of these is organized into basic elements and compound elements. Thus, the function package contains the system behavior, which can be reused in other models. And the component package contains the elements of the platform model, which can also be reused.

3.1.1.2 Class Diagrams

These diagrams are used to model the static system structure, which defines its elements, relationships, ports and interfaces. The elements describe two aspects:

- *Components for platform* model that will be part of physical system structure, these describe the basic SystemC entities (such as modules and channels).
- *Structures for application model* which encapsulate the behavior of the system, declaring attributes and methods of a function, they also represent the elements hierarchy. The application structure has ports, which provide the means for connecting the model elements, and It has interfaces, which are used to model a set of public operations that can be provided or implemented by various elements.

3.1.1.3 Composite Structure Diagrams

There diagrams describe the internal structure elements of application and platform models. There diagrams show the components (SystemC modules), channels, ports and connectors, and how the communication takes place among them. This communication is carried out through ports, which provide/require a service, doing invisible the internal structure at the external elements, allowing improving the research designs and facilitating the generation of code.

3.1.1.4 State Diagrams

State diagrams are used in the functional architecture, modeling the system dynamic aspects. The transition among states is triggered by events (sensitive signals). These diagrams define the system behavior at a high abstraction level.

3.1.1.5 Activity Diagrams

Activity diagrams describe the internal workings of the methods described by state diagrams; that is, they offer the possibility to specify more thoroughly the system operations. Additionally, these diagrams allow bringing the application model to SystemC methods. There diagrams are very similar to flow charts, which can implement decision points and loops in the system behavior.

3.1.2 UML profile

To extend the capabilities of research tool a set of extensions called profiles was selected. In particular two profiles –UML/SystemC and UML/MARTE– have been applied.

3.1.2.1 SystemC profile

This profile is disposed to map UML models developed in SystemC code. It defines a set of constraints and similarities between both languages, as shown in Table 1. This table shows that the SystemC profile has been divided into two parts: the first one it related to model physical architecture (structural) and the second one to their behavior.

UML	SystemC	Stereotypes
STRUCTURAL		
Class	Module	<<sc_module>>
Class	Primitive Channel	<<sc_prim_channel>>
Class	Hierarchical channel	<<sc_channel>>
Class	Signal	<<sc_signal>>
Class	Fifo	<<sc_fifo>>
Port	Port	<<sc_port>>
Port	Input/Output	<<sc_in/out>>
Connector	Connector	<<sc_connector>>
Interface	Interface	<<sc_interface>>
BEHAVIOR		
State machines	Method	<<sc_method>>
State machines	Thread	<<sc_thread>>
Operation	Constructor	<<sc_constructor>>
Operation	Event	<<sc_event>>

Table 1. SystemC Profile

3.1.2.2 MARTE profile

MARTE profile will allow modeling some hardware devices and real-time constraints. For modeling hardware components, MARTE has the Hardware Resource Modeling (HRM) sub-profile, with which can represent certain resources, such as: a set of processing resources (<<HwComputing>>), devices involved in the communication process (<<HwCommunication>>), memory resources (<<HwStorage>>), assistive devices that are not so critical (<<HwDevice>>), among others [15].

MARTE also offers another subprofile to behavior model called Software Resource Modeling (SRM). This sub-profile can represent entities that compete for computing resources by <<SwConcurrency>>, synchronization mechanisms to control the flow of execution by <<SwInteraction>>, interfaces between peripherals and software implementation support <<SwBroking>> [15]. Furthermore, MARTE allows adding time's constraints and events to the functional model

3.2 Code Generation

The next step in the transformation process is the cod generation. This is accomplished through a series of analysis to different system representations. The first representation is described by UML diagrams with MagicDraw tool [16]; this makes it possible to generate a second code representation XMI (XML Metadata Interchange). XMI is a standard language which allows the easy exchange of data among modeling tools, specializing in models based on UML [17]. This XMI code is captured by our tool, which is integrated in the Eclipse environment, where it applies a XSLT Stylesheet (eXtensible Stylesheet Language Transformations) by Saxon-B open source processor which performs a filtering code, and changes it to another XMI document. The new document contains only XMI information, eliminating irrelevant data and providing continuity in the next step.

Then, within the same working environment, a data structures generator, called DOM was applied. It transforms the XMI document to a tree-like structure in Java. With this representation, the model hierarchy is captured, obtaining the structured elements (hardware, attributes and methods). This structure is organized into arrays with predefined classes. Figure 2 shows a fragment of the data structure model built to express the system.

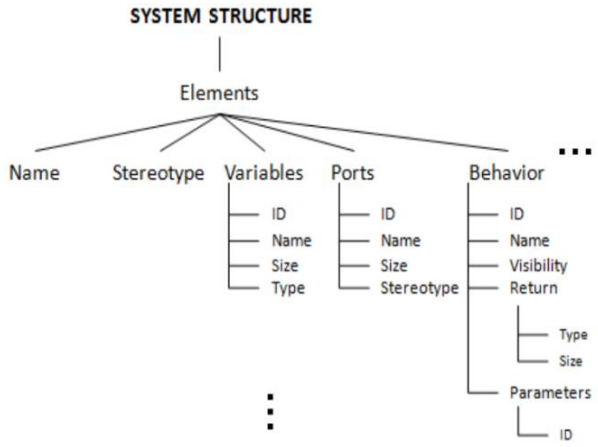

Figure 2. ***Data structure.***

Tthe data structure fits into a SystemC template using the template engine Freemaker. This is an engine to generate HTML output, but can also be used to generate the standard text code [17]. The data structure defines the model, while the template indicates how this model should be organized in a format source. Thus, the data structure, the template and the java application produce the output source code in specific language, which in this case is SystemC.

A template with Freemaker syntax based on the system data structure and target language, which allows expressing the system in SystemC code was created. For the sake of simplicity, in Figure 3 shows a small part of the template.

```
#include "${SubMod}.h"
class ${modelo.NAME}: public ${modelo.IDENT}{
public:
// module port declaration
${port.TYPE}<${port.INTERF}<${port.SIZE}>>${port.NAME};

//submodule declaration
${SubMod.CLASS} *${SubMod.NAME};

//process declaration
public:
${(Funct.RETURN)}${Funct.NAME}(${par.TYPE}${par.NAME}){
/*Functionality goes here*/ }
private:
${(Funct.RETURN)}${Funct.NAME}(${par.TYPE}${par.NAME}){
/*Functionality goes here*/ }
    . . .
// constructor
SC_HAS_PROCESS(${modelo.CLASS_NAME});
${modelo_.CLASS }(sc_module_name name:sc_module(name){
  //module local channel implementation
  ${Channel.NAME}=new${Channel.TYPE}(${Channel.DATA});

  //submodule port binding
  ${SubMod.NAME}.${SubMod.PORTS} (${SubMod.BINDING});
    . . .
}

//member variables
private:
${var.type}<${var.size}> ${var.name}=${var.value};
    . . .

};
```

Figure 3. ***Freemaker template.***

3.3 Simulated model

Finally, system model in SystemC language was obtained. This model allows the simulation to validate platform architecture and application. This simulation is carried out under the same Eclipse environment, which should include the SystemC-2.2.0 library [18]. Additionally, more features to generated code to make measurements of any of the quality factors mentioned at the beginning can be manually added.

4. Case study: Wireless Body Sensor Network

This case study aims to model a wireless body sensor network. It consists on a series of small smart devices, called nodes, which are spatially distributed on body; it communicates wirelessly with other nodes; it has the ability to sense vital signs and some computing power.

This model system consists on 4 nodes and a wireless channel. A node called Sink, which is in charged of gathering information and to sense the cardiac activity (EKG Node). The other nodes will sense the oxygen saturation (SaO_2 Node), motion (Accelerometer Node) and blood pressure (Pressure Node). Each node consists on several modules, such as Central Processing Unit (CPU), a radio unit, a serial communication channel, a memory, and an analog-digital converter a sensing module (ADC), among others. Figure 4 shows the modules which compose each node.

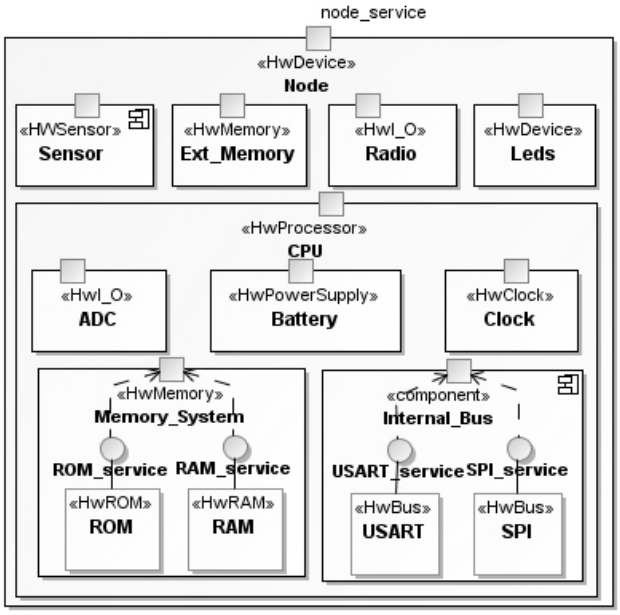

Figure 4. ***Node modules.***

Each module is represented by a class, which contains attributes, methods, and ports. Figure 5 shows the CPU class.

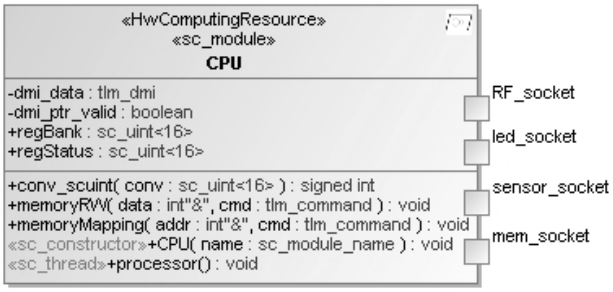

Figure 5. ***CPU Class.***

This module was stereotyped as *<<HwComputingResource>>* using the MARTE profile and it was stereotyped as *<<sc_module>>* using the SystemC profile. Also, the module methods can be stereotyped with the SystemC profile, as simulation processes (sc_thread or sc_method). These processes are functions within the modules that are "registered" in the simulation kernel [19]. Furthermore, a method to be the class constructor (*<<sc_constructor>>*) can be stereotyped.

The connection among the internal modules of a node is performed by the composite structure diagram. Communication is done through ports, which either provide or require interfaces. Figure 6 shows the internal structure of the accelerometer node.

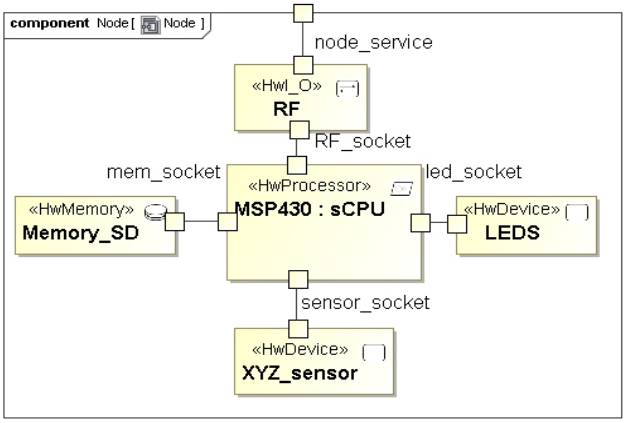

Figure 6. ***Node Composite Structure Diagram.***

Figure 7 shows the general nodes behavior. The behavioral model is developed using state diagrams. Model was applied to some restrictions on MARTE such as: <<TimeDomain>> which defines a time limit on states to implement its processes; <<GaEventTrace>> which indicates signals are activated by external events; and <<ResourceUsage >> which specifies that state makes use of physical resources.

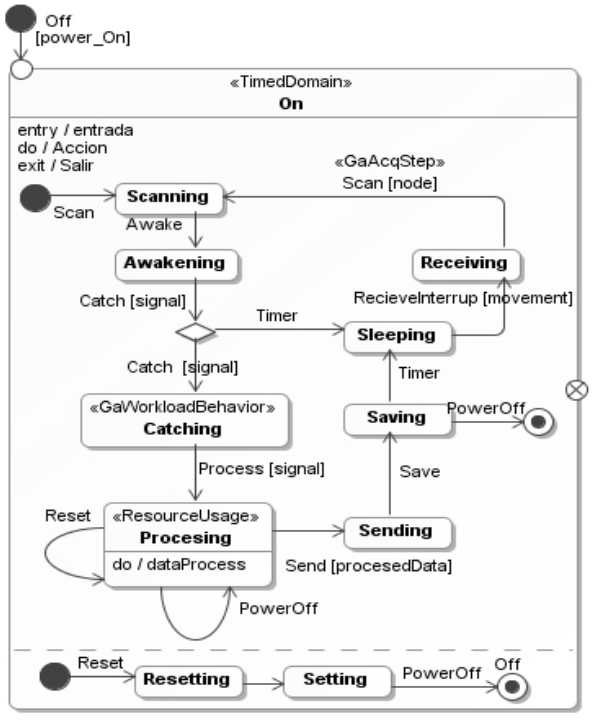

Figure 7. ***NodeBehavior - StateDiagram .***

Finally, figure 8 shows an example of CPU model in SystemC language as a result of automatic code generation derived from UML diagrams.

```
1  #ifndef MSP430_H
2  #define MSP430_H
3  #include "systemc.h"
4  #include "ADC.h"
5  #include "Clock.h"
6  ...
7  class MSP430: public sc_module {
8  public:
9  //Module Port Declaration
10 tlm:tlm_b_initiator_socket< > RF_socket;
11 tlm:tlm_b_initiator_socket< > led_socket;
12 ...
13 //Submodule Declaration
14 ADC *adc1;
15 Clock *clock1;
16 Internal_Bus *USART1;
17 ...
18 //Functions
19 public:
20 signed int conv_scuint(sc_uint<16> conv){ }
21 void memoryRW(int &data, tlm::tlm_command cmd){ }
22 ...
23 //Constructor
24 SC_HAS_PROCESS(CPU);
25 CPU(sc_module_name name):sc_module(name){
26 sc_constructor(CPU);
27 sc_thread(processor);
28 ...
29
30 //Submodule Implementation
31 adc1 = new ADC("adc1");
32 clock1 = new Clock("clock1");
33 ...
34 //Sub-Module Port Binding
35 adc1.ADC_init_socket(ADC_target_socket);
36 clock.time_init_socket(time_targer_socket);
37 ...
38 }
39 //Attibutes
40 private:
41 tlm::tlm_dmi dmi_data;
42 sc_uint<16> regBank;
43 ...
44 };
45 #endif
```

Figure 8. ***CPU SystemC code generated.***

Figure above describes the CPU module header file (CPU. h file). In the first lines, the modules that compose CPU module were indicated. Lines 10 to 12 declare module ports stereotyped with SystemC profile, which allow the data flow among modules. Lines 14 to 17 instances of the modules were declared. The functions were defined in lines 20 and 21, which can be public or private, and their functionality were modeled using state diagrams as shown in Figure 7. The constructor is declared between the lines 24 and 38 it carried out registration functions in the simulation kernel, and it also carried out the interconnections among modules. Finally on lines 40, 41, and 42 module private variables were declared.

5. Conclusions

In this paper, a design process for automatic code generation, to improve productivity and quality in system design was followed. It was necessary to merge the capabilities' UML to model systems with the power to simulate of SystemC language. In this process designs flexible designs due to its modularity, and the separation between platform model and application model was achieved. UML allows modeling through graphical notations and approach our models to a specific domain, due to the profiles that can handle this language, making language UML valuable for the design of embedded systems and real-time systems.

As future work it has been pretended to study the restrictions that MARTE profile offers to perform modeling real time systems. Also, it is intend to continue improving the rules for both modeling and code generation, in order to ensure the right transformation to SystemC models.

6. Acknowledgment

Research supported by COLCIENCIAS, TIC Ministry at Colombia, and ARTICA (excellence research center) with the project "Design Methodology of Embedded Systems with High Reliability and Performance Focused on Developing of Critical Applications," Colombia.

7. References

[1] W. Wolf. "High–Performance Embedded Computing: Architectures, Applications and Methodologies". Morgan Kaufmann. 2007.

[2] Alberto Sangiovanni-Vincentelli "Quo Vadis, SLD: Reasoning About the Trends and Challenges of System Level Design", Proceedings of the IEEE, Vol. 95 No. 3, March 2007.

[3] A. Sangiovanni-Vincentelli. "Is a Unified Methodology for System-Level Design Possible?". IEEE Design and Test of Computers Special Issue on Design in the Late and Post-Silicon Era, 25(4):346-358, July 2008.

[4] Per Andersson, Martin Höst. "UML and SystemC – A Comparison and Mapping Rules for Automatic Code Generation", Embedded Systems Specification and Design Languages, Chapter 14, Editioral Springer, 2007.

[5] P. Andersson, M. Höst, M. Bergström. "UML to SystemC Transformation in the MARTES Project". Embedded Systems Specification and Design Languages – FDL'07, 2007.

[6] Correa B.A., Eusse J.F., Múnera D., Vélez J F., Aedo J.E. "High Level System-on-Chip Design using UML and SystemC". Electronics, Robotics and Automotive Mechanics Conference (CERMA).

[7] E. Riccobene, P. Scandurra, A. Rosti, and S. Bocchio. "An HW-SW Co-design Environment based on UML and SystemC". 2008

[8] Jorgiano Vidal, Florent de Lamotte, Guy Gogniat, Philippe Soulard, Jean-Philippe Diguet: "A co-design approach for embedded system modeling and code generation with UML and MARTE". Design, Automation & Test in Europe Conference & Exhibition, 2009.

[9] M. Mura, A. Panda, M. Prevostini. "Executable Models and Verification from MARTE and SysML: a Comparative Study of Code Generation Capabilities". Workshop, 2008.

[10] L. Murillo, M. Mura, M. Prevostini. "Model-based Design Space Exploration for RTES with SysML and MARTE". Forum on Specification, Verification and Design Languages, 2008.

[11] L. Murillo, M. Mura, M. Prevostini. "Bridging the Gap between Model Driven Engineering and HWSW Codesign". Master Thesis, 2009

[12] M. Mura, M. Prevostini. "Code Generation from Statecharts: Simulation of Wireless Sensor Networks". Conference on Digital System Design Architectures, Methods and Tools, 2008.

[13] Open source Tool for graphical UML2 Modelling www.papyrusuml.org

[14] Éric Piel, Rabie Ben Attitalah, Philippe Marquet, Samy Meftali, Smaïl Niar, Anne Etien, Jean-Luc Dekeyser, and Pierre Boulet. "Gaspard2: from MARTE to SystemC Simulation". DATE 08, Munich, Germany, March 2008.

[15] "A UML Profile for MARTE: Modeling and Analysis of Real-Time Embedded systems, Beta 2". OMG Adopted Specification. June 2008.

[16] Visual UML modeling tool www.magicdraw.com

[17] "MOF 2.0/XMI Mapping, Version 2.1.1". OMG Available Specification. December 2007

[18] The Open SystemC Initiative (OSCI). www.systemc.org

[19] D. Black, J. Donovan, B. Bunton, A. Keist. "SystemC: From the Ground Up". Springer Science+Business Media, LLC. 2010.

Context Free Grammars For Drawing The Outline Of Binary Trees Using L-System

Abraham Meshach Ponraj
Depertment of Computer Science
Madurai Kamaraj University
Madurai 625 021
S.India
E-mail: ponrajcomputer@gmail.com

Abstract *- A drawing of a binary tree T maps each node of T to a distinct point in the plane and each edge (u v) of T to a chain of line segments with end points u and v. Several approaches are found in the literature which includes path based, Rings based, HV and level based etc. In this paper, we introduce the context free grammar using L-System. It is observed that these grammars are easy to implement and modify. The major advantages of the new systems are: easy to implement, easy to modify and the width of the edge is inversely proportional to the depth of each node. Thus it makes the visualization process easier and efficient from the stand point of human cognitive system.*

Keywords: Graph Drawing – Binary Trees- L System

Introduction

An L-system or Linden Mayer system is a parallel rewriting system [4, 5]. Linden Mayer system is a language, which means a set of strings that is made by the application using certain rules. L-System documents are text files containing L systems L-System editor recognizes L-System documents with the extension .lin, multiple instances of L System documents can be opened in L System Editor. Linden Mayer systems consist of strings of symbols [6, 7]. The starting string is called the axiom. Each generation, zero or more transitions are applied to the string, based on a list of rules.

Each rule consists of an "input" and an "output"; the input is the search substring and the output is the substring it is to be replaced. The main concept of the generative process is string rewriting, in which the letters that comprise an initial string are replaced by other letters according to pre-defined rules. This string rewriting process is usually repeated for several generations.

In the interpretative process the letters of one or multiple generations of string are interpreted and visualized. For instance, letters of a string can be visualized by mapping them to attributes of objects or alternatively by interpreting them as turtle graphic commands. Linden Mayer System is the geometric representation of formal grammars. Grammars themselves are sets of simple rules used to transform strings of characters. We have used the following symbols:

F--- move forward, drawing a line

f--- move forward without drawing a line

+--- Turn left (by rotating clockwise on the spot)

- --- Turn right (by rotating anti-clockwise on the spot)

-

[--- remember the current position

] --- return to the last remembered position

The L system type will be set according to the extension [8]. Context-free production rules refer only to an individual symbol. Context-sensitive production rules apply to a particular symbol only if the symbol has certain neighbors. The system is said to be deterministic if there is exactly one production for each symbol. Similarly a system is said to be Stochastic if there are several, and each is chosen with certain probability during each iteration.

An L-system consisting of 4 parts:-

- A set of variables (*i.e.* the symbols that can be replaced by production rules).
- A set of constants (*i.e.* the symbols that do not get replaced. The constants the following symbols: !, [,], +, -.).

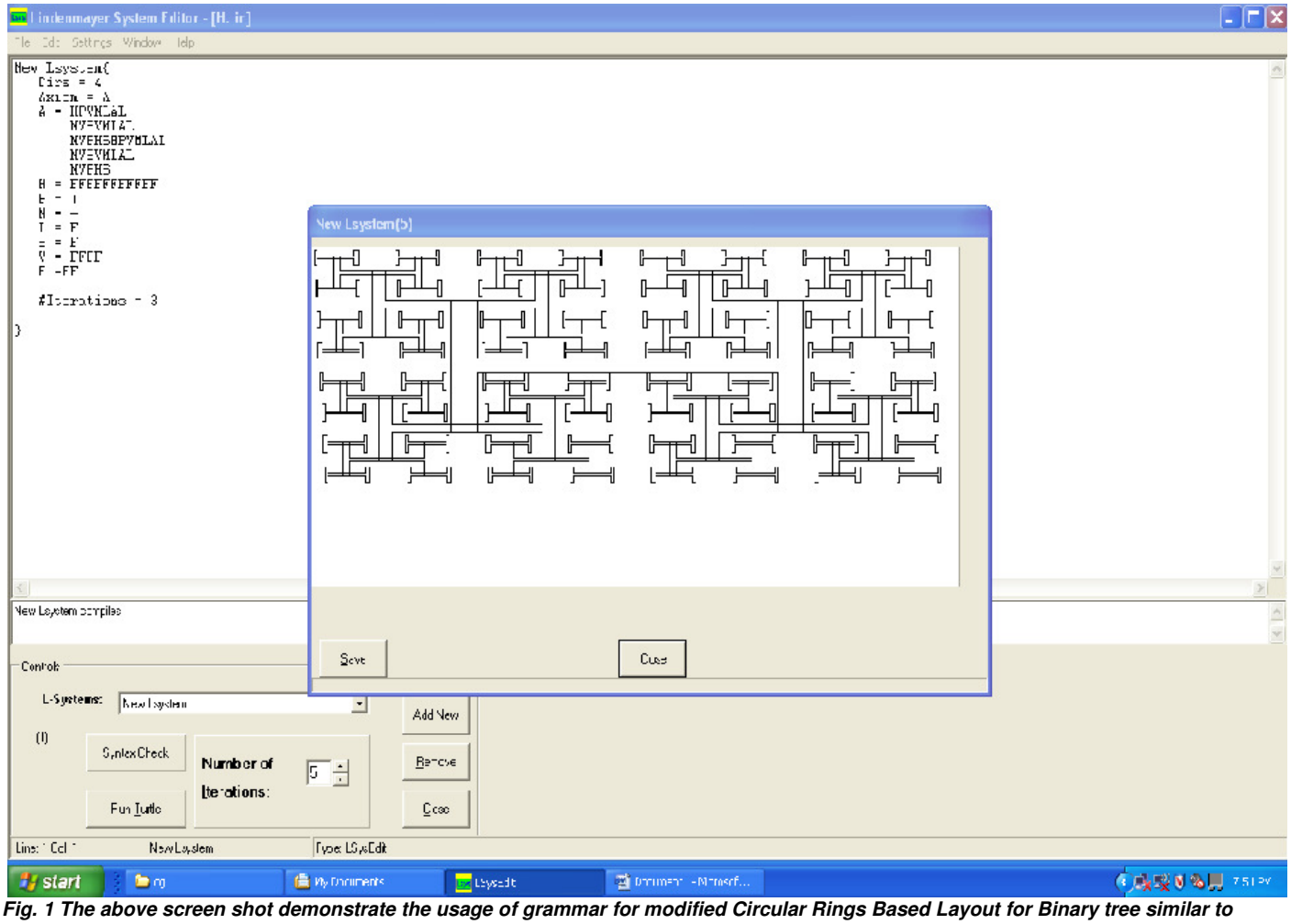

Fig. 1 The above screen shot demonstrate the usage of grammar for modified Circular Rings Based Layout for Binary tree similar to Botanical tree. The root node is at the center. Please note the variation in the width of the edges which serves as the grouped labeling.
A detailed explanation is given in APPENDIX- A

➢ A single axiom (*i.e.* the string composed of some number of variables and/or constants. The axiom is the initial state of the system).

➢ A set of production rules- it may be defining the way variables can be replaced with combinations of constants and other variables. A production consists of two strings - the predecessor and the successor.

L-system grammars are very similar to the semi-The grammar L-Systems are now commonly known as parametric L systems, defined as a tuple,

G = (V, S, ω, P)

Where,
V (the alphabet) is a set of symbols containing elements that can be replaced (variables) S is a set of symbols containing elements that remain fixed (constants)
ω (start, axiom or initiator) is a string of symbols from V defining the initial state of the system

P is a set of production rules or productions defining the way variables can be replaced with combinations of constants and other variables. A production consists of two strings, the predecessor and the successor

2. Graph Drawing of Binary trees

Binary Tree which is a special case of a general tree is the back bone for several representation in computer algorithms. Tree drawing using L-system is concerned with the automatic generation of geometric representions of relational information, often for visualization purposes [1, 2, 3] using turtle graphics. The typical data structure for modeling hierarchical information is a tree whose vertices represent entities and whose edges correspond to relationships between entities. Visualizations of hierarchical structures are only useful to the degree that the associated diagrams effectively

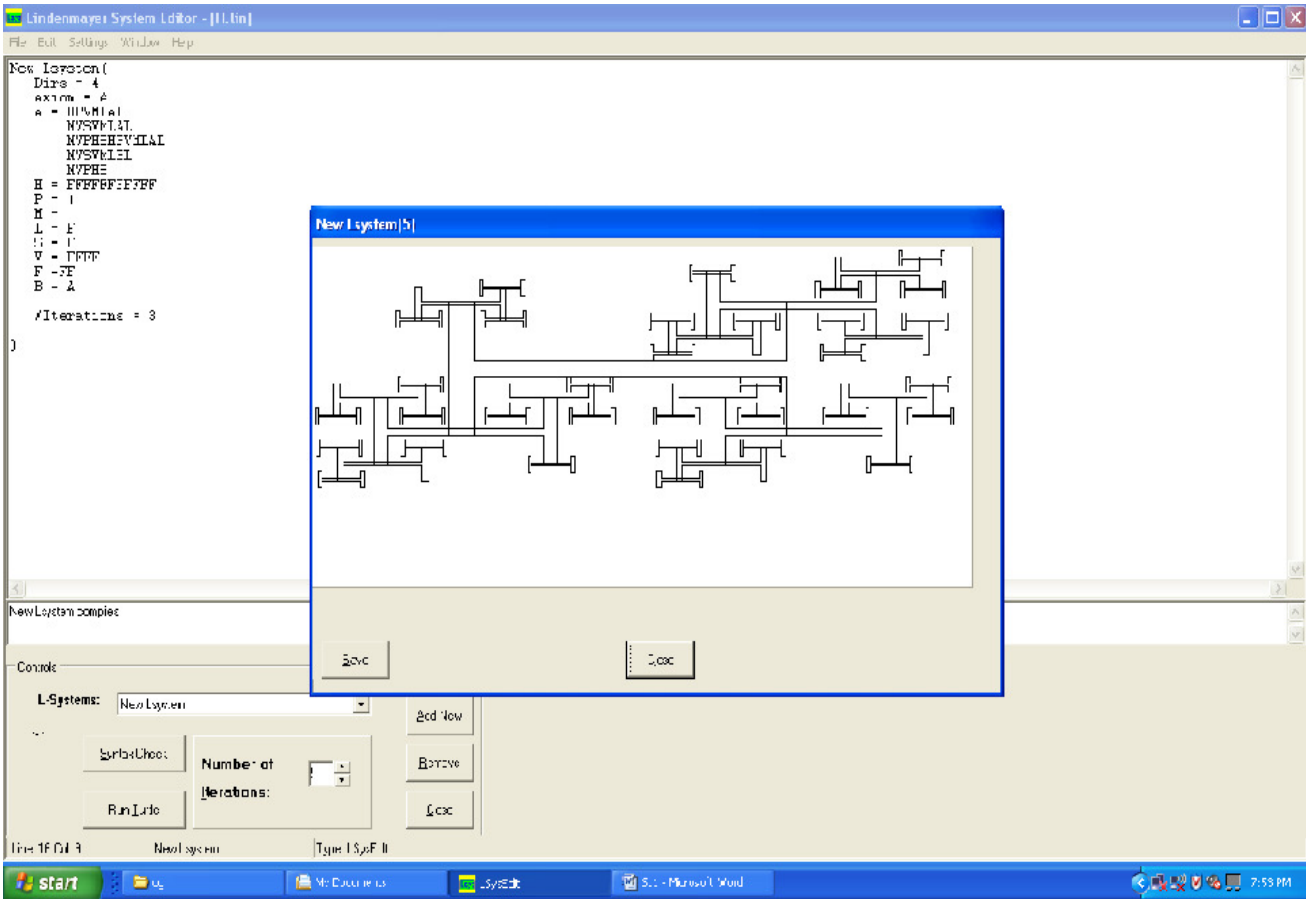

Fig 2 - Prunning the 4th corner 1

convey information to the people that use them. A good diagram helps the reader to understand the system, but a poor diagram can be confusing. Thus a good diagram should have no over lap between the nodes. In addition to this, the edges should be sepatated to a maximum distance with in the given area. This type of binary tree drawings have several applications in Web-site Design and Browsing (structure of a Web-site),Business Administration (organization charts), Artificial Intelligence (knowledge - representation is a hierarchies), Logic Programming (SLD-trees), , Biology (evolutionary trees), and Chemistry (molecular drawings), Decision Support Systems (activity trees) Software Engineering (program nesting trees, object oriented class hierarchies).

A drawing convention is a basic rule that a drawing must satisfy to be admissible [4, 5]. A polyline drawing is a drawing in which each edge is drawn as a connected sequence of one or more line segments, where the meeting point of consecutive line-segments is called a bend.

An orthogonal drawing is one in which each edge is drawn as a chain of alternating horizontal and vertical segments. An upward drawing is defined as a drawing where no child is placed higher in the y- direction than its parent. A non upward drawing is a drawing which is not upward. A grid drawing is one in which each vertex is placed at integer coordinates. Assuming that the plane is covered by horizontal and vertical channels, with unit distance between two consecutive channels, the meeting point of a horizontal and a vertical channel is called a grid-point. The computer screen can be viewed as a grid of pixels placed at integer coordinates.

Grid drawings guarantee at least unit distance separation between the nodes of the tree, and the integer coordinates of the nodes and edge-bends allow the drawings to be rendered in a (large-enough) gridbased display surface, such as a computer screen, without any distortions due to truncation and round-off errors.

The smallest rectangle with horizontal and vertical sides parallel to the axes, that covers the entire grid drawing, is called the enclosing rectangle. A planar drawing is a drawing

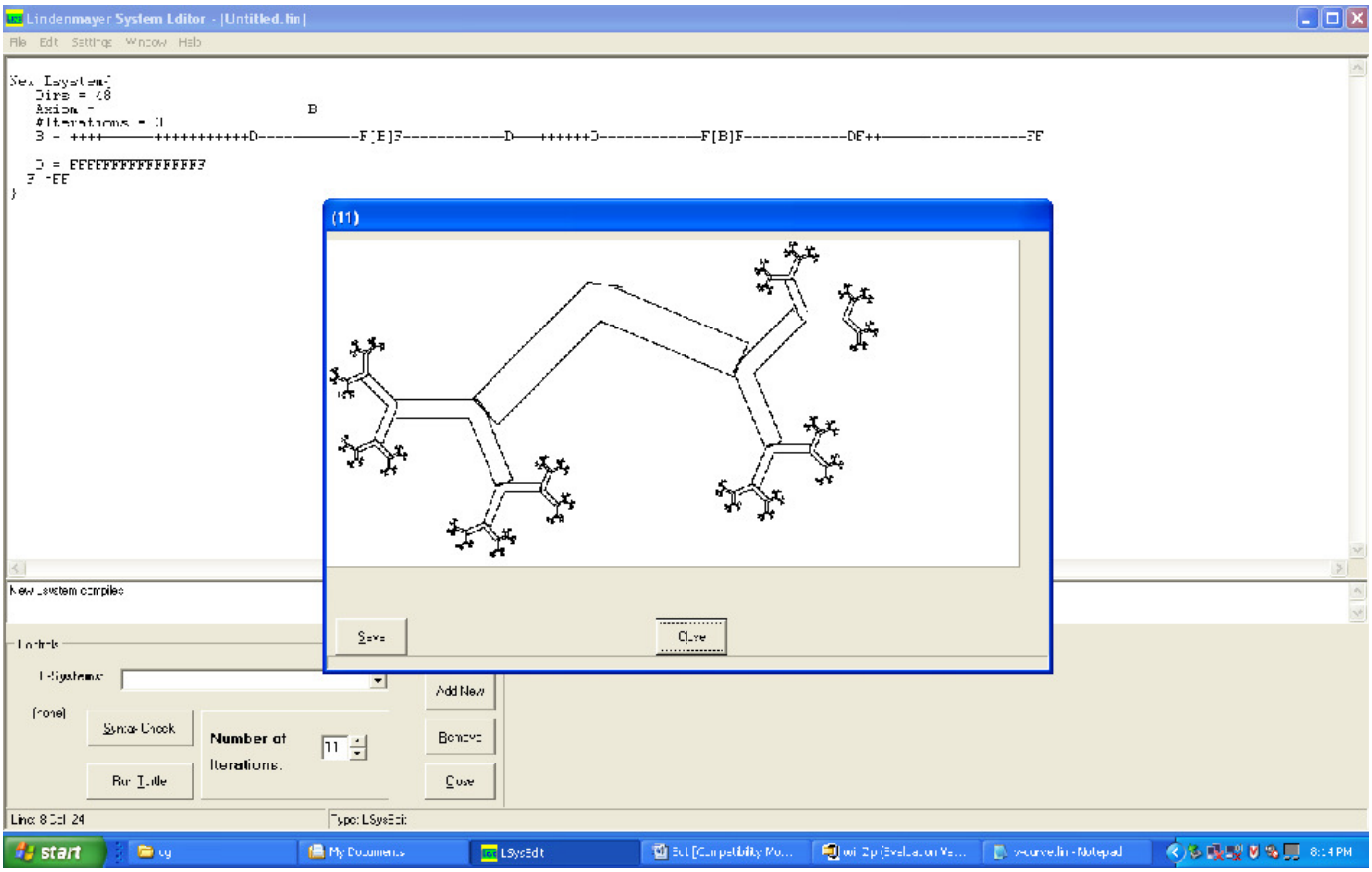

Fig 3- A Grammer for level based *1*

.

in which edges do not intersect each other in the drawing. Planar drawings are normally easier to understand than non-planar drawings, *i.e.* drawings with edge-crossings. Since any tree admits a planar drawing, it is desirable to obtain planar drawings for trees The so called straight-line tree drawings have each edge drawn as a straight line segment. It is natural to draw each edge of a tree as a straight line between its end-nodes.Straight-line drawings are easier to understand than poly line drawings.

2.1 Level-Based Approach

The Level-Based Approach can be used on both binary and general trees and it is characterized by the fact that in the drawings produced, the nodes at the same distance from the root are horizontally aligned. A layered drawing of a graph is a drawing such that the vertices are constrained to lie on geometric layers which can be lines, circles, or other kind of curves. Partitioning the vertices into distinct layers can be an effective way to emphasize some structural properties of the graph; in many cases this is required in some real -world applications to convey the so called semantic constraints.

Radial drawings are often used in drawing graphs, even though they do always guarantee planarity.

The Horizontal-Vertical Approach can be used on both binary and general trees. In this approach, a divide-and-conquer strategy is used to recursively construct an upward, orthogonal, and straight-line drawing of a tree, by placing the root of the tree in the top-left corner, and the drawings of its left and right sub trees one next to the other (horizontal composition) or one below the other (vertical composition). The resulting drawing also exhibits the sub tree separation property within an O (n log n) area.

Horizontal- Vertical Approach can be used on both binary and general trees. In this approach, a divide-and-conquer strategy is used to recursively construct an upward, orthogonal, and straight-line drawing of a tree, by placing the root of the tree in the top-left corner, and the drawings of its left and right sub trees one next to the other (horizontal composition) or one below the other (vertical composition).

The resulting drawing also exhibits the sub tree separation property within an O(n log n) area.

2.2 Path-Based Approach

The Path-Based Approach uses a recursive winding paradigm to draw a binary tree T by laying down a small chain of nodes monotonically in the x-direction leading to a distinguished node v, and then ”winding” by recursively laying out the subtrees rooted at the children of v in the opposite direction.

2.3 Rectangular Drawing

A rectangular drawing of a plane graph G is a planar drawing of G such that each edge is drawn as a horizontal or vertical segment and each face is drawn as a rectangle. Every graph with a rectangular drawing is bi- connected and has at least four vertices of degree 2 on its outer face.

2.4 Ortho-Radial Grid

An ortho-radial grid is a grid composed of concentric circles and half-lines starting at the center of the circles. In an ortho-radial grid, a radial segment is a connected part of a half-line that does not include the center S of the circles, and a circular segment is a connected part of a circle. In an ortho-radial grid a rectangle is a closed curve consisting of two nonzero length circular segments and two (possibly coincident) non- zero length radial segments.

2.5 Rectangular-Radial drawing

A rectangular-radial drawing of a plane graph G is a planar drawing of G such that each edge is drawn as a single radial or circular segment and the boundary of each face is drawn as a circle or rectangle. Rectangular-radial drawings are topologically equivalent to drawings on a cylinder.

3.Summary and Conclusion

In this paper, an easy implementation is given using L-System to draw the layout for binary tree with variable width in edge. This methodology can be very much helpful in VLSI design where each edge represent the clock pulse and a D.C power supply in a planner graph drawing. Wider the width of the edge can represent grater power consumption in the VLSI layout. The growth of these binary trees is exponential in time. As given in the Fig.1, the variable H and V can be increased with few more F in order to change the shape of the tree. More nodes can be added by increasing the number of iterations. Similarly, one can prune one or more sides of the tree by introducing late substitution. For example, we have introduced a dummy variable B to prune the growth in Fig.2. We have also introduced the grammar for ‘v’ type of tree similar to botanical tree growth as given in Fig.3.

4. Reference

[1] S. T. Teoh and K. L. Ma. RINGS: A technique for visualizing large hierarchies. In Proceedings 10th International Symposium on Graph Drawing, volume 2528 of Lecture Notes in Computer. Sci., pages 268-275. Springer, 2002.

[2] G. G. Robertson, J. D. Mackinlay, and S. K. Card. Cone trees: animated 3d visualizations of hierarchical information. In CHI '91: Proceedings of the SIGCHI conference on Human factors in computing systems, pages189-194. ACM Press, 1991.

[3] G. Melancon and I. Herman. Circular drawings of rooted trees. Technical Report INS-9817, Netherlands' National Research Institute for Mathematics and Computer Sciences, 1998.

[4] E. H. Chi and S. K. Card. Sense making of evolving web sites using visualization spreadsheets. In Proceedings of the Symposium on Information Visualization, pages 18-25.
IEEE Press, 1999.

[5] Grzegorz Rozenberg, Arto Salomaa “ Lindenmayer systems: impacts on theoretical computer science, computer “ - Page no:3

[6] Oliver Deussen, Bernd Lintermann “Digital design of nature: computer generated plants and organics” - Page no: 65

[7] Przemyslaw Prusinkiewicz, Aristid Lindenmayer, James Hanan.” The algorithmic beauty of plants” Page no: 66

[8] Grzegorz Rozenberg, Arto Salomaa “Lindenmayer systems: impacts on theoretical computer science, computer” Page no: 254.

APPENDIX – A - GRAMMER FOR CIRCULAR RING BASED APPROACH FOR FIGURE 1

circular ring based{
1 Dirs = 4
2 Axiom = A
3 A = HPVMLAL
4 MVSVMLAL

```
5     MVPHSHPVMLAL
6     MVSVMLAL
7    MVPHS
8   H = FFFFFFFFFFF
9    P = +
10  M = -
 11 L = F
 12  S = F
 13  V = FFFFFFF
14   F =FF
}
```

Dirs = 4 means, the angle + is 90 degrees and - is -90 degrees for the turtle to change it's direction from the current direction We have used a recursive procedure and call axiom A RECURSIVELY at the four corners of the H curve as given in line numbers 2 to 7 The horizontal length of H can be adjusted by increasing the number of F in line number 8. An increase in the number of F L and S as given in line 11 and 12, will increase the width of H

Global Grids and Cloud Toolkits

Safiye Ghasemi[1], Seyyed Mohsen Hashemi[2]

[1] Department of Computer, Sepidan Branch, Islamic Azad University, Sepidan, Iran
ghasemi.ss@gmail.com

[2] Islamic Azad University, Science and Research Branch, Tehran

***Abstract*- In the past few years, many overlying concepts of distributed computing eminently cluster, grid and cloud computing have appeared. In recent years, extensive researches have been conducted in the area of simulation to model large complex systems and understand their behavior, especially in parallel and distributed systems. Distributed computing combines multiple computers, geographically dispersed in a cost effective way and presents a single unified resource to the end user with huge storage and computational power. Due to their complexity, grid computing and cloud computing applications need to be tested before running on an appropriate infrastructure. However, access to such infrastructures is not feasible or available to everyone. Therefore, various simulation tools were developed to ease the cost and complexity of testing these applications. Therefore, the aim of this paper is to analyze and compare various simulation tools for some distributed systems such as grid computing and cloud computing.**

***Keywords*- Simulation tools, Cloud computing, Grid computing, middleware.**

I. INTRODUCTION

Grid and cloud computing are as current decade computing technologies consisting of various unambiguous resources which are supported by different organizations. Management of such systems seems to be too complex. Therefore researchers use different methodologies and tools to analyze, evaluate and predict their proposed algorithms and methods. The most of printed researches have been evaluated on real grid environment infrastructures or by using tools of these technologies.

These distributed systems offer abundant computational power, enabling us to tackle the most challenging applications, such as weather forecasting and earthquake simulations. They are extremely complex systems of geographically distributed and independently managed resources. Some of the numerous aspects that need to be addressed are: resource management, heterogeneity, fault tolerance, network performance, security, adaptability, scalability and transparency.

An increasing number of simulation tools have been designed and developed. A simulation tool can be run at any speed relative to the real world according to various possible scenarios. The results give information about the behavior of real systems and enable researchers to understand and improve their applications without the cost and effort of using a real testbed. Simulators model the logic of specific systems and can execute faster than the real execution would be. The results of the simulation are saved to support post-simulation analysis of the system behavior.

In the last few years, a lot of research has been carried out in the area of simulating large-scale parallel and distributed systems and in particular grid and cloud environments. We have carried out a study of a number of tools used for simulating these environments. We summarize the results of our study in this paper and we give an overview of the architecture of these tools and then give more focus to the network support provided by these tools (such as how the network is modeled, the flexibility of these models, the supported network protocols, etc.).

This paper presents: (1) the first describes some simulation tools for studying applications of grid and cloud computing, (2) a comparison of the introduced tools, (3) some existed grid and cloud middlewares, (4) the comparison of introduced middlewares and (6) conclusions and summary of survey.

II. GRID AND CLOUD SIMULATION TOOLS

There are many infrastructures for grid and cloud computing to be used in scientific and industrial applications. According to their remarkable complexities, it is essential to check the applications on such infrastructures before running in real environment. Difficulties on accessing such infrastructures, researchers attend to develop simulation tools to decrease the cost and complexity of testing programs. These tools open up the possibility of evaluating the hypothesis (application benchmarking study) in a controlled environment where one can easily reproduce results. Simulation-based approaches offer significant benefits to IT companies (or anyone who wants to offer his application services through clouds) by allowing them to: (i) test their services in repeatable and controllable environment; (ii) tune the system bottlenecks before deploying on real clouds; and (iii) experiment with different workload mix and resource performance scenarios on simulated infrastructures for developing and testing adaptive application provisioning techniques.

In recent years the role of implementation and hosting of a program have been discarded and the infrastructural services by cloud computing has been replaced. Evaluating the performance of cloud environment provisioning policies, application workload models, and resources performance models in a repeatable manner under varying system and user configurations and requirements is difficult to achieve. The remainder of current paper consists of introduction and investigation of some grid and cloud simulators.

A. GridSim

The tool has been introduced by Buyya[12] to explore the performance of quality in wide distributed environments such as grid and P2P networks. The Java-based discrete-event grid simulation toolkit supports modeling and simulation of heterogeneous grid computing resources (both time- and space-shared), users and application models. It provides primitives for creation of application tasks, mapping of tasks to resources, and their management. The GridSim toolkit provides facilities for the modeling and simulation of resources and network connectivity with different capabilities, configurations, and domains. It supports primitives for application composition, information services for resource discovery, and interfaces for assigning application tasks to resources and managing their execution. These features can be used to simulate resource brokers or grid schedulers for evaluating performance of scheduling algorithms or heuristics.

A layered and modular architecture for grid simulation leverages existing technologies and manages them as separate components. To simulate grid resource brokers using the GridSim toolkit, the developers need to create new entities that exhibit the behavior of grid users and scheduling systems. The user-defined entities extend the GridSim base class to inherit the properties of concurrent entities capable of communicating with other entities using events. All components in GridSim communicate with each other through message passing operations.

The implementation of GridSim toolkit in Java is an important contribution since Java provides a rich set of tools that enhance programming productivity, application portability, and a scalable runtime environment. As the JVM (Java Virtual Machine) is available for single, multiprocessor shared or distributed machines such as clusters, GridSim scales with them due to its concurrent implementation. This toolkit uses processing elements with different speeds for modeling the computing resources. Then, one or more of them can be put together to create a machine. Similarly, one or more machines can be put together to create a grid resource. Thus, the resulting grid resource can be a single processor, shared memory multiprocessors, or a distributed memory cluster of computers.

Another positive property of GridSim can be mentioned as operating the capabilities of a data grid as well data duplicating, querying for replicated data and for accessing to them.

The toolkit can model topologies of networks by using routers and connectors, consider the traffic, reserve processing units and evaluate the quality of network.

B. SimGrid

SimGrid is a toolkit that provides core functionalities for the simulation of distributed applications in heterogeneous distributed environments. The goal of SimGrid is to support research in the area of distributed and parallel application scheduling on distributed computing platforms ranging from workstations to grid environments. SimGrid is based on event driven simulation. It provides a set of abstractions and functionalities to build a simulator corresponding to the applications and infrastructures characteristics. In SimGrid resources are modeled by their latency and service rate. These characteristics may be set as constants or evolve according to previously collected traces. The topology is fully configurable. Indeed, this is the responsibility of the user to define the topology and may be use collections of links to simulate complex mechanisms like routers. All actions (computations or communications) are referred as tasks. The user is responsible to schedule computations and communications on the correct resources. SimGrid considers execution time prediction errors allowing the user to understand the behavior of the scheduling algorithms under complex situations where execution time cannot be accurately predicted.

SimGrid is a C-based discrete event job scheduling simulation library. SimGrid provides highly accurate network model for TCP and non-TCP transport. Network topology can be built to represent real system for data-intensive application simulation.

Abstractions in SimGrid are agent, location, task, path and channel. An agent makes scheduling decision. A location is the place an agent executes in the simulated topology. A task is an activity which can either be computation or a data transfer. A path is a collection of communication resources representing a set of physical network links. A channel is the opened communication ports by agents at locations. SimGrid engine is scalable and can implement several valid simulation models. The toolkit can be run on various operating systems as well Windows, AIX and Linux, and can be programmed by any of Java, Ruby, Lua or C languages, which has the best performance when C is used.

SimGrid is a project in both research and development context.

In comparison to GridSim, SimGrid has fewer abilities. The toolkit can not support system such as the GridSim does. The serial engine of the simulator and non-object oriented environment are some reasons. Furthermore this tool can not support data grid computing services like data duplication.

C. CloudSim

CloudSim is a framework developed by the GRIDS laboratory of University of Melbourne which is an extensible simulation toolkit that enables modeling and simulation of cloud computing environments. The CloudSim toolkit supports modeling and creation of one or more virtual machines (VMs) on a simulated node of a Data Center, jobs, and their mapping to suitable VMs. It also allows simulation of multiple Data Centers to enable a study on federation and associated policies for migration of VMs for reliability and automatic scaling of applications.

CloudSim offers the following features: first, support for modeling and simulation of large scale cloud computing infrastructure, including data centers on a single physical computing node; second, a self-contained platform for modeling data centers, service brokers, scheduling, and allocations policies. The availability of virtualization engine,

which aids in creation and management of multiple, independent, and co-hosted virtualized services on a data center node; and the flexibility to switch between space-shared and time-shared allocation of processing cores to virtualized services are some of unique features of the tool. Separateness of programming section and simulation test can be considered as a positive point of the toolkit. But the tool can not simulate huge applications of internet.

The CloudSim is implemented at the next level by programmatically extending the core functionalities exposed by the GridSim layer. CloudSim provides novel support for modeling and simulation of virtualized Cloudbased data center environments such as dedicated management interfaces for VMs, memory, storage, and bandwidth.

Allocation of application-specific VMs to Hosts in a Cloud-based data center is the responsibility of the Virtual Machine Provisioner component. This component exposes a number of custom methods for researchers, which aids in implementation of new VM provisioning policies based on optimization goals. The system parameters such as the required number of processing cores, memory and storage as requested by the cloud user form the basis for such mappings. Other complicated policies can be written by the researchers based on the infrastructure and application demands.

D. CloudAnalyst

Some developments on CloudSim are needed to enable the simulator to model the huge applications of web. CloudAnalyst, built on CloudSim, allows description of application workloads, including information of geographic location of users generating traffic and location of data centers, number of users and data centers, and number of resources in each data center. Using this information, CloudAnalyst generates information about response time of requests, processing time of requests, and other metrics. By using CloudAnalyst, application developers can determine the best strategy for allocation of resources among available data centers, strategies for selecting data centers to serve specific requests, and costs related to such operations.

In CloudAnalyst the events are grouped at three levels. In the first level, there are user bases, which represent a cluster of users which are handled as a single unit. In the next level, user requests generated from each regional user base are grouped based on a grouping factor, which is kept independent of the user base size. In the last level, requests simultaneously processed by a single virtual machine are grouped. The last two grouping factors are configurable by CloudAnalyst users, and it is also possible not to group simulation elements.

Another important component of CloudAnalyst is the network model. Modeling of bandwidth is probably the most complex task, especially considering the nature of a network such as the Internet. In the current version of CloudAnalyst we use a hypothetical parameter, available bandwidth, which is assumed to be the quota of Internet bandwidth available for the application being simulated, ignoring other external factors. Events such as traffic generation are produced using a Poisson distribution.

SimJava is the infrastructure framework used in CloudSim and so some features are used directly in CloudAnalyst.

There are several highly desirable features of the toolkit such as Ease of use, ability to define a simulation with a high degree of configurability and flexibility, graphical output, repeatability and ease of extension. The technologies CloudSim used are Java, CloudSim, Java swing and SimJava.

III. THE COMPARISON OF SIMULATION TOOLS

There is very little or no support in existing grid computing simulation toolkits for modeling of on-demand virtualization enabled resource and application management. Further, cloud environments promise to deliver services on subscription-basis in a pay-as-you-go model to cloud customers. Hence, cloud infrastructure modeling and simulation toolkits must provide support for economic entities such as cloud brokers and cloud exchange for enabling real-time trading of services between customers and providers. Among the currently available simulators discussed in this paper, only GridSim offers support for economic-driven resource management and application scheduling simulation.

With the advancement of cloud computing technologies rapidly, there is a new need for tools to study and analyze the benefits of the technology and how best to apply the technology to large-scaled applications.

In cloud computing there is an additional layer called virtualization, which is known as an execution and host environment for services belongs to cloud environment. Table 1 depicts a summarized comparison of introduced simulation tools.

TABLE I
LISTING OF FUNCTIONALITIES AND FEATURES FOR SOME GRID AND CLOUD SIMULATORS

Properties/ Simulators	CloudAnalyst	CloudSim	SimGrid	GridSim
Network Representation	Yes	Yes	Yes	Yes
Processing Node	Yes	Yes	Yes	Yes
Virtual Organization	Yes	No	No	No
Economical Modeling	Yes	Yes	No	Yes
Virtual Machine	Yes	Yes	No	No
language	Java	Java	C, XML	Java

Modelling bandwidth for a complex network like the Internet is an extremely difficult task. The CloudAnalyst "available bandwidth" is a hypothetical measure of the "available" bandwidth between regions. That is the bandwidth available between regions purely for the simulated application, disregarding all other traffic.

Then when calculating the network data transfer delay, the Internet Characteristics takes into consideration the current level of application traffic and the available bandwidth in deciding how long it should take to complete the transmission of data.

IV. MIDDLEWARES OF GRID AND CLOUD COMPUTING

Middlewares provide users with seamless computing ability and uniform access to resources in the heterogeneous environment. Several software toolkits and systems have been developed, most of which are results of academic research projects, all over the world. In order to provide users with a seamless computing environment, these middleware systems need to solve several challenges originating from the inherent features of the grid and cloud environments. One of the main challenges is the heterogeneity in such environments, which results from the multiplicity of heterogeneous resources and the vast range of technologies encompassed by the grid and cloud computing. Another challenge involves the multiple administrative domains and autonomy issues because of geographically distributed grid computing resources across multiple administrative domains and owned by different organizations. Other challenges include scalability and dynamicity/ adaptability. Middleware systems must tailor their behavior dynamically and use the available resources and services efficiently and effectively.

The remainder of this paper provides an insight into the different grid and cloud computing middleware systems existing today, followed by the comparison of these systems.

A. Globus

The Globus is one of the powerful tools for creating, controlling and management of grid environment, which provides open source software toolkit that can be used to build computational grids and grid computing based applications. This open source software toolkit allows sharing of computing power, databases, and other tools securely online across corporate, institutional and geographic boundaries without sacrificing local autonomy. The core services, interfaces and protocols in the Globus toolkit allow users to access remote resources seamlessly while simultaneously preserving local control over who can use resources and when. The fifth version of the project serves many services to grid system managers like security, resource management and information management.

The Globus architecture has three main groups of services accessible through a security layer. These groups are Resource Management, Data management and Information Services. The local services layer contains the operating system services, network services like TCP/IP, cluster scheduling services provided by Load Leveler, job-submission, query of queues, and so on. The higher layers of the Globus model enable the integration of multiple or heterogeneous clusters. The core services layer contains the Globus toolkit building blocks for security, job submission, data management, and resource information management. The high-level services and tools layer contains tools that integrate the lower level services or implement missing functionality.

The project like Linux with open sources has been grammatically matured. Some of main grid envirinment application which uses Globus as their low level software are AppLeS, Ninf, Nimrod-G, NASA IPG, Condor-G, Gridbus Broker, UK eScience Project, GriphyN and EU Data Grid.

B. Cloudbus

Cloudbus can be considered as the 21st century vision of computing tool. The CLOUDS lab has been designing and developing cloud middleware to support science, engineering, business, creative media, and consumer applications on cloud environments.

In recent years users can observe various cloud computing of providers from all over the world for providing resources like computers, data and etc. Resources available in the cloud are acquired by means of third party brokering services that mediate the access to the real infrastructure.

The Cloudbus Toolkit is a collection of technologies and components that comprehensively try to address the challenges involved in making this vision a concrete reality.

Technologies such as Aneka or Workflow Engine provide services for executing applications in the cloud. These can be public cloud computing, private intranets, or data centers that can all be uniformly managed within an InterCloud realm. The InterCloud model will: (a) promote interlinking of islands of clouds through peering arrangements to enable inter-cloud resource sharing; (b) provide a scalable structure for clouds that allow them to interconnect with one another and grow in a sustainable way; (c) create a global Cyberinfrastructure to support e-Science and e-Business applications.

Cloudsim and Aneka as the components used in Cloudbus, enable users to model developed clouds. These components can define and develop various policies in all software stack components.

C. Aneka

A .Net based service-oriented platform for desktop grid computing that provides a configurable service container hosting pluggable services for discovering, scheduling and balancing various types of workloads and a flexible and extensible framework or API supporting various programming models including threading, batch processing, MPI and dataflow. Users and developers can easily use different programming models and the services provided by the container to run their applications over desktop grids managed by Aneka.

The framework provides a highly modular architecture whose node consists of an instance of a configurable container that hosts several compulsory services and any number of optional services. The compulsory services provide functions such as security, persistence mechanisms, and communication protocols, and are together called as the base infrastructure. The optional services include specific executors for different types of programming models and associated schedulers.

In addition Aneka is a market oriented cloud development and management platform with rapid application development and workload distribution capabilities. It is an integrated middleware package which allows you to seamlessly build and manage an interconnected network in addition to accelerating development, deployment and management of distributed applications using Microsoft .Net frameworks on these networks. The middleware is market oriented since it allows you to build, schedule, provision and monitor results using

pricing, accounting, QoS services and SLA services in private and public network environments.

C. Alchemi

The Alchemi grid computing framework was conceived with the aim of making grid construction and development of grid software as easy as possible without sacrificing flexibility, scalability, reliability and extensibility.

Virtual machines alike clusters are designed for a limited number of resources, but the exponential growth of Internet connections demand considerably more volumes. Typically only one-tenth of processing power is used has given rise to interest in harnessing the vast amounts of processing power that is available in the form of spare CPU cycles on Internet- or intranet-connected desktops. This new paradigm has been dubbed grid computing.

Alchemi is a Windows-based grid computing framework implemented on the Microsoft .Net Platform that provides the runtime machinery and programming environment required to construct desktop grids and develop grid applications. It allows flexible application composition by supporting an object-oriented grid application programming model in addition to a grid job model. Cross-platform support is provided via a web services interface and a flexible execution model supports dedicated and non-dedicated execution by grid nodes. Actually the Microsoft .Net framework provides a powerful toolset that can be leveraged for all of these, in particular support for remote execution (via .Net Remoting and web services), multithreading, security, asynchronous programming, disconnected data access, managed execution and cross-language development, making it an ideal platform for grid computing middleware.

V. A COMPARISON ON INTRODUCED MIDDLEWARES

Each middleware mentioned previously has a usage. Typically Globus is a project for composition of services. Table 2 depicts the comparison between middlewares of former section.

Studying attributes of these tools and comparing them show that their abilities are the same in many parts. Their main differences are come from the architecture and implementation model. Globus, Aneka and Cloudbus provide service brokers, while Alchemi does not support any service broker. Alchemi and Gridbus are as brokers of grid computing.

The communication module of Globus is based on Nexus which supports synchronous message passing. Globus provides security services by GSI which is based on SSL and X.509V3 documents. In the existing layers of Alchemi in Gridbus uses security services of .Net and other components of Gridbus which are provided by Globus GSI.

TABLE II
COMPARISON OF VARIOUS ATTRIBUTES OF MIDDLEWARES

properties	Globus	CloudBus	Aneka	Alchemi
Focus	Low level services	Virtual machine modeling, cloud infrastructure	Cloud infrastructure and services	Cloud infrastructure and services
Implementation Model	Hourglass model at system level	Hourglass model at user level	Hourglass model at user level	A low level of integration
Implementation Technologies	C , Java	C , C#	C , C#	C#, .Net
Runtime Platform	Unix	Unix, .NET, Windows	Unix, Windows, Mac, .NET	Unix, Mac Windows, , .NET
Architecture	Layered and Modular	Layered	Utility Model and Layered	Hierarchical

VI. CONCLUSION

There has been considerable research aiming at the development of grid and cloud computing middleware systems and most of these systems have been successfully applied in other grid and cloud related projects and applications. Furthermore none of grid computing simulators can model the infrastructural and application level requirements of cloud computing.

Current research introduces some famous simulators in grid and cloud environments and also middlewares of these distributed systems. Then a comparison is provided according to some features such as service provision, service types, virtualization policies, SLA, GUI and used framework.

To sum up, none of the tools can be mentioned as the best of all. Researchers should select the appropriate one according to the application they need and their other requirements.

REFERENCES

[1] R. Buyya, S. Pandey and C. Vecchiola, 'Cloudbus Toolkit for Market-Oriented Cloud Computing', Cloud Computing and Distributed Systems (CLOUDS) Laboratory Department of Computer Science and Software Engineering, The University of Melbourne, Australia, 2009.

[2] Bhathiya Wickremasinghe, 'CloudAnalyst: A CloudSim-based Tool for Modelling and Analysis of Large Scale Cloud Computing Environments', MEDC Project Report, 2009.

[3] The EC-GIN Consortium, "Survey of Grid Simulators, Network-level Analysis of Grid Applications", Europe-China Grid InterNetworking, 2008.

[4] Benjamin Quetier and Franck Cappello, "A survey of Grid research tools: simulators, emulators and real life platforms", University of Paris South, 2004.

[5] R. Buyya and S. Venugopal. 'The Gridbus Toolkit for Service Oriented Grid and Utility Computing: An Overview and Status Report', Grid Computing and Distributed Systems Laboratory Department of Computer Science and Software Engineering, The University of Melbourne, Australia, 2003.

[6] Richard M. Fujimoto, 'Parallel and distributed simulation systems', a wiley-interscience publication, 2000.

[7] R. N. Calheiros, R. Buyya, et al., 'CloudSim: A Novel Framework for Modeling and Simulation of Cloud Computing Infrastructures and Services', GRIDS Laboratory, Department of Computer Science and Software Engineering, The University of Melbourne, Australia, 2009.

[8] Bhathiya Wickremasinghe, 'CloudAnalyst: A CloudSim-based Tool for Modelling and Analysis of Large Scale Cloud Computing Environments', MEDC Project Report, 2009.

[9] Europe-China Grid InterNetworking, 'Survey of Grid Simulators Network-level Analysis of Grid Applications', European Sixth Framework STREP, 2006.

[10] H. Casanova, A. Legrand, M. Quinson , "SimGrid: a Generic Framework for Large-Scale Distributed Experiments".

[11] V. Mendez, F. Garcıa, 'SiCoGrid: A Complete Grid Simulator for Scheduling and Algorithmical Research, with Emergent Artificial Intelligence data algorithms', Universidad de Zaragoza, Computer Science Departament, Computer Architecture area, Technical Report RR-06-11. DIIS. UNIZAR. 2005.

[12] Rajkumar Buyya, Manzur Murshed, "GridSim: a toolkit for the modeling and simulation of distributed resource management and scheduling for Grid computing", School of Computer Science and Software Eng, 2001.

SESSION

SIMULATION

Chair(s)

TBA

A Graphical User Interface for Simulating Robust Military Village Searches

Ryan Friese[1], Paul Maxwell[1, 3], Anthony A. Maciejewski[1], Howard Jay Siegel[1, 2]
[1]Electrical and Computer Engineering Department
[2]Computer Science Department
Colorado State University, Fort Collins, CO 80523-1373 USA
[3]United States Army

Abstract —*In the current military environment, village searches are conducted daily. To accomplish a village search task in accordance with orders provided by higher headquarters, the mission leaders must plan and allocate resources (e.g., soldiers, robots, military working dogs, unmanned aerial vehicles) efficiently. The plans these leaders create are based on personal experience and planning data found in military field manuals. The Robust People, Animals, and Robots Search (RoPARS) planning tool for village search developed at Colorado State University can assist military leaders in the planning process. The tool consists of a graphical user interface and a resource allocation engine. This tool allows a user to create a simulation for a given village. These simulations allow military leaders to visualize how a given plan would be executed and to develop plans for the mission that are robust against uncertainty in the environment.*

Keywords: graphical user interface, simulation, village search, robustness, resource allocation

1. Introduction

Military leaders are often forced to make decisions about how to allocate and utilize a variety of resources available to them. Under the stresses and constraints of warfare, making these decisions can be difficult. To help military leaders, we can use computers to formulate plans that will ensure the solution will be within the mission constraints. Currently, there is no such tool available, and decision makers must rely on their own personal experience to formulate mission plans.

The Robust People, Animals, and Robots Search (**RoPARS**) planning tool for village searches developed at Colorado State University is part of the People-Animals-Robots (**PAR)** multi-disciplinary research project. The PAR project is organized by the Colorado State University Information Science and Technology Center (**ISTeC)** [1]. RoPARS will be able to assist military leaders allocate resources and make decisions throughout the planning process.

Village searches are an important daily mission for the military. A village search consists of multiple search targets (e.g., buildings) and multiple search resources (e.g., soldiers, military working dogs, robots, unmanned aerial vehicles). The planners must be able to efficiently allocate the search resources to search the targets while staying within the mission's constraints. The overall mission constraint we are concerned with is mission deadline time (**MDT**), but there are many important intermediate constraints. These intermediate constraints take the form of **boundary lines** (physical or virtual lines that indicate allowable search areas for the search teams), **phase lines** (physical or virtual lines that represent a synchronization barrier controlling forward movement of search teams), and direction of advance (indicates search direction). Figure 1 shows an example of a village with these constraints.

To create these mission plans, leaders use their own experience and simple data tables provided in military field manuals (e.g. [2, 3]). There are a number of uncertainties that are present during each mission, such as changes in search rate, movement rate, weather, temperature, enemy presence, and road blockages. These uncertainties cause variation in the rate at which movement and searches are conducted. Thus, creating an exact solution is infeasible. The RoPARS planning tool provides a way for leaders to account for these uncertainties and create a solution that is robust against them. In this environment, we say a solution is **robust** [4, 5] if we meet the specified MDT even with the uncertainties in search and movement rates. We quantify robustness by the probability we will meet the MDT. For a more detailed explanation of how we define robustness for the military village search problem, the reader is referred to [6].

The RoPARS planning tool consists of a graphical user interface (**GUI**) and a resource allocation engine. The tool is a simple geographical information system (**GIS**) that imports Environment Systems Research Institute (**ESRI**) shapefiles of a search area, it allows user input to the plan, creates a resource allocation using "static" or "offline" allocation heuristics (e.g., [7]) and graphically displays the resulting plan at a user-selected rate.

This research was supported by the National Science Foundation under grant number CNS-0905399, and by the Colorado State University George T. Abell Endowment

Figure 1. Example village search mission with eight target buildings (T_j), a unit boundary, a phase line, and a direction of advance. Taken from [6].

The need for a GUI is important because it allows users to read existing shapefiles of a search area, and then recreate the village from them. By using these existing files, users do not have to spend their own time creating these villages by hand, which can be an extremely time consuming process. With this tool, we make the planning process quicker and more efficient. We currently do not know of other tools that leverage these existing files in the way we do. Although we are presenting this tool for use in a military village search situation, the GUI can be adapted for use in the search and rescue domain [8].

The main contribution of this paper is to introduce and demonstrate the graphical user interface for the RoPARS planning tool. This will show that by using a simple interface, which utilizes existing imaging files, leaders can create efficient plans in a faster and simpler way.

The remainder of the paper is organized as follows. Section 2 reviews related work in the fields of military combat simulation. Background on the different tools that helped to create the GUI is discussed in section 3. A description of the workings, features, and operation of the GUI are detailed in section 4. Section 5 contains our conclusions and future work.

2. Related work

While our work is directed towards military village search, it is similar to the problems presented by search and rescue missions. There has been much work done in developing software to help aid in planning of search and rescue missions. At a broader level of abstraction, there has been much work done creating geographical information systems GUIs.

ESRI developed one of the most popular current GIS software packages [9]. ArcGIS is a multi-feature software package for displaying and manipulating geographic information. Similar to our software, ArcGIS allows users to import shapefiles and view their contents. It also contains many features that are unrelated to the village search problem. Although ArcGIS is a very powerful and useful software, our GUI is much simpler and allows for easy manipulation of a search area.

The software in [10] is used by the United States Coast Guard in search and rescue missions around the United States and the Caribbean. The GUI is actually an extension of [9] and so it is able to use all the features provided by the ArcGIS program. This program attempts to simplify the user interaction with the ArcGIS software by providing a wizard-based interface and by minimizing keystrokes. It also has animated display capabilities. Like our software, this software allows users to add constraints to the search mission. Where the program differs from ours is that it primarily deals with water-based missions, as well as searches that take place over a large area. It does not have the same level of granularity that our software provides, i.e., building-by-building searches.

Another search and rescue program is [11]. This software, unlike [10], is designed to handle not only water-based search missions, but also land-based missions. While it is able to allow users to view the plans for a search and rescue mission, it requires the users to create these missions themselves. Users must create the search routes as well as handle the allocation of search resources. Avoiding such human intensive actions is the motivation for developing our RoPARS tool.

Outside of the realm of search and rescue, the authors of [12] demonstrate software used for road routing in a cooperative multi-transportation system. The program is a GIS system that works at the "village" or city level, much like our work. It displays the best road routing for a given system, and is similar to the way we display search routes for a given village search. Because this program is dealing with road routing it has no reason to take into account building locations, nor does it have to display any animations.

The authors in [13] present software that utilizes computer aided design (**CAD**) drawings, GIS technology, and a virtual reality (**VR**) environment to simulate evacuation dynamics. The simulated evacuations are created for individual buildings and each person inside the building will have a unique escape route. Much like our software, the authors utilize GIS to extract spatial features of an area to formulate a plan. This simulation software allows users to focus on an individual building instead of a larger area.

As a supplement to GIS, the authors of [14] conducted a survey on the integration of wireless sensor networks with GIS. Wireless sensor networks provide data on a variety of environmental factors such as temperature, humidity, and location of objects. All of these factors could be utilized by our software to create plans that are more effective.

In summary the wide variety of software that uses GIS concepts varies in its designs and purposes, such as general display and modification of geographic data, search and rescue mission planners, building evacuation simulators, and

road routing systems. While all useful in their domains, none contain all the features required for military village search missions.

3. Background

The RoPARS tool was implemented using C++. We chose C++ as our language due to the fact there are existing libraries and frameworks we could use to handle some of the lower level details of a graphical user interface and the reading in of shapefiles. To create the graphical user interface, **Qt** [15], a cross-platform software and user interface framework was employed. The Qt framework contains the tools necessary for drawing and handling interactions with the GUI. By handling most of the infrastructure code, Qt allowed us to focus on creating features for the GUI instead of the framework operations of the GUI. Qt has a framework that handles the drawing of custom shapes, as well as a framework that can handle various types of animations. The GUI utilizes both of these frameworks.

The GUI is able to visually display a search area. The geographical information for the search area is contained in an ESRI shapefile. Many shapefiles of military interest can be downloaded from the urban tactical planner suite [16]. **Shapefiles** are a popular geospatial vector data format for geographic information systems. A shapefile stores non-topological geometry and attribute information for the geospatial features in the set. These features are stored as independent shapes within the file, with each shape comprised of a set of vertices that define its shape. Because these shapes are independent of one another, they can be non-contiguous and overlapped. Shapefiles can be used to define features such as roads, buildings, and waterways.

The RoPARS GUI currently requires one shapefile representing the roads in a search area and one shapefile representing the buildings. While shapefiles at the very least provide geospatial information, they do not necessarily explicitly provide attributes about the features such as road lengths or the total ground surface area a building occupies (both of these attributes are required for creating a search plan). The GUI becomes more powerful and informative as the data in the shapefile grows. If the provided shapefiles are rich in information, the GUI can use this information to be more detailed and accurate. Currently, due to the sparseness of data contained in the available shapefiles, both road lengths and total ground surface area occupied by a building may have to be calculated after loading the shapefiles into the GUI. To load in shapefiles, the GUI makes use of the C library provided by [17].

4. GUI description

4.1. Overview

The graphical user interface for the RoPARS planning tool is what allows users to create, and visualize search plans in a quick and efficient manner. Because time is often a precious commodity on the battlefield, leaders need a simple yet powerful interface to run simulations and generate resource allocations quickly. The GUI essentially has two main operating modes. The first is the village definition mode, and the second is the simulation/playback mode. The village definition mode is where a user selects shapefiles, inputs mission constraints (e.g., boundary and phase lines, buildings to search, and search teams) and creates data files for the resource allocation engine. The playback mode allows the user to view a plan created by the resource allocator.

4.2. Village definition mode

Village definition mode allows the user to create the search scenario. First, a user must input shapefiles describing the search area. Two shapefiles must be input: one for the roads in the search area and one for the buildings in the area. The GUI will then parse the shapefiles and display the village. The user is then able to modify the village to match the constraints required by the mission. There are currently four modifications a user can apply to the village. The first modification a user can perform is selecting which buildings to search in the village. A selected building will be colored blue, as shown by the screenshot in Figure 2. The next two modifications allow the user to partition the village with the military graphical control measures boundary and phase lines. The village in Figure 2 contains one boundary line, indicated by the vertical green line running through the middle of the village. The village also contains a single phase line as shown by the horizontal red line. Finally, a user is able to add search teams into the village. Figure 2 shows the village currently contains three human teams, one canine team, and one robot team. Each team's individual search attributes are also visible.

Aside from allowing the user to add modifications to the village, the GUI must also calculate additional information about the village for use in search plan creation. The first piece of information calculated is the approximate ground surface area occupied by each building. The ground surface area is used by the resource allocator to determine how long a search team will take to search a building. The buildings input from the shapefile can be virtually any shape and are not guaranteed to be convex. Thus, to calculate the ground surface area, each shape must first be triangulated (i.e., split up into many small triangles). It is then a simple procedure of calculating the area of all the triangles comprising the shape and adding them together. To triangulate the shapes, the ear-clipping algorithm provided by [18] is used to allow both convex and concave shapes to be triangulated. This is not an exact procedure and error does occur, often in the form of a calculated area bigger than what the building actually occupies. This error will occur if the building has, for example, a courtyard in the middle of it. We assume this error is negligible, although courtyards are not part of the actual building, search teams may still search through them while exploring the rest of the building.

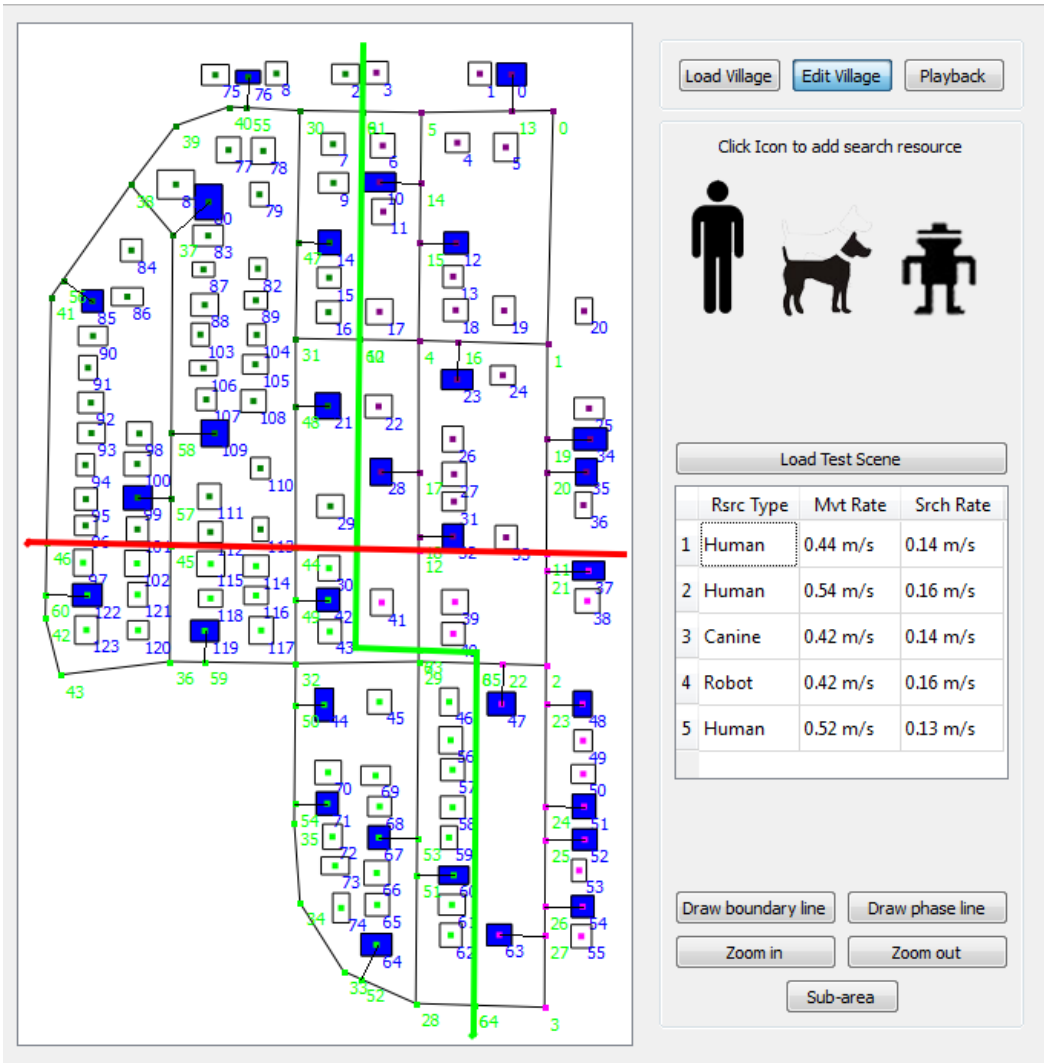

Figure 2. RoPARS tool GUI screen capture of an example village search scenario with a vertical boundary line (green), a horizontal phase line (red), thirty target buildings (blue), and five search teams and their search attributes.

After calculating the building areas, the approximate GPS centroid for each building must also be calculated. This information is useful in the resource allocation engine for heuristics that use distance as a metric [19]. The centroid is calculated by taking the center of the bounding box for a given building. Again this is not an exact procedure and produces minor error, as the calculated centroid is actually for the bounding region of a building, not the building itself. This error occurs most often on buildings that are irregularly shaped, and is less likely for buildings that are square or rectangular. We assume this error is also negligible, even though the GPS centroid might be outside the building (e.g., a courtyard or lawn), it still indicates the point about which the building is located.

When finished calculating the ground surface area and GPS centroid for the buildings, the road network must be represented. The **road network** consists of road segments and road nodes. A **road segment** is a stretch of road between two road nodes. **Road nodes** are created using three criteria. The first is where two road segments intersect each other with the road node being placed at the intersection. The second is when a building is going to be searched; a road node is placed at the spot on a road segment closest to the building. The last criterion for creating road nodes is a limit on the length of any given road segment (e.g., 200 meters). Any road segment longer than the length criterion is subdivided into multiple segments.

With the road network represented, the GUI displays the search area, allowing a user to view and constrain the search area. Users are allowed to select buildings they want to search. Every time a new building is selected, the road network either adds a new road node for the building to

connect to, or connects the building to an existing road node. The road network is updated so that the minimum number of road nodes are used to meet the three road network criteria.

Users can further constrain the search area by adding in boundary and phase lines. A **boundary line** splits the search area into separate smaller areas. A search team that is assigned to one area is not allowed to cross a boundary line and enter another area. A **phase line** represents a synchronization line for the teams searching the village. This means that a search team cannot cross a phase line until all other search teams, regardless of which boundary area they area in, are ready to cross that phase line. A user is able to draw in multiple boundary lines and phase lines. Every time a new line is input, the GUI must calculate on what side of the line every road node and building is located. The GUI then color-codes the buildings to show which boundary and phase area they are located.

The final constraint a user is able to add to the search area is the search teams used in the mission. A user is able to add three different types of search teams to the search area. These are human search teams, military working dog search teams, and robot search teams. Every time a new search team is added, a dialog box is opened allowing the user to change certain properties of the team (Figure 3). These properties of a search team are the mean movement rate, the standard deviation of the movement rate, the mean search rate, and the standard deviation of the search rate. Each of these values can be edited for each search team, and are supplied to the resource allocator to create search plans. If the user chooses not to enter specific values for each team, default values are used instead. These default values are taken from military field manuals such as [2, 3].

After a user is finished constraining and adding search teams to a search area, the GUI creates three data files for the resource allocator. The first file is the **road network file**. This file is essentially an adjacency table that contains the information on how the nodes in the road network are connected to each other, i.e., which road nodes are connected, and the distance in meters between them. The second file is the **building data file**. This file contains the information about the buildings to be searched, as well as each of those buildings' approximate ground surface area, and GPS centroid. The buildings are also organized according to boundary area and phase line area. The third file is the **search resource file**. This file contains information about the search teams, it specifies the type of teams, and each team's movement and search attributes. These three files are used by the resource allocator to create robust and efficient search plans.

4.3. Playback mode

Once the resource allocation engine has finished creating a search plan, it creates an allocation file that the GUI uses to display and playback the search plan. This allocation file contains information for each team, showing which road segments a team traverses and how long it takes the team to traverse each segment, and which buildings a team searches as well as how long it takes to search each building. Taking this information, the GUI constructs animations for each team that visually show the search path each team takes. This timing data is based on the expected values of the completion time probability mass functions used in the allocator [19]. Because the timing data from the resource allocation engine is used, all of the teams' locations with respect to each other are representative of what they would be like in the real world. These animations also accurately show how every team must be ready to cross a phase line before any one team does cross the line.

Users also are allowed to change the rate at which the playback runs. It can be played back as slow as real time and as fast as 500x. Not only does the GUI playback the search paths for each team, but also it traces out the search path as a team advances (Figure 4). After the playback is finished, a user can still see what path a team followed as well as which buildings that team searched. There is also the option for the user to select specific teams and only display those teams' search paths. This allows users to inspect individual team search plans. After viewing a search plan, a user can go back and add or remove constraints from the village, and then generate a new search plan for comparison purposes.

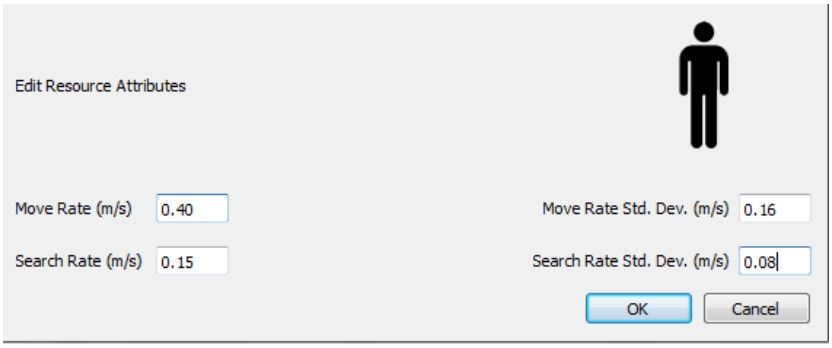

Figure 3. RoPARS tool GUI screen capture of a search resource edit attributes dialog.

5. Conclusions

Determining how to utilize and allocate resources for a military village search is a common but complex problem. Currently military officers must use simple field manuals and personal experience to create these plans. This is a time-consuming process and creates plans of varying quality. We have presented the GUI for the RoPARS tool to demonstrate how computer- aided planning can assist in creating robust search plans. This GUI provides a simple and intuitive yet powerful interface for users to quickly define a search area, and then see an animation of the resulting search plan.

Future work in this area includes augmenting the GUI to allow dynamic updating and display of a search plan while it is conducted on the ground, possibly through the use of wireless sensor networks [14]. This would allow commanders to see mission progress, as well as modify the current plan, should unforeseen difficulties develop during the search. Such difficulties could include roadblocks, insurgent activity, or environmental factors. There also are various general improvements to the GUI such as multithreading the entire application, allowing for the input of more environmental constraints/variables, and displaying the satellite imagery of the search area underneath the graphical representation.

Acknowledgements. The authors would like to thank A. Al-Qa'wasmeh and B. Khemka for their comments.

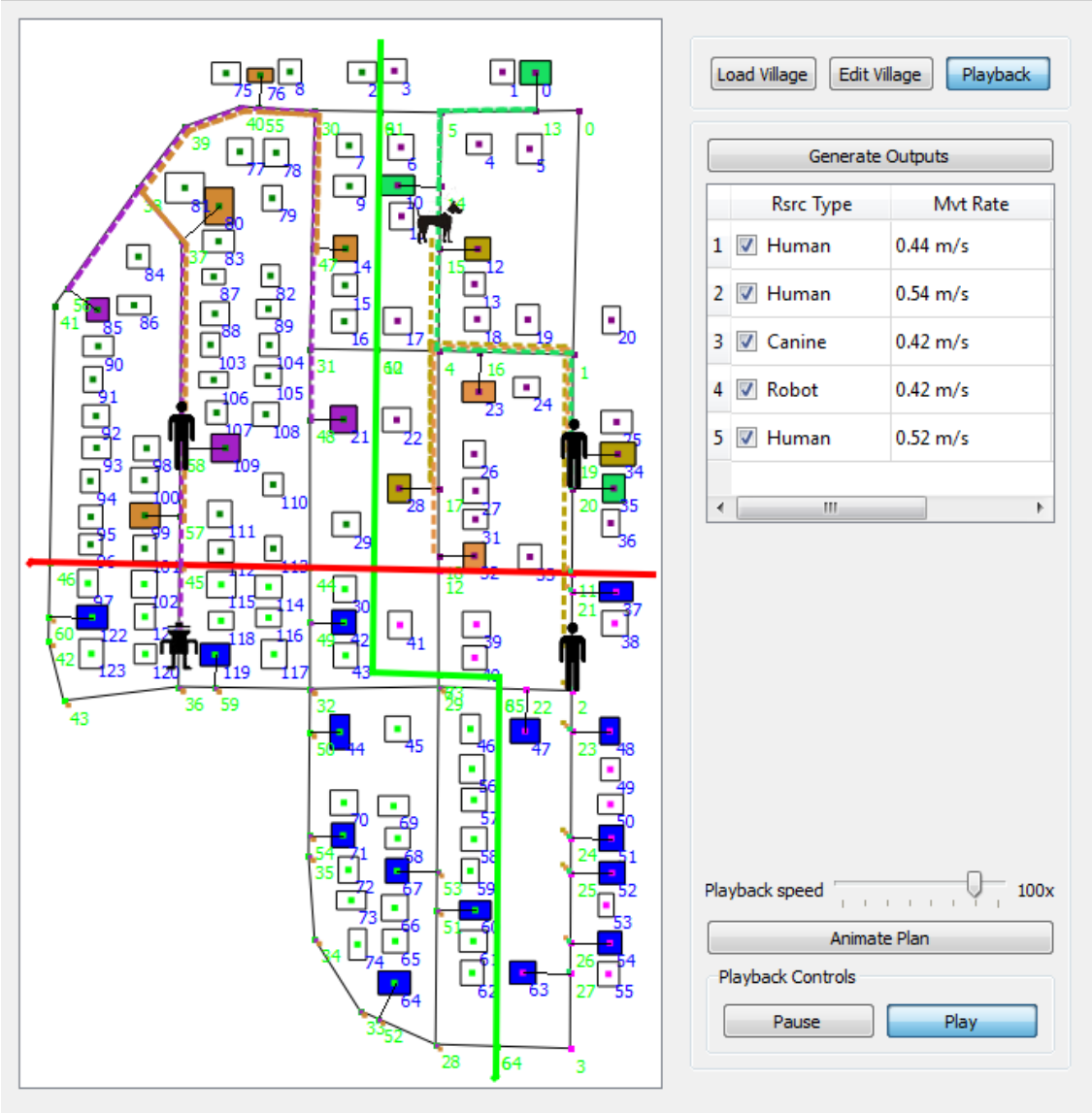

Figure 4. RoPARS tool GUI screen capture of an example resource allocation in playback mode with five search resources and their associated colored movement paths.

References

[1] Colorado State University, *The Information Science & Technology Center*, http://www.ISTeC.ColoState.edu, accessed Feb. 15, 2011.

[2] *FM 34-8-2 Intelligence Officer's Handbook,* U. S. Army Training and Doctrine Command, Ft. Monroe, VA, May 1998.

[3] *FM 3-31.1 Army and Marine Corps Integration in Joint Operations*, U. S. Army Training and Doctrine Command, Ft Monroe, VA, Nov. 2001.

[4] S. Ali, A. A. Maciejewski, H. J. Siegel, and J. Kim, "Measuring the robustness of a resource allocation," *IEEE Transactions on Parallel and Distributed Systems*, Vol. 15, No. 7, Jul. 2004, pp. 630-641.

[5] S. Ali, A. A. Maciejewski, and H. J. Siegel, "Perspectives on robust resource allocation for heterogenous parallel systems," *Handbook of Parallel Computing: Models, Algorithms, and Applications*, S. Rajasekaran and J. Reif, eds., Chapman & Hall/CRC Press, Boca Raton, FL, 2008, pp. 41-1-41-30.

[6] P. Maxwell, R. Friese, A. A. Maciejewski, H. J. Siegel, J. Potter, and J. Smith, "A demonstration of a simulation tool for planning robust military village searches," *Huntsville Simulation Conference (HSC'10)*, Oct. 2010.

[7] V. Shestak, J. Smith, A. A. Maciejewski, and H. J. Siegel, "Stochastic robustness metric and its use for static resource allocations," *Journal of Parallel and Distributed Computing*, Vol. 68, No. 8, Aug. 2008, pp. 1157-1174.

[8] P. Maxwell, H. J. Siegel, and J. Potter, "The ISTeC People-Animal-Robots laboratory: Robust resource allocation," *2009 IEEE Int'l Workshop on Safety, Security, and Rescue Robotics*, Nov. 2009.

[9] Environmental Systems Research Institute, *"ESRI ArgGIS10,"* http://www.esri.com /software/arcgis/arcgis10/, accessed Feb. 1, 2011.

[10] United States Coast Guard, *Search and Rescue Optimal Planning System (SAROPS)*, http://www.uscg.mil/acquisition/international/sarops.asp, accessed Jan. 28, 2011.

[11] SAR Technology Inc. *SAR Technology: 'Incident Commander Pro'*, http://sartechnology.ca/sartechnology/ST_ProgramOverview.htm, accessed Jan. 28, 2011.

[12] G. Qin, Q. Li, and X. Deng, "Aided plan and optimization of road routing in cooperative multi-transportation system," *2008 International Conference on Modeling, Simulation, and Visualization Methods (MSV'08)*, Jul. 2008.

[13] F. Tang, A. Ren, A. Fu, and Z. Xu, "An integrated simulation framework for evacuation dynamics with CAD, GIS, and VR views," *2010 International Conference on Modeling, Simulation, and Visualization Methods (MSV'10)*, Jul. 2010.

[14] M. A. Salam, O. M. Soysal, and H Schneider, "Integration of wireless sensor networks in geographical information systems: a survey," *2010 International Conference on Modeling, Simulation, and Visualization Methods (MSV'10),* Jul. 2010.

[15] *Qt – Cross-Platform application and UI framework*, http://www.qt.nokia.com, accessed Sep. 10, 2009.

[16] United States Army Corps of Engineers, *Engineering Research and Development Center*, http://www.erdc.usace.army.mil, accessed Feb. 10, 2011.

[17] Shapfile C Library V1.2, http://shapelib.maptools.org, accessed Sep. 15, 2009.

[18] D. Eberly, *Geometric Tools*, http://www.geometrictools.com/Documentation/TriangulationByEarClipping.pdf, accessed Oct. 8, 2010.

[19] P. Maxwell, A. A. Maciejewski, H. J. Siegel, J. Potter, and J. Smith, "A mathematical model of robust military village searches for decision making purposes," *2009 International Conference on Information and Knowledge Engineering (IKE'09)*, Jul. 2009, pp. 311-316.

Development of a Fall Dynamics Probabilistic Distribution Database for Biomechanical Simulation

Hiroyuki Kakara[1, 2], Yoshifumi Nishida[2], Yusuke Miyazaki[3], Hiroshi Mizoguchi[1, 2], and Tatsuhiro Yamanaka[2, 4]

[1]Department of Mechanical Engineering, Faculty of Science and Technology, Tokyo University of Science, Noda, Chiba, Japan

[2]Digital Human Research Center, National Institute of Advanced Industrial Science and Technology, Tokyo, Japan

[3]Department of Mechanical Science and Engineering, Kanazawa University, Kanazawa, Ishikawa, Japan

[4]Ryokuen Children's Clinic, Kanagawa, Japan

Abstract - *This paper describes the development of a fall dynamics probabilistic distribution database and a biomechanical simulation to investigate possible measures for preventing childhood serious fall injuries. Data of children's activities were first collected at a sensor home, a mock daily-living space. The sensor home comprises a video-surveillance system embedded into a daily-living environment and a wearable acceleration-gyro sensor. Falls were then detected from sensor data using a custom-developed fall detection algorithm, and videos of detected falls were extracted from long-time recorded video. The extracted videos were used for analyzing fall posture. Characteristic values associated with fall dynamics were determined from the fall-posture analysis and accumulated into a database. Using the developed database, a user can perform conditional searches of fall data by inputting search conditions, such as a child's attributes and fall situation. Finally, a biomechanical simulation of falls was conducted with initial conditions set using the database.*

Keywords: Daily fall, Childhood injury prevention, Fall database, Fall dynamics, Biomechanical simulation

1 Introduction

Falls account for the largest share of the causes of childhood unintentional injuries and the costs of medical care due to injuries. According to a 2008 report on child injury prevention by the World Health Organization [1], over a half of non-fatal injuries are the result of falls, while the main cause of injury-related deaths are not falls. In 2004, injuries by falls in the United States cost 95 billion dollars, accounting for the largest share (> 25%) of the medical costs associated with injuries and deaths. Similarly, in Japan, among children 0 to 4 years of age, falls account for over 50% of non-fatal injuries, as shown in Fig. 1 [2], while the leading causes of mortality are traffic-related injuries and drowning [3]. Additionally, head injuries account for approximately 45% of injuries by falls [4], and head injuries due to falls often lead to serious injuries. Thus, it is important to deal with not only fatal injuries but also non-fatal injuries. In particular, reducing the risk of injury due to falls is the one of the most urgent issues since this type of injury is the most common and associated with the high medical costs.

Generally, there are three approaches to preventing injury due to falls: 1) prevent the occurrence of falls by training children, 2) create an environment in which a child cannot fall, or 3) create an environment that is resistant to injuries from falls. The first two approaches seem to be effective because they focus on the occurrence of falls. However, in the case of children, falls occur naturally in the course of development, and children fall even in flat, obstacle-free spaces. Therefore, it is almost impossible to prevent children from falling, and eliminating the experience of falling is detrimental for a child's growth and development. From this perspective, the present study deals with the third approach, creating an environment that is resistant to injuries from falls.

When creating an environment that is resistant to injuries from falls, it is necessary to predict and assess the severity of these types of injuries. A typical method is a biomechanical simulation of falling [4] [5]. A simulation allows investigators to reproduce fracture phenomenon taking the material properties of the human body into consideration. A reliable simulation, however, also requires information regarding the circumstances surrounding a fall, and such

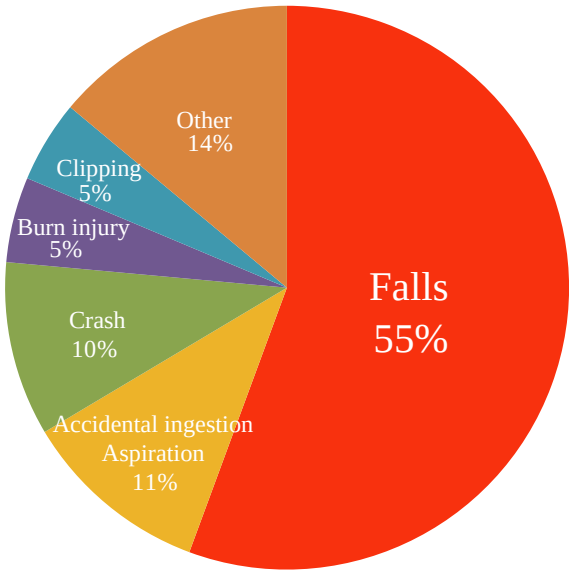

Fig. 1 Causes of injury

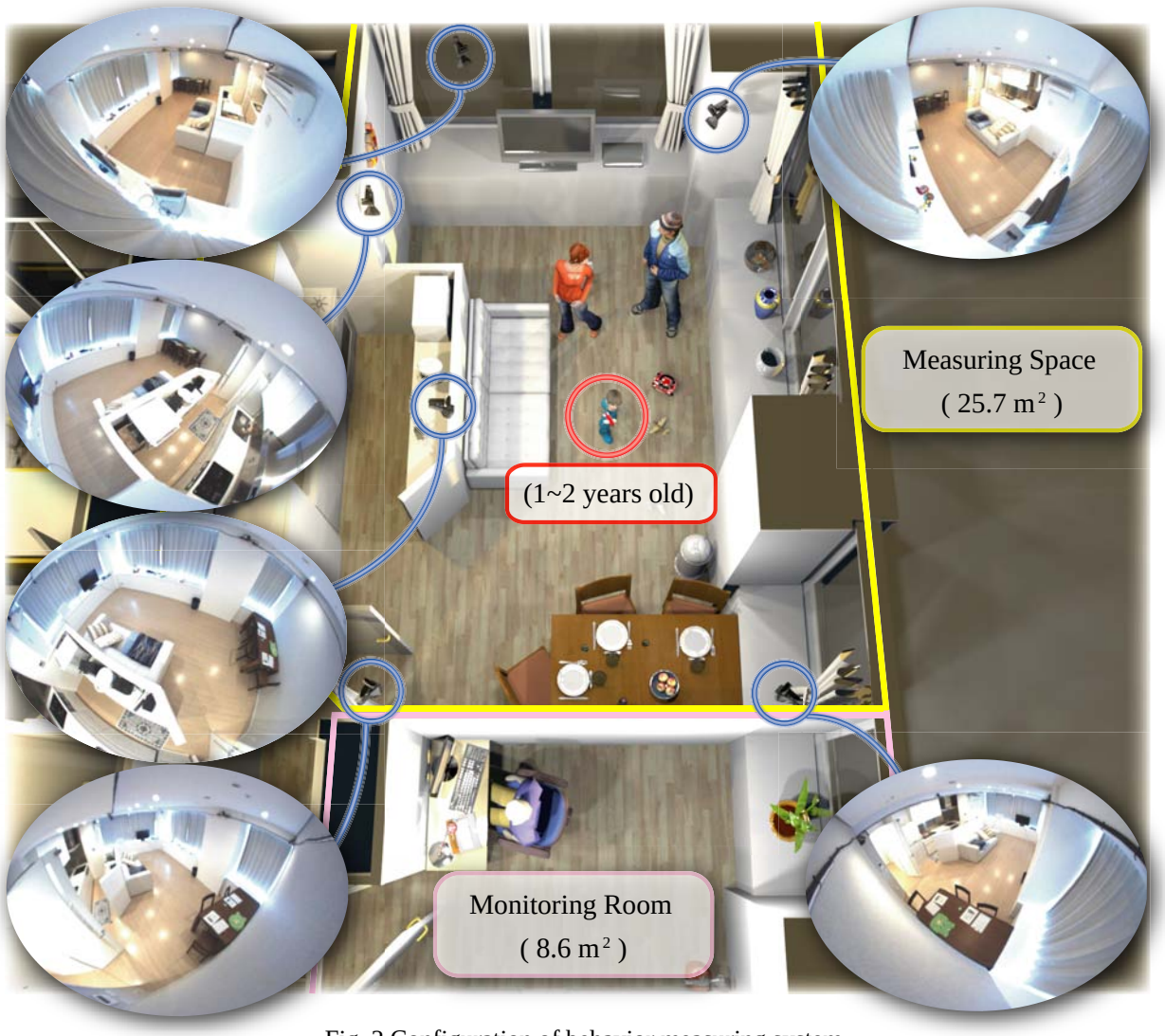

Fig. 2 Configuration of behavior measuring system

situational data are not currently available.

Many studies on falls have already been conducted. For example, some fall detection algorithms have been developed [7-9] and studies to prevent the occurrence of falls by understanding the incidence, causes, and circumstances of falls [10] have been conducted. However, these studies are focus on elderly people and moreover the dynamics of falls remain to be clarified.

The objective of the present study was to develop a database of fall dynamics that occur in a daily living space. This database was designed to allow a user to perform conditional searches of fall data by inputting search conditions, such as a child's attributes and fall situation. This database will enable more realistic fall simulations and these realistic simulations will, in turn, assist in the development of safer and more functional products.

The fall dynamics database was developed as follows. First, two systems were developed: 1) a system that measures child's behavior, and 2) a system which extracts fall videos from the recorded behavior data using a fall detection algorithm. Next, data of activities and extracted fall videos were collected. Finally, characteristic values associated with fall dynamics were calculated by motion analysis, and the database was created by accumulating the fall data.

2 Development of the behavior measuring system and the experiment

2.1 The behavior measuring system

The behavior measuring system was developed in an ordinary apartment to obtain unintentional fall data in a daily living space. The configuration of the system is shown in Fig. 2, and comprises a video-surveillance system and Bluetooth adapter embedded into a sitting-dining room, and a PC in a bedroom adjacent to the sitting-dining room. The video cameras and Bluetooth adapter are connected to the PC. The Bluetooth adapter is used for communication between the PC

and an acceleration-gyro sensor. The system is capable of measuring two kinds of data:

- Sensor data (167 Hz, for fall detection)
- Video data (30 fps, for motion analysis)

The video data are synchronized with the sensor data by adding the frame number to the sensor data each time the PC receives the sensor data. In consideration of safety, safety measures were implemented, such as pillow shams on sharp corners or hinge covers.

2.2 The experiment

Data from the daily activities of children were obtained in the behavior measuring experiment conducted under the following conditions:

- Subjects: 1- to 2-year-old children
- Measurement time: Approximately 60 minutes
- Subject number per single measurement: 1 child

The age group of children was selected considering that children at this age fall frequently. The measurement time was set in consideration of child's fatigue. All parents signed a consent form for the recording and release of data prior to the experiment. The height and weight of each child (i.e., database search conditions) were first measured and then each participant was dressed in the experimental garment shown in Fig. 3. To make wearing the sensor less cumbersome for the children, the sensor was placed in the back pocket of the

Fig. 3 Experimental garment

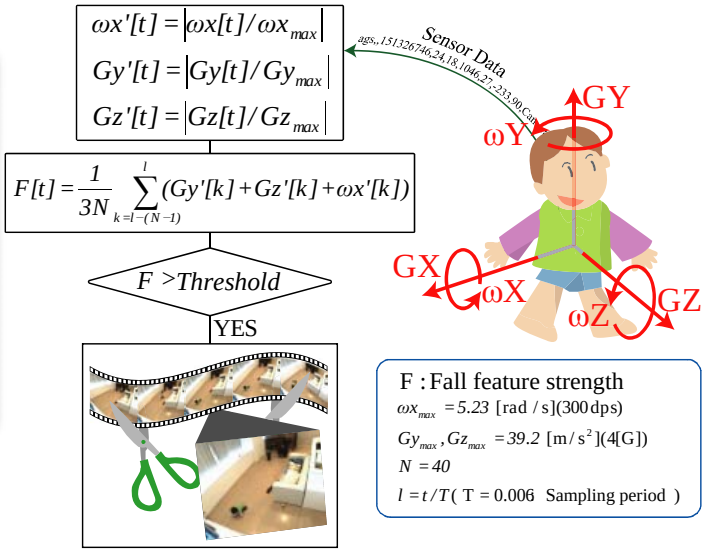

Fig. 5 Fall detection algorithm

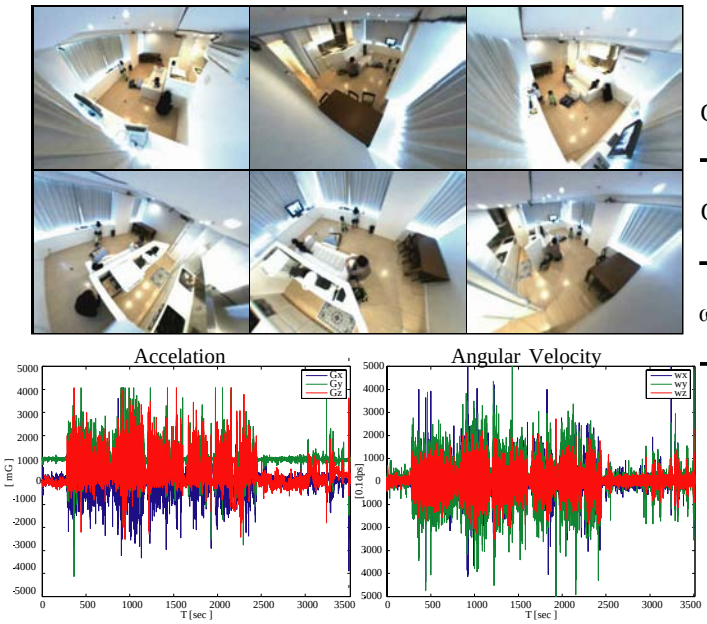

Fig. 4 Example of measurement results

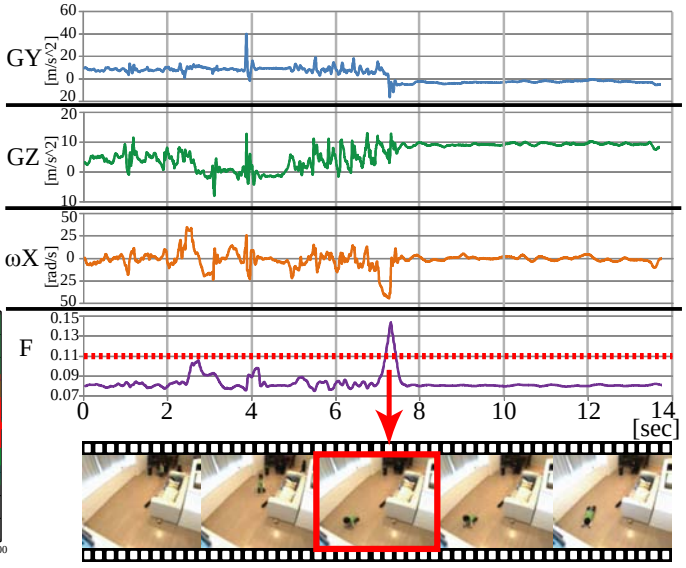

Fig. 6 Fall detection example

garment.

The measurements began immediately once the initial preparations were completed. In the sitting-dining room, there were many toys to stimulate lively behavior, and the children played with their parents as usual using these toys. Moreover, because the focus was obtaining unintentional fall data, intentional falls were unnecessary.

2.2.1 Example of measurement results

To date, measurements have been conducted with 6 children between 11 and 28 months of age, and 67 occurrences of falls have been obtained. An example of behavior data is shown in Fig. 4.

3 Fall detection algorithm

After the measurement, fall videos were extracted using data from the acceleration-gyro sensor. The fall detection algorithm shown in Fig. 5 was developed to extract fall videos automatically. Rapid changes in acceleration or angular velocity occur during falls. Particularly, Gy (acceleration of a body's lengthwise direction), Gz (acceleration of a body's anterior-posterior direction), and ωx (angular velocity about body's abscissa axis) show fall feature more obviously. Results indicated that fall features distribution among these three data varied substantively depending on the development stage of the child. For example, the fall features of toddling children tend to appear in Gy because they tend to fall assuming a seated posture. On the other hand, fall features of more active children tend to appear in Gy or ωx because they tend to fall forward. Thus, these three data (Gy, Gz, and ωx) were considered for detection of falls by both toddling and active children, and a fall detection algorithm was subsequently developed that calculates the fall feature strength, F.

Earlier studies have developed fall detection algorithms [7-9]. However they can't be applied to this case because of following reasons. First, child's fall postures differs from adult's ones largely, so it is difficult to detect falls by a simple threshold processing of acceleration data. Fall features don't appear at the completely same instant in sensor data. To deal with this point, the algorithm developed by us utilizes integration of acceleration and angular velocity. Second, child's body is very small and its figure is quite different from that of adult, so it is difficult to detect falls using only image processing. Thus, we developed a new fall detection algorithm using the acceleration-gyro sensor.

As the first step shown in Fig. 5, the algorithm calculates dimensionless Gy, Gz, and ωx by dividing absolute values by sensor maximum values (Gy_{max}, Gz_{max}, and ωx_{max}). Each of the sensor maximum values are shown in Fig. 5.

Next, the algorithm adds three dimensionless values in order to calculate the comprehensive scale of F. Moreover, considering that there is a maximum time lag of 200 [msec] among the three values, the algorithm integrates 40 data (for 240 [msec]) and adds the integration to the comprehensive scale. In order to normalize the comprehensive, the algorithm divides F by "3N". The "3" indicates the added data number (Gy, Gz, and ωx), and "N" indicates the integrated data number (40). As a result of this operation, the maximum value of F becomes 1.

Finally, the algorithm performs threshold processing. If F exceeds a given threshold, the system determines that a fall has occurred and extracts fall videos by referring to the frame number data added after the sensor data.

Sample Gy, Gz, ωx, and calculated F data are shown in Fig. 6. F changes rapidly and eventually exceeds a threshold (0.11); an actual fall occurred at this point.

4 Fall motion analysis

Fall motion was analyzed using extracted fall videos, and daily fall dynamics were calculated. Commercial motion analysis software (Frame-DIAS IV) was used to calculate the 3D position of each body area. The following data were

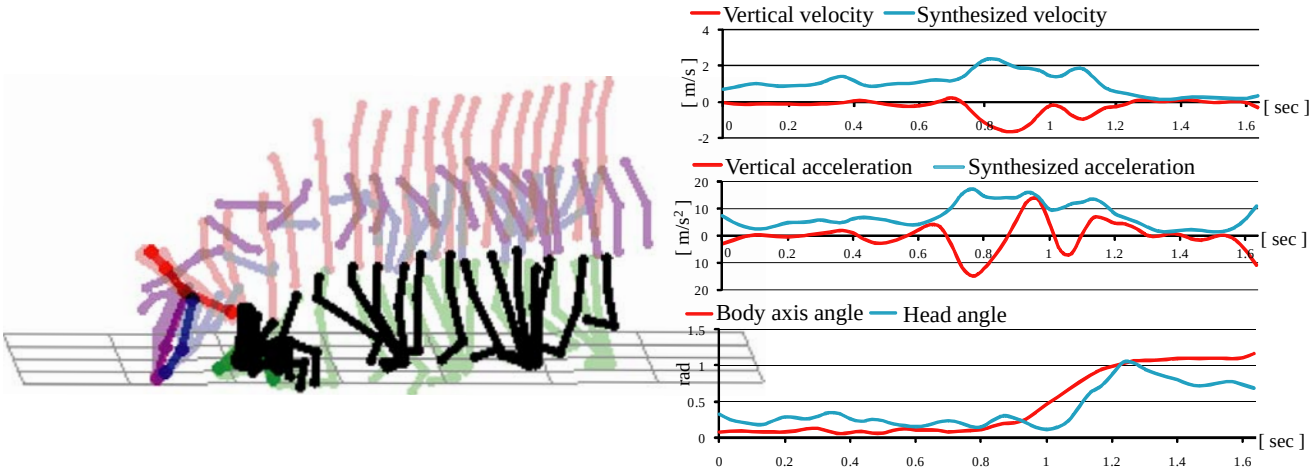

Fig. 7 Posture analysis example

obtained from the fall motion analysis:

- 3D position of body axis (top of head → tragus → base of neck → center of the abdomen)
- Head velocity (vertical direction & synthesis)
- Head acceleration (vertical direction & synthesis)
- Head angle (∟ top of head- tragus - vertical direction)
- Body axis angle (∟ base of neck - center of the abdomen - vertical direction)

An example of the fall motion analysis is shown in Fig. 7.

5 Database of fall dynamics probabilistic distribution

5.1 Data accumulation

The database was developed by accumulating fall data, and includes the following information: 1) fall dynamics data as stated in Section 4, 2) children's attributes such as age, height, weight, and 3) fall situation such as landing body site, last behavior, and cause of fall. The first two sets of data are used as search conditions. The developed database browser is shown in Fig. 8.

5.2 Functions of the database

The database browser has a search condition setting area on the left, and a table which shows the search results on the right. A probabilistic distribution of retrieved fall dynamics data is displayed in the lower portion of the browser. The details of the implemented function are described in the following section.

5.2.1 Conditional search of fall data

In the developed database, conditional searches of fall data are possible by inputting the following search conditions.

- Subject's attributes: age, gender, height, weight, dominant hand and foot
- Fall situation: landing body site, last behavior, and cause of fall

By inputting any one of these search conditions, the corresponding data can be retrieved.

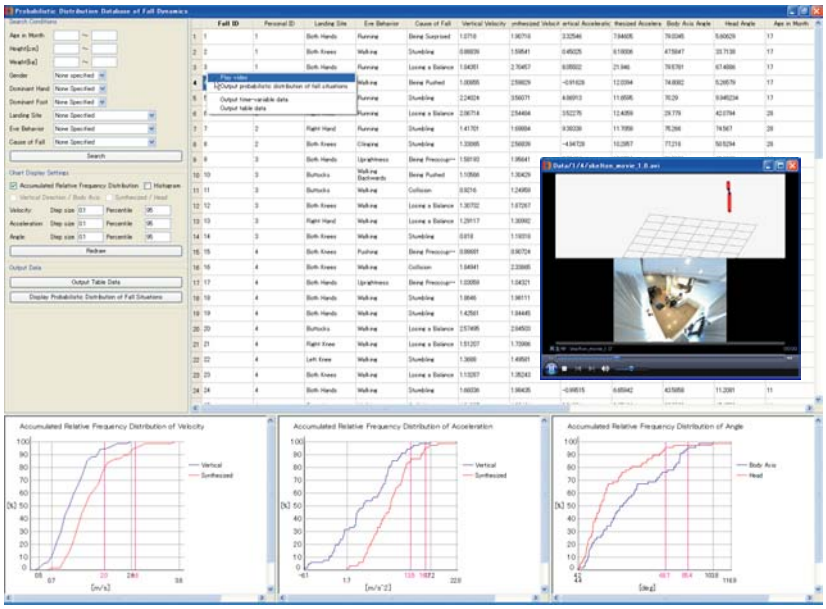

Fig. 8 Database browser

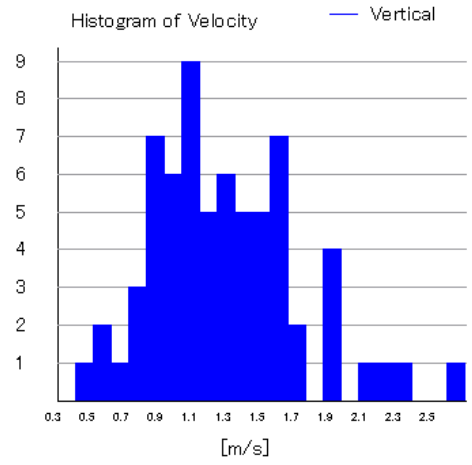

Fig. 9 Histogram

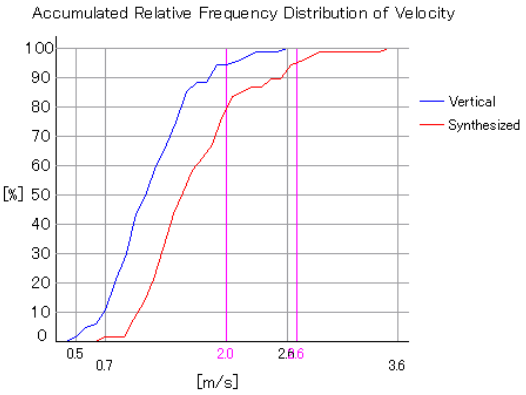

Fig. 10 Accumulated relative frequency distribution

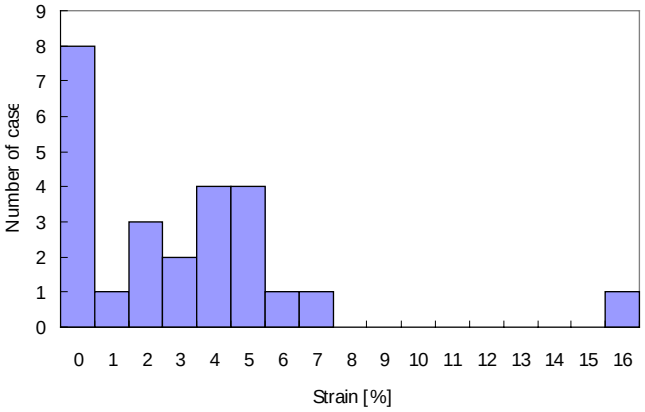

Fig. 11 Histogram of ultimate strain

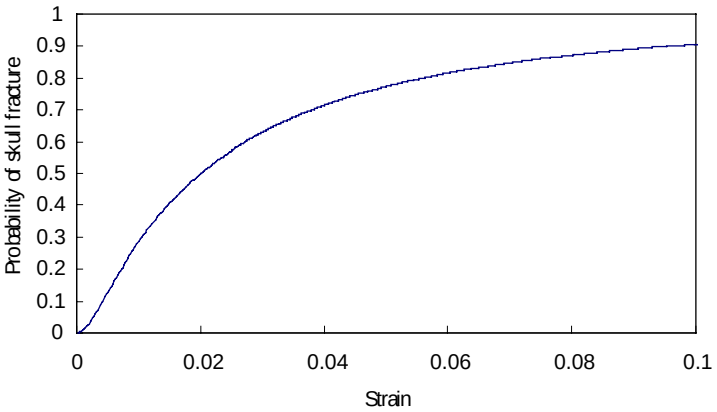

Fig. 12 A probabilistic distribution of skull fracture occurrences

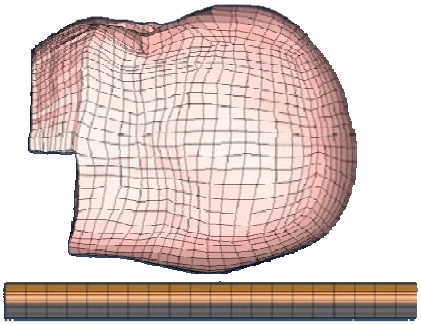

Fig. 13 Example of the simulation

Table 1 Event probability of cranial bone fractures

Floor material	Concrete	Wood flooring	Cushion floor	Shock absorbing floor
Maximum principal strain	0.00466	0.00414	0.00270	0.00148
Bone fracture rate	12%	10%	5%	2%

5.2.2 Visualizing the probabilistic distribution

The developed browser can display the probabilistic distribution of fall dynamics, representing values of velocity, acceleration, and angle. The browser calculates and automatically displays the probabilistic distributions and subsequently updates them each time a user performs a search. The browser has two types of probabilistic distributions: the histogram and accumulated relative frequency distribution. An example of the histogram is shown in Fig. 9, and an example of a chart of the accumulated relative frequency distribution, which is equal to the percentile curve, is shown in Fig. 10. Thus, this database browser enables the user to conduct not only worst-case analysis, but also analysis based on percentile in consideration of the probabilistic distribution.

5.2.3 Displaying individual fall videos and motion analysis videos

By selecting a cell in the right-hand table, the corresponding fall video and the resultant video of the motion analysis are shown.

5.2.4 Outputting time-variable data of fall dynamics

By selecting a cell in the right-hand table, the browser outputs the time-variable dynamics data of the corresponding fall. CSV files of probabilistic distributions can also be obtained by selecting one of the charts.

5.3 Example of a biomechanical simulation

A biomechanical simulation was conducted, which reproduced the impact of a head hitting the floor, and the strain at the point of bone fracture (ultimate strain) was calculated. The initial conditions of the simulation were set using the database.

A histogram of data points for parietal and occipital cranial bones under three-point bending, as reported by Brittany Coats and Susan Margulies, is shown in Fig. 11 [11]. The histogram shown in Fig. 12 was made using these data. This chart represents the relationship between the ultimate strain and a probabilistic distribution of skull fracture occurrences. Thus, if ultimate strain data are input, the event probability of bone fractures can be obtained.

A simulation of a child falling and the hands land first is shown in Fig. 13. The developed database has 16 occurrences of hands-first landing falls. To conduct the worst-case analysis, maximum velocity (2.5 [m/s]) data are extracted from the developed database. The resultant data are shown in Table 1, and indicate that the biomechanical simulation predicts the probabilities of bone fracture.

6 Conclusions

This paper describes the development of a fall dynamics database and biomechanical simulation using the developed database. A system for measuring children's daily behavior and a fall video extracting system were developed and

subsequently used to create the database. Fall dynamics for the database were calculated using fall motion analysis, and, to date, measurements have been compiled from 6 children between 11 and 28 months of age. The developed database has four principal functions: 1) conditional search of fall data, 2) visualization of the probabilistic distribution, 3) display of individual fall videos and motion analysis videos, 4) output of a time-variable data file of fall dynamics. Data from this database enables not only worst-case analysis, but also analysis based on percentile in consideration of the probabilistic distribution. Finally, using the developed database, a biomechanical fall simulation was conducted to estimate the probability of bone fracture due to falling. Future versions of the system will include a pattern recognition method for fall detection, in order to improve detection accuracy. Additional simulations will also be conducted under various situations using the developed database.

7 References

[1] World Health Organization. "World Report on Child Injury Prevention," (edited by M. Peden, K. Oyegbite, J. Ozanne-Smith, A. A. Hyder, C. Branche, A. F. Rahman, F. Rivara and K. Bartolomeos). 2008

[2] National Institute of Advanced Industrial Science and Technology. "Project of Building a Safety-Knowledge-Recycling-Based Society 2009"

[3] Ministry of Health, Labor and Welfare. "Accidental Deaths (Specified Report of Vital Statistics) 2009"

[4] National Institute of Advanced Industrial Science and Technology. "Kids Design Circle [Online]," http://www.kd-wa-meti.com/ (accessed April 4, 2011)

[5] Y. Miyazaki, Y. Murai, Y. Nishida, T. Yamanaka, M. Mochimaru and M. Kouchi. "Head Injury Analysis In Case of Fall from Playground Equipment Using Child Fall Simulator"; The impact of Technology on Sport, Vol. III, pp.417-421, 2009

[6] Y. Miyazaki, Y. Nishida, Y. Motomura, T. Yamanaka and I. Kakefuda. "Computer Simulation of Childhood Head Injury Due To Fall From Playground Equipment"; The 2nd Asia Pacific Injury Prevention Conference, November 2008

[7] A. K. Bourke, J. V. O'Brien and G. M. Lyons. "Evaluation of a threshold-based tri-axial accelerometer fall detection algorithm"; Gait and Posture, Vol. 26 Issue 2, pp. 194-199, November 2006

[8] T. Zhang, J. Wang, P. Liu and J. Hou. "Fall Detection by Embedding an Accelerometer in Cellphone and Using KFD Algorithm"; IJCSNS International Journal of Computer Science and Network Security, Vol. 6 No. 10, pp. 277-284, October 2006

[9] L. Hazelhoff, J. Han and P. H. N. de With. "Video-Based Fall Detection in the Home Using Principal Component Analysis"; ACIVS 2008, pp298-309, October 2008

[10] S. Robinovitch, F. Feldman, D. Wan, O. Aziz and T. Sarraf. "Video recording of real-life falls in long term care provides new insight on the cause and circumstances offalls in older adults"; Proceedings of the XIX Conference of the International Society for Posture & Gait Research Bologna, pp. 80, June 2009

[11] B. Coats and M. Susan. "Material Properties of Human Infant Skull and Suture at High Rates"; Journal of Neurotrauma, Vol. 23, pp. 1222-1232, 2006

Patient-Specific Computational Simulation of the Mitral Valve Function Using Three-Dimensional Echocardiography

Y. Rim[1], S. T. Laing[1], P. Kee[1], K. B. Chandran[2], D. D. McPherson[1] and H. Kim[1]
[1]Department of Internal Medicine, The University of Texas Health Science Center at Houston, Houston, Texas, USA
[2]Department of Biomedical Engineering, The University of Iowa, Iowa City, Iowa, USA

Abstract - *Abnormal mitral valve (MV) morphology may lead to high stress generation. Computational simulation of the MV apparatus may help us better understand and characterize the biomechanics and physiology of MV function and disease-related alterations. The MV apparatus geometry was identified using three-dimensional (3D) transesophageal echocardiographic (TEE) patient data. These data were converted into a 3D computational MV model. Computational simulation of the MV function was performed using finite element analysis with an experimentally-determined material model. Functional and morphological characteristics were evaluated and compared to the 3D TEE data. The MV simulation demonstrated the complex 3D MV shape with good agreement to 3D TEE, and determined regions of stress concentration in the MV components. Asymmetric stress distribution was clearly displayed on the MV leaflets indicating realistic and physiologic alteration of MV morphology and function. This novel computational simulation strategy may provide a powerful tool for patient-specific structural evaluation of the MV.*

Keywords: Mitral valve, Finite element analysis, Three-dimensional echocardiography, Computational modeling, Patient-specific, Simulation

1 Introduction

The mitral valve (MV) apparatus has a complex anatomical structure consisting of two asymmetric leaflets, a saddle-shaped annulus, chordae tendineae, and papillary muscles [1]. It is important to assess the physiologic characteristics of the MV apparatus. Abnormally increased stress distribution in the mitral leaflets may play a major role in pathological alteration, improper remodeling and malfunctions of the MV apparatus.

Three-dimensional (3D) echocardiography can provide detailed morphology of the MV leaflets and annulus contributing to our understanding of MV function and anatomy. It is more suitable to conduct 3D assessment for the evaluation of MV function because of the complex MV structure [2]. Surgeons are now using 3D transesophageal echocardiography (TEE) prior to MV repair to evaluate MV geometry and focus the surgical procedure, particularly for MV prolapse. Current clinical 3D echocardiography can demonstrate excellent volumetric morphology of the MV apparatus and provide information on the regurgitated flow jet across the MV leaflets using Doppler ultrasound in real time allowing evaluation of mitral regurgitation [3]. However, biomechanical information such as high stress concentration and abnormal bending curvature within the MV apparatus structure is not available from 3D echocardiography alone. Numerical evaluation methods such as finite element analysis can be utilized to assess biomechanical characteristics of the MV apparatus.

Finite element analysis is an effective method for morphologic evaluation and stress determination of native aortic and mitral valves [4-6] as well as bioprosthetic valves [7, 8]. This is due in part to our understanding that localized concentration of mechanical stress and large flexural deformation are closely related to tissue degeneration and calcification in heart valve diseases [9-11]. Specifically for MV pathology, annular shape and geometric distribution of chordae tendineae play an important role with respect to functional valvular abnormalities [12-14].

The combination of 3D echocardiography and computational simulation can provide a powerful tool to evaluate complex structural and functional information of the MV apparatus.

In this study, we develop an integrated modeling platform to create a precise MV geometry model using patient 3D TEE data, and perform computational evaluation of the MV function. This computational evaluation strategy, with rigorous validation, may help us better understand the dynamics of MV function and provide a comprehensive noninvasive imaging and evaluation techniques potentially improving the diagnosis and treatment of MV pathology.

2 Materials and Methods

The MV apparatus including the anterior and posterior leaflets, the mitral annulus and the location of the papillary muscles was identified using 3D TEE data of a patient. This study was approved by the Institutional Review Board of The University of Texas Health Science Center at Houston.

2.1 Finite element modeling of the MV

A Philips iE33 ultrasound unit (Philips Medical Systems, Bothell, WA) with a 3D TEE transducer was

utilized to obtain the 3D geometry of the MV and its apparatus. Following our standard 3D TEE echo protocols, 3D TEE was performed to acquire the best MV geometry. The 3D TEE data was stored in digital format and converted into a 3D computational MV model.

Fig. 1 demonstrates the algorithms to convert 3D echocardiographic data of the MV apparatus into a finite element model followed by computational dynamic simulation. The 3D coordinate data of the MV apparatus structure was digitized, and the MV leaflets and annulus geometry segmented and traced in a multiple number of sagittal binary images of the MV structure. The 3D geometry of the leaflets was created using a B-spline surface modeling method. All the algorithms to create 3D MV geometry were developed using MATLAB software (The Mathworks Inc., Natick, MA). The 3D MV leaflets geometry was imported to ABAQUS (SIMULIA, Providence, RI), and meshed using S4R element type (4-node shell elements). The main and two secondary chordae tendineae were added to the MV model by connecting the location of the papillary muscles and the edge of two leaflets [15]. Each chordae tendineae was modeled using a series of 3D line elements (T3D2 element type).

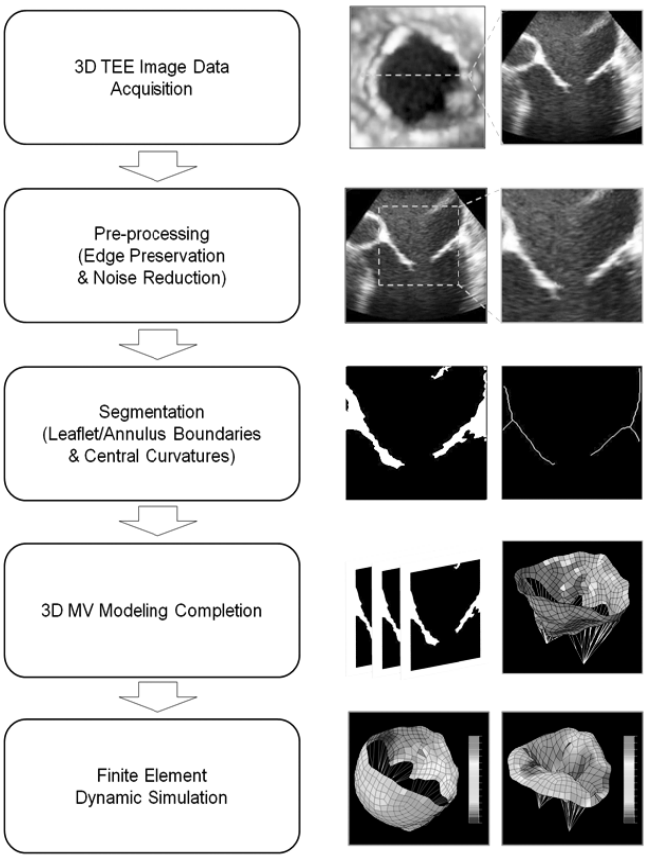

Figure 1. Flowchart of MV modeling and finite element dynamic simulation

2.2 Material modeling of the MV

The MV leaflets were modeled as a hyperelastic material. The nonlinear hyperelastic mechanical behavior of the leaflet tissue was modeled using a Fung-elastic constitutive model [16]. Material parameters were determined by fitting the biaxial mechanical test data of the anterior and posterior leaflet tissue from a previous study [17]. The Levenberg-Marquardt nonlinear least squares algorithm was used for the curve fitting.

Elastic properties of the MV leaflets were defined by nearly incompressible, nonlinear and anisotropic strain energy function W with four parameters (c, A1, A2 and A3) as the shear components are small enough to be negligible [17]. The strain energy function used in this study is as follow.

$$W = \frac{c}{2}[e^{Q} - 1], \quad Q = A_1 E_{11}^2 + A_2 E_{22}^2 + 2A_3 E_{11} E_{22} \quad (1)$$

In nearly incompressible hyperelastic material, the relationship between the Cauchy stress and the Green-Lagrange strain is given by

$$\sigma_c = (2E_{11} + 1)c\exp(Q)(A_1 E_{11} + A_3 E_{22}) \quad (2)$$

$$\sigma_r = (2E_{22} + 1)c\exp(Q)(A_3 E_{11} + A_2 E_{22}) \quad (3)$$

The stress-strain relationships were defined along the circumferential (σ_c) and radial (σ_r) directions, and the parameters obtained by fitting the previously reported experimental data [17]. The leaflet thickness was set to 0.69 mm for the anterior leaflet and 0.51 mm for the posterior leaflet.

The chordae tendineae were modelled using a linear elastic and isotropic material model with a Young's modulus of 470 MPa and a Poisson's ratio of 0.48 [18]. Density and cross-sectional area of the chordae tendineae were set to 1,100 kg/m^3 and 0.4 mm^2, respectively [18].

Validation studies pertaining to implementation of these material properties into ABAQUS were performed by biaxial test simulation with a single element model. Computer-predicted stress-strain relationship from the single element biaxial test simulation was compared with the experimental data.

Following the vigorous validation studies, we performed dynamic simulation of the MV apparatus model created from a patient 3D TEE data.

2.3 Boundary conditions for MV simulation

Boundary conditions were assigned to the finite element MV apparatus model such that all the degrees of freedom were restricted along the saddle-shaped mitral annulus. The locations of the papillary muscles were also fixed. Pressure change in the left ventricle and left atrium is shown in Fig. 2 [19]. Time-varying physiological pressure difference across the MV was applied on the anterior and posterior leaflet surface as pressure loads.

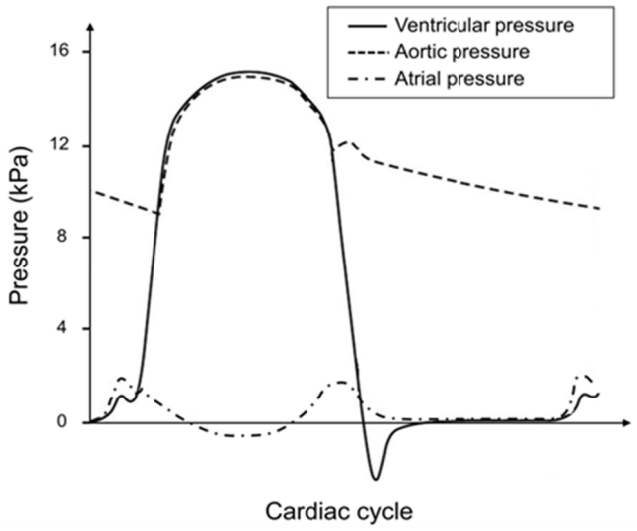

Figure 2. Pressure change across the MV during a cardiac cycle

During the closing phase, coaptation of the MV leaflets was modeled using the surface-to-surface contact algorithm with the penalty contact method in ABAQUS.

3 Results

3.1 Finite element modeling of the MV

The 3D echocardiographic image data were successfully converted to a 3D finite element MV model. Fig. 3a depicts the extracted 3D volumetric MV structure when the valve is closed and open. The mitral annulus and two leaflets are clearly visible from the ventricular view. A 3D surface model of the MV apparatus was created with the user-defined semi-automated algorithm, and then imported to ABAQUS followed by meshing and adding the chordae tendineae. Fig. 3b and 3c demonstrate the consequent structural model of the MV apparatus with a total of 656 shell elements for the leaflets and 296 line elements for the chordae tendineae. Anomaly of the MV leaflet morphology was clearly observed in both 3D TEE image data and the finite element model. Surface smoothness of the leaflets was excellent allowing successful surface mesh subsequently. No mesh distortion was observed.

3.2 Validation studies of the material modeling

The anterior and posterior leaflets have different material characteristics. We have implemented the experimentally determined material properties of the anterior and posterior leaflets from a previous study [17] into the finite element model. The posterior leaflet is more extensible than the anterior leaflet. Validation studies of the material modeling of the MV leaflets were performed. In Fig. 4, x- and y-axis represent the Green-Lagrange strain (E) and the Cauchy stress (σ), respectively. Nonlinear

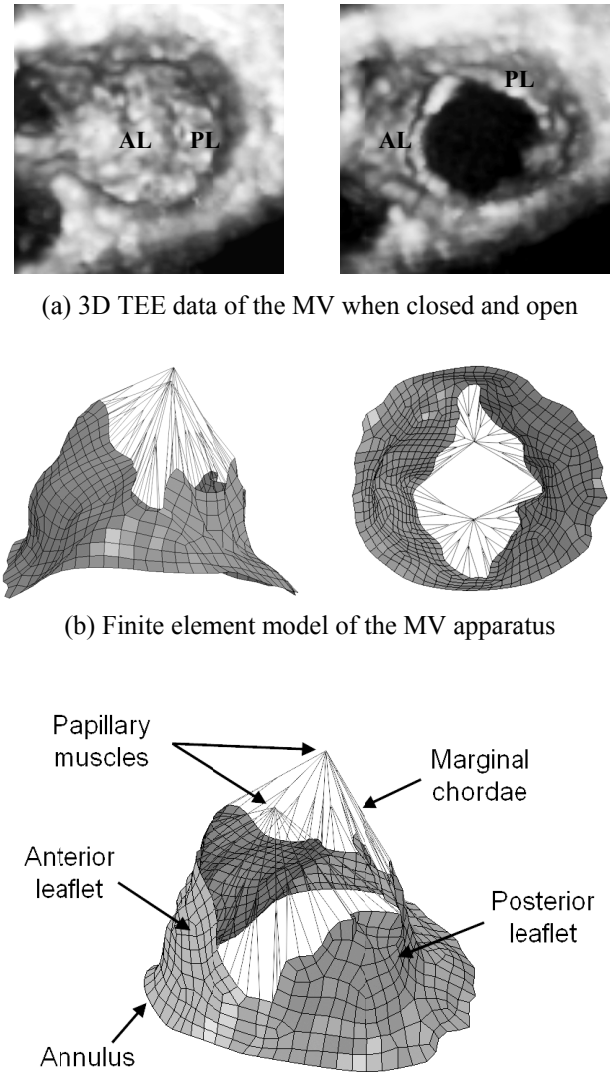

(a) 3D TEE data of the MV when closed and open

(b) Finite element model of the MV apparatus

(c) Components of the 3D finite element MV model

Figure 3. Computational MV apparatus model created by using patient 3D TEE data

regression curves (solid lines) fitted to the Fung-elastic constitutive model [Eq. (1)-(3)] showed good agreement to the experimental stress-strain relationships data for both anterior and posterior leaflets ($r^2 \geq 0.91$). The open circles and triangles demonstrate the previously reported biaxial mechanical test data [17], and the computer-predicted data obtained from single element biaxial test simulations using the implemented Fung-elastic constitutive model and the material parameters are shown in solid circles and triangles. These validation data indicate that the Fung-elastic constitutive model has been successfully implemented in the ABAQUS platform and this model can be utilized for simulations of the complex MV function.

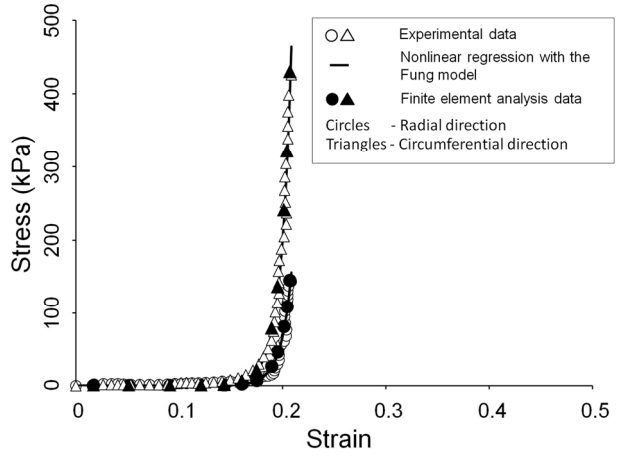

(a) Anterior leaflet

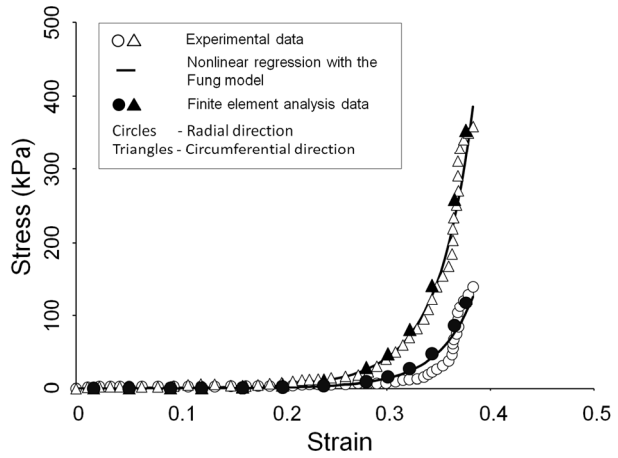

(b) Posterior leaflet

Figure 4. Stress-strain relationships of the anterior and posterior leaflets

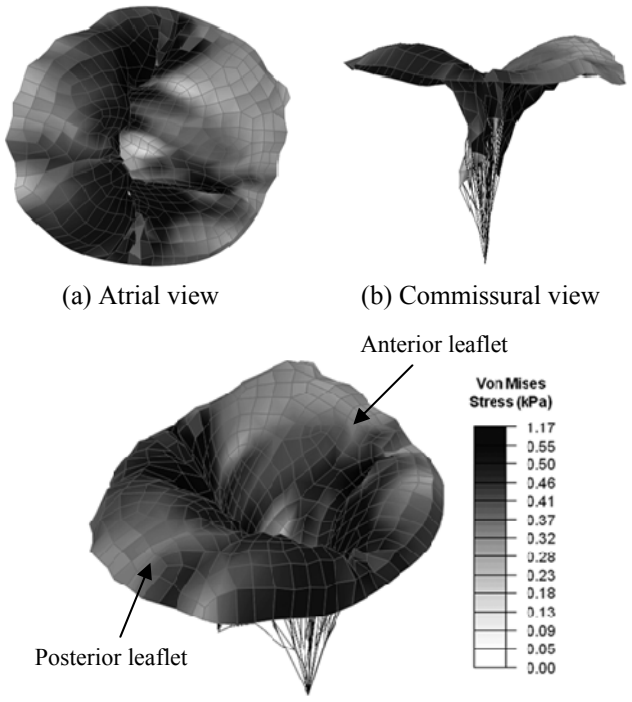

(a) Atrial view (b) Commissural view

(c) Oblique view

Figure 5. Von Mises stress distribution in the MV apparatus at the closed position

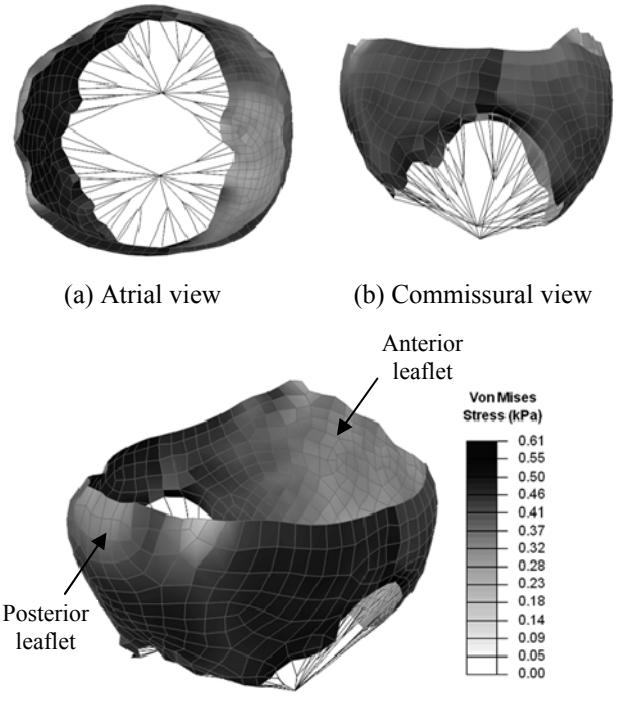

(a) Atrial view (b) Commissural view

(c) Oblique view

Figure 6. Von Mises stress distribution in the MV apparatus at the open position

3.3 Dynamic simulation of the MV function

We performed dynamic simulation of the MV function over the cardiac cycle. The von Mises stress distributions in the MV leaflets and annulus at the closed and open positions are shown in Figs. 5 and 6.

The largest stress values were distributed in the vicinity of the commissures at the fully closed position (Fig. 5). For this particular patient data, the highest stress value was observed near the regions with extremely high curvature where self-contact (i.e. contact between the elements in the same leaflet) occurred in both the anterior and posterior leaflets. The maximum stress value was located at the self-contact region in the anterior leaflet (1.17 kPa). The stress distribution was centralized at the belly region and spread toward the annulus. It was clear that the regions with relatively high stress values corresponded to the highly stretched regions or the self-contact regions with large curvature for both the leaflets. It is noteworthy that the

anterior and posterior leaflets showed different stress distribution patterns and values.

At the fully open position, relatively large stress values (0.46-0.61 kPa) were distributed near the commissural areas where the two leaflets were connected (Fig. 6). The posterior leaflet was under relatively larger stress than the anterior leaflet at this position. The stress distribution had a similar pattern as the strain distribution in both the leaflets.

4 Discussion

With the integrated modeling platform developed in this study, we acquired 3D TEE data of a patient including the anterior and posterior leaflets, the annulus and the location of the papillary muscles to create a 3D virtual MV apparatus model. The MV leaflets geometry was segmented in a multiple number of sagittal binary images, three-dimensionally reconstructed, and meshed. The chordae tendineae were added to complete the finite element modeling of the MV apparatus. The material characteristics of the anterior and posterior leaflets were modeled as a nonlinear hyperelastic material, and successfully implemented into ABAQUS and validated by single element biaxial mechanical test simulations. Computational simulation of the MV function was performed using finite element dynamic analysis.

Even though many studies have been reported in computational simulations of the MV, most of the previous studies performed simulations with geometrically simplified models due to the complexity of the MV apparatus [18, 20-22]. Precise 3D geometry of the MV apparatus acquired from 3D echocardiography can be utilized for computational evaluation of MV functional characteristics. Computational simulation combined with 3D echocardiography can help us better understand the features of dynamic morphologic and structural alterations of the MV apparatus capturing the consequences of valve function in microseconds. Moreover, the use of patient-specific MV apparatus geometry may be a crucial factor to determine the extent and severity of abnormality of each structural component, such as extreme local stress concentration in the leaflets, annulus, or chordae tendineae during valve function. The integrated modeling platform developed in this study allows us to create a geometrical MV apparatus model from patient 3D TEE data for computationally accurate and physiologic evaluation of the MV function.

Abnormally deformed MV leaflet morphology was clearly observed in both the 3D echocardiogram and the corresponding 3D structural MV model. Validation studies of the material modeling of the MV leaflets showed good agreement between the experimental data, curve fitting data, and finite element-predicted data. Using these MV modeling techniques and material models, we were able to perform finite element dynamic analysis of the MV function of a patient. The dynamic simulation demonstrated different stress distribution patterns between the anterior and posterior leaflets. In addition, the largest stress values were observed around the self-contact regions in both the leaflets indicating that abnormal distortion of leaflet morphology could induce extremely high stress in the leaflet.

There are several limitations in the present study. Material parameters for the Fung-elastic constitutive model were determined by fitting the porcine MV tissue data. However it is not feasible to obtain material properties of patient MV tissue at present. In the future studies, we will employ improved material properties for modeling of the MV leaflets and chordae tendineae when experimental data of human tissue are available.

To our knowledge, this is the first study to conduct a computational simulation using 3D echocardiographic image data of a patient to evaluate biomechanical characteristics of the MV structure over the cardiac cycle. The presented modeling algorithm and simulation techniques can help us understand the dynamics of MV function. This computational MV evaluation strategy may provide comprehensive noninvasive imaging with valuable biomechanical information of the MV during valve function potentially improving the diagnosis and treatment of MV pathology. This methodology has the potential to quantitate the extent of disease-related functional alterations and restoration towards normal valvular function following MV repair.

5 References

[1] S. Y. Ho, "Anatomy of the mitral valve," *Heart*, vol. 88 Suppl 4, pp. iv5-10, Nov, 2002.

[2] J. Hung, R. Lang, F. Flachskampf, S. K. Shernan, M. L. McCulloch, D. B. Adams, J. Thomas, M. Vannan, and T. Ryan, "3D echocardiography: a review of the current status and future directions," *J Am Soc Echocardiogr*, vol. 20, pp. 213-233, Mar, 2007.

[3] J. Kwak, M. Andrawes, S. Garvin, and M. N. D'Ambra, "3D transesophageal echocardiography: a review of recent literature 2007-2009," *Curr Opin Anaesthesiol*, vol. 23, pp. 80-88, Feb, 2010.

[4] R. Gnyaneshwar, R. K. Kumar, and K. R. Balakrishnan, "Dynamic analysis of the aortic valve using a finite element model," *Ann Thorac Surg*, vol. 73, pp. 1122-1129, Apr, 2002.

[5] K. J. Grande, R. P. Cochran, P. G. Reinhall, and K. S. Kunzelman, "Mechanisms of aortic valve incompetence: finite element modeling of aortic root dilatation," *Ann Thorac Surg*, vol. 69, pp. 1851-1857, Jun, 2000.

[6] K. S. Kunzelman, D. W. Quick, and R. P. Cochran, "Altered collagen concentration in mitral valve leaflets: biochemical and finite element analysis," *Ann Thorac Surg*, vol. 66, pp. S198-205, Dec, 1998.

[7] G. Burriesci, I. C. Howard, and E. A. Patterson, "Influence of anisotropy on the mechanical behaviour of bioprosthetic heart valves," *J Med Eng Technol*, vol. 23, pp. 203-215, Nov-Dec, 1999.

[8] H. Kim, J. Lu, M. S. Sacks, and K. B. Chandran, "Dynamic simulation of bioprosthetic heart valves using a stress resultant shell model," *Ann Biomed Eng*, vol. 36, pp. 262-275, Feb, 2008.

[9] M. R. Aupart, D. G. Babuty, L. Guesnier, Y. A. Meurisse, A. L. Sirinelli, and M. A. Marchand, "Double valve replacement with the Carpentier-Edwards pericardial valve: 10-year results," *J Heart Valve Dis*, vol. 5, pp. 312-316, May, 1996.

[10] M. S. Sacks, "The biomechanical effects of fatigue on the porcine bioprosthetic heart valve," *J Long Term Eff Med Implants*, vol. 11, pp. 231-247, 2001.

[11] M. S. Sacks, and F. J. Schoen, "Collagen fiber disruption occurs independent of calcification in clinically explanted bioprosthetic heart valves," *J Biomed Mater Res*, vol. 62, pp. 359-371, Dec 5, 2002.

[12] S. Bhattacharya, and Z. He, "Role of annulus tension in annular dilatation," *J Heart Valve Dis*, vol. 18, pp. 481-487, Sep, 2009.

[13] B. Gao, W. Sun, S. Mathew, and Z. He, "Effects of papillary muscle position on anterior leaflet stretches under mitral valve edge-to-edge repair," *J Heart Valve Dis*, vol. 18, pp. 135-141, Mar, 2009.

[14] Z. He, and S. Bhattacharya, "Papillary muscle and annulus size effect on anterior and posterior annulus tension of the mitral valve: an insight into annulus dilatation," *J Biomech*, vol. 41, pp. 2524-2532, Aug 7, 2008.

[15] J. H. Lam, N. Ranganathan, E. D. Wigle, and M. D. Silver, "Morphology of the human mitral valve. I. Chordae tendineae: a new classification," *Circulation*, vol. 41, pp. 449-458, Mar, 1970.

[16] R. J. Okamoto, H. Xu, N. T. Kouchoukos, M. R. Moon, and T. M. Sundt, 3rd, "The influence of mechanical properties on wall stress and distensibility of the dilated ascending aorta," *J Thorac Cardiovasc Surg*, vol. 126, pp. 842-850, Sep, 2003.

[17] K. May-Newman, and F. C. Yin, "Biaxial mechanical behavior of excised porcine mitral valve leaflets," *Am J Physiol*, vol. 269, pp. H1319-1327, Oct, 1995.

[18] E. Votta, F. Maisano, S. F. Bolling, O. Alfieri, F. M. Montevecchi, and A. Redaelli, "The Geoform disease-specific annuloplasty system: a finite element study," *Ann Thorac Surg*, vol. 84, pp. 92-101, Jul, 2007.

[19] S. Kaul, "The extents of mitral leaflet opening and closure are determined by left ventricular systolic function," *Heart*, vol. 90, pp. 126-128, Feb, 2004.

[20] K. H. Lim, J. H. Yeo, and C. M. Duran, "Three-dimensional asymmetrical modeling of the mitral valve: a finite element study with dynamic boundaries," *J Heart Valve Dis*, vol. 14, pp. 386-392, May, 2005.

[21] F. Maisano, A. Redaelli, M. Soncini, E. Votta, L. Arcobasso, and O. Alfieri, "An annular prosthesis for the treatment of functional mitral regurgitation: finite element model analysis of a dog bone-shaped ring prosthesis," *Ann Thorac Surg*, vol. 79, pp. 1268-1275, Apr, 2005.

[22] V. Prot, B. Skallerud, G. Sommer, and G. A. Holzapfel, "On modelling and analysis of healthy and pathological human mitral valves: two case studies," *J Mech Behav Biomed Mater*, vol. 3, pp. 167-177, Feb, 2010.

DARS: A Discrete Event Mobile Ad Hoc Routing Simulator

S. A. Kress, K. L. May, M. E. Moorman, G. Dimitoglou
Department of Computer Science
Hood College
Frederick, Maryland 21701, USA
{sak14, klm33, mem19, dimitoglou}@hood.edu

***Abstract*—The dynamic nature of Mobile Ad Hoc Networks (MANETs) makes them difficult to design, analyze and implement. Using simulations it becomes simpler, more cost-effective and easier to test, verify and reproduce results and develop better understanding of the performance, routing and particular characteristics of MANET environments. To address this need, the Dynamic Ad hoc Routing Simulator (DARS), an open source, platform independent discrete event simulation platform was developed. One goal for DARS was to balance the need for an intuitive, simple-to-deploy and easy to use versatile tool with a feature-rich graphical user interface. Another goal was to provide the necessary extensible infrastructure to perform reliable, scalable and realistic routing simulation experiments. After achieving both of the these goals, we present the potential of DARS as a useful tool for both research and educational purposes.**

Keywords-discrete event simulation; networking; wireless networks; routing protocols; mobile ad hoc networks

I. Introduction

Mobile ad hoc networks (MANETs) are wireless collections of network nodes. They are amorphous in structure since the nodes are mobile, therefore continuously moving and changing the network topology. The proliferation of highly capable mobile devices and the ubiquity of wireless network infrastructures has made MANETs an attractive solution with widespread applications and scope. Such networks can be deployed in a range of environments, ranging from large-scale, highly dynamic networks to small-scale, power-constrained networks. Examples range from uses in the military battlefield and emergency response to gaming [15], law enforcement and commercial applications for the exchange of information between taxicabs in a vehicle ad hoc network (VANET) [7, 12].

Designing applications for MANETs presents many different opportunities and challenges. Routing is a particularly interesting area since deploying MANETs requires the use of special routing protocols that enable participating nodes to route and exchange packets. Unlike other networks, ad hoc environments do not start with, or maintain, a known topology therefore the routing protocols have to discover the environment to operate. The possible large scale of such networks, with thousands or millions of nodes, makes it necessary to have the means to simulate an environment and study the performance and behavior of routing protocols.

This paper describes the Dynamic Ad Hoc Routing Simulator (DARS) which was developed to provide a platform-independent, easy to use, reliable and extensible, routing layer discrete event simulation platform. DARS has been implemented in Java, and offers a versatile front-end user interface (UI) that provides intuitive, drag-and-drop access to the back-end simulation engine. Besides extensive logging capabilities and interactive and batch mode scenario execution, some of the key features include simulation animation, pausing and replay.

The simulator was designed to serve both as a learning tool and an experimentation platform for students and researchers alike. It includes two routing protocols: Ad hoc On Demand Distance Vector (AODV) and Destination-Sequenced Distance-Vector Routing (DSDV) and comes with extensive code and user's guide documentation to support those interested in using it or extending its capabilities by developing new protocols. This paper is organized as follows: Section 2, provides some background of MANET protocols and simulators. Section 3 includes the description of the simulation environment including the software architecture and an overview of the main features. In Section 4 a sample simulation run is described, using AODV as the routing protocol. Finally, Section 5 concludes the paper with a summary and some ideas for possible improvements and future work.

II. Background

A. Mobile Ad Hoc Routing Protocols

Mobile ad-hoc networks are wireless networks with message exchanges based on multi-hop links. The lack of any other infrastructure (ex. router or base station) requires each node to act as a router by receiving and forwarding packets to and from other nodes. The implementation of routing is based on sets of rules (a protocol) that define the necessary node mechanisms and packet propagation methods. Numerous such protocols have been developed, each using a different strategy for determining the optimal path and moving packets between source and destination nodes. Unlike non-mobile networks that may use static routing protocols, in MANETs, dynamic routing protocols are used to match the dynamic nature of the environment which manifests with continuously changing routing tables. These protocols are typically classified under two categories, *Distance Vector* and *Link-State* protocols.

Distance-vector routing requires from nodes to act as routers and periodically, or when network topology changes occur, inform their neighbors of the updated routing tables. Link-state routing protocols on the other hand require from a node acting as a router to inform all other nodes in a network of any topology changes. In MANETs, routing protocols can be further classified as on demand (reactive) and table-driven (proactive) routing protocols

Reactive protocols do not maintain routing information unless there is communication. When a node attempts to communicate with another node, then the protocol searches for the route and establishes the connection to facilitate the message exchange. This is usually achieved by flooding the network with routing requests [22]. The Ad hoc On-Demand Distance Vector (AODV) protocol is one of the most commonly studied and used distance vector, reactive protocols. Its implementation is simple, based on on-demand route discovery, route maintenance and hop-by-hop routing making it well-suited to dynamic network topologies. Some of the advantages of AODV are its simplicity and scalability to very large number of nodes due to its efficient (on-demand) bandwidth utilization and its robustness against nodes that disappear from the topology -- a common occurrence in MANETs. The limitations of the protocol are based on its inherent inability to reuse routing information, a relatively high route discovery latency due to its on-demand nature and its susceptibility to security attacks [13].

Proactive routing protocols maintain destinations and routes in routing tables before they are required and periodically distribute them to the entire network. This type of routing protocol often has the properties of link-state routing and only vary on the routing information that is being updated in each routing table. The Destination-Sequenced Distance Vector (DSDV) Routing protocol is such a protocol. Each node maintains in a routing table extensive routing and node information which is frequently advertised and either fully or incrementally transmitted to each of the node's neighbors. The design objective and advantage of DSDV was to guarantee loop-free paths [11]. Another advantage is maintaining only optimal paths instead of multiple paths to every destination. However, the continuous routing information advertising results in high bandwidth consumption, making DSDV inefficient, not scalable and not suitable for larger networks.

When comparing the two protocols it is obvious that DSDV works better in smaller networks while AODV seems more of a a general purpose protocol. Each one is a good representative of the two different classes, reactive and proactive protocols. As such, we decided to use them as the two example protocols that come with the first release of DARS.

B. Simulators

The examination of the operation and routing behavior of a real MANET can become very challenging. As topology sizes expand by including more nodes and the network structure changes as mobility increases, it becomes very difficult to obtain timely, meaningful and reproducible information from a real MANET environment. This means that the cost and difficulty of troubleshooting, verifying or improving the operation of the network also increase.

The use of simulation lends itself well when studying MANET routing protocols. This has led to the development of a number of simulation platforms varying in complexity, scope granularity and availability.

ns-2 is one of the most widely used open-source discrete event network simulators in the research community. It is based on the OSI model and was designed to simulate wired networks. Support for wireless networks and mobility models has been introduced either as extensions or by integration with other projects (i.e. CMU Monarch Project [20], Blueware [3], Graph Mobility project [21] and Obstacle Mobility [9]).

GloMoSim [23] is the second most popular open-source, discrete-event, OSI standard compliant, wireless network simulator. It is based on message-passing and was written in Parsec, a C-based simulation language [2]. While new protocols and modules have to be written in Parsec, the simulator has also been enhanced by the integration of external projects (i.e. Obstacle Mobility [9]) that have increased its usefulness. The lack of GloMoSim good documentation and a user interface has been addressed by QualNet [16], a commercial ad hoc network simulator that supports and extends protocols and models offered in GloMoSim.

Another commercial discrete-event network simulator is OPNet [6]. Written in C++ it offers a mature user interface, concurrent simulation scenarios execution and it supports an extensive list of protocols There are other simulators, such as J-Sim [10, 18], OMNet++ [8], GTNets [17], each offering a variety of models, options and features but they have received less attention by practitioners and researchers.

From the leading simulators, *ns-2* is powerful but complex, not very modular and computationally intensive. GloMoSim has poor documentation and was developed using Parsec [2], a non-mainstream programming language which makes its adaptability and use in the classroom less attractive. Overall, many of the community developed and open source simulators tend to lack good documentation and support. Commercial simulators mitigate these shortcomings but they are closed source and often less flexible in extending their capabilities.

Given the breadth and complexity of MANET simulation, we realized that it would be too ambitious to attempt to develop an all encompassing simulation platform that would mitigate all the issues with existing simulators. Inspired by the development of the AODV Simulator [19], we decided to focus on creating an extensible infrastructure that is focused on the simulation of MANET routing algorithms and protocols.

III. Simulation Environment

A. Software Architecture

DARS has been designed to enable users to interactively experiment with routing protocols, devise their own mobile topologies, develop communication scenarios and examine the generated network behavior.

The architecture of DARS is based on a two-tier architecture. The first tier is the graphical user interface (GUI) which enables users to interact with the simulator while also providing the simulation animation rendering capabilities. The second tier is the simulation's main tier which includes an Event Handler module, the Simulation engine, a Node/Protocol

Interface Module, a Logging System and an an Error Handler module.

The Event Handler acts as a bridge between the tiers. It processes user events that occur on the GUI and is designed to interact with any GUI front-end that can generate and pass the necessary user events to the Simulation Engine. The Simulation Engine is the simulator's core component which performs the necessary discrete event computations and provides the necessary internal coordination, processing and replay capabilities The Node/Protocol Interface is designed to interact with the different routing definitions that describe how each protocol deals with node communication, path selection, and message exchanges. Finally, the Logging System creates a time-ordered record of all events and activities that take place during a simulation execution.

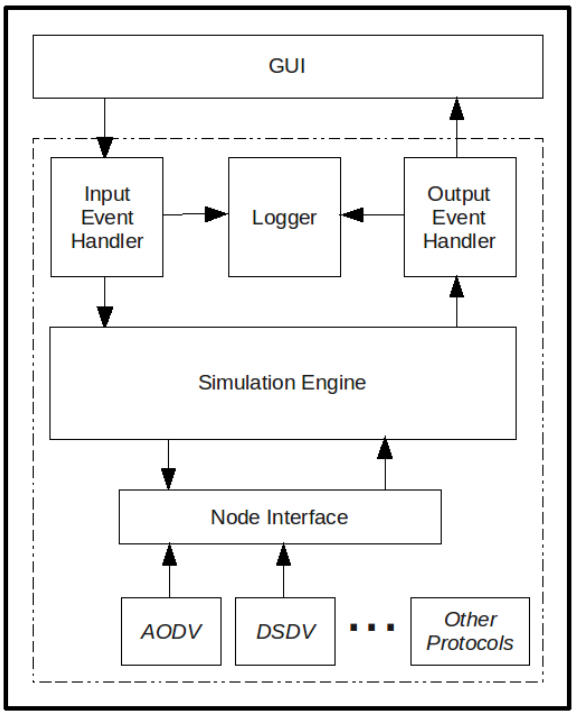

Figure 1. The DARS two-tier software architecture and its modules.

B. Features

DARS was developed as a platform independent application with three distinct overarching objectives.

First, to provide the necessary extensible infrastructure to perform reliable, scalable and realistic routing simulation experiments.

Second, to enable users via a GUI to setup, configure, and access both the simulation parameters and execution results.

Third, to provide a a user-friendly and intuitive GUI that could animate the routing process and provide to the user all the necessary information, including error handling, to assess the progress of the simulation. Following are some of the features and capabilities provided in DARS:

- **Intuitive Interface with Realistic Visualizations.** The DARS GUI provides a set of easy to use interface controls with drag-and-drop functionality, menu-driven navigation and keyboard shortcuts, giving easy access to topology configuration and node parameters. Distinct canvas areas enable users to focus on the GUI area of interest. The top area of the interface contains simulation control buttons and sliders. The middle (main) canvas area is where the network topology is configured and displayed During a simulation session, this graphic display provides the real-time animation of the MANET. The animation feature, while computationally intensive, provides a realistic view of the network. For larger networks, users have the option to disable the animation and conserve resources. The bottom canvas area is the DARS logger console, displaying detailed, timestamped, text-based information of the session in progress.
- **High Granularity of Node Control.** DARS allows the user to add, edit attributes and remove single or multiple nodes before and even during the simulation execution.
- **Flexible Topology Configuration.** Users, using drag-and-drop operations on the GUI, have complete freedom to setup, edit, save for later use and remove network topologies of any configuration. Node location and parameters are customizable and it is also possible to deploy random topologies with multiple nodes. Node parameters can be set manually or automatically for single or multiple nodes, or group of nodes using random but valid data within ranges.
- **Extensive Logging Capabilities.** DARS provides both real-time and off-line detailed logging of all events that take place at each increment of the simulation session including the state of each node and all the transmitted messages. The generated, verbose logs can be displayed on the GUI and filtered out according to the desired level of detail. These filtering options provide an invaluable tool for real-time monitoring and post-session analysis.
- **Simulation Replay.** The logs are constructed in such a way that can be later reloaded on DARS and have an exact replay of a previously executed simulation. During the replay, users are able to interact in real-time with the simulation, change and manipulate parameters to obtain different information.
- **Multiple Simulation Execution Modes and Real-Time User Interaction.** In interactive mode, users can, during an active simulation session make any number of changes in the simulation parameters (e.g. simulation speed), the network topology, node properties or even add messages to be transmitted between nodes. It is also possible to pause an active session, make changes and then resume the simulation with the new changes going into effect. In batch mode, a user may reload an existing simulation session and just execute it from start to finish. In blended mode, the user may begin by loading a previously executed session but the user elaborates upon the loaded configuration by changing node or topology parameters.
- **Real Time Routing Tables.** DARS provides the ability to look at any nodes routing table at every given point during the simulation. The routing table will dynamically change based on the surrounding topology and the given protocol in use. Multiple routing tables can also be displayed simultaneously.

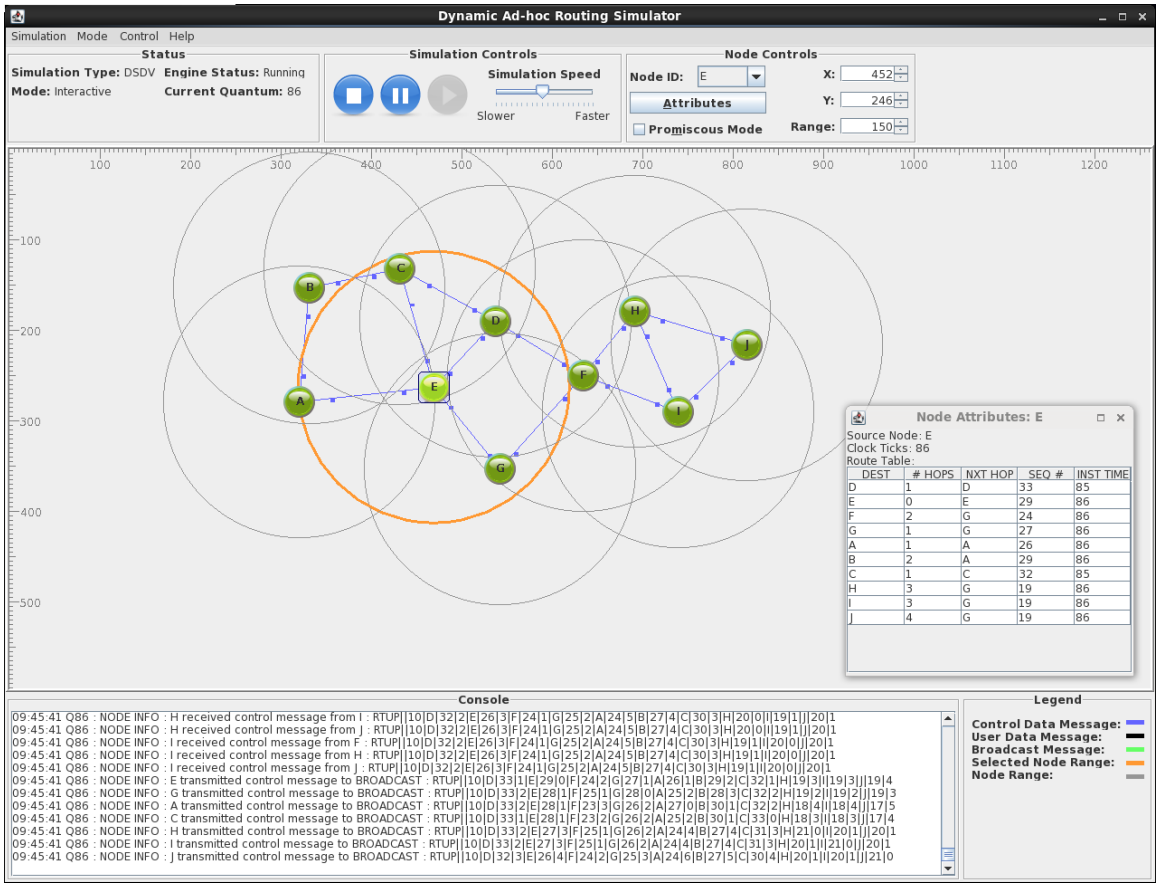

Figure 2. The DARS GUI consists of three panes: (a) the top pane which has simulation controls, (b) the middle pane which displays the network topology and the simulation animation during execution, and (c) the bottom pane which shows the real-time simulation log entries.

- **Extensibility via an exposed Application Programming Interface (API).** The DARS architecture is modular and has been designed to allow users to extend the system both in the front and the back-end. The GUI module can be easily changed or even replaced with a completely different interface. Similarly, users are able to extend the two current available classes of protocol types (one proactive and one reactive) by adding more protocols within these two classes (e.g. Clusterhead Gateway Switch Routing [5], Distributed Bellman-Ford Routing Protocol [4], Hierarchical State Routing [14], Robust Secure Routing Protocol [1] etc) or by adding a new protocol class type (e.g. adaptive, flow-oriented, power aware, etc.). Adding a protocol is simple, well-documented and requires just three steps: (a) using a "Node Factory" class to create a new node, (b) extending a "Node Class" to actually implement a protocol and (c) creating a dialog box that describes the node attributes.

IV. Experimentation with DARS: AODV

To exercise the features of DARS, two protocols have been included with the initial release: AODV and DSDV.

Fig. 3 shows an animation snapshot of the main pane from the execution of the AODV routing protocol.

In this instance, ten mobile nodes were deployed. The circles around the nodes represent the communication signal strength and the lines connecting the nodes indicate that route connectivity has been established between nodes and messages can be exchanged. Users have the ability to display in real-time the routing table information of any node on the network. In AODV, routes are discovered on an "as-needed" basis and only a limited horizon of one hop is maintained instead of the entire route.

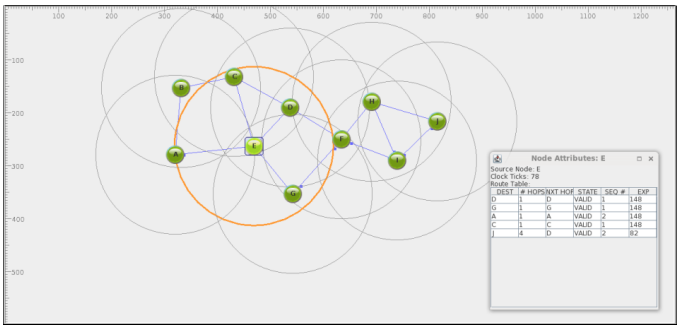

Figure 3. A snapshot of an AODV-based MANET simulation execution with ten nodes.

The numbered tick marks on the left and top side of the pane are used to provide coordinate information on the location of a node. While in this example the particular network is very small in size and the location of the nodes is obvious, DARS can accommodate network topologies with thousands of nodes, exchanging large numbers of messages.

V. Conclusion and Future Work

Simulations are very useful to understand and examine issues in mobile ad hoc networks. A variety of simulation platforms exist but the majority were developed for wired network topologies. The proliferation of interest in wireless networks has generated the need to enhance these platforms and extend them in order to accommodate network node mobility. Some of these platforms have been successful in attracting MANET researchers but each platform seems to have its own shortcomings. The most common limitation is the increased complexity of many platforms or the difficulty in extending features and capabilities.

We developed DARS, a discrete event simulator, with the goal of creating a versatile, extensible and scalable but simple to use simulation platform. For the first release we included two routing protocols to ensure the feasibility of running MANET topologies on the simulator. Preliminary results are very encouraging and DARS has met the original software requirements and will hopefully also meet the requirements of a wider user base.

For the immediate future, there are numerous potentially interesting areas of work. First, it would be useful to have a verification study that would evaluate and benchmark DARS against certain criteria and against other simulation platforms that can handle the mobility and dynamism of ad hoc networks. Second, the usefulness of DARS will increase if more routing protocols are added to the existing suite. A geographically aware and a secure routing protocol would be two desirable top candidates that could enrich the current version of the simulator. Third, it would be very beneficial to conduct a performance study with extensive testing in order to establish the extent of the capabilities of the software and the physical requirements and boundaries (e.g. RAM, CPU) imposed by hardware. Currently, only anecdotal evidence of preliminary load and stress testing results have indicated that DARS scales well (thousands of nodes) but a more systematic and comprehensive analysis should be undertaken.

Overall, DARS seems to have fulfilled the motivating objective of creating an intuitive, versatile and extensible simulation tool for mobile ad hoc networks. The software source, documentation and executables for various platforms can be found on the project page at: http://dars.sourceforge.net/

References

[1] Afzal, S.R., Biswas, S., Koh, J., Raza, T., Lee, G. and Dong-kyoo Kim, RSRP: A Robust Secure Routing Protocol for Mobile Ad hoc Networks, Proceedings of Wireless Communications and Networking Conference, 2008. WCNC 2008. IEEE, pp. 2313-2318, March 31 2008-April 3 2008.

[2] Bagrodia, R., R. Meyer, M. Takai, Y., Chen, X. Zeng, J. Martin and H. Y. Song, Parsec: A parallel simulation environment for complex systems, Computer 31 (1998), pp. 77–85.

[3] Barr, R., (2002) Blueware: Bluetooth simulator for ns, Technical report, MIT, Cambridge (2002).

[4] Bartsekas, D. P., Gallagher, R.G. (1987) Distributed Asynchronous Bellman-Ford Algorithm, Data Networks, pp. 325-333, Prentice Hall, Enlgewood Cliffs, 1987, ISBN 0-13-196825-4.

[5] Ching-Chuan Chiang, Hsiao-Kuang Wu, Winston Liu, Mario Gerla (1997) Routing in Clustered Multihop, Mobile Wireless Networks with Fading Channel, IEEE Singapore International Conference on Networks, SICON'97, pp. 197-211, Singapore, 16.-17. April 1997, IEEE.

[6] Desbrandes, F., S. Bertolotti and L. Dunand, Opnet 2.4: An environment for communication network modeling and simulation, in: Proceedings of European Simulation Symposium. Society for Computer Simulation, 1993, pp. 64–74.

[7] Giordano, S. (2002) Mobile Ad Hoc Networks, in Handbook of Wireless Networks and Mobile Computing (ed I. Stojmenović), John Wiley & Sons, Inc., New York, USA. doi: 10.1002/0471224561.ch15

[8] Imre, S., Keszei, Horv´ath, Holl´os, Barta and Kujbus, Simulation environment for ad-hoc networks in OMnet++, in: IST Mobile Summit 2001, 2001, pp. 135–140.

[9] Jardosh, A., E. M. Belding-Royer, K. C. Almeroth and S. Suri, Towards realistic mobility models for mobile ad hoc networks, in: MobiCom '03: Proceedings of the 9th Annual International Conference on Mobile Computing and Networking (2003), pp. 217–229.

[10] J-Sim, http://sites.google.com/site/jsimofficial/, (visited 20-March-2011).

[11] Perkins, C. E. and Bhagwat. P. (1994). Highly dynamic Destination-Sequenced Distance-Vector routing (DSDV) for mobile computers. In Proceedings of the conference on Communications architectures, protocols and applications (SIGCOMM '94). ACM, New York, NY, USA, 234-244.

[12] Perkins, C.E. (2001). Ad hoc networking: an introduction. In Ad hoc networking. Addison-Wesley Longman Publishing Co., Inc., Boston, MA, USA 1-28.

[13] Ning.P. and Sun.K. (2003) How to misuse AODV: A case study of insider attacks against mobile ad-hoc routing protocols. Technical report, Comput. Sci. Dept., North Carolina State Univ., Raleigh, NC, USA, 2003.

[14] Guangyu Pei and Mario Gerla and Xiaoyan Hong AND Ching-Chuan Chiang, A Wireless Hierarchical Routing Protocol with Group Mobility, IEEE WCNC'99, New Orleans, USA, September 1999.

[15] Riera, S. M., O. Wellnitz and L. Wolf, (2003) A zone-based gaming architecture for ad hoc networks, in: NETGAMES '03: Proceedings of the 2nd workshop on Network and system support for games (2003), pp. 72–76.

[16] QualNet, http://www.scalable-networks.com/, (visited 25-March-2011).

[17] Riley, G. F., The Georgia Tech network simulator, in: MoMeTools '03: Proceedings of the ACM SIGCOMM workshop on Models, methods and tools for reproducible network research (2003), pp. 5–12.

[18] Sobeih, A., Wei-Peng Chen, Jennifer C. Hou, Lu-Chuan Kung, Ning Li, Hyuk Lim, Hung-Ying Tyan and Honghai Zhang, J-Sim: A Simulation and Emulation Environment for Wireless Sensor Networks, in the IEEEWireless Communications Magazine, August 2006.

[19] The AODV Simulator, http://aodvsimulator.sourceforge.net/, (visited 25-March-2011).

[20] The CMU Monarch Project's Wireless and Mobility Extensions to NS. (1998), http://www.monarch.cs.rice.edu/, (visited 25-March-2011) .

[21] Tian, J., J. Hahner, C. Becker, I. Stepanov and K. Rothermel, (2002) Graph-based mobility model for mobile ad hoc network simulation, in: Annual Simulation Symposium, 2002, pp. 337–344.

[22] Tseng Y.C., Shen C.C, and Chen W.T. (2003) Mobile IP and ad hoc networks: An integration and implementation experience. Technical report, Dept. of Comput. Sci. and Inf. Eng., Nat. Chiao Tung Univ., Hsinchu,, Taiwan, 2003.

[23] Zeng, X., R. Bagrodia and M. Gerla, Glomosim: A library for parallel simulation of large-scale wireless networks, in: Workshop on Parallel and Distributed Simulation, 1998, pp. 154–161.

Real Time Simulation for the Optimisation of Asset Management and Production Operations

J. Baulch[1] **and Dr. E. van Voorthuysen**[2]
[1]School of Mechanical and Manufacturing Engineering, University of New South Wales, Sydney, New South Wales, Australia
[2]School of Mechanical and Manufacturing Engineering, University of New South Wales, Sydney, New South Wales, Australia

Abstract - In today's highly competitive manufacturing environment, businesses are constantly exposed to a level of commercial risk. This level of risk is influenced by market trends, actions of competitors and operational decisions made within the company itself. The repercussions of some internal decisions can be quite damaging financially, for example lost sales. One area that continues to be problematic is the reliability of critical assets.

With increasingly sophisticated simulation platforms, it is possible to build models that closely mimic the behavior of complex systems to predict future performance and the associated costs based on historical failure data and current process data. Users are then able to make critical operational decisions in real time, for example, repair versus replace, when to maintain and overhaul, improvement action, level of resources required both human and in terms of machine spares and rescheduling of maintenance and production to meet additional orders.

A simulation model has been developed as part of a case study to be used for operational decision support of a complex food processing line.

Keywords: Simulation, Asset Management, Reliability, Operations, Optimisation

1 Introduction

Simulation is being used increasingly to assess a range of outcomes associated with a specified change to a system. Traditionally discrete event simulation has been used to explore how physical changes to a system associated with revision and redesign of plant layouts affect production output, the optimization of spares and human resource scheduling, the investigation and improvement of processes and procedures and of course, the optimization of maintenance strategies.

In the majority of today's industries organizations are forced to deal with multiple concurrent strategies, market and competitive influences, changes in regulations for example OH&S or environmental and technological trends and advances. As part of the asset management strategy there are many operational decisions associated with these forces that need to be made over a variety of time frames including very short term opportunistic decisions to long-term improvement and replacement decisions. It is a key objective to be able to predict the likely outcome or range of outcomes that may result from changes in these influences or actions and build a business case to support the associated investment decisions. Decisions are then made based on the most likely and economically beneficial outcome in terms of return and net present value. The competitiveness of a company is directly affected by its ability to optimize equipment lifecycles and the associated costs.

Traditionally companies have avoided investment in maintenance on the basis that it has been difficult to predict the benefit of investment in maintenance and process improvement. The proposed solution is an adaptive simulation tool that can be used in real time to predict various outcomes by mimicking the performance, behavior and condition of the assets in a variety of operational and commercial scenarios. This simulation model is to be coupled with a real time reliability and performance monitoring system. The simulation model is adaptive in the sense that the internal and external conditions are not static; rather the environment and problem itself are dynamic. To confidently generate accurate forecasts the user must recognize this and be aware that the variables that drive the model are continuously updated when new information becomes available. This allows the user to analyze proposed changes to maintenance activities and strategies or system parameters and gain more likely outputs for performance and return.

It is an operationally strategic priority for a company to monitor reliability and condition of critical components in real time based on units of usage or output in order to confidently forecast and ultimately prevent forthcoming failures in a cost efficient manner. A major constraint in achieving this is the volume of data that must be managed to drive the model. In order to sustain the flow and integrity of the data a custom built Excel based user interface will monitor the reliability profile of critical assets and ultimately feed this information into the simulation model.

The capability of this model is driven in part by what the industrial partners of this project require and in part by the increased degrees of freedom established by the unique

information and knowledge that can be extracted from historical, current and forecasted data. Currently most models in literature focus on one area, maintenance strategies. This model has been designed so that the main simulation engine can be used to predict outcomes minimize the amount of commercial risk that a company can expose itself to for a number of operational decisions such as changes to production, maintenance schedules or operating procedures. In addition to this it is designed with an interface to eliminate the complexities of simulation from the investigative process, as most users will not be experts. This essentially presents the user with a push button system that generates the specific output required to make decisions on the fly.

An asset management case study is currently underway where the fore mentioned model is being developed and tested to assist with the operational decision making of a high-speed food processing line.

2 Literature Review

Simulation models built to mimic and explore maintenance activities have been widely reported in literature and cover a diverse range of specific purposes. These include the following;

- Maintenance planning and scheduling ([1] – [6])
- Evaluation of maintenance and replacement strategies ([7] – [13])
- Repair capacity ([14])
- Shutdown strategy ([15])
- Inventory and stores management ([3], [9] and [16])
- Maintenance staffing ([17] – [19])

Although there have been many different ideas and models proposed regarding maintenance and its functional areas there are some common findings amongst the large majority of authors.

- Common rationale
  - Optimisation of maintenance activities
  - Optimisation of key maintenance functions
  - Optimisation of scheduling maintenance activities
  - Minimizing the costs associated with maintenance
  - Aim to improve productivity, availability, reliability and throughput
- A short-term focus: The models appear to be used to offer a solution for a current scenario.
- Dynamic behavior is largely ignored. This coincides with short-term focus.

At the time that these models were built they may have been more than suitable for the purpose and business drivers of that era. However, due to tougher financial and production demands, both internal and external to the organization there is a need for adaptive real time simulation based decision tools with a wider operational and long term focus. Critical operational decisions and strategies need to be made and reviewed on a regular basis due to frequently changing customer demands and production requirements.

3 The Model

As part of the asset management and process improvement process and ultimately as part of the decision and simulation modeling process it is critical to know what data is required to drive the model and how to analyze this data to make it useful in a simulation model. Following this it is important to realize what information and in turn what knowledge is created by this analysis. This will then create understanding about the problem, its solution(s) and associated risks that will allow for informed decisions to be made, ones that have been tested in a simulated environment (Fig 1). This process is critical for determining where issues may lie within a system and generating a solution for these issues. An example is failure data leading to the derivation of the failure PDF and in turn being able to forecast future failures. It is important to realize that the reverse of this process can also work. In other words, when a level of performance of the system is desired the model can suggest the required level of reliability and capability of critical subsystems and components. The user can decide whether or not to pursue the proposed improvements and the best method to achieve these.

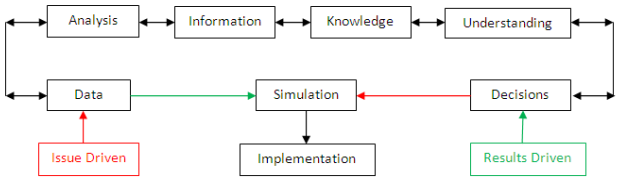

Fig. 1. The process used for understanding and decision support for both issue driven and results driven problems.

The model that has been built is largely driven by the reliability of the critical assets and their physical layout. Raw failure and process data is collected for each of the major assets. The failure data is then analyzed using the Weibull distribution to quantify the stochastic and dynamic behavior of the assets. The critical modules and sub-modules are then statistically and mathematically characterized in terms of reliability and performance based on historical and current process data. This analysis can highlight areas of undesirable performance, whether it is related to failures, capacity or capability. Fig. 2 outlines this process. The production line to be simulated consists of seven major assets that can be

configured ten different ways to process five different product categories. A schematic of the line is shown in Fig. 3.

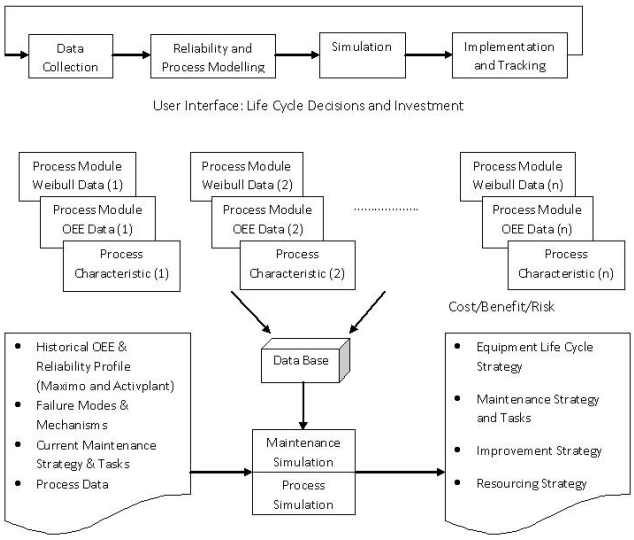

Fig. 2. The continuous process for reliability improvement driven by the simulation of maintenance strategies and production operations.

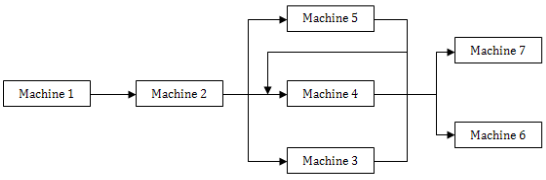

Fig. 3. The schematic of the production line. This line can be set up in ten different configurations depending on the batch type and volume required. For the purpose of confidentiality the assets are referred to by a pre allocated numbering system.

The logic map (Fig. 4) shows the flow of events and how and where assets are seized for maintenance activities or failure repairs. The model is programmed to remove failures from the failure queue when the associated maintenance task has been completed and vice versa. The purpose of this is to reset the failure distribution after maintenance or repair just as in real life. The user will have the ability to add, remove and alter maintenance plans and tasks within the model to represent changes in current maintenance strategies over time.

It is critical for the user to be able to anticipate the level of asset utilization. This level of utilization is associated with a particular amount of investment on maintenance strategies. It is important for the user to be able to determine when to cease spending on maintenance in terms of which tasks are carried out and how frequently. It is expected that this will vary throughout the year in line with the amount of demand and utilization of the asset. A chart mapping the ratio of asset reliability to maintainability versus asset availability can be plotted (Fig. 5). The marginal return of the extra investment in reliability and maintainability decreases to a point where it is no longer economical to continue investment to achieve a higher level of availability. The simulation model will be used in conjunction with this analysis with the aim of optimizing the amount of investment on maintenance with respect to the desired level of availability throughout periods of varying demand.

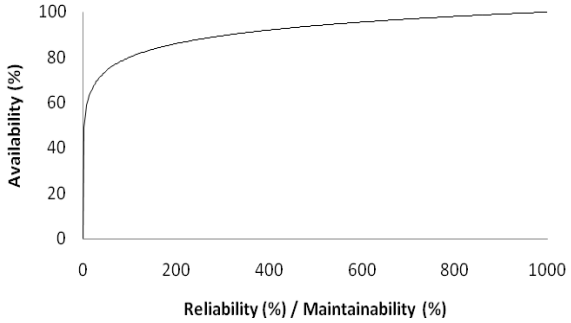

Fig. 5. The ratio of asset reliability to maintainability versus asset availability (adopted from [22]). By strategically positioning the asset on the curve a business will be able optimize the level of investment in maintenance strategies through periods of fluctuating demand.

The user can also investigate operational decisions associated with production. By adjusting the production schedule the user will be able to estimate the level of production that can be achieved and can determine when urgent orders added to the schedule are expected to be completed and how the remaining production will be affected.

If equipment modifications, upgrades and replacements are to be investigated the user can adjust the process inputs for the particular asset and be able to estimate a range of outcomes based on the expected performance improvements. In addition to this the user can determine if adjustments will be required to other assets so that bottlenecks and other flow issues on the line can be identified and plans can be devised to try and prevent these potential flow issues. The additional changes can be made to the model and re-simulated so management is able to make informed decisions about how to implement new equipment and manage the existing equipment to maximize output and avoid potential issues.

A range of inputs was entered into the model to test the accuracy of the simulation engine. These inputs included a typical production schedule based on historical production figures, which in turn influences asset utilization, historical failures distributions, process abnormalities and a typical maintenance schedule. Other data included machine processing speeds, conveyor speeds and lengths to maintain an accurate buffer between processes, a level of quality, the number of machine operators and maintenance personnel required for the production line.

The model has been tested against one year of historic data to validate the simulation engine. A total of fifteen yearlong cases were run with a warm-up time of five hundred hours. The results of the simulation came out very close to the real

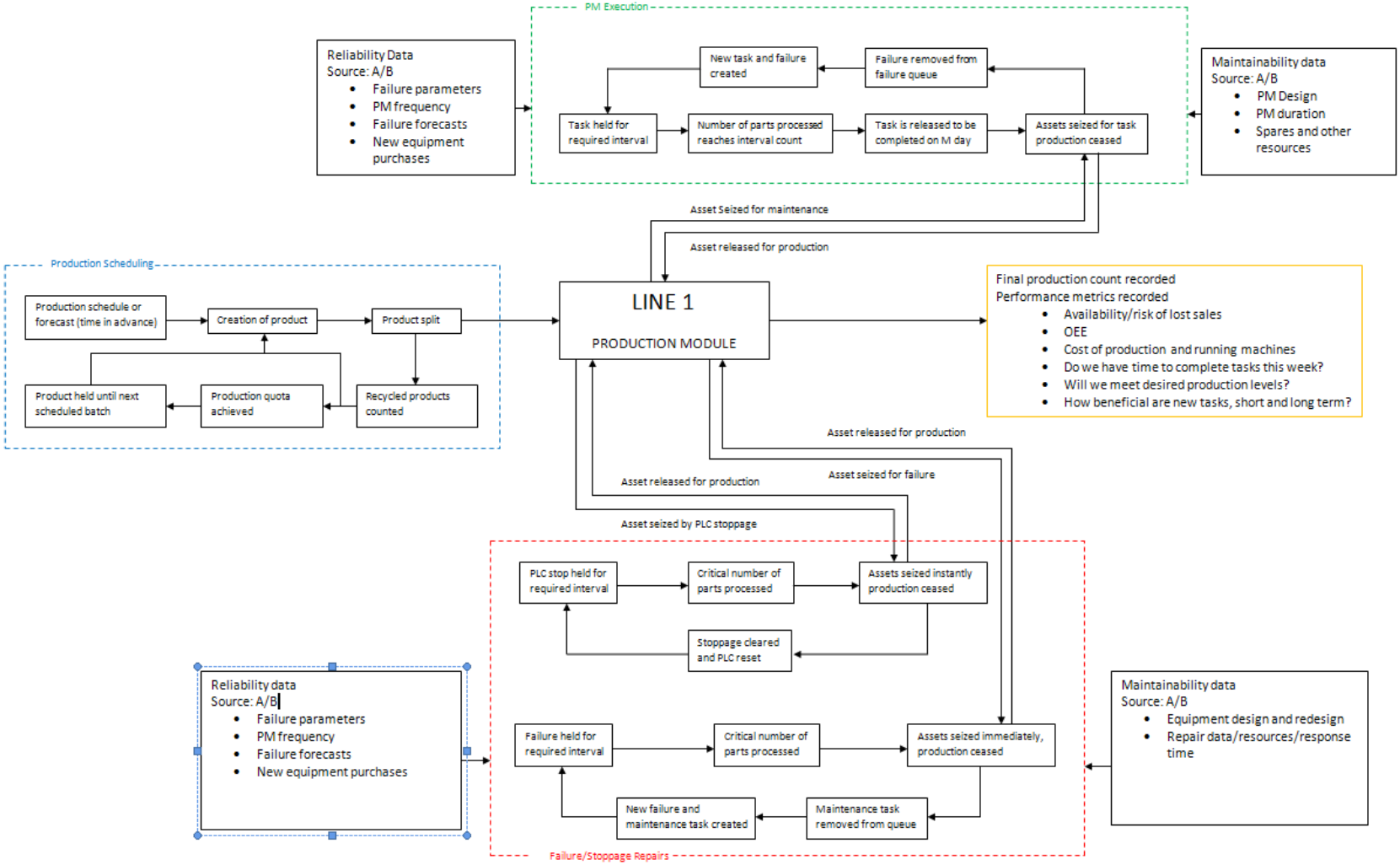

Fig. 4. The simulation logic map outlines how and what causes events occur during the simulation, examples of the input required and output to be assessed (input data sources have been withheld for the purpose of confidentiality).

output. The mean error between the simulated cases and the real output was less than one percent. The causes for this small error have been narrowed down to the use of average production schedules and likely slight differences in machine speed settings. This is supported by the average machine utilization generated by the model over the twelve-month simulated period (Table 1).

TABLE I
A COMPARISON OF SIMULATED MACHINE AND REAL MACHINE UTILIZATION

Asset Number	Simulated Utilization (%)	Real Utilization (%)
M1	39.7	38.3
M2	41.7	39.0
M3	18.2	18.0
M4	14.3	12.3
M5	31.7	31.1
M6	17.8	20.9
M7	31.6	35.7

The results of the simulation show that the model is an accurate representation of the real system and hence allows this model to be used as a realistic engine for the purpose of predicting future outcomes in terms of maintenance and improvement decisions. The model will be able to be used to predict outcomes for decisions to be made over the short, medium and long terms. In the short term it will be used for the scheduling and management of critical PMs, investigating opportunistic maintenance decisions, scheduling of urgent corrective or production work, re-routing and re-prioritizing production. Short-term maintenance costs can then be minimized and in turn the level of commercial risk can be estimated and managed. Medium term decisions regarding machine utilization, upgrades and redesign of equipment and redesign, addition, removal and the frequency of PMs can be considered. These decisions are directed towards the long-term reliability, performance and capability of the equipment in addition to managing maintenance costs and commercial risk. In the long term the user may need to investigate the replacement of these machines and commissioning of new equipment in order to maintain levels of return and system performance in addition to changing demand and product specifications.

4 Conclusion

Although a large number of simulations models have been reported in literature that are used to solve maintenance and maintenance sub functional issues it is clear that there is a need for adaptive operational driven simulation models that have a wider and longer focus on decisions that can shape the way a company may conduct its business in the short, medium and long terms. In addition it is evident that there is a need for simulation based decision tools that can be used in real time to assess various decisions shortly before they need to be made.

A validated and verified simulation engine has been presented that is capable of tackling the various dynamic scenarios that a business may face throughout time. Through the use of this simulation tool the user will have the ability to assess various scenarios faced and choose the best path that will generate the business the greatest ROI, optimized OEE and expose the business to a minimal amount of commercial risk.

5 Acknowledgment

The authors would like to thank the commercial partner of this project (for the purpose of confidentiality the business will not be named) for continual support throughout the duration of the case study.

6 References

[1] Y. Sun, "Simulation for Maintenance of an FMS: An Integrated System of Maintenance and Decision Making," *International Journal of Advanced Manufacturing Technology*, vol. 9, no. 1, pp 35-39, Jan. 1994.

[2] S. Duffuaa & A. Andijani, "An Integrated Simulation Model for Effective Planning of Maintenance Operations for Saudi Arabian Airlines (SAUDIA)," *Production, Planning and Control*, vol. 10, no. 6, pp. 579-584, Sep. 1999.

[3] S. Duffuaa, M. Ben-Daya, K. Al-Sultan & A. Andijani, "A Generic Conceptual Simulation Model for Maintenance Systems," *Journal of Quality in Maintenance Engineering*, vol. 7, no. 3, pp 207-219, 2001.

[4] R. Mortenson, "Maintenance Planning and Scheduling using Network Simulations," *Proceedings of the 1981 Winter Simulation Conference*, pp. 333-340, 1981.

[5] A. Ali, X. Chen, Z. Yang, J. Lee & J. Ni, "Optimized Maintenance Design for manufacturing Performance Improvement Using Simulation," *Proceedings of the 2008 Winter Simulation Conference*, pp. 1811-1819, 2008.

[6] N. Brown & S. Powers, "Simulation in a Box (A Generic Reusable Maintenance Model)," *Proceedings of the 2000 Winter Simulation Conference*, pp. 1050-1056, 2000.

[7] F. Azadivar & J. Shu, "Use of Simulation in Optimization of Maintenance Policies," *Proceedings of the 1998 Winter Simulation Conference*, pp. 1061-1067, 1998.

[8] M. El Hayek, E. van Voorthuysen & D. Kelly, "Optimizing Life-Cycle Cost of Complex Machinery with Rotable Modules using Simulation," *Journal of Quality in Maintenance Engineering*, vol. 11, no. 4, pp. 333-347, 2005.

[9] M. El Hayek, "Optimizing Life-Cycle Maintenance Cost of Complex Machinery Using Advanced Statistical Techniques," Ph.D. Thesis, School of Mechanical and Manufacturing Eng., Univ. of New South Wales, Sydney, Australia, 2006.

[10] Roux, O., Jamali, M., Kadi, D. & Châtelet, E. (2008). "Development of Simulation and Optimization Platform to Analyze Maintenance Policies Performances for Manufacturing Systems," *International Journal of Computer Integrated Manufacturing*, vol 21, no 4, Jun, pp. 407-414.

[11] A. Oyarbide-Zubilliga, A. Goti, & A. Sanchez, "Preventive Maintenance Optimization of Multi-Equipment manufacturing Systems by Combining Discrete Event Simulation and Multi- Objective Evolutionary Algorithms," *Production*, 355, 2008.

[12] W. Yun, I. Moon and G. Kim, "Simulation-Based Maintenance Support System for Multi-Functional Complex Systems," *Production, Planning and Control*, vol. 19, no. 4, pp. 365-378, Jun, 2008.

[13] R. Harvey, D. McElveen, P. Miyares & T. Schuppe, "C-141 Depot Maintenance: Using Simulation to Define Resource Requirements," *Proceedings of the 1992 Winter Simulation Conference*, pp. 1145-1152, 1992.

[14] R. Gatland, E. Yang & K. Buxton, "Solving Engine Maintenance Capacity Problems with Simulation," *Proceedings of the 1997 Winter Simulation Conference*, pp. 892-899, 1997.

[15] J. Mathew & C. Rajendran, "Scheduling of Maintenance Activities in a Sugar Industry using Simulation," *Computers in Industry*, vol. 21, no. 3, pp. 331-334, Apr, 1993.

[16] R. Sarker & A. Haque, "Optimization of Maintenance and Spare Provisioning Policy using Simulation," *Applied Mathematical Modeling*, vol. 24, no 10, pp. 751-760, Aug, 2000.

[17] E. Mjema, "An Analysis of Personnel Capacity Requirement in the Maintenance Department by using a Simulation Method," *Journal of Quality in Maintenance Engineering*, vol. 8, no. 3, pp. 253-273, 2002.

[18] F. Shin, B. Ram, A. Gupta, X. Yu & R. Menassa, "A Decision Tool for Assembly Line Breakdown Action," *Proceedings of the 2004 Winter Simulation Conference*, pp. 1122-1127, 2004.

[19] Q. Chang, J. Ni, P. Bandyopadhyay, S. Biller & G. Xiao, "Maintenance Staffing Management," *Journal of Intelligent Manufacturing*, vol. 18, no. 3, pp. 351-360, Jun, 2007.

[20] E. J. Van Voorthuysen & R. A. Platfoot, "Flexible data acquisition system to support process identification and characterization," *Proceedings of the Institution of Mechanical Engineers, Part B: Journal of Engineering Manufacture*, vol. 214, no. 7, pp. 569-579, 2000.

[21] E. J. Van Voorthuysen & R. A. Platfoot, "Process Improvement Planning Using Path Modelling and Simulation," *Proceedings of the Institution of Mechanical Engineers, Part B: Journal of Engineering Manufacture*, vol. 215, no. 8, pp. 1107-1115, 2001.

[22] M. J. Neale, *Component Failure, Maintenance and Repair*, Butterworth and Heinemann. Oxford, 1995.

Implementing a Flexible Simulation of a Self Healing Smart Grid

Kendall E. Nygard, Steve Bou Ghosn, Davin Loegering,
Md. Minhaz Chowdhury, Md. M. Khan, Ryan McCulloch,
Anand Pandey
Department of Computer Science
North Dakota State University
Fargo, ND, USA
{Kendall.Nygard, Steve.Boughosn, Davin.Loegering, Md.
Chowdhury, Mahbuburrahman.Khan, Ryan.Mcculloch,
Anand.Pandey}@ndsu.edu

Prakash Ranganathan
Department of Electrical Engineering
University of North Dakota
Grand Forks, ND
prakashranganathan@mail.und.nodak.edu

Abstract—We describe the design and implementation of an agent based simulation for a smart grid. The design supports the evaluation of procedures for self healing.

The main design goal is to support the testing and comparing of alternative decision models that can specify grid-management actions that can be applied in scenarios that call for self healing. We first describe the agent and decision model design of our simulation .We thenpresent the main features and innovations of our simulator, including such as respresenting the topology of the power grid, flexibility of the design, dynamic agent generation,scalability, and decision model independence. We also describe our work in progress.

Keywords- Multi-agent System; SmartGrid; Distributed computing; intelligent systems; Self-healing

I. INTRODUCTION

Agent-oriented software designs provide multiple advantages in Smart Grid simulations [1]. This type of design involves multiple interacting agents at supervisory and subservient levels, where each device, assessment, prediction, modeling, response, and decision-making procedure is associated with an agent. The agents are distributed, communicate and collaborate with each other, and take automatic actions to correct problematic conditions in the electrical grid. Our agent-oriented design is also scalable, with inherent provisions for handling distributed systems that are larger and more complex than those currently modeled.

There have been previous efforts to create simulation systems for a smart grid environment [2] [3][4]. In [2] the authors created a hardware simulation of a simple microgrid using MATLAB and Simulink to implement the functionality of low level electric circuits. They basically established the viability of an intelligent distributed autonomous system with autonomous agents that model a microgrid. Their agent implementation was very rudimentary, involving voltage monitoring to activate circuit breakers and to secure critical loads. The work was the advancing of a concept, with little agent interaction, analysis or evaluation. They did establish that a microgrid can be managed as part of the global grid and can work autonomously in islanded mode. In [3] an adaptive self-healing framework for power grids based on intelligent agent technologies is proposed, but the work did not into a working simulation. In [4], a promising flexible agent based simulation of a dynamic smart city is described.

The primary Smart Grid issues that can be addressed using the simulator are as follow:

- Which types of decision models are the most appropriate for handling self healing for specific alterative situations that can arise in a smart grid?
- Which types of decision models can maximize reliability and efficiency for a given power system?
- Which types of decisions can be made rapidly enough to avoid cascading failures, while still being deliberate enough to maintain the system efficiency?

Previous smart grid simulation research work falls short of providing satisfactory answers to these questions. Moreover, previous simulation designs have little flexibility to support to the simulating of different test cases. In particular, there is a strong need for simulation models to adequately handle dynamic as well as static topologies.

Our simulation design is highly flexible and scalable. It supports the creation new grid topologies from primitive elements and intelligent agent mappings through a convenient and easy to use graphical interface. The simulation can be manipulated at run time through various actions, including the shutting down of devices or the forcing of component failures. Finally, and importantly, the type of decision model used by the system agents can be configured, and entirely new models can be developed, run, and tested in the simulator. We see considerable potential for the simulations that we describe to help in the building a smarter electrical Grid architecture.

This paper is divided as follows: section II discusses the agent model and design used to implement our MAS (multi-agent system). Section III explains a general overview of how decision models are used and implemented in our simulation. Section IV discusses the main features and innovations of the simulator, gives an overview of its use, and describes potential benefits in Smart Grid research.

II. Agent Model Implementation and Design

In this section we describe the agent design used in the implementation of our simulation. We use a three layer design, in which the two upper layers are agent based. The bottom layer (the physical layer) is a simple hardware simulation. Our aim with the bottom layer is to mimic the behavior of the electrical components themselves. Components modeled at this layer include relays, transformers, capacitors, power lines, consumers and generators, all running as autonomous units with no intervention or added intelligence. This separation between the intelligent agent layer and the physical simulation allows scenarios to to run at the hardware level like the grid normally operates today, and, using intelligence agent support, to run with intelligent management.

At the physical layer we do not model full detail such as the modeling described in [2]. As an alternative, we treat the physical components as abstract black boxes and concern ourselves only with the basic power, voltage, and current metrics that are input and output to and from devices. This is because our focus is on the agent-based upper layers where our concern with how agents can solve fault situations, such as power outages, by assuming specific roles and collaborating with one another. For these kinds of purposes, knowing the details of the fault on an individual electrical component basis is not necessary in evaluating strategies for handling the fault by employing the decision models that generate the strategies.

In the middle layer of our design reside the supervised agents, including the Distributed Energy Resources (DER) agents, User agents, Device agents, and Control Agents. These agents collaborate with each other to achieve global goals, and are described below

User agents: These agents act on behalf of consumers. For example, if there is an outage they engage in a negotiation with DER agents to obtain a power lease to address the outage.
DER agents: These agents act on behalf of power generation sources that are independent of the primary power distribution circuits. These sources are typically small companies or special consumers that also participate in the power market. Examples include wind power generation facilities, or geothermal generators, etc. DER agents act on behalf of their generators by engaging in power supply negotiations with users.
Device Agents: These agents are in charge of performing operations on devices. Examples include rerouting power by changing the distribution of power sent through the lines of a relay, disabling a certain power line on that same relay, shutting down a transformer or closing a circuit breaker to secure a critical load or island on some portion of the grid.
Control agents: These agents constantly monitor a section of the grid, collecting data and information from the devices and power lines in that geographical area. These results are sent in real time to a fusion point and aggregated. The results after fusion represent the status of the system at a certain moment in time. That fusion point where all data is received and aggregated is in the management agent, which is described below.

Middleware is required for the agents in the middle layer to communicate with the physical components in the first layer. This is achieved by encapsulating the bottom layer within an agent called the environment agent. The environment agent contains all information about the grid topology and all device status information at any given time. Middle layer agents query the environment agent to acquire information about the physical grid. They also send write/modify requests to the environment agent when they seek to alter the behavior of the physical grid. This simulates at an abstract level how the agents would be integrated with smart meters and other sensors in a real grid.

The top layer is administrative and hosts the management agents that make the high level decisions. The control agents send all data representing the status of the system at a given time to the management agent. Having received the relevant data, the management agents organize and analyze the data and detect situations in the grid that require self healing. When such a situation is detected, it creates a strategy to heal the system. This strategy is expressed as a set of corrective behaviors that prescribe a set of roles to be performed by the middle layer agents. Like the environment agent, the management agent has knowledge of the microgrid topology. It knows, for example, how components are physically connected, but it does not know if a line has failed or its current voltage level value. That information is sent in real time to the management agent by the control agents. The management agent is the primary decision maker in the simulation. However, the other agents in the middle layer still have certain autonomy to carry out the high level decisions generated by the management agent. Middle layer agents must make the specific decisions needed to carry out the higher level actions. Figure 1 illustrates the layered structure.

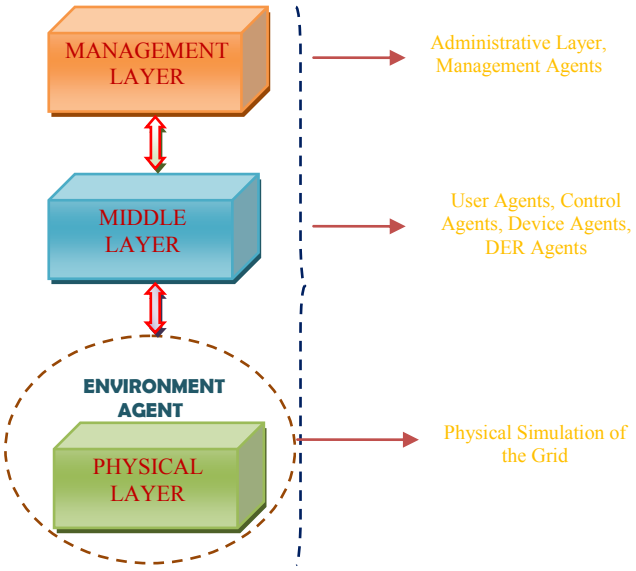

Figure 1. Multilayered MAS (Multi-agent system) design

Figure 2 shows the communication flows between layers and illustrates the kinds of intelligence that is integrated into each layer. The management agent is on top and on the bottom we have the basic physical components simulated in the environment agent with no intelligence. The middle layer agents have some intelligence but they are limited in comparison with the management agent.

The framework used to implement our MAS is the Java Agent Development Framework (JADE). The primary reason we chose JADE is due to its strong compliance with agent communication standards like the IEEE standard for the Foundation for Intelligent Physical Agents (FIPA). This ensures portability and interoperability between many different systems and platforms. Other reasons are its convenience and ease of use. JADE runs agents in containers, which are agent groupings, and related agents usually run in the same container.

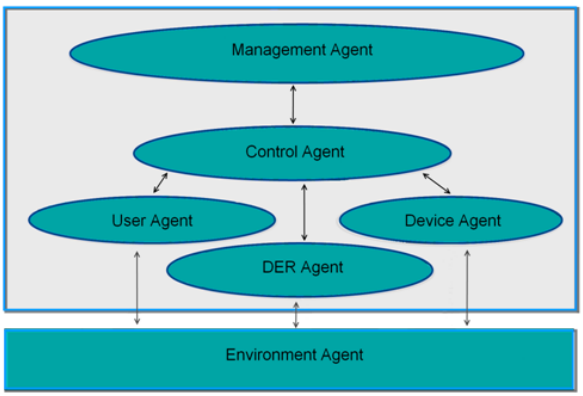

Figure 2. Flow of Communication between agents in our MAS

III. Decision Models Implementation Design

Decision models are at the core of our simulation, and as such there are many levels of decisions that can be taken by agents. The highest level decisions are made exclusively by the management agents. Management agents can use different decision models depending on the testing configuration. For example, it is possible to test a certain scenario using an Integer Linear Programming (ILP) decision model and then compare it against a Naive Bayesian decision model.

The decision process works in the following way: First, the management agent receives all relevant data representing the status of the system at a given time. Within the decision framework there is a special layer called the data presentation layer that is in charge of receiving the data collected from the control agents, and structuring it to make it compatible with the selected decision model. A decision model based on Bayesian logic might need the information presented in a different way than a one based on an ILP. If a researcher creates a new decision model and wants to integrate it into the simulator he/she must usually also create a data presenter that is appropriate for that model. An exception to this case is when one of the default data presenters already available in the simulator would work. In this way the data presenter layer of the decision model can be compared to the data presentation section of the application layer in the popular ISO networking model.

Once the Management agent receives the formatted data, it determines if the status of the power grid is normal or there is a need for self healing. In the latter case, it uses the decision model to generate a strategy that identifies corrective actions that can be taken to solve the detected problem in a high performance way. The decision model translates the results obtained into a set of corrective behaviors consisting of mappings of various middle layer agents to appropriate roles. The final output that the decision model generates is a set of actions and the agent responsible for accomplishing them, in the format that our MAS understands. The layer within the decision model that is in charge of converting the generated results to this format is called the Results Translator.

An example of a set of corrective behaviors could be:

DeviceAgent1 Set Line 2 in Relay +200Watts
DeviceAgent2 Close Circuit
DeviceAgent8 Shutdown Device
DERAgent6 Generate +100Watts

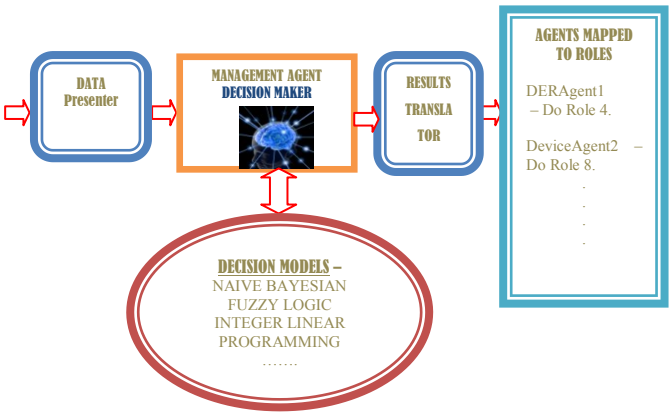

Figure 3 Decision Model Design used in the Simulator

IV. Simulation Features And Design

In this section we discuss the main features of our simulation and explain the innovations that our simulator introduces when compared with previous smart grid simulations. We also provide a tour of the simulator, its basic configuration and use, and illustrate the potential benefits it brings to researchers testing self healing scenarios for a smart grid.

First we describe the design and run modes in which the simulator operates. In design mode, the simulator is configured with the details of a desired test scenario. At a minimum, designing a scenario requires inputting or loading a microgrid topology and the agent assignments to different components or sections of the microgrid. From this mode the user can save the design information to an XML file for later use. This makes it convenient for others to verify results or to run other tests on the exact same topology. In run mode, a test case created in design mode is loaded and then a simulation run is made. As the simulation proceeds the physical

infrastructure is emulated and the agents are active, monitoring and collaborating.

The main strengths of our simulation are as given below.

- Physical Layer Independence
- Power Grid Topology Design Flexibility
- Scalability
- Flexible Agent Mapping
- Dynamic Agent Generation
- Decision model Independence
- Active Control of the Testing Environment.

We describe of these strengths in turn.

Physical Layer Independence.

The physical hardware simulation is in a different layer than the agents, which allows considerable independence between them. Separating them allows us to run the simulator as a purely hardware simulation of the physical grid with no external intervention or intelligence. It is then possible to run the same configuration using agents and intelligence, and then assess how the control exercised by the agents improves the efficiency of the self-healing process of the power grid.

Topology Design Flexibility.

A primary goal in the simulation was to design it to provide flexibilitye to allow researchers to test a wide variety of grid topologies. We adopt a node/arc representation. The arcs modelpower lines and the nodes can represent consumers, generators or devices (like relays or transformers). This design allows researchers to generate a large variety of topologies.

Topology design of a microgrid is done in design mode using GUI tools, as illustrated in Figure 4. A toolbar along the left side of the window allows the user to drag and drop a variety of nodes onto the main grid layout area and connect them with power lines. The nodes can models consumers, generators, or devices and components like relays or transformers. The simulator has the flexibility to easily incorporate new types of components into the system as required. After a microgrid topology is designed, all the topology design information can be saved to an XML file for later use. The XML dialect is illustrated in Figure 5.

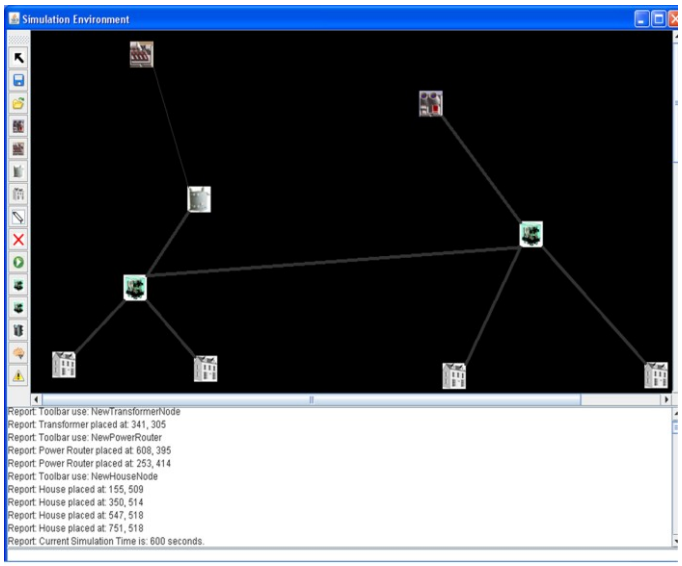

Figure 4 Simulation GUI design mode

Scalability.

Design choices at the microgrid level provide for easy scaling of the system. Multiple microgrids can be interconnected to create larger microgrids and large scale grids. Within multiple microgrids a user can specify the positions of the internal and external connection points. Each of the microgrids in the simulator runs in an independent JADE container.

```
<Simulation.SimulationComponent>
  <position>
    <x>341</x>
    <y>305</y>
  </position>
  <inputPowerLines>
    <Simulation.PowerLine>
      <distance>155</distance>
      <maximumVoltage>2000.0</maximumVoltage>
      <maximumCurrent>2000.0</maximumCurrent>
      <maximumPower>2000.0</maximumPower>
      <startPosition>
        <x>294</x>
        <y>158</y>
      </startPosition>
      <endPosition>
        <x>342</x>
        <y>306</y>
      </endPosition>
      <name>line1</name>
      <idComponent1>Coal0</idComponent1>
      <idComponent2>Transformer2</idComponent2>
      <lineFailed>false</lineFailed>
      <lastPowerValueBeforeFailure>0.0</lastPowerValueBeforeFailure>
      <traceableFailed>false</traceableFailed>
      <trackInputPower>0.0</trackInputPower>
    </Simulation.PowerLine>
  </inputPowerLines>
  <type>DEVICE</type>
  <node class="Simulation.Transformer">
    <name>Transformer2</name>
    <numStates>2</numStates>
    <nodeFailed>false</nodeFailed>
    <queueVoltage class="linked-list"/>
    <queueCurrent class="linked-list"/>
    <queuePower class="linked-list"/>
    <GS/>
    <subtype>Transformer</subtype>
    <maximumVoltage>1000.0</maximumVoltage>
    <maximumCurrent>1000.0</maximumCurrent>
    <maximumPower>1000.0</maximumPower>
    <failureProbability>0.2</failureProbability>
    <deviceFailed>false</deviceFailed>
```

Figure 5 Section of XML file storing design information

Once a user has generated several microgrids and established the connections between them, there is great flexibility under the JADE platform for executing the simulations over the microgrids. The constituent microgrids can be set to run on the same computer or distributed computer. Figure 6 illustrates multiple interconnected microgrids. The only limits to the scalability of the system are the processing power and related resources available to the user. The simulator itself has no specific limits, since different instances of it can be run to support each microgrid, and interconnected microgrids can communicate and interact with each other.

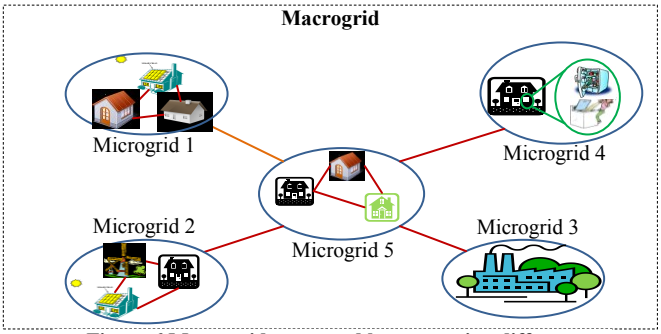

Figure 6 Macrogrid generated by connecting different microgrids

Flexible Agent Mapping and Dynamic Agent Generation.

After a user has designed the topology of their grid and specified the design parameters, he/she can design and develop the desired agent support. The toolbar can be used place agents within the network. A user can specify that available devices will be monitored or manipulated by agents by selecting the agent tool in the toolbar and clicking on thedesired component to associate the agent with the device. Associations between agents certain consumers or generators are carried out with mappings in the same way.

As an example of the flexibility of this control, a user could have an agent assigned to monitor a certain device in one run, and then retest the same scenario without the agent monitoring that same device, to be evaluate how that particular change affects the results.

One of the main features of our simulation is that the agents are dynamically generated in the supporting agent platform (JADE). When the user shifts the simulation from design to run mode the system will start the simulation of the physical grid and will automatically launch the JADE framework, dynamically creating the agents that the user mapped. The system is pre-configured to determine which kind of agent is required for each node. If, for example, the agent is placed on a consumer for which it knows it should create a user agent, on a generator a DER agent, and on a device a device agent, etc. Agent associations are illustrated in Figure 6. The agent-component mappings are saved to the XML file that stores design information.

In the case of a control agent, since it monitors a complete section or area in the grid instead of a single component, the set of components it monitors is determined by associating it with the nearest power line and then applying a hop-range parameter that can be set by the user, to decide the range within which components are monitored by that control agent. Only components within a hop-range number of hops from the original power line are monitored.

Every microgrid created in the simulator runs in a separate JADE container. Figure 7 provides an illustration. Agents that the user specified in design mode are created dynamically and placed in the microgrid JADE container and the system automatically creates an environment agent for the microgrid and at least one management agent.

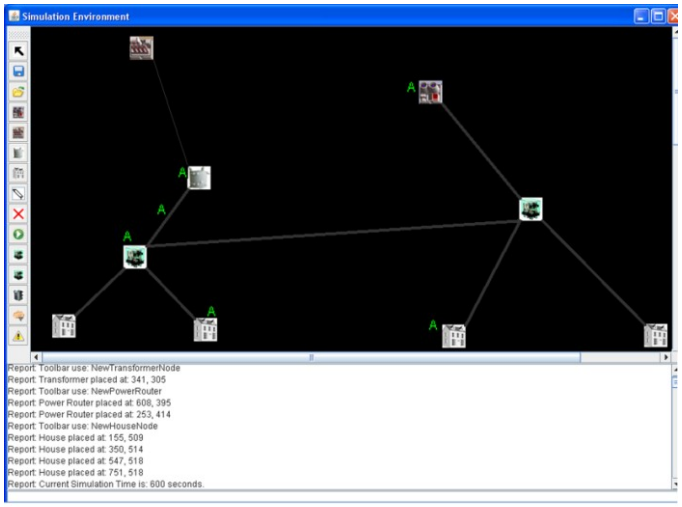

Figure 6 Design GUI showing agent associations

Decision model Independence.

A major innovation of our simulation system when compared to previous efforts is that of having the decision models independent within the design. Multiple customized decision models can be configured in the simulator. For example a management agent could be configured to use ILP (Integer Linear Programming) as its decision model to test a particular scenario and evaluate the efficiency and performance of how agents respond when using that decision model, and then test the same situation by configuring a heuristic decision model or one based on a Naïve Bayesian method, then compare the results. We anticipate the development of many decision models that will run seamlessly and be evaluated in the simulator

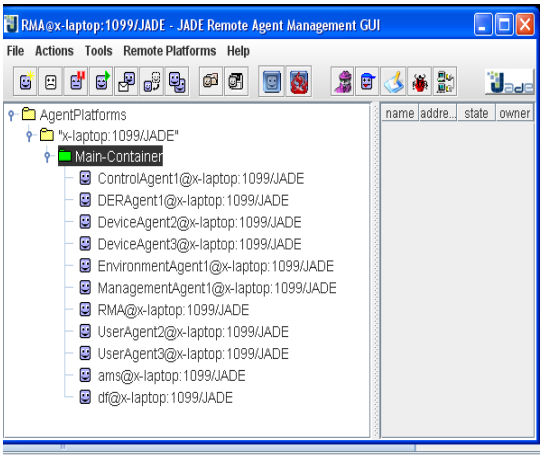

Figure 7 Jade running with a container created for the Microgrid and the agents dynamically generated

Standard interfaces will allow researchers to design their own models and smoothly plug them in, without the need to know the details of the internal implementation of the simulator. An ILP model will be the first decision model to be integrated and evaluated by the [5].

The decision models for lower level agents are also configurable. For example DER and user agents use a

prototype power negotiation model to establish power leases. That model is configurable with a simple default model that is based on the lowest price. More complex power negotiation models are under development.

Active Control of the Testing Environment.

The simulator allows users to configure parameters and settings when designing a physical microgrid and to change those parameters dynamically during run mode. An illustration of run mode is in Figure 8. Some examples of these parameters are the maximum power a given generator can produce the power demands of consumers, and the capacities of power lines. Parameters can be set and modified at both design and run time. For example, in design mode users can set an initial power/voltage/current that a component can output when the simulation starts, but in run mode it is possible to modify and reconfigure the voltage/power/current settings of a component in real time. Parameters set at design mode are saved with the rest of the configuration. When in run mode, a user can also generate different failures in the grid, such as forcing a power line failure or a relay to malfunction. These actions can be used to observe the resulting effect and in particular the self-healing operations taken by whatever decision model is currently configured.

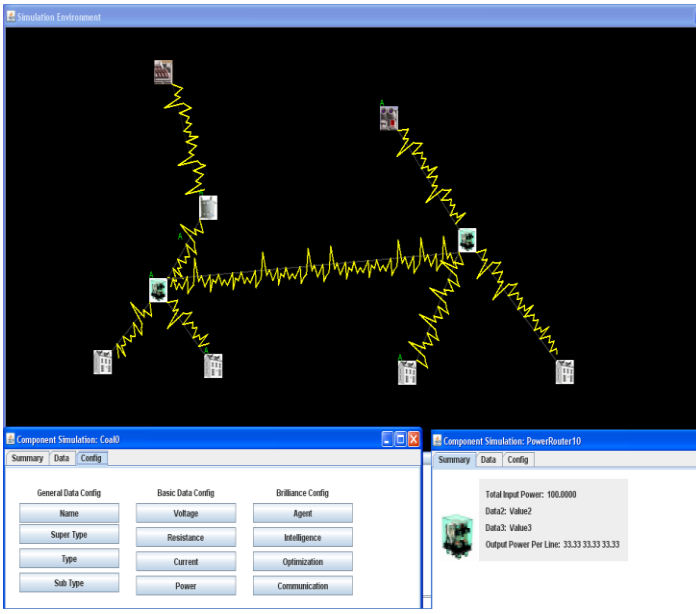

Figure 8 Simulation in run mode

V. CONCLUSIONS AND FUTURE WORK

The implemented simulation system satisfies the requirements of flexibility and scalability described in the design guidelines in [1]. It provides a powerful and versatile testing environment that allows the use of different testing configurations for every run, and gives the user control to manipulate the environment to determine how the agents would react to that particular situation. Furthermore, an important feature is that it allows users to choose which decision model should be used and to compare how agents behave differently in different situations using different decision models. Researchers are also able to design their own decision models and plug them into the system for testing.

Our work in progress includes heuristic decision models and the ILP model described in [5]. After these models are fully implemented, we will run them and evaluate their performance in the simulator and compare their performance and efficiency for alternative power grid self healing scenarios.

VI. REFERENCES

[1] S. Boughosn, P. Ranganathan, S. Salem, J. Tang, D. Loegering, and K. Nygard., Agent-oriented Designs for a Self Healing Smart Grid, 1st IEEE international Conference on Smart Grid Communications, Gaithersburg, Maryland, 2010.

[2] M. Pipattanasomporn and S. Rahman, Multi-Agent Systems in a Distributed Smart Grid: Design and Implementation, *Proc. Proc. IEEE PES 2009 Power Systems Conference and Exposition (PSCE'09),* 2009.

[3] Z. Noorian, H. Hosseini, and M. Ulieru, "An Autonomous Agent-based Framework for Self-Healing Power Grid," *Proc. IEEE Conference on Systems, Man and Cybernetics,*, 2009.

[4] S. Karnouskos, T. Nass de Holanda (2009): Simulation of a smart grid city with software agents, *European Modeling Symposium* EMS, Athens, 2009.

[5] K. Nygard, Prakash Ranganathan et.al, Optimization Models for Energy Reallocation in a Smart Grid, IEEE INFOCOM 2011, Machine to Machine Communications and Networking Workshop, Shanghai, China, April 10-15 2011, to appear.

[6]

Simulation of Spatial Self-Organization in a Stepping Stone Environment

Bilal Gonen[1], **Guy Hoelzer**[2]
[1]Computer Science and Engineering Department, University of Nevada, Reno, Reno, Nevada, U.S.A.
[2]Biology Department, University of Nevada, Reno, Reno, Nevada, U.S.A.

Abstract— *Self-organization is the process where a structure or pattern appears in a system without a central authority or external element imposing it through planning. In various areas, simulation is a safe and low-cost alternative to complex problems. We developed a free online simulation tool which computes and displays spatial self-organizing behavior of individuals in a stepping stone environment.*

Keywords: bioinformatics, simulation, spatial self-organization

1. Introduction

Self-organization is the process where a structure or pattern appears in a system without a central authority or external element imposing it through planning. This globally coherent pattern appears from the local interaction of the elements that make up the system, thus the organization is achieved in a way that is parallel (all the elements act at the same time) and distributed (no element is a coordinator) [1].

The concept of self-organization is central to the description of biological systems, from the subcellular to the ecosystem level. There are also cited examples of "self-organizing" behaviour found in the literature of many other disciplines, both in the natural sciences and the social sciences such as economics or anthropology [2] [3] [4] [5] [6] [7]. Self-organization has also been observed in mathematical systems such as cellular automata. Sometimes the notion of self-organization is conflated with that of the related concept of emergence. The link between emergence and self-organization remains an active research question [1].

Originally, the term "self-organizing" was used by Immanuel Kant in his Critique of Judgment [8], where he argued that teleology is a meaningful concept only if there exists such an entity whose parts or "organs" are simultaneously ends and means. Such a system of organs must be able to behave as if it has a mind of its own, that is, it is capable of governing itself [1].

The idea that the dynamics of a system can tend by itself to increase the inherent order of a system has a long history. One of the earliest statements of this idea was by the philosopher Descartes, in the fifth part of his Discourse on Method [9], where he presents it hypothetically [1].

According to Scott Camazine, in biological systems self-organization is a process in which pattern at the global level of a system emerges solely from numerous interactions among the lower-level components of the system. Moreover, the rules specifying interactions among the system's components are executed using only local information, without reference to the global pattern [10].

In various areas, simulation is a safe and low-cost alternative to complex problems. We developed a free online simulation tool which computes and displays spatial self-organizing behavior of individuals in a stepping stone environment. For the public consumption by the research community, we made it a free online simulator at `www.evosimulator.com`. The simulator is developed in C#, .Net, and Silverlight 4.0 to provide more visual insight to the users. In this paper, we use a real-world example. We simulated "Beetle World" which is an experiment conducted in our biology department. In this experiment, plates are used as stepping stones, and beetles are used as individuals. First, Section-2 gives an overview of the steps in the simulation. Then, the online simulation tool is described in Section-3.

2. EvoSimulator

In this section, the EvoSimulator algorithm is explained in detail. The program is developed in object-oriented approach. There are five classes used in this simulator, i.e., Generation, Grouplist, Group, Plate, and Beetle. There are several user-inputted parameters for this simulation. These parameters are;

- Number of plates
- Number of beetles per plate
- Number of alleles
- Number of generations

When we started building this simulation tool, we were simulating an experiment where beetles move between plates. In that experiment, plates represent stepping stones. In each generation, for the next offspring, to ensure the fixed amount of beetles to be produced in each plate, the same amount of beans are put into each plate. This ensures that the same number of offspring to be produced in each plate, since one bean can hold at most one beetle egg. Each plate is connected to two other plates. We also connect the first and last plates to each other forming a circular linear shape. Number of alleles is also a user-inputted parameter for our simulation. The beetles inherit their chromosome

from their mother. Algorithm1 shows the main steps in EvoSimulator algorithm.

Algorithm 1 $EvoSimulator\_main\_function$

```
1: Create beetles and position plates
2: Call splitMaster function
3: for genID = 1 to numOfGenerations do
4:     Create an object of Generation class;
5:     Call makeChildrenForAllPlates function;
6:     Call fillVacancies function;
7:     Call killParentBeetles function;
8:     Call splitMaster function;
9: end for
```

2.1 Creating Beetles and Positioning Plates

The plates in the simulation are placed in a circular chain shape. Each plate has two neighbor plates. N being the number of plates, to make it circular shape, plate-1 is neighbor to plate-2 and plate-N. Then we create beetles. We set the gender of beetles to either male or female with equal probability. Each beetle has a unique ID number assigned to them so that we can keep track of them during the simulation. Each beetle has also an allele assigned to them when they are created. We also set the number of children that a beetle will produce during its life span. This number is produced by using poisson distribution. As the lambda parameter of poisson distribution, we used 1.8 in our simulation. We then place the beetles in plates in equal quantity. This number of beetles per plate is set by user before the simulation begins.

2.2 Grouping The Plates

We split the plates into subdivisions based on their FST values. FST (Fixation index) is a measure of population differentiation, genetic distance, based on genetic polymorphism data. It is simply the correlation of randomly chosen alleles within the same sub-population relative to that found in the entire population. It is often expressed as the proportion of genetic diversity due to allele frequency differences among populations [1].

As the grouping heuristic, we used a top-down approach. That is, we put all the plates into one group, and begin splitting the groups into subgroups. In each generation, we create an empty group and we put all the plates into that group. Then, we call the splitMaster function which is illustrated in algorithm-2. In this function, there are two types of functions; (i) Analyze function which computes from where to split the group that maximizes the overall FST. (ii) Split function that actually splits the group into two groups. Based on the number of groups in the system, these two functions operate differently. The reason is that the plates are placed in a circular shape. We need to compute not only from which plate to split the group, but also from which plate should the first group start. Algorithm-3 is the pseudo-code of the splitTheOnlyGroup function. This process is displayed in figure 1. We set the minimum size for a group as 2. That is there must be at least two plates in a group. The AnalyzeTheOnlyGroup function finds both first-cut and split points which gives the maximum FST. After the group is split into two groups, the splitMaster function calls the splitGroupListWhenMultipleGroups function. This function iterates through all the groups, and within each group it checks each possible split point to find out which group to split and which point to split that maximizes the overall FST. Algorithm-4 is the pseudo-code of the splitGroupListWhenMultipleGroups function. And the process of splitting grouplist when multiple groups is illusrated in figure 2.

Algorithm 2 $splitMaster$

```
1: while groups still can be splitted do
2:     if there is only one group then
3:         Call AnalyzeTheOnlyGroup function;
4:         Call splitTheOnlyGroup function;
5:     else
6:         Call AnalyzeMultipleGroups function;
7:         Call splitGroupListWhenMultipleGroups function;
8:     end if
9: end while
```

Algorithm 3 $splitTheOnlyGroup$

```
1: for first_cut = 0 to numOfPlates do
2:     calculate fromPlateIndex;
3:     calculate toPlateIndex;
4:     for i = fromPlateIndex to toPlateIndex do
5:         Find a split point that maximizes the FST
6:     end for
7: end for
```

Algorithm 4 $splitGroupListWhenMultipleGroups$

```
1: for group_ID = 0 to numOfGroups do
2:     if plateCountInThisGroup > minGroupSize + 1
       then
3:         Find a split point in group that maximizes FST
4:     end if
5: end for
```

2.3 Creating New Generations

There are three main steps happening in each generation. Those are;

- Produce offspring and put them into plates.
- Fill Vacancies in the plates.

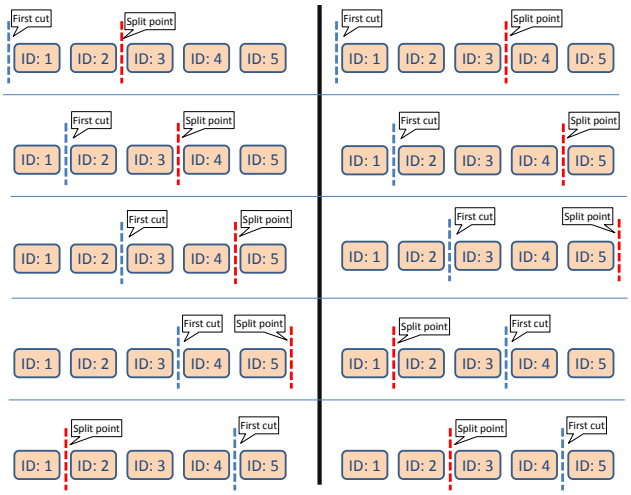

Fig. 1: Process of splitting the grouplist initially

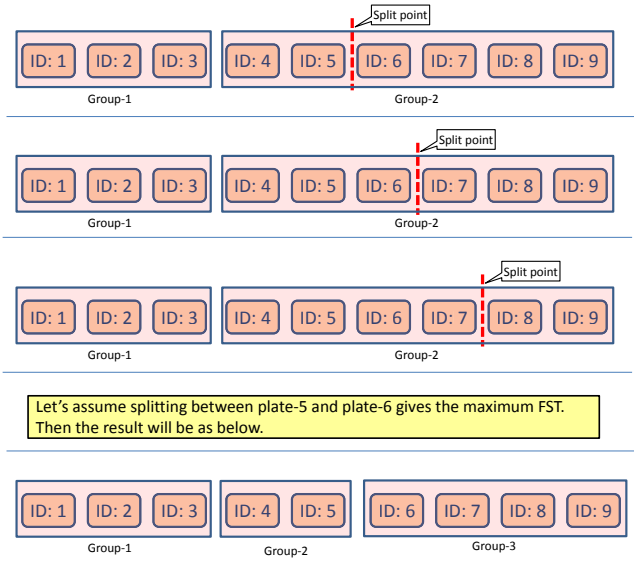

Fig. 2: Process of splitting grouplist when multiple groups

- Kill parent individuals.

2.3.1 Produce Offspring and Put Them Into Plates

In the simulation, we check every beetles in every plates. If the beetle is a female, then we get the number of children to produce from that female beetle. The number of children is generated for each female beetle by using poisson distribution. And this number is assigned to them when the beetles are created. Before producing any child from that parent, we make sure if there is some vacant spot in any plate around the female parent to place her child. We use Gaussian distribution to determine how far away the child will be from their mother. After determining which plate to put the child, we check the plate to see if the plate has reached to its maximum number of children already. If

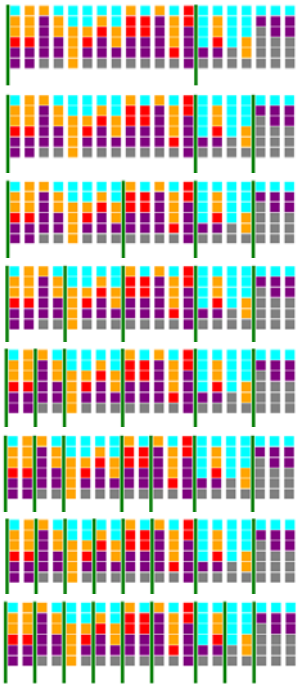

Fig. 3: groups

so, then we generate another moving distance number using normal distribution to put the child into another plate. We repeat this process until either we find a vacant spot in a plate, or we fail to find a vacant spot for some user-defined number of times. As long as we find vacant spot for the female parent to put her children, we keep repeating this process for the number of children to produce from that female parent. If we are able to find a vacant spot to place a child, then we produce a child from the parent and put the child into the plate. At the end of this repetition, if we are unable to find a vacant spot to place a child, then we don't generate any more child from the parent, and go to the next female parent in the plates.

2.3.2 Fill Vacancies in The Plates

After we fill in the plates with child beetles, there may be some vacant spots in the plates. To fill in those vacant spots in the plates, we try to find a female parent from other plates. We determine which plate to search by using gaussian distribution. When we find a female parent, we produce a child beetle from it, and put into the vacant spot. At the end of this process, all of the plates hold the same number of child beetle.

2.3.3 Kill Parent Beetles

In this step, we remove parent beetles from the plates. However, they still remain in the memory of the simulation with their ID numbers so that we can display some statistical

Fig. 4: Entry point for the parameters

information by using historical data.

3. EvoSimulator Tool

EvoSimulator is a free online simulation tool which computes and displays evolutionary behavior of individuals in a stepping stone environment. As mentioned above, there are several user-inputted parameters for this simulation. These parameters are; Number of plates, Number of beetles per plate, Number of alleles, and Number of generations. Figure-4 displays the entry point for these parameters in the simulator tool.

Figure-5 is a screenshot of the simulator after running it. The histogram shows that when the number of groups increases, the FST of the population also increases. Each vertical column below the histogram represents a plate, and each colored square represents a beetle. Colors of the beetles represent the chromosome type (alleles).

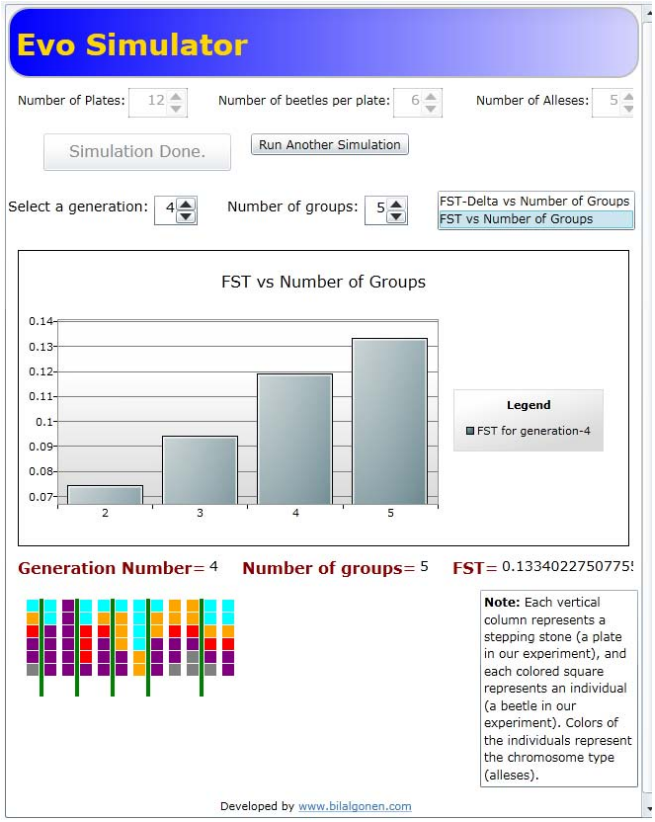

Fig. 5: A screenshot of the simulator after running it

4. Conclusion

We developed a free online simulation tool to simulate spatial self-organizing behavior of individuals in a stepping stone environment. After several experiments, we observed that if we run the simulation long enough the spatial configuration of genetic variations in the population self-organizes.

References

[1] http://en.wikipedia.org.
[2] V. Castets, E. Dulos, J. Boissonade, and P. De Kepper, "Experimental evidence of a sustained standing turing-type nonequilibrium chemical pattern," *Phys. Rev. Lett.*, vol. 64, no. 24, pp. 2953–2956, Jun 1990.
[3] G. Nicolis and I. Prigogine, *Self-organization in nonequilibrium systems*. New York: Wiley, 1977.
[4] T. et al., *Proc. Natl. Acad. Sci. U.S.A. 99*, p. 9645, 2002.
[5] H. Wager, *Philos. Trans. R. Soc. London Ser. B 201*, p. 333, 1911.
[6] J. D. M. J. J. Tyson, *Development 106*, p. 421, 1989.
[7] S. M. Y. M. D. Bertness, S. D. Gaines, *Ecology 79*, p. 1382, 1998.
[8] I. Kant, *Critique of judgment*, 1987.
[9] "Rene descartes, discourse on method, 1637."
[10] S. Camazine, N. R. Franks, J. Sneyd, E. Bonabeau, J.-L. Deneubourg, and G. Theraula, *Self-Organization in Biological Systems*. Princeton, NJ, USA: Princeton University Press, 2001.

OpenSIM (Open Simulation engine for Interoperable Models) for Weapons Effectiveness Analysis

Kangsun Lee, Joonho Park and Chanjong Park
Department of Computer Engineering, MyongJi University
San 38-2 NamDong, YongIn, Kyunggi-Do
449-728, Republic of Korea

Abstract *– As modern weapon systems become complex in dynamics and operational environments, evaluating their effectiveness becomes a hard task, accordingly. In order to analyze the effectiveness of a weapon system realistically, we have to consider not only dynamics of the weapon system, but also natural environments under which the weapons are operated, and operational strategies with which the weapons are utilized, as well. These factors are hard to control in real world, and thus, simulation technology has been massively used as an alternative for the effectiveness analysis. OpenSIM(Open Simulation Engine for Interoperable Models) is a simulation environment for weapons effectiveness analysis. OpenSIM provides 1) a modeling framework to represent weapon systems, environments and operational strategies, 2) various simulation services including scheduling, journaling, and logging, 3) linkage to other simulation systems, such as live and virtual simulators, and commercial engineering tools,. In this work, we present tools and services of OpenSIM and illustrate how OpenSIM can aid weapon engineers to perform complex modeling and simulation tasks for weapons effectiveness analysis.*

Keywords: Weapons Effectiveness Analysis, Simulation Engine, Integrated Simulation Environment, Hybrid Simulation

1 Introduction

Modern weapon systems are very complex in their structure and dynamics. They operate with sensors, commands and shooters distributed over the network, and cooperate based on complex engagement strategies [1]. Effectiveness of weapon systems can vary according to various factors on natural environments (i.e. sea, ground, air) and operational environments (i.e. engagement strategies). These factors are hard to control in real world, and thus, simulation technology has been massively used to measure/predict the effectiveness of a weapon system. In order to simulate a weapon system and assess its effectiveness in various war conditions, we need a set of models to represent weapons dynamics, natural environment, and operational environments. These models require us to employ different modeling methods. For example, dynamics of the weapon system are usually represented with a set of mathematical equations. Natural environments and operational environments are represented as a set of states and state transition rules. Simulating different types of models together challenges us to coordinate the advancement of simulation time and data flow. M&S (Modeling and simulation) tasks can be more complicated when the weapon systems interoperate with existing Live, Virtual and Constructive simulators [2].

A simulation environment can be defined as a suite of tools and services that assist developers and analysts to perform modeling and simulation activities [3]. An integrated simulation environment for weapons effectiveness analysis can greatly help weapon engineers and analysts to perform complex M&S tasks. However, there have been insufficient research works on *what constitutes a simulation environment for weapons effectiveness analysis*. In this paper, we identify requirements for the M&S environment of weapons effectiveness analysis, and present OpenSIM (Open Simulation engine for Interoperable Models) as a solution.

This paper is organized as follows. Section 2 reviews related works and identifies M&S requirements for the weapons effectiveness analysis. Section 3 presents OpenSIM and explains how the OpenSIM can help weapon engineers and analysts to measure/predict the effectiveness of a weapon system. Tools and services in OpenSIM will be presented with a simple example. Section 4 concludes this paper with future works to achieve.

2 Related Works

Modeling and simulating weapon systems are very complex tasks. Several simulation environments have been developed to ease the complexity involved in theM&S tasks.

JMASS (Joint Modeling and Simulation System) [4] is a modeling and simulation system that provides capabilities for defining models, combining models into simulations, executing simulations, and post-processing the results. JMASS provides several tools and predefined C++ components that simplify the configuration of models and provide access to common simulation services, such as timing, event queuing, and inter-component communication.

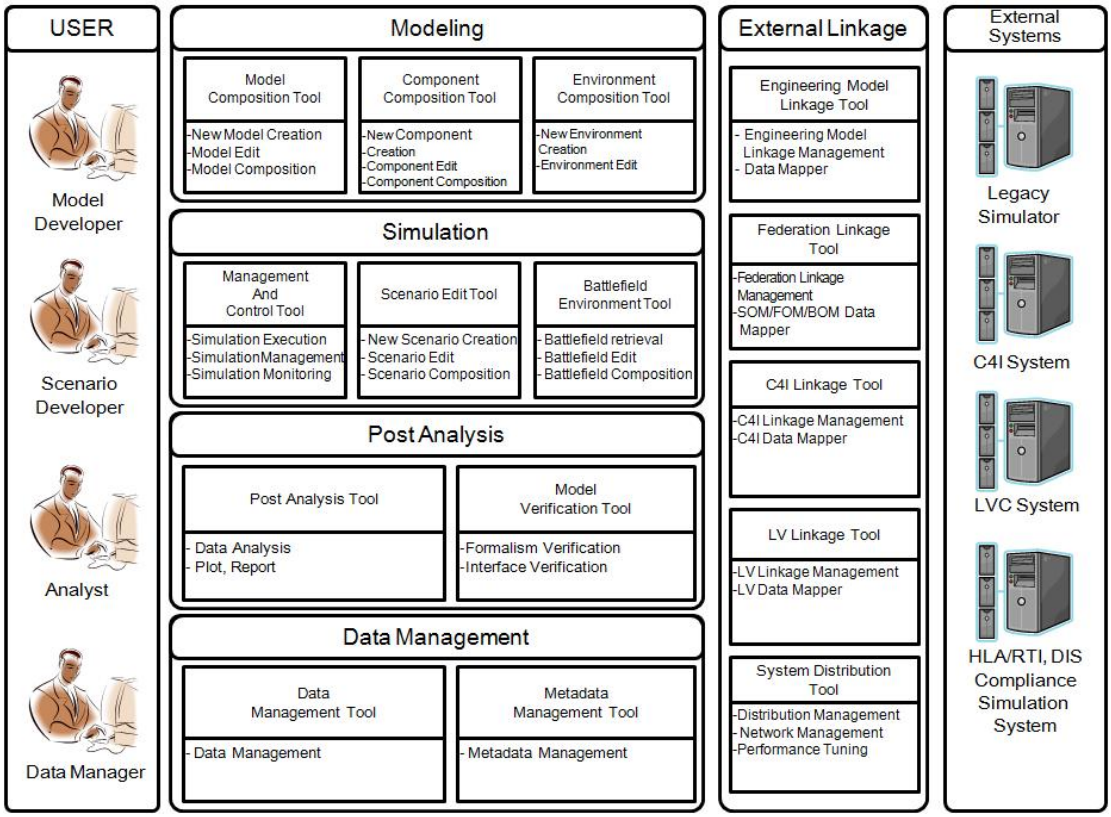

Figure 1. OpenSIM : Overview

JMASS is used to build digital system models for engineering and engagement-level simulations.

In OneSAF, simulation behaviors and models are data driven, to support customization and "what-if" analysis. System capabilities are exposed by powerful visual tools. High degree of interoperability through DIS (Distributed Interactive Simulation) and HLA (High Level Architecture) [6] is provided in OneSAF.

Based on the existing M&S environments in the military community, we can identify services that could be used for leveraging M&S activities for weapons effectiveness analysis:

- A standard modeling framework + formalism: Weapons effectiveness analysis involves many models of different types. A standard modeling framework can provide useful constructs to build different types of models. Adding formalism to the modeling constructs can make the structure, behaviors and interfaces of the model "seeable". Weapon engineers can utilize these information to locate reusable M&S assets.
- Simulation services: Besides the basic simulation services such as scheduling, journaling, and logging, weapon engineers need explicit supports for hybrid simulations in order to coordinate time advancement between engineering-level simulations (i.e. simulation of weapon models) and engagement-level simulations (i.e. simulation of natural and operational models), transparently.
- Linkage to Legacy simulation systems and Commercial engineering tools: Simulating weapons effectiveness often requires interoperation with various legacy simulators, such as Live, Virtual and Constructive simulators and Command/Control systems. Many existing weapon models have been constructed with commercial engineering tools, such as MATLAB®/SIMULINK®. Linkage to the commercial tools is also desirable to improve reusability of the existing weapon models.

OpenSIM realizes these features with a set of tools, services, standard interfaces. Details can be found in Section 3.

3 OpenSIM(Open Simulation engine for Interoprable Models)

OpenSIM (Open Simulation engine for Interoperable Models) is an integrated simulation environment for weapons effectiveness analysis. OpenSIM provides a suite of tools and services for developing, executing and analyzing simulations of weapon systems, as shown in Figure 1. OpenSIM is *open* to different types of models, different levels of simulations, and different types of legacy systems. We introduce the modeling framework, simulation services, and linkage capability of OpenSIM in Section 3.1 – 3.3.

3.1 Modeling Framework

A modeling framework guides modelers to organize a system into a set of small components that can be separately executable on different computers. The modeling framework of OpenSIM has been devised based on DEVS(Discrete Event System Specifications) formalism [7]. DEVS is a formal modeling method to hierarchically describe entities and behaviors of a system. DEVS provides two types of models for hierarchical composition. An *atomic model* depicts a system as 3 sets (a set of inputs, a set of outputs, a set of states) and 4 functions (external transition function, internal transition function, output function and time advance function). A *coupled model* consists of a set of atomic models, coupling information among the atomic models, and input/output ports. DEVS has been successfully used in defense modeling and simulation developers and resulted many applications with various computer languages, such as, C++ and Java [8,9].

Figure 2 shows our modeling framework based on DEVS. In order to assess the effectiveness of a weapon system, we have to consider 1) dynamics of the weapon system, 2) environments where the weapon system are deployed, 3) engagement strategies where the weapon system are operated. As illustrated in Figure 2, our framework organizes a weapon simulator with three models: weapon model(s), environment model(s) and engagement model(s). A model can be further composed of components and subcomponents, which are described with 3 states and 4 transition functions. The proposed modeling framework helps developers to chop the whole simulator into small-sized components which can be independently executable on different computers. [10]

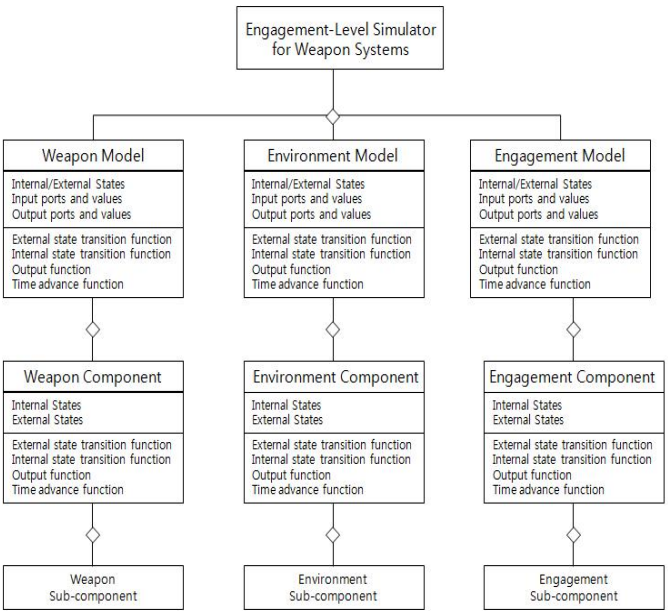

Figure 2. OpenSIM Modeling Framework

The modeling framework can also facilitate reuse of weapon simulators. For example, the environment model of a torpedo can be reused in a missile simulator, even though we can't reuse the torpedo simulator as a whole. Users can see all semantic information on the models in terms of the structures and behaviors (i.e. states and state transitions) and utilize the information to locate reusable model candidates.

OpenSIM provides a set of tools and services to enable the proposed modeling framework. Modelers specify weapon models, environment models and engagement models on easy-to-use GUIs on OpenSIM. An example is shown in Figure 3. An aircraft is composed of *Navigator, Radar* and *Missile*. *Navigator*, *Radar* and *Missile* are modeled with Atomic Components of OpenSIM with 3 states and 4 transition functions. An aircraft couples *Navigator*, *Radar* and *Missile* as shown in Figure 3.

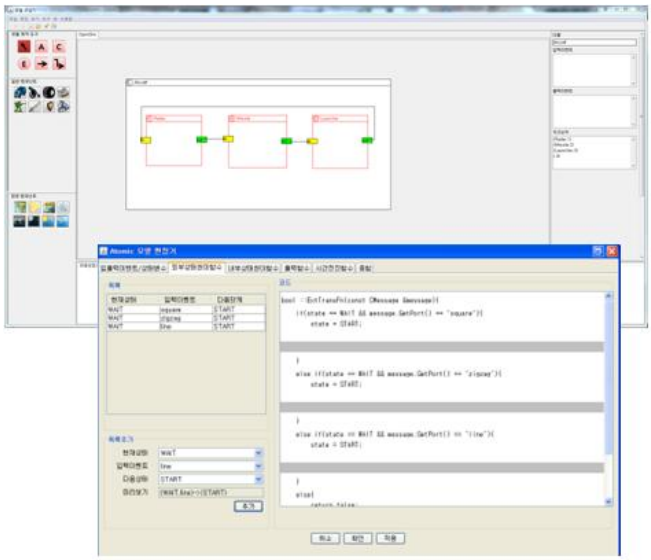

Figure 3. Modeling Tools in OpenSIM

All these information are fed to *Translator* of OpenSIM, which automatically generates the correponding C++ codes, as shown in Fugure 4. OpenSIM also offers services to build environement models. For example, *Atmosphere services* allow environment models to reference atmospheric data at a given altitude and location. Various utility services are provided to help developers build models. Data structures and algorithms, mathematical solvers, and random number generators are the examples.

3.2 Simulation Services and Tools

OpenSIM provides a set of services to simulate weapon systems in natural and operational environments. Followings are parts of OpenSIM simulation services.

- Scheduling services: OpenSIM manages time to support hybrid simulation. Weapons change behaviors continuously, while their operational strategy changes with discrete amount of time.

```
class Radar: public Op_ModelA {// Radar ModelA
public:
    Radar();
    Radar(std::string name);
    virtual ~Radar();

   //External, Internal function
   virtual bool ExTransFn(const Message);
   virtual bool InTransFn();
   // Output, Time advance function
   virtual bool OutputFn(Message &);
   virtual TimeType TimeAdvanceFn();
};

class Missile: Public Op_ModelA { // Missile ModelA
……
};

//Navigator ModelA
class Navigator: Public Op_ModelA {
……
};

//AirCraft ModelC = Navigator+Radar+Missile
class AirCraft: public Op_ModelC {
 public:
   AirCraft();
  virtual ~AirCraft();
}

AirCraft::AirCraft() {
  Navigator* navigator;
  Radar* radar;
  Missile* missile;

  navigator = new Navigator("Navigator");
  radar = new Radar("Radar");
  missile = new Missile("Missile");

  //Register components and Set ports
  AddComponent(3, navigator, radar, missile);
  AddInPort(1, "in");
  AddOutPort(1, "out");

  // Coupling Information
  AddCoupling(this, "in", navigator, "in");
  Addcoupling(navigation, "done", radar, "in");
  AddCoupling(radar, "detected", missile, "in");
AddCoupling(missile, "shot", this, "out);
```

Figure 4. Automatic Code Generation (in part)

Scheduling services process events in time order and allow continuous and discrete-event simulations to occur together.

- Internal high-speed communication services: OpenSIM provides services to run models in either single- or multi-threaded modes to speed up simulation.
- Resolution Services: Weapons effectiveness analysis involves various models with different levels of detail. Model developers can specify the level of detail for their models. Analysts can switch simulation levels of detail, on the fly, by using the resolution services.
- Journaling Services: Attributes can be selected for periodic output during a simulation. Journaling services sample the values of selected attributes during a simulation and save the sampled values to a specified file format in OpenSIM.
- Message Logging Services: Message Logging services write messages logged during a simulation to the corresponding output medium.

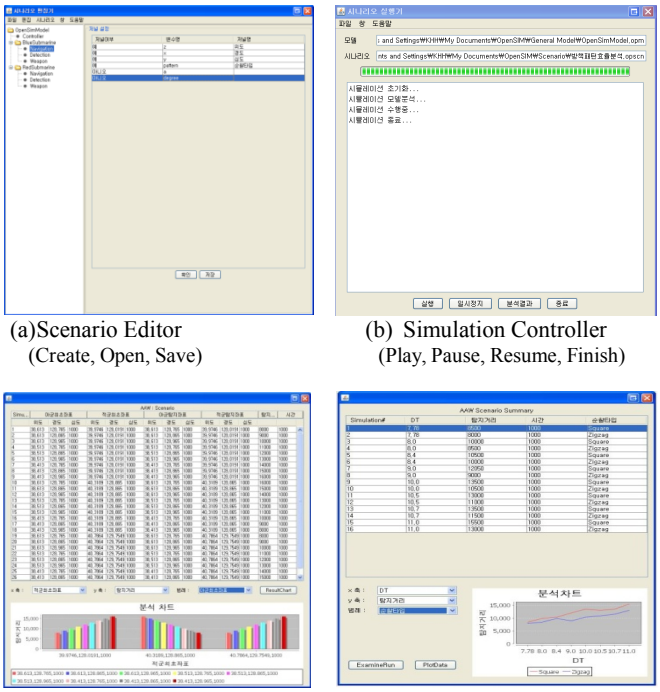

(a)Scenario Editor (Create, Open, Save)

(b) Simulation Controller (Play, Pause, Resume, Finish)

(c) Analysis Tools (Plots, Reports)

Figure 5. Simulation and Analysis Tools in OpenSIM

OpenSIM provides a set of tools to help analysts define simulation scenarios, manage and monitor simulations, as shown in Figure 5. A set of analysis tools are also provided to help analysts view simulation results.

3.3 Linkage Services

In this section, we briefly introduce OpenSIM linkage services.

- Linkage to existing HLA Federations: Weapon models may interoperate with existing HLA Federations. OpenSIM provides gateway services to connect existing HLA federations. Gateway services should coordinate the advancement of logical and/or real time, and provide translation between different data models.
- Linkage to Web: Weapons effectiveness analysis may involve various devices, platforms, and even organizations dispersed over the network. Web services are expected to provide an ideal solution for integrating various simulation artifacts disparate platforms, systems, and organizations [11]. A SOAP interface and its services enable various web applications to communicate with the models within OpenSIM.
- Linkage to LVC Simulators: OpenSIM LVC gateway services automate integration with LVC standards, such as HLA, DIS (Distributed Interactive Simulation), and TENA (Test and Training Enabling Architecture) [12].

- Linkage to Engineering Tools: Dynamics of weapon systems are usually described with complex mathematical equations. Commercial tools, such as MATLAB®/SIMULINK® [13] are very popular to many engineers in M&S community to represent dynamics of weapon systems with mathematical equations. OpenSIM allows engineers to develop and test weapon models using MATLAB/SIMULINK. By using linkage services, the weapon mathematical models are connected to engagement and environment models within OpenSIM [14].

Most of the linkage services are under development. Common basic services, such as SOM/FOM translation services, are being identified. The SOM/FOM translation services provide data translation between various systems (i.e. Engineering Tools, LVC simulators, etc) in a uniform manner.

4 Conclusion

Measuring the effectiveness of weapon systems involves complex M&S tasks – Different types of models should be simulated with engineering-level, engagement-level, and their combined levels. Linkage to the legacy systems, such as LVC simulators, and commercial engineering tools make the M&S tasks even more intractable. An integrated simulation environment can help weapon engineers/analysts to semi-automate subsets of the required M&S tasks. OpenSIM provides a suite of tools and services for developing, executing and analyzing simulations, and linking the legacy systems and engineering tools for weapons effectiveness analysis. OpenSIM is under development, and we would like to test out OpenSIM with various weapons for continuous improvement. Some of the important research issues have not been addressed in this work – How to manage a model repository? How to compose complex weapon systems of systems by taking ontology into consideration? We would like to study these issues in the future.

Acknowledgement

This work was supported by Defense Acquisition Program Administration and Agency for Defense Development under the contract UD080042AD, Republic of Korea

5 References

[1] Department of Defense Report to Congress, "Network Centric Warfare", July 27, 2001, http://www.dod.mil/nii/NCW/

[2] Lalit K. Piplani, Joseph G. Mercer and Pichard O. Roop, "System Acquisition Manager's Guide for the use of Models and Simulations ", Management College, 1994

[3] Voratas kachitvishyanukul et. Al, "Simulation Environment for the New Millennium", Proceedings of the 2001 Winter Simulation Conference, pp. 541 – 547

[4] JMASS Developer's Reference Guide, JMASS 6.0, 2002

[5] Program Executive Office - Simulation, Training, and Instrumentation (PEO STRI), OneSAF International Users Manual Version 2.0, March 20, 2009

[6] IEEE Std 1516-2000, IEEE standard for modeling and simulation (M&S) high level architecture (HLA) – federate interface specification, 2000

[7] Zeigler B.P. and Kim T. G., and Praehofer H., "Theory of Modeling and Simulation", 2nd edition, Academic Press, New York, 2000

[8] Chang Ho Sung, Su-Youn Hong, and Tag Gon Kim, "Layered Approach to Development of OO War Game Models Using DEVS Framework", Proceedings of the Summer Computer simulation Conference, 2005, pp. 65-70

[9] L.F.Perrone, F.P.Wieland, J.Liu, B.G.Lawson, D.M.Nicol, and R.M.Fujimoto, "Application of the DEVS framework in Construction Simulation, Proceedings of the Winter Simulation Conference", 2006, pp 2077-2086

[10] Hyunhwi Kim, Kangsun Lee, et. al, "An ASW (Anti-Submarine Warfare) Simulator on Smart Phones", Proceedings of the World Multiconference on Systemics, Cybernetics and Informatics , 2010, pp. 333-337

[11] Hyung Gi Song, Kangsun Lee, "sPAC (Web services performance analysis center): Performance analysis and estimation tool of web services", Lecture Notes in Computer Science, 2005, pp. 109-119

[12] TENA – Test and Training Enabling Architecture, https://www.tena-sda.org/display/intro/Home

[13] MATLAB® and SIMULINK®, http://www.mathworks.com/products/

[14] Chang Ho Sung, Jeong Hee Hong and Tag Gon Kim, "Interoperation of DEVS Models and Differential Equation Models using HLA/RTI: Hybrid Simulation of Engineering and Engagement Level Models", 2009 Sping Simulation MultiConf., San Diego, CA, USA, Mar., 2009 , pp. 387-392

[15] Kyung-Min Seo, Hae Sang Song, Se Jung Kwon and Tag Gon Kim, "Measurement of Effectiveness for an Anti-torpedo Combat System Using a Discrete Event Systems Specification-based Underwater Warfare Simulator", Journal of Defense Modeling and Simulation, 2011

Computer Simulation of Water-Oil Separation in Cylindrical and Square Hydrocyclones

Carlos Rosales[1], Miguel Barron[2], Isaias Hilerio[3], and Dulce Medina[4]
Departamento de Materiales, Universidad Autonoma Metropolitana
Av. San Pablo No. 180, Col. Reynosa- Tamaulipas, 02220 Mexico City, Mexico
[1]al209384607@alumnos.azc.uam.mx , [2]bmma@correo.azc.uam.mx, [3]ihc@correo.azc.uam.mx
[4]dyolotzin@correo.azc.uam.mx

Abstract - *Computational Fluid Dynamics is employed to predict the efficiency of separation of water-oil mixtures in cylindrical and square hydrocyclones. Computer simulations are conducted using the Large Eddy Simulation model for turbulence. Mass flowrates of oil are trackeded for the upper and lower exits of each hydrocyclone. Finally, the results are compared for each hydrocyclone with the purpose of evaluate the separation efficiency.*

Keywords: Cilindrical hydrocyclone, Computational Fluid Dynamics, Large Eddy Simulation, square hydrocyclone, water-oil separation.

1. Introduction

Around 1891 hydrocyclones (HC) are employed by first time as small-scale separators, but until 1945 these devices become industrialy employed. Nowadays, HC have a wide range of applications, e.g. mass transfer devices, solid-liquid, liquid-liquid and solid-gas separators, in industries such as construction, mining, food, petrochemical and so on.

A lot of experimental, theoretical and computer work has been carried out in order to analyze the effect of the design parameters in water-oil separation efficiency of cylindrical HC. In computer simulations, Grady *et al.* [1] employed the Reynolds Stress model to predict the velocity fields and the separation efficiency in cylindrical HC. In [2] Paladino *et al.* studied the behavior of multiphase flow in HC. Huang [3] analyzed the phase distribution in a HC considering high oil inlet concentration. Chou *et al.* [4] studied the effect of the geometrical design of HC in the separation efficiency.
From past reports it has been concluded that the main parameters which determine the operating conditions in cylindrical HC are: the density of the involved phases, the inlet pressure, the upper exit diameter, and the lower exit diameter.

Currently, the bulk of research is focused on cylindrical HC, and little attention has been paid to another geometries, such as spherical or square ones. Related to square HC, Wang *et al.* [5] did a comparison between cylindrical and square geometries in HC to separate solid-liquid mixtures. In a recent work, Raoufi *et al.* [6] evaluated the separation efficiency of these HC.

Given that the application of square geometries in HC is relatively new, in this work is compared the water-oil mass flow rates in the exits of cylindrical and square HC. The performance of both HC is numerically explored using Computational Fluid Dynamics (CFD) software.

2. Mathematical model

Mass conservation is modeled through the well known continuity equation [7]:

$$\frac{\partial \rho}{\partial t}+\frac{\partial}{\partial x}(\rho v_x)+\frac{\partial}{\partial y}(\rho v_y)+\frac{\partial}{\partial z}(\rho v_z)=0 \qquad (1)$$

where

ρ = fluid density
v_i = ith component of velocity
t= time
x,y,z= spatial coordinates

Momentum conservation of a newtonioan fluid is governed by the Navier-Stokes equations (NS) [7]:

$$\frac{\partial}{\partial t}(\rho v_i)+\frac{\partial}{\partial x_j}(\rho v_i v_j)=-\frac{\partial p}{\partial x_i}+\frac{\partial}{\partial x_j}\left\{\mu_{eff}\left(\frac{\partial v_j}{\partial x_j}+\frac{\partial v_j}{\partial x_i}\right)\right\} \qquad (2)$$

where

p= pressure
μ_{eff} = effective fluid viscosity
x_j = jth component of x coordinate

The Large Eddy Simulation (LES) model is selected as turbulence model. LES finds the velocity profiles by means of filtering operations of the velocity fields. The instantaneous velocity u_t is defined as the

sum of the filtered velocity $\overline{u_i}$ and the residual component $\overline{u'}$:

$$u_i = \overline{u_i} + \overline{u_i'} \tag{3}$$

Equation (3) is applied to the NS equations [8]. From the resulting transformation, a new term which contains the stress tensor τ^{sgs}_{ij} is created and defined as

$$\tau^{sgs}_{ij} = -\mu t\left(\frac{\partial \overline{u_i}}{\partial x_j} + \frac{\partial \overline{u_j}}{\partial x_i}\right) \tag{4}$$

The resulting filtered NS equations are as follows:

$$\frac{\partial \overline{u_i}}{\partial t} + \frac{\partial\left(\overline{u_i u_j}\right)}{\partial x_j} = -\frac{1}{\rho}\frac{\partial \bar{p}}{\partial x_i} + \frac{\partial}{\partial x_j}\left(\mu \frac{\partial \overline{u_i}}{\partial x_j}\right) - \frac{\partial \tau j}{\partial x_j} + gi \tag{5}$$

here g_i is the ith component of gravity.

3. Computer simulations

A commercial CFD software is employed to construct the 3D geometries and solve the transient NS equations. Figures 1 and 2 show the geometry and dimensions of the square HD. Figure 3 shows the geometry and dimensions of the cylindrical HD.

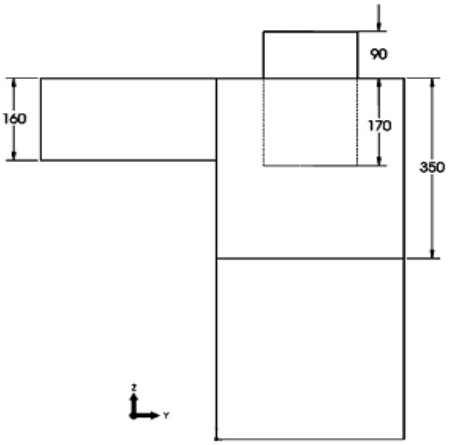

Fig. 1 Geometry and dimensions (in mm) of the square hydrocyclone [5].

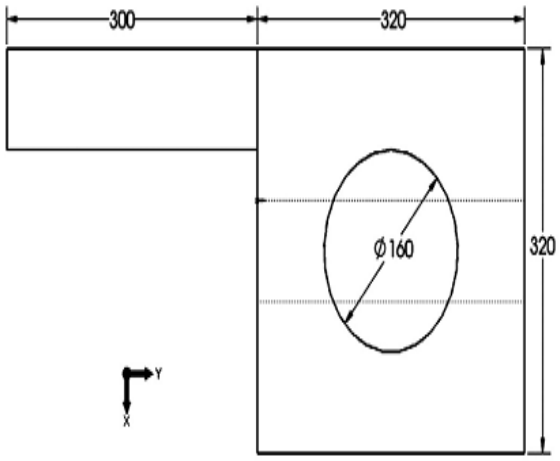

Fig. 2 Geometry and dimensions (in mm) of the square hydrocyclone [5].

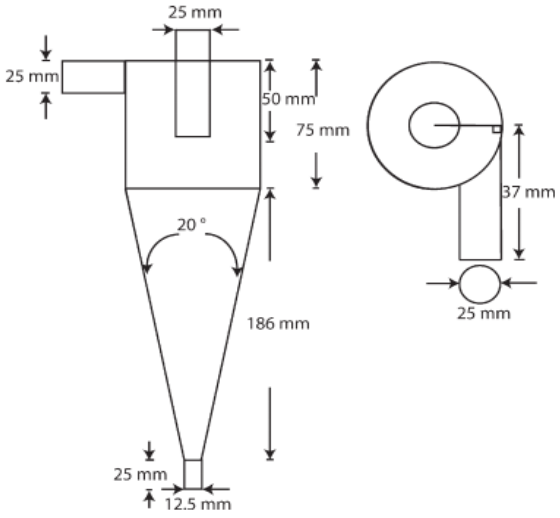

Fig. 3 Geometry and dimensions of the cylindrical hydrocyclone [11].

In Figures 4 and 5 are depicted the mesh employed in the square and the cylindrical HD, respectively.

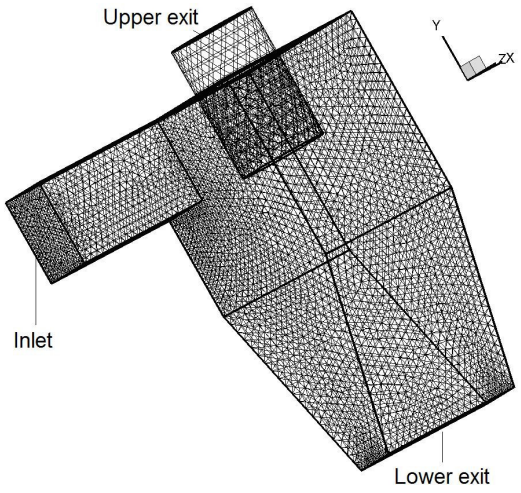

Fig. 4 Mesh of the square hydrocyclone.

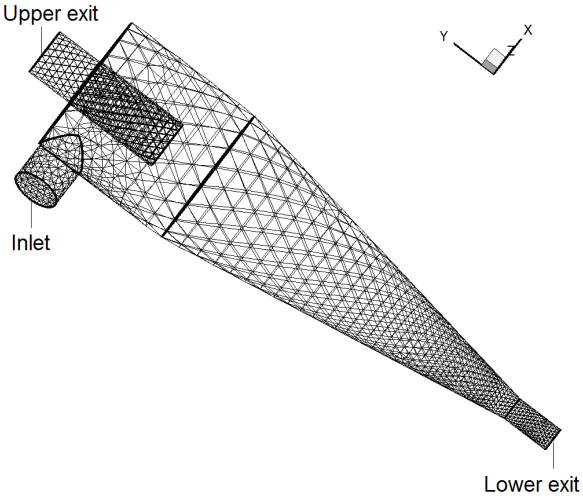

Fig. 5 Mesh of the cylindrical hydrocyclone.

In Table 1 are shown the properties of the considered fluids, i.e. oil and water.

Table 1. Properties of the considered fluids

Property	Value
Oil density (kg/m^3)	500
Oil viscosity (kg/m-s)	1.06
Water density (kg/m^3)	998.2
Water viscosity (kg/m-s)	0.001

The process is assumed isothermal. For simplicity in the numerical simulations, just two phases are considered, namely water and oil. An inlet velocity of 10 m/s for the water-oil mixture is considered.

4. Analysis of results

An inlet mixture with 50% in volume of water and 50% in volume of oil is assumed. Computer runs of 10 s are carried out in both the square and the cylindrical HD.

Figure 6 shows that the mass flow rate of oil leaving the square HD. It is appreciated that the oil mass flow rate is greater in the lower exit than that correspondig to the upper exit.

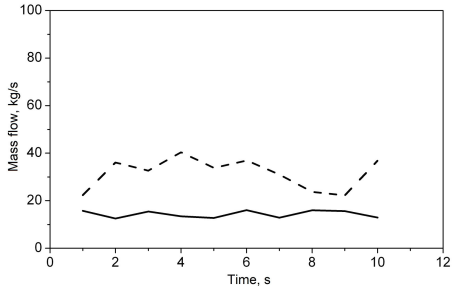

Fig. 6. Mass flow rate of oil in the upper exit (solid line) and the lower exit (dashed line) of the square hydrocyclone.

In accordance with the above figure, there is not a good separation between water and oil given that the flow of oil must be greater in the upper exit than in the lower one due to the lower density of oil compared with water. Maybe this anomalous behavior is originated by the loss of momentum caused by the geometry of the square HD, particularly the sharp angles between adjacent walls.

In Figure 7 are shown the mass flow rates of oil leaving the cylindrical HD. On the contrary to the square HD, in the cylindrical one the mass flow rate of oil is greater in the upper exit than in the lower one. This the behavior expected due to the low density of oil.

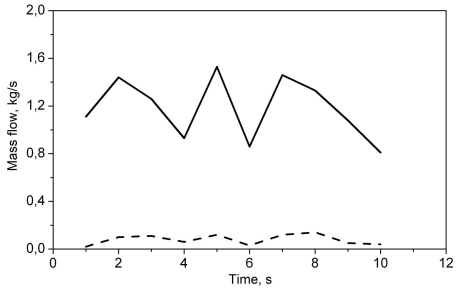

Fig. 7. Mass flow rate of oil in the upper exit (solid line) and the lower exit (dashed line) of the cylindrical hydrocyclone.

A comparison between Figures 6 and 7 indicates that the water-oil separation is better in the cylindrical HD than in the square one. Perhaps the loss of momentum in the square HD could be prevented by incresing the inlet velocity in this HD.

5. Conclusions

In accordance with the computer simulations, a proper water-oil separation is obtained in the cylindrical HD compared with that obtained in the square one. Possibly, the loos of momentum in the square HD due to its geometry originates its inefficient separation.

In future work it could be tested if the loss of momentum in the square HD could be prevented by incresing the inlet velocity in this HD.

References

[1] S. A. Grady, G. D. Wesson, M. Abdullah, E. E. Kalu, "Prediction of 10-mm hydrocyclone separation efficiency using Computational Fluid Dynamics", *Filtration and Separation*, Vol. *40*, pp. 40-46. 2003.

[2] E. E. Paladino, G. C. Nunes, L. Schwenk, "CFD analysis of the transient flow in a low-oil concentration hydrocyclone", *AIChE Annual Meeting, Conference Proceedings,* pp. 646-657. *2005.*

[3] S. Huang, "Numerical simulation of oil-water hydrocyclone using Reynolds-Stress model for Eulerian multiphase flows", *The Canadian Journal Of Chemical Engineering,* Vol. 10, pp. 829-834. 2008.

[4] L.Y.Chu,W.M.Chen,X.Z.Lee, "Effect of structural modification on hydrocyclone performance", *Separation and Purification Technology,* Vol. 21, pp. 71-86. 2000.

[5] S. Wang, M. Fang, Z. Luo, X. Li, M. Ni, K. Cen, "Instantaneous separation model of a square cyclone", *Powder Technology,* Vol. 102 pp. 65–70. 1999.

[6] A. Raoufi, M. Shams, H. Kanani, "CFD analysis of flow field in square cyclones", *Powder Technology,* Vol. 191, pp. 349-357. 2009.

[7] R. B. Bird, W. E. Stewart, E.N. Lightfoot. *Transport Phenomena,* 2nd Ed., Wiley, New York, 2002.

[8] S.B. Pope, *Turbulent Flows,* 1st eddition, Cambridge University Press, Cambridge, 2000.

[9] J. Smagorinsky,"General circulation experiments with the primitive equations: I. The basic experiment", *Monthly Weather Review,* Vol. 91, pp. 99-164. 1963.

[10] A.Yakhot, A.Ozag, V.Yakhot, M.Israeli, "Renormalization group formulation of Large Eddy Simulations", *Journal of Scientific Computing*, Vol. 4, pp. 139-158. 1989.

[11] J.A. Delgadillo, R.K. Rajamani, "Exploration of hydrocyclone designs using Computational Fluid Dynamics", *Int. J. Miner Process,* Vol. 84, pp. 252-261. 2007.

Computer Simulation of Slag Splashing in a Steelmaking Converter

Miguel Barron[1], and Isaias Hilerio[2]
Departamento de Materiales
Universidad Autonoma Metropolitana Azcapotzalco
Av. San Pablo 180, Col. Reynosa-Tamaulipas
Mexico, D.F., 02200 MEXICO
[1]bmma@correo.azc.uam.mx, [2]ihc@correo.azc.uam.mx

Abstract - *Some variables that influence the slag splashing phenomenon in an oxygen steelmaking converter are numerically analyzed in this work. The effect of lance height, jet velocity, jet exit angle and slag viscosity on the washing and ejection mechanisms of slag splashing is studied in this work employing two-dimensional transient computational fluid dynamics simulations. A parameter here called average slag volume fraction is proposed for the quantitative evaluation of the slag splashing efficiency. Besides, a qualitative comparison is made between the computational fluid dynamics results and physical model results from literature.*

Keywords: Computational fluid dynamics, basic oxygen furnace, oxygen steelmaking, refractory lining, slag splashing.

1. Introduction

Wear of refractory lining in oxygen converters for raw steel manufacturing is a factor which greatly influences the production costs in current industrial plants. In recent years slag splashing has emerged as a new technology to extend the lifetime of the refractory lining of converters by reducing the wear associated to thermal and chemical attack by slag and mechanical impact by scrap [1]. In the slag splashing process, molten slag remaining in the bottom of the vessel after the draining of steel is splashed to the converter sidewalls using a supersonic jet of nitrogen. Molten slag freezes at the converter walls forming a protective coating that decreases the wear of the refractory lining. Nitrogen is injected into the converter through a water-cooled vertical lance which has several inclined convergent-divergent nozzles.

Three main stages have been identified in the formation of the slag protective coating: transport of molten slag to the converter sidewalls, adherence of the molten slag to the sidewalls, and freezing and hardening of the slag layer [2]. Related to the transport of the molten slag to the converter sidewalls, two mechanisms are present: wash coating, and ejection coating [3]. The first one occurs due to the bulk movement of the molten slag to rise above the initial level, and the second one due to the ejection of slag droplets which adhere to the vessel sidewalls [4].

Several experimental studies on slag splashing are reported in the literature. These studies employ physical scale models of the converter, and cold liquids and air replacing molten slag and nitrogen, respectively [3, 5-6]. In [3] it is reported that large nozzle inclination and lance heights increase the splashing, and the main mechanism of splashing changes from ejection to washing as the viscosity of the liquid is increased. In [5] it is reported that the amount of slag splashed is increased as the lance is raised but beyond at a critical value of the lance height splashing decreases. In [6] it is shown that when the jet flow rate is increased or the liquid viscosity is decreased, the lower regions of the walls are splashed at a much greater rate. It is also shown that by changing the lance height, more liquid is deposited in the upper regions of the vessel at the expense of lower regions.

Numerical studies of gaseous jets impinging on a liquid surface are carried out using Computational Fluid Dynamics (CFD) simulations [7-9]. Agreement is reported between numerical and water model results, unfortunately these studies are mainly focused on the jet-surface interaction and the prediction of the surface topography, rather than liquid splashing. Few CFD studies are reported in the literature on the direct simulation of slag splashing using dimensions of actual converters and properties of molten slags.

In this work it is analyzed the influence of some variables on the slag splashing process using CFD simulations. The variables considered here are the lance height, jet velocity, jet exit angle and slag viscosity, and the dimensions of the converter correspond to an actual industrial converter of 150 metric tons. A dimensionless parameter here called

average slag volume fraction is proposed for the quantitative evaluation of the slag splashing efficiency. A qualitative comparison is made between the CFD results and experimental results from literature.

2. Mathematical model

In the slag splashing process, molten slag resting in the converter bottom is splashed to the converter sidewalls using a supersonic jet of gaseous nitrogen. The momentum of the nitrogen jet is transferred to the slag, which causes the slag to be stirred and ejected by the action of a standing wave and high shear forces, respectively [3]. Predominance of one of the coating mechanisms, i.e. washing or ejection, depends on factors such as the jet characteristics (velocity, exit angle), the operating conditions (lance height, molten slag depth) and the slag properties (viscosity, density, temperature). Inertial, gravitational, viscous and interfacial forces are acting on both phases, i.e. gaseous nitrogen and molten slag, causing a nonisothermal multiphase flow. To model this complex system here considered, equations which govern the fluid flow, the mass balance, the turbulence and the multiphase flow are required. Fortunately, nowadays such equations are well known, however, numerical solutions are mandatory.

The flow of an incompressible newtonian fluid is governed by the well-known Navier-Stokes equations, which in vector form are expressed as follows [10]:

$$\frac{\partial(\rho u_i)}{\partial t}+\frac{\partial(\rho u_i u_j)}{\partial x_j}=-\frac{\partial p}{\partial x_i}+\frac{\partial}{\partial x_j}\left\{\mu_{eff}\left(\frac{\partial u_i}{\partial x_j}+\frac{\partial u_j}{\partial x_i}\right)\right\} \quad (1)$$

where ρ is the fluid density, u_i is the i^{th} component of the fluid velocity u, t is time, x_j is j spatial coordinate, p is pressure, and μ_{eff} is the effective fluid viscosity. To maintain the mass balance in the system, the continuity equation [10] $\partial u_j/\partial x_j = 0$ must be solved. Turbulence is simulated by means of the classical two equations K-ε model [11]:

$$\rho v_j \frac{\partial K}{\partial x_j}=\frac{\partial}{\partial x_j}\left(\frac{\mu_t}{\sigma_K}\frac{\partial K}{\partial x_j}\right)+\mu_t\frac{\partial v_j}{\partial x_i}\left(\frac{\partial v_i}{\partial x_j}+\frac{\partial v_j}{\partial x_i}\right)-\rho\varepsilon \quad (2)$$

$$\rho v_j \frac{\partial \varepsilon}{\partial x_j}=\frac{\partial}{\partial x_j}\left(\frac{\mu_t}{\sigma_\varepsilon}\frac{\partial \varepsilon}{\partial x_j}\right)+C_1\mu_t\frac{\varepsilon}{K}\frac{\partial v_j}{\partial x_i}\left(\frac{\partial v_i}{\partial x_j}+\frac{\partial v_j}{\partial x_i}\right)-C_2\frac{\varepsilon}{K}\rho\varepsilon \quad (3)$$

In the Navier-Stokes equations the effective viscosity is determined from $\mu_{eff}=\mu_0+\mu_t$, where μ_0 is the laminar viscosity and μ_t is the turbulent viscosity. μ_t is obtained from $\mu_t=\rho C_\mu K^2/\varepsilon$, where K and ε are calculated by solving Eqs. (2) and (3), and C_μ= 0.09. Boundary conditions for K and ε at the inlet nozzle is calculated as follows [12]: $\kappa_{in}=0.01 u_{in}^2$, $\varepsilon_{in}=2K_{in}^{3/2}/D_n$ where U_{in} and D_n are the inlet nominal velocity and the nozzle diameter, respectively.

The Volume of Fluid (VOF) model to issue the multiphase flow is based on the assumption that two or more phases are not interpenetrating. For each additional phase q its volume fraction α_q is introduced as a variable. In each control volume the volume fractions of all phases sum to unity. The tracking of the interface between the phases is accomplished by solving the continuity equation for each phase [13]:

$$\frac{\partial \alpha_q}{\partial t}+\vec{v}\bullet\nabla\alpha_q=0 \quad (4)$$

3. Computer simulations

The physical dimensions of the considered converter, shown in Table 1, correspond to an actual industrial converter of 150 metric tons of capacity. The coordinate system and meshing of the converter are shown in Fig. 1. Just one nozzle, locate in the left side of the converter, is considered.

Some simplifications are needed in order to tackle the complex numerical task without excessive computer costs. An isothermal two-dimensional system is assumed. The coupled Navier-Stokes equations, the continuity equation, the turbulence model and the VOF model are numerically solved using the CFD technique. Transient isothermal two-dimensional computer simulations are carried out using a time step of 0.0001 s and a mesh consisting of 14075 trilateral cells. Total integration time is 5 s. The variables considered relevant to the slag splashing phenomenon which are studied in this work are the lance height, jet velocity, jet exit angle and slag viscosity. Table 2 shows the values of the above variables employed in the computer simulations, which correspond to actual values in industrial converters.

Table 1. Dimensions of the converter.

PARAMETER	VALUE
Height	7.2 m
Diameter	4.8 m
Lance diameter	0.2 m
Nozzle diameter	0.043 m
Number of nozzles	1

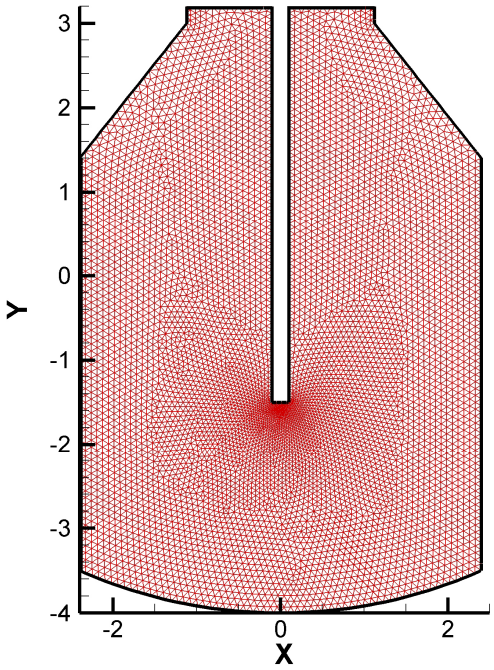

Figure 1. Coordinate system (m) and meshing of the converter.

Table 2. Values of the variables.

VARIABLE	VALUES
Lance height, h	1, 2, 3 m
Jet velocity, v	1, 1.5, 2 Mach number
Jet exit angle, α (see Fig. 2)	5, 10, 15 degrees
Slag viscosity, μ	0.01, 0.1, 0.5 kg/(m s)
Molten slag depth, h_s	0.5 m

4. Analysis of results

Numerical results are shown in this Section for an integration time of 5 s. In Fig. 2 one can be observe the distribution of phases in the converter for the following values of variables: lance height, 2 m; jet velocity, 1.5 Mach; jet exit angle, 10°; and slag viscosity, 0.1 kg/(m s). The blue and the red phases represent nitrogen and molten slag, respectively. Besides, in Fig. 2 are depicted the velocity vectors exhibiting two recirculatory zones. The red vector corresponds to the incoming supersonic nitrogen jet. The two mechanisms of slag coating, i.e. washing and ejection, are clearly seen in this figure. The slag splashing pattern shown in Fig. 2 is similar to those reported in the literature [3-4, 14].

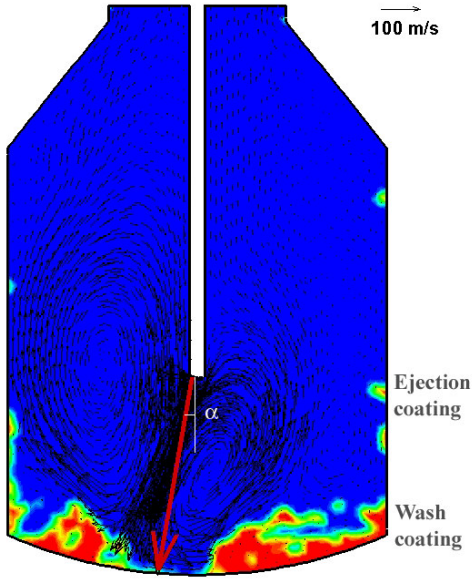

Figure 2. Distribution of phases and velocity vectors in the converter. Mechanisms of slag coating are marked. Blue phase is nitrogen, red phase is molten slag.

A dimensionless parameter $\bar{v}_s$ here called *average slag volume fraction* is proposed for the quantitative evaluation of the slag splashing efficiency. This parameter is calculated for the left vertical sidewall, and is defined as follows:

$$\bar{v}_s = \frac{\int_{H\,min}^{H\,max} v_s(h)dh}{H_{max} - H_{min}} \qquad (5)$$

where v_s is the local value of the slag volume fraction for a given time, and H_{min}= -3.5 m and H_{max}= 1.4 m (see Fig. 1) are the vertical coordinates of the start and end of the left vertical sidewall, respectively. The physical meaning of $\bar{v}_s$ corresponds to an average volume fraction of molten slag in the left sidewall due to the slag splashing by the combined action of washing and ejection mechanisms. It attempts to measure the efficiency of slag splashing: $\bar{v}_s = 0$ means absolutely no coating of the left sidewall, whereas $\bar{v}_s =$ 1 implies full coating of the aforementioned sidewall.

From now on the variables studied are the lance height, jet velocity, jet exit angle and slag viscosity with the values considered in Table 2.

4.1 Influence of lance height

Figs. 3-4 show the distribution of phases and the average slag volume fraction as a function of the lance height, respectively. Splashing is increased as the lance height is increased, however, beyond a certain value of the lance height, splashing decreases. This behavior is consistent with that reported in physical model experiments [3,5,15]. Small lance height causes a deep cavity in the molten slag and a large recirculation zone [4] which favours the prevalence of the wash coating mechanism. Large lance height promotes drop generation [16-17] and the ejection coating mechanism is favoured.

4.2 Influence of jet velocity

The depth of the cavity formed in the molten slag depends on the momentum of the nitrogen jet. In its turn, the jet momentum depends on the nitrogen mass flow rate and the velocity. Figs. 5-6 show the effect of the jet velocity on the distribution of phases and slag splashing. As the jet velocity is increased the slag splashing is increased. Low jet velocity promotes the stirring of the slag, and the wash coating mechanism dominates. High jet velocity generates high shearing forces and high drop generation [16- 17], therefore in this case the ejection mechanism becomes dominant. Anyway, as the jet velocity is increased the slag coating efficiency is raised, as is seen in Fig. 6. Results of physical models corroborate these findings [4,5].

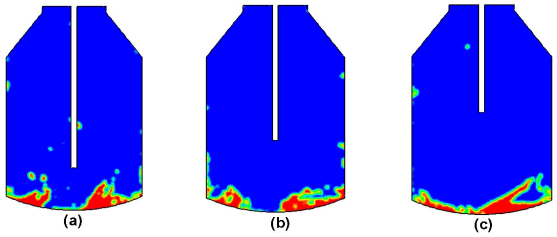

Figure 3. Effect of lance height on slag splashing. (a), (b) and (c) correspond to lance heights of 1, 2 and 3 m, respectively, for v= Mach 1.5, α= 10°, μ= 0.1 kg/(m s), h_s= 0.5 m.

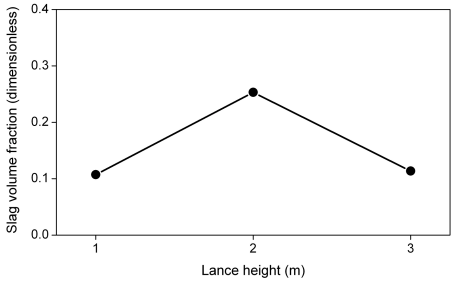

Figure 4. Average slag volume fraction as a function of the lance height.

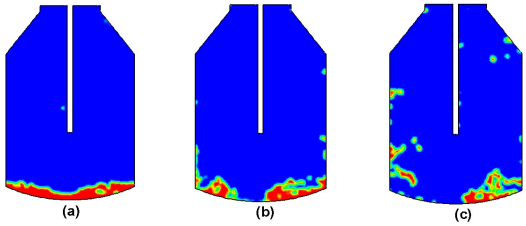

Figure 5. Effect of the jet velocity on the slag splashing. (a) Mach 1, (b) Mach 1.5, (c) Mach 2 , for h= 2 m, α= 10°, μ= 0.1 kg/(m s), h_s= 0.5 m.

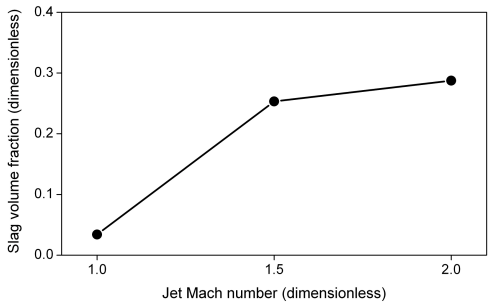

Figure 6. Average slag volume fraction as a function of the jet velocity.

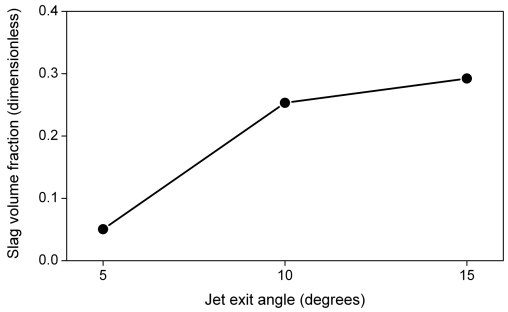

Figure 8. Average slag volume fraction as a function of the jet exit angle.

4.3 Influence of jet exit angle

When the lance nozzle is inclined the jet exits from the nozzle and enters to the converter with an angle α (see Fig. 2). As the exit angle is increased, the vertical component of the jet velocity is decreased and the horizontal component is increased. In this case the shearing forces are increased and an overall increase in the amount of slag splashed is observed [3,4]. Of course, when the angle becomes too large and goes beyond a critical value, the jet does not impact the slag anymore. The value of the critical angle depends on the lance height and the molten slag depth. In [4] it is reported that the critical value of the jet exit angle is 45°. Beyond 45° the slag splashing would be decreased.

4.4 Influence of slag viscosity

The influence of the slag viscosity is observed in Figs. 9-10. In accordance to Fig. 10, as viscosity is increased the efficiency of slag coating is decreased. This is explained by the fact that for higher viscosities higher shearing forces are needed for drop generation and the formation of a standing wave. From this point of view, a low viscosity of the molten slag would be desirable, unfortunately slags with low viscosity have little adherence to the converter sidewalls and tend to flow down [4]. On the other hand, the viscosity of a molten slag mainly depends on temperature, composition and the presence of solid phases. Then, in some plants the slag is subjected to a conditioning process for optimizing its viscosity through the addition of materials such as magnesia and ferrous oxide. Comparing Figs. 4, 6, 8 and 10 one can observe that the slag viscosity is, among the variables studied, that which gives the highest slag coating efficiency.

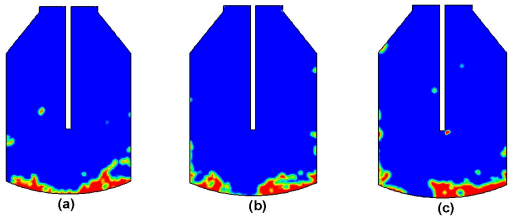

Figure 7. Effect of the jet exit angle on the slag splashing: (a) 5°, (b) 10°, (c) 15°, for v= Mach 1.5, h= 2 m, μ= 0.1 kg/(m s), h_s= 0.5 m.

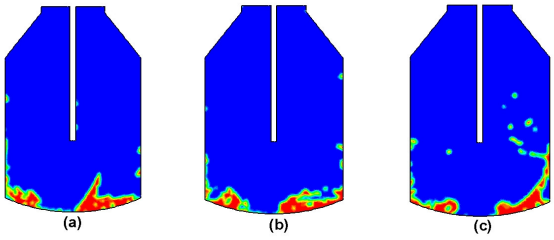

Figure 9. Effect of the slag viscosity on the slag splashing. (a) 0.01, (b) 0.1, (c) 0.5 kg/(m s), for v= Mach 1.5, h= 2 m, α= 10°, h_s= 0.5 m.

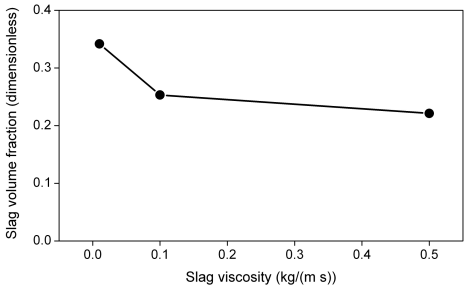

Figure 10. Average slag volume fraction as a function of the slag viscosity.

5. Conclusions

The slag splashing phenomenon has been studied by means of Computational Fluid Dynamics simulations. A parameter to carry out a quantitative evaluation of the coating efficiency of the slag splashing process is proposed. The effect of variables such as the lance height, jet velocity, jet exit angle and slag viscosity on the coating efficiency was elucidated. Numerical results of this work are in qualitative agreement with those reported in the literature for physical models. Among the studied variables, the most influential one is, apparently, the slag viscosity.

6. References

[1] C.J. Messina, J.R. Paules. The Worldwide Status of BOF Slag Splashing Practices and Performance. *Steelmaking Conference Proceedings*, Pittsburgh, PA, 1996, 153-55.

[2] T. R. Galiullin, E. V. Protopopov, V. V. Sokolov, A. G. Chernyatevich. Gas-Jet Conditions in the Slag Coating of Oxygen-Converter Linings. *Steel in Translation*, 38 (2008) 97-100.

[3] K.D. Peaslee. Physical Modelling of Slag Splashing in the BOF. *Iron and Steel Engineer*, 73 (1996) 33-37.

[4]. K.C. Mills, Y. Su, A.B. Fox, Z. Li, R.P. Thackray, H.T. Tsai. A Review of Slag Splashing. *ISIJ International,* 45 (2005) 619-633.

[5] M.J. Luomala, T.M.J. Fabritius, E.O. Virtanen, T.P. Siivola, T.L.J. Fabritius, H. Tenkku, J.J. Härkki. Physical Model Study of Selective Slag Splashing in the BOF. *ISIJ International,* 42 (2002) 1219-1224.

[6] K.D. Peaslee, W. Chen. Important Factors for Effective Slag Splashing. *CIM Conference Proceedings*, Edmonton, Canada, 2004.

[7] L. Salinas, R. Fuentes. Interaction between a Gaseous Vertical Descending Jet and a Liquid Surface-A Theoretical and Experimental Study. *Copper 99 Conference Proceedings*, Phoenix, AZ, 1999.

[8] A. Nguyen, G. Evans. Computational Fluid Dynamics Modelling of Gas Jets Impinging onto Liquid Pools. *Applied Mathematical Modelling*, 30 (2003) 1472-1484.

[9] M. Ersson, A. Tilliander, L. Jonsson, P. Jonsson. A Mathematical Model of an Impinging Air Jet on a Water Surface. *ISIJ International,* 48 (2008) 377-384.

[10] R.B. Bird, W.E. Stewart, E.N. Lightfoot. *Transport Phenomena*, 2nd Ed., Wiley, New York, 2002.

[11] B.G. Thomas, Q. Yuan, S. Sivaramakrishnan, T. Shi, S.P. Vanka, M.B. Assar. Comparison of Four Methods to Evaluate Fluid Velocities in a Continuous Slab Casting Mold. *ISIJ International,* 41 (2001) 1262-1271.

[12] G. Solorio-Díaz, R.D. Morales, J. Palafox-Ramos, L. García-Demedices, A. Ramos-Banderas. Analysis of Fluid Flow Turbulence in Tundishes Fed by a Swirling Ladle Shroud. *ISIJ International,* 44 (2004) 1024-1032.

[13] C.W. Hirt, B.D. Nichols. Volume of Fluid (VOF) Method for the Dynamics of Free Boundaries. *Journal of Computational Physics*, 39 (1981) 201-225.

[14] K.M. Goodson, N. Donaghy, R.O. Russell. Furnace Refractory Maintenance and Slag Splashing. *Iron and Steelmaker*, 22 (1995) 31-34.

[15] O. Olivares, A. Elias, R. Sanchez, M. Diaz-Cruz, R.D. Morales. Physical and Mathematical Models of Gas-Liquid Fluid Dynamics in LD Converters. *Steel Research*, 73 (2002) 44-51.

[16] N. Standish, Q. L. He. Drop Generation due to an Impinging Jet and the Effect of Bottom Blowing in the Steelmaking Vessel. *ISIJ International,* 29 (1989) 455-461.

[17] Q. L. He, N. Standish. A Model Study of Droplet Generation in the BOF Steelmaking. *ISIJ International,* 30 (1990) 305-309.

[18] V. A. Sheremet, A. V. Kekukh, S. V. Troshii, A. P. Stovpchenko, A. S. Brodskii, O. I. Pavlyuchenkov. Experience in the Use and Comprehensive Maintenance of Converter Refractory Linings. *Refractories and Industrial Ceramics*, 47 (2006) 75-77.

SESSION

MODELING

Chair(s)

TBA

Modeling with Uncertainty – Interval Computations Using Fuzzy Sets

J. Honda, R. Tankelevich

Department of Mathematical and Computer Sciences,

Colorado School of Mines, Golden, CO, U.S.A.

Abstract – *A new method of interval computations using fuzzy sets and stochastic processes is proposed. It is concerned with the development of a practical technology that can be used by engineers and researchers to facilitate the process of decision making under uncertainty, in a state of "bounded rationality". The methodology called Interval Resolution considers a model and interval values specified by the researcher for each model parameter of interest, and returns the feasible interval ranges for all model's parameters. The process continues with the researcher refocusing on different subsets of parameters as needed and can end up with collapsing some intervals. Fuzzy sets and Monte Carlo methods are used to compute the feasible ranges. A modeling software, Interval Solver, and a descriptive langua ge are proposed and implemented along with the IR Integrated Development Environment. A number of applications have been considered. Theoretical and experimental analysis of computational efficiency is under way.*

Keywords: Interval computations, models with uncertainty, fuzzy sets, decision making, bounded rationality

1 Introduction

In general field of modeling and engineering, researchers and designers always deal with uncertainties in setting model parameters. Making decisions about the proper parameters and factors requires interval analysis. Researchers in the mathematical modeling and engineering design community have identified interval analysis as a potentially powerful design tool, and called for their further development [1, 2, 3]. However, efficient practical methods are still to be devised that can handle the complexities of models used in many engineering applications.

Here we present a technology called *Interval Solver* that can facilitate finding the relations between the model's characteristics, with uncertainties given as conditions of the model. Using *Interval Solver*, one can define the model in the form of implicit interval equations. Initial estimates of the intervals are given by the modeler. By changing the intervals of uncertainties for a subset of the variables, one can find out how the other intervals are affected. New *feasible* intervals are computed by *Solver*. Now, the modeler can decide on what intervals are to be controlled next and make the appropriate changes. A new set of feasible intervals for all variables are recalculated by *Solver*. The process continues until the intervals (maybe, completely collapsed) are found that are considered as the most agreeable with the objectives of the engineering design or the model validation.

The underlying concept of this methodology is in compliance with the principle of *bounded* rationality developed by Herbert Simon [4] who identified the importance of the fact that in the presence of uncertainty, humans will attempt to isolate a closed subsystem that contains only a limited number of parameters and a limited range of consequences. Modeling tools should assist and improve the effectiveness of this human response to bounded rationality.

The *Interval Solver* methodology can be applied to various modeling situations. As just a single example, consider chemical and biological modeling using kinetic equations. The experimental results are often used to validate the model; however, the observed concentrations of the reagents and other measurable quantities leave the researcher with a significant uncertainty in the ways of how to interpret the results. In [5], certain chemical kinetics equilibrium problems have been solved correctly with interval techniques applied to analysis of sensitivity of such characteristics as the dimensionless numbers, some scalars, such as the max/min concentrations, or max/min spatial and temporal derivatives, or concentrations (spatial/temporal derivatives) at the boundaries of the chemical reactors, and others.

In engineering, designers often use bounded parameters during the preliminary design phase to provide flexibility, and/or to express uncertainty about what the design

component "should look like". Resolving intervals of uncertainty helps to devise a proper set of parameters adjusted *ad hoc.*

The main difficulty of finding intervals satisfying the model is in solving the inverse model, namely, in finding the feasible ranges of parameters and input variables of the model given the intervals of its output values. By changing an interval for one of the variables, any other intervals become affected and should automatically change to comply with the new intervals.

The methods of interval and soft computing seem to be appropriate for this problem. There is a significant body of research in this field (a comprehensive analysis of the state of art in the interval and soft computing field can be found in [6].

The approach implemented in *Interval Solver* is based on combining the fuzzy sets presentation of intervals and stochastic modeling that work well with interval computations.

Use of fuzzy sets and statistical method of resolving intervals makes it a robust method capable of handling "difficult" model characteristics such as nonlinearity, discontinuity, non-algebraic functions, etc [7].

2 Interval Resolution

We consider a model with N degrees of freedom represented by variables x_i, $i \in [1, N]$. Each variable is given with its interval, $X_i = [x_{i,\min}, x_{i,\max}]$. There is an operator, $\Re$, applied to a k-th set of intervals $\{ X_i \}^k$ to produce an updated set of intervals $\{ X_i \}^{k+1} = \Re (\{ X_i \}^k)$ such that any repeated applications of $\Re$ to the same set of intervals does not change them thus approaching the *fixed* point in interval resolution. We call intervals corresponding to fixed point *balanced* or *feasible*.

It is assumed that the model the interval analysis is applied to is a mathematical description of a problem which can be presented as a function $\mathbf{F}(\boldsymbol{V})$ that takes some inputs as a mathematical vector $\boldsymbol{V}$ to produce an output vector $\boldsymbol{W}$:

$$\boldsymbol{W} = \mathbf{F}(\boldsymbol{V}).$$

Figure 1 depicts this relationship.

This is considered to be a model of a problem for which an appropriate set of values $\boldsymbol{V}$ should be found to satisfy a certain constraints for output $\boldsymbol{W}$. The typical process is based on the *What If* paradigm. What happens to $\boldsymbol{W}$ if a value of $\boldsymbol{V}$ *is* somehow changed? Again, more typically, in such analysis one keeps the output $\boldsymbol{W}$ within a specific interval of values while trying different combinations of input values $\boldsymbol{V}$.

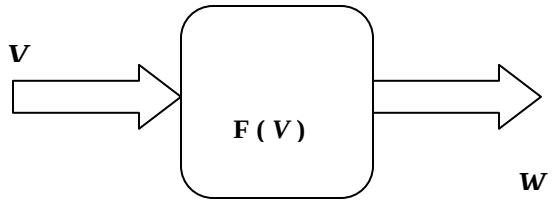

Figure 1. A typical process of modeling and sensitivity analysis

With the interval method, the decision making is the process where both input $\boldsymbol{V}$ and output $\boldsymbol{W}$ are treated similarly. Both input and output variables belong to the same set of variables $\boldsymbol{X} = \boldsymbol{V} \cup \boldsymbol{W}$ thus allowing to use input and output variables interchangeably: $\boldsymbol{\Phi(X) = 0}$ where implicit function $\boldsymbol{\Phi (X) = F (V) - W}$.

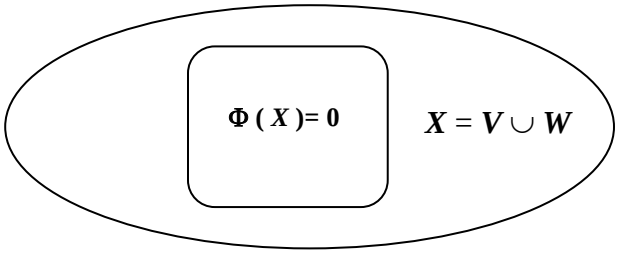

Figure 2. The interval based sensitivity analysis

As Figure 2 shows all variables can be used interchangeably either as input or output, so it is possible to use either **V** or **W** to see how they affect each other.

Each variable is taken from a given interval. The proposed decision making process finds all possible combinations of **V** and **W** that satisfy the equation $\boldsymbol{\Phi(X) = 0}$, thus producing all *feasible* subintervals defining all possible solutions.

Example. Given

$$\boldsymbol{y - ax^2 = 0} \ (\boldsymbol{x, y \in X})$$

and intervals from which x and y can be taken, find all possible pairs (x, y) satisfying the given equation.

Let $a = 1$, given intervals for $x = [-3,3]$ and for $y = [1,4]$, the interval resolution produces the following feasible intervals for x:

[-2,-1], [1,2] (the original interval is split onto two subintervals)

and for *y*:

[1,4] (this interval is not changed by this process).

This result can be interpreted as application of the operator $\Re$ to given intervals for *x* and *y*:

{[[-2,-1], [1,2]], [1,4] } = $\Re${[-3,3], [1,4]}

One can consider any values in the resulted intervals for both *x* and *y* as *productive* in the sense that there is at least one solution trajectory that passes through the point represented by this value. Now, any desirable changes can be made in the obtained intervals and applying the operator $\Re$ again, thus producing a new set of intervals until the desirable combination of *x* and *y* can be found.

The process involved in the single $\Re$ application converges to the completely balanced set of intervals.

The proposed interval analysis uses Monte Carlo method as a general approach to any problem having *N* degrees of freedom represented by variables x_i, $i \in [1, N]$. Each variable is given with its interval, $X_i = [x_{i,\min}, x_{i,\max}]$. Randomly selected values from the X_i intervals are processed to calculate the left hand side function in the $\mathbf{\Phi(X) = 0}$ equation. The selected values from the X_i intervals are given the weights from 0 to 1 depending on how close the calculated function approaches 0. This represents another important feature of the method – the use of fuzzy sets.

The membership function, μ, for the implicit non-linear model of *M* equations:

$$\Phi_k(x_1, x_2, \dots, x_N) = 0, \qquad i = 1, 2, \dots, M$$

represents the "soft" intersection of the fuzzy sets for each equation (the product of their membership functions) and is calculated as a single multidimensional bell curve:

$$\mu = \prod_{k=1}^{M} e^{-{F_k}^2(x_1,x_2,\dots,x_N)/\sigma^2} = e^{-\sum_{k=1}^{M} {F_k}^2(x_1,x_2,\dots,x_N)/\sigma^2}$$

To estimate the performance of the method let's start with finding a specific point x_0 with and resolution Δx in an interval of *x* having the unit length.

If the uniform distribution of probability is used then the probability of finding the point x_0 is

$\mathbf{Pr}[x = x_0] = \Delta x$.

Next, consider a two variable problem, such as in *Example* above. The probability of finding a point in the feasible interval will be given as a ratio of the total length of feasible intervals to the length of the original interval. In the case of *x*, it will be $\mathbf{Pr}[x \in [-2,-1] \cap [1,2]\ ] = 4/6$.

The probability of finding a bound for a variable x_0 of a feasible interval in a system having *n* degrees of freedom is given as the product of probabilities $\mathbf{Pr_i}$ to find a point in *n*-1 feasible intervals times the probability $\mathbf{Pr}_0$ to find a single point in the given interval. Assuming that all original intervals are normalized to the unit length then the probability to find a bound is:

$$\mathbf{Pr}[x0 = \text{bound}] = \Delta x \prod_{i=1}^{n-1} \Delta I_i$$

where ΔI_i is a feasible interval for x_i ($0<\Delta I_i <=1$).

Assuming ΔI_i = ½ and $m = 1/\Delta x$, the previous formula becomes

$\mathbf{Pr}[x_0 = \text{bound}] = 2^{n-1}/m$.

Some numerical examples illustrate this analysis as shown further. The major advantage of using the Monte Carlo method applied to the fuzzy set of a non-linear model is the fact that it seems working (1) with any type of mathematical models, (2) converges much faster than other deterministic methods and, at the same time, (3) provides the full scope of the feasible intervals even if the original intervals become split onto many subintervals after applying operator $\Re$.

3 Graphical Interface

Graphical user interface is a significant part of *Interval Solver* technology. The intervals both original and feasible are produced under user's control. Given initial intervals for variables *x* and *y*

($x \in$ [-1,1], $y \in$ [-2,2]))

in the above quadratic model, the feasible intervals for the both variables can be depicted in many graphical forms. The linear diagrams as shown in Figure 3(a, b) are one of the possible graphical methods.

The feasible intervals found as ($x \in$ [-1,1], $y \in$ [-0,1]) are depicted as thick lines while the thin lines represent the original intervals (Figure 3, a).

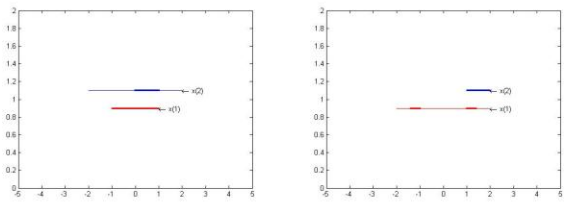

(a) (b)

Figure 3. Interval resolution for a quadratic equation

The user can try other intervals. For intervals [-2 2; 1 2] the solution ($x \in$ [-1.41,-1]$\cap$ [1,1.41], $y \in$ [1,2]) obtained is shown in Figure 3, b.

Another simple example concerns the relationship between the intervals of variables in the dimensionless expression for diffusivity in chemical reactions:

$$D = \frac{D_0 \varepsilon}{uLT}$$

with six variables,

$$D, D_0, \varepsilon, u, L, T.$$

A set of initial (arbitrary) intervals can be set. An example of the interval distribution, both initial and feasible is shown in Figure 4.

This small model can be resulted from the decomposition of a larger chemical model including differential equations of chemical kinetics. Each part of the model can be resolved separately and then iteratively matched with other submodels.

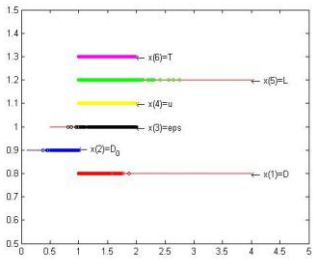

Figure 4. Interval resolution for diffusivity equation

4 Interval Solver

Interval Solver is a technology developed to facilitate the Interval Resolution methodology. Several algorithms were investigated as potential candidates for use by the technology.

Simple Monte Carlo Algorithm

This basic implementation of the Interval Solver method conducts *N* random walks. Each walk takes as input a system of implicit equations, i.e. $\mathbf{\Phi(X)=0}$, and randomly generated values for each parameter of the model, i.e. the solution vector **X**. The values are selected so that they are within the corresponding user prescribed intervals for each parameter in **X**. The values in **X** are applied to each equation of the model. The results of this application are then evaluated using the soft membership function according to [7]. This results in a fuzzy membership value expressing how "close" **X** is to being an exact solution (i.e. generating $\mathbf{\Phi(X)=0}$). The solution, and its corresponding fuzzy membership value are stored in a data structure for graphical presentation after the *N*-th random walk. Below is a diagram of the algorithm:

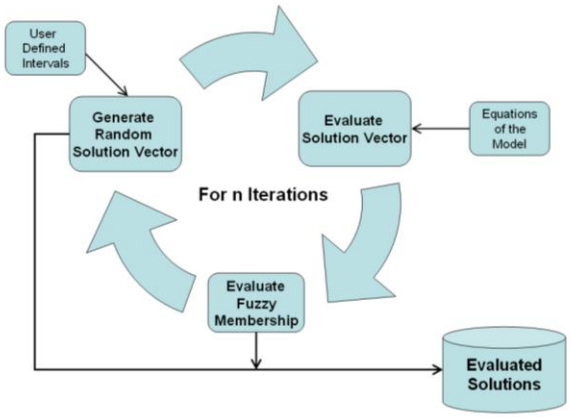

Figure 5. Diagram of the Simple Monte Carlo Method

Bubble Monte Carlo Algorithm

The bubble Monte Carlo approach improves on the simple Monte Carlo algorithm efficiency by guiding the random walk process over successive iterations, or epochs. In the beginning, *K* number of solutions are generated. The minimum and maximum bounds for each variable are tested during this first iteration. Therefore, it is a requirement that $K>2V$, where *V* is the number of parameters in the model.

The solution vectors for these boundary tests are randomly generated and saved for the boundary test variable which is assigned the maximum or minimum bound. The remaining $K-2V$ solution vectors are generated at random, using the prescribed intervals. The solution vectors are evaluated and fuzzy membership estimated in the same manner as the simple Monte Carlo algorithm, and the algorithm proceeds through *N* epochs.

Each epoch has a certain threshold value, μ_T, which is assigned using a function of the current epoch. After the

solution vectors are evaluated and fuzzy membership estimated, the solution vectors for the next epoch are assigned using $\boldsymbol{\mu_T}$ and the solution vectors from the current and previous epochs. More specifically, say $\boldsymbol{\mu_{k,n}}$ is the fuzzy membership value for the k^{th} solution vector of the n-th epoch (n being the current epoch). Then, assigning values for the *k-th* solution vector of the n+1 epoch uses the following decision structure:

- If $\boldsymbol{\mu_{k,n-1} < \mu_{k,n}}$ **and** $\boldsymbol{\mu_{k,n} >= \mu_T}$
  Then the current epoch improved on the previous epoch's solution, and is above $\boldsymbol{\mu_T}$. So permute each parameter of the k^{th} vector of the current epoch (n)by a random amount. This permutation is a function of $\boldsymbol{\mu_T}$ so the permutation amount decreases as the epochs increase.
- If $\boldsymbol{\mu_{k,n-1} >= \mu_{k,n}}$ **and** $\boldsymbol{\mu_{k,n} >= \mu_T}$
  Then the current epoch did not improve on the previous epoch's solution and is above $\boldsymbol{\mu_T}$. So permute each parameter of the k^{th} vector of the previous epoch (n-1) by a random amount.
- If $\boldsymbol{\mu_{k,n} < \mu_T}$
  Then the current epoch solution vector has membership below $\boldsymbol{\mu_T}$. So randomly assign each parameter of the k^{th} vector to be between the initial minimum and maximum bounds.

After assignment, the vectors are evaluated using the model, and fuzzy membership is estimated. The solution vector and its membership are stored in a data structure for graphical display after the last epoch, and then the next iteration proceeds.

The algorithm has a higher efficiency than the simple algorithm. This is due to the fact that the permutation function and solution vector acceptance are both functions of $\boldsymbol{\mu_T}$. More specifically, large changes in the solution vectors are allowed in the first epochs, while $\boldsymbol{\mu_T}$ is low; thereby allowing a comprehensive scan of the entire range. As epochs increase, and $\boldsymbol{\mu_T}$ increases towards 1, the permutation amount decreases; thereby allowing for greater exploration of the feasible solution intervals, and less exploration of the infeasible regions.

As described in the next section, this method was found to be more efficient than the basic Monte Carlo approach.

5 Experimental results

The properties of the above *Interval Solver* algorithms were examined using various statistical methods. Some of them are discussed here for the same quadratic model as above (Figure 3 a).

Analysis of Simple Monte Carlo Algorithm

The "Simple Monte Carlo" algorithm was used as baseline for a general analysis of the method, and benchmark for the more advanced algorithms.

The random walk is a significant part of the *Interval Solver* algorithms A random vector $\mathbf{X} = [x, y]$ and the corresponding fuzzy set's membership function, μ, are evaluated.

The graphs of the envelopes of $\mu(x)$ are shown in Figure 6. The peaks are the points where the variables produce the best fit for the given model. The peaks equal to 1.0 represent the points belonging to the sought feasible interval. The peaks lower than 1.0 belongs to the fuzzy interval of solutions.

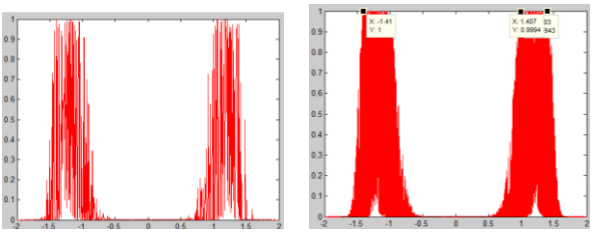

Figure 6. The $\mu(x)$ envelopes with number of samples 1000 and 10,000

In the case of 10,000 samples, statistical accuracy of funding the interval boundaries = 0.003/4=0.1%. Exhaustive search with the same number of steps (100 by 100) has the accuracy 4/100=4%. (The boundaries are presented as data tips on the graph.) This result agrees with the theoretical analysis. In order to improve on the simple algorithm's efficiency, we noted the following observations and relationships:

1. As demonstrated in the table below, *reducing* the exact solution membership value increases the probability that the random walk will encounter an exact solution (as defined by the lowered membership value). T**he** probability of finding at least one exact solution, with *reduced accuracy*, belonging to the feasible intervals is estimated as a deviation $\Delta\mu = 1.0 - \mu$:

Δμ	0.001	0.1	0.2	0.4	0.6
Pr(Δμ)	**0.0128**	**0.135**	**0.2**	**0.3**	**0.42**

Table 1: Reduced Accuracy (Δμ) versus exact solution encounter probability (Pr(Δμ))

Numerous experiments confirm the linear character of the probability of finding a single solution as a function of its accuracy.

Corollary to this then is the notion that *increasing* the exact solution membership value reduces the probability that the random walk will encounter non-exact solutions.

2. The probability of finding, at least, a single (exact) solution vs. the model's space dimension, *N*, (number of degrees of freedom) is confirmed to be the following function:

$\Pr(\Delta\mu=0.001) = a / 2^{N-2}$.

(In the case of the above quadratic model, $a = 0.0128$.)

3. Since we deal with the one dimensional search space the probability of finding at least one point with μ close to 1 is high:

$$\mathbf{Pr}[x0 \;=\; \text{bound}] \;=\; \Delta x \prod_{i=1}^{n-1} \Delta I_i$$

Analysis of the Bubble Monte Carlo Algorithm

These results imply that it is possible to develop an algorithm which identifies and expands the feasible intervals by slowly increasing μ (decreasing Δμ) so that the length of the subinterval(s) traversed by the random walks are iteratively decreased until only the final exact solutions remain. The previously described bubble Monte Carlo algorithm implements these findings.

The following table summarizes the efficiency of the various algorithms in identifying the feasible intervals for the same quadratic model as above (Figure 3 a). For the purposes of this experiment, we found the number of solution points required to "identify" the feasible interval length to within 98% of the analytically derived length of 2.0 for X, and 1.0 for Y.

Algorithm	Solutions Required
Simple Monte Carlo	3500
Bubble Monte Carlo	1500

Table 2: Efficiency of two algorithms described above

6 Interval Solver (software)

A software implementing the *Interval Solver* methodology was developed to analyze the performance of the various *Interval Solver* algorithms, and to demonstrate how the proposed method might be practically implemented. Figure 7 shows an example of the *Interval Solver* GUI with a model's run.

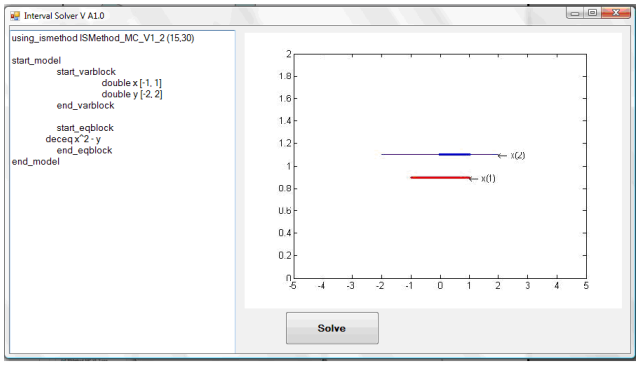

Figure 7. The panel of GUI of Interval Solver software

The left panel is used to enter the desired interval solver algorithm, equations of the model, the list of variables and the initial intervals. On the right, the graphical output is presented. Below, the control panel is located.

7 Conclusion

We presented here a new method, *Interval Solver*, that provides an efficient, robust methodology of interval analysis through its novel use of fuzzy sets in the Monte Carlo simulation settings.

8 References

[1] J. Aughenbaugh and C. Paredis, "Why Are Intervals and Imprecision Important in Engineering Design?" *Reliable Engineering Computing Workshop, Savannah, GA, USA, 2006*, 2006.

[2] M. Bruns, C. Paredis, and S. Ferson, "Computational Methods for Decision Making Based on Imprecise Information," 2006.

[3] National Research Council (U.S.). NetLibrary, Inc., *Theoretical foundations for decision making in engineering design*, Washington D.C.: National Academy Press, 2001.

[4] H. Simon, *Administrative behavior : a study of decision-making processes in administrative organizations*, New York: Free Press, 1997.

[5] M. Stadtherr, *Interval analysis: Application to chemical chemical engineering design problems.* In: A. Iserles (ed.) Encyclopedia of Optimization. Kluwer Academic, Norwell, MA (2001)New York.

[6] Chenyi Hu, Ralph Baker Kearfott, Andre de Korvin, Vladik Kreinovich, editors. *Knowledge Processing with Interval and Soft Computing*. London : Springer Verlag, 2008. ISBN: 978-1-84800-325-5.

[7] Zadeh, L.A., "Fuzzy Sets as a Basis for a Theory of Possibility", *Fuzzy Sets and Systems*, 100 (Supplement), 1999, pp. 9-34.

New Trends in Modeling and Identification of Loudspeaker with Nonlinear Distortion

Pascal Brunet and Bahram Shafai
Department of Electrical and Computer Engineering, Northeastern University, Boston, MA, USA

Abstract— *This paper provides recent developments in modeling and identification of nonlinear systems pertinent to loudspeaker with nonlinear distortion effect. It is known that when small loudspeakers are driven at high playback levels the nonlinear characteristics of these speakers become a major source of sound degradations. Consequently it is essential to find a good model that matches to the loudspeaker response for the purpose of predicting and preventing the nonlinear distortion. This becomes particularly important for the purpose of improving sound quality of mobile phones. This paper presents the loudspeaker operation, the issues of concern, and nonlinear modeling techniques that can reliably be used for its identification process. Frequency domain and state-space modelings are considered and emphasis is given towards polynomial nonlinear state-space models which can better tie to nonlinear identification of loudspeaker.*

Keywords: nonlinear systems, loudspeaker, modeling, identification, best linear approximation

1. Introduction

Acoustic transducers are part of our everyday life, and we use them intensively throughout the day using our cellphones, listening to the radio in our car, looking at the TV or playing games on computer at night. In all cases, sound distortion is present and has negative impact on the sound quality, diminishing listening pleasure and, worse, speech intelligibility. In some cases, texting is the only way to get your message across. In particular, cellphones, teleconference systems, PC systems use small loudspeakers driven at high-amplitude to get enough sound level greatly increasing nonlinear distortion. It is particularly critical when it comes to hands-free or speaker-phone situations. So, nonlinear distortion becomes increasingly prevalent, and yet there is still no satisfactory model for this phenomenon. The study of loudspeaker and its characterization based on sine response remained common approach for many years. Sine sweep, step by step or continuous, have been used to measure frequency response and distortion. For non-linear behavior characterization single tone is used to measure harmonic distortion and two tones are used for intermodulation and difference distortion. Many different and sophisticated variations of these basic measurements are used, but sine response doesn't predict reliably the music or speech quality. Multitone and random noise excitations, along with coherence analysis have been introduced [1] but have not gained in popularity. The different distortion measurements (harmonic distortion, intermodulation, multitone distortion, non-coherent power) are not related to each other by an underlying model, and remain purely symptomatic. It is natural to think that the loudspeaker industry could benefit from the modern techniques of nonlinear system identification to obtain a comprehensive and accurate model for diagnosis, quality control, simulation, prediction and ultimately, linearization. Following the advancements in nonlinear system theory, during the last 30 years, many attempts have been made in the identification and linearization of loudspeaker [2]-[3]. However due to the wide range of audio frequencies (20 Hz to 20kHz) and high human ear sensitivity, the loudspeaker identification and linearization remain an elusive goal. This paper reviews recent developments in the domain of loudspeaker identification and explores new possibilities to improve modeling that is better match to the loudspeaker response. First we present the loudspeaker operation principles and the major causes of distortion, then we explore the successive modeling approaches that have been investigated in the last 30 years. Finally we provide new directions of research in the frequency domain and propose two techniques based on state-space for modeling of loudspeaker which can effectively be used in identification process.

2. Preliminary Development

In this section, we give a brief overview of the loudspeaker operation and the modeling approaches that have been investigated in the last 30 years.

2.1 Loudspeaker Mechanism

The most common type of driver is electro-dynamic. The driving part, the motor, is a moving coil into a static magnetic field. The audio signal goes through the coil and creates a variable magnetic field that interact with fixed magnets and generate a mechanical force that is roughly proportional to the electrical current. The acoustic radiation is insured by a lightweight cone (diaphragm) attached to the coil. An elastic suspension maintains the coil and the attached cone in place into the frame ("basket"). The cone is also mechanically connected to the basket by an elastic

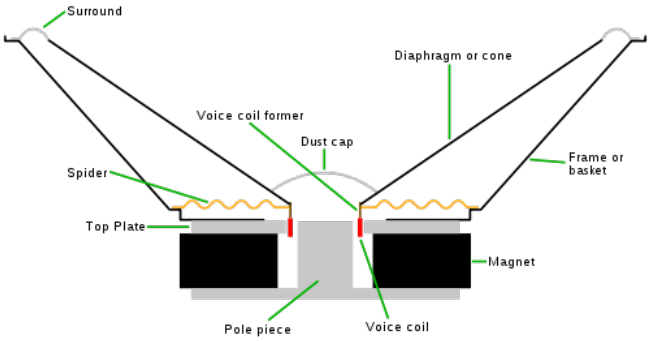

Fig. 1: Loudspeaker mechanism.

suspension called surround (see fig. 1). Designing a driver combines acoustic, mechanical, electrical and material science. A simplified linear model based on lumped parameters describes the loudspeaker mechanism at low frequencies. It is composed of 2 differential equations.

$$u(t) = Ri(t) + L\frac{di}{dt} + Bl\frac{dx}{dt} \quad (1)$$

$$Bli(t) = m\frac{d^2x}{dt^2} + r\frac{dx}{dt} + kx(t) \quad (2)$$

Where u(t) is the input voltage, i(t) the current, x(t) the cone displacement and R, L, Bl, m, r, k are electromechanical parameters of the loudspeaker. It is important to note that the force factor Bl, the voice coil inductance L and the stiffness k are nonlinear function of the displacement x. Therefore nonlinearity is intrinsic to the driver's principle of operation. Beside the changing parameters just mentioned, there is a wide variety of non-linear behaviors [4]. For example, at high frequencies the cone and dome no longer behave as rigid bodies. They exhibit breakup modes and eventually the vibrations become nonlinear. Another distortion inherent to the fundamental principle of operation is the Doppler effect due to the fact that the sound is emitted from the diaphragm which is a moving source.

2.2 Approaches of System Identification

White Box (1980's): The first attempts of system identification applied to loudspeaker were based on the lumped model described by equations (1) and (2). A simple system identification method delivers a first prediction of the mechanical behavior of the loudspeaker for low frequencies, and small signals. It was applicable up to the cone breakup frequency where the cone still behaves as a rigid piston. The measurement method is based on sine excitation and proceeds in two successive parts, involving added mass or loudspeaker enclosure. In a seminal paper [2], the most prominent nonlinearities (force factor Bl(x), self-inductance L(x), stiffness k(x)) are approximated by polynomials, then expressed in term of Volterra series. Extensions of this work are reported in [5] (see also the references therein). The white box approach is limited to low frequencies and low order nonlinearities (typically 2 or 3).

Black-Box (1990's): Unlike white box approach, the black box scheme uses input/output model with no physical insight. One technique uses NARMAX in the time domain [6], described by:

$$y_t = f(y_{t-1}...y_{t-n}, u_t...u_{t-m}, e_{t-1}...e_{t-d}) + e_t \quad (3)$$

Where u and y represent input and output, e represents noise and f(.) is a nonlinear function (e.g. polynomial). Other attempts were made in the frequency domain, using a general Volterra model [7]. Volterra models are interesting because of their standard and general approach. They relate immediately to the frequency domain and provide generalized frequency responses, but their complexity is such that the order is limited practically to 3.

Block Model (2000's): Recent trends use a simplified Volterra model with diagonal kernels $h_n(t,...t) \equiv h_n(t)$, incorporating Hammerstein scheme as shown in 2 with the output of the system represented by:

$$y(t) = \sum_{n=1}^{Q} u^n(t) * h_n(t) \quad (4)$$

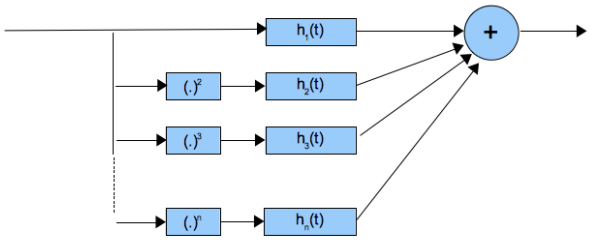

Fig. 2: parallel-hammerstein.

This model deviates from physical intuition, however attempts were made in [8] to obtain a proper identification of each path, more exactly of each transfer function h_n. Independently, a modified Wiener-Volterra model was proposed in [3] (see fig. 3), that has the property of having an exact inverse. This makes it suitable for loudspeaker linearization by derivation of a predistortion filter. It is interesting to note that the parallel-Hammerstein and the Wiener-Volterra models cover the full acoustic frequency range contrary to previous models.

2.3 Analysis

As we pointed out in the introduction, we are dealing with loudspeaker, not only for music and entertainment but also for communication. In the case of complex signals like speech or music, distortion sounds generally like a modulation noise that degrades the clarity of the signal. To demonstrate this effect, music has been played through a

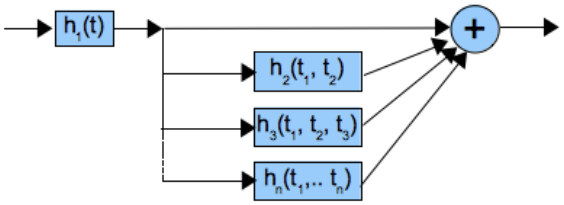

Fig. 3: Modified Wiener Volterra.

loudspeaker and the added non-linear distortion has been measured as the non-coherent power present in the acoustical signal [1]. Fig. 4 shows both the spectrum of the musical signal and the spectrum of the added distortion noise.

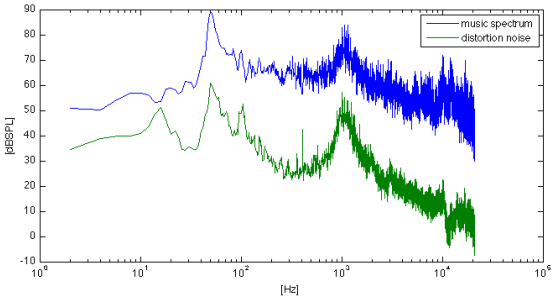

Fig. 4: Music spectrum and Distortion Noise from a Loudspeaker.

3. Proposed New Methodologies

In this section we present new models that can reliably be used in identification of loudspeaker.

3.1 Frequency Domain Block Model

In the last decade many papers have been published on the frequency domain approach ([9], [10] and references therein). The general approach is the following

1) Find the best linear approximation
2) Identify the added nonlinearity

which is practical and well-suited for weakly nonlinear systems.

This approach is justified by the following fact that a Volterra system subjected to Gaussian random input is equivalent to a linear system with an added noise source at the output (see fig. 5). The linear part Y_R contains all the contributions coherent with the excitation and the nonlinear part Y_S gathers all the contributions which are not coherent to the input. For each frequency $\omega, Y_S(\omega)$ is the sum of contributions like:

$$H_3(\omega_1, \omega_2, \omega - \omega_1 - \omega_2)U(\omega_1)U(\omega_2)U(\omega - \omega_1 - \omega_2) \quad (5)$$

Where H_3 is the Volterra generalized frequency response of order 3 and $\omega_1 + \omega_2 \neq 0$. For a random input U,

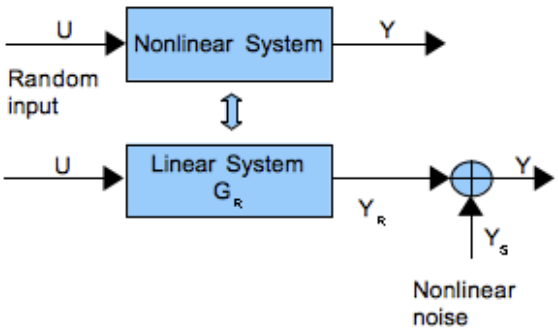

Fig. 5: Nonlinear system with random input and its equivalent linear system + nonlinear noise source.

each contribution is random, and Y_S cannot be distinguished from a noise. Note that odd degrees of nonlinearity can add coherent contribution to Y_R (e.g. insert $\omega_1 + \omega_2 \neq 0$ in (5)) that modify the best linear approximation G_R . Using this result a general purpose and flexible block model is proposed as shown in fig. 6. It is a parallel structure with

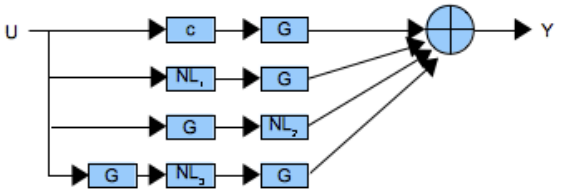

Fig. 6: Generic nonlinear model for frequency domain identification.

each branch representing a typical situation. The 1st branch is simply the linear case (c is a pure real gain). In the following branches NL_i are static polynomials systems. The 2nd branch is Hammerstein system. The 3rd branch is a Wiener system. The 4th branch is a cascade approximation of a nonlinear feedback. Note that linear block G is the same in all branches. That model is identified in successive steps. First the best linear approximation of the overall system is identified and inserted as G in all branches. Then the active branches are selected based on their power contributions. Finally the polynomial NL_i of the selected branches are identified. This approach seems well suited to loudspeaker identification. In particular, the nonlinear feedback that is part of electrodynamic loudspeaker mechanism can be identified. Our immediate goal is to apply this model to loudspeaker identification and compare it with previous methods.

3.2 Nonlinear State-Space Modeling

The most general representation of nonlinear system in state space notation can be expressed as:

$$\begin{aligned} \dot{x}(t) &= f(x,u,t) \\ y(t) &= h(x,u,t) \end{aligned} \tag{6}$$

for continuous-time system, where $x \in \mathbb{R}^n$, $u \in \mathbb{R}^m$ and $y \in \mathbb{R}^l$. The analysis and design of nonlinear system (6) is not a trivial task. Therefore, more attention has been given to special class of nonlinear systems. In particular, the class of nonlinear systems affine in the input attracted systems and control community for obvious reasons. The state equation of this class is given by:

$$\dot{x}(t) = f(x) + g(x)u \tag{7}$$

and the output equation is assumed linear in state i.e. $y(t) = Cx(t)$. It is not difficult to show that under the assumption of $f(x) = 0$ and continuous differentiability of f(x) and g(x), one can recast (7) in the pseudolinear form

$$\dot{x}(t) = A(x)x + B(x)u \tag{8}$$

which resemble linear system; however, the system matrices are state dependent. It should be pointed out that the choice of the matrix A(x) is not unique. Note also that the nonlinearity is in multiplicative format. Due to this structure, control theoretical concepts can be developed to mimic the classical state-space design approaches. For example the state feedback design and its optimal control format based on Linear Quadratic Regulator (LQR) leads to state dependent Ricatti equation (SDRE), which can be solved to specify the feedback gain. Therefore it is also interesting to pursue research in identification schemes based on this model structure.

A. Polynomial Nonlinear State Space Model

Recently the following class of Lipschitz nonlinear systems has attracted a considerable attention [11]:

$$\begin{aligned} \dot{x}(t) &= Ax + Bu + Ep(x,u) \\ y(t) &= Cx + Du + Fq(x,u) \end{aligned} \tag{9}$$

where $p(t) \equiv p(x,u)$ and $q(t) \equiv q(x,u)$ satisfy the Lipschitz condition. Note that in this case the nonlinearity is in additive format. It can be shown that applying functional expansion of the function **f** and **h** in (6) with various kinds of basis functions, one can arrive at (9). In this paper, a set of polynomial basis functions is chosen due to computational simplicity and its advantage in our application. The polynomial Nonlinear State Space (PNSS) model is defined by (9) consisting of the linear terms in x(t) and u(t) with constant coefficient matrices A, B, C, D, E, F and the vectors $p(t) \in \mathbb{R}^{n_p}$ and $q(t) \in \mathbb{R}^{n_q}$ containing nonlinear monomials in x(t) and u(t) of degree two up to a chosen degree r, where the coefficient matrices E and F contain the coefficients associated with those monomials. Note that the monomials of degree one are included in the linear part of the PNSS model structure. When a full polynomial expansion is carried out, all monomials up to degree r must be taken into account. First, a vector z is defined as the concentration of the state vector and the input vector as

$$z(t) = [x_1(t) \dots x_n(t) u_1(t) \dots u_m(t)]^T \tag{10}$$

As a consequence, the dimension of the vector z(t) is given by n_z= n+m. Then, using the conventional index notation for monomials we define:

$$p(t) = q(t) = z(t)_{\{r\}} \tag{11}$$

Note that the vector $z(t)_{\{r\}}$ as defined in (11) should contain all monomials with a degree between two and r. For instance, the vector $z_{\{3\}}$ with n_z= 2 denotes

$$z_{\{3\}} = [z_{(2)} z_{(3)}]^T = [z_1^2, z_1 z_2, z_2^2, z_1^3, z_1^2 z_2, z_1 z_2^2, z_2^3]^T \tag{12}$$

where we define $z_{(r)}$ as the vector of all the distinct monomials of degree r composed from the elements of vector z. The number of elements in vector $z_{(r)}$ is given by the following binomial coefficient

$$N_r = \binom{n_z + r - 1}{r} \tag{13}$$

Thus, the vector $z_{\{r\}}$ has the length

$$L_r = \binom{n_z + r}{r} - 1 - n_z \tag{14}$$

and corresponds to considering all the distinct nonlinear combinations of degree r, which is the default choice for the PNSS model structure. The total number of parameters required by the model in(9) , is given by

$$N = \left[\binom{n + m + r}{r} - 1 \right] (n + l) \tag{15}$$

B. Bilinear and State Affine Models

The class of bilinear state space models is described by

$$\begin{aligned} \dot{x}(t) &= Ax + Bu + \sum_{k=1}^{m} N_k u_k x(t) \\ y(t) &= Cx + Du \end{aligned} \tag{16}$$

It is well known that bilinear state space models are universal approximates for continuous-time nonlinear systems within a bounded time interval. Unfortunately, this approximation does not hold in discrete time case. A more general class of state space models known as state affine models admit this approximation for discrete-time systems [12]. A state affine model of degree r for discrete-time

systems is defined as

$$x(t+1) = \sum_{i=1}^{r-1} A_i u^i(t) x(t) + \sum_{i=1}^{r} B_i u^i(t)$$
$$y(t) = \sum_{i=1}^{r-1} C_i u^i(t) x(t) + \sum_{i=1}^{r} D_i u^i(t) \qquad (17)$$

These models results in a natural way when describing sampled continuous-time bilinear state space systems [13]. The advantage of this model is that the states x(t) appear linearly in the state and output equations. As a consequence, subspace identification techniques can be used to estimate the model parameters. It is also interesting to see that state affine models form a subset of the PNSS model class.

4. Identification Procedure

It should be pointed out that a parallel treatment of previous section for discrete-time nonlinear system can be established. This is convenient for system identification process. In this case, without loss of generality, we see similar state space notation as follows:

$$x(t+1) = Ax + Bu + Ep(t)$$
$$y(t) = Cx + Du + Fq(t) \qquad (18)$$

Due to the fact that nonlinearities are concentrated in the states, one can simplify PNSS representation by considering only $z(t) = x(t) = [x_1(t) \dots x_n(t)]^T$ and construct $\mathrm{x(t)}_{\{\mathrm{r}\}}$ which reduces the computational complexity. The identification procedure for PNSS model consists of three major steps. First, best linear approximation (BLA) of the system under test is determined non-parametrically in mean square sense. Then, a parametric linear model is estimated from BLA using frequency domain subspace identification method [14]. This is followed by solving a nonlinear optimization of the linear model. The last step consist of estimating the full nonlinear model by using again a nonlinear search algorithm that minimizes the model output error in regard to the measured output. The following steps summarizes the frequency domain subspace identification technique:

1) The BLA is obtained by a classical FRF measurement using periodic excitation (e.g. multitone) [9].
2) The FRF estimate is extended to the full unit circle and the Impulse Response coefficients $\hat{h}_i$ are obtained by IDFT of the FRF
3) The Hankel matrix is defined from the Impulse Response:

$$\hat{H} = \begin{pmatrix} \hat{h}_1 & \hat{h}_2 & \cdots & \hat{h}_r \\ \hat{h}_2 & \hat{h}_3 & \cdots & \hat{h}_{r+1} \\ \vdots & \vdots & \ddots & \vdots \\ \hat{h}_q & \hat{h}_{q+1} & \cdots & \hat{h}_{q+r-1} \end{pmatrix}$$

with number of rows $q > n$ and number of columns $r \geq n$, n being the order of the system.
4) The Singular Value Decomposition of the Hankel matrix is calculated and the system order is determined by selection of the n largest singular values.
5) The system matrices $\hat{A}, \hat{C}$ are estimated directly from the n left singular vectors.
6) The remaining system matrices $\hat{B}, \hat{D}$ are estimated by least-square optimization of the state-space model with respect to the measured FRF

5. Conclusion

This paper summarized the available techniques for modeling and identification of loudspeaker with its unavoidable nonlinear distortion phenomenon. Various frequency and state-space approaches have been analyzed. It is shown that when a general, black-box model of a nonlinear device is required, the PNSS model is a perfect tool to approximate the nonlinearity. This enables the identification procedure to be performed in a straightforward fashion using three simple steps; namely, best linear approximation, estimate a linear model, and finally solve a standard nonlinear optimization problem.

References

[1] P. Brunet and S. Temme, "A new method for measuring distortion using a multitone stimulus and non-coherence," in *Audio Engineering Society Convention 121*, no. 6877, Oct 2006.

[2] A. J. M. Kaizer, "Modeling of the nonlinear response of an electrodynamic loudspeaker by a volterra series expansion," *J. Audio Eng. Soc*, vol. 35, no. 6, pp. 421–433, 1987.

[3] K. Lashkari, "A novel volterra-wiener model for equalization of loudspeaker distortions," in *Acoustics, Speech and Signal Processing, IEEE International Conference on*, vol. 5, May 2006.

[4] W. Klippel, "Tutorial: Loudspeaker nonlinearities—causes, parameters, symptoms," *J. Audio Eng. Soc*, vol. 54, no. 10, pp. 907–939, 2006.

[5] ——, "The mirror filter-a new basis for reducing nonlinear distortion and equalizing response in woofer systems," *J. Audio Eng. Soc*, vol. 40, no. 9, pp. 675–691, 1992.

[6] H.-K. Jang and K.-J. Kim, "Identification of loudspeaker nonlinearities using the narmax modeling technique," *J. Audio Eng. Soc*, vol. 42, no. 1/2, pp. 50–59, 1994.

[7] M. J. Reed and M. J. Hawksford, "Practical modeling of nonlinear audio systems using the volterra series," in *Audio Engineering Society Convention 100*, May 1996.

[8] M. Rebillat, R. Hennequin, E. Corteel, and B. F. G. Katz, "Prediction of harmonic distortion generated by electro-dynamic loudspeakers using cascade of hammerstein models," in *Audio Engineering Society Convention 128*, May 2010.

[9] J. Schoukens, J. G. Nemeth, P. Crama, Y. Rolain, and R. Pintelon, "Fast approximate identification of nonlinear systems," *Automatica*, vol. 39, no. 7, pp. 1267 – 1274, 2003.

[10] J. Schoukens, R. Pintelon, T. Dobrowiecki, and Y. Rolain, "Identification of linear systems with nonlinear distortions," *Automatica*, vol. 41, no. 3, pp. 491 – 504, 2005.

[11] J. Paduart, L. Lauwers, J. Swevers, K. Smolders, J. Schoukens, and R. Pintelon, "Identification of nonlinear systems using polynomial nonlinear state space models," *Automatica*, vol. 46, no. 4, pp. 647 – 656, 2010.

[12] E. Sontag, "Realization theory of discrete-time nonlinear systems: Part 1-the bounded case," *Circuits and Systems, IEEE Transactions on*, vol. 26, no. 5, pp. 342 – 356, May 1979.

[13] W. J. Rugh, *Nonlinear System Theory: The Volterra-Wiener Approach.* Johns Hopkins Univ Press, 1981.

[14] T. McKelvey, H. Akcay, and L. Ljung, "Subspace-based multivariable system identification from frequency response data," *Automatic Control, IEEE Transactions on*, vol. 41, no. 7, pp. 960 –979, Jul 1996.

Modeling of DNA Replication

Xiaoli Yang[1], Ge Rong[1], and Charles C. Tseng[2]
[1]Department of Electrical and Computer Engineering, Purdue University Calumet, Hammond, IN, USA
[2]Department of Biological Sciences, Purdue University Calumet, Hammond, IN, USA

Abstract - *In this paper, we introduce an interactive computer program using a modeling and simulation technology to provide students with hand-on experiences in learning the DNA replication process. With the interactive program, students are able to actively control and visualize the coordinated actions of two DNA polymerase III coenzymes within the replication machinery for both leading and lagging strand syntheses at the replication fork.*

Keywords: DNA replication, DNA polymerase III holoenzyme, replication fork, interactive computer program, modeling, simulation

1 Introduction

DNA replication is one of the most fundamental properties for all living organisms. The process is complicated and often presents a challenging subject for biology students [1]. Because of the directionality and complementary nature of the double stranded DNA (dsDNA), along with 5'-3' unidirectional activity of the DNA polymerase III holoenzyme, it is difficult to understand the detailed process of DNA replication.

Although the graphic presentations in today's biology textbooks are excellent for visualization, the static diagrams are inadequate for students to comprehend the complete machinery involved. Recently, animations are available on some websites, but the animated motions do not provide students with "hands-on" experiences. To initiate an innovative method for genetics and molecular biology education, we created a computer generated DNA model which reflects all key characteristics of the molecule. Based on the model, we implemented our computerized program for visualizing DNA replication as a continuous process. With the interactive capability, the program provides users with hands-on experiences by controlling the replication steps during the learning process. It is hoped that the new approach will serve as a model system to supplement learning science that requires abstract conceptualization.

2 The DNA Model and Its Physical Simulation

The DNA model incorporates a physical simulation engine similar to ragdoll physics [2, 3] which is embedded in every element of the model to assure smooth model movements. Elements are connected together and kept a desired distance from one another. The system can therefore ensure that elements do not scramble together once the model starts moving. For molecular simulation, a DNA strand is regarded as a series of linked nodes, and the double helix is composed of two interwinding strands with hydrogen bonds attracting the complementary bases. Each node behaves independently and interacts with its neighboring nodes on the same string (Fig. 1).

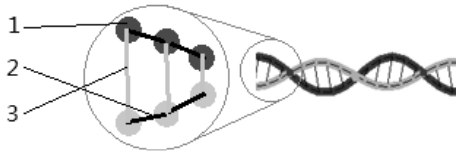

Fig. 1. DNA model and its basic structure. 1: node, 2: linkage between nodes, 3: hydrogen bonds between different nucleotide bases.

The interactive node was designed at the nucleotide base level, consisting of A (adenine), C (cytosine), G (guanine), and T (thymine). Another base U (uracil) was used to replace T for simulating the RNA strand. Different molecules can be visualized in different colors and manipulated for various behaviors and motions. Although the nodes may be correctly placed initially, the distance between them may become invalid after some integration steps. In order to obtain the correct distance, we move the nodes by setting an internal force among nodes (Fig. 2). This is done by pushing the nodes directly away from each other or by pulling them closer depending on whether the erroneous distances are too small or too large from threshold distance). The force (F) is determined by the equation (1):

$$f = \frac{(D - T)}{D} * E \qquad (1)$$

where T is the threshold distance, D is the current distance between each pair of nodes, and E is a quadratic scaling factor

for enlarging repulsive force. If the f value is negative, the distance should be extended and *vice versa*.

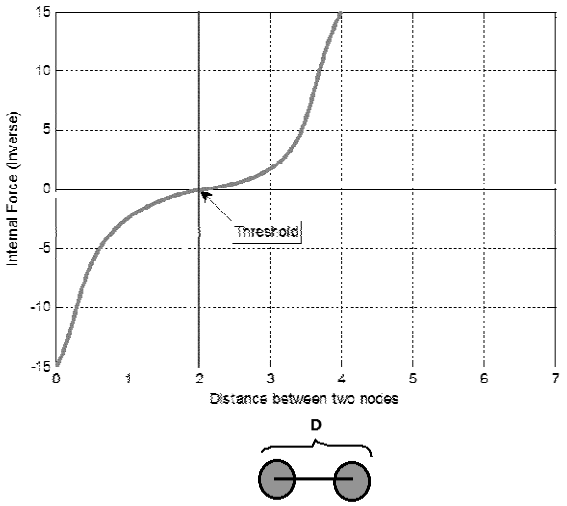

Fig. 2. The plot of a quadratic equation to simulate internal force between nodes. The threshold value indicates the ideal distance between the nodes (D)

The molecular process was simulated by separating the entire procedure into dozens of steps for user visualization and interaction. Related proteins (including enzymes), RNA primers, leading and lagging DNA strands were also modeled and rendered during the procedure. We developed our model under the Microsoft .NET platform as well as an interactive program to simulate DNA replication. Users may control the entire process and perform the following functions: moving step forward or backward, pausing, reading description and instructions, and interacting with models. A demonstration mode aimed to enhance the teaching effectiveness is provided.

Simulation can be run with good performances on any computer with CPU higher than 1 GHz and RAM higher than 256Mb.

3 Levels of Modeling

To understand the DNA replication mechanism, it is necessary to divide the learning process into two major levels: Level 1 is to introduce the individual steps which characterize the specific events during the process, and level 2 is to combine the individual steps into a cohesive DNA replication process for learning the overall process [4, 5].

3.1 Modeling Level I: Individual DNA Replication Steps

Using E. coli as an example, the individual steps of DNA replication is shown in Fig. 3. The DNA molecule has

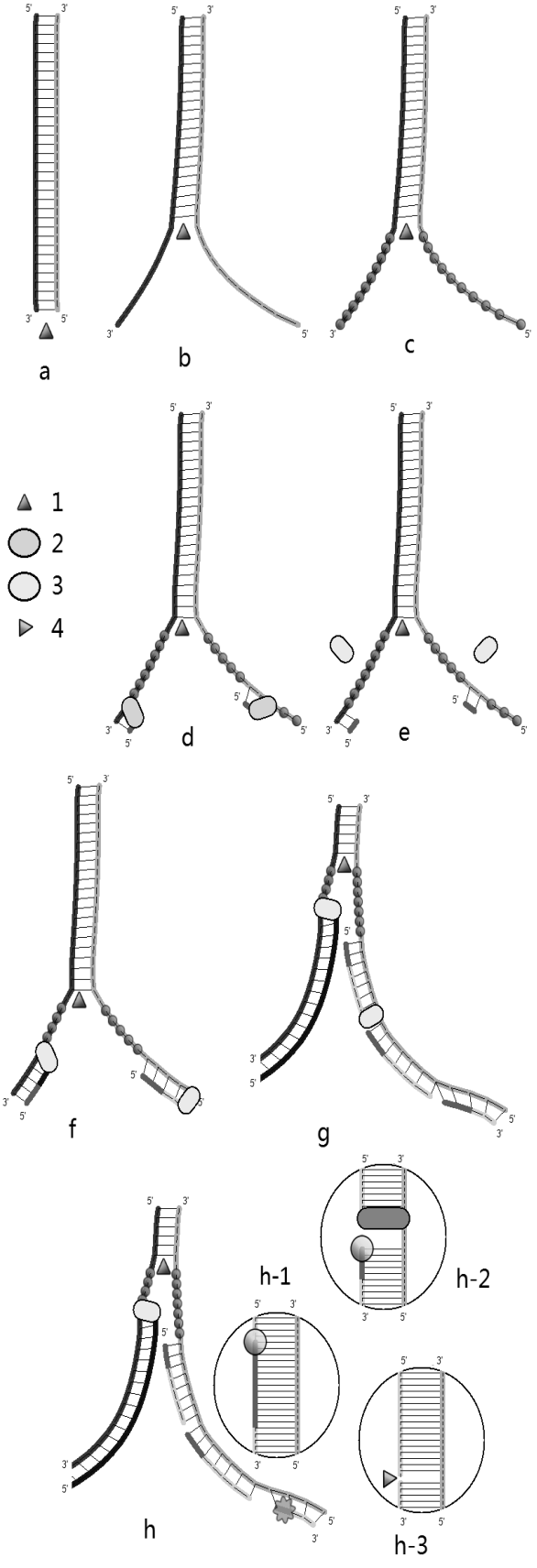

Fig. 3. Individual DNA replication steps. (a) antiparallel structure of dsDNA with a helicase below, (b) action of the helicase, (c) function of the single strand binding protein, (d) RNA primer synthesis by RNA primase, (e-g) continuous and discontinuous syntheses of leading (left) and lagging (right) strands, respectively, and (h with h1, h2, and h3) shows the removal of the RNA primase; and the RNA primer which is replaced with new DNA by DNA polymerase I followed by nick sealing by DNA ligase. 1: Helicase, 2: RNA primase, 3: DNA polymerase III, and 4: DNA ligase.

an antiparallel structure with two strands running in opposite directions, 5' to 3' and 3' to 5' (a). The helicase shown is to break hydrogen bonds between bases (b). The binding of SSB (single strand binding protein) is to prevent the renaturation of the newly separated single strands (c). Separation of dsDNA by the helicase generates a replication fork (b, c) which advances as the replication process continues. RNA priming is accomplished by the action of RNA primase which does not require a primer for RNA synthesis (d). DNA synthesis using both DNA templates starts with RNA primer extension by the DNA polymerase III core enzyme (d). The DNA polymerase III core enzymes, which form a DNA holoenzyme for both leading and lagging strand synthesis (Fig. 2), is here intentionally separated (d) for the sake of explanation at this level. The continuous synthesis of the leading strand and discontinuous synthesis of the lagging strand are visualized stepwise (f-h). The lagging strand synthesis also involves the joining of Okazaki fragments sequentially. Final steps (h1-h3) include the removal of the RNA primase and the RNA primer which is replaced with new DNA by DNA polymerase I. The linking of Okazaki fragments is completed when the nick is sealed by DNA ligase (h3).

3.2 Modeling Level II: Overall DNA Replication Process

Since single stranded DNA (ssDNA) can easily be broken and the consequence may be a complete break of the chromosome, it is essential to limit amount of ssDNA during replication [1]. This can be achieved by joining multiple DNA polymerases to form a holoenzyme during DNA synthesis at the replication fork (Fig. 4 a-g). The holoenzyme consists of two copies of DNA polymerase III core enzyme connected by a copy of the clamp loader (γ complex). As the helicase unwinds the dsDNA at the replication fork, the leading strand template is acted immediately by the DNA polymerase for continuous replication (except for the initial RNA primer synthesis by the RNA primase), whereas the lagging strand template is spooled out, bound by SSB, and followed by RNA primer synthesis with the RNA primase intermittently (discontinuous synthesis).

The resulting RNA primer-DNA template hybrid is recognized by the sliding clamp loader with a sliding clamp for DNA synthesis using leading and lagging strand templates separately. The sliding clamp, which encloses the DNA

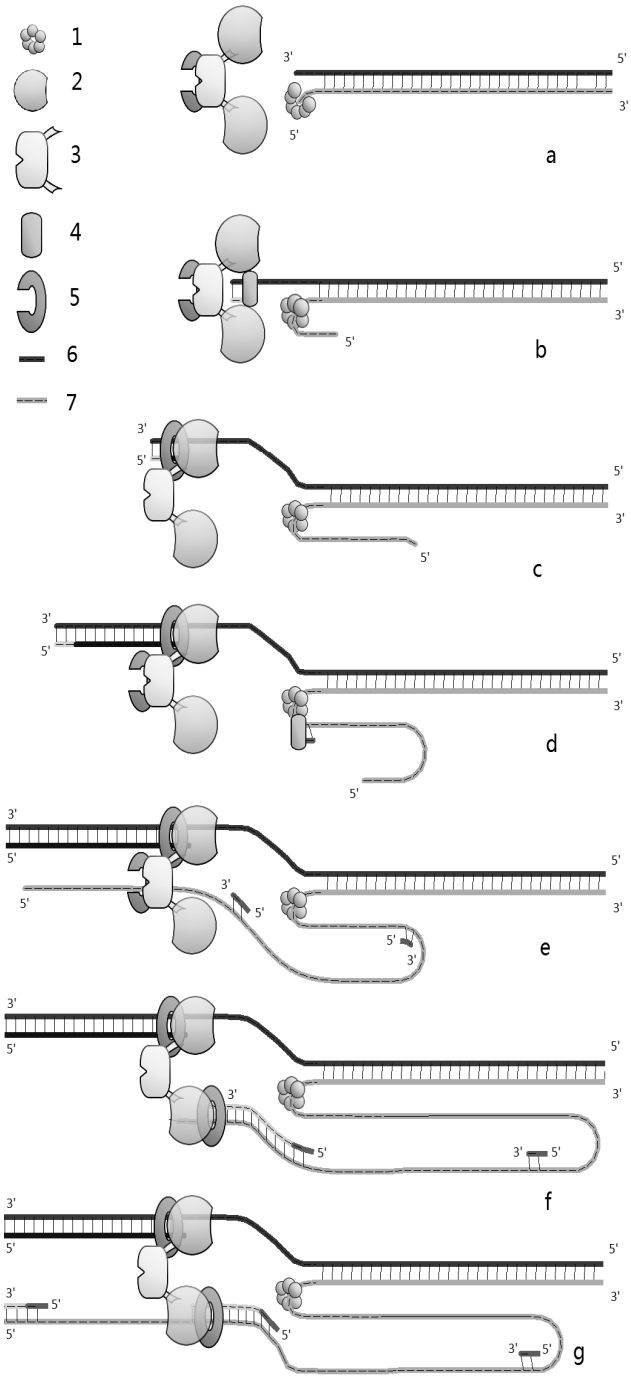

Fig. 4. Overall DNA replication process, showing initial binding of RNA primase to the leading strand template unwinded by helicase (a), the leading strand synthesis (b, c) followed by the lagging strand synthesis (d), synthesis of first Okazaki fragment (e-f), followed by the initiation of second Okazaki fragment (g). 1: helicase, 2: DNA polymerase III core enzyme, 3: clam loader with tau protein, 4: RNA primase, 5: sliding clamp, 6: leading strand template, 7: lagging strand template

during replication, is first attached to the clamp loader and then to one of the DNA polymerase III core enzymes for synthesis of the leading strand. Similarly, another sliding clamp is used for generating the lagging strand. In this way, the DNA holoenzyme, with its weakly associated helicase, brings all DNA replicates elements such as DNA polymerase core enzymes, clamp loader, DNA duplex (including leading and lagging strand template), sliding clamps, and RNA priming by RNA primase followed by RNaseH, DNA polymerase I, and DNA ligase for completing of DNA replication.

4 Conclusions

STEM (science, technology, engineering, and mathematics) education is vital to today's society. Because of the abstract nature of most scientific concepts, STEM is often considered difficult fields that many students try to avoid. Current teaching methods involve listening (classroom lecturing), reading (textbooks and papers) visualizing (photos, drawings, and animations), home work for problem solving, and experimentations (laboratory). To supplement the above methods, our interactive computer program was designed for students to have hands-on experiences during the learning process. The significance of this project includes:

4.1 Through dynamic and controllable models, DNA replication can be visualized by students to reveal each step of the process.
4.2 The methodology is suitable for developing dynamic models of other molecular structures which can be controlled by students for performing different functions according to the guided instructions.
4.3 With the software package, students may learn the complicated concept at any time and practice outside the classroom.
4.4 There will be no time constraint for students to complete the learning process; therefore, it is ideal for individualized learning.
4.5 The tutorial tool can be used for teaching part of general biology, cell biology, genetics, and molecular biology at the college level.

5 References

[1] Watson, J.H., T. A. Baker, S. P. Bell, A. Gann, M. Levine, Richard Losick. Molecular Biology of the Gene. 6th ed. Cold Spring Harbor Laboratory Press, New York, 2008.

[2] Witkin, A, D. Baraff, Physically Based Modeling: Principles and Practice, Siggraph '97 course notes, 1997.

[3] Thomas J., Advanced Character Physics, IO Interactive, 2DK-1463 Copenhagen K, Denmark, 2000.

[4] Corn J.E. and J.M. Berger. Regulation of bacterial priming and daughter strand synthesis through helicase-primase interactions. Nucleic Acid Res. 34:4082-4088, 2006.

[5] Benkovic S. J., A. M. Valentine, F. Salinas. Replisome-mediated DNA replication. Annual Rev. Biochem. 70:181-208, 2001.

Channel Assignment Model in Wireless Mesh Networks

Shaharuddin Salleh and Nur Atikah Salahudin
Department of Mathematics, Faculty of Science
Universiti Teknologi Malaysia, 81310 Johor Bahru, Malaysia
{ss@utm.my, atikahsalahudin@yahoo.com}

Abstract – *A wireless mesh network is a multi-hop network consisting of nodes called mesh routers and mesh clients. The network is self-organized and it is capable of covering a large geographical area for purposes like data gathering, communication and information processing. For communication, the nodes in the network are allocated with one or more channels based on the IEEE 802.11 protocol. Channels in a wireless mesh network are allocated in such a way to minimize the bandwidth with the constraint of avoiding the electromagnetic interferences. In this paper we propose a model called XION which allocate channels based on minimum bandwidth with the adjacency channel constraint. Our model is efficient in performing minimization in the number of channels and schedules the tasks in the network with minimum completion time.*

Keywords: Wireless mesh network, channel assignment, graph edge coloring and task scheduling.

1. Introduction

A wireless mesh network (WMN) is multi-hop wireless network consisting of nodes called mesh routers and mesh clients [1]. The nodes in WMN can be in static position or mobile, and they are capable of communicating with other nodes through the built-in radio transmitters and receivers. Mesh routers are normally in stationary position, and they provide coverage for the mesh clients which can be static or mobile. WMN has attracted research due to its many current and potential applications such as in the community networks, broadband home networking, video-on-demand (VoD), last-mile Internet access and video surveillance.

Communication in the multi-hop wireless mesh network is provided through non-overlapping channels operating under the IEEE 802.11 protocol. A radio channel is required before communication between two nodes in a WMN can be established. A single channel allows one way delivery of message or data, and it may not be sufficient to satisfy the high volume of communication demand between the nodes in the network. Therefore, WMN relies on multiple channels on each node in the network in order to fulfill this requirement. To achieve this mission, every node in WMN is equipped with multiple Network Interface Cards (NICs) which allow tuning to one of the available channels. A pair of nodes can communicate with each other if their NICs are tuned to the same channel in the transmission range of each other and that the channels are not in the interference state. The use of the same channel by several nodes at the same time when they are within the transmission range may result in electromagnetic interference. Therefore, different channels are assigned to links that originate from the same node in order to avoid the interference.

Channel assignment in a wireless mesh network is a graph theoretical application associated with the assignment of limited resources to the mesh routers and mesh clients. The resources consist of radio channels which are assigned according to frequencies. The number of channels, or the bandwidth, in a particular node is limited according to the average demand in the node. Therefore, an efficient system for managing the assignment of channels is important in order to optimize their assignments.

In this paper, we propose a scheme called XION which schedules tasks in a multi-channel wireless mesh networks. The paper is organized into six sections. Section is the introduction while Section 2 describes the problem. A survey on some scheduling models is discussed in Section 3. Section 4 describes our channel assignment model, and this is supported by a simulation work in Section 5. Finally, Section 6 is the summary and conclusion.

2. Problem Formulation

The problem in this work can be stated as follows: Given a network in the form of a connected graph $G(V, E)$ with n nodes and m edges, where $V = \{v_i\}$ for $i = 1, 2, ..., n$ and $E = \{e_{ij}\}$ for $i, j = 1, 2, ..., m$. How can the channels be assigned in order to support data communication between the pairs of nodes in the network with minimum completion time?

3. Channel Assignment

Channels are limited resources in the network and they are assigned from the allocated bandwidths. The main objective in channel assignment is to assign the channels with minimum bandwidth, that is, to assign as few channels as possible but satisfy the demand in the network.

We refer a wireless mesh network as the connected graph $G(V, E)$ with n nodes and m edges, where $V = \{v_i\}$ for $i = 1, 2, ..., n$ and $E = \{e_{ij}\}$ for $i, j = 1, 2, ..., m$. The nodes in the graph are the nodes in the network while the edges between the pairs of nodes denote the nodes are within the

transmission range of each other to enable them to communicate directly.

Channels are assigned to the nodes in such a way to avoid the electromagnetic interference. To achieve this objective, the channels are assigned with the adjacency, co-channel and co-site constraints in order to avoid the interference. In our present model, we only consider the channel adjacency constraint.

3.1 Single Channel Communication

Single channel communication refers to communication between a pair of nodes in the network using a single channel. At any given time, the channel can be used for one-way transmission of data. However, the opposite way transmission on the channel is possible at a different timeslot so as to avoid data collision.

Single channel communication in a network is achieved by assigning different number of channels to the nodes in the network. A variable x_{ik} is defined as follows:

$$x_{ik} = \begin{cases} 1 & \text{if } v_i \text{ is assigned with channel } k \\ 0 & \text{otherwise} \end{cases}$$

In our model, each node v_i in the network is assigned with k channels where k is the degree of the node in the graph. Hence, the distribution of channels among the nodes is not even as it depends on the adjacency matrix of the graph. We also consider the adjacency constraint whereby no two links that originate from the same node can use the same channel at the same time. Obviously, the adjacency constraint is the edge coloring problem in graph theory.

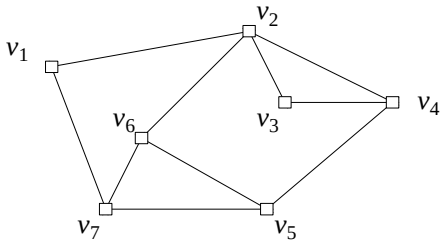

(a) Initial setup.

Figure 1. A mesh network with seven nodes.

Figure 1 shows a connected graph with seven nodes which represents a simple wireless mesh network. From the adjacency constraint, radio interference originates from the assignment of the same channel from a node. Therefore, the assignment of different channels from a single node will avoid this problem. This produces the assignment of channels on the links as shown in Figure 2.

In Figure 2, v_1 and v_2 can communicate directly using channel 1, while v_2 and v_4 are served by channel 2. With the adjacency constraint, the channels are assumed to be assigned according to the edge coloring concept where no two edges from the same node use the same channels. It can be seen that v_2 communicates with its adjacent nodes v_1, v_3, v_4 and v_6 using channels 1, 4, 2 and 3, respectively. Therefore, the node is assigned with these four channels, and the number of allocated channels coincides with the degree of the node. It can be seen that a total of four channels is required which is the cardinality of the graph, and they are assigned according to Table 1.

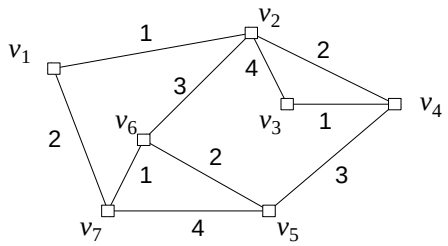

Figure 2. Single channel communication for the graph in Figure 1 using four channels.

Table 1. Channel assignments for Figure 1(b).

x_{ij}	Channels			
	1	2	3	4
v_1	1	1	0	0
v_2	1	1	1	1
v_3	1	0	0	1
v_4	1	1	1	0
v_5	0	1	1	1
v_6	1	1	1	0
v_7	1	1	0	1

3.2 Multiple Channel Communication

A single channel may not be able to support the high volume of data transfer between the nodes in the network. This is because a single channel allows one-way communication and this results in slow movement of data. For speeding up the data transfer, the use of multiple channels in a link allows duplex type of communication where the movement of data between the nodes can be performed in two opposite directions simultaneously.

Figures 3 shows the case of two channels per link between the pairs of nodes. The channels are assigned in such a way that no two adjacent edges share the same channel. It is obvious that eight channels are required in the 2-channel case, and their assignments at the nodes are shown in Tables 2. In a similar assignment, It follows that Figure 4 shows the assignment of channels for the case of links with three channels each. It can easily be generalized that the channel adjacency constraint allows $m-$channel links in a graph whose cardinality is k is km.

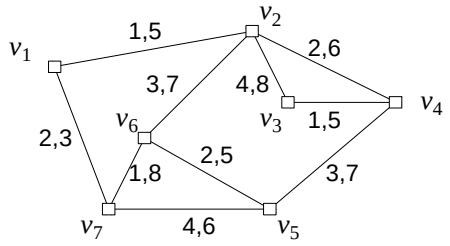

(a) 2-channel communication.

Figure 3. A mesh network with two channels on each link.

Table 1. Channel assignments for the graph in Figure 2.

x_{ij}	Channels							
	1	2	3	4	5	6	7	8
v_1	1	1	0	0	1	0	0	0
v_2	1	1	1	1	1	1	1	1
v_3	1	0	0	1	1	0	0	1
v_4	1	1	1	0	1	1	1	0
v_5	0	1	1	1	1	1	1	0
v_6	1	1	1	0	1	0	1	1
v_7	1	1	0	1	0	1	0	1

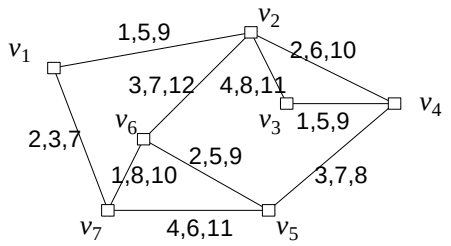

Figure 4. Links with 3 channels each.

4. XION Scheduling Model

We discuss a data movement model in a wireless mesh network. Communication between a pair of nodes in a wireless mesh network follows a path with the minimum number of hops. Therefore, the total time required to move a message or data between a pair of nodes is also the shortest path between the two nodes, assuming the weight on each edge of the graph is 1.

Our communication model is called XION. In this model, we assume a node can cast data using different routes at the same time with the cost of 1 unit of time at every single hop. This is necessary since a stopover at a node always costs some overhead in terms of switching and startup. Hence, if the route from the source to its destination involves 3 hops then the time required is 3 units. It is also assumed that a node can cast or receive data at the same time.

4.1 Single Channel Communication

Communication using a single-channel link is possible by utilizing all the available channels in the nodes. However, optimal results are obtained by choosing routes with the minimum number of hops and minimizing the number of channels through constantly reusing the same channels. We study the case in this section.

Figure 5 shows the case of sending two units of data from v_1 to v_4 using one-way communication links. Two shortest routes are required in order to minimize the casting time, one unit of data on $v_1 \to v_2 \to v_4$ while the other unit on $v_1 \to v_7 \to v_5 \to v_4$. Data is moved from v_1 to v_2 using channel 1 in timeslot 0, that is, from $t = 0$ to $t = 1$, and this is written as 1:0-1 in the figure. Obviously, the first route $v_1 \to v_2 \to v_4$ ends at $t = 2$ while the second route ends at $t = 3$. Therefore, only two channels are required and the total time taken is three units, as illustrated in the figure.

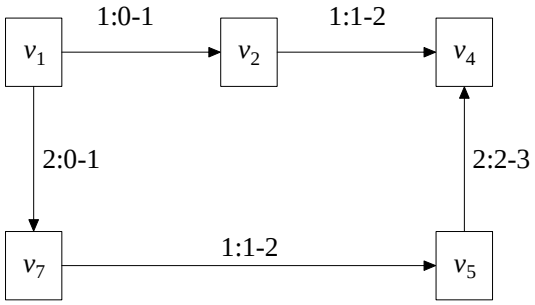

Figure 5. One-way communication between v_1 to v_4.

The XION algorithm is outlined as follows :

// Algorithm XION. Channel assignment for scheduling tasks between (v_a, v_b) ;
Input:
Graph $G(V, E)$, $V = \{v_i\}$ and $E = \{e_{ij}\}$ with n nodes and m edges;
Process:
Let timeslot $t = 0$;
Determine the shortest path $R = (v_a, v_b)$;
For $r = 1$ to R
    For $k = 1$ to C ;
        If the lowest available channel satisfies the adjacency constraint;
            Assign the channel to the path;
            Break;
        endif
        Go to the next available channel;
    endfor
endfor

Figure 6 shows two-way communication between v_1 to v_4. Supposed 2 units of data each need to be sent from v_1 to v_4 and v_4 to v_1. The single channels in the communication links allow data to be sent in duplex manner but at different

timeslots in order to avoid data collision. The simple simulation, as illustrated in the figure, requires two channels and four timeslots whose results are similar to the one-way communication model in Figure 6. The difference here is the links in the network are used twice at two different timeslots.

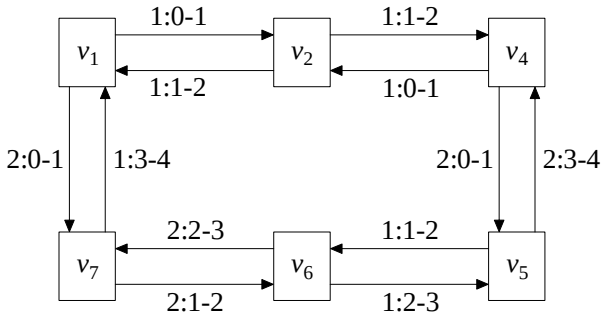

Figure 6. Two-way communication between v_1 and v_4.

We also consider another case where some units of data are to be sent between several pairs of nodes in the network. Figure 7 shows the case where two units of data each need to be sent between the nodes: $(2: v_1 \rightarrow v_4)$, $(2: v_2 \rightarrow v_7)$ and $(2: v_3 \rightarrow v_5)$. All the three pairs have the completion time of $t = 3$, with the first two using two channels and the third with three channels.

Figure 8 shows the performances in the data communication of the above case through Gantt chart. The chart serves as the parallel computing model where each path is processed by a processor.

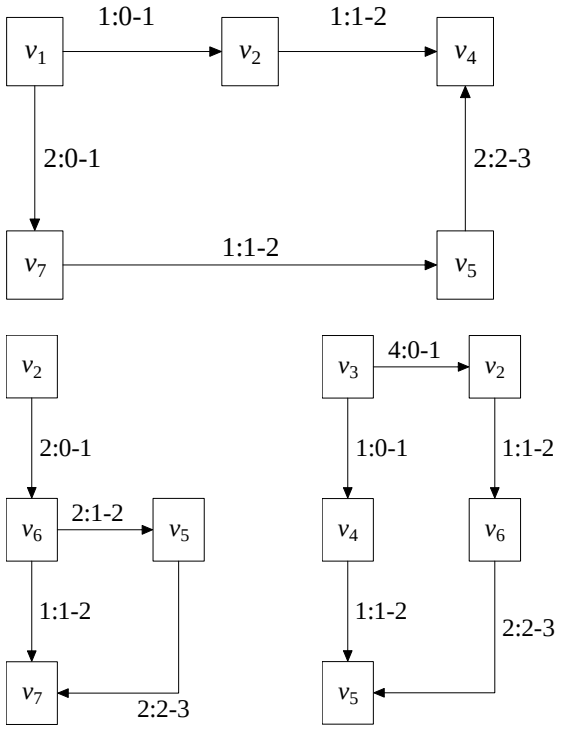

Figure 7. Multiple data movement between three pairs of nodes.

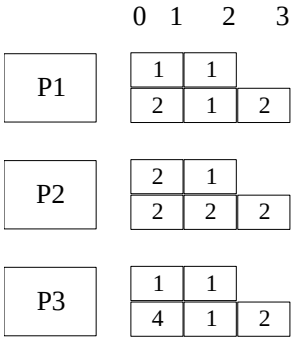

Figure 8. Gantt chart of the performances in Figure 5.

5. Experimental Results

Simulations have been performed on several graph shapes and sizes whose nodes and edges are randomly determined. The nodes are scattered at random locations. Some models with few nodes are modeled as sparse graphs, while some other are dense.

Table 2 shows seven samples of connected graphs which model seven wireless mesh networks. Each graph has the number of nodes and edges as shown in columns 2 and 3, respectively. A run with XION produces channel assignment results in column 4. Random communication is performed between pairs of nodes in the graph to producing a schedule with their completion time shown in column 5.

Table 2. Results from some sample graphs.

Model	#Nodes	#edges	#channels	timeslots
1	4	6	2	3
2	7	10	2	4
3	10	16	4	4
4	15	21	6	5
5	20	32	8	5
6	25	48	8	7
7	30	52	8	11

6. Summary and Conclusion

Channel allocation in wireless mesh networks contributes significantly to the performance, stability and effectiveness of the network. In most cases, the main objectives include minimizing the bandwidth and proper allocation in such a way to avoid the electromagnetic interferences. Our paper describes this two main issues as well as proposing a schedule which minimize the completion time of task assignment through an effective channel allocation scheme called XION.

For simplicity, XION only considers the channel adjacency constraint in this initial work. Through simulation, XION is successful in producing the desired results in the form of minimum number of channels and minimum completion time for task communication between the pairs of nodes in the network.

We propose to study the problem further by adding the other two main constraints, namely, co-site and co-channel. These two constrints add to the reality and practical situation of wireless mesh networks. It is also expected that the network behaves properly under many inherent graph properties like minimum spanning tree and strongly connectedness, which contribute towards problems in routing and scheduling.

Acknowledgement

This research has been financially supported by the Fundamental Research Grant Scheme no. 4F010 under the Malaysian Ministry of Higher Education (MOHE) and Universiti Teknologi Malaysia. The authors would like to thank the ministry and university for the support.

REFERENCES

[1] F.Akyildiz, X.Wang and W.Wand (2005), "Wireless mesh networks: a survey", Computer Networks, 47(4)445-487.

[2] H.Huang, X.Cao, X.Jia and X.Wang (2009), "Channel assignments using block design in wireless mesh networks", Computer Communications, (32)1148-1153.

[3] Yong Ding and Li Xiao (2010), "Channel allocation in multi-channel wireless mesh networks", Journal of Computer Communications, doi:10.1016/j.comcom.2010.10.011 (article in press).

[4] W.Si, S.Selvakennedy and A.Y.Zomaya (2010), "An overview of channel assignment methods for multi-radio multi-channel wireless mesh networks", (70)505-524.

[5] S.Salleh, A.Zomaya, S.Olariu and B.Sanugi (2005), "Numerical simulation and case studies using Visual C++.Net", Wiley-Interscience, USA.

BIM-Based Parametric Modeling: A Case Study

Duygu Yenerim[1], **and Wei Yan**[2]
[1, 2] Department of Architecture, Texas A&M University, College Station, Texas, United States of America

Abstract – *Parametricism has come to scene as an important style in both architectural design and construction where conventional Computer-Aided Design (CAD) tool has become substandard. Building Information Modeling (BIM) is a recent object-based parametric modeling tool for exploring the relationship between the geometric and non-geometric components of the model. The aim of this research is to explore the capabilities of BIM in achieving variety and flexibility in design extending from architectural to urban scale. This study proposes a method by using User Interface (UI) and Application Programming Interface (API) tools of BIM to generate a complex roof structure as a parametric family. This project demonstrates a dynamic variety in architectural scale. We hypothesized that if a function calculating the roof length is defined using a variety of inputs, it can later be applied to urban scale by utilizing a database of the inputs.*

Keywords: Parametric Variety, Parametric Modeling, Building Information Modeling, Application Programming Interface, Architectural Design, Urban Design

1 Introduction

Architects, planners, designers, and engineers who have a role in designing and implementing physical constructs have come to believe that diagrams play an important role in representing design thinking and managing collaboration among them [1]. In architecture, drawings mostly represent the design decisions on building form, spatial configurations, orientation, materials, and users, and the relationship among buildings, environments, and people. Computer-Aided Design (CAD) is a conventional design tool that produces drawings by creating lines, arcs and other geometric shapes. However, in order to make any changes in design, CAD requires performing changes on each related component in the drawings. This may affect time spent on design and construction [2].

In recent years, parametricism has become an important style in architectural design and construction. Today, parametric design technology has come to a stage where conventional CAD tools not only has been losing its power but also has become substandard. The idea of parametric design and thinking is seeking and exploring for relationships between components that determine both geometric and non geometric properties of a model [3].

Building Information Modeling (BIM) is a recent tool for object-based parametric modeling which means that instead of designing each instance such as walls or windows, the designer identifies an object family and its parameters including angles, dimensions and other properties helping it to relate to other objects.

Creating a variety in typology is the second important concern taken into consideration as a design problem; it has started off with *Modernity and Minimal Dwelling* in 1920s by embracing the concept of flexibility along with variety [4]. Owing to the parametric relationships, designers not only can achieve the concept of *variety* in a continuous and dynamic way, but they can also create *flexibility* from small scale interiors and architectural designs to a larger scale [5]. Object-oriented modeling of BIM and parametric variety as an inclusive concept, which encompasses flexibility and adaptability, structures the framework of the discussion.

The purpose of this research is to pursue the capabilities of BIM in achieving variety and flexibility spanning from architectural to urban scale. In order to do so, we performed an experiment in architectural scale by modeling a building complex through using BIM technology. This complex is composed of three buildings with six different S-shaped roofs. These roofs are different from each other but they share the same parameters. Radius and curvic lengths of the arcs are changing from one roof to the other. Therefore, the roof is the component that ensures the dynamic variety according to the changing floor dimensions beneath. The aim is to build a model which can adjust itself according to the change in floor dimensions. This method is experimented in architectural scale and explored if it can be applied to urban scale. We hypothesized that if a function calculating the roof length is defined using a variety of inputs, it can later be applied to urban scale by utilizing a database of the inputs.

The expected outcome is to be beneficial for larger scale designers. This research is important because the process of creating a variety in a larger scale is time consuming and the solutions may not always be successful. For instance, for settlement design, one of the major problems that architects come across frequently is creating a variety in houses. Every dweller has different needs and expectations; therefore they want their houses to be unique. Using BIM parametric

modeling User Interface (UI) and Application Programming Interface (API) tools will shorten the process of design and offer endless solutions.

2 Background

Parametric model and *parametric design* are overlapping terms that denote a slight difference in their meanings; *parametric model* refers to the medium that is utilized to establish variation of geometrical components of objects whereas *parametric design* is the design action by utilizing parametric models [6]. Integrating parametric design thinking into design process results in flexible solutions with endless and continuous potential of forms [7,8,9]. Parametric modeling also allows having control over an object. According to Robert Woodbury, the idea of parametric modeling refers to creating models which are clearly defined by its parameters; thereby, the end product of design generated with predefined parameters are established successfully [10].[1] Moreover, integrating algorithms in parametric modeling enables to deal with more complex forms and leads a variety in object geometry [12].

The purpose of this research was to investigate BIM technology in parametric design and its capabilities in achieving variety spanning from architectural to urban scale.

2.1 The capabilities of BIM-based parametric modeling

In traditional design and drawing system which includes both pencil and CAD-based applications, it is easy to create a model of a building, whereas it is difficult to make adjustments or changes to the models [10, 13]. If the length of a wall is changed, designer needs to update all drawings individually: plans, sections, elevations, and the 3D model. This is the main difference between BIM design applications and CAD systems. Ability of automatically updating the objects comes from the parametrically defined interface between object and user which is called object based modeling [3].

BIM is essential for object-based parametric modeling which was first developed in 1980s [3]. It was defined as "an instance of populated data model of buildings that contains multi-disciplinary data specific to a particular building [through its lifecycle.]" [14]. Object-oriented design embraces the design around objects and methods together [15]. Besides its benefits in design, using BIM is an accurate way of documenting and implementing big chunks of data on individual buildings to relevant stakeholders. The National Building Information Modeling Standard (NBIMS) committee states that BIM can incorporate eight data sets: (1) designer data, (2)legal data, (3)geospatial data, (4)financial data, (5)specifier data, (6)environmentalist data, (7)sustainers data, and (8)owner/occupier data [3,14].

2.2 Parametric modeling for continuous and systematic variety

Variety is an important concept in architecture. The term refers to "[a] different form *of* some thing, quality, or condition; something which differs or varies from others of the same class or kind; a kind or sort" [16]. Especially in housing design, the building should provide an opportunity to offer a choice of selection from a variety of configuration and layout [17]. This has been a concern starting from the era of modernism. Due to its capability of adapting the model to the changes performed by users, BIM is a very effective environment for designers to create objects which can vary based on changing specifics of the model. A single building can be replicated in a continuous and systematic variety by creating BIM parametric family in UI and integrating API tool to generate a function between parametric family objects.

2.3 Parametric modeling in urban scale

BIM design tool is currently used for architectural scale. However, parametric modeling is starting to be used in urban scale as well. For instance, Zaha Hadid Architects apply parametric design into both architectural and urban scales (Figure 01). They designed the urban fabric of Kartal-Pendik in Istanbul in 2006. The design includes buildings, pedestrian and vehicle path systems. The model was generated in Autodesk® Maya® and the end product includes the exterior geometry of buildings.

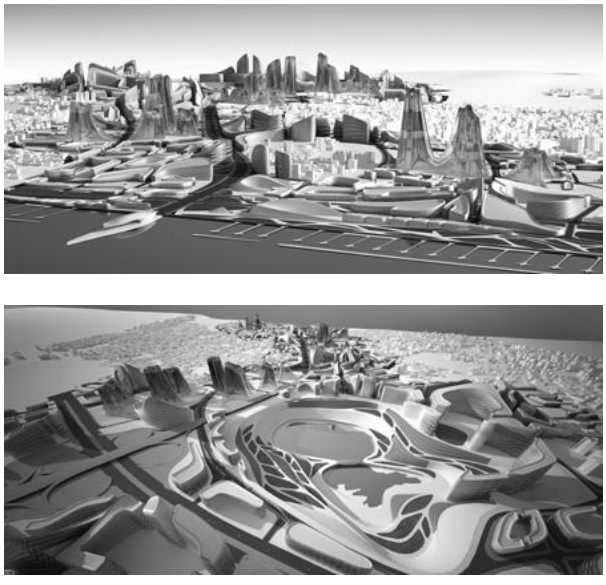

Figure 01: Kartal-Pendik Masterplan in Istanbul, Turkey by Zaha Hadid Architects [18].

[1] Parametricism has been the recent movement in architecture and there are studies showing that parametric design has a theory underneath. Patrik Schumacher defines the term as "the great new style after modernism" [11].

In this research paper, after experimenting the proposed method and tools in architectural scale, we suggested that BIM could be a beneficial tool for larger scale projects as it provides enough detail, information and variety in building scale.

3 Methods and implementations

In this research, BIM tool Autodesk® Revit® 2011 was used to model an architectural project. It contains all the parametric information about the building allowing it to reflect any changes applied by the designer. In addition, an external database was used in order to set constraints and control these changes such as dimensional information on how to make adjustments to the model in order to obtain various and flexible end products. The external database for this research was designed in Microsoft® Excel® and the interaction between BIM and MS Excel was coded using Microsoft® Visual C#.

In this project, the roof is the component that provides parametric variety in the design of the building geometry through changing design decisions on values of its parameters: angles and radii of arcs, length, and width. The method that we experimented in this project consists of two levels: (1) creating the roof as a BIM parametric family by math functions in UI and (2) establishing an algorithm between floors and the roof structure by API functions.

3.1 Roof as a BIM parametric family

In Autodesk® Revit®, *category*, *family* and *type* are three terms that constitute the basis of modeling by defining objects and their hierarchy in a project. *Category* refers to the main group of elements such as a wall, door, floor, roof, window, furniture or beams. The term *family* is used for a set of objects under a category that (a) possess same properties which are called *family parameters*, and (b) have similar formal representation in the project [19,20]. For instance, a door category dwells several door families such as single flush, double flush, double panel, double glass, single sliding, double sliding door families. These door families possess similar parameters which enable users to create a variety of different *types* in one family.

In this study, the roof structure is created as a parametric *family* from scratch. Each building in the complex has two different S-shaped roofs. Each S-shaped roof consists of two arcs, and for each roof, the radius and length of these two arcs are changing. Parametric modeling was tested to achieve numerous geometric forms along with its structural columns. This study of the roof shapes was done through varying curvature, length and width of the two arcs.

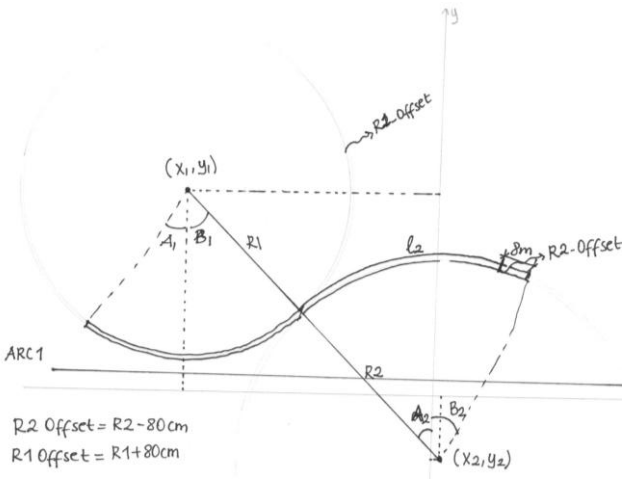

$$R2\ Offset = R2 - 80cm \quad (1)$$

$$R1\ Offset = R1 + 80cm \quad (2)$$

$$R1 + R2 = \sqrt{(X1 - X2)^2 + (Y1 - Y2)^2} \quad (3)$$

$$l_2 = 2.\pi.R2.(\frac{A_2 + B_2}{360°}) \quad (4)$$

$$l_1 = 2.\pi.R1.(\frac{A_1 + B_1}{360°}) \quad (5)$$

Figure 02: Diagrammatic drawing of a S-shape roof and its parametric rules.

In order to create roof as a parametric family in Autodesk® Revit® (Figure 02), we started off with creating the roof as a family; it was followed up with defining the coordinates and drawing the two arcs tangent to each other in the Generic Model family template along with fixing their centers. Coordinates of center points and radii were added as parameters. However, the major problem in this level was how to constrain these two arcs in order to keep them tangent to each other, no matter what their radii are. By using the math function, Pythagorean Theorem, we made the radii and the coordinates of the center point of arcs dependant on each other (Figure 02 and 03). In other words, by plugging in different values to the origins of the circles or the radius of the circle on the left (R1), the value of the radius of the circle on the right (R2) changes automatically.

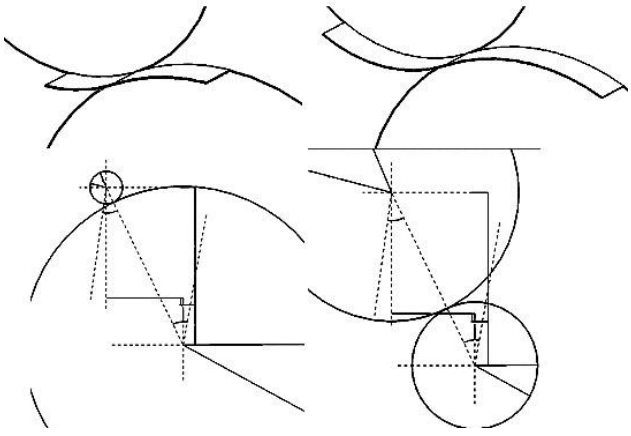

Figure 03: Changing the length of the arcs (upper figure) and varying the shape of the roof (lower figure)

The offset value of each circle showed the thickness of the roof and they were also defined by the value of one of the radii (R1). To be more flexible on the shape of the roofs, we identified two angles for each arc and added them as parameters. The change on the value of the angle had an impact on the length of the arcs. This step allowed us to get a variety of roof structures (Table 01).

Table 01: Parametric variables of parametric roof family

Family Types

Name:

Parameter	Value	Formula
Materials and Finishes		
Material_ARC2 (default)	<By Category>	=
Material_ARC1 (default)	<By Category>	=
Dimensions		
Y2 (default)	5464.56	=
Y1 (default)	16085.92	=
X2 (default)	336.72	=
X1 (default)	10154.35	=
R2_Offset (default)	4383.72	= R2 - 80 cm
R2 (default)	4463.72	= sqrt((X1 - X2) ^ 2 + (Y1 - Y2) ^ 2) - R1)
R1_Offset (default)	10080.00	= R1 + 80 cm
R1 (default)	10000.00	=
EXTRUDE (default)	2600.00	=
ARC2_LENGHT (default)	2801.29	= 2 * pi() * R2 * ((ARC2_ANGLE_A + ARC2_ANGLE_B) / 360°)
ARC2_ANGLE_B (default)	10.000°	=
ARC2_ANGLE_A (default)	25.957°	=
ARC1_LENGHT (default)	5926.61	= 2 * pi() * R1 * ((ARC1_ANGLE_A + ARC1_ANGLE_B) / 360°)
ARC1_ANGLE_B (default)	25.957°	=
ARC1_ANGLE_A (default)	8.000°	=

The roof structure was designed parametrically in order to easily create/design indefinite varieties of buildings with this roof, no matter what the dimensions of the floors were (Figure 04). However, the challenge was that we were not able to make adjustments on the roof at the project level. This was the limitation of this parametric roof family.

3.2 API for creating the relation between Roof and Floor

To overcome this challenge, we moved to the next step which was to constitute algorithmic relationships between object families. Revit® API allows us handle this limitation using MS Visual C#. If the code was successful, any change on the length of the floor could reflect proper change in the length of the roof. The challenging part of this project was that the length of the roof was actually the arc lengths not the projection on the X axis (Figure 04). Consequently, changing the length of the roof by modifying the length of the floor would not give the right solution unless the angles were set up properly.

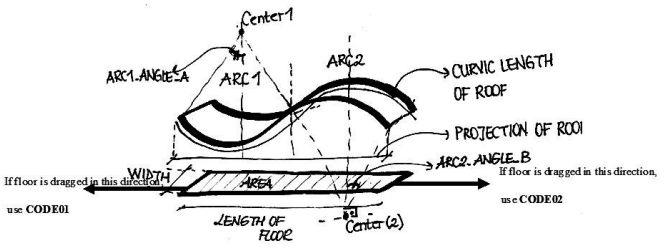

Figure 04: Diagrammatic drawing of the function between roof and floor.

In order to create a correlation between the roof and the floor length, we performed experiments on the length of projected roof on the X axis and prepared a database with different arc angles (Table 02). This database includes angles of each arc, and shows the length increase or decrease according to the selected angle for each arc. Since angles more than 45° are not appropriate for a roof design in this project, two constraints were applied to the arc angles in order to limit the values to any degree between 0° and 45°. These two constraints are that angle of arc cannot get (1) any value larger than 45 and (2) any negative value.

Table 02: Excel Sheet for the external database of the roof angle-length relations

Data	A0	A5	A10	A15	A20	A25	A30	A35	A40	A45
A0	314.189	357.036	393.223	432.593	468.682	538.051	544.14	576.948	609.756	681.934
A5	343.027	385.874	422.061	461.431	497.52	536.889	572.978	605.786	638.594	710.772
A10	369.962	412.81	448.997	488.366	554.455	563.825	599.914	632.722	665.53	737.707
A15	399.49	442.337	478.524	517.894	583.982	593.352	629.441	662.249	695.057	767.234
A20	425.736	468.583	504.77	544.14	610.229	619.598	655.687	688.495	721.303	793.481
A25	451.982	494.83	531.017	570.386	636.475	645.845	681.934	714.742	747.55	819.727
A30	478.229	521.076	557.263	596.633	662.722	672.091	708.18	740.988	773.796	845.974
A35	501.194	544.042	580.229	619.598	685.687	695.057	731.146	763.954	796.762	868.939
A40	524.16	567.007	603.194	642.564	708.653	718.022	754.111	786.919	819.727	891.905
A45	547.126	589.973	626.16	665.53	731.618	740.988	777.077	809.885	842.693	914.87

However, even with the constraints and the database table, there were still infinite number of solutions for the angles, given a floor length. Therefore, two separate codes were created, which were to be run based on the direction of the change on the floor (Figure 04 and Table 02). When the change was applied, part of the roof on the other side of the floor and its arc angle were kept constant, whereas the other part of the roof was modified. Base case arc angles were fixed at 5° for ARC2 and 10° for ARC1 in the project.

Basic algorithm was developed to find the appropriate length of the roof by referring to the database, which contains the pre-calculated length values and their corresponding angles. To find the appropriate roof angle, all length values in the Excel table were tested by the program with the use of a loop function.

4 Findings and discussion

Although there are other methods used in both architectural and urban design, what has been missing from achieving parametric variety for more complex forms, BIM-based modeling allowed for adaptation to the overall design for any changes occurred in any components and fast creation of variety in building design. These two abilities of parametric modeling are the innovations in design.

Autodesk® Revit® as a parametric BIM tool offers two options in modeling: (1) User Interface (UI) and (2) Application Programming Interface (API). UI provides an

environment for user interactive geometry and prototype design. However, as a limitation, UI did not allow linking two or more different objects: roof and floor. Therefore, we used API tool to overcome this limitation.

It is possible to create roof and floor parametric models from scratch by using API but it would be time consuming. Therefore, integrating UI and API is more feasible to develop parametric BIM models: (1) designing complex geometries in UI and (2) applying complex calculations and algorithms in API.

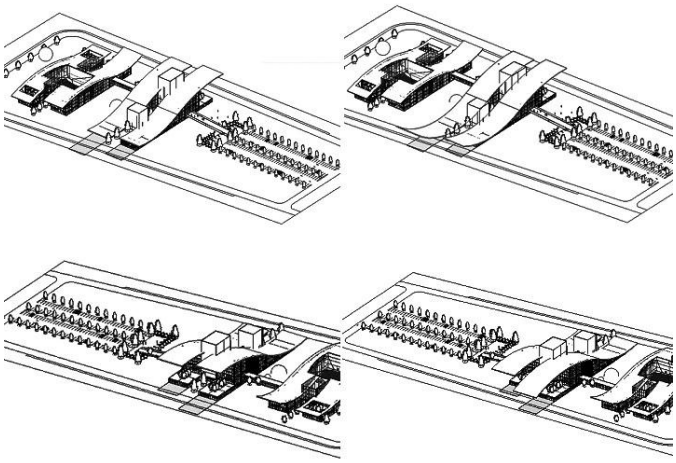

Figure 05: In Upper Figure, Existing roof on the left and modified roof after running the Code 1on the right and In Lower figure, Existing roof on the left and modified roof after running the Code 2on the right.

The hypothesis was that if a function calculating the roof length is defined using a variety of inputs such as length of floors, it can later be applied to urban scale by utilizing a database of inputs. We picked a geometric shape which was challenging due to its relation with the floor (Figure 05). Overall, the findings demonstrate that BIM-based parametric modeling of an architectural project provided fast creation of continuous variety in design form.

This application has several potential limitations due to the existing tools. First, since the parametric roof *family* was modeled by utilizing Generic Model family template under mass *category*, Autodesk® Revit® does not allow us to label it under the roof *category*. Therefore, created roof is a massing model which ends up with typological variety by changing the values of its parameters.

Second, the shape of the roof and the floor caused problems while linking their length parameters. To overcome this limitation, we implemented a set of experiments on the projection of s-shaped roof on X axis and developed a database that links angles of the roof (ARC1_ANGLE_A and ARC2_ANGLE_B) and expected projection on the X axis.

5 Conclusions

In this research, we parametrically modeled an architectural project to test if we could achieve a continuous variety on design form. A roof of a building complex is used as a case study that provides parametric variety in the design geometry form of the building through changing design decisions on values of its angles and radii of arcs, length, and width. The method that we experimented on this project consists of two levels: (1) creating the roof as a BIM parametric family by math functions and (2) establishing an algorithm between floors and the roof structure by API programming. Parametric modeling is a useful tool to achieve that kind of complexity in design problems.

The significance of this research is that the potential applicability of this method to urban scale. However, the number of parameters and codes for urban scale modeling can be much larger. New parameters can be utilized and played with according to (1) the function of buildings such as residential, commercial, industrial, (2) the size of buildings, (3) the lot of buildings, and (4) inhabitant preferences can also be added.

One of the major benefits of BIM-based urban design is that exterior shapes of buildings are designed together with their interior spaces. In other words, other parametric design software only allows designers to consider urban sphere, but not focus on individual buildings. However, through BIM designers can deal with the individual building scale together with the urban scale with other tools.

6 Future work

BIM parametric design and API applications are very powerful in architectural scale and may be adapted to urban scale. This adaption requires more relationships to be defined between different components to achieve enough level of variety in buildings. Larger the scale, more functions and more spatial complexity come to the stage.

Future work can be to apply this method to a larger scale design. For instance, informal settlements are one of the major challenges for developing countries and the United States has experienced this through the settlements developed along the US – Mexico border called the Colonias. A great percentage of these houses are substandard and need to be redesigned. Residents of the houses have different needs and requirements thereby, variety in houses are needed. This method suits this goal. A single family house may be designed parametrically integrating powerful programming methods for adding or removing rooms, dividing or multiplying spaces, and can be designed successfully in a significantly short time period.

7 References

[1] Ellen Yi-Luen Do and Mark D. Gross. "Thinking with Diagrams in Architectural Design." Artificial Intelligence Review (Kluwer Academic Publishers), 15, 135-149, 2001.

[2] Marco Vanucci. "Open Systems: Approaching Novel Parametric Domains"; From Control to Design: Parametric/ Algorithmic Architecture. ACTAR, 118-129, 2008.

[3] Chuck Eastman, Paul Teicholz, Rafael Sacks and Kathleen Liston. "BIM Handbook: A Guide to Building Information Modeling for Owners, Managers, Designers, Engineers, and Contractors". John Wiley & Sons, Inc., 2008.

[4] Tatjana Schneider and Jeremy Till. "Flexible Housing". Architectural Press, 2007.

[5] Patrik Schumacher. "Parametricism as Style-Parametricist Manifesto"; 11th Architecture Biennale, Venice, 2008.

[6] Barrios Hernandez and Carlos Roberto. "Cognitive Models for Parametric Design [Modelos Cognitivos para el Diseño Paramétrico]"; Proceedings of the 11th Iberoamerican Congress of Digital Graphics México D.F. (SIGraDi), 239-242, 2007.

[7] Kyle Steinfeld, Pravin Bhiwapurkar, Anna Dyson and Jason Vollen. "Situated Bioclimatic Information Design: A New Approach to the Processing and Visualization of Climate Data"; Proceedings of the 30th Annual Conference of the Association for Computer Aided Design in Architecture (ACADIA), 88-96, October, 2010.

[8] Ming Tang and Jonathon Anderson. "Mathematically Driven Forms and Digital Tectonic: A Formula for Realizing the Digital"; Proceedings of the 30th Annual Conference of the Association for Computer Aided Design in Architecture (ACADIA), 103-109, October, 2010.

[9] Daniel Baerlecken, Martin Manegold, Judith Reitz and Arne Kuenstler. "Integrative Parametric Form-Finding Processes"; New Frontiers: Proceedings of the 15th International Conference on Computer-Aided Architectural Design Research in Asia CAADRIA 2010 (Computer-Aided Architectural Research in Asia), 303–312, 2010.

[10] Robert Woodbury. "Elements of Parametric Design". Routledge Taylor & Fransis Group, 2010.

[11] Patrik Schumacher. "Let the Style Wars Begin"; Architects Journal (EMAP Ltd), 231.16, 41-45, May 2010.

[12] Carlos L. Marcos. "Complexity, Digital Consciousness and Open Form: A New Design Paradigm"; Proceedings of the 30th Annual Conference of the Association for Computer Aided Design in Architecture (ACADIA), 81-87, October, 2010.

[13] Eddy Krygiel and Bradley Nies. "Green BIM: Successful Sustainable Design with Building Information Modeling", edited by Willem Knibbe, Jennifer Leland, Scott Johnson, Rachel McConlogue and Liz Welch. 1st ed. Wiley Publishing, Inc., 2008.

[14] Vladimir Bazjanac. "Impact of the US National Building Information Model Standard (NBIMS) on Building Energy Performance Simulation"; Proceedings: Building Simulation Beijing, China, 1377-1382, 2007.

[15] Micheal Pinedo and Benjamin P. C. Yen. "On The Design and Development of Object-Oriented Scheduling Systems"; Annals Operations Research. 70, 359-378, 1997.

[16] Oxford University. "Oxford Language Dictionaries Online: English"; http://www.oed.com (Oxford University Press) (accessed April 24, 2011), 2010.

[17] Tatjana Schneider and Jeremy Till. "Flexible Housing: Opportunities and Limits"; Arq., 9, 157-166, 2005.

[18] Zaha Hadid Architects. "Kartal Pendik Masterplan, Istanbul"; http://www.zaha-hadid.com/category/masterplans (accessed November 24, 2010), 2006.

[19] Autodesk® Revit® Architecture 2010. "Imperial Tutorials". http://images.autodesk.com/adsk/files/rac_help.pdf. (accessed May 10, 2011) 2009.

[20] Autodesk® Revit® Architecture 2010. "User's Guide". http://images.autodesk.com/adsk/files/rac_help.pdf. (accessed May 10, 2011) 2009.

A Six State HMM for the S&P 500 Stock Market Index

Jaroslav Lajos, K. M. George, N. Park
Computer Science Department
Oklahoma State University
218 Mathematical Sciences
Stillwater, Ok 74078

Abstract – *The Hidden Markov models (HMMs) provide a flexible general purpose approach for modeling various dynamic systems that can be observed through univariate or multivariate time series, even though the underlying system state is not directly observable. In this paper we provide a basic introduction to the Hidden Markov Models (HMMs) and a rationale for choosing them to model the dynamic behavior of the various stock market equities and indices. In order to illustrate the applicability of the HMMs to the stock market, we define a general algorithm which is then used to develop a specific six-states HMM of the S&P 500 index.*

Key Words: HMM, stochastic, modeling, stock market, S&P 500.

1 Introduction

Various financial models of the equity markets have been proposed and studied in the domain of economics. Most of these are based on the concept of discrete-time stochastic processes (i.e. time series) which provide a general framework for estimating models from empirically collected historical data.

Most of the models are linear and can be categorized as either Autoregressive moving average (ARMA) models or state-space models. Even though they are conceptually different, it has been shown that the ARMA and the state-space models are statistically equivalent. In general, the linear models are not sufficiently adequate in predicting the number of features associated with the bear and bull markets. In order to address these problems, a class of nonlinear Markov-switching models has been developed [8].

The Hidden Markov Models (HMMs) provide a flexible general purpose approach for modeling various dynamic systems that can be observed through univariate or multivariate time series. The unique characteristic of HMMs is the fact that the underlying system state is not directly observable. It can only be estimated using some related observable parameter [1, 2, 3].

In this research, we utilize the existing Hidden Markov chain mathematical techniques to model the dynamic behavior of selected stock market equities. In particular, various methods will be researched and developed for stock market HMM parameter selection, estimation, model training, simulations, forecasting and validation. Furthermore, these methods will be developed with the overall goal of providing practical techniques for investment decision making that can improve and potentially optimize stock market investment returns.

Section 2 of this paper provides a basic overview of HHM. This includes a list HMM applications, HMM definition, fundamental HMM problems and algorithms, and HMM MATLAB functions. Section 3 describes our HMM approach to stock market modeling. This includes a general ten step algorithm and a detailed description of a specific six-state HMM of the S&P 500 index. Section 4 presents the simulation results and final conclusions with further work presented in Section 5.

2 HMM Overview

The HMMs have been extensively used in various scientific fields. This success can be attributed to the HMMs' rich theoretical foundations

and rigorous mathematical structures. Some of the more common applications are:

- Speech recognition and machine translation,
- Bioinformatics and Biophysics (DNA sequencing, gene predictions, etc.),
- Communication modeling (communication channels, internet traffic, etc.),
- Financial modeling,
- Environmental studies (earthquake predictions, weather predictions, etc.), and
- Behavioral studies (homicides, suicides, etc.) [2, 3].

The HMM approach combines the concept of finite state automata with the theory of stochastic processes. Thus, it can categorize as a form of a probabilistic finite state system where the actual states are not directly observable. They can only be estimated using various external observables associated with the hidden states.

The key components of HMM are the following:

1) finite set of hidden states,
2) finite set of observation symbols,
3) initial state probability distribution vector,
4) state transition probability matrix, and
5) observation probability matrix.

2.1 HMM Definition

The formal mathematical definition of the HMM is specified in terms of a state transition probability matrix, and an observation probability matrix using conditional probability notation. For example the statement $P(A|B)$ represents the probability of observing event *A* given the occurrence of event *B*.

An HMM is defined as a quintuple $\lambda = (S, V, A, B, \pi)$ where: [2]

- $S = \{s_1, s_2, \dots, s_N\}$ is a set of *N* possible states; a state at time *t* is usually denoted by $q_t \in S$
- $V = (v_1, v_2, \dots, v_M)$ is a set of *M* possible observation symbols; an observation at time *t* is usually denoted by $o_t \in V$
- *A* is an *NxN* state transition probability matrix defined by:

$$A = \{a_{ij} | \, a_{ij} = P(q_{t+1} = s_j | q_t = s_i)\}$$

- *B* is an *NxM* observation probability matrix defined by:

$$B = \{b_{ij} | b_{ij} = P(o_t = v_j | q_t = s_i)\}$$

- π is an *N* dimensional initial state probability distribution vector defined by:

$$\pi = \{\pi_i | \pi_i = P(q_1 = s_i)\} = P_S(s_i)$$

Note: The following conditions must be satisfied:

1. $\sum_{j=1}^{N} a_{ij} = 1, \;\; 1 \le i \le N$
2. $\sum_{j=1}^{M} b_{ij} = 1 \, , \;\; 1 \le i \le N$
3. $\sum_{i=1}^{N} \pi_i = 1$

In addition to the standard HMM, several other types and variations have been proposed and used for modeling. The following lists some of these variants:

- Input-Output HMM,
- Nth order HMM,
- HMM with silent states,
- Left-to-right and right-to-left HMM,
- Hierarchical HMM,
- Coupled HMM, and
- Autoregressive HMM.

2.2 HMM Fundamental Problems

The HMM implementation usually involves the following three fundamental problems: [1, 2]

1. *Evaluation Problem*: Given an HMM $\lambda = (S, V, A, B, \pi)$ and a sequence of observations $O = o_1, o_2, \dots, o_T$, what is the probability that the observed sequence was generated by the model? That is, determine $P(O|\lambda)$.
2. *Decoding Problem*: Given an HMM $\lambda = (S, V, A, B, \pi)$ and a sequence of

observations $O = o_1, o_2, \ldots, o_T$, what is the most likely hidden state sequence $Q = q_1, q_2, \ldots, q_T$ that could produce the observations? That is, find a state sequence $Q = q_1, q_2, \ldots, q_T$ that maximizes the observational probability $P(O, Q|\lambda)$. It is usually implemented using the Viterbi Algorithm.

3. *Learning Problem*: Given a set of observation sequences $\{O_1, O_2, \ldots, O_n\}$, find the HMM $\lambda = (S, V, A, B, \pi)$ that best explains the observation sequences. That is, find values for $\lambda = (S, V, A, B, \pi)$ that maximize $P(O|\lambda)$. Thus, this is a problem of estimating the most likely HMM parameters for the given set of observation sequences. It is usually implemented using the Baum-Welch Algorithm.

2.3 HMM Software Packages

There are several existing software implementations of the various HMM algorithms. In our simulations we have utilized both the MATLAB and the R statistical HMM packages. MATLAB is proprietary, whereas R is open source software.

MATLAB implements the HMM (S, V, A, B, π) via five functions as described below; where Q represents a sequence of states and O a sequence observations.

1. [O, Q] = *hmmgenerate*(length, A, B): Generates a sequence Q of states and a sequence O of observations.

2. [A, B] = *hmmestimate*(O, Q): Calculates maximum likelihood estimates of transition and observation probabilities.

3. [A, B] = *hmmtrain*(O, Ai, Bi): Calculates maximum likelihood estimates of transition and observation probabilities from the given initial estimates Ai of transition and Bi of observation probabilities. (uses the Baum-Welch algorithm).

4. Q = *hmmviterbi*(O, A, B): Calculates the most probable sequence Q of states for a given sequence O of observations.

5. P = *hmmdecode*(O, A, B): Calculates the sequence P of posterior state probabilities.

3 HMM Approach for Modeling Stocks

This section describes both the general HMM consideration and also the specific parameter choices used in the HMM simulation.

First we provide a ten step summary of the overall HMM simulation algorithm. There are four main phases to implementing the algorithm:

- selection of HMM input parameter (steps: 1, 2, 3, and 4.),
- selection of initial HMM training parameters (steps: 5 and 6),
- the HMM training process (steps: 7, 8, and 9), and
- the final interpretation of the model simulation results (step 10).

3.1 Summary of the HMM Simulation Algorithm

This section provides a ten step summary of our overall HMM simulation approach to modeling stock equities and indexes.

1. Select stock security to be modeled (examples: DJI, SPX, IBM).

2. Using some observable stock related parameter(s), define a set V of M observation symbols (example: partition % daily price changes into *n* intervals).

3. Select a time frame and, using appropriate historical information, compute the corresponding observation sequence O (training data set).

4. Select the number of states parameter N (S = {1, 2, …, N}).

5. Estimate the initial state transition probability matrix A (guess, use *hmmestimate*, two level data set partitioning, etc.).

6. Estimate the initial observation probability matrix B (guess, use *hmmestimate*, two level data set partitioning, etc.).

7. Calculate maximum likelihood estimates for the transition and the observation probabilities: [A, B] = *hmmtrain*(O, Ai, Bi).

8. Calculate the most probable sequence Q of states for the given sequence O of the model observations: Q = *hmmviterbi*(O, A, B).

9. Calculate the sequence P of posterior state probabilities for the sequence O of the model observations: P = *hmmdecode*(O, A, B).

10. Interpret the model results and use P and Q sequences to make trading decisions. Compare returns to a benchmark S&P 500.

3.2 Input Parameter Selection

The selection of the input parameter consists of choosing the following:

- stock equity or index to be modeled,
- the observation parameter(s) and the associated time series, and
- number of states.

For the purpose of this study we'll model the dynamic behavior of the S&P 500 index during the time frame from 1985 to March 2011. The following chart shows the corresponding closing prices.

Figure 1: S&P 500 Closing Prices

From the mathematical perspective, the purpose of HMM estimation is to discover a good-fit inverse relationship between the state and the observed parameters so that the model can then be used effectively to predict the actual hidden state probability distributions from the known sequences of the observed parameter. For this reason, the selection of the observation parameter is perhaps the most important part of a successful HMM development. It should have a high degree of functional relationship to the unknown state parameter. The observation parameter can be univariate or multivariate. The following list illustrates some possible choices for type this parameter:

- time series of price changes of the selected stock or index,
- time series of price changes with trading volume changes,
- time series of price changes coupled with some fundamental data (EPS, etc.),
- time series of price changes coupled with some economic indicators (GDP, etc.), and
- time series Intervals: 1-minute, 15-minutes, hourly, daily, etc.

For our current simulation we have selected the observation sequence consisting of the S&P 500 daily closing price fluctuations, represented as a percentage of the previous day closing price. The following graph shows the corresponding time series.

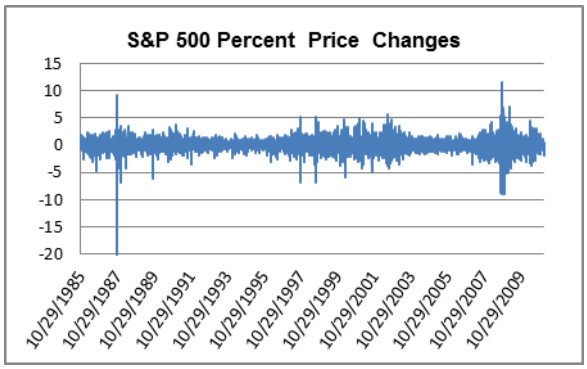

Figure 2: S&P 500 Percent Price Changes

This observable parameter has a large number of possible outcomes, thus it must be quantized into a smaller set of discrete values. We accomplish this by subdividing the overall interval (-100%, 100%) into a discrete set of six subintervals, each corresponding to

an observable value. The particular quantization used in our simulation is defined Table 1.

Table 1: Discretization of the Observable

Observation	Start of Interval	End of Interval
O1	-100%	-3%
O2	-3%	-1%
O3	-1%	-0%
O4	0%	1%
O5	1%	3%
O6	3%	100%

The occurrence frequency of the six observation symbols is illustrated in the following graph of their 40- day moving average.

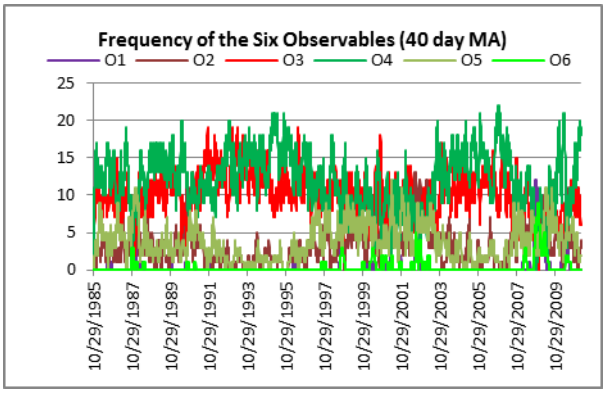

Figure 3: Frequency of the Six Observables

Both the above and previous graphs clearly reveal a correlation between increase in volatility and major market downturns.

The final input parameter to be considered is the number of states. We have experimented with different numbers of states and found that the number of six states provides a good choice for modeling the S&P 500 index. In general, a larger number of states yields a more accurate model; however, the HMM algorithms become computationally more intensive as this number increases.

3.3 The Initial HMM Training Parameter

The next step in implementing our HMM simulation is to select the initial state transition probability and the initial observation probability matrices. This choice is also very critical to developing a good model. However, for the purpose of the current simulation, we will use the simple defaults given in the following tables.

Table 2: Initial State Transition Probability Matrix

	State1	State2	State3	State4	State5	State6
State 1	0.9000	0.0200	0.0200	0.0200	0.0200	0.0200
State 2	0.0200	0.9000	0.0200	0.0200	0.0200	0.0200
State 3	0.0200	0.0200	0.9000	0.0200	0.0200	0.0200
State 4	0.0200	0.0200	0.0200	0.9000	0.0200	0.0200
State 5	0.0200	0.0200	0.0200	0.0200	0.9000	0.0200
State 6	0.0200	0.0200	0.0200	0.0200	0.0200	0.9000

Table 3: Initial Observations Probability Matrix

	O1	O2	O3	O4	O5	O6
State 1	0.1667	0.1667	0.1667	0.1667	0.1667	0.1667
State 2	0.1667	0.1667	0.1667	0.1667	0.1667	0.1667
State 3	0.1667	0.1667	0.1667	0.1667	0.1667	0.1667
State 4	0.1667	0.1667	0.1667	0.1667	0.1667	0.1667
State 5	0.1667	0.1667	0.1667	0.1667	0.1667	0.1667
State 6	0.1667	0.1667	0.1667	0.1667	0.1667	0.1667

3.4 The HMM Training Process

The final phase of our HMM simulation algorithm (steps: 7, 8, and 9) is to compute the following:

- the maximum likelihood estimates for the transition and the observation probabilities ([A, B] = *hmmtrain*(O, Ai, Bi)),
- the most probable sequence Q of states for the given sequence O of the model observations (Q = *hmmviterbi*(O, A, B)), and

- the sequence P of posterior state probabilities for the sequence O of the model observations (P = *hmmdecode*(O, A, B)).

The final HMM model result are summarized in the next section.

4 The Six-States S&P 500 HMM Simulation Results

The final HMM simulation results for the S&P 500 index are presented in this section. They consist of the following items:

- state transition probability matrix,
- observation probability matrix,
- sequence of the most likely states, and
- sequence of the posterior state probability distributions.

The following tables and graphs illustrate these results.

Table 4: Trained State Transition Probability Matrix

	State1	State2	State3	State4	State5	State6
State 1	0.9822	0.0178	0.0000	0.0000	0.0000	0.0000
State 2	0.0555	0.9383	0.0038	0.0000	0.0024	0.0000
State 3	0.0000	0.0020	0.9897	0.0083	0.0000	0.0000
State 4	0.0000	0.0000	0.0000	0.9765	0.0208	0.0026
State 5	0.0000	0.0000	0.0360	0.0000	0.9640	0.0000
State 6	0.0000	0.0000	0.0000	0.0000	0.0095	0.9905

Table 5: Trained Observations Probability Matrix

	O1	O2	O3	O4	O5	O6
State 1	0.2169	0.1987	0.1190	0.1764	0.1229	0.1661
State 2	0.0109	0.2716	0.2543	0.2939	0.1529	0.0165
State 3	0.0551	0.2570	0.1875	0.1799	0.2498	0.0706
State 4	0.0000	0.0342	0.4037	0.5196	0.0425	0.0000
State 5	0.0032	0.0733	0.3654	0.4570	0.1011	0.0000
State 6	0.0025	0.1339	0.3269	0.3484	0.1855	0.0028

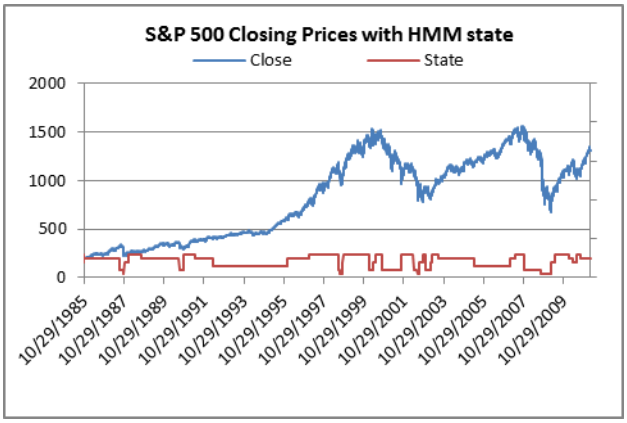

Figure 4: S&P 500 Closing Prices with HMM state

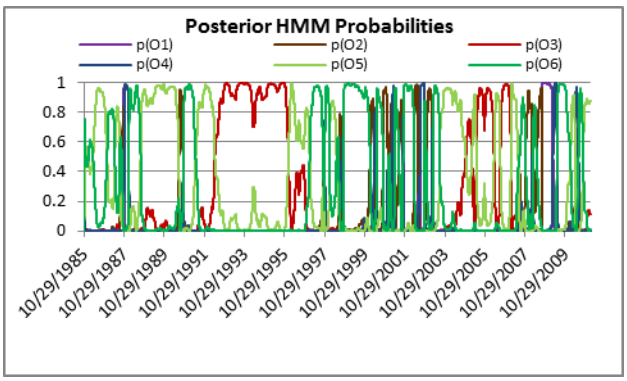

Figure 5: Posterior HMM Probabilities

Table 6: Price Changes/Returns for the Six-States S&P 500 HMM

	Count	Days	Change	Avg, Chg.
State 1	2	141	-484.32	-3.43
State 2	7	678	-879.24	-1.30
State 3	9	333	-22.74	-0.07
State 4	2	1385	466.49	0.34
State 5	8	2308	907.82	0.39
State 6	11	1709	1338.64	0.78

These results provide a large amount of information that can be used to analyze the various aspects of the dynamic behavior of the S&P 500 index. They can also be used for forecasting future prices and formulating various investment strategies.

For example, one could use the model results to formulate the following investment strategies based

on whether the current state has positive or negative return expectations:

1. Buy when there is a transition to a positive return state and sell when there is a transition to a negative return state.

2. Buy when there is a transition to positive return state and sell short when there is a transition to a negative return state.

3. Sell short when there is a transition to a negative return state and cover the short sale when there is a transition to a positive return state.

5 Conclusions and Further Work

In this paper we have presented a basic overview of the Hidden Markov Model and showed how it can be implemented using existing software packages.

Next we have presented a general ten step algorithm for developing an HMM for stock market equities and indexes. We used this algorithm to develop a six-state model for the S&P 500 index. Finally, we illustrated the wealth of dynamic information that the model provides.

Due to the complexities associated with our HMM research, we had to limit the scope of the topics. The additional topics of more in-depth analysis, forecasting, model validation, model optimization, and advance investment strategy formulations will be presented in subsequent papers.

6 References

[1] Oliver C. Ibe, Markov Processes for Stochastic Modeling, Elsevier Academic Press, 2009, San Diago, California, USA.

[2] Lawrence R. Rabiner, "A Tutorial on Hidden Markov Models and Selected Applications in Speech Recognition", Proceedings of the IEEE, pp. 257-286, Vol. 77, No. 2, February 1989.

[3] Walter Zucchini and Iain L. MacDonald, Hidden Markov Models for Time Series, Chapman & Hall/CRC, 2009, Boca Raton, FL, USA.

[4] Gerald Appel, *Technical Analysis: Power Tools for Active Investors*, FT Prentice Financial Times, March 2005.

[5] Alfred V. Aho and Jeffrey D. Ullman, *The Theory of Parsing, Translation, and Compiling, Volume I: Parsing*, Prentice-Hall, Inc., 1972

[6] Alfred V. Aho, John Hopcroft, and Jeffrey D. Ullman, *The Design and Analysis of Computer Algorithms*, Addison-Wesley Publishing Company, June 1976.

[6] Pierre Bremaud, *Markov Chains: Gibbs Fields, Monte Carlo Simulation, and Queues*, Springer-Verlag New York, Inc., 1999.

[7] Samuel Eilenberg, *Automata, Languages, and Machines*, Vol. B, Academic Press, 1976.

[8] Frank J. Fabozzi, Sergio M. Focardi, and Petter N. Kolm, *Financial Modeling of the Equity Market*, John Wiley & Sons, Inc., January 2006.

[9] Sergio M. Focardi and Frank J. Fabozzi, *The Mathematics of Financial Modeling and Investment Management*, John Wiley & Sons, Inc., March 2004.

[10] Robert G. Gallager, *Discrete Stochastic Processes*, Kluwer Academic Publishers, 1996.

[11] Mika Hirvensalo, *Quantum Computing*, Springer-Verlag, 2nd edition, February 2004.

[12] Paul G. Hoel, Sidney C. Port, and Charles J. Stone, Introduction to Probability Theory, Houghton Mifflin Company, 1971.

[13] W. M. L. Holcombe, *Algebraic Automata Theory*, Cambridge University Press, 1982.

[14] John E. Hopcroft and Jeffrey D. Ullman, *Introduction to Automata Theory*, Languages and Computation, Addison-Wesley Publishing Company, Inc., 1979.

Empirical Evaluation of Modeling Languages Using Multi-Lift System Case Study

Abbas Rasoolzadegan, Ahmad Abdollahzadeh
Intelligent Systems Laboratory (http://ce.aut.ac.ir/islab)
Information Technology and Computer Engineering Faculty
Amirkabir University of Technology (Tehran Polytechnic)

Abstract - *This paper empirically investigates the advantages and limitations of modeling languages by specifying the multi-lift system as a non-trivial case study. The multi-lift system is a suitable test bed to demonstrate the expressive power of modeling languages in specifying such a concurrent, reactive, and complex system. English, UML, and Object-Z have been chosen, respectively, as informal, semi-formal, and formal modeling languages to specify the software requirements of the multi-lift system. These modeling languages are then compared and evaluated based on their likelihood to produce a specification with some defined characteristics. The conclusion is that informal languages such as English cannot be used to produce software models, because they are prone to ambiguity. Each of the formal and semi-formal languages has some unique advantages and limitations. Semi-formal models should be supplemented with formal ones to produce high quality software.*

Keywords: Modeling languages, Object-Z, UML.

1 Introduction

A model is the mathematical meaning of a description of a domain, or a prescription of requirements, or a specification of software, i.e., is the meaning of a specification of some universe of discourse. Modeling is the process of identifying appropriate phenomena and concepts and of choosing appropriate abstractions in order to construct a set of models which reflect appropriately on the universe of discourse being modeled. In software engineering we create successions of models: $domain \rightarrow requirements \rightarrow software\ designs$. Thus the combined universes of domain engineering, requirements engineering, and software design constitute the universe of discourse of software engineering [4]. Model and modeling play a crucial role in the software development process. In software engineering, models are used to describe both the problem (requirements) and the solution (design) in order to gain a better understanding of the issues involved. Once a model has been constructed it can be analyzed to uncover flaws and expose fundamental issues [5]. This role of models cannot possibly be assumed by code. The idea is not new, but there is a recent trend towards more use of models in mainstream circles of software engineering.

Models must be written using some language or notation. A language consists of syntax and semantics. Software models should be precise, be abstract to avoid bias towards any specific implementation, and be written in terms of user-observable phenomena. Programming languages cannot be used to write them, because programs describe one way to meet the needs of a product, but not necessarily the actual requirements of stakeholders. This means that we need specialized notations to model software systems. Software modeling languages are divided into three big groups: informal, semi-formal, and formal. Informal group includes all natural languages (such as English) which are prone to ambiguity. Semi-formal languages (such as UML) have a formal syntax, which is usually diagrammatic, but no formal semantics. Formal languages (such as Object-Z) are usually textual and have a formal or mathematical syntax and semantics.

In this paper, advantages and limitations of modeling languages are investigated empirically by specifying the multi-lift system using English, UML, and Object-Z. Multi-lift system is a commonly used test bed to demonstrate the expressive power of various modeling languages in specifying concurrent reactive systems. It is not a trivial case study because of the complexity caused by inherent concurrent interaction in the system. The multi-lift system includes parallel, distributed, embedded, and real-time software. In a real-time software system the correctness of the system behavior depends not only on the logical results of the computations, but also on the physical instant at which these results are produced [1]. An embedded computer system is a system that uses a computer as a component, but whose prime function is not that of a computer. Parallel and distributed software systems have their own complex features such as the concurrent interactions between various system components, the

reactive nature of the systems, and various message passing schemes between system components.

The conclusion of the empirical evaluation of modeling languages is that each modeling language has some unique advantages and limitations. Using only one of them as the sole modeling approach will not guarantee high quality software. Literature review also confirmed this conclusion [4], [8]. As a result, we can supplement semi-formal models with formal ones to introduce precision in the development process and to sweeten formal languages usage. Such a combination leads to develop the software with the desired quality [11-14]. Proposing a new approach to integrate semi-formal and formal models is left for future work.

The rest of this paper is organized as follows: Section 2 presents informal specification of requirements and expected properties of given multi-lift system. This system is rather an "ideal" one in which some of the technical corners are cut. In section 3 formal specifications of the system's requirements is presented using Object-Z. Section 4 specifies these requirements visually in UML. Finally, Section 5 draws conclusions and discusses future work.

2 Informal Specification

A lift system for a multi-floor building consists of multiple elevators. The elevators are supposed to be used in a building having floors numbered from 1 to *MaxFloor*. There are two direction buttons on each floor (except the top floor and the lobby) for the passengers to call for going up and down. There is only one 'down' button at the top floor and one 'up' button in the lobby. Inside each elevator there is a panel of floor buttons each of which indicates a destination floor. Door is one of important parts of a lift system. When an elevator car stops in a particular floor, its door is opened for passenger to come out and come in to the car. Arrival sensor is used in every floor for detecting the elevator. Once an elevator reaches a particular floor, the floor's arrival sensor detects the elevator and stops the car. Any button can be pushed at any time. Any external floor button is turned on from the time it is pushed until an elevator with the same travel direction stops at the floor and opens the door. Any internal 'on' button of a lift is turned off when the elevator visits the corresponding floor.

The multi-lift system that is defined in this paper has the basic functions that all elevator systems have such as moving up and down, open and close doors, and of course, pick up passengers. When a car stops at a floor, the door is opened and the car lantern, which indicates the current move direction of the car, is illuminated for notifying the passengers of the current move direction of the car. In order to certify system safety, the emergency brake will be triggered and the car will be forced to stop under any unsafe conditions. The lift system is responsible for controlling the lifts. Passengers interact with the lift system by pressing buttons on the individual floors or on the control panel inside the elevators. Initially, all lifts stay on the ground floor of the building. If a passenger enters a lift and presses the button for the *k-th* floor the request information is sent to the system. Then the lift moves up to the *k-th* floor. When the lift arrives at the destination, it opens the door for a certain period *M* seconds of time, then closes it again, and becomes idle. Moreover, when a passenger on *m-th* floor calls a lift by pressing the up or down button, the most suitable lift is moved to the *m-th* floor by the lift system and the door is opened on arrival. The passenger may request to go to a particular floor by pressing the corresponding button on the control panel inside the lift. If there is no passenger interaction on the control panel within *M* seconds, then the lift will close the door and go idle at that floor.

3 Formal Specification

Formal specification of the multi-lift system is presented using Object-Z [2] which is a state-based language that favors a model-oriented style of specification. It is an extension to Z to facilitate the structuring of a model in an Object Oriented (OO) style. It provides the class schema as a structuring mechanism (a collection of an internal state schema and operation schemas) and support for OO notions such as object, inheritance, and polymorphism. Object-Z is the most successful OO extension to Z among the ones that emerged in early 1990s [2].

In this section, just the main components of the lift system are presented due to the space limitations. More information about the details of the formal specification has been elaborated in [16]

LiftButton

$\upharpoonright(num, state, \text{INIT}, Press, TurnOff, Blink)$

$Button[\textbf{redef}\ \ Press]$

$num : \mathbb{N}$

$state : ButtonStatus \mid Blink$

$1 \leq num \leq \#floors$

Press

$\Delta(state)$

$state = Off \land\ num \in liftb.floorsServiced \land\ num \neq liftb.current$

$state' = On \land\ liftb.AddIntReqToIntList \bullet [floorNum? = num]$

Blink

$\Delta(state)$

$state' = Blink$

FloorButton

$\upharpoonright(direction, state, \text{INIT}, Press, TurnOff)$

$Button[\textbf{redef}\ \ Press]$

$direction : MotionDirection$

$floor : Floor$

$selt \in floor.buttons$

Press

$\Delta(statc)$

$state = Off \land state' = On$
$floor.Press \bullet [md? = direction]$

Passenger

$\upharpoonright()$

$id : \mathbb{N}$

Press

$button? :\downarrow Button$

$button?.Press$

TurnOff

$button? :\downarrow Button$

$button?.TurnOff$

Floor

$\upharpoonright(\textsc{Init}, GetNum, Press, TurnOff)$

$num : \mathbb{N}$
$fmdi : \mathrm{seq}\ FMotionDirectionIndicator_{\textcircled{C}}$
$flpi : \mathrm{seq}\ FLiftPositionIndicator_{\textcircled{C}}$
$buttons : \mathbb{P}\ FloorButton_{\textcircled{C}}$
$centc : CentralController$
$building : Building$

$1 \le num \le \#floors$
$1 \le \#buttons \le 2$
$\#fmdi = \#lifts$
$\#flpi = \#lifts$
$\forall\ lpi : \mathrm{ran}\ flpi \bullet lpi.flr = self$
$\forall\ mdi : \mathrm{ran}\ fmdi \bullet mdi.fr = self$
$\forall\ b : buttons \bullet b.floor = self$
$self \in centc.floors$
$self \in building.floorsb$

Init

$\forall\ m : \mathrm{ran}\ fmdi \bullet m.\textsc{Init}$
$\forall\ l : \mathrm{ran}\ flpi \bullet l.\textsc{Init}$
$\forall\ b : buttons \bullet b.\textsc{Init}$

GetNum

$num! : \mathbb{N}$

Press

$md? : MotionDirection$

$centc.PutReqToQ \bullet [extReq? = (num, md?)]$

TurnOff

$md? : MotionDirection$

$\exists\ button \in buttons \bullet button.direction = md? \Rightarrow button.TurnOff$

LocalController

$\upharpoonright(ds, \textsc{Init}, OpenDoor, ClosеDoor, UpdateDispatchingStrategy, Move, GetId, GetLiftInfo, AddExtReqToExtList, DeleteExtReqFromExtList, UpdateFloorsServiced, UpdateStandbyFloor, Stop, LiftMoved)$

$id : \mathbb{N}$
$liftInfo$
$ds : DispatchingStrategy$
$centcont : CentralController$
$extRequestList : Requests$
$standbyFloor : \mathbb{N}$
$lift : Lift$

$id = lift.num$
$self \in centcont.loccents$
$self = lift.lc$

Init

$extRequestList = \varnothing$
$standbyFloor = 1$

OpenDoor

$lift.OpenDoor$

CloseDoor

$lift.CloseDoor$

Move

$ds = Closed \land \neg(lift.IsWeightOver)$
$lift.md = Up \rightarrow$
$\quad (\exists\ r : extRequestList \bullet r.1 > lift.current) \lor$
$\quad (\exists\ i : \mathrm{dom}\ lift.fbuts \bullet (i > current \land fbuts(i).state = On)) \Rightarrow$
$\quad lift.Move \bullet [direction? = Up]$
$lift.md = Down \Rightarrow$
$\quad (\exists\ r : extRequestList \bullet r.1 < lift.current) \lor$
$\quad (\exists\ i : \mathrm{dom}\ lift.fbuts \bullet (i < current \land fbuts(i).state = On)) \Rightarrow$
$\quad lift.Move \bullet [direction? = Down]$
$[extRequestList = \varnothing \land lift.intRequestList = \varnothing] \bullet$
$\quad lift.fbuts(lift.standbyFloor).state = On$

Stop

$[lift.fbuts(lift.current).state = On] \bullet$
$\quad lift.DeleteIntReqFromIntList \bullet [floorNum? = lift.current] \land$
$\quad lift.fbuts(lift.current).TurnOff$
$\lor$
$[\exists\ r \in extRequestList \bullet (r.1, r.2) = (lift.current, lift.md) \bullet$
$\quad DeleteExtReqFromExtList \bullet [extReq? = (lift.current, lift.md)] \land$
$\quad centcont.TurnOffFloorBut \bullet [(floorNum?, md?) = (lift.current, lift.md)]$
$\lor$
$[lift.md = Up \land \exists\ r \in extRequestList \bullet$
$(r.1 = lift.current \land r.2 \neq lift.md) \land \nexists\ b : lift.fbuts \bullet$
$(b.num > lift.current \land b.state = On) \land \nexists\ r \in extRequestList \bullet$
$r.1 > lift.current] \bullet$
$\quad lift.MotionDirectionChanged \land$
$\quad DeleteExtReqFromExtList \bullet [extReq? = (lift.current, lift.md)] \land$
$\quad centcont.TurnOffFloorBut \bullet [(floorNum?, md?) = (lift.current, lift.md)]$
$\lor$
$[lift.md = Down \land \exists\ r \in extRequestList \bullet$
$(r.1 = lift.current \land r.2 \neq lift.md) \land \nexists\ b : lift.fbuts \bullet$
$(b.num < lift.current \land b.state = On) \land \nexists\ r \in extRequestList \bullet$
$r.1 < lift.current] \bullet$
$\quad lift.MotionDirectionChanged \land$
$\quad DeleteExtReqFromExtList \bullet [extReq? = (lift.current, lift.md)] \land$
$\quad centcont.TurnOffFloorBut \bullet [(floorNum?, md?) = (lift.current, lift.md)]$
$lift.stop \land OpenDoor$

UpdateDispatchingStrategy

$\Delta(ds)$
$newDS? : DispatchingStrategy$

$ds' = newDS$

GetLiftInfo

$liftInfo!$

AddExtReqToExtList

$\Delta(extRequestList)$
$extReq? : Requests$

$extRequestList' = extReq \cup extRequestList \land$
$lift.fbuts(floorNum?).state = Blink$

DeleteExtReqFromExtList

$\Delta(extRequestList)$
$extReq? : Requests$

$extRequestList' = extRequestList \setminus \{extReq?\}$

UpdateFloorsServiced

$newSet? : \mathbb{P}\,\mathbb{N}$

$lift.floorsServiced = newSet?$

UpdateStandbyFloor

$floorNum? : \mathbb{N}$

$lift.standbyFloor = floorNum?$

GetId

$id! : \mathbb{N}$

LiftMoved

$centcont.UpdateFloorsIndicators \bullet$
$[(liftNum?, floorNum?, md?) = (lift.num, lift.current, lift.md)]$

CentralController

$\upharpoonright(INIT, PutReqToQ, GetReqFromQ, ResponseToExtReq, TurnOffFloorBut, UpdateFloorsIndicators)$

$locconts : \mathrm{seq}\, LocalController$
$reqQ : RequestQueue$
$strategy :\downarrow ExternalRequestAllocator_{\circledS}$
$tmcc : TrafficManager_{\circledcirc}$
$csg : ControlStrategyGenerator_{\circledcirc}$
$floors : \mathrm{seq}\, Floor$
$buildingc : Building$

$\#locconts = \#lifts$
$\forall\, l : \mathrm{ran}\, locconts \bullet l.centcont = self$
$csg.ceco = self$
$strategy.centralcontroller = self$
$tmcc.cctrl = self$
$\forall\, f : \mathrm{ran}\, floors \bullet f.centc = self$
$buildingc.cc = self$

INIT

$csg.INIT$

PutReqToQ

$extReq? : Requests$

$reqQ.Join \bullet [item? = extReq?]$

$ResponseToExtReq \mathrel{\widehat=} [reqQ.size \neq 0] \bullet$
$(reqQ.Leave \wedge\ strategy.AllocateExternalRequest) \bullet$
$([item! = extReq?] \wedge\ locconts(liftNum!).AddExtReqToExtList) \bullet$
$([extReq? = item!] \wedge\ reqQ.Remove) \bullet [item? = item!]$

TurnOffFloorBut

$floorNum? : \mathbb{N}$
$md? : MotionDirectiom$

$floors(floorNum?).TurnOff(md?)$

UpdateFloorsIndicators

$liftNum? : \mathbb{N}$
$floorNum? : \mathbb{N}$
$md? : MotionDirectiom$

$\forall\, f : \mathrm{ran}\, floors \bullet$
$(f.fmdi(liftNum?).state = Off \Rightarrow f.fmdi(liftNum?).TurnOn)$
$\wedge\, f.fmdi(liftNum?).content = md? \wedge$
$f.flpi(liftNum?).content = floorNum?$

4 Semi-formal Specification

In this section the multi-lift system is specified and designed using UML which is an industry-standard language for specifying, visualizing, constructing, and documenting the artifacts of software systems, as well as other non-software systems. UML simplifies the complex process of software design, making a "blueprint" for construction, and is now the standard notation for software architecture. The use of the UML notation for grasping the static structure of the system and for highlighting the system behavior greatly assists the understanding of the formal model. This effectively outlines an integrated approach to modeling the parallel, complex, and distributed software systems. UML provides both the structural views and behavioral views of the system. In this section, a brief UML documentation package is given based on informal and formal models presented before. More detailed information has been explained in [16].

According to the requirements document of our study, the use case diagram of the multi-lift system includes six use cases as shown in Figure 1.

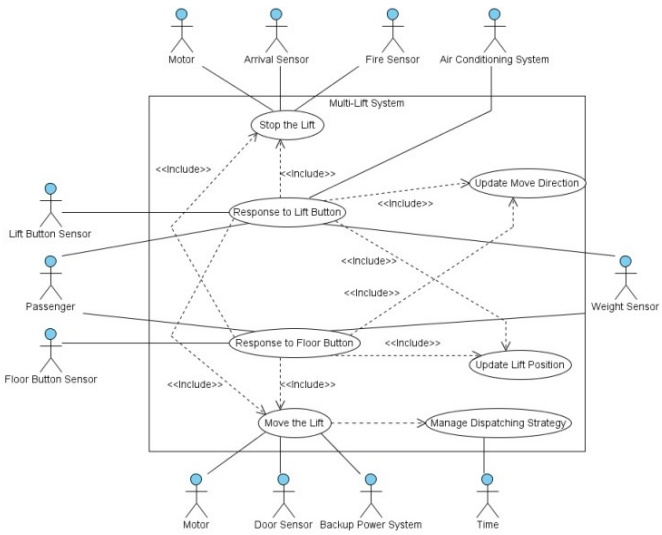

Figure1. Use case diagram of multi-lift system

As an instance, Figure 2 shows the sequence diagram illustrating the scenarios of the use case "Response to Floor Button". Figure 3 illustrates one of the activity diagrams corresponding to the narrative (various scenarios) of the use case "Response to Lift Button".

As the main characteristic states of the lift are the move direction and the door status, in Figure 4, a product of the state spaces of *MoveDirection* and *DoorStatus* forms the state diagram of the lift system. Transitions between states are labeled with Object-Z operations with instantiated preconditions. The instantiated preconditions for each operation are also partitioned and labeled so that they can be presented in a reusable fashion.

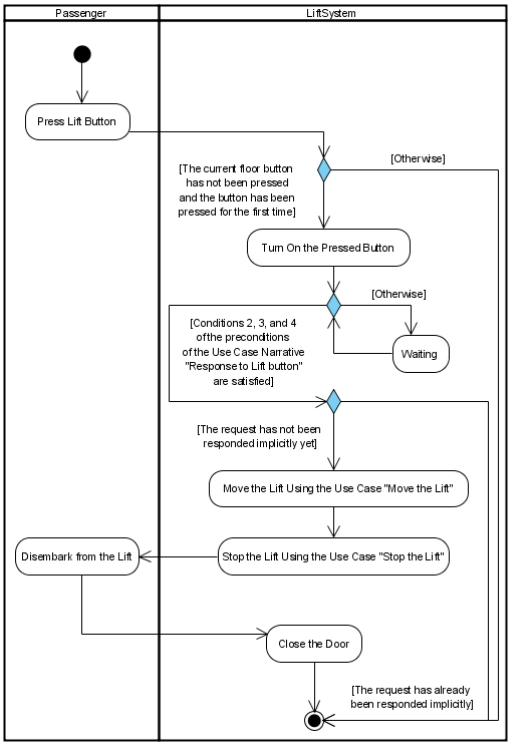

Figure3. Activity diagram corresponding to the narrative of the use case "Response to Lift Button"

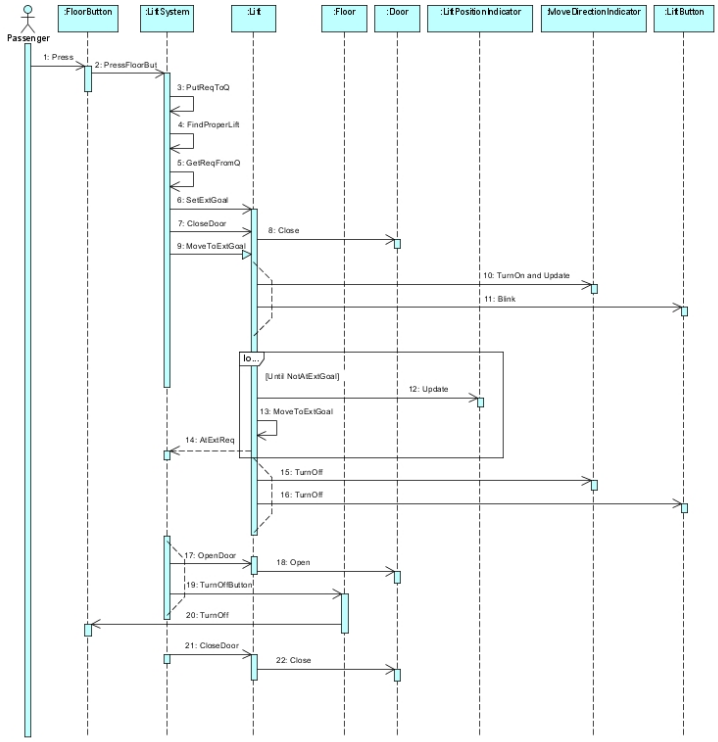

Table1. Comparison of the mentioned modeling languages

Criteria \ Modeling Language	English	UML	Object-Z
Produce readable models	2	3	1
Requires least amount of technical skills	3	2	1
Facilitates development process	1	2	3
Produce testable models	1	2	3
Produce specification decoupled from design	1	2	3
Has least potential for ambiguity	1	2	3
Helps to know when to stop each development phase	1	2	3
Has tool support	1	2	2
Produces maintainable models	1	2	2
Encourage rigorous understanding of requirements	1	2	3
Helps check internal data consistency	1	3	2
Helps validate requirements	1	3	2
Helps verify requirements	1	2	3
Subject to automatic analysis	1	2	3
Helps to know whether all requirements are captured	1	2	3
Total scores for all criteria	18	33	37

Message No. 1:

$$PressButton \mathrel{\widehat{=}} PressUp \vee PressDown$$

Message No. 10:

$$MoveDirectionIndicator.Update \mathrel{\widehat{=}} MoveDirectionIndicator.TurnUp \vee MoveDirectionIndicator.TurnDown$$

Message No. 12:

$$LiftPositionIndicator.Update \mathrel{\widehat{=}} LiftPositionIndicator.Increase \vee LiftPositionIndicator.Decrease$$

Message No. 19:

$$TurnOffButton \mathrel{\widehat{=}} DownOff \vee UpOff$$

Figure2. Sequence diagram corresponding to the narrative of the use case "Response to Floor Button"

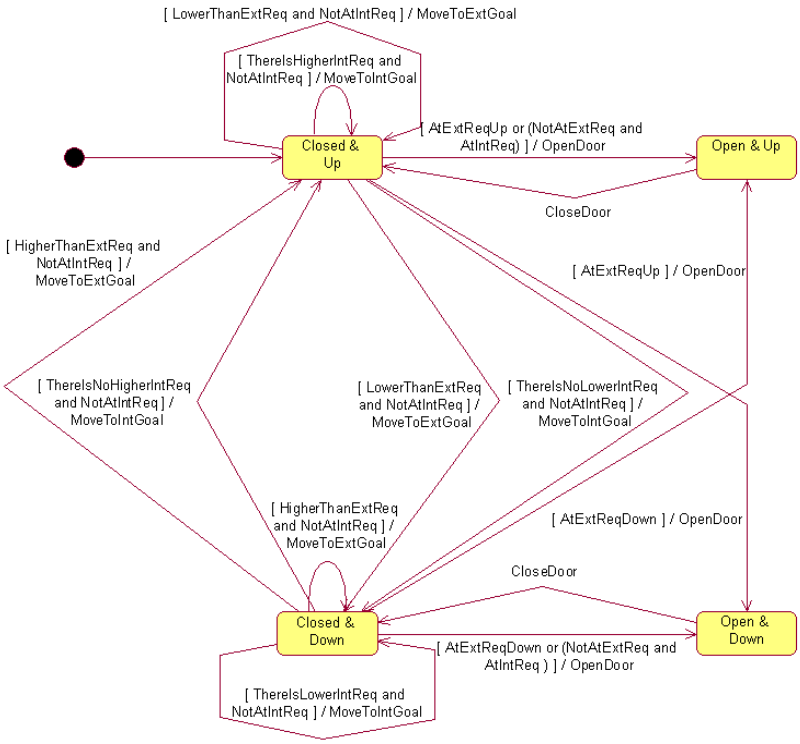

$$AtExtReqDown == \exists g : extGoal \bullet current - first(g) \wedge second(g) - Down \qquad NotAtExtReq == \nexists g : extGoal \bullet current = first(g)$$

$$AtExtReqUp == \exists g : extGoal \bullet current = first(g) \wedge second(g) = Up \qquad LowerThanExtReq == \exists g : extGoal \bullet current < first(g)$$

$$higherThanExtReq == \exists g : extGoal \bullet current > first(g) \qquad NotAtIntReq == fbuts(current).state \neq On$$

$$ThereIsHigherIntReq == \exists i : \mathrm{dom}\, fbuts \bullet (i > current \wedge fbuts(i).state = On)$$

$$AtIntReq == fbuts(current).state = On \qquad ThereIsNoHigherIntReq = \neg ThereIsHigherIntReq$$

$$ThereIsLowerIntReq == \exists i : \mathrm{dom}\, fbuts \bullet (i < current \wedge fbuts(i).state = On)$$

$$ThereIsNoLowerIntReq = \neg ThereIsLowerIntReq$$

Figure4. State diagram of the Lift System

5 Discussion

Table 1 summarizes the relative merits of each of the three modeling languages (English, UML, and Objec-Z) in producing useful artifacts to support various phases of the development cycle according to our empirical experiment on specifying the multi-lift system. A point system ranges from 1 (worst) to 3 (best) whereby a score of 3 for one of the three languages indicates that it best addresses the criteria of merit compared to the other two languages. A language is better than another language for a particular basis of comparison if the former scores a higher point than the latter. Two languages scoring the same number of points for a given criteria of merit imply that none clearly addresses the criteria better than the other. Even though a language may score the same number of points for two different bases of comparison, it does not imply that the language performs equally well in both areas of comparison. For each basis of comparison, the languages are rated relative to one another.

The actual values of the total scores for each language give us some intuitive ideas on how the languages rated comparatively. Overall, the English as an informal language is the least effective tool to produce high quality models for specification and design. The Object-Z as a formal language seems to offer the best alternative. What has been evident throughout the discussion on the relative merits of the various modeling languages is that none of them is ideal in all respects. In other words, each language has some unique advantages and limitations. Using only one of them as the sole modeling approach leads not to a high quality software

The results obtained by this empirical experiment confirm the discussions and results raised from the literature review. According to the literature, formal modeling languages such as Object-Z take a precise approach to software development, delivering reliable software; however, in addition to high cost involvements, they require a level of expertise that is not common in commercial development communities. These limitations lead to decreasing their practicality [4]. Semi-formal modeling languages such as UML that are widely used in practical large-scale software development do not take a rigorous approach to reliability of software in development [8]. Moreover, the increasing importance of developing high quality software beside increasing necessity of *Requirements Engineering* [4] as well as need for further abstraction leads to increasing use of various types of models [4-5]. Models are used at different phases of software development, ranging from requirements to detailed design for specification, analysis, validation (rather than simulation or prototyping [6]), and verification of customer requirements, problems, and solutions. This is the idea behind *Model-Driven Software Engineering* (MDSE), an approach that advocates models, rather than code, as the primary artifacts of software developments. *Model transformation* and *model refinement* have key roles in MDSE [7].

Investigation of advantages and limitations of semi-formal and formal modeling languages, theoretically (by surveying the literature) and empirically (by defining suitable case studies), shows that combination of various types of modeling languages ensures achieving high quality (such as reliable, yet flexible and reusable) software [9-10], [15]. Regarding to the above-mentioned conclusion, we are going to propose a new approach to integrate Object-Z and UML notations using a bidirectional and precise transformation. Accordingly, software is initially modeled using Object-Z. These formal models, along with formal refinement ensure correctness. With an iterative and evolutionary approach, formal models are transformed to UML. Applying design patterns on visualized models improves some other aspects of quality such as flexibility, reusability, and scalability. The improved models are then re-formalized. By specifying the multi-lift system manually in this paper, we provide a suitable test bed to empirically assess the systematic approach that will be proposed in the future. The new approach will be applied on the existing formal specification produced by Object-Z. Then the output will be compared with the current visual specification presented by UML. The more these two models are similar, the more the new approach will be precise.

6 References

[1] Kopetz, H. (1997) *Real-Time Systems: Design Principles for Distributed Embedded Applications*, Springer, first edition.

[2] Duke, R., Rose, G. (2000) *Formal Object-Oriented Specification Using Object-Z*. MacMillan Press.

[3] Booch, G., Rumbaugh, J., and Jacobson, I. (1999) *The Unified Modeling Language User Guide*, Addison-Wesley Professional.

[4] Bjørner, D. (2006) *Software Engineering 3: Domains, Requirements, and Software Design*, Springer.

[5] Williams, J.R. (2009) *Automatic Formalization of UML to Z*, MSc Thesis, Department of Computer Science, University of York.

[6] Pressman, R. (2009) *Software Engineering: A Practitioner's Approach*, 7th edition, McGraw Hill.

[7] Schmidt, D.C. (2006) "Model-driven engineering", IEEE Computer, vol. 39, no. 2, pp. 25-31.

[8] Porres, I. (2001) *Modeling and Analyzing Software Behavior in UML*, PhD thesis, Department of Computer Science, Abo Akademi University, Finland.

[9] Amálio, N. (2006) *Generative frameworks for rigorous model-driven development*, PhD thesis, Dept. of Computer Science, University of York.

[10] Razali, R., Snook, C., Poppleton, M., Garratt, P. (2008) "Usability Assessment of a UML-based Formal Modeling Method Using Cognitive Dimensions Framework", Human Technology: An Interdisciplinary J. on Humans in ICT Environments.

[11] Baresi, L., Pezzè, M. (2001) "On Formalizing UML with High-level Petri Nets", In Concurrent Object-Oriented Programming and Petri Nets, Lecture Notes in Computer Science (LNCS) 2001, pp. 276-304, Springer.

[12] Risco-Martin, J.L., de la Cruz, J.M., Mittal, S., and Zeigler, B.P. (2009) "eUDEVS: Executable UML with DEVS theory of modeling and simulation", Simulation, vol. 85, Issue 11/12, pp. 750-77.

[13] Kim, S.K., Carrington, D.A. (1999) "Formalizing the UML class diagram using Object-Z", LNCS 1723/1999, 753.

[14] Kim, S.K., Carrington, D.A. (2000) "A formal mapping between UML models and Object-Z specifications" In ZB'00: Proc. of 1st Int. Conf. on B and Z users on Formal Specification and Development in Z and B, pp. 2-21, Springer.

[15] Stevens, B. (2006) "Implementing Object-Z with Perfect Developer", J. of Object Technology, vol. 5, no. 2, pp. 189-202.

[16] Rasoolzadegan, A., Abdollahzadeh, A. (2011) *Specifying a Parallel, Distributed, Real-Time, and Embedded System: Multi-Lift System Case Study*, Technical Report, Information Technology and Computer Engineering Faculty, Amirkabir University of Technology, Tehran, Iran.

Modelling of Railway Network Using Petri Nets

MANDIRA BANIK[1], RANJAN DASGUPTA[2]
[1]Dept. of Computer Sc. & Engg., National Institute of Technical Teachers' Training & Research, Kolkata, West Bengal, India (student)
[2]Dept. of Computer Sc. & Engg., National Institute of Technical Teachers' Training & Research, Kolkata, West Bengal, India

Abstract - *This paper deals with the use of Petri nets in modelling railway network and designing appropriate control logic for it to avoid collision. Here, the whole railway network is presented as a combination of the elementary models – tracks, stations and points (switch) within the station including sensors and semaphores. We use generalized mutual exclusion constraints and constraints containing the firing vector to ensure safeness of the railway network. In this research work, we have actually introduced constraints at the points within the station. These constraints ensure that when a track is occupied, we control the switch so that another train will not enter into the same track and thus avoid collision.*

Keywords: Petri nets, safeness constraints, firing vectors, asynchronous systems.

1 Introduction

Modelling of complex systems for better understanding is a very wide-spread research activity and researchers all over the world are trying to model more and more complex systems. Several tools have also been developed for this purpose and Petri Net [1] is one of such tools used for quite some time to model various asynchronous systems. Railway network is considered as a very complex system and appropriate modelling of it to avoid collision is of very high importance. In [3], Giua and Seatzu have used Petri Net to model railway network and developed some expression of constraints to avoid collision. However the paper does not include the situation when there is a train already in a track and another train is in the input line. In our research work, Giua and Seatzu model has been augmented to avoid collision in such cases.

2 Brief overview of Petri Nets

2.1 Definition of Petri nets

Petri net is a formal modelling technique and consists of places, transitions and arcs directed from either places to transitions or transitions to places, representing flow relations. Pictorially, places are drawn as circles and transitions as boxes or bars (Figure 1). Arcs are labelled with weights. Labels for unity weights are generally not given. A place from which a directed arc goes to a transition is called input place of that transition. A place, to which there is a directed arc from a transition, is called output place of that transition. A Petri net is given a state by marking its places with tokens. A marking M is a function [9] that assigns to each place a non negative integer representing number of tokens at that place. In graphical representation, black dots in circles denote tokens in places. Petri Nets may formally be defined as [1] –

A Petri net is a 5-tuple - (P, T, F, W, M_0) where :

$P = \{ p_1, p_2, \ldots, p_m \}$ is a finite set of places,

$T = \{ t_1, t_2, \ldots, t_n \}$ is a finite set of transitions,

$F \subseteq (P \times T) \cup (T \times P) \}$ is a set of arcs (flow relations),

$W: F \rightarrow \{1, 2, 3, \ldots\}$ is a weight function,

$M_0: P \rightarrow \{0, 1, 2, 3, \ldots\}$ is the initial marking,

$P \cap T = \varnothing$ and $P \cup T \neq \varnothing$.

where, $(P \times T)$ and $(T \times P)$ denotes the ordered pair of sets P and T.

By changing distribution of tokens on places the occurrence of events (transitions) may be reflected. The flow of tokens in Petri net are governed by the following rules [2] -

- A transition t is said to be enabled if each input place p of t contains at least the number of tokens equal to the weight of the directed arc connecting p to t.
- A firing of an enabled transition t removes from each input place p the number of tokens equal to the weight of the directed arc connecting *p* to *t.* It also deposits in each output place *p* the number of tokens equal to the weight of the directed arc connecting *t* to p – giving a new marking.

There are also some high-level Petri nets – timed Petri net [6][7], coloured Petri net [8] etc.

2.2 Applications of Petri nets

Petri nets are used for a very wide variety of applications. Specially they are well-suited for systems those are concurrent, asynchronous, distributed, parallel and nondeterministic [1]. In [6], the author presents how timed Petri net is used to model the GPRS charging system

and to analyze its performance when the system works in the normal status and how it handles the maximum supportable busy hour call attempts of the GPRS network. [7] also depicts application of timed Petri net to model traffic signal control where two separate subnets are designed for signal indications (green, yellow, and red) and the transitions between indications (one light becomes red before another becomes green). Besides these, Petri nets have been successfully applied in modelling and performance analysis of communication protocols, flexible manufacturing systems, sequence controllers, distributed-software systems, distributed-database systems, multiprocessor systems, fault-tolerant systems, programmable logic and VLSI arrays [1] etc. Using Petri nets dynamic behaviour of the systems can also be studied [2].

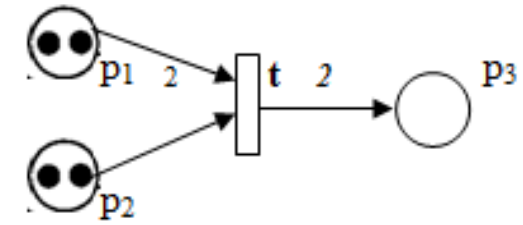

(a)

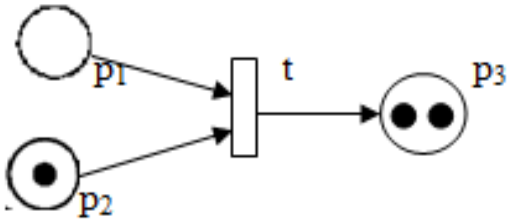

(b)

Figure 1: The marking (a)before firing of enabled transition t (b)after firing of t

2.3 Generalized Mutual Exclusion Constraints (GMECs)

(Un)controllable and/or (un)observable transitions may be used in many applications, for example, in the railway network problem. Uncontrollable transitions are transitions that cannot be disabled by any control action and unobservable transitions are transitions whose firing cannot be directly detected or measured [3]. In [3], generalized mutual exclusion constraints (GMECs) has been utilized for expressing collision avoidance constraints for designing controllers for Petri nets with (un)controllable and/or (un)observable transitions. A generalized mutual exclusion constraint [5] is a linear constraint that limits the weighted sum of tokens in some places of a Petri net. GMECs are used for expressing constraints that states which system state i.e., what marking will be allowed to achieve, for example, safeness in the railway model. A GMEC may be enforced adding to the net a single control structure consisting in a new place called monitor place.

2.4 Constraints containing Firing Vector

Constraints may contain both marking and firing vector elements. These constraints represent that an event (modelled by a transition) can occur at a system's state governed by the marking vector elements, if that system's state allows it to occur [4]. Firing vector q denotes which transition is the next to fire when the Petri net is going from one marking to another marking. It is an nx1 column vector of 0's and an only one, where n is the number of transitions. Now depending on whether a system's state allows a transition t_j to occur, jth element of firing vector

$q_j = 1$ indicating transition t_j is enabled and

$q_j = 0$ indicating transition t_j is not enabled.

3 Railway network problem

The whole railway network is presented as a combination of the elementary models - tracks, stations and points within the station [3].

3.1 Track model

A railway track is shown in Figure 2. Here the track is divided into three segments – α1, α2, α3. Trains can go on this single track in left or right direction. The track includes sensors and semaphores. Sensors A and B detect the passage of train in both directions [3]. The passage of a train directed rightward (from segment α1 to segment α2) can be stopped and also can be detected by semaphore A. Semaphore B does the same for the train directed leftward (from segment α3 to segment α2).

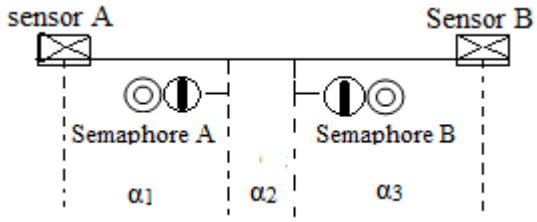

Figure 2: A Railway Track

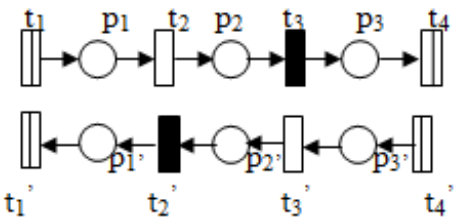

Figure 3: Petri net model of the track of Figure 2

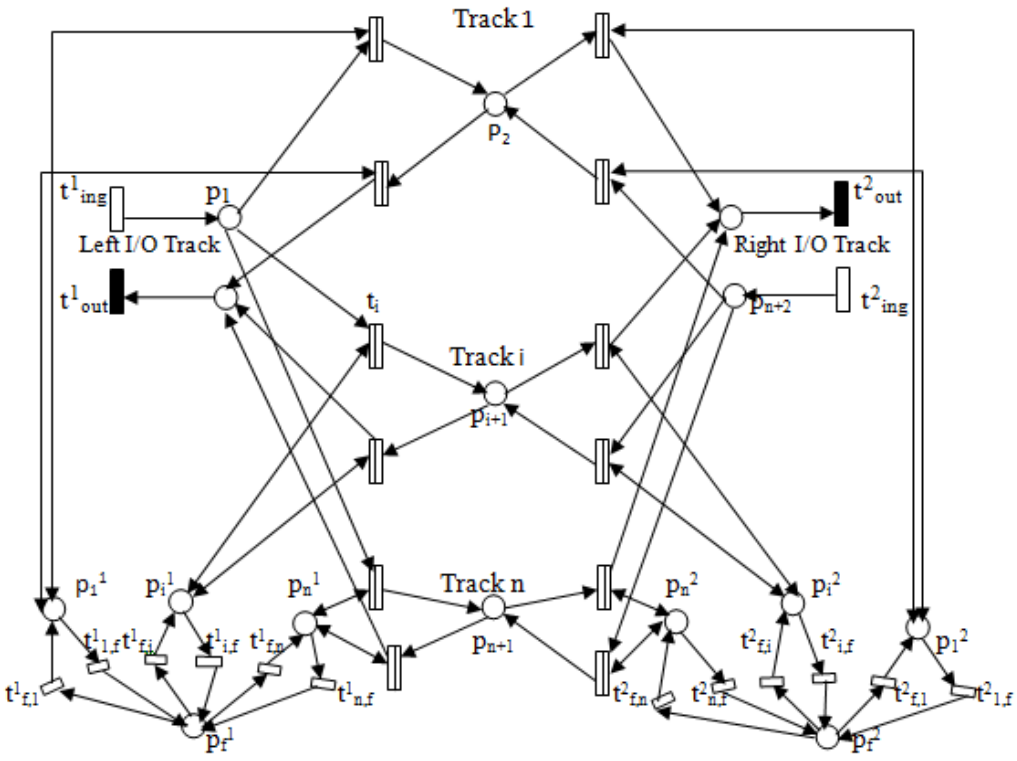

Figure 4: The simplified Petri net model of an n-tracks railway station

In the Petri net model of the track shown in Figure 3, there are two sets of places (p_1, p_2 ,p_3 and $p_{1'}$,$p_{2'}$, $p_{3'}$) and transitions(t_1, . . , t_4 and t_1', . . ,t_4') , representing flow of trains in right and left directions respectively. Each couple of places p_i , p_i' are used to represent segment α_i of the track i.e., the marking of p_i or p_i' indicates the presence of a train directed rightward or leftward in segment α_i. Transitions denote the passage of a train from one segment to another in a certain direction.

In the Petri net model, transitions may be (un)controllable and/or (un)observable so as to represent sensors and semaphores. A both controllable and observable transition represents a semaphore [3]. For example, transitions t_2 and t_3' in Figure 3 correspond to semaphore A and semaphore B respectively: transitions t_2 and t_3' are controllable and observable to denote that at those points of the net the presence of trains can be detected and controlled (their transit can be forbidden) by the corresponding semaphores. Transitions t_1, t_4, t_1' and t_4' represent sensors as a sensor can only detect the passage of train. Transitions t_2' and t_3 are uncontrollable and unobservable.

3.2 Railway station model

Figure 4 can be referred for the Petri net model of an n-tracks railway station. The station [3] consists of n+2 different stretches among which there are n inner tracks (tracks 1, . ,i, . ,n) and two input/output (I/O) tracks on the left and right side. The controllable and observable transitions t^1_{ing} and t^2_{ing} fires when a train enters into the station, while the uncontrollable and unobservable transitions t^1_{out} and t^2_{out} fires to denote the exit of a train from the station.

Now depending on the position of the points a certain track in the station is enabled and trains may be routed to that track. The Petri net models of the points (switch) of the n-tracks station are given by the two subnets on bottom left and on bottom right of Figure 4. The superscripts 1 and 2 are used to indicate places and transitions relative to the left and the right points, respectively. The models represent points (switch) with n possible tracks. Consider for left points. When place p_i^1 (i =1, . . ,n) is marked, left points is connected to track i and trains on the left I/O track may be directed to that track. Actually, transition t_i fires (train enters in track i) if both of its input places p_1 and p_i^1 are marked. But, if place p_f^1 is marked, no train can cross the points. Points position is changed among points places p_i^1 (i=1, . . ,n) by firing transition $t^1_{f,i}$, to enable different paths. Same is for the right points. Place p_f^1 or p_f^2 is marked when the enabled path is being changed or points are switched off.

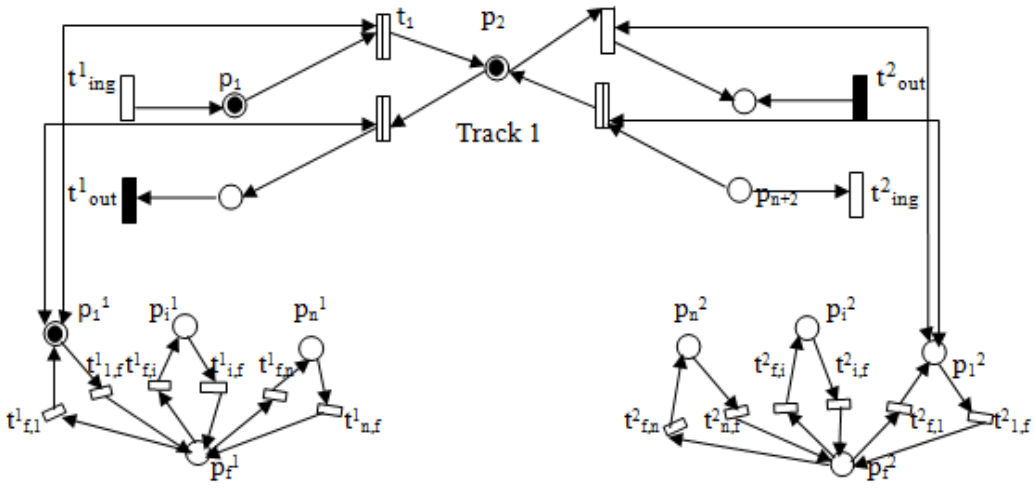

Figure 5: Petri net model of a part of the n-tracks railway station

3.3 Control logic for Tracks and Stations

3.3.1 Safeness of tracks

The collision avoidance constraints can be written as GMECs to ensure that each couple of places p_i and p'_i in Figure 3, representing the same segment of a single-track cannot contain tokens simultaneously, and moreover each place never has more than one token. The GMEC is [3] -

$$m_i + m_i' <= 1$$

relative to a segment of a track. Here, m_i denotes the marking of place p_i. Same constraints can be applied for the tracks of the station also.

Because of the presence of the uncontrollable and/or unobservable transitions in the railway network model, a more restrictive constraint has been developed in [3]. That constraint ensures safeness, but imposes too restriction [3] if applied to the places corresponding to tracks within a station.

So a better solution is to develop a new set of station admission rules or constraints, some of which also include the firing vectors.

3.3.2 Station admission rules

A simplified Petri net model of the station is given in Figure 4. The *station admission rules* can be described as [3]

- No more than n trains should be simultaneously present in the station including the I/O tracks. It can be written as GMEC -

$$\sum_{i=1}^{n+2} m_i <= n$$

- No train may arrive from outside entering the left (or right) I/O track if one inner track is nonempty and the left (or right) points is enabling the flow of trains towards the nonempty track.

$$q^1_{ing} + m_{i+1} + m_i^1 <= 2, \quad i= 1, \ldots ,n \quad \text{(for left side)}$$
$$q^2_{ing} + m_{i+1} + m_i^2 <= 2, \quad i= 1, \ldots ,n \quad \text{(for right side)}$$

For example, if a train exists in inner track 1(place p2 is marked) and the left points is connected to track 1(p_1^1 is marked) then t1ing cannot fire, otherwise an accident occurs. It is applicable for right side also. This case is generalized for n-tracks in the above equations that control the entrance of trains in the station.

4 Limitation of the railway network model

The Petri net model described in section 3 takes care for the selection of vacant tracks among various available tracks. However it does not include successive incoming of trains in the presence of train in station as described here. For example, consider the case in Figure 5. A train exists in inner track 1(place p_2 is marked) and a train also is in the left I/O track (place p_1 is marked) and the left points is connected to track 1(p_1^1 is marked). Now t_1 fires as both of its input places (p_1 and p_1^1) are marked, entering the train in the left I/O track in track 1 and a collision occurs. Same thing will happen for the right side also. Thus the given station admission rules in section 3.3 regulate only the input of trains in the station, not the points within it and that may result in an accident.

5 Proposed model for revised station admission rules

The limitation is addressed here. This accident can be avoided if the left points is not connected to track 1 when trains exist on both track 1 and left I/O track. Now token can be deposited on place p_1^1 only by firing transition $t^1_{f,1}$ of left points model (see Figure 5). So to make p_1^1 not to

be marked, we impose constraints on firing of $t^1_{f,1}$. The constraint is $t^1_{f,1}$ cannot fire if both places p_1 and p_2 are marked simultaneously. This is written as following inequality –

$$q^1_{f,1} + m_1 + m_2 <= 2$$

Thus the points can be regulated. We generalize this constraint for the n-tracks railway station to regulate the points within station to ensure safeness. We develop the following generalized constraints –

$q^1_{f,i} + m_1 + m_{i+1} <= 2$, i= 1, . . . ,n (for left side)
$q^2_{f,i} + m_{n+2} + m_{i+1} <= 2$, i= 1, . . . ,n (for right side)

which imply that if both places p_1(or p_{n+2}) and p_{i+1} are marked, $t^1_{f,i}$ (or $t^2_{f,i}$) cannot fire to make point place p_i^1(or p_i^2) (i= 1, . . . ,n) marked (see Figure 4). That is the left (or right) points corresponding a nonempty inner track cannot be enabled if train exists in the left (or right) I/O track.

6 Conclusion

Modelling with Petri net is being considered as one of the very helpful tools to detect collision in a railway network problem. Following the design model of Giua and Seatzu in [3], in this research work we have augmented the model by introducing constraints at the points (switch). This ensures that when a track is occupied, we control the switch so that another train will not enter into the same track and thus avoids collision.

7 References

[1] Tadao Murata, "Petri Nets: Properties, Analysis and Applications", Proceeding of the IEEE, Vol 77, No. 4, April 1989.

[2] Richard Zurawski and Meng Chu Zhou, "Petri Nets and Industrial Applications: A Tutorial", IEEE Transactions on industrial electronics, vol. 41, no. 6, December 1994.

[3] Alessandro Giua and Carla Seatzu, "Modeling and Supervisory Control of Railway Networks Using Petri Nets", IEEE Transactions on automation science and engineering, vol. 5, no. 3, July 2008.

[4] J. O. Moody, K. Yamalidou, M. D. Lemmon, and P. J. Antsaklis, "Feedback Control of Petri Nets Based on Place Invariants", *Automatica*, vol. 32, no. 1, pp. 15–28, Jan. 1996.

[5] Maria Pia Fanti, Alessandro Giua and Carla Seatzu, "Generalized Mutual Exclusion Constraints and Monitors for Colored Petri Nets", IEEE 2003.

[6] Jiacun Wang, "Charging Information Collection Modeling and Analysis of GPRS Networks", IEEE Transactions on systems, man, and cybernetics—part c: applications and reviews, vol. 37, no. 4, July 2007.

[7] George F. List and Mecit Cetin, "Modeling Traffic Signal Control Using Petri Nets", IEEE Transactions on intelligent transportation systems, vol. 5, no. 3, September 2004.

[8] K. Jensen, "Coloured Petri Nets: A High-level Language for System Design and Analysis", In:G. Rozenberg (ed.): Advances in Petri Nets 1990, Lecture Notes in Computer Science Vol. 483, Springer-Verlag 1991, 342-416.

[9] C Ghezzi, M Jazayeri and D Mandrioli, "Fundamentals of Software Engineering", PHI.

Grey forecasting model for diesel vapor detection and alarm system

Yan Gao[1], Xiaozhou Lü[1,2] and Wenke Lu[1]
[1]College of Information Science and Technology, Donghua University, Shanghai, 201620, P.R.China
[2]Department of Electronic Engineering, University of Washington, WA, 98105, United States

Abstract—*A grey forecasting mathematic model using to determine the recording duration time for diesel vapor detection and alarm system is presented. In order to detect the concentration of volatilized diesel vapor and alarm the risks in engine room of ships, we have developed a diesel vapor detection and alarm system based on catalytic combustion sensor[1]. In this work, we build a grey forecasting mathematic model to determine the recording duration time for the system, design an experiment to obtain the data and write MATLAB codes to solve the model. The result show that we determine a recording duration time with a high accuracy.*

Keywords: Grey forecasting model, Diesel vapor detection and alarm system, Gas sensor

1. Introduction

The leaked diesel oil in engine room of ships volatilizes continuously. When the concentration of volatilized diesel vapor reaches the lower flammability limits(LEL), security risks will occur if there is no timely measures being taken, especially under some circumstances such as higher temperatures in engine room or occurs in an ignition source. Therefore, it is necessary to place sensors in engine room to detect the concentration of diesel oil vapor and alarm the risks.

In our previous work[1], we derived the calculation formula of the volume of diesel in different concentration and determined the coefficient of the formula via analysis of the physical, chemical and volatilization properties of diesel. We then designed an experiment based on the calculated data of the formula and obtained the sensitive data between catalytic combustion sensor output and diesel volume. Furthermore, we derived the function between sensor output and diesel volume based on the experiment data. After fitted the curve and analyzed the linearity, we found that the catalytic combustion sensor could met the design requirements. Then we designed a diesel vapor detection and alarm system in engine room based on catalytic combustion sensor and applied it in ships. In the system, we set 25%(LEL) as the pre-alarm point and 50%(LEL) as the alarm point. In the actual application, however, we found that such setting existed too many false pre-alarm. The concentration of diesel vapor reached pre-alarm point but did not reach alarm point. If we set 50%(LEL) as the pre-alarm point, there will be no time to take measures. Therefore, we need to forecasting the concentration of next time to pre-alarm risks in advance and determine the recording duration time. After a research, we found that the grey forecasting could solve this problem.

Grey forecasting is a branch of grey system. Grey system theory was pioneered by Julong Deng. He published the first paper about grey system theory titled "The Control Problem of Grey System" in the international journal system & control letter, 1982 [2]. Up to now, grey system theory has been successfully applied to medicine [3], [4] image processing [5], robot [6], industry technology [7], [8], [9], [10], digital watermarking technology, petroleum drilling and so on. Grey forecasting involve sequence forecasting, calamities forecasting, seasonal calamities forecasting, topological forecasting and systematic forecasting. It has been widely applied in agriculture, mechanism and climate due to less data (the need data for grey forecasting is as few as 4 datum in every series), leaving out of consideration of data distribution and simply calculating. The typical model of grey forecasting is Grey Model(1,1) [11], [12] which can be written by GM(1,1). It can forecast the next data based on the foregone data in real-time.

This paper begins with the building of the grey forecasting mathematic model. Then it presents the data obtained from the experiment and writhe MATLAB codes to solve the model. The recording duration time is determined by the result of the solved model.

2. Building grey forecasting model GM(1,1)

2.1 Model building

Supposing $x^{(0)}$ is the raw series, written as

$$x^{(0)} = (x^{(0)}(1), x^{(0)}(2), \cdots, x^{(0)}(n)), \tag{1}$$

Let $x^{(1)}$ be the Accumulated Generating Operation(AGO) series of $x^{(0)}$ written as

$$x^{(1)} = AGO(x^0) \tag{2}$$

Provided that

$$x^{(1)} = (x^1(1), x^1(2), \cdots, x^1(n)) \tag{3}$$

where

$$x^{(1)}(k) = \sum_{m=1}^{k} x^{(0)}(m), k = 1, 2, \cdots, n \tag{4}$$

Supposing $z^{(1)}$ is the MEAN series of $x^{(1)}$, written as

$$z^{(1)} = MEAN(x^{(1)}) \tag{5}$$

Provide that

$$z^{(1)} = (z^{(1)}(2), z^{(1)}(3), \cdots, z^{(1)}(n)) \tag{6}$$

where

$$z^1(k) = 0.5x^{(1)}(k) + 0.5x^{(1)}(k-1), k = 1, 2, \cdots, n \tag{7}$$

We define the model of grey differential of GM(1,1) is

$$x^{(0)}(k) + az^{(1)}(k) = b \tag{8}$$

where a is said to be developing coefficient; b is said to be the grey input; $x^{(0)}(k)$ is grey derivative, which is corresponding to $\frac{dx^{(1)}}{dt}$; $z^{(1)}(k)$ is background value, which is corresponding to $x^{(1)}(t)$.

Therefore, the white differential of GM(1,1) can be written as

$$\frac{dx^{(1)}}{dt} + ax^{(1)} = b \tag{9}$$

The response of the equation (9) is

$$\begin{aligned} \hat{x}^{(1)}(k+1) = &\quad (x^{(0)}(1) - \frac{b}{a})e^{(-ak)} + \frac{b}{a} \\ \hat{x}^{(0)}(k+1) = &\quad (x^{(1)}(k+1)) - \hat{x}^{(1)}(k) \end{aligned} \tag{10}$$

The flowchart of GM(1,1) show as in fig.1 .

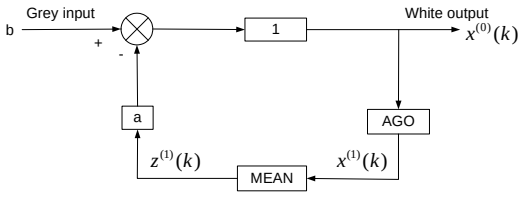

Fig. 1: The flowchart on GM(1,1).

2.2 Parameter identification

Substituting $k = 2, 3, \cdots, n$ into (8), we have

$$\begin{aligned} x^{(0)}(2) + az^{(1)}(2) &= b \\ ax^{(0)}(3) + az^{(1)}(3) &= b \\ &\vdots \\ x^{(0)}(n) + az^{(1)}(n) &= b \end{aligned} \tag{11}$$

The above equations can be written as

$$\boldsymbol{y}_N = \boldsymbol{BP} \tag{12}$$

where

$$\boldsymbol{y}_N = [x^{(0)}(2), x^{(0)}(3), \cdots, x^{(0)}(n)]^T \tag{13}$$

$$\boldsymbol{B} = \begin{bmatrix} -z^{(1)}(2) & 1 \\ -z^{(1)}(3) & 1 \\ \vdots & \vdots \\ -z^{(1)}(n) & 1 \end{bmatrix} \tag{14}$$

$$\boldsymbol{P} = \begin{bmatrix} a \\ b \end{bmatrix} \tag{15}$$

Here, $\boldsymbol{B}$ is said to be data matrix; $\boldsymbol{y_N}$ is said to be data vector; $\boldsymbol{P}$ is said to be parameter vector. The equation (12) can be solved as

$$\boldsymbol{P} = \begin{bmatrix} a \\ b \end{bmatrix} = (\boldsymbol{B}^T\boldsymbol{B})^{-1}\boldsymbol{B}^T\boldsymbol{y}_N \tag{16}$$

Solving the equation, we have

$$a = \frac{\sum_{k=2}^{n} z^{(1)}(k) \sum_{k=2}^{n} x^{(0)}(k) - \sum_{k=2}^{n} z^{(1)}(k)x^{(0)}(k)}{(n-1)\sum_{k=2}^{n} z^{(1)}(k)^2 - (\sum_{k=2}^{n} z^{(1)}(k))^2} \tag{17}$$

$$b = \frac{\sum_{k=2}^{n} x^{(0)}(k) \sum_{k=2}^{n} z^{(1)}(k)^2 - \sum_{k=2}^{n} z^{(1)}(k) \sum_{k=2}^{n} z^{(1)}(k)x^{(0)}(k)}{(n-1)\sum_{k=2}^{n} z^{(1)}(k)^2 - (\sum_{k=2}^{n} z^{(1)}(k))^2} \tag{18}$$

By letting

$$\begin{aligned} C &= \sum_{k=2}^{n} z^{(1)}(k), \\ D &= \sum_{k=2}^{n} z^{(0)}(k), \\ E &= \sum_{k=2}^{n} z^{(1)}(k)x^{(0)}(k), \\ F &= \sum_{k=2}^{n} z^{(1)}(k)^2, \end{aligned} \tag{19}$$

We have

$$\begin{aligned} a &= \frac{CD - (n-1)E}{(n-1)F - C^2} \\ b &= \frac{DF - CE}{(n-1)F - C^2} \end{aligned} \tag{20}$$

Letting

$$\begin{aligned} \Delta_a &= CD - (n-1)E \\ \Delta_b &= DF - CE \\ \Delta &= (n-1)F - C^2 \end{aligned} \tag{21}$$

The parameter a, b can be written as

$$\begin{aligned} a &= \frac{\Delta_a}{\Delta} \\ b &= \frac{\Delta_b}{\Delta} \end{aligned} \tag{22}$$

3. Experiment

We carried out the experiments in an airtight acrylic chamber of a volume 60 cm^3 which is shown as in Fig.2. The acrylic chamber has an air inlet which can pulls the fresh air in and an outlet which can extracts diesel vapor out. We put a small heater, install a fan and set a sensor which is fixed in a bracket into the chamber. The sensor is connected to a computer through a control unit.

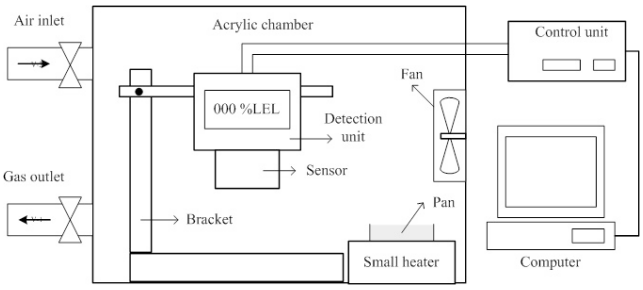

Fig. 2: Schematic diagram of experiment.

We put 6.80ml fresh diesel into a pan and put it on the small heater. The diesel will be heated to 100℃. The concentration of diesel vapor is increasing and will be detected by the sensor. The output of the sensor will be record every 5 minutes as output value to computer through control unit. After recorded 5 data, we put the diesel vapor out by gas outlet and put another 6.80ml fresh diesel in and repeat the experiment. This time, we recorded the data every 10 minutes. The experiment will carry out three times and the recording duration time will be 5 minutes, 10 minutes and 15 minutes. The recorded data of the experiments will be recorded shown as in Table 1.

Table 1: The sensor output in different recording duration time

Output($LEL\%$)	t_1	t_2	t_3	t_4	t_5
$x_1(\Delta t = 5min)$	1	3	8	11	15
$x_2(\Delta t = 10min)$	6	12	19	26	34
$x_4(\Delta t = 20min)$	12	27	35	51	60

4. Results and discussion

We write MATLAB coeds to solve the model. The result is shown as in table 2.

Table 2: Estimated value, average errors and average accuracy of three series

Output($LEL\%$)	t_5	$\hat{t_5}$	$\varepsilon(avg)$	P°
$x_1(\Delta t = 5min)$	15	18.4513	9.9428%	90.0572%
$x_2(\Delta t = 10min)$	34	36.2887	0.9482%	99.0518%
$x_4(\Delta t = 20min)$	60	66.9879	3.1358%	96.8642%

From table 2 we can obtain that the average accuracy is large than 90% whenever Δt is equals 5 minutes, 10 minutes or 20 minutes. It reveals that the grey forecasting model GM(1,1) has a better accuracy ($> 90\%$) in forecasting concentration of diesel vapor in engine room. We also obtain that it will get a high accuracy ($> 99\%$) when Δt is equals 10 minutes. Therefore, we choose 10 minutes as the recording duration time (Δt) in this work. Actually, it is enough to take measures timely for a seaman within 10 minutes in practical using.

5. Conclusions

In this work, we have built a mathematic model (GM(1,1)) based on grey forecasting in order to determine recording duration time for diesel vapor detection and alarm system in engine room. We have designed experiment to obtain data for the grey model of GM(1,1) and write MATLAB codes to solve the model. The results showed that the best recording duration time (Δt) is 10 minutes which have a high accuracy larger than 99%.

References

[1] X. Lu and W. Lu, "Building output-input function of catalytic combustion sensor to diesel vapor," *Measurement*, vol. 43, no. 4, pp. 596–602, 2010.

[2] J. Deng, "The congrol problem of grey systems," *Systems & control letters*, no. 5, pp. 288–294, 1982.

[3] X. Tan and Y. Li, "Using grey relational analysis to analyze the medical data," *Kybernetes*, vol. 33, no. 2, pp. 355–362, 2004.

[4] X. Tan, J. Deng, H. Pan, and S. Liu, "Grey system and grey data management in medicine," in *Grey Systems and Intelligent Services, 2007. GSIS 2007. IEEE International Conference on*, Nanjing, 11 2007, pp. 163–166.

[5] Y. Feng and K. Cao, "Grey relevance feedback for interactive content-based image retrieval," *The Journal of Grey System*, vol. 13, no. 1, pp. 215–228, 2001.

[6] C. C. Tsung and S. C. Long, "Efficent path planning of manipulator based on grey prediction," *The Journal of Grey System*, vol. 12, no. 1, pp. 19–27, 2000.

[7] J. Lin and Y. Tarng, "Optimization of the multi-response process by the taguchi method with grey relational analysis," *The Journal of Grey System*, vol. 4, no. 4, pp. 355–370, 1998.

[8] J. Lin, K. Wang, B. Yan, and Y. Tarng, "Grey-based taguchi method for optimizing the multi-response process," *The Journal of Grey System*, vol. 11, no. 3, pp. 257–277, 1999.

[9] J. L. K. W. B. Y. Y. Tarng", "Optimization of the electrical discharge machining process based on the taguchi method with fuzzy logics," *Journal of Materials Processing Technology*, vol. 102, no. 1-3, pp. 48–55, 2000.

[10] C. Lin, J. Lin, and T. Ko, "Optimisation of the edm process based on the orthogonal array with fuzzy logic and grey relational analysis method," *The International Journal of Advanced Manufacturing Technolgoy*, vol. 19, no. 4, pp. 271–277, 2002.

[11] J. Deng, "A novel grey model gm(1,1):generalizing gm(1,1)," *The Journal of Grey System*, vol. 12, no. 1, pp. 1–8, 2001.

[12] J. Deng, "Undulating grey moedel(ugm) gm(1,1)," *The Journal of Grey System*, vol. 13, no. 3, pp. 201–205, 2001.

Hybrid Micro-Power Energy Station; Design and Optimization by Using HOMER Modeling Software

Iyad. M. Muslih[1], Yehya Abdellatif [2]

[1]Department of Mechanical and Industrial Engineering, Applied Science University, Amman, Jordan
[2] Department of Electrical and Computer Engineering, Applied Science University, Amman, Jordan.

Abstract - Hybrid Optimization Model for Electric Renewables (HOMER) software was utilized to find the optimum design of a hybrid micro-power energy station by minimizing the cost of energy based on different capacity shortage percentages. A full investigation of site conditions and restrictions was done to optimize the design and implementation of a hybrid power station. In addition, this paper took into consideration the economic impact and design tradeoffs in order to optimize the cost and performance of the energy system. Many combinations of conventional and renewable energy resources were considered for this hybrid energy station. From the analysis of the HOMER model results, the optimum hybrid power station was suggested, based on the current fuel price, wind speed, and solar conditions. The optimization function objective is to minimize the Net Price Cost (NPC) and the Cost of Energy (COE) with zero percentage of capacity shortage.

Keywords: Renewable Energy**,** Optimization**,** Cost of Energy**,** Hybrid Station, HOMER.

1 Introduction

The significant increase in demand for energy by several emerging nations has driven the global energy consumption to unprecedented levels. As a result, the cost of energy has reached new levels and is expected to continue to rise. The ramifications of this large increase in energy cost, will pose serious challenges to the economies of most developing nations. In addition, harmful emissions from fossil fuel are causing serious environmental and health problems, and are believed to be the main culprit behind the global warming phenomenon. [1]

For economical and environmental reasons and to reduce dependency on imported energy, many countries need to invest in alternative and renewable energy. It is possible to combine traditional technology with renewable energy technologies in order to minimize fossil fuel energy production cost by effective utilization of renewable energy resources for energy production.

The U.S. National Renewable Energy Laboratory (NREL) developed a micro-power Hybrid Optimization Model for Electric Renewables (HOMER) to assist engineers in finding the best design of a micro-power system among various power generation systems across a wide range of applications [2] [3]. A micro-power system is a system that generates electricity and/or heat to serve a primary load. By using HOMER, it is much easier to design a system that is capable of matching the energy availability from different technologies (such as wind, solar, and diesel generators) with the local load profile. [4][5]

Several studies have been done demonstrating the ability to design hybrid configurations of renewable energy systems in order to maximize the performance while minimizing the cost. These studies stopped short of the complete analysis of all aspects of the hybrid power components by not addressing the optimization and implementation of the system. This paper will address all possible combinations of PV solar energy, wind energy, and diesel power generators that can satisfy the load demand. All variables with full detailed specifications were considered for all available energy resources in the selected location for the hybrid station. [6-11]

2 Methodology

Hybrid Optimization Model for Electric Renewables (HOMER) software is utilized to find the optimum sizing of the Hybrid station by minimizing the cost of the hybrid power system with a specific load demand based on different capacity shortage percentages.

This research will consider two aspects of the design process; the simulation and optimization aspects. In the simulation process, every possible power system will be simulated for each hour of the day to determine the technical feasibility for each combination of micro-power systems. This simulation process is performed on the basis of a life cycle cost which includes the total cost of installing and operating the system

over the project's lifespan. In the optimization process, the model simulates the various configurations of the simulation process and suggests the single most technically feasible

configuration at the lowest life cycle cost, where the minimization of the objective function is formulated based on different technical and economical constraints of the local area.[2]

3 Study Area and Load Profile

The study area in this research is a village, Kamsha, which is located in Jordan. The village power needs is presently supplied through the national electricity grid.

The location of the suggested hybrid micro-power station is located at (32' 07" N and 35' 54" E) and the elevation of the site is 2951 ft above sea level [12]. The location is shown in Figure 1.

Figure 1. The suggested location of the hybrid micro-power station

The AC load is a combination of electricity loads mainly used for domestic lighting and powering TV and radio sets, refrigeration units and electrical motors used for water pumping for domestic use.

The AC load profile considered for a block of homes in the village has a scaled annual load average of 35 kWh/d with a 4.5 KW peak load and a load factor of 0.321.

The daily load profile is given in Figure 2 with a maximum load of 12 KW for the hours between 17 and 22 of the day. The daily load is duplicated for all days of the year with a random variability from day to day as 15%. The load profile for the year is shown in Figure 2.

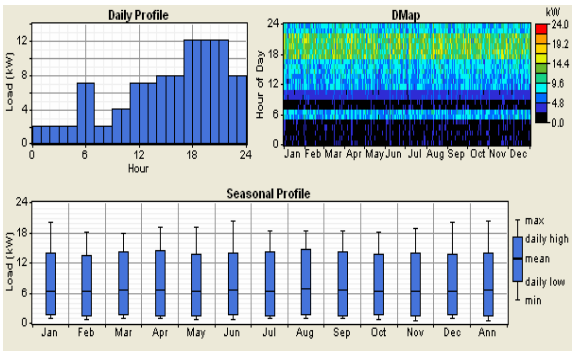

Figure 2. Daily and seasonal electrical load profiles.

4 The Proposed Micro-Power System

The schematic diagram of the proposed micro-power system in this study is shown in Figure 3.

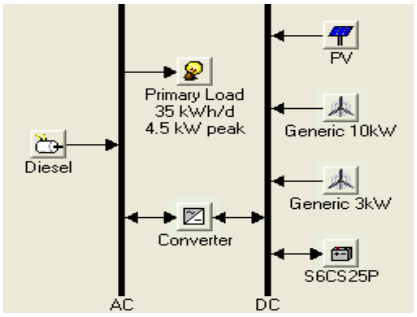

Figure 3. Diesel, Wind and Solar Hybrid Configuration

This study considers three different types of power supply technologies based upon the availability of local resources in the area: a solar PV unit, two small size wind power generation units, a diesel power generation unit. The system includes a set of storage batteries, a converter and other hardware parts necessary of the hybrid system.

4.1 Diesel Unit

Given the fact that the energy available from wind turbines and solar PVs is highly intermittent and occurs mostly at certain times of the day; the diesel power generator was used as a primary power generation option, to increase the reliability of the hybrid supply station.

An AC diesel power generation unit of a size of 8 KW is considered. The capital cost of the unit is 6500 dollars and the operation and maintenance (O&M) is 0.2 dollars/h. The

lifetime is 15000 in operating hours. The replacement cost of the diesel unit is 5500 dollars. The price of fuel at the time of study is taken as 0.8/L in US dollars with no limit on diesel consumption per year. The fuel properties of the diesel power generator were set as: a lower heating value of 43.2 MJ/kg, a density of 820kg/m^3, a carbon content of 88% and sulfur content of 0.33%. The efficiency curve of the unit is shown in Figure 4. [2][13]

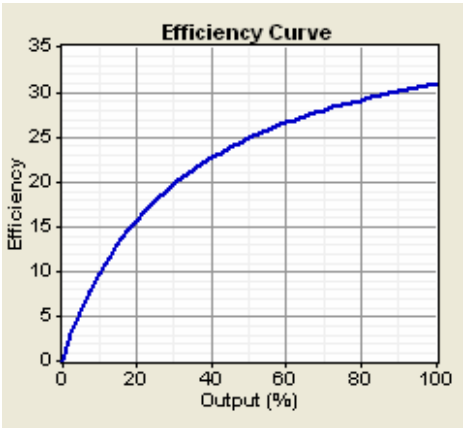

Figure 4. The efficiency curve of the diesel power generator.

4.2 PV Solar Unit

The daily radiation and clearness index for the selected location of the hybrid power station is shown in Figure 5. [2][14][15]

The PV modules used in the proposed system are assumed to have a capital cost of 3,400 dollars/KW without considering other auxiliary components of system. The modules life time is estimated by the manufacturer to be 25 years with an O&M of 100 dollars/year. A horizontal axis monthly adjustment is considered to increase the effectiveness of PV unit. [16]

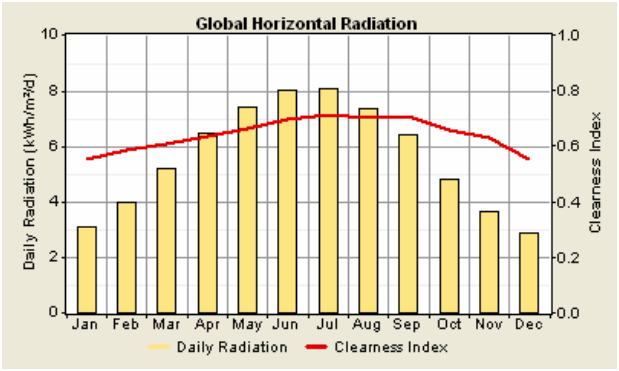

Figure 5. Daily radiation and clearness index of the location.

4.3 Wind Unit

The wind data collected for the suggested location and the wind scaled speed with monthly averages for the year are given in Figure 6. [2][14][15][17]

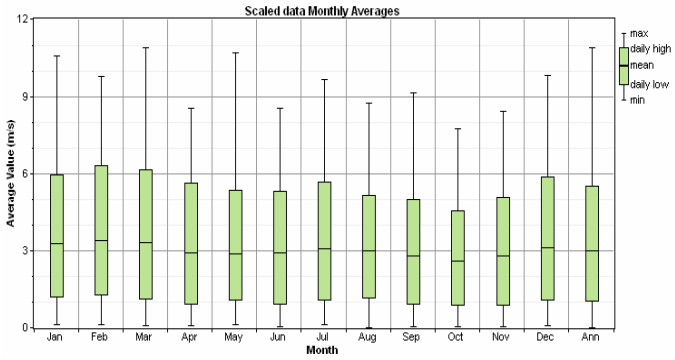

Figure 6. Wind speed with monthly averages for the year.

For the wind power generation, two units of small size wind turbine are considered, 3 KW and 10 KW. For the 3 KW unit, the capital cost is 11000 dollars with a life time of 15

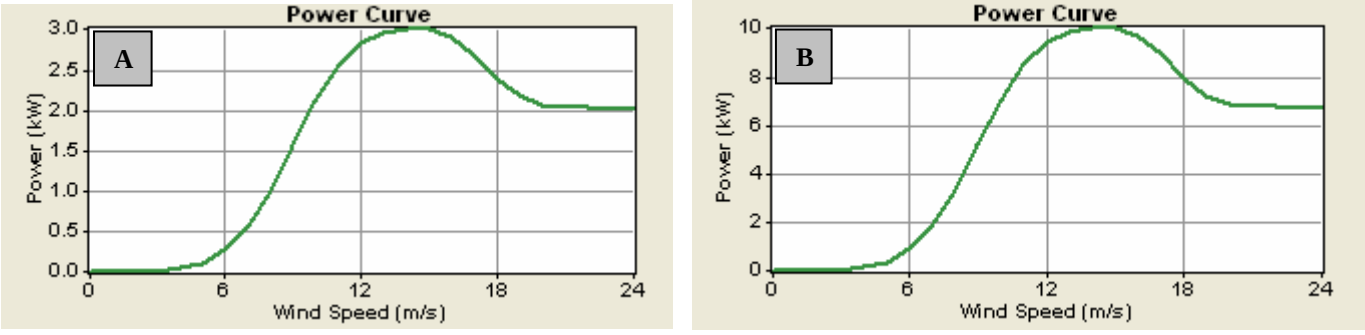

Figure 7. The power curve for: (a) 3 KW wind turbine, (b) 10 KW wind turbine.

years, a hub height of 20 m, and a replacement cost of 7000 dollars. The O&M is taken as 300 dollars /year. The power curve of this 3 KW unit is shown in Figure 7-a.

For the 10 KW unit, the capital cost is 27000 dollars with a life time of 15 years, a hub height is 20 m, and a replacement cost of 23000 dollars. The O&M is taken as 350 dollars /year. The power curve of this 10 KW unit is shown in Figure 7-b. [18-19]

4.4 Storage Battery Bank

The battery type used in the proposed system is Surrette 6CS25P from the manufacture Rolls/Surrette. The Nominal voltage is 6 V and Nominal capacity of 1,156 Ah (6.94 KWh). The minimum state of charge is 40% and maximum charge rate is 1 A/Ah with a maximum charge current of 41 A. The lifetime throughput is 9,645 KWh. The cost of one battery is taken as 1200 dollars and a life time of 4 years with a replacement price of 1100 dollars and the O&M cost is 50 dollars/year. The relation between the battery capacity in Ah and the discharge current in A is given in Figure 8-a. The relation between the cycles of failure and the depth of discharge is given in Figure 8-b.[2][20]

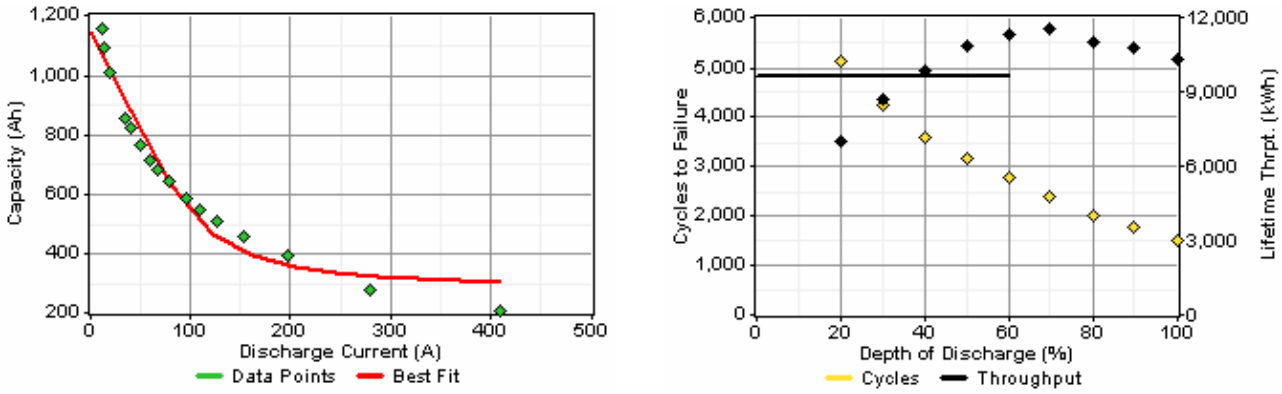

(a) (b)

Figure 8. (a) The relation between the battery capacity and the discharge current. (b) The relation between the cycles of failure and the depth of discharge.

4.5 Converter

A converter is required for the system in which DC components serve an AC load or vice-versa. The size of the used converter is taken as 10 KW with a capital cost 12500 dollars and the O&M coast is 100 dollars/year. The converter efficiency is 90% with a lifetime of 20 years and the converter can operate simultaneously with an AC generator. The capacity of the rectifier relative to inverter is 100% with an efficiency of 85%.[2]

5 Results and Analysis

All possible hybrid configurations were used as input values for HOMER in order to find the optimum configuration based on the available resources. The model has the capability to calculate the net present cost (NPC) and the cost of energy (COE) from the installation and operation of different power generation technologies over the given life cycle of the project which is considered as 25 years.

For each possible case of energy type combinations, the total net present cost (NPC), the system capacity mix, and the energy mix are analyzed. It should be noted that the total NPC is HOMER's main economic output on which different system types are ranked.

Considering a wind speed of 4 m/s and a fuel price of 0.8 dollars/L, the optimum hybrid system based on the NPC and COE is given in Table 1. The system is made of an 8 KW of PV, an 8 KW diesel power generator, 12 batteries and a 4 KW converter. The capital cost of the system is 63,100 dollars and the operating cost is 3484 dollars. The total NPC is 105601 dollars and the COE is 0.678 dollars/KWh which is less than the national grid tariff for Jordan which is 1.59 dollars/KWh.[21]

Table 1. All possible hybrid power configurations considering a wind speed of 4 m/s and a fuel price of 0.8 dollars/L.

PV (kW)	G10	G3	Dsl (kW)	S6CS25P	Conv. (kW)	Disp. Strgy	Initial Capital	Operating Cost ($/yr)	Total NPC	COE ($/kWh)	Ren. Frac.	Capacity Shortage	Diesel (L)	Dsl (hrs)	Batt. Lf. (yr)
6		1	8	8	4	LF	$ 62,500	3,332	$ 103,148	0.662	0.82	0.00	1,614	1,297	12.0
8			8	12	4	LF	$ 63,100	3,484	$ 105,601	0.678	0.81	0.00	1,658	1,331	12.0
	1		8	8	4	LF	$ 58,100	5,055	$ 119,756	0.769	0.72	0.00	2,816	2,250	12.0
			8	8	2	CC	$ 28,600	7,848	$ 124,334	0.798	0.00	0.00	6,363	3,826	12.0
10	1			16	6	CC	$ 97,700	3,064	$ 135,074	0.867	1.00	0.00			12.0
6			8		4	CC	$ 41,900	10,017	$ 164,081	1.053	0.40	0.00	7,863	6,223	
6		1	8		4	CC	$ 52,900	9,670	$ 170,851	1.096	0.51	0.00	7,267	5,783	
			8			CC	$ 16,500	13,639	$ 182,868	1.174	0.00	0.00	11,049	8,760	
	1		8		4	CC	$ 48,500	11,848	$ 193,015	1.239	0.45	0.00	8,811	7,036	

And by considering a wind speed of 5 m/s and a fuel price of 0.8 dollars/L, the optimum hybrid system based on the NPC and COE is given in Table 2. The system is made of a 6 KW of PV, a 3 KW wind turbine, an 8 KW diesel power generator, 8 batteries and a 4 KW converter. The capital cost of the system is 62,500 dollars and the operating cost is 3322 dollars. The total NPC is 103148 dollars and the COE is 0.662 dollars/KWh which is lower than the previous case.

Taking both the wind speed and diesel price as the two major variables in the system; the optimal configuration of the hybrid station can be suggested as shown in figure 9-a, 9-b, 9-c. with 0% capacity shortage, 5% capacity shortage, 10% capacity shortage, respectively. The shortage percentage is shown on the gird of each figure

Table 2. All possible hybrid power configurations considering a wind speed of 5 m/s and a fuel price of 0.8 dollars/L.

PV (kW)	G10	G3	Dsl (kW)	S6CS25P	Conv. (kW)	Disp. Strgy	Initial Capital	Operating Cost ($/yr)	Total NPC	COE ($/kWh)	Ren. Frac.	Capacity Shortage	Diesel (L)	Dsl (hrs)	Batt. Lf. (yr)
8			8	12	4	LF	$ 63,100	3,484	$ 105,601	0.678	0.81	0.00	1,658	1,331	12.0
6		1	8	8	4	LF	$ 62,500	4,080	$ 112,271	0.720	0.74	0.00	2,213	1,777	12.0
			8	8	2	CC	$ 28,600	7,848	$ 124,334	0.798	0.00	0.00	6,363	3,826	12.0
		1	8	8	2	CC	$ 39,600	7,393	$ 129,781	0.833	0.14	0.00	5,550	3,500	12.0
6			8		4	CC	$ 41,900	10,017	$ 164,081	1.053	0.40	0.00	7,863	6,223	
10	2			20	6	CC	$ 125,500	4,019	$ 174,521	1.120	1.00	0.00			12.0
6		1	8		4	CC	$ 52,900	10,075	$ 175,790	1.128	0.46	0.00	7,596	6,032	
			8			CC	$ 16,500	13,639	$ 182,868	1.174	0.00	0.00	11,049	8,760	
		1	8		2	CC	$ 30,000	13,844	$ 198,870	1.276	0.09	0.00	10,857	8,638	

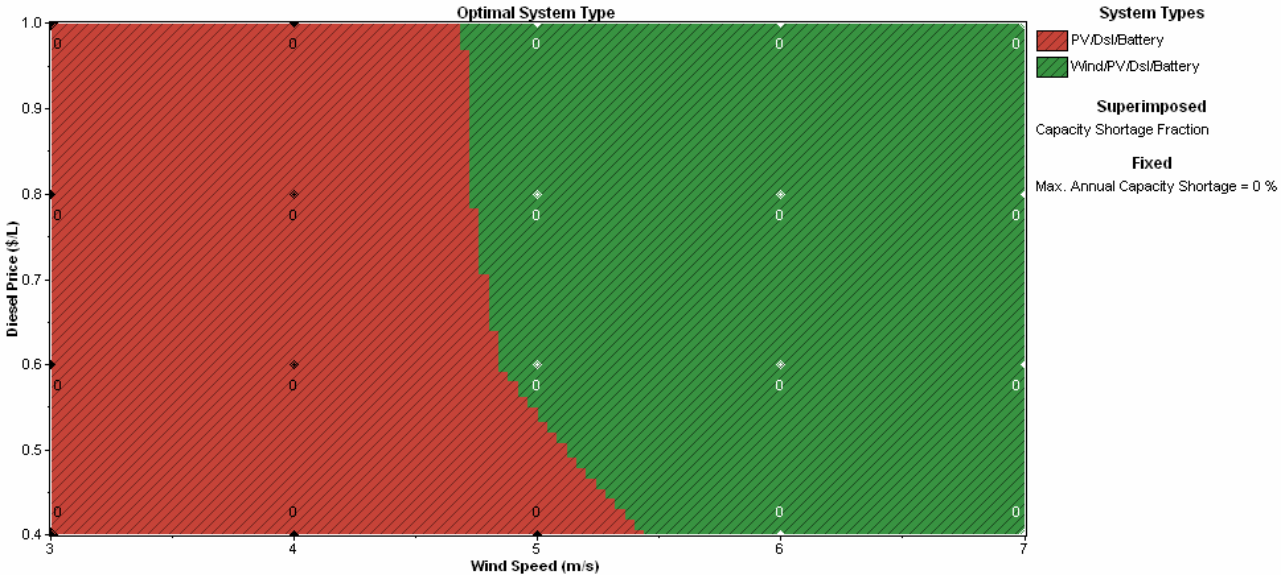

(a)

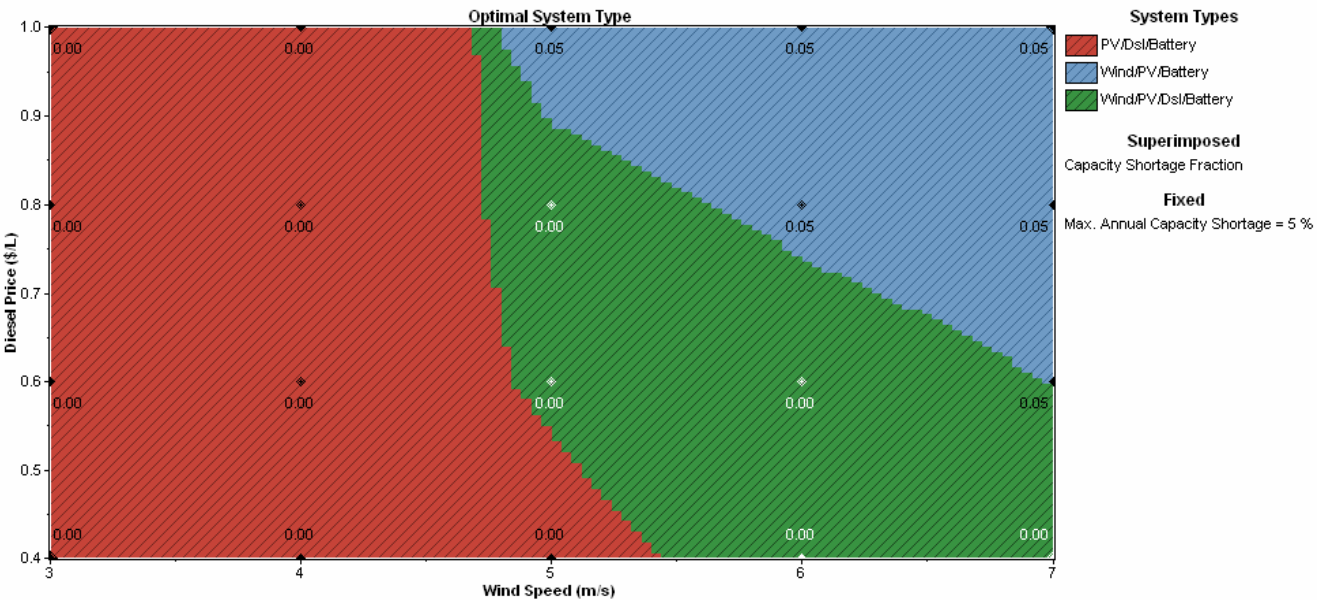

(b)

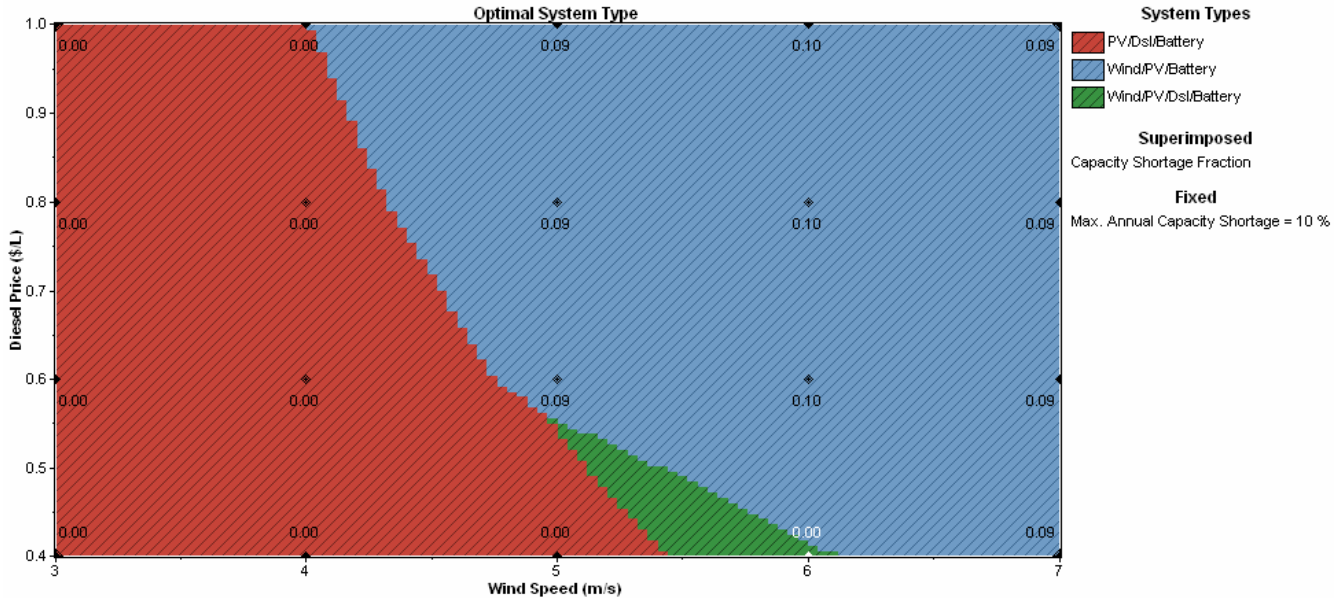

(c)

Figure 9. Optimal configuration of the hybrid station with; (a) 0% capacity shortage, (b) 5% capacity shortage, (c) 10% capacity shortage, respectively.

6 Conclusions

Based on the results and analysis of the HOMER model, the optimum hybrid power station based on the current fuel price, the average wind speed, and the local site conditions is made of; a 6 KW of PV power generation unit, a 3 KW wind turbine unit, an 8 KW diesel power generator, 8 Surrette 6CS25P batteries and a 4 KW converter and a 4 KW rectifier.

The capital cost of the system is 62,500 dollars and the operating cost is 3322 dollars. The total NPC is 103148 dollars and the COE is 0.662 dollars/KWh with zero percentage capacity shortage which less than the current national gird price.

The optimization of the design and implementation of hybrid renewable energy systems is dependent on the geographic location and not just on the available renewable energy resources. A location is selected in Jordan where the government suggested the area to be one of few promising locations for renewable energy systems with a well developed infrastructure to facilitate the implementation, operation and management of the optimal hybrid power station.

It should be noted that, although the application and implementation of renewable energy systems for domestic or commercial application are primarily dependent on the availability of the renewable resources on the specific site of concern, there are number of economic considerations and design tradeoffs to be taken into consideration in order to optimize cost and performance.

7 References

[1] Salah abdallah, et al. "National grid, Diesel and Photovoltaic Power Generation Systems in Jordan: An Engineering and Economical Evaluation " Energy Sources Part B: Economics, Planning & Policy, Oct2010, Vol. 5 Issue 4, p370-383, 14p.

[2] National Renewable Energy Laboratory, HOMER Getting Started Guide Version 2.68, NREL, 2010.

[3] Iqbal MT, A feasibility study of a zero energy home in Newfoundland, Renewable Energy, 29 (2) 277289, 2004

[4] Designing High Reliability Power Systems for PEMEX Using HOMER, Arturo Romero Paredes Rubio, World Renewable Energy Congress VIII, Denver, Colorado, 2004.

[5] Georgilakis PS, State-of-the-art of decision support systems for the choice of renewable energy sources for energy supply in isolated regions, International Journal of Distributed Energy Resources, 2 (2) 129-150, December 2005

[6] Shaahid SM, El-Amin I, Rehman S, Al-Shehri A, Bakashwain J, Ahmad F, Potential of autonomous/off-grid hybrid wind-diesel power system for electrification of a remote settlement in Saudi Arabia, Wind Engineering, 28 (5) 621-628, 2004.

[7] Iqbal MT, Pre-feasibility study of a wind-diesel system for St. Brendan's, Newfoundland, Wind Engineering, 27 (1) 3951, 2003

[8] Rehman S et al, Feasibility study of hybrid retrofits to an isolated off-grid diesel power plant, Renewable & Sustainable Energy Reviews, 11 (2007) 635-653

[9] Juhari Ab. Razak, Kamaruzzaman Sopian & Yusoff Ali, Optimization of Renewable Energy Hybrid System by Minimizing Excess Capacity. International Journal of Energy, Issue 3, Vol. 1, 2007, pp. 77 – 81

[10] Kamel, S. & Dahl, C.,The Economics of Hybrid Power Systems for Sustainable Desert Agriculture in Egypt, Energy, Vol. 30, 2005, pp 1271-1281.

[11] Ashok, S. Optimised Model for Community-Based Hybrid Energy System. Renewable Energy, Vol. 32, No. 7, 2007, pp. 1155-1164.

[12] Google Earth. 1600 Amphitheatre Parkway, Mountain View, CA 94043, United States. http://www.google.com/earth/index.html as of 25-2-2011

[13] http://www.hondapowerequipment.com/gen.htm as of 25-2-2011

[14] The Hashimite Kingdom of Jordan, Meteorological Department, Climate Division, Jordan Climatic Data, 2007.

[15] Surface Meteorology and Solar Energy; A renewable energy resource web site Rel.6.0.http://eosweb.larc.nasa.gov/cgi-bin/sse/sse.cgi?+s01#s01T as of 25-2-2011

[16] The Potential of Solar Energy Application in Jordan. 1983. Assessment and Analysis of Available Energy Resources, Royal Scientific Society, Vol.3, Amman-Jordan.

[17] Habali, S.A.; Hamdan, M.A.S.; Jubran, B.A. and Zaid, Adnan.I.O. 1987. Wind Speed and Wind Energy Potential of Jordan, Solar Energy 38(1): 59-70.

[18] http://www.gepower.com/prod_serv/products/wind_turbines/en/index.htm

[19] http://www.mpshq.com/products/wind_turbines/index.html as of 25-2-2011

[20] http://www.surrette.com/content/specifications-renewable as of 25-2-2011

[21] Jordan National electrical Company. http://www.nepco.com.jo/english_etariff.html

SESSION

ANALYSIS AND PERFORMANCE EVALUATION

Chair(s)

TBA

Towards an Evaluation Framework for Pervasive Computing System

Yasir Malik, Mona Soliman and Bessam Abdualrazak
DOMUS Laboratory
Department of Computer Science, University of Sherbrooke, Sherbrooke, Quebec, Canada

Abstract— *This paper presents a evaluation framework model for pervasive computing systems. Evaluation of pervasive computing system has struggled due to diversity of technology and absence of common standard guidelines & methodologies to design and evaluate the systems. We propose a evaluation framework model for qualitative and quantitative evaluation of pervasive computing system. In our model, we incorporated important system, user, contextual and environmental factors that are necessary for comprehensive evaluation. The proposed model is step towards forming standard evaluation guidelines that can be use during formative and summative evaluation and, can facilitate designer and industry for successful transfer of technology.*

Keywords: Pervasive Computing, Evaluation Framework, Standardization, System Factors, Human Factor

1. Introduction

Pervasive computing is shifting the computing paradigm toward everywhere computing. The emergence covers distributed & mobile computing, sensor networks, human computer interaction and artificial intelligence under umbrella of pervasive computing. Weiser[1]envisioned pervasive computing where computing devices integrated smartly in their deployed environments to facilitate user with their everyday living. Nearly two decades since Weiser's vision was introduced [34], very few practical or even promising systems have been deployed and generated significant impact and received acceptance.

Evaluation is an essential process for successful deployment, assessment and acceptance of new technologies. Evaluation of pervasive computing system has struggled due to the complexity, openness and diversity of technology. There is consensuses among researchers that traditional performance approaches are no longer applicable for pervasive computing environments. In effort for pervasive system evaluation various methods and solutions are currently being used and subsequently published in literature. However due to the multidisciplinary research in pervasive computing it is difficult to answer "*what and how to evaluate*", hence one box solution is impractical although desirable [28]. Our studies concludes that the evaluation methods presented in literature have some limitation in one way or other, because of either they are developed for some specific applications or have only considered some factors and discounted other in evaluation.

As the technology is improving there is a great need of standard evaluation model to position pervasive computing systems and define directions for future research. Due to fundamental difference with traditional computing system in terms of user interaction and involvement, we observed that pervasive system should be designed and evaluated keeping its user in mind, so that the system do not disturb the everyday living of user and smartly integrates itself in their lives. Ciarletta and Dima's in [11] presented a user driven design model for pervasive systems. The key feature of their model was the user representation at each system design stage, however it is limited to the design issues of pervasive system and provide not information on evaluation. In this paper we proposed a evaluation framework model for pervasive computing system. In our model, we utilize and extend their model and identified most important factors to be considered while designing and evaluating. Key features of our model that can make a significant improvement in the design and evaluation process of pervasive system are:

- *Consideration of environmental factors that cannot be ignored due to the nature of pervasive systems.*
- *Contextual factors to better observe the behavior of user and system within the context it will be used.*
- *User factors that play an important role in designing and evaluating the system.*
- *Ground work for integrating technology acceptance and adoption model or successful transfer of technology.*

The factors presented in this paper lay the groundwork for establishing an evaluation framework for pervasive computing system. The rest of the paper is organized as follows. In the next section we have presented a brief summary of all surveyed paper focusing on pervasive computing evaluation, next we present our evaluation framework model along with discussion on the factors for evaluation. Finally in section 4 we summarized the paper and discuss future goals.

[1]http://sandbox.parc.com/weiser/

2. Related Work

This section presents the review of some presentative work that address different evaluation challenges and their solutions. There is clear consensuses among the researchers that traditional performance approaches are no longer applicable for pervasive computing environment. Gabriele in [22] suggested that due to high QoS requirements, proactive performance tuning activities and interdependencies between user behavior & system hinder conventional evaluation techniques to fit in the box. Scott and Jennifer identified some major challenges in pervasive computing evaluation like, applicability of metrics, scale, ambiguity and unobtrusiveness [31]. Some authors like [26][6][9] presented some approaches to gather data and selecting the metrics from scenarios that are driven by real problem than by technology for qualitative and quantitative evaluation. Efforts have also been made to explore formative and summative evaluation approaches for pervasive systems such as [7][12][25][21]. However the fact that these approaches cannot make a significant impact is because their focus were entirely on gathering user requirement before designing a working system or vice-versa.

Due to the importance of human behavior and contextual factor in the design of pervasive computing environments, a concept of living laboratory was presented in [4][19] to evaluate pervasive environments. Results of living laboratories are helpful to identify pitfalls and improvement opportunities required in the interactional aspect, however they are not satisfactory (1) when deployed outside the lab environment (2) users who participate (student or volunteers) in such studies are not real users of application therefore the interaction and intentional level of these individuals cannot be generalized. To capture true user experience researchers turned to *In-situ* evaluation, and brought system to interact with real user in the context the technology or application will be used. Researchers utilize techniques like (wizard of Oz, experience sampling, analyzing data from sensors, cultural probes etc to conduct evaluation[30]. In-suit evaluation techniques seems promising for pervasive computing systems, however as (1)studies are done on prototypes therefore it is expected, result may differ when evaluated with complete system, (2) the time period of 2-3 weeks is not sufficient, also (3) the question how to effectively analyze and utilize the data in evaluation is still not answered.

All the aforementioned evaluation method, have some limitation in one way or other. Because either they are developed for some specific applications of pervasive computing, have only considered some factors and discounted other in evaluation, not accounted user acceptance and adoption in evaluation process etc. A scrutiny of all the presented work has encouraged us to develop a comprehensive evaluation framework that cover almost every aspect of and related to pervasive computing system.

3. Evaluation Framework Model

To find the answer for "*what and how to evaluate*" we survey state of art to determine the ultimate interest of researchers when they made design decision and evaluate their prototypes. As compare to traditional computing system, pervasive systems rely on user intention, context and operating environment. We came to the conclusion that there is a great need of evaluation framework that consider user, system, contextual and environmental factor for the comprehensive evaluation of system. We develop a evaluation framework model for pervasive computing evaluation (See Figure 1) and identify the most important user and system aspects and established a list of quantitative and qualitative parameters for evaluation (summarized in Table 1 [36]). The system-centric parameters gauges the efficiency and effectiveness of the design decisions and presents the assessment of how the system performs and expands under normal and abnormal conditions, as well as the resources employed to achieve the target performance. Similarly user-centric parameters are used to indicate how well the behaviors of a system correspond to user intentions and expectations, and how much effort it takes on users part to interact with the system. Knowing the complexity and the diversity of pervasive computing system different measurements and results collected may not truly reflect the pervasive computing system if comparison are made among systems with vastly different designs approaches and/or application domains. It is therefore crucial to identify not only quantifiable parameters that can be measured and evaluated, but also using non-quantifiable parameters to characterize important aspects of these systems. In addition, we believe it is equally important to consider the contextual and environment factor into account for a comprehensive evaluation of pervasive systems. Following we present the key evaluation aspects from system, user, contextual and environmental prospective that lay groundwork to develop a comprehensive evaluation framework and to construct technology acceptance model [14].

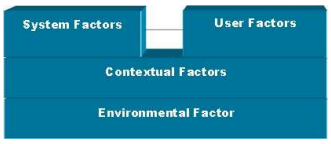

Fig. 1: Evaluation Framework Model

3.1 Environmental Factors

Pervasive computing systems are envisioned to be smartly fabricated into people's lives and environments. Unlike traditional computing systems where environment was considered irrelevant for design and evaluation, it plays an important role in design and development of pervasive computing system. In diverse disciplines, techniques and principles

Table 1: Summary of Quantitative and Qualitative Parameters of System and User

	Quantifiable Parameters	Non-quantifiable Characteristics
System-Centric Parameters	System Performance Communication Performance and cost Software Footprints Power Profiles Data storage & manipulation Quality of context Programming efficiency Reliability Fault-tolerance Scalability Maintainability Effectiveness	Node-level characteristics Service & application Context Characteristics Security & Privacy Knowledge representation Architectural characteristics Standardization Extensibility Backward compatibility Proactivity Adaptability characteristics
Parameters Concerning System and User	Adaptability Self-organization Error Explicitness	Economical consideration

have been developed for environmentally friendly execution and deployment of technologies [20]. Although pervasive systems are intended to bring comfort in our daily living, however it has some positive and negative effects on the environment too. Hence it is significantly important for pervasive computing researchers to consider environmental factors during the design of software and devices for pervasive environments. The importance of the matter has been articulated in literature but to the best of our knowledge no standard guidelines or techniques are developed to date to support design and evaluation.

The environmental factors can be derived from technical and non technical domains. From the technical domain designer and evaluators should consider the implicit and explicit implication of deployed technologies, such as device safety and installation constraints present in the environment, environmental conditions (such as heat, cold and humidity) for the devices[2], energy consumption, physical waste and recycling of devices, user safety against non-ionizing radiations from mobile communication, environmental dynamics, potential health or environmental effects, stress imposed on the user, restriction of consumers and patients, threats to ecological sustainability and dissipation of responsibility in computer-controlled environments [24].

Non Technical factors can be accounted from diverse disciplines such as government regulating authorities, architecture, transportation engineering [28], green technology concept, potential impact of applying technologies (Human Health Impacts, local natural environment impacts, social and cultural impacts, global impacts, and resource sustainability) identified in Environmental Technology Assessment Manual[3](EnTA). We believe the aforementioned environmental factors in one way or another can play important role in design and assessment of pervasive computing system.

[2]Pervasive device with built-in computing and communication abilities

[3]EnTA manual is Prepared by John E. Hay and Mathew Noonan for the United Nations Environment Programme Division of Technology, Industry and Economics Consumption and Production Unit, Paris, France and International Environmental Technology Centre, Osaka, Japan

3.2 Contextual Factors

Pervasive computing demands application that can support highly dynamic environments and required less user intervention. To meet such challenges applications should be designed considering context in mind. There is rapid development in design of context aware applications that can react autonomously on behalf of users [18][10][27]. Although the research in context-aware computing is growing yet there is an impoverished understanding of what context is and how it can be used. This result in various understanding and definitions of context presented in literature [5][8][15][29][33]. Context is one of the most distinctive characteristics of pervasive computing system. Thus when there is change in context due to any reason the performance of the system could be questioned, this could be the service provided by the system did not adapt with the current context of user or the service is not relevant to the situation. We suggest that the pervasive computing applications and its services should be designed and evaluated considering contextual factors into account. Grace et al in [23] presented a context based evaluation model and suggested to evaluated the technologies within the context they will be used. The model does not support pervasive computing evaluation as, the contextual factors considered in their model do not completely comply with pervasive system. The contextual factors solely depend on the definition of the context.

For the purpose of understanding we consider the most important type of context (Location, Time, Identity, Activity and Environment)[5]. To broaden the scope and considering the interdependency of environment and context we have also considered environment as a type of context, as the change in environmental factor can also bring change in context. The contextual factor in environment could be different due to the change in location, identities, activities and time, this will result a change in context. A context-aware application that adapt environments for its user, or provide specific service depending on the context of the environment must account the contextual factor to provide

efficient and effective service execution.
Contextual factors can be determined by creating the scenarios in the real environments, understanding human behavior, social situations, purpose of application & services and environmental factors. More factors can be considered depending on the requirement and purpose of application and most importantly definition of context. As such there are no scales to check the performance of contextual factors except the quality of the context, a complete characterization of context in a system, and dimension of the context that are of interest. The number of different dimensions of context can be used to correlate the complexity of system and utilization of context, for instance whether they used proactively or reactively greatly affect the responsive time and resource usage of the system.

3.3 System Factors

In this section, we have briefly describe and discuss the important system evaluation factors. These factors are by no means complete but are best suited for the purpose of effective performance evaluations. We deem as the pervasive computing research grow and more experiences are shared in its evaluation, more factors and aspects will be introduced. These system evaluation factors are determined from our experience in designing taxonomy of pervasive computing system [2]. Following we present the system evaluation factors.

3.3.1 Infrastructure

Infrastructure factors cover the conceptual design and functional structure of all hardware and software components in pervasive systems. As one of the primary characteristic of pervasive systems is communication and computing capabilities that are integrated into environment to provide the services from personal to global scale. From the communication point of view the architectural characteristics at the system level, node-level characteristics, communication performance & cost and economical considerations are of more importance while evaluating the system. The diverse nature of pervasive computing makes it difficult for software designers to adapt one common model that can meet all its requirements. The major challenges that make the software design difficult are ability of software architectures to support interoperability due to various network and software technologies, user needs and service mobility [13]. The key aspects that should be considered while evaluating the software architecture are modularity, software dynamics, management, design compatibility, embedded intelligence, interpretability etc. Details of key measuring parameters can be found in [2].

3.3.2 Integration

Pervasive computing systems by its nature require integration of many different subsystems with very different characteristics. These subsystems include computational facilities, communication devices, mechanical or chemical sensors and actuators, smart appliances, and existing control systems. Plenty of research efforts have been spent on solving various integration issues, and different implementers have tried on different approaches. Based on the approach taken, systems usually exhibit different architectures and therefore present vastly different characteristics. We believe that integration is among the important factor that needs to consider for comprehensive evaluation. The important aspect like maintainability, standardization, reliability, fault-tolerance, architectural characteristics and scalability would be valuable for evaluating the integration methods and to better analyze and check the performance of utilities provided in middleware, patterns and efficiency of integration between application components and middleware.

3.3.3 Service Availability

The goal of pervasive computing system is to provide its user with rich set of services that are embedded in the user's physical environment and integrated seamlessly with their everyday tasks. Unlike services that are provided by internet, pervasive computing services are invisible, intelligent and invoked automatically depend on the events happening in the environment, user context or conditions that satisfy their invocation. In our observation potential aspects that could make significance difference in evaluation would be ubiquitous nature of service (i.e. any where any time), contextual factors in executing the service, service composition, service interoperability and quality etc.

3.3.4 Interaction

In pervasive computing system, human-computer interaction and machine to machine interaction is the important components and they are becoming highly dynamic and implanted in environment. A system should adapt the interaction and presentation using various components available for interfacing based on behavior sensing, service mobility and events happening in the environment. The main objective is to make the system usable and interactive for its user, the easier the system is, and most likely people will use and adapt it. Unlike traditional computing system, interaction in pervasive computing is done implicit and explicitly with the user, for that reason there are so many human aspects that must be considered for the effective design and evaluation. The interaction in pervasive system is not just interacting with the monitor, the scope is far bigger when it comes to implicitly interaction, where user is observed from implanted sensors in the environment for their activities, gestures and behaviors. The systems that do no account these aspects may lose its credibility and user may not adopt it. The potential aspects that need to be consider while evaluating would be human to machine and machine to machines with keeping the conceptual factors in mind.

3.3.5 Extensibility and Backward Compatibility

Extensibility is a major consideration for most computing paradigms, and certainly one of the fundamental factors when evaluating any pervasive computing system. It describes how well the design and the architecture of a system can accommodate new components in the future and the new technologies which come with them. Backward compatibility on the other hand describes the capability of a system to integrate or collaborate with legacy systems or technologies. Many pervasive computing systems such as smart houses, structure integrity monitoring or urban computing facilities, are expected to have much longer lifespan as compared to traditional computing systems. Many systems are also intertwined with physical plants that require deployment at the time of construction or risk incurring high cost during deployment. With increase development in the technologies and applications for pervasive computing system the extensibility and compatibility factor will play a vital role in its evaluation. For instance the geographic span of different pervasive computing system can very up to several orders of magnitudes, this will result in significant impact on the operation behavior and organization of the system. The designer and assessor must take these considerations into account for successful deployment and operation of their system. The extensibility and backward compatibility can be evaluated by examining characteristics such as the support for dynamic upgrade in firmware and applications; whether there are mechanisms to improve the flexibility in the architecture of the system, such as the use of adapters; whether the nodes support multiple interfaces and standards; and whether they are configurable and the extent that they can be adjusted.

3.3.6 Invisibility

Pervasive computing system tends to implant computing device to improve well being and autonomy to the environment and making them invisible to the user. Invisibility can be achieved by using and considering the environmental and contextual factors. Impact of invisibility should be considered to quantify its implicit and explicit effects on its user and system.

3.3.7 Maintainability

The large number of simple and cheap components employed in most pervasive computing systems translates to short mean time to failure (MTTF) and makes failure a norm in the operation. To make sure the system remain operational over a period of time, considerable resources need to be allocated for continuous maintenance. To understand the true cost of real-world deployments, we need to measure MTTF, the recovery time, the cost of replacement parts and other maintenance related parameters such as the man-hour required to replace or fix the failed entities, and the size of maintenance crew needed to keep the system operational.

3.3.8 Security and Privacy

Pervasive computing is supposed to be "calm" and invisible. In order to bring intelligence to an environment that can satisfy users' desires and needs, the system has to be highly personalizing and customizable. This in turn depends on the capability to acquire and dissimilate data about users to various parts of the system. Typical pervasive computing systems holding a lot of fine-grained personal information, such as real-time locations, medical history and biometrics, personal preferences and schedule, concerns over security and privacy have reached a new height. Any serious discussion on practical deployment would need to address the concerns over the security and privacy first. Examples of characteristics critical to the security and privacy in pervasive computing systems include the expressiveness of security policy and the strength of security enforcing mechanism. As regarding to the privacy control, researchers have suggested appropriate measures and policies on the protection of content, identity and locations are needed.

3.4 User Factors

Pervasive computing systems are designed to serve users and facilitate them in their daily activities. They have to satisfy user's needs and conform to the environmental constraints where users locate, and compatible with their physical and mental characteristics. Therefore, when evaluating pervasive computing systems, it is crucial to consider and evaluate factors not only from the system perspective, but also from the user perspective. Following we have discussed some user factors that we think are essential for pervasive computing design and evaluation. These factors are derived from our personal experience in [3][17] and also considering standard guideline presented in [32]. These factors have qualitative and quantitative importance in evaluation and can be utilized to develop constructs of Technology acceptance model. Table 2 summarize the key factors and aspects could be considered for evaluation.

3.4.1 Personal Factors

Personal factors define the individual characteristics of the user and their surroundings. It considers user's lifestyle and focus on aspects of sensory aspects that could affect or stimulate the user's senses, for instance noise, light, comfortable positions, etc. Pervasive systems have to be adjusted to the user's characteristics. Despite the fact that every person is unique, the "standard user" doesn't exist. But there are some aspects of personal factors that have to be taken into account, to design a system that will be useful for our target population (for instance assistive technology for people with special needs). Following we have presented some of these aspect that we considered important for design

and evaluation and can help to define the constructs of technology acceptance model.

3.4.2 Demographics Aspects

The demographic factors represent the statistical socio-economic characteristics of a population, such as age, sex, education level, occupation, country custom anthropometry data, and so on. Populations are diverse and their habit and lifestyle differ from country to another. It will be worthy to design and evaluate pervasive system considering the demographic factors of user in mind. Demographic factors can be useful in defining the constructs of technology acceptance model and regular feedback will help designers to tune the system for target population.

3.4.3 Comfort Aspects

The comfort is one of the most important aspects in pervasive system. Indeed a person will use the system only if he/she feels comfortable with it. This aspect represents the state of well being the user feels when he/she use the system. To be adopted by the user the system has to be comfortable. The term comfortable is exclusively not the user's postural comfort, but also sensory and visual comfort. Indeed interacting with pervasive system affects all our senses, this is why a system that make the user uncomfortable to achieve his/her goal, will likely be rejected by user. The consideration of comfort aspect in evaluation will help in finding the right direction for user acceptance of technology.

3.4.4 Skills Aspects

Skills factors are also considered important in the design of pervasive computing system. Most of the pervasive computing applications required user to understand the basic computing technologies of today i.e. PC or Cell Phone. Skills factor actually help to understand the user abilities to perform some task. It is commonly said *"Learning-by-Doing"* if we know the potential of the user, we can improve his learning abilities by helping him/her to perform some task. It is worthy to look into the experience aspect of user, the target population may contain novice and experienced user of current technologies (e.g. use of PDA). The experienced people may have another point of view, which can be relevant, for the system, due to their learning and experience of past as compare to novice user. Additionally, it is interesting to consider the user's mental workload and capacity. The system will be much appreciated if it is concise and it doesn't require more cognitive load. To understand such details, comprehension aspects, performance, and use without error aspects have to be considered in design and evaluation.

3.4.5 Organic Factors

Organic factors relate to the physiological function of body and psychological aspect of user, these factors are not quite considered and evaluated in traditional computing system. However in pervasive computing system it is significantly important to consider and evaluate these factors. Physiological aspects can consider user's impairment such as a loss of an organ (impairment after accident) which is likely to be a problem for user to interact with the system and could limit their activities. Among other user body organ, brain is the most important and central part and it play a major role in user performance. The impairment in it is considered like a loss of user's capacity, their intellectual functions and confidence [1]. It is valuable to consider mental workload and capacity in the design of pervasive system (e.g.Cognitive Orthotic) [16]. Additionally psychological factors enable us to understand the user's personality, frame of mind, and their feelings toward the system. For instance people who have technophobia will likely not show interest in learning and adapting new technology.

3.4.6 Health Factors

Health aspect should be carefully considered in design and evaluation process of pervasive systems. Health aspect relates to the user's health state. It gives the information about user diseases, or allergies if any. Health aspects have to be considered, to address the difficulties user can face while using the system. The user's health performance could limit him/her in performing some activities. If a user doesn't show any impairment, but present some difficulties in performing some activities while using the system, the system must notice this change in user's performance, collect the related data (for instance by consulting it's vital signs and user's medical history) to propose some services.

3.4.7 Social and Community Factors

It represents the factors affecting or piloting directly or indirectly the life we lead in the society. Although demographic aspects are part of in personal factors, it can also be covered in social factors, given that social status and work is a part of social factors. For instance in case of pervasive healthcare application for elderly, the demographics and social factors can play an important role, for instance, in some countries especially in oriental ones, people are closer to their family with social and cultural bonding, their acceptance of the technology will likely be difficult compare to the people living in occidental countries, where social and cultural norms are not as strong compare to oriental ones. Moreover, religion is a aspect that should be taken into consideration, given that it is an aspect that could have an impact on social life and technology usage [35]. For the purpose of understanding take the example of Buddhist people who practice religion, it is likely they don't accept

new technologies easily, because they are closer to the nature and count more on their family. Similarly, if the system doesn't fit with the country's policy, it won't be used by the citizens. Furthermore, it is worthy to consider user's soft skills, interpersonal aspect which can tell about user's traits of personality and abilities they present while contacting other people in everyday life.

4. Conclusion

Pervasive computing systems are gaining attention in academia and industry. It is significantly important to predict and understand its acceptance and adoption level among its users. In this paper, we have presented a evaluation framework model for comprehensive evaluation of pervasive computing system. We suggested that, there is a great need that pervasive system are designed and evaluated considering its user, environment and context in mind. In our model, we have incorporated and discussed important system, user, contextual and environmental factors that should not be overlooked during the evaluation process of pervasive systems. We have also discussed the importance of user acceptance of the pervasive technology. The acceptance measures user's willingness to use a system, and how users adopt and tolerate the system. In other words, it describes user's satisfaction, easy of learning, attitude towards acceptability of system. The goal of evaluation should not only to emphasize if a particular system is accepted by its intended users or not. We have an even higher interest in identifying the reasons for why this system is accepted or rejected. Our model can provide a groundwork to construct and integrate technology acceptance and adoption model that will facilitate designer and industry for successful evaluation and transfer of technology. Using the guidelines presented in the model, we are working on a formal model of the evaluation framework. The framework will provide further insights into how to interpret the results of evaluation as well as strengthen design and implementation of evaluation framework.

References

[1] B. Abdulrazak, B. Chikhaoui, C. Gouin-Vallerand, and B. Fraikin, "A standard ontology for smart spaces," *IJWGS*, vol. 6, no. 3, 2010.

[2] B. Abdulrazak, Y. Malik, and H.-I. Yang, "A taxonomy driven approach towards evaluating pervasive computing system," in *ICOST '10: Proceedings of the Eight International Conference On Smart homes and health Telematics*. South Korea: Springer Berlin / Heidelberg, 2010, pp. 32–42.

[3] B. Abdulrazak, M. Mokhtari, and B. Grandjean, "Usability of an assistive robot manipulator: Toward a quantitative user evaluation," vol. 306, no. 1, pp. 211–220, 2004.

[4] G. D. Abowd, C. G. Atkeson, A. F. Bobick, I. A. Essa, B. MacIntyre, E. D. Mynatt, and T. E. Starner, "Living laboratories: the future computing environments group at the georgia institute of technology," in *CHI '00: CHI '00 extended abstracts on Human factors in computing systems*. New York, NY, USA: ACM, 2000, pp. 215–216.

[5] G. D. Abowd, A. K. Dey, P. J. Brown, N. Davies, M. Smith, and P. Steggles, "Towards a better understanding of context and context-awareness," in *HUC '99: Proceedings of the 1st international symposium on Handheld and Ubiquitous Computing*. London, UK: Springer-Verlag, 1999, pp. 304–307.

[6] J. J. Barton and J. Pierce, "Finding the right nails: Scenarios for evaluating pervasive systems," in *Pervasive '07: Common Models and Patterns for Pervasive Computing Workshop*. Canada: Springer-Verlag, 2007.

[7] V. Bellotti and I. Smith, "Informing the design of an information management system with iterative fieldwork," in *DIS '00: Proceedings of the 3rd conference on Designing interactive systems*. New York, NY, USA: ACM, 2000, pp. 227–237.

[8] P. J. Brown, "The stick-e document: a framework for creating context-aware applications," in *Proceedings of EP'96, Palo Alto*. also published in it EP–odd, June 1996, pp. 259–272.

[9] M. Burnett and C. P. Rainsford, "A hybrid evaluation approach for ubiquitous computing. environments," in *In Workshop: Evaluation Methodologies for Ubiquitous Computing*, 2005.

[10] H. Chen, T. Finin, and A. Joshi, "An ontology for context-aware pervasive computing environments," *Knowl. Eng. Rev.*, vol. 18, no. 3, pp. 197–207, 2003.

[11] L. Ciarletta and A. Dima, "A conceptual model for pervasive computing," in *ICPP '00: Proceedings of the 2000 International Workshop on Parallel Processing*. Washington, DC, USA: IEEE Computer Society, 2000, p. 9.

[12] S. Consolvo, L. Arnstein, and B. R. Franza, "User study techniques in the design and evaluation of a ubicomp environment," in *UbiComp '02: Proceedings of the 4th international conference on Ubiquitous Computing*. London, UK: Springer-Verlag, 2002, pp. 73–90.

[13] C. A. da Costa, A. C. Yamin, and C. F. R. Geyer, "Toward a general software infrastructure for ubiquitous computing," *IEEE Pervasive Computing*, vol. 7, no. 1, pp. 64–73, 2008.

[14] F. Davis, "Perceived usefulness, perceived ease of use, and user acceptance of information technology," *MISQ Central MIS Quarterly*, vol. 13, no. 3, 1989.

[15] A. Dey, G. Abowd, M. Pinkerton, and A. Wood, "Cyberdesk: A framework for providing self-integrating ubiquitous software services," in *Knowledge-Based Systems*. ACM Press, 1997, pp. 47–54.

[16] S. Giroux, H. Pigot, B. Paccoud, D. Pache, E. Stip, and J. Sablier, "Enhancing a mobile cognitive orthotic: A user-centered design approach," *International Journal of Assistive Robotics and Mechatronics*, vol. 9, no. 1, pp. 36–47, 2008.

[17] S. Helal and B. Abdulrazak, "Toward a scalable home-care delivery for frail elders and people with special needs," in *ICORR '07: Proceedings of the Tenth International Conference On on Rehabilitation Robotics*. Noordwijk aan Zee: IEEE, 2007, pp. 994 – 998.

[18] K. Henricksen and J. Indulska, "Developing context-aware pervasive computing applications: Models and approach," *Pervasive and Mobile Computing*, vol. 2, no. 1, pp. 37 – 64, 2006.

[19] S. S. Intille, K. Larson, J. S. Beaudin, J. Nawyn, E. M. Tapia, and P. Kaushik, "A living laboratory for the design and evaluation of ubiquitous computing technologies," in *CHI '05: CHI '05 extended abstracts on Human factors in computing systems*. New York, NY, USA: ACM, 2005, pp. 1941–1944.

[20] R. Jain and J. Wullert, II, "Challenges: environmental design for pervasive computing systems," in *MobiCom '02: Proceedings of the 8th annual international conference on Mobile computing and networking*. New York, NY, USA: ACM, 2002, pp. 263–270.

[21] X. Jiang, J. I. Hong, L. A. Takayama, and J. A. Landay, "Ubiquitous computing for firefighters: field studies and prototypes of large displays for incident command," in *CHI '04: Proceedings of the SIGCHI conference on Human factors in computing systems*. New York, NY, USA: ACM, 2004, pp. 679–686.

[22] G. Kotsis, "Performance management in ubiquitous computing environments," in *ICCC '02: Proceedings of the 15th international conference on Computer communication*. Washington, DC, USA: International Council for Computer Communication, 2002, pp. 988–997.

[23] G. A. Lewis and L. Wrage, "A process for context-based technology evaluation: Examples for the evaluation of web services technology," in *ICCBSS '06: Proceedings of the Fifth International Conference on Commercial-off-the-Shelf (COTS)-Based Software Systems*. Washington, DC, USA: IEEE Computer Society, 2006, p. 63.

[24] H. Lorenz, S. Claudia, and K. Andreas, "Assessing the human, social, and environmental risks of pervasive computing," *International*

Table 2: Summary of User Aspects and Key Elements

User Factors	Aspects	Elements
Personal Factors	Demographic Aspects	Age
		Sex
		Anthropometry
		Social Status and Work
	Comfort Aspect	Postural Comfort and Pressure
		User Effort
		Satisfaction
		Economical Consideration
		Sensory Comfort
		Visual Comfort
	Skill Aspect	Experience
		Use without error
		Mental workload Conciseness
		Symbol interpretation and denomination
		Ease of Learning
		Use without error
		Capacity
		Language abilities
		Willingness
		Openness to experience
Organic Factors	Physiological and Psychological Aspects	Intellectual functions
		Activity limitation
		Impairments
		Confidence
User Factor	Health Aspects	Allergies
		Diseases
		Health state
Social	Social Aspects	Community life
		Religion and spirituality
		Political life and citizenship
		Community social and civic life
		Language
		Interpersonal aspects
		Soft ski

Journal of Human and Ecological Risk Assessment, vol. 10, pp. 853–674, 2004.

[25] L. Mamykina, E. Mynatt, and M. A. Terry, "Time aura: interfaces for pacing," in *CHI '01: Proceedings of the SIGCHI conference on Human factors in computing systems*. New York, NY, USA: ACM, 2001, pp. 144–151.

[26] J. Mankoff, "Crossing qualitative and quantitative evaluation in the domain of ubiquitous computing. presented at the chi 2005 workshop on usage analysis: Combining logging and qualitative methods," 2005.

[27] G. K. Most?faoui, J. Pasquier-Rocha, and P. Br?zillon, "Context-aware computing: A guide for the pervasive computing community," *Pervasive Services, IEEE/ACS International Conference on*, vol. 0, pp. 39–48, 2004.

[28] S. Neely, G. Stevenson, C. Kray, I. Mulder, K. Connelly, and K. A. Siek, "Evaluating pervasive and ubiquitous systems," *IEEE Pervasive Computing*, vol. 7, pp. 85–88, 2008.

[29] T. Rodden, K. Chervest, N. Davies, and A. Dix, "Exploiting context in hci design for mobile systems," in *in Workshop on Human Computer Interaction with Mobile Devices*, 1998.

[30] J. Scholtz and S. Consolvo, "Conducting in situ evaluations for and with ubiquitous computing technologies," *International Journal of Human-Computer Interaction*, vol. 22, pp. 103–118, 2007.

[31] C. Scott and M. Jennifer, "Challenges for ubicomp evaluation," Technical report ucb-csd-04-1331, 2004.

[32] T. B. Ustün, S. Chatterji, J. Bickenbach, N. Kostanjsek, and M. Schneider, "The international classification of functioning, disability and health: a new tool for understanding disability and health." *Disability and rehabilitation*, vol. 25, no. 11-12, pp. 565–571, 2003.

[33] A. Ward, A. Jones, and A. Hopper, "A new location technique for the active office," *IEEE Personal Communications*, vol. 4, no. 5, pp. 42–47, 1997.

[34] M. Weiser, "The computer for the 21st century," *SIGMOBILE Mob. Comput. Commun. Rev.*, vol. 3, no. 3, pp. 3–11, 1999.

[35] S. P. Wyche and R. E. Griner, "Extraordinary computing: religion as a lens for reconsidering the home," in *CHI '09: Proceedings of the 27th international conference on Human factors in computing systems*. New York, NY, USA: ACM, 2009, pp. 749–758.

[36] H.-I. Yang, C. Chen, B. Abdulrazak, and S. Helal, "A framework for evaluating pervasive systems," *Int. J. Pervasive Computing and Communications*, vol. 6, no. 4, pp. 432–481, 2010.

Leveraging Diverse Regression Approaches and Heterogeneous Machine Data in the Modeling of Computer Systems Performance

André A. Cesta[1], Adriano Takara[2], and Danilo A. Moschetto[2]
1 Matera Systems-Eldorado Partnership, Campinas, SP, Brazil
2 Eldorado Research Institute, Campinas, SP, Brazil

Abstract —*Regular forms of Amdahl's law and the Super Serial model fail to be predictive of machine performance for heterogeneous processor datasets. In order to address this problem we successfully express Amdahl's law and the Super Serial model in terms of common denominator processor characteristics such as threads and clock speed.*

The revised forms of Amdahl's law and the Super Serial model allow leveraging heterogeneous machine data as input to capacity or scalability models. The authors choose to use regression for its formalism in verifying models.

The main scientific contributions are: (1) Generalized Amdahl's law and Super Serial model taking into account threads, clock speed, processor cores and cache size; (2) Empirical models for performance gains due to cache memory; (3) Alternatives on variable segmentation (e.g. truncating memory at saturation point). (4) A Hybrid regression method combining all the previous.

Keywords – performance, modeling, hardware, capacity, regression.

1 Introduction

Instead of beginning with the adapted forms of Amdahl's law[5] and the Super Serial Model[11] we will take a gentler path where these two adaptations are inserted amid the broader context of heterogeneous systems performance modeling.

Usually, performance predictions are derived via a single approach (e.g. frequentist or mechanistic - by reference to physical causes). Example: one can build a model based on Amdahl's law an equation that predicts the scalability of a computer system as a function of installed processors: p and a coefficient: σ. The resulting model proves accurate only for the processor considered; degenerating for heterogeneous ones (c.f. regression $C_A(p)$). Utilizing this model in conjunction with a total memory variable proves difficult (Amdahl's does not take memory into account).

In order to address these problems, we adapt Amdahl's law and the Super Serial model to forms based on threads and clock speeds (common denominators for all processors). The improvements in model quality are significant (c.f. regression $C_A(t,c)$). We then proceed to apply these adapted equations in performance modeling where they are further improved to take cache, inter core and inter processor aspects into account. The equation results are used as terms of hybrid multiple linear regression models based on different regression approaches (frequentist, empirical, mechanistic). The training datasets are always low cardinality and heterogeneous hardware data.

To understand the method proposed, some prior knowledge on the following subjects is assumed: statistics; multiple linear regression[12]; hardware capacity models [8] and laws such as Amdahl's[5] and Super Serial[11]. Article [8] introduces the laws and models homogeneous machines using only mechanistic techniques.

Assuming the reader is familiar with regression theory the notation we use should match the standard:

$$\widehat{y_i} = \beta_0 + \beta_1 x_1 + \beta_2 x_2 + \ldots + \beta_{p-1} x_{p-1} \qquad (1)$$

The quality of the regression may be indicated by the coefficient of determination adjusted ($R^2 adj \in [0,1]$), where a higher number indicates a more assertive model.

The resulting models were verified to be generic, robust and accurate for the few variables chosen (c.f. 3.8 and 6).

1.1 Historical context

Benchmarks are the standard for measuring equipment performance under specific workloads. Several benchmarks are available ranging from narrow tests (e.g. memory access) to broad ones (e.g. video encoding). While lending themselves to multiple interpretations, benchmarks cannot reliably predict the performance of new software packages or new hardware elements. In these cases experimentation is required.

Once enough experimental benchmark data has been accumulated for the new system in question, multiple forms of inference can take place that will reduce the amount of further laboratory work. Typical inferences are: *(1)* predicting system performance when one resource is increased and others are fixed[5][8]; *(2)* Predicting system performance on unforeseen hardware based on benchmarks for other software on the same hardware[7].

1.2 The new method

The modeling method presented here does not preclude any of the previous methods which can be done either directly in the case of *(1)* or via introduction of new empirical regression variables such as benchmarks in the case of *(2)*. The presented method is concerned mainly with what the latter inference forms cannot achieve due to their lack of modeling for differences across hardware systems.

The main goal or our models: predicting a software package's performance on completely unforeseen, but reasonably optimally configured hardware, using for this purpose data on performance from the same software on different platforms and the intrinsic differences among the platforms.

Having a model that works on *heterogeneous* systems allows any prior experimentation, even on other hardware platforms to be leveraged directly into predictions for new or hypothetical hardware. This has implications into the fields of hardware and software design and their matching with regards to: sizing, scalability and capacity planning.

1.3 Regression as a modeling technique

The revised expressions of Amdahl's law and the Super Serial model would be suitable as inputs to many types of models: neural networks, regression, Bayesian, etc. We choose to verify the practical value of the new equations with multiple linear regression for the following reasons: formalism, ease of interpretation, match to the nature of most relevant variables (mostly quantitative ordinal), low requirements on training dataset cardinality (´00s), capacity to combine multiple approaches (frequentist, empirical and mechanistic).

In the case of performance models with qualitative variables (e.g. operating system, motherboard make) we suggest logistic regression (not yet validated with the method) or combining regression predictions with other qualitative modeling techniques.

Other not selected methods were neural networks and Bayesian methods. Neural networks have been successfully used with a similar purpose on heterogeneous micro-architectures[1], but they are hard to interpret and require vast amounts of data for training, which make them prohibitive for us (macro architectures are difficult to simulate[14] in order to collect thousands of records). Bayesian methods would also require vast amounts of data in order to attain accuracy (c.f. 4).

1.4 Case study dataset and benchmark

In order to verify the theoretical results and exercise our method, a case study was developed. For this case study we selected public Internet data on hardware performance (a performance index) for a well-known ERP system. The use of public data avoids bias and allows for easy reproduction of experiments by other researchers. For commercial reasons we avoid mentioning the ERP vendor name or machine brands here.

From empirical observation we see this index to be a capacity index y directly proportional to the number of concurrent users (correlation 0.9988), while still maintaining a pre-defined Quality of Service – QoS (average response time below 1 second).

Assume the simulated users execute a fixed mix of transactions. Consider that the amount of users simulated is continuously raised until the last point where the QoS is maintained. This last point yields the actual machine index which is, on the vast majority of tested cases, CPU bound.

If the system whose performance one tries to model using this regression method does not count with a similar benchmark, first of all it would be necessary to apply one.

1.4.1 Case study dataset variables selection

Our choice of variables is given by the table below.

Table 1. Variables utilized in the case study

Var	Description	Var	Description
p	Total Processors	$l1$	Total L1 Cache KB
pc	Total Processor Cores	$l2$	Total L2 Cache KB
t	Total Threads	$l3$	Total L3 Cache KB
c	Processor Clock GHz	m	Total Memory GB

There are also extra variables qualifying the cache size $l1$, $l2$, $l3$ with regards to their location (per processor, per 2 cores, etc).

Variables pc, t, c are more fine grained than those typically found in capacity or scalability analysis (p).

This is the minimal set of variables required to verify that our adaptations of Amdahl's law and the Super Serial model explain the performance variability.

We have deliberately not included any of the variables related to brands, makes or microprocessor designs in the model. This makes modeling more challenging, since we have highly heterogeneous systems. While these ignored variables are not necessary to verify the new formulas, they are certainly useful to improve the models.

2 Hybrid regression method

In order to avoid the problems of classical regression, we propose a hybrid method, consisting of well defined steps, each one leading to an intermediate regression of varied approach (frequentist, empirical, mechanistic).

2.1 Method pre requisites

The dependent variable being predicted must be a benchmark index, please refer to 1.4 for some characteristics of reliable capacity benchmarks.

The initial datasets should be pruned of configurations identified as non-optimal such as machines with bottlenecks other than the ones being the focus of the modeling: processing power related variables in our case. These

records can be reintroduced later if the model built proves robust[4] enough in areas of the modeled space occupied by non-optimal machines. Such pruning is not a problem since we want to predict performance of balanced machines. One should be aware of collinearity problems though (many variables will be linear with performance). In case one requires predicting capacity for machines with easily detectable out-of-balance configurations on memory, motherboard, etc, we refer them to our model with memory as a bottleneck (c.f. 3.7) as a starting point.

2.2 Hybrid method: step by step

The regression model is built in two phases. The first one is the variable selection and transformation that is performed by repeating the following cycle, until R^2adj and stderr improvements diminish considerably.

Phase 1, Single Variables

1 – Calculate the regression on a single variable without transforming it, starting with the ones the study focuses on.

2 – Analyze the regression quality: R^2_{adj}, stderr, residuals, variable significance (t test).

3 – Verify if the variable alone requires an empirical transformation to align it with *y*. Among the common transformations[12] we have square root, log, segmentation or truncation; or any of the previous and other functions combined.

One must pay attention to manifestations of mechanistic aspects. Two such aspects are worth mentioning:

(1) Variables which are predictive but not exactly linearly correlated with y probably indicate a potential for interaction with other variables (e.g. c and t).

(2) Variables that influence performance, but only up to a certain point are typical in such models. This is the case of memory (c.f. 3.3). Consider variable segmentation.

Phase 2, Variable Combinations

The second phase deals with composite variables that represent real world interactions. For instance, multiple threads running at a certain clock generate processing power.

The main difference between this step in our process and the variable creation from the stepwise regression method is the empirical knowledge employed. For instance, cache size interacts directly with the capacity of processing instructions per second (less memory fetches are needed) although it does not add new memory space.

These composite variables are modeled using the same steps presented in the first phase.

3 Modeling an ERP system

In order to verify the proposed method and adaptations to Amdahl's law and Super Serial model (SS) we developed a case study based on an ERP's system performance data (c.f. 1.4.1). The dependent variable may be seen in 1.4.

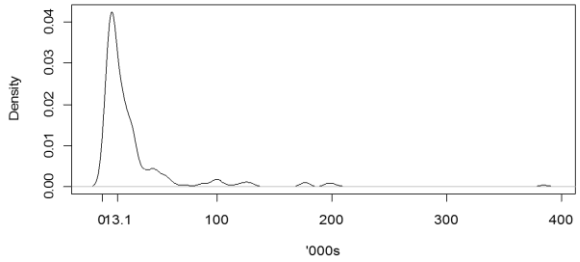

Figure 1: Kernel density estimate for ERP capacity index

The capacity index ranges from 0 to 380k, with a median index value of 13.1k what can be achieved, nowadays, with a quad core machine at 3GHz.

The long tail makes the analysis challenging because: (1) there is not enough data on this tail - only 15 machines above 100k; (2) mechanistic capacity models tend to accumulate errors towards scaled up subjects - the larger the hardware the larger the portion ignored by the model; (3) Regression tends to be highly influenced by the leverage of a few large machines.

3.1 Data cleansing and preparation

Firstly all machines older than 2005 were removed. This left 248 benchmarks out of which five were discarded as influential observations (three of the five discards dated before 2007). The remaining 243 machines were used for modeling.

3.2 Classical regression

The method starts with a naïve frequentist regression adding all input variables without any transformation or combination. The $l2$ and $l3$ cache were omitted for not being total values per machine, but instead provided on a per core basis, per 2 cores, per processor, etc.

Regression on*:* $y = p + pc + t + c + l1 + m$. *Results:* $R^2_{adj} = 0.8996$; $stderr$ *=12660.* Interpretation: the R^2_{adj} is good while the errors are large. Memory was the most significant predictor.

3.3 Single variable modeling

This section follows the method steps outlined in 2.2 (Phase 1) We describe only the parts that differ here. Variables directly linked to processing power (c, t) are best analyzed first.

Regression on c: R^2_{adj}=0.0066, a very low value. Interpretation: high end machines may use multiple low clock processors. No transformation was applied.

Regression on t: R^2_{adj}=0.7438, a high value for a single variable. Some low end machines already make use of the highest clocks possible, so improvements can only be achieved by adding threads. No transformation applied to t since it should be more meaningful when combined with other variables and graphical analysis indicates it is linear with *y*.

Regression on m: R^2_{adj}=0.8486; stderr =15560, the highest R^2_{adj} for a single variable. Correlation of 0.92 with y. This is both good and bad, since it means the ERP scales well with memory, but can lead to multicollinearity problems with other predictors aligned with y (c.f. 3.7).

3.4 Composing variables

This section matches the method steps outlined on 2.2 (Phase 2).

The following variables have a clear relationship: p, $pc, t, c, l1, l2, l3$. Additionally there is information on how the total caches ($l1, l2, l3$) apply: per core, per 2 cores, etc. These variables are in a sense a mid-level description of the processors and the elements they describe are physically located on the processors.

The following regressions were made as references to evaluate combinations of the form: f(c, t), culminating on the adapted Amdahl and SS of clock and threads:

Regression $y = t + c$: $R^2_{adj} = 0.7791$; stderr=18789. An inclined plane of hardware manufacturer strategies.

Regression $tghz^{.75} = (t \cdot c)^{0.75}$: $R^2_{adj} = 0.8854$ with stderr = 13530. After some transformation attempts 0.75 proved to be the most adequate exponent related to the difficulty in scaling software and hardware.

In possession of a performance measure ($tghz^{.75}$) and with secure knowledge that memory is not very meaningful past saturation point, we could segment[12] memory into $m1, m2$ and find improved results. We are not performing this transformation because we will achieve better results.

3.5 Amdahl's law for threads and clock

Amdahl's law governs software system's capacity *and*[8] scalability. It expresses these as a function of the number of processors p and $\sigma = ts \div (tp + ts)$, a constant that is related to the fraction of program parts that cannot be executed in parallel where ts is the time to complete the serial tasks of the program on a *serial* processor and tp is the time to complete all parallelizable parts of the program on a on a *serial* processor. Amdahl's law for capacity or scalability on processors is expressed on these terms by:

$$C_A(p) \cong S_A(p) = \frac{p}{1 + \sigma(p-1)} \quad (2)$$

$$\lim_{p\to\infty} C_A(p) = \frac{1}{\sigma} \quad (3)$$

Note that if $p = 1$ the capacity is proportional to p and that for values of p above 1 we have a slightly lower capacity due to the penalty for adding more processors. This is expressed for a program that is not entirely parallelizable by: $\sigma(p-1)$. Regression on $C_A(p)$: $R^2_{adj} = 0.4596$; stderr=29390. The σ can be calculated using the regression and trial and error. The regression results did not improve because we are dealing with *heterogeneous* processors (each p value on the dataset has different capacity).

In order to obtain more accurate results we need to adapt the law above to the case of heterogeneous processors. Some work has been performed on adapting it to multiple equivalent cores[3][10], but it is not useful here since our cores are different as well.

We have to express the law in terms of lower common denominators, namely threads and clock speed. All modern machines have threads running at a certain clock speed and are able to process instructions in parallel using threads.

The simplest abstraction that can be made that holds for the whole law demonstration is that each thread behaves like a *small serial* processor in Amdahl's definition.

$$C_A(t) \cong S_A(t) = \frac{t}{1 + \sigma(t-1)} \quad (4)$$

Regression on $C_A(t)$: $R^2_{adj} = 0.7443$, an improvement from 0.45 from $C_A(p)$, but not significant. The problem is that the dataset contains heterogeneous machines with threads of different clock speeds. If the speedup formula at the basis of Amdahl's demonstration is revisited (speedup is defined as time for a serial processor to complete $ts + tp$ divided by time for a parallel processor to complete $ts + tp/p$ or $ts + tp/t$ on our case, we see that doubling the clock doubles the speed of any machine, i.e. doubles the speed on both the serial and the parallel processors equally. On the limit as t increases to infinity the capacity of the machine is $1/\sigma$, and doubling the clock will double this capacity as it will execute the serial and the parallel tasks in half the time.

This whole reasoning is confirmed by [8], from which we adapt the quotation: "*For σ=0.20, Amdahl's Law predicts that adding a second processor will yield a relative capacity of 1.67. That is, the maximum throughput with two processors will*" not be 2, but "*1.67 times that with one processor." ... "on the limit*" with a large number of processors "*the scalability will be* $1/\sigma$*"* =1/0.20=5. "*If, instead of adding a second processor, we replace the single processor with one twice as fast, the throughput will then be exactly twice that with the slower processor. This is because the faster processor reduces the time required for both the serial and parallel portions of the workload.*" and the new capacity limit will be 10 instead of 5. "*Because of this, it is generally more cost effective to use a faster single processor than to add processors to achieve increased throughput in cases where Amdahl's Law applies*".

Adapted Amdahl's law and equation for the case of clock speed c and threads t capacity or scalability.

$$C_A(t, c) \cong S_A(t, c) = c \cdot \left(\frac{t}{1 + \sigma(t-1)}\right) \quad (5)$$

Regression on $C_A(t, c)$: $R^2_{adj} = 0.9069$; stderr=12200. Note: Sigma needs to be re-optimized. Comparing to regression $tghz^{.75} = (t \cdot c)^{0.75}$: $R^2_{adj} = 0.8854$; stderr =

13530. A law is better than empiricism, but notice that if we make t = 1 we reduce Amdahl's equation above to $t.c = tghz$. Back to empiricism. Applying $C_A(t,c)^{1.1}$ makes R^2_{adj} become 0.9105 and the errors decrease. But we will leave the law without the exponent for the time being. This empirical exponent points out to something Amdahl does not take into account and on a regression would accumulate as errors towards scaled-up hardware…

3.6 Adaptation of the Super Serial model

The only characteristic that differs from Amdahl's law to Super Serial[8] is a penalty for inter processor communication. The SS model deals with this penalty by adding another term to the denominator: $\gamma \cdot p \cdot (p-1)$, a term proportional to the number of communication paths among processors and a constant γ.

$$C_{ss}(c,t,p) = c \cdot \left(\frac{t}{1 + \sigma \cdot [(t-1) + \gamma \cdot p \cdot (p-1)]} \right) \quad (6)$$

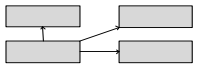

Figure 2. Representation of the model used in (6)

Notice the formula already appears half adapted to clock and threads. An explanation is necessary to complement the details in[8]: the figure above shows p processors as rectangles with each processor having p-1 communication/synchronization pathways in between it and others. In a steady state situation, the amount of inter processors communication work stealing processor cycles is $p \cdot (p-1)$ times a small constant γ to compensate for the fact that this is not taking place all the time and to indicate a small cost penalty for the communication.

Regression on $C_{ss}(c,t,p)$: $R^2_{adj} = 0.9084$; stderr=12100. All constants required re-optimization. We will improve this further with a second adaptation to allow communication penalty among threads in one core to all other cores (pc) or processors (p):

$$C_{ss}(c,t,p,pc) = \frac{t}{c \cdot \dfrac{}{1 + \sigma \cdot [(t-1) + \vartheta \cdot \frac{t}{pc} \cdot pc \cdot (pc-1) + \gamma \cdot \frac{t}{p} \cdot p \cdot (p-1)]}} \quad (7)$$

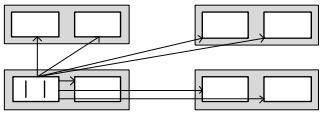

Figure 3. Representation of the model used in (7)

Term: $\cdot \frac{t}{pc} \cdot pc \cdot (pc-1)$: The diagram depicts processors again as outer rectangles; cores as inner white rectangles and threads as small vertical line segments inside inner rectangles. The actual communication is proportional to the amount of threads per processor core (t/pc); it takes place from each thread in the core to all separate cores (pc -1), so the arrows have weight 2 representing one path for each thread in the highlighted core. Communication happens for all cores at the same time on a steady state situation ($\cdot pc$). This also explains why the processor penalty term was multiplied by t/p. This is the Super Serial model adapted to threads and clock. Coefficients were re-optimized on a triple variable optimization.

Regression $C_{ss}(c,t,p,pc)$: $R^2_{adj} = 0.911$; stderr=11920.

3.7 Bottleneck modeling

Notice that the latest models do not make use of the dangerous memory (m) variable. We know m to be important only up to a saturation point, beyond which it can be ignored for this ERP system. So we are only interested in cases of machines with m low enough to become a bottleneck.

Imagine having memory and a CPU based predictor as a regression, which geometrically defines an inclined plane of expected ERP capacity indexes; we know, however, that as memory drops we have a bottleneck and this plane should look more like a cliff around the bottleneck area.

How to segment memory around its saturation point. For systems that scales linearly on memory, one defines a linear coefficient μ that if applied to a capacity estimate $\hat{y}_i$ brings it to the scale of recommended memory for that processing capacity. The capacity estimate must not use memory as a variable and can be any of the regressions before or even just one of their terms:

$$\mu = mean(m_i \div \hat{y}_i) \quad (8)$$

The recommended memory rm for a machine is then given by: $rm = \text{adj} \cdot \mu \cdot \hat{y}_i$. An adjustment factor adj assuming values around 1.0 (e.g. 0.9, 1.1) is used to compensate for conservative or liberal memory averages on the dataset. If on average there is memory surplus, this factor will probably be less than 1 as the saturation is reached before the average. The factor needs to be optimized so as to produce the best regression results. Typical regression terms derived from memory segmentation are:

$m1 = memory\ before\ saturation\ point.$

$m2 = memory\ after\ saturation\ point.$

$mbottle = if\ m2 > 0\ then\ 1\ else\ 1/(rm \div m1)$[13].

Regression:

$$C_{bss}(c,t,p,pc) = p + pc + t + c + l1 + m1 + \log m2 + C_{ss}(c,t,p,pc) + mbottle \cdot \hat{y} \quad (9)$$

Where $\hat{y}$ is an estimate from an equation similar to the above, but without memory related terms. Such regression achieves $R^2_{adj} = 0.9367$ and stderr = 10060.

This cannot be improved further for the 282 machines on the initial dataset without including additional variables such as operating system, processor registers, etc.

3.8 Empirical cache modeling

There are no steady state mechanistic models available for cache. A different empirical model is needed for each type of cache location (e.g. *l2* cache on core and *l3* on processor). Instead of building one model for each combination of cache locations, we have selected the largest subset containing 153 heterogeneous machines with similar cache location (*l1* and *l2* cache on the cores and *l3* cache on the processor or absent). These continue to be a heterogeneous mix of operating systems, microprocessor architectures, DBMS, etc.

The selected subset received empirical modeling on performance boosts due to cache hits and performance decreases due to cache synchronization penalties, which yielded final and best results of R^2_{adj} of 0.98 and stderr of 3445 (small machines suffered smaller errors). These results were similar to those obtained by other researchers using regression either with many more variables for micro-processors[2][9] or with less variables, but homogeneous machines[8].

For single term regressions based on the empirical and mechanistic cache models below we obtained: $R^2_{adj} = 0.9689$ and $stderr = 4301$. The high R^2_{adj} value shows that our adapted version of mechanistic equations explain the performance variability

For hybrid multiple term regressions combining frequentist, empirical and mechanistic approaches we obtain best values of : $R^2_{adj} = 0.9801$ and $stderr = 3445$. This shows how worthy the method is, but points out to the need to introduce more variables (motherboard speed, processor registers, operating system) to be able to further decrease error. We could frequently find machines on the dataset with exactly the same regression variables and results, but differing in their real capacity indexes by 3000 due to other ignored variables.

Firstly, we improve ϑ and γ on our Super Serial model adaptation $C_{ss}(c,t,p,pc)$ to use *l*1, *l*2 and *l*3. The γ coefficient is complemented becoming: $\gamma \cdot \log(1 + l3/(t/p))$, a penalty proportional to the amount of cache on the processor. The log function was empirically chosen. Likewise, ϑ is split into two (τ and φ) to account for separate inter-core communication penalties for *l*1, *l*2 cache amounts.

$$C_{ss2}(c,t,p,pc,l2,l3) = \frac{t}{c \cdot \left(1 + \sigma \cdot \left[(t-1) + \tau \cdot \log\left(\frac{l1}{t/pc}\right) \cdot \frac{t}{pc} \cdot pc \cdot (pc-1) + \varphi \cdot \log\left(\frac{l2}{t/pc}\right) \cdot \frac{t}{pc} \cdot pc \cdot (pc-1) + \gamma \cdot \log\left(1 + \frac{l3}{t/p}\right) \cdot \frac{t}{p} \cdot p \cdot (p-1)\right]\right)} \quad (10)$$

Regression (10) results: $R^2_{adj} = 0.9493$; stderr=5496

Let's model now cache boost on this architecture, since we have only modeled cache penalty so far:

Regression: $C_{ss2}cache = C_{ss2}(c,t,p,pc,l2,l3) \cdot \log\left(\log\left((1 + (l3 \cdot p)^{el3}) \cdot (l2 \cdot pc)^{el2} \cdot (l1 \cdot pc)^{el1}\right)\right)$: $R^2_{adj} = 0.9689$; stderr=4301. Remember that for this subset of 151 machines we have similar locations for cache (see above). The factor added at the end of the new $C_{ss2}cache$ model is the log log of the interaction of all cache sizes of the machine, with each one raised to a power exponent that is optimized to match the individual cache importance.

This brings us to the last point of our case study: Regression $p + pc + t + c + l1 + l2 + l3 + C_{ss2}cache$; $R^2_{adj} = 0.9801$ and stderr = 3445 on 151 machines. Part of the residual analysis is depicted below:

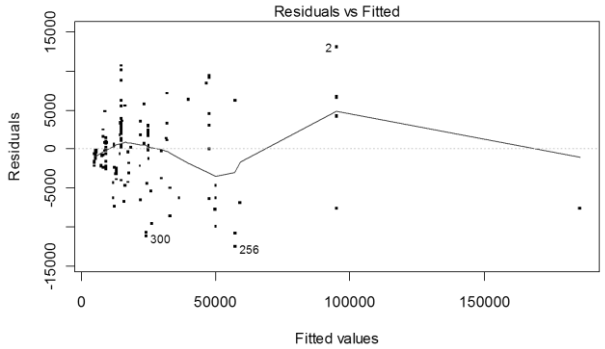

Figure 4. Residual analysis of C_{ss2}cache

Notice that the errors are much smaller for low end machines. Machines with capacity index less than 11k had stderr 1984 for instance. The errors fluctuate a little more for the few larger machines with higher capacity index (with the trend line always below 5000), perhaps due to the influence of the few observations available.

We did not wish to remove them yet since a larger error for such large machines is less of a problem and the subject predicted is machine capacity. This is common for mechanistic models and not so common for pure frequentist model (large errors on larger systems and being generic enough to cover the whole scale). The errors seem to be normally distributed as shown below.

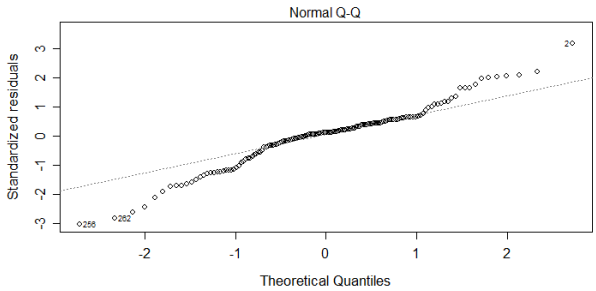

Figure 5. Residual analysis of C_{ss2}cache

We performed another regression with a new memory truncation and proceeded to modeling memory as a botleneck which did not improve on this regression in terms of errors, but became more realistic. A validation with a test dataset composed of the last capacity indexes was consistent with the residual analysis above.

4 Related work

Our approach belongs to an unexplored niche. In [2], the authors used statistical regression to optimize micro-architectures (registers, queues, etc). Given the 22 billion possible variable combinations, experimenting would not be feasible; even with simulation the authors had to resort to sampling. A regression on a sample of size 4000 of simulated data was performed to predict both performance and energy consumption, resulting in errors among 4% e 4.5% (larger datasets usually imply smaller errors).

In [9] the author presents a project along the same lines, but with more modern regression techniques (MART - *Multiple Additive Regression Trees*). The goal is again to predict micro-architecture processor performance which is achieved with values R^2 around 0.97.

If obtaining large samples is not an issue (as it is on our case) one can also consider using neural networks[1]. The variables and results are similar to [2] and [9] and the training data set is from the Spec benchmark.

In [8], the authors present various modeling techniques based on single curve fitting aided by regression to minimize fitting error. Some of the equations and laws (Linear, Amdahl's[5], Super Serial[11], Gustafson's[6] and throughput in relation to demand on bottleneck resource[13]) are the same as the ones adapted in this article.

Other approaches diverge even further from modeling, such as use of discrete simulation for prediction purposes only. Among these we highlight article [14] as a direct alternative to our method.

5 Acknowledgements

This research project was realized by Instituto de Pesquisas Eldorado and Dell Computadores do Brasil under the scope and support of the Brazilian Informatics Law (Brazilian Federal Law # 8248/91). This article would not have been possible without the invaluable support and machine donations by Dell.

6 Conclusion

Theoretical advances and applications: Amdahl and Super Serial capacity and scalability models can be written in terms of threads and CPU clock, lending themselves to modeling heterogeneous hardware system performance. Empirical cache models can be created to improve the former. All of these can be employed in regression models with additional variables. The resulting technique proves useful for: machine sizing, capacity planning, migrating to different hardware platforms, technical education on hardware design, etc.

Results: The adapted versions of Amdahl's law and the Super Serial model are significantly more predictive on these datasets. Take for instance the adaptation of Amdahl's law which improved values of: $R^2_{adj} = 0.4596$ and stderr=29390 in the case of Amdahl(*processors*) to values of: $R^2_{adj} = 0.9069$; stderr=12200 in the case of Amdahl(threads, clock) (c.f. 3.5, 3.6).

The results from generic hybrid regression were also very good given the challenging dataset of heterogeneous machines used and the reduced number of variables (c.f. 1.4.1). Please read the short session at the end of 3.8 for quantitative details.

Future work: our method allows further improvements by addition of lower level variables such as number of processor registers, queue lengths drawing from [2][9] and high level ones such as motherboard, memory speeds, operating system.

7 References

[1] A. Beg. "Predicting Processor Performance with a Machine Learnt Model", in 50th IEEE International Midwest Symposium on Circuits and Systems (MWSCAS/NEWCAS'07), Montreal, Canada, 2007, pp. 1098-1101.

[2] B. C. Lee, D. M. Brooks. "Accurate and efficient regression modeling for microarchitectural performance and power prediction", in Proceedings of the 12th international conference on Architectural support for programming languages and operating systems (12th ASPLOS-XII), 2006, pp. 185-194.

[3] E Yao, Y Bao, G. Tan, M. Chen. "Extending Amdahl's law in the multicore era". in SIGMETRICS Performance Evaluation Review, 37(2), 2009, pp. 24-26.

[4] G. Box. "Robustness is the Strategy of Scientific Model Building", Robustness in Statistics. eds., R.L. Launer and G.N. Wilkinson, Academic Press, p. 202, 1979.

[5] G. M. Amdahl. "Validity of the Single-Processor Approach To Achieving Large Scale Computing Capabilities", in Proceedings of AFIPS, Atlantic City,NJ, AFIPS Press, 1967, pp. 483-485.

[6] J. L. Gustafson. "Reevaluating Amdahl's Law", in Communications of the ACM, vol. 31, no. 5, 1988, pp. 532-533.

[7] K. Hoste, L. Eeckhout, H. Blockeel. "Analysing commercial processor performance numbers for predicting performance of applications of interest", in SIGMETRICS, 2007, pp. 375-376.

[8] L. G. Williams, C. U. Smith. "Web Application Scalability: A Model-Based Approach", in Computer Measurement Group Conference (CMG), 2004, 215-226.

[9] L. L. Peng, B. Ramadass. "Accurate and efficient processor performance prediction via regression tree based modeling", in Journal of Systems Architecture, Volume 55, Issues 10-12, Pages 457-467, October-December 2009.

[10] M. D. Hill, M. R. Marty. "Amdalh's Law in the Multicore Era", in IEEE Computer, 2008, pp. 33-38.

[11] N. J. Gunther. "The Practical Performance Analyst", iUniverse.com, 2000.

[12] N. R. Draper, H. Smith. "Applied Regression Analysis", Wiley-Interscience, 1998.

[13] R. Jain. "The Art of Computer Systems Performance Analysis: Techniques for Experimental Design, Measurement, Simulation, and Modeling", New York, NY, John Wiley, 1990.

[14] S. Kounev. "J2EE Performance and Scalability -From Measuring to Predicting", SPEC BENCHMARK WORKSHOP 2006, Austin, Texas, Jan, 2006.

Simulation Modeling for Quality Enhanced Software Process Based on Rework Analysis

Jian Zhai[1], **Bei Zhang**[1], **and Qiusong Yang**[1]
[1]National Engineering Research Center of Fundamental Software,
Institute of Software, Chinese Academy of Sciences, Beijing, China

Abstract— *Quality is a critical attribute of software. A software process with sophisticated design and analysis would benefit the quality of the output software greatly. To enhance the quality of a software process, some quality assurance activities need to be incorporated into the process. As a consequence, the quantity of rework activities as well as the cost and duration of the process would be increased. In this paper, we quantitatively analyze and predict the impacts of such reworks by a novel simulation modeling approach, in which, the factors related to rework are carefully described, and the impacts of rework in cost and duration as well as quality are further analyzed. At last, a case study is given to illustrate the usage of the approach, whose capability, rationality, and availability are indicated by the simulation results.*

Keywords: process; rework; quality; simulation; cost estimation

1. Introduction

For decades, most software organizations have continuously suffered from a common problem: it is difficult to ensure in advance that the quality of an output software product of a certain software project would satisfy the consumers' requirements in every aspect, so that the phenomenon of delaying, overcost, poor-quality or something similar are unavoidably generated. To solve or relieve such a problem, many attempts have been introduced, among which, software process techniques are the most important ones. Research on software process techniques implies that the quality of software product would be greatly contributed by its developing process. And software process with careful design and analysis would be necessary for high-quality software products in most cases.

Based on the concept of software process improvement referred by CMMI [8], the most famous software process assessment reference model, to enhance the quality of a software product, there should be corresponding quality enhancing activities adapted in the original software process to refine it. Furthermore, by inserting certain activities to critical stages, the updated software process should be more able to successfully meet the relevant quality requirements. The inserted activities could be peer review, quality assurance, process adjustment and some related activities or recursions. Since the quality criterion is enhanced and some new quality related activities are added, there would be more rework activities in the newly updated process if the other factors remain the same, so that the resource assignment, cost, schedule, etc. of the process should be re-estimated correspondingly. Under such situations, carefully modeling and closely analyzing rework turns out to be a necessity.

In fact, rework is a common phenomenon in actual software development: almost all software projects include rework activities more or less. But surprisingly, few of the classical books in software engineering or software process engineering discuss rework concretely, including CMMI. Actually, most researches on rework exist in the form of empirical studies of software engineering. In a technical report from CMU/SEI [1], rework is defined as all corrective work performed after a review or test. An empirical study reports that for organizations from CMM level 2 to level 5, the average amount of percentage of rework falls from 23.2% to 6.8% in terms of time consuming [3], which means rework cannot be completely avoided, and the analysis of rework is significant as well.

The nature of rework activities is complicated. It may be related to various internal or external factors, such as the maturity level of an organization, the capability of operators for activities, the techniques that aid the development, the requirement of the quality of output products, the restriction from the cost or schedule, and so on. The empirical studies focus on the relationship between the maturity level of organizations and the rework activities with an implicit assumption that the other factors are fixed. In fact, the maturity level is a macro view factor for an organization, whose improvement is a hard and long-term update, whereas the analysis of the interactions among the key factors in a micro view, such as the human capability, the quality requirement, and so on, would be an easier, more light-weighted, and more efficient way for an organization to understand and control the rework activity, which would significantly benefit a software project and even a software organization.

To quantitatively and qualitatively analyze and estimate the key factors in a software project affected by rework activities, software process simulation modeling is a viable approach. As a kind of simulation technique that have been widely used in many other disciplines, software process simulation is increasingly used in analyzing software pro-

cesses. In academia, simulation may help validating research initiatives on software process, some of which can hardly be validated in real context, due to the ever changing external environment and cost concerns. In practice, when facing alternatives decisions for a certain issue in software development, simulation may help a process designer or project manager to observe the impacts of them in advance and in detail to choose the best according to his own judgement. As a result, simulation techniques have been used to address a variety of issues in software process modeling ranging from the strategic management of software development, supporting process improvements to software project management training [6].

In this paper, we introduce as-TRISO/ML, a software process simulation modeling language extended from s-TRISO/ML [10], to model and quantitatively analyze the performance of quality enhanced software processes, especially for discovering the relationship between the cost/schedule/quality of a process and the newly generated rework activities. In other words, in the proposed simulation model, rework activities and related internal/external factors are carefully modeled, and the mechanism and effect of rework have been further discussed and estimated. In addition, a case study is given in this paper to illustrate the usage of the simulation approach. Furthermore, the simulation results of the case study will indicate the capability, rationality and availability of the approach by comparing with the results of another simulation with different factor assignments.

In what follows: Section 2 introduces the related works, including those on the rework phenomenon of a process, the software process simulation modeling. Section 3 briefly introduces as-TRISO/ML. Section 4 describes the abstract activities and human resources in simulation models of processes. Section 5 gives a case study of the simulation modeling and analyzes the results. At last, section 6 draws conclusion.

2. Related Work

2.1 Rework

Rework is a common phenomenon in software development. Nearly all software projects include rework activities in certain degree. Unfortunately, rework receives less than enough attention from both industry and academia. Some empirical reports of software development observe and analyze the quantity and influence of rework [1], [7], [3]. The authors notice that the quantity of rework can be decreased from low maturity level organizations to high level ones, but it cannot be completely removed from a software process in practice. Based on such situation, rework is mentioned in some software development life cycles, but in such models rework activities are always treated as a nominal and abstract step only rather than an explicit description.

[2] notices such problem, and tries to formalize rework in software processes. In the study, the authors describe the nature of rework in Little-JIL software process programming language [9]. In fact, the aims of this paper are both to model structure of rework and to verify Little-JIL language. Though the deep analysis of rework is overlooked in this study, its formalization enables us to better understand rework, and to further our analysis of rework.

2.2 Software Process Simulation Modeling

The software process simulation techniques can be divided into two categories, the traditional simulation and the ones aided by new technique. The representatives of traditional simulation are system dynamics (SD) [4] and discrete event simulation (DES) [5], whereas the range of new technique aided simulation is wider, for which stochastic process algebra based process simulation [10] is a delegate.

The traditional simulation techniques tend to be powerful and complex, and are difficult to handle and expensive and employ in practice. In opposite, the latter category of simulation techniques tend to be easy-to-use and light-weighted. For example, stochastic process algebra based process simulation can be executed upon an executable descriptive software process model, and get quantitative results of cost and schedule prediction. A summary of the state-of-the-art of software process simulation modeling can be found in [11].

The research of [10] is closely related to this study. In [10], the authors introduce a stochastic simulation modeling language, and analyze the possible cost and duration of a software process by a stochastic simulation approach. The weakness of the research in [10] is that the semantics of the given simulation modeling language is not expressive enough to describe the complex nature of software process, so that some operations, such as conditional choice, and some types of activity, such as rework, cannot be properly handled by such a language.

3. as-TRISO/ML: A Software Process Simulation Modeling Language

To analyze the effect of rework activities and simulate quality enhanced software processes, a software process simulation modeling language named as-TRISO/ML is employed in this paper. As-TRISO/ML is an extension of s-TRISO/ML introduced in [10] for stochastic simulation of software process. As-TRISO/ML inherits the basic structure and the rigorous formal foundation from s-TRISO/ML, so that a process modeled by as-TRISO/ML can be simulated stochastically for the performance analysis. Whereas the difference between the two languages is that a mechanism to support values and functions transferring in a process is added into as-TRISO/ML, which is mandatory for rework activities description and analysis.

In as-TRISO/ML, the graphical notations are defined similarly with those in s-TRISO/ML. The diamond notations stand for the executing sequence controlling nodes, which include sequential, parallel, choice, and conditional choice. And the ellipse notations stand for the activities, which include actual activities and virtual activities. The examples of the notations are shown in Fig. 1. In as-TRISO/ML, actual activities and virtual activities are separated strictly. The actual activities are executed by human resource, operated in certain duration and finished in time or deferred. The duration of an actual activity would be determined by a distribution parameter r. In opposite, the virtual activities in model do not occur in actual software process, and the function of these activities in a model is to indicate the executing sequence or the others relationships in the actual activities.

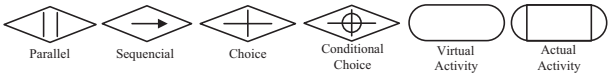

Fig. 1: Graphical elements of as-TRISO/ML

Furthermore, activities recursion can be included in processes defined by as-TRISO/ML. Take Fig. 2 for example. The process roots from a virtual activity $VA0$, of which the sub layer activities $VA1$, $VA2$, $VA3$ and $AA7$ are executed sequentially. Virtual activity $VA1$ leads an activity recursion, in which actual activities $AA1$ and $AA1'$ are executed in order first. After $AA1'$ is finished, there is a virtual activity VA_R, followed by a conditional choice operation to be dealt with. If $AA1.q$, a parameter outputted by $AA1$, is less than a given value $p1$, a threshold of the recursion, then the virtual activity $VA1$ and its sub-activities would be executed once again until the relationship between the two parameters is changed. If the relationship $AA1.q >= p1$ is satisfied, the conditional choice turns to an empty virtual activity $VA1_E$, which stands for the finish of the recursion and the next activity of the process is executed. Similarly, $VA2$ leads to a recursion with the same structure. Next, $VA3$ leads to a parallel execution of two pairs of sequential actual activities. At last, actual activity $AA7$ is executed.

4. Modeling the Quality Enhanced Software Process

4.1 Classification of Activities

Generally speaking, by the difference of the objectives, the activities in a process can be largely divided into three types, which are **functional activity** (FA), **quality assurance activity** (QA), and **management activity** (MA). The objective of FA is to implement the functional requirements of a software project and output the related artifacts. The typical FAs include activities of requirement, design, coding and test, as well as the sub-activities of them. The objective

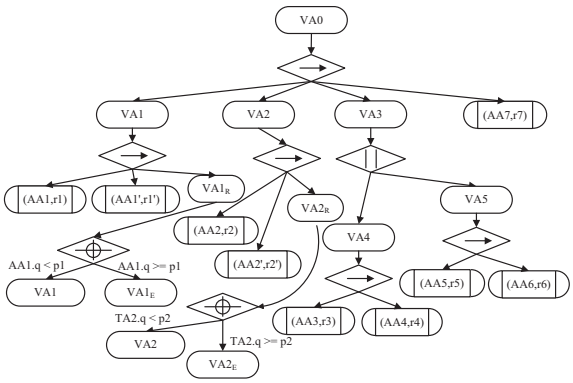

Fig. 2: A software process described by as-TRISO/ML

of QA is to check, assess and confirm the quality of the outputs from the functional activities to ensure the output artifacts meet the pre-agreed requirements. And the objective of MA is to organize and structure the other two types of activities, and assign the appropriate resources to them.

To enhance the quality of software product outputted by a software process, one of the most important and direct updates is to insert more QAs into a process, such as peer review, quality control and so on. Under the same condition, an inevitable consequence of such update is that the more quality weaknesses are found, the more additional FAs or rework would be needed theoretically. And the quantity and time of rework activities would depend on several factors, such as the capability of the operator of FA, the capability of the operator of QA, the complexity of FA, the quality requirement of FA and so on. It can be assumed that the more rework activities occurs in an FA, the higher quality the outputs of the FA can be reached, and the quality of the outputs would eventually meet the quality requirement. In such situation, a pair of FA and the corresponding QA, as well as the activity recursions, can ensure the quality of FA's outputs to be good enough, and such structure of FA and QA can be treated as an integrated activity, called **trustworthy activity** (TA).

4.2 Definition of Operators

For an operator of activities in a process, the attributes of him can be described by a matrix $Op : (\tilde{P}, \tilde{Q}, \tilde{W})^T$, where Op stands for the name of the operator, and the vectors $\tilde{P}$, $\tilde{Q}$ and $\tilde{W}$ are all quadruples, and separately stand for the expected productivity, the expected quality of output, the wage for the four stages of a development including requirement, design, coding and testing. The expression for attributes of operators is as matrix 1 shows.

$$Op : (\tilde{P}, \tilde{Q}, \tilde{W})^T = \begin{pmatrix} p_{req} & q_{req} & w_{req} \\ p_{des} & q_{des} & w_{des} \\ p_{cod} & q_{cod} & w_{cod} \\ p_{tes} & q_{tes} & w_{tes} \end{pmatrix} \quad (1)$$

In such a matrix, the units of the attributes can be customized in practical use. For different types of development and different granularity, the units of productivity might be "pages per day", "lines per hour", "test cases per week" or something alike. And the unit of wage should be at the same time unit of productivity. The expected quality is a ratio without unit, which stands for percentage of the workload for the qualified part of the outputs out of the total workload of the execution. Here, the productivity and the expected quality of an operator could be described in various forms, including const value, normal distribution with given expectation and variance, some other types of distributions, and so on. The flexibility of the attribute definition depends on the description of the instability and the volatility of operators.

Qualitatively, an operator with higher capability would have higher productivity, higher expected quality and higher wage. For operators with similar wage, the productivity and the expected quality are under an inverse relationship, which offers opportunities to choose more felicitous operators for projects with different concerns and restrictions. It does not require all the values be assigned in an attribute matrix. The assignment depends on the capability of the operator for different development stages and the historical project data or other results of empirical studies. The details for the value assignment are beyond the scope of this paper, and will not be discussed here.

4.3 Definition of Activities

The activities should be described for the further simulation and analysis. In this study, FA is described by a triple as expression $FA : (T, S, C)$, in which T and C stands for the type and the complexity of the FA, and S stands for the expected scale of the FA's output. For TAs, they are combination of one FA and one QA, so that they can be described by a quadruple $TA : (T, S, C, R)$, in which T, S, C are the attributes of the inside FA, and R stands for the quality requirement of the inside QA.

For example, tuple $TA1 : (DES, 10, 1, 0.9)$ means $TA1$ is a trustworthy activity for design, its expected scale of the output is 10 pages and its complexity is 1; for quality requirement, it cannot be finished until its correct percentage is proven to reach or exceed 90%.

As for assignment of human resources for process activities, there needs only one operator for a FA, whereas it needs two operators for a TA: one for the inside FA, and the other for the inside QA. An assignment is described by a tuple (FA, Op) or (TA, Op, Op'). To simplify the simulation model, the capability of the QA's operator is unified and fixed as expression 2 shows:

$$Op' : (\tilde{P}', \tilde{Q}', \tilde{W}')^T = \begin{pmatrix} p_{req}^{QA} & 1 & w_{req}^{QA} \\ p_{des}^{QA} & 1 & w_{des}^{QA} \\ p_{cod}^{QA} & 1 & w_{cod}^{QA} \\ p_{tes}^{QA} & 1 & w_{tes}^{QA} \end{pmatrix} \quad (2)$$

Expression 2 assumes that the correctness of QA is 100%; in other words, a QA operator can correctly find all the weaknesses in the inside FA's outputs, avoiding missing reports and error reports.

For a TA, if the quality of the output of the inside FA fails to reach the quality requirement, the TA, including the inside FA and QA, should be reworked to enhance the output quality. Here it is assumed that rework could always increase the quality of output by certain percentage, and the rework only takes upon the erroneous part of the output; in other words, the workload of rework would decrease time and again.

4.4 Analysis for the Process Quality

From the description above, the quality of whole process, which is structured by single activities, could be estimated by the combination of quality of involved activities. Quantitatively, the quality of output of a certain type FA, without a corresponding QA, depends on the assigned operator's expected quality of output for such type of FA. And the quality of output of a TA depends on the quality requirement R. Depending on the way of combination of activities, the quality of process can be estimated by the following rules.

- For process or virtual activity structured by sequential activities, the quality of process would equal the continued product of the quality of each activity.
- For process or virtual activity structured by parallel/choice activities, the quality of process would equal the minimum one of the quality of all activities.
- For process or virtual activity structured by both sequential and parallel/choice activities, the above rules can be used recursively.

For example, there is a process structured by four sequential FAs, whose quality are $\{0.8, 0.85, 0.8, 0.9\}$. By the first rule, the quality of process would be $Q_{Process} = 0.8 \times 0.85 \times 0.8 \times 0.9 = 0.4896$. And for the same process, the FAs are shifted to TAs, whose quality are $\{0.9, 0.9, 0.9, 0.9\}$, then the quality of process would be $Q_{Process} = 0.9 \times 0.9 \times 0.9 \times 0.9 = 0.6561$, which is 34% enhanced in quality from the update.

5. Simulation Modeling

Based on the above description of operators and activities, the simulation model can be further built by as-TRISO/ML language. Since the estimations of operator's productivity and quality can hardly be fixed on a certain value, in the simulation model, the two variables are arranged to a normal distribution, in which the attributes are described by the expectation and variance of the distribution. Higher expectation of the distribution means better operator, whereas higher variance of it means higher instability of the operator. Qualitatively, an operator with higher expectation and lower variance would have higher capability. On the other hand,

the wage of operators, the scale and complexity of activities are treated as fixed values rather than stochastic variables in the simulation.

To build a simulation model of quality enhanced software process requires the following steps:

1) Describe a quality-enhanced software process by as-TRIOS/ML modeling language. First model all of the FAs or functional activities, then select the quality sensitive FAs, and then insert QAs or quality assurance activities to generate TAs or trustworthy activities, in order to enhance the overall quality of the process.
2) Instantiate the as-TRISO/ML process model, i.e. assign the complexity, scale, and quality requirement of the proper actual activities.
3) Assign operators for the activities, i.e. introduce the parameters related to operators into the simulation model.

5.1 Process Modeling and Its Instantiation

Due to the limited space, this paper skips the first step of simulation modeling, and directly takes the software process model described by Fig.2 for example. As is described, the as-TRISO/ML model describes a waterfall-like software process, in which only the first two activities are quality-sensitive and include explicit quality assurance activities inside. Then, the model should be instantiated and the operators should be assigned. Table 1 shows the assigned parameters related to process activities. The type, scale, complexity and operator of each activity are assigned separately in the table. Here, the activity $AA1$ and $AA2$ have an explicit quality threshold, which means they require the correct percentage must reach or exceed 95%; otherwise it must be reworked. In opposite, all of the passed thresholds of the rest AAs are 0, because there is no QA inserted for them in the process model, and they would be executed only once.

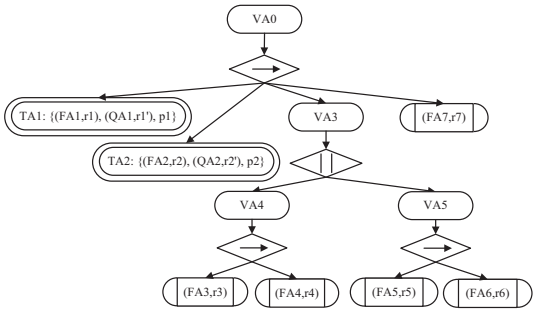

Fig. 3: Simplified process model graph

To simplify the presentation of the graph, this paper introduces a notation with twin lines to indicate the recursion or the TAs, in which the parameters needed by the recursion should be marked clearly and the caption of them should be TA plus the serial number. In addition, all the captions of the actual activities (AAs) in the process are updated by their actual features, either FAs or QAs. The simplified graph is showed in Fig. 3.

Table 1: The parameters assignment of the model

ID	Type	Scale	Complexity	Operator	Threshold
FA1	Req	20 pages	1	Op1	0.95
QA1	QA	20 pages	1	Op0	-
FA2	Des	5 pages	2	Op2	0.95
QA2	QA	5 pages	2	Op0	-
FA3	Cod	10 KLOC	0.8	Op3	0
FA4	Tes	10 KLOC	0.6	Op4	0
FA5	Cod	8 KLOC	0.8	Op5	0
FA6	Tes	8 KLOC	0.6	Op6	0
FA7	Tes	18 KLOC	0.5	Op7	0

On the other hand, the operators' attributes are shown in Table 2. Since the operators are assigned to only one task in the process, the focused attribute would be a certain row of his attribute matrix. For example, $Op1$ is assigned to a requirement activity in the process, so that in his matrix only the row related to requirement is significant, whereas the rest could be ignored in this process. To simulate the instability of operators capability, the productivity and quality of operators are described by a normal distribution $N(E, \sigma^2)$, in which, the expectation of the distribution E stands for the expected or average value of the attribute, and the variance σ stands for the possible deviation from the expectation. The normal distribution briefly describes the capability of human: E indicates the most possible value of the capability, for which the higher the better, and σ indicates the degree of instability of the capability, for which the lower the better. The property of normal distribution tells that the probability that the stochastic value falls into the intervals $E \pm \sigma$, $E \pm 2\sigma$ and $E \pm 3\sigma$ are 68%, 95% and 99% respectively, which implies that the value of the distribution would be around the expectation in most situations.

Table 2: The related attributes of the operators

ID	Matrix Row	Productivity	Quality	Wage
Op0	QA_{REQ}	$N(10, 1^2)$	1	600
Op0	QA_{DES}	$N(10, 1^2)$	1	600
Op1	Requirement	$N(2, 0.5^2)$	$N(0.8, 0.1^2)$	500
Op2	Design	$N(1, 0.2^2)$	$N(0.9, 0.08^2)$	800
Op3	Coding	$N(0.6, 0.1^2)$	$N(0.9, 0.05^2)$	700
Op4	Test	$N(0.4, 0.08^2)$	$N(0.85, 0.06^2)$	400
Op5	Coding	$N(0.55, 0.1^2)$	$N(0.88, 0.04^2)$	500
Op6	Test	$N(0.5, 0.1^2)$	$N(0.9, 0.08^2)$	550
Op7	Test	$N(1, 0.15^2)$	$N(0.9, 0.03^2)$	800

After the assignment of parameters of activities and operators, the duration parameter r of each activity could be computed by formula 3.

$$r = \frac{Activity.Complexity \times Activity.Scale}{Operator.Productivity} \tag{3}$$

in which, $Operator.Productivity > 0$.

The formula means the value of r is direct proportion to the complexity and scale of the activity itself, and inverse proportion to the productivity of the assigned operator. Since the productivity of operators obeys normal distribution, the value of duration obeys the reciprocal of normal distribution, whose analytic expression is rather complex and unpractical, so simulation is a proper method to analyze it.

5.2 Simulation Analysis

After all of the above preparation, the simulation model can be executed in our prototype simulation environment called *TRISO/IT*. TRISO/IT is an integrated toolkit for software process modeling, simulation, and analysis. In TRISO/IT, the modeling is user-friendly, and the simulation and analysis are very efficient. It would take only several seconds to run the simulation model described in Fig.2 for hundreds of thousands of times and output the simulation results on an Intel Core i5 2.4G processor with 4G RAM. Furthermore, by the increase of the model scale, the execution time would increase in a liner way.

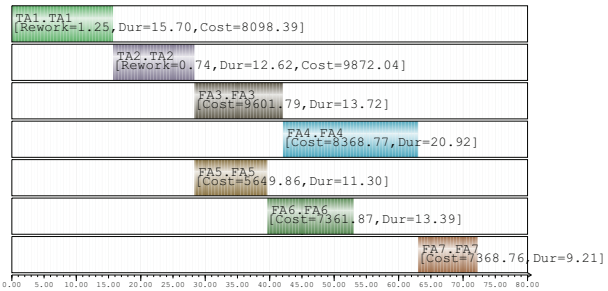

Fig. 4: The Gantt Chart generated from the simulation

Fig. 4 shows the Gantt Chart generated from the simulation result of the described process. The figure describes the expectation of the duration and cost and the average rework time of activities, as well as the temporal relationship among the activities. It can be found that the first trustworthy activity, which is a combination of one functional activity and one quality assurance activity, would take 15.70 days and cost 8098.39 units of money to be finished in expectation, and the expected rework times is 1.25 times, which means, in average, it needs 1.25 times of execution to achieve the quality requirement of such a TA. Similarly, trustworthy activity TA2 would take 12.62 days and 9872.04 units of money with 0.74 time of rework. All the rest activities are only functional activities without any corresponding quality assurance activities added, and the expected duration and cost are marked in the figure for each FAs. From the figure, we find that the expected duration of the process is 72.24 days and the expectation of the total cost is 56371.59 units of money.

In addition, to evaluate the availability of the approach and compare the simulation results, we run the simulation model once again with different parameter settings. In the second simulation, the quality requirements of the two TAs are assigned to be 0, which means they can be finished in exactly one execution with any level of quality of outputs, and the quality of outputs only depends on the quality of the internal FA's operator. In other words, the rework activities would be absent in such a process. From the process quality estimation rules, the quality of the first process with rework is $Q_1 = 0.95 \times 0.95 \times REST = 0.9025 \cdot REST$, and the quality of the second process without rework is $Q_2 = 0.8 \times 0.9 \times REST = 0.72 \cdot REST$. In the expressions, $REST$ indicates the quality combination of FA3 to FA7, which remains the same in the two models. Comparing Q_1 and Q_2, it can be found that the quality of the former is significantly better than that of the latter.

Fig. 5 shows the Gantt Chart of the second simuation. In the figure, the expected duration and cost of TA1 is 12.80 days and 6601.90 units of money, saving 2.9 days and 1496.5 units of money. Similarly, in such a process, TA2 is shorter in duration, lower in cost. In a macro view, the total duration of the process is 68.12 days, and the total cost of it is 53970.18 units of money.

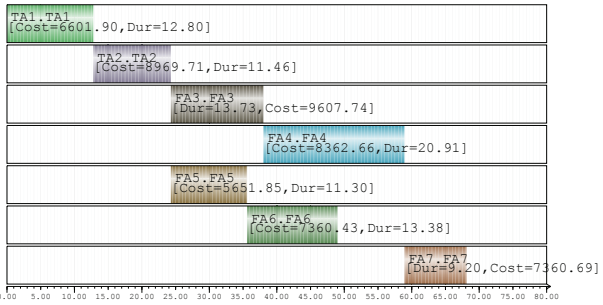

Fig. 5: The Gantt Chart generated from the non-rework simulation

Furthermore, the distribution of duration and cost of simulated models could be analyzed. Fig. 6 shows the distribution of duration of the two process models. In the figure, the vertical axis indicates the probability, and the horizontal axis indicates the number of days. The left curve stands for the second simulation and the right curve stands for the first. The marked points on the two curves are the expectation of execution durations. From the figure, the probability to finish the whole process within the expected number of days is 57.70% for both simulations. And for 95% confidence interval of the distribution, the duration of the first and the second process would not exceed 84.95 days and 80.24 days.

Similarly, the cost distribution is shown in Fig.7, in which the vertical axis indicates the probability and the horizontal axis indicates the money cost. The left curve stands for the second simulation and the right curve stands for the first. The marked points on the two curves are the expectation of cost of the two processes. The probabilities to finish the whole

process within the expected cost are 56.96% and 57.27% for the first and second simulation respectively. And for 95% confidence interval of the distribution, the cost of the first and the second process would not exceed 64106.39 and 61307.70 units of money.

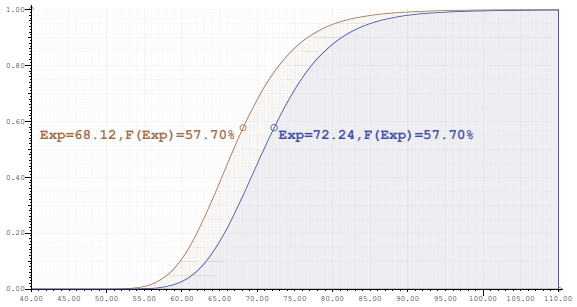

Fig. 6: The comparison of the two duration distributions

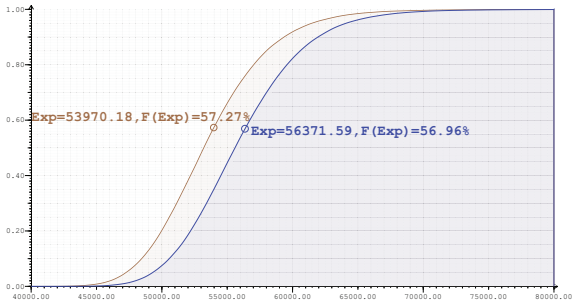

Fig. 7: The comparison of the two cost distributions

From the statistics of the simulation, it is clearly show that the process cost and duration are significantly affected by the rework activities. As the cost and duration of the process are increased in a quality enhanced process, the quality of such a process is improved accordingly. The simulation approach may quantitatively help users make a trade-off between the cost/duration and the quality of a process in order to reach a balance in an integrated consideration at last.

6. Conclusion

Quality is an important factor for software. Software process would greatly benefit the quality of the output software, if the process is carefully designed and closely analyzed. It is obvious that adding quality assurance activities into a software process would improve the quality of the output software, if the other factors remain the same. On the other hand, if the quality of a process is enhanced, the quantity of rework activities as well as the cost/duration of the process will increase. In such situation, it is important to estimate the effect of such reworks and balance the cost/duration of the process and the quality of the products.

In this paper, a novel simulation modeling approach is introduced to quantitatively analyze and predict the impacts of rework in a software process within certain resources and constraints. To analyze quality enhanced software processes, the factors related to rework, such as the quality requirement, the expected quality of operators and so on, are carefully described and modeled in the approach. With the process model and the description of critical factors, the simulation could be executed then to analyze the impacts of reworks. The case study shows the procedure of the simulation modeling approach. In addition, the comparison between the results from two times of simulation with different factor settings exhibits the capability and the availability of the approach.

7. Acknowledgement

This work is supported by the National Natural Science Foundation of China under grant No. 90718042, 60903051, 61073044, the Hi-Tech Research and Development Program (863 Program) of China under grant No.2007AA010303, 2007AA01Z186, Collaboration Project Between Chinese Academy of Sciences and Guangdong Province under grant No.2009B091300131, as well as the National Basic Research Program (973 program) under grant No. 2007CB310802.

References

[1] K. Butler and W. Lipke. Software process achievement at tinker air force base. Technical Report Technical Report CMU/SEI-2000-TR-014, Carnegie-Mellon Software Engineering Institute, Sept. 2000.

[2] A. G. Cass, S. M. S. Jr., and L. J. Osterweil. Formalizing rework in software processes. In F. Oquendo, editor, *Software Process Technology*, volume 2786 of *Lecture Notes in Computer Science*, pages 16–31. Springer Berlin / Heidelberg, 2003.

[3] M. Diaz and J. King. How cmm impacts quality, productivity, rework, and the bottom line. *CrossTalk: The Journal of Defense Software Engineering*, Mar. 2002.

[4] A. Law. *Simulation Modeling and Analysis*. McGraw-Hill, 2000.

[5] D. Liu, Q. Wang, J. Xiao, J. Li, and H. Li. Rvsim: A simulation approach to predict the impact of requirements volatility on software project plans. In Q. Wang, D. Pfahl, and D. M. Raffo, editors, *ICSP*, volume 5007 of *Lecture Notes in Computer Science*, pages 307–319. Springer, 2008.

[6] R. J. M. Marc I. Kellner and D. Raffo. Software process simulation modeling: why? what? how? *Journal of Systems and Software*, 46(2):91–105, 1999.

[7] E. D. N. T. Haley, B. Ireland and R. Dion. Raytheon electronic systems experience in software process improvement. Technical Report Technical Report CMU/SEI-95-TR-017, Carnegie-Mellon Software Engineering Institute, Nov. 1995.

[8] C. P. Team. Cmmi for development, version 1.2 - improving processes for better products. Technical Report Technical Report CMU/SEI-2006-TR-008, Carnegie-Mellon Software Engineering Institute, 2006.

[9] A. Wise. Little-jil 1.5 language report,. Technical report, Department of Computer Science, University of Massachusetts, 2006.

[10] J. Zhai, Q. Yang, F. Su, J. Xiao, Q. Wang, and M. Li. Stochastic process algebra based software process simulation modeling. In Q. Wang, V. Garousi, R. J. Madachy, and D. Pfahl, editors, *ICSP*, volume 5543 of *Lecture Notes in Computer Science*, pages 136–147. Springer, 2009.

[11] H. Zhang, B. A. Kitchenham, and D. Pfahl. Software process simulation modeling: An extended systematic review. In J. Münch, Y. Yang, and W. Schäfer, editors, *ICSP*, volume 6195 of *Lecture Notes in Computer Science*, pages 309–320. Springer, 2010.

Optimizing Operation Scheduling for In-Memory Databases

Christian Schwarz, Vadym Borovskiy, Alexander Zeier
Hasso Plattner Institute, University of Potsdam, Potsdam, Germany

Abstract—*A Computer system is a sophisticated combination of software and hardware components that work closely together to solve today's problems. While algorithms within a software component itself can be implemented and optimized by a small group of developers, algorithms for an entire software stack are more complex and their development gets expensive. To speed up the development of in-memory database specific scheduling algorithms for operating systems, we implemented a simulation model based on SAP's TREX in-memory column database. This simulation is used to optimize query scheduling and execution algorithms without the necessity of modifying every component within the existing system. To quantify the advantages and drawbacks of the different scheduling algorithms, we use the Star Schema Benchmark to measure the cost reduction per user with regards to the implemented operating system scheduling techniques.*

Keywords: Database Simulation, In-Memory Database, Operation Scheduling

1. Introduction

Multi-core processors and many core systems are a reality today. While the gaming industry adopted and used those techniques from the early days, it has taken enterprise systems longer to see the benefits of parallel algorithms. The reason is that enterprise systems typically use a multi-tier architecture, where each component can be scaled-out regarding to the customer's needs. To take advantage of those parallel computing resources available different approaches are used: increasing either the number of parallel processes within the system or the degree of parallelism within the systems algorithms.

The first approach enables the enterprise systems to serve more users in parallel, while maintaining the systems performance characteristics. With the increasing workload on the enterprise system, synchronization between different processes and resource contention become more challenging issues. A drawback that has to be discussed as well is that even if a system's performance characteristics would not change for a single process it is not possible to gain speed up from the parallel processing units for the single user enabling more complex operations, such as forecasting functions or what-if analysis within sub-second response times. During peak loads, the system can handle more transactions, while during non-peak situations a lot of resources will not be used.

The second approach, increasing parallelism within the systems algorithms requires more development effort. Existing algorithms must be modified and developed to take advantage of parallelism and new algorithms not fixed to sequential processing. Thus not only the number of users can be increased, it enables speeding up single queries and new, more complex operations can be developed that had been unthinkable before.

The availability of huge main memory within a single-server system enables in-memory databases to become reality in today's enterprise environments. Their performance characteristics allow the vision of combined workload scenarios and the end of data warehouses [1]. The missing hard disk I/O waiting time makes operation scheduling an important issue for in-memory databases. While the bottleneck moves from the storage media closer to the CPU, queries and their corresponding database operations have to be scheduled in an intelligent manner to maximize the performance benefits for the user. While it is a complex task to implement new scheduling algorithms in a real world operating system, an implementation within a detailed simulation model of such systems is more feasible to evaluate the benefits and drawbacks of new algorithms, such as scheduling techniques.

For the work of this paper, we implemented a detailed simulation for the in-memory database system TREX, which is the main component of SAP's Business Warehouse Accelerator [2]. The implemented simulation model includes multiple scheduling algorithms that are benchmarked against each other. We give a detailed description of our simulation model in section 2. In section 3 we present the implemented scheduling strategies. The used benchmark is presented in section 4 followed by the evaluation of the implemented algorithms in section 5. Section 6 presents related work in the area of database simulation, parallel query execution and scheduling algorithms, followed by our conclusion in section 7.

2. Simulation Model

Based on SAP's TREX in-memory column database, we build a simulation model funded on the principles of network queuing model techniques and parallel discrete event simulation [3], [4]. The model consists out of six major parts: tenants and users, queries and operations, servers and processors. All of those parts represent their real world instances.

Tenants and users build the SQL query generating part of the simulation. While the data of multiple tenants are served

by the same database process, tenants are not to be able to share data between each other. To isolate tenants within the shared process, data of different tenants is isolated into different tables [5]. A tenant is defined by its amount of data and the number of users corresponding to its data. A user generates queries that have to be processed by the database. After the user receives the response to its query, he spends a specific think time and sends the next query afterwards. The think times of the users are gamma distributed which represents a typical distribution in web based scenarios [6].

Queries, generated by the user get parsed into an acyclic data flow execution graph containing database operations. **Operations** are defined by their inputs, outputs and required resources, such as memory bandwidth and CPU cycles. Those resources are traced during multiple executions of the benchmark queries. Details about query processing are presented in subsection 2.1.

A Server is defined by its available main memory and the number of installed processors. The server uses a specific scheduling algorithm to schedule its operations. While the arrival rate is defined by the users of all tenants placed on the server, the number of available service centers working on operations is limited by the available processors within the server. A **processor** has a predefined memory bandwidth and a fixed clock rate. While the bandwidth determines the maximum amount of data that can be transferred in a certain amount of time, clock rate limits the number of CPU cycles the processor can execute per second. Each processor can only work on one operation at the same point in time. Multi core CPUs are modeled as independent processors.

2.1 Query Processing Details

After a query has been send to and received by the database, a query execution plan is created. A simplified example of a query execution plan for Star Schema Benchmark Query 4.2 (shown in Figure Figure**??**) is shown in Figure 2. TREX uses data flow execution techniques to minimize communication overhead and to optimize inter operator parallelism within a multi core server. Operations having all inputs available can be scheduled for execution. During their execution they will create outputs and consume memory bandwidth and CPU cycles. Like in TREX each operation is is executed by a separate operating system thread. The maximum number of parallel threads within the system can be defined in the TREX engine and thus in the simulation. While each query gets one guaranteed execution thread, a thread pool with a defined maximum number of spare threads for scheduling of parallel operations within the same query is available and shared between all queries. If spare threads are available, queries can execute operations in parallel that do not depend on each other.

A scheduled operation consumes up to the maximum of available resources for its scheduled execution. If the operation has to consume more than the available resources

```
SELECT d_year, s_nation, p_category,
  SUM(lo_revenue - lo_supplycost)
  AS profit
FROM date, customer, supplier, part,
  lineorder
WHERE lo_custkey = c_custkey
  AND lo_suppkey = s_suppkey
  AND lo_partkey = p_partkey
  AND lo_orderdate = d_datekey
  AND c_region = 'AMERICA'
  AND (p_mfgr = 'MFGR#1'
    OR p_mfgr = 'MFGR#2')
GROUP BY d_year, s_nation,
  p_category ORDER BY d_year,
  s_nation, p_category
```

Fig. 1: SQL for Star Schema Query 4.2

within its scheduled time frame, it will partly consume them and has to be rescheduled. An operation that finishes before the end of its time frame allows the next operation to be scheduled immediately for a full schedule time frame without waiting for the predefined scheduled time slot. An operation can only be scheduled on one processor at a time, which is a limitation of the used database. Thus operations represent the minimum unit of parallelism within our model.

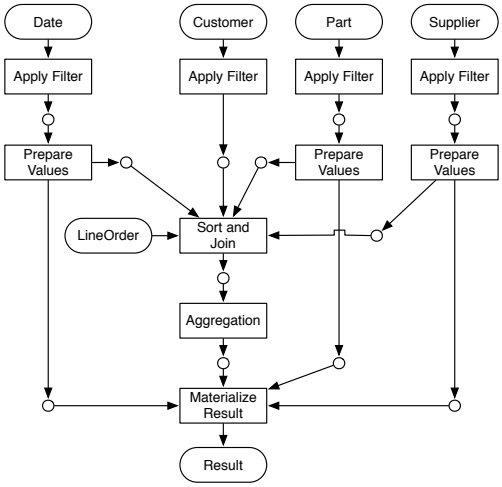

Fig. 2: Simplified Query Execution Plan for Star Schema Query 4.2

While bandwidth and required CPU cycles differ between different tenant sizes and queries, we executed each query several times for tenants with scaling factors between 0.05 up to 20. Each query from the used benchmark was executed and traced more than 200 times to capture the required detail for each operation. The required CPU cycles and memory bandwidth for each operation of a specific query type was

extracted to build a function that calculates the required resources within the simulation. During those benchmark runs, the noise from other system processes, such as cron jobs, was below 1.2 %, therefore we decided not to model them in our simulation.

3. Scheduling Algorithms

To evaluate the influence of operating system scheduling on the performance of in-memory databases, we implemented several scheduling algorithms. The details of those algorithms are presented in this section.

The random scheduler *(random)* maintains a single queue for the server that contains all operations that have to be executed. If a processor becomes available, it reduces the list of operations to a list of operations that can be scheduled at this time. From this new list of operations a random operation is chosen for execution on the available processor. If the operation was finished within its scheduled time frame, it will be removed from the original list.

Two **first in - first out strategies** were implemented for this paper, append-fifo *(afifo)* and hot-standby-fifo *(hsfifo)*. Both maintain a single list of operations for the server and differ in the way an operation is handled that could not be scheduled is handled. If a processor becomes available for execution, both schedulers start at the beginning of their operation queues and search until all operations are checked or an executable operation has been found. If an operation can be scheduled it is removed from the list and sent to the processor for execution. If an operation cannot be scheduled, the append-fifo scheduler puts the operation to the end of its operation list. The hot-standby scheduler checks the next operation without changing the original operations position in the list. After an operation was executed, it gets appended to the end of the list, if it could not consume all of its required resources during its execution time frame.

The finisher *(fin)* works like the hot-standby-fifo, with an infinite time frame for execution. A scheduled operation is executed until it could consume all of the required resources. The fin scheduler does not require any reschedules of operations.

The operation aware scheduler *(ops)* is based on knowledge collected during test runs for the simulation model. It uses the same technique as the hot-standby-fifo scheduler for maintaining operation queues. The operation aware scheduler maintains multiple queues for different database operations. Based on the insights from our test runs that the aggregation within the database queries consumes the majority of the resources required within a query (Figure 3), aggregations are kept in a separate queue from all other operations. If an aggregation and a non-aggregation operation can be scheduled, the aggregation has the processor for a 2.5 times longer time frame than other operations and a counter is increased. This is done, until the counter reaches two. In that case, the operation that was inserted into the schedulers queues earlier gets scheduled. If a non-aggregating operation is scheduled the counter will be reset to zero. Because aggregations represent the most resource consuming operations, make intensive usage of CPU caches and represent the last operations of all used analytical queries, this raises the odds to complete nearly finished queries within the given SLOs.

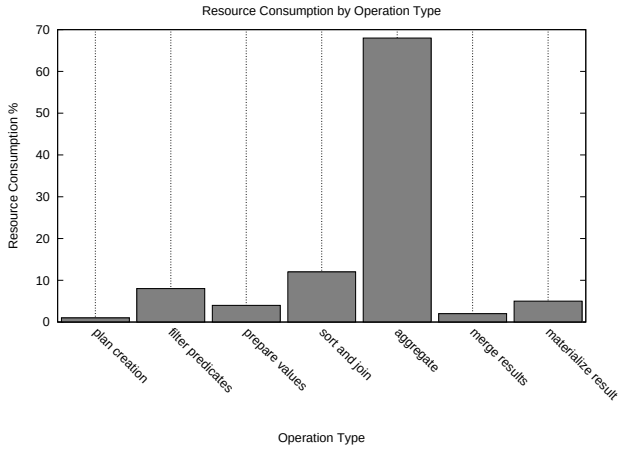

Fig. 3: Average resources consumption by operation type

4. Benchmark Definition

The implemented scheduling algorithms will be benchmarked in a multi-tenant web-based analytics scenario. This includes a service level objective (SLO); a specified percentage of all executed queries has to be processed within the specified response time goal. We used queries from the Star Schema Benchmark (SSB) [7], which itself is a modified version of the TPC-H benchmark for analytic workload [8]. The SSB consists out of four so called query flights, each flight representing a drill down operation into the tenant's data. A tenant's data consists of four dimension tables (customer, part, supplier, date) and one fact table (lineorder). The size of those tables is modified by the scaling factor. Multiple tenants with varying scaling factors and a corresponding number of users are used.

A user of a specific tenant will send all SSB queries of a randomly selected query flight in sequential order. The selection of the query flight is distributed equally among all users of the tenant. The think time between receiving a query result and sending the next query to the database system is gamma distributed between 1 and 25 seconds with the highest probability between 5 and 6 seconds for all users. The probabilities for all think times are shown in Figure 4.

During our test runs in the real system, where we collected the information about the required resources of each operation within the queries, we measured a background noise below 1.5 %. Due to this negligible number, we decided

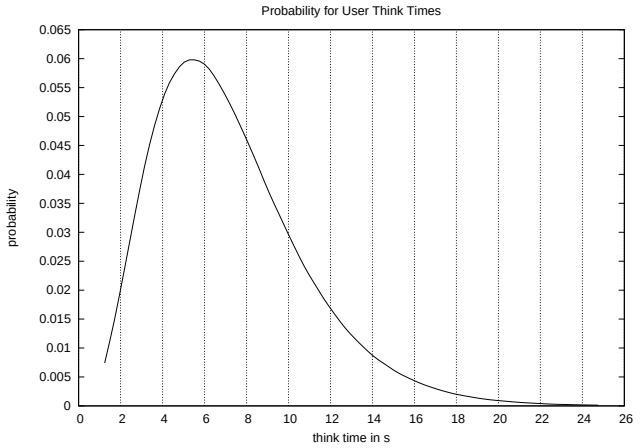

Fig. 4: Think time probabilities for all users

not to simulate any non query related operations within the system.

5. Evaluation

To evaluate the difference between our scheduling algorithms, we simulated them with different schedule time frames. During the simulation we had to fulfill the following service level objectives:

- response time goal is 1 second
- 99 percent of all queries have to be answered within the response time goal
- every query has to be processed

The optimization goal was to serve as many users as possible with a single server instance. We increased the number of users, until the service level objectives could not be met anymore for a simulated sliding window of 5 minutes.

Two different strategies are used to determine the number of users per tenant. The first one is the *constant user scaling*, where each tenant has the same number of users, regardless of its scaling factor. The second one is the *logarithmic user scaling*. Each tenant has a different number of users, depending on its data size. Tenants with more data have more users than smaller tenants with less data. This shifts the workload to more long running queries.

The results for the constant user scaling are shown in Figure 5. As to be expected, the fin scheduler is not influenced by the size of the schedule time frame, because an operation that is scheduled would be executed until it is finished. Our optimized scheduling algorithm uses its knowledge about the internal query structure. It achieves up to 21 % more users in system throughput, than all other scheduling algorithms. The *hsfifo* stays above the *afifo* algorithm, because the aggregation operations of all queries stay in front of the fifo queue until they get executed for the first time, instead being appended at the end, before the first run. This increases the chance to finish a query within the given SLOs. The *rand* scheduler is the worst for the constant user scaling, because the odds of finishing a query reduce if more queries arrive at the server.

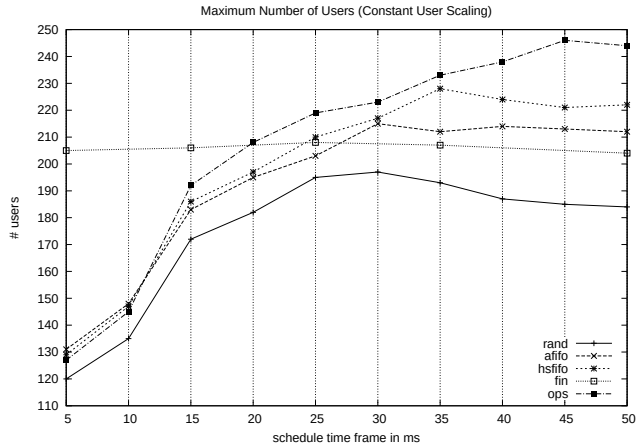

Fig. 5: Maximum number of users with constant user scaling

Figure 6 shows the results for the logarithmic user scaling method. Based on the higher average required resources per user, the number of users that can be served by the system is decreased for all scheduling algorithms. The main difference to the constant scaling regarding the overall performance consists in the fact that both fifo algorithms deliver nearly the same result. The average aggregation takes more resources which reduces the *hsfifos* benefit. Our optimized scheduling algorithm still performs up to 16 % better than all other algorithms.

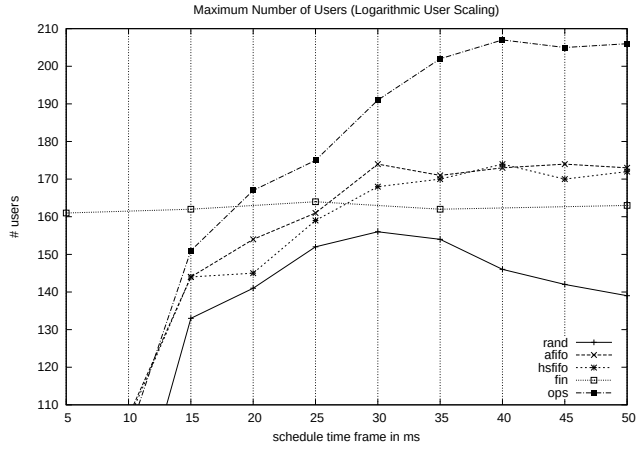

Fig. 6: Maximum number of users with logarithmic user scaling

If we compare both scaling variants, all scheduling algorithms decrease their throughput by nearly the same factor. The rand scheduler decreases by 21 %, *afifo* by 19 %, *hsfifo* by 24 %, *fin* by 22 % and *ops* by 17 %. Nevertheless, the *ops* algorithms seem to be less fragile, when it comes to

different query load situations. In both user scaling variants, the numbers of users that can be served increases with the size of the scheduling time frame, because the chance to finish a short running operation increases and less rescheduling operations are necessary. That there is a necessity to reschedule operations if they take to many resources is shown by the bad performance of the *fin* algorithm. If it is used, aggregations block other short running operations from finishing in time.

6. Related Work

Using simulation models to evaluate algorithms is a prominent methodology when it comes to parallelism within a database system. While parallel databases such as Bubba [9] and Gamma [10] had to use complex simulation models that captured the important hardware and software components of a computer system, the details to build a simulation model of all components of an in-memory database are less complex.

Discrete event simulation represents a technique to model problems in computer science [11]. The main idea is to use a reference dataset captured from a real world system to simulate system components as a network of queues and service centers. That is why a variety of simulation frameworks such as Simjava [12], Ptolemy [13] and Parsec [14] exist. To optimize existing and developing new algorithms, application system specific simulators have been built to incorporate the specifications of existing systems, such as a simulator for large-scale networks [15]. Within this paper we tried to build a detailed simulator for in-memory databases. Using a white box query execution model to understand the internal parallelization of the examined SAP TREX database helps us to implement new algorithms within a short period of time.

The optimization of database queries and their execution is a heavily researched topic [16], [17]. During the last years the availability of multi core processors increased the need of having optimized operating system scheduling algorithms for a large number of cores [18]. In the area of real-time database workload management two different types of algorithms can be defined: static and dynamic. Static algorithms require the knowledge of the set of tasks that have to be scheduled as well as their constraints. Dynamic algorithms can be split into algorithms for resource sufficient environments and resource insufficient environments [19]. An orthogonal differentiation can be applied as well: internal and external workload management. Internal management algorithms control the available resources like main memory and processing units, while external management is based on admission control to manage the queries that have to be executed by the database in parallel. To develop algorithms for internal workload management, early studies used simulation models for disk based databases [20], [21]. The usage of priority based algorithms to schedule the least available resources seem to be sufficient for disk based systems [22].

The problem to build an optimized scheduling mechanism for high performance in-memory database systems that takes both, operating system requirements and database operations into account is not solved yet.

7. Conclusion and Outlook

In this paper we presented the benefits of simulation for software developers at the example of an in-memory database scheduling algorithm. Understanding and modelling a complex system improves the implementation speed for new algorithms and enables the developers to evaluate and to validate new algorithms without the need to implement them in a complex system. Within our simulation we developed an optimized scheduling algorithm for in-memory databases that increases the overall performance while the transaction throughput of the database system gets higher. We took advantage of the predictability of in-memory databases that are not restricted to slow disk I/O and our simulation could focus on the new bottleneck of in-memory databases, such as memory bandwidth and available CPU resources. The implemented scheduling algorithm outperformed all other implementations by 10 to 20 % in regard to the number of users that could be served by the system, reducing the costs per system user.

To validate those first results more tests have to be done. The chosen tenant layout has to be modified and the scaling of users needs to be re-evaluated with real companies. The built simulation needs to be revalidated with other scenarios and more transactional workloads to make it a framework for in-memory database development and simulation.

References

[1] H. Plattner, "A common database approach for oltp and olap using an in-memory column database," *SIGMOD '09: Proceedings of the 35th SIGMOD international conference on Management of data*, Jun 2009.

[2] T. Legler, W. Lehner, and A. Ross, "Data mining with the sap netweaver bi accelerator," *Proceedings of the 32nd international conference on Very large data bases*, pp. 1059–1068, 2006.

[3] E. Lazowska, J. Zahorjan, G. Graham, and K. Sevcik, *Quantitative system performance: computer system analysis using queueing network models*, 1984.

[4] A. Ferscha and S. Tripathi, "Parallel and distributed simulation of discrete event systems," *Parallel and distributed computing handbook*, pp. 1003–1041, 1996.

[5] D. Jacobs and S. Aulbach, "Ruminations on multi-tenant databases," *BTW Proceedings*, 2007.

[6] G. Bai and C. Williamson, "Time-domain analysis of web cache filter effects," *Performance Evaluation*, vol. 58, no. 2-3, pp. 285–317, 2004.

[7] P. O'Neil, E. O'Neil, and X. Chen, "The Star Schema Benchmark (SSB)," *Pat*, 2007.

[8] T. P. P. Council, "TPC Benchmark H - standard specification revision 2.12.0," pp. 1–139, Jun 2010. [Online]. Available: http://tpc.org/tpch/default.asp

[9] H. Boral, W. Alexander, L. Clay, G. Copeland, S. Danforth, M. Franklin, B. Hart, M. Smith, and P. Valduriez, "Prototyping bubba, a highly parallel database system," *IEEE Transactions on Knowledge and Data Engineering*, vol. 2, no. 1, p. 24, 1990.

[10] D. DeWitt, S. Ghandeharizadeh, D. Schneider, A. Bricker, H. Hsiao, and R. Rasmussen, "The gamma database machine project," *IEEE Transactions on Knowledge and Data Engineering*, pp. 44–62, 1990.
[11] C. Cassandras, "Discrete-event systems," *Handbook of networked and embedded control systems*, pp. 71–89, 2005.
[12] F. Howell and R. McNab, "simjava: A discrete event simulation library for java," *SIMULATION SERIES*, vol. 30, pp. 51–56, 1998.
[13] S. Ha, J. Buck, E. Lee, and D. Messerschmitt, "Ptolemy: A framework for simulating and prototyping heterogeneous systems," *en.scientificcommons.org*, Jan 1992. [Online]. Available: http://en.scientificcommons.org/42882643
[14] M. Takai, Y. Chen, X. Zeng, J. Martin, and H. Yoon, "Parsec: A parallel simulation environment for complex systems," *IEEE Computer*, vol. 31, pp. 77–85, 1998.
[15] X. Zeng, R. Bagrodia, and M. Gerla, "Glomosim: a library for parallel simulation of large-scale wireless networks," *ACM SIGSIM Simulation Digest*, vol. 28, no. 1, pp. 154–161, 1998.
[16] W. Hasan, "Optimization of sql queries for parallel machines," 1995.
[17] L. Mackert and G. Lohman, "R* optimizer validation and performance evaluation for distributed queries," *VLDB '86: Proceedings of the 12th International Conference on Very Large Data Bases*, Aug 1986.
[18] J. Anderson, J. Calandrino, and U. Devi, "Real-time scheduling on multicore platforms," *Real-Time and Embedded Technology and Applications Symposium, 2006. Proceedings of the 12th IEEE*, pp. 179–190, 2006.
[19] J. Stankovic, C. Lu, S. Son, and G. Tao, "The case for feedback control real-time scheduling," *Real-Time Systems, 1999. Proceedings of the 11th Euromicro Conference on*, pp. 11–20, 1999.
[20] K. Brown, M. Carey, D. DeWitt, M. Mehta, and J. Naughton, *Resource allocation and scheduling for mixed database workloads*, 1992.
[21] M. Carey, R. Jauhari, and M. Livny, "Priority in dbms resource scheduling," *Proceedings of the Fifteenth International Conference on Very Large Data Bases: August 22-25, 1989, Amsterdam, The Netherlands*, p. 397, 1989.
[22] D. McWherter, B. Schroeder, A. Ailamaki, and M. Harchol-Balter, "Priority mechanisms for oltp and transactional web applications," 2004.

3-D Computer Aided Modeling and Analysis of Moving Load on a Bridge with Rough Surface

I. M. Muslih[1], I. Abu-Alshaikh[1]
[1]Department of Mechanical and Industrial Engineering, Applied Science University, Amman, Jordan

Abstract *- Computer modeling and simulation in mechanical engineering are essential for problems with many changeable parameters and complicated closed form solutions. In this study, modeling of the dynamic response of a moving load on a bridge with rough surface is demonstrated by using computer aided design software as an engineering modeling tool. The modeling is based on static and dynamic analysis. The vertical displacement of the body and forces applied to the bridge were both determined. The results from the modeling analysis were found to be in agreement with the results obtained from the analytical method for a one moving load case. Once the model is constructed and proved to be correct, it can be used in many other dynamic studies of moving loads with different variables where closed form solutions are not applicable.*

Keywords: Moving Load, Dynamic Analysis, CAD analysis, Pro/Engineer, Surface roughness.

1 Introduction

Three-dimensional complex mechanical engineering modeling has become more feasible and cost effective in the industrial field due to the recent increase in computing power, advanced computer aided design and simulation, and advanced implementation of physical and engineering concepts in commercial modeling software.[1][2][3]

In this study, the focus is particularly on the dynamic response produced by automobiles, modeled as moving loads, on a bridge with a rough surface and the forces produced by these moving loads on the bridge itself. Studying the dynamic response of the moving loads based on the nature of the problem at hand may include; analytical methods, numerical and finite element methods, [2][4]. Three-dimensional analysis and simulation was carried out due to the three-dimensional nature of the problem and to construct a workable model that can be used later in more complicated dynamic problems. The chosen software was *Pro-Engineer WildFire 4.0* for its advanced CAD system and advanced dynamic tools suitable for this study.

Both analytical solution and computer modeling of the dynamic response of the suspension system mechanism of the moving load due to base excitation of a rough surface were carried out and compared.

2 Mathematical Modeling

To carry out the dynamic analysis in this study; First, the bridge roughness was molded and then the analytical solution for both the vertical displacement of the moving load and the dynamic force produced by the suspension-system mechanism on the bridge was determined. The computer modeling analysis for the suspension-system mechanism of the moving load was compared with the results from the previous analysis.

The roughness of the bridge was modeled as a sinusoidal function of the expression:

$$y(t) = Y \sin(wt) \qquad (1)$$

Where, Y is the roughness amplitude and w is the moving body frequency. The suspension system has a spring with stiffness K and damper constant C as shown in Figure 1. and D is the cycle length.

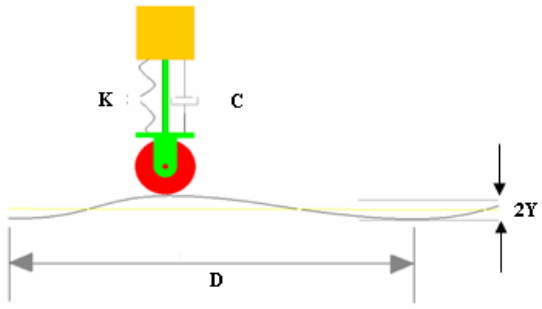

Figure 1 Modeling of the suspension system

The Analytical solution for the dynamic response of the suspension system with bridge roughness can be determined based on the equation:

$$\sum F = ma = m\ddot{x} = -F_s + (-F_d) = 0 \qquad (2)$$

Modeling the suspension system as a base excitation, the spring force is expressed as;

$$F_s = k(x - y) \qquad (3)$$

and the damper force is expressed as;

$$F_d = c(\dot{x} - \dot{y}) \qquad (4)$$

where, ***x*** is the body vertical displacement and y is the base displacement.[5][6]

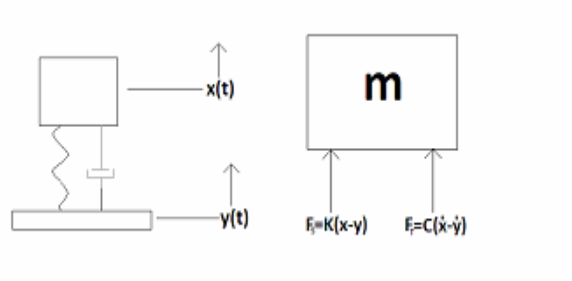

Figure 2 Forces and displacements definition.

By considering the bridge roughness model as the base excitation displacement, the equation of motion is;

$$m\ddot{x} + c\dot{x} + kx = cYw\cos(wt) + kY\sin(wt) \qquad (5)$$

The above equation can be expressed as:

$$m\ddot{x} + c\dot{x} + kx = A\sin(wt - \alpha) \qquad (6)$$

Where,

$$A = Y\sqrt{(k^2 + (cw)^2}\,\alpha \qquad (7)$$

And ,

$$\alpha = \tan^{-1}\left[\frac{-cw}{k}\right] \qquad (8)$$

The solution of equation (6) is;

$$x(t) = X\sin(wt - \phi) \qquad (9)$$

Where,

$$X = Y\left[\frac{1 + [2\xi r^2]^2}{[1 - r^2]^2 + [2\xi r]^2}\right]^{1/2} \qquad (10)$$

$$r = \frac{w}{w_n} \quad \text{and} \quad w_n = \sqrt{\frac{k}{m}} \qquad (11)$$

And,

$$\xi = \frac{c}{2\sqrt{km}} \qquad (12)$$

$$\phi = \tan^{-1}\left[\frac{2\xi r^2}{1 + (4\xi^2 - 1)r^2}\right] \qquad (13)$$

The two forces acting on the moving body from the base could be combined as one excitation force with a phase shift as follows.

$$F = F_T\sin(wt - \phi) \qquad (14)$$

Where,

$$F_T = mXw^2 \qquad (15)$$

3 CAD Modeling and Analysis

The parameters used in the theoretical analysis were implemented in Pro/Engineer WildFire 4.0 to perform a simulation analysis for the problem in hand and compare the results from both methods. [7]

A Pro/Engineer 3D Modeling tool, which is the Extrusion tool, was used to model the mechanism parts. The moving body mass, wheel part and the suspension base part were modeled as shown in Figure 2 to simulate the automotive suspension mechanism parts.

The rough bridge sinusoidal equation was implemented in Pro/Engineer modeler tool to exactly model the bridge as in the theoretical part.

A guide for the mechanism to force the body into moving in the direction of the rough bridge is modeled and added to the system by using the slider connection tool in Pro/Engineer. All the mechanism parts modeled were assembled in Pro/Engineer in the assembly file. The

suspension base was assembled in such way so slides inside the guide. The mass was assembled to slide over the suspension base using the slider connection tool as in Figure 3 (a) and (b). The wheel was assembled to role over the bridge using the pin connection tool as in Figure 3 (c).

A spring with a stiffness constant equals to ***K*** was created by using the Pro/Engineer spring tool. A damper of ***C*** value was created by using Pro/Engineer damper tool. To deal with the interaction and contact between the wheel and the rough bridge or road, a cam-follower connection was created to enable the wheel to roll over the bridge as shown in Figure 4. A mass of ***m*** in kg was applied to the mass part using the mass property tool. Also, the gravity acceleration was defined in the direction shown in the Figure 4.

The initial condition was created to start the simulation run at the beginning of the bridge by running a static analysis to determine the static deflection value to be used as an initial condition for the run to have only vibration from the rough bridge. A servo motor was created to implement a velocity of ***V*** to the moving object in the direction of the guide. A dynamic analysis was carried out to find the mass displacement response and the force on the system.

4 Results and Discussion

A car with mass of 1007 kg, a damper constant of C = $2x10^4$ N.sec/m and a spring constant of K = $4x10^5$ N/m where adopted as a case study based on real data.

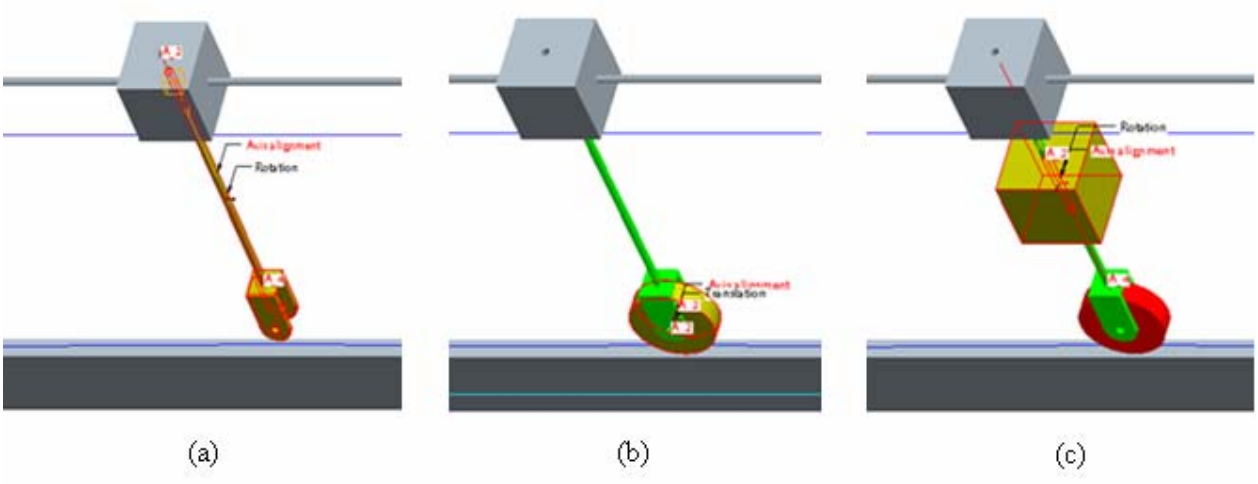

Figure 3 Modeling of the suspension system parts in the moving load model

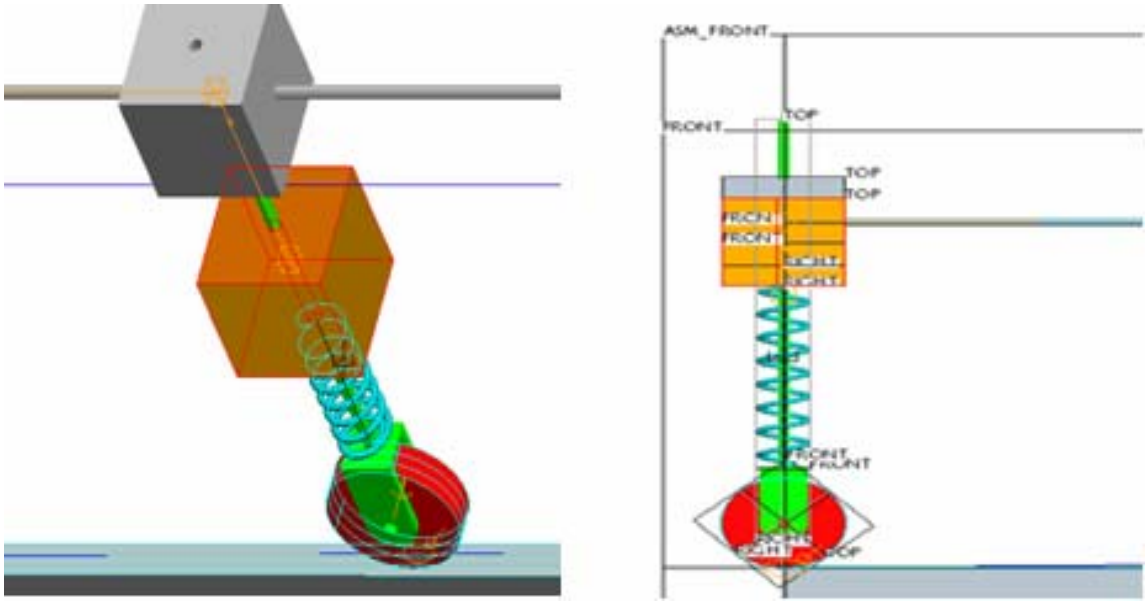

Figure 4 Complete modeling of the moving system

By using the analytical solution provided above, the damping ratio is equal to $\xi = 0.49$.

From this damping ratio, it is concluded that this is a case of an under-damped forced vibration because of $\xi < 1$. The frequency ratio is r = 0.876 where, w_n = 19.93 rad/sec , and w = 17.545 rad/sec. Also the maximum displacement of the car is X = .0294 m with a phase shift of Φ = 0.253 rad.

The final car displacement response equation is determined to be:

$$x(t) = 0.0294 \sin(17.454t - 0.253) \qquad (16)$$

The final force response is as follows;

$$F = 9.02x10^3 \sin(17.454t - 0.253) \qquad (17)$$

A Matlab program has been used to plot the response equations from the theoretical analysis and produced the results shown in Figure 5 and Figure 6 for both the displacement and force response where the maximum force recorded was ± 9.02x10^3 N and the maximum displacement recorded was 0.029 meter [8].

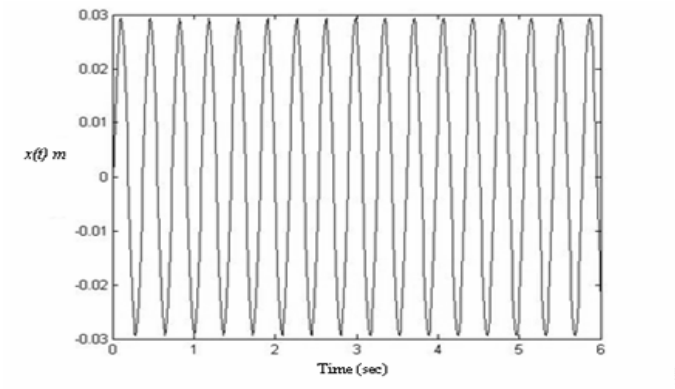

Figure 5 X-displacement – Analytical solution

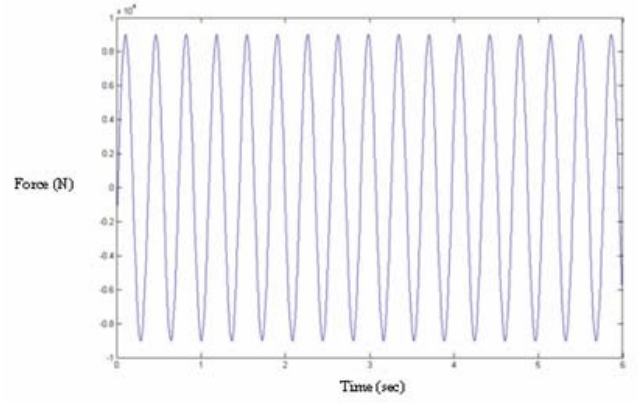

Figure 6 Force response – Analytical solution

The Pro/Engineer simulation model for the same case study produced the results shown in Figure 7 and Figure 8, respectively. The maximum force recorded was approximately ± 9.021x10^3 N which is only 0.01% in difference from the theoretical result. It should be noticed that in the Pro/Engineer modeling, the value of the mass weight was added to the force calculated.

The maximum displacement recorded was 0.028 meter which is 3.44% of the theoretical value. Pro/Engineer analysis has the distance between the mass and the reference coordinate system added from which the distance response is measured.

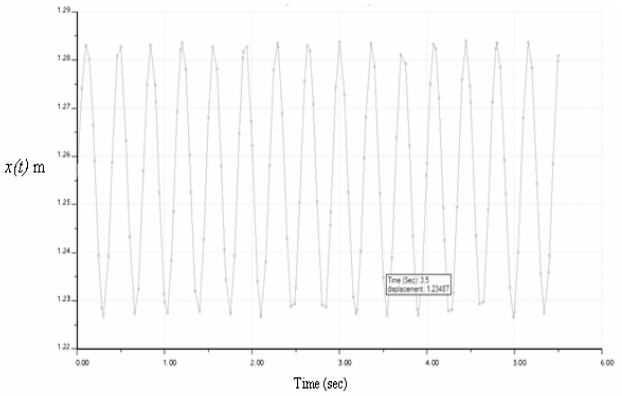

Figure 7 X-displacement – Modeling results.

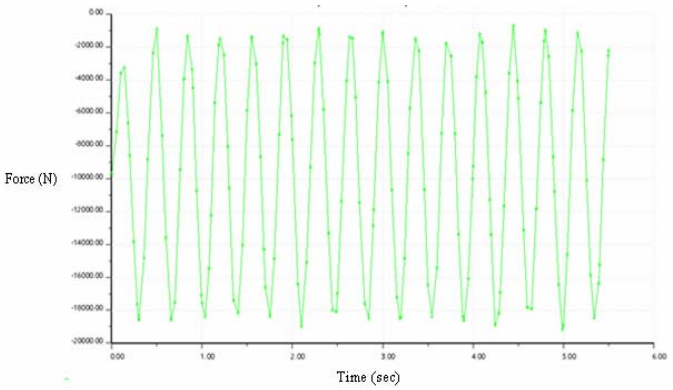

Figure 8 Force-response – Modeling results

5 Conclusions

In system dynamic modeling, there is no direct way to model the response of moving bodies with different velocity values and masses. Closed form solutions can be obtained for some simple cases. By using the capabilities of an available CAD software, a dynamic response model is

built to simulate the moving load problem where the mechanical model can be used to simulate any moving load with varying speeds of automobiles moving in the same or opposite directions on a bridge with rough surface. The forces generated in the system due to the dynamic moving load can be calculated

The produced model can be used as a block and saved in the database of the software. It can be called upon need during the process of bridge design analysis.

6 References

[1] Pesterev, A. V. and Bergman, L. A., "Response of Elastic Continuum Carrying Moving Linear Oscillator" ASCE Journal of Engineering Mechanics, Vol. 123, pp. 878{884 (1997).

[2] Abdel-Rohman, M. and Al-Duaij, J., "Dynamic Response of Hinged-Hinged Single Span Bridges with Uneven Deck" Journal of Computers and Structures, 59(2), pp. 291–299, 1996.

[3] Pesterev, A.V. and Tavrizov, G.A. "Structural Analysis Method for Dynamic Analysis of Conservative Structures" The International Journal of Analytical and Experimental Modal Analysis, Vol. 9, No. 4, pp. 302{316 (1994).

[4] Green, M.F. and Cebon, D., "Dynamic Response of Highway Bridges to Heavy Vehicle Loads: Theory and Experimental Validation," Journal of Sound and Vibration, Vol. 170, No. 1, pp. 51{78 (1994).

[5] Mechanical Vibrations, Singiresu S. RaoT, 4th Edition, 2003, Prentice Hall

[6] Engineering Vibration, Daniel J. Inman, 3rd Edition, 2007, Prentice Hall

[7] Pro/Engineer-documentation, Thttp://www.ptc.com/appserver/mkt/products/home.jsp?k=403TH.

[8] MATLAB, 2010. MATLAB help. The MathWorks, Inc. http://www.mathworks.com/access/helpdesk/help

Evaluation of Noise Reduction Techniques in two-dimensional Echocardiography Images in the Left Ventricular by Image Processing Algorithms Using Matlab Software

A. Elnaz golchin [1], **B. Saeed darvishi** [2]

[1]Department of Biomedical Engineering, Islamic Azad University- Science and research branch, Tehran, Iran
[2]Department of Biomedical Engineering, Islamic Azad University- Science and research branch, Tehran, Iran

Abstract - *Echocardiography images are usually corrupted by speckle noise. This noise reduces the image contrast and blurs the explanation of important spots in medical diagnosis. Since the speckle noise is destructive, the denoising procedure on the image, in comparison to other noises, is more difficult. It seems that the old techniques of noise suppression are not appropriate for removing the speckle noise. This paper presents the comparison of old techniques of improving the two-dimensional cardiograph images' quality in the left ventricular by Median, Adaptive wiener and Kaun filters to the latest methods of denoising based on the wavelet transformation and wavelet packets. Then the resulted data are compared with the results of other noise suppression techniques. In the filters' comparison phase the PSNR factor has been used and the level of PSNR increase between the noisy image and the filtered image signifies the success rate of filtering.*

.

Keywords: Image Processing, Echocardiography, Speckle Noise, Filters.

1 Introduction

Medical images are usually damaged by noise in their acquisition and transmission. The main objective of image denoising techniques is to remove such noises as much as possible while retaining important signal features and increase the physician's care and it is significant in diagnosing diseases. Ultrasonic images, a sample of which is echocardiography, are very important in medicine, and this importance is due to its being economical, transferable, and uses the unionization rays [1].

Speckle filtering is a central pre-processing step for the feature extraction, analysis, and recognition of heart problems. Based on the noise type which is multiplicative (speckle noise) or mass (Gaussian noise), in retrieval procedure, all the efforts is done to reconstruct and restore the image which is degraded under the effect of this knowledge. So the restoration techniques move toward the degradation modeling and applying the reverse processes to restore the original image. The probable model produced for the speckle noise is as follows [5,6]:

$$g(n,m) = f(n,m)u(n,m) + \zeta(n,m) \qquad (1)$$

g,f are respectively original and observed image. u shows the multiplicative and ζ shows the mass part of the speckle noise. m,n implicate the vertical and horizontal brandies of sample image .When we are dealing with echocardiograph image, we just pay attention to multiplicative image, like the following relation:

$$g(n,m) = f(n,m)u(n,m) \qquad (2)$$

Recently wavelet transform is used as a tool for image processing to reduce speckle noise. Speckle noise is a high-frequency component of the image and appears in wavelet coefficients. this paper the wavelet Universal threshold technique (Visushrink) has been used for this purpose.[1]

2 A review on the studied data

2.1 Ultrasound

Human ears hear sound waves with frequencies between 20 Hz and 20 kHz. Higher frequencies are called ultrasound and

in diagnostic ultrasonography which is used in medicine, waves with frequencies that vary between 1 MHz and 20 MHz are used. Echocardiography images are ultrasound images from the heart.

2.2 Transducer and piezoelectric crystal

Ultrasound transducers use a piezoelectric crystal to produce and receive ultrasound waves (Figure 1). When electric current enters, the crystal moves and produces an ultrasound wave. The frequency that is released by a transducer depends on the nature and the width of the piezoelectric material. Whenever an ultrasound wave reaches a piezoelectric crystal, an electric current is produced; therefore the crystal is used as a receiver and a transmitter.

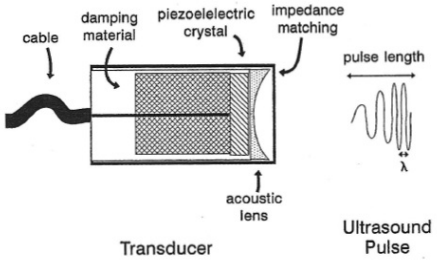

Figure1:Transducer

2.3 Some of The standard views of the transducer's location

2.3.1 Parastenal view : Parasternal Long Axis View is often the first view during echocardiography. It is also the most common view used to guide the M-Mode cursor while taking measurements of the left ventricle, aorta and left atrium. The view also gives a good visualistion of mitral and aortic valves.[9] parasternal have 2 palans, short axis plan and long axis plan figure2,3 :

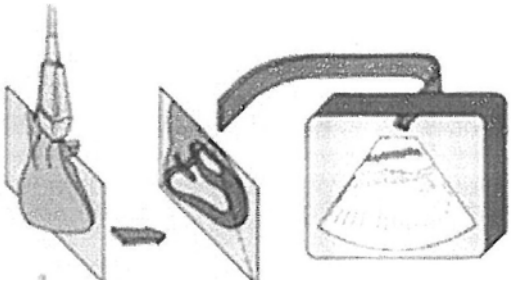

Figure2: parasternal long axis plan

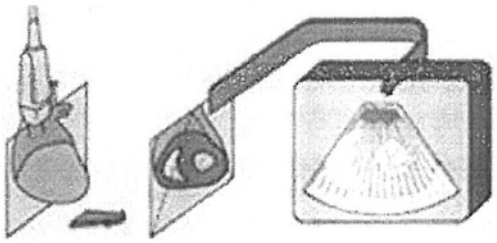

Figure3: parasternal short axis plan.

2.3.2 Apical view : The transduceris palced on heart' Apex. Apical view has 2 plans , 2 chamber view and 4chamber view.(Figure4,5).

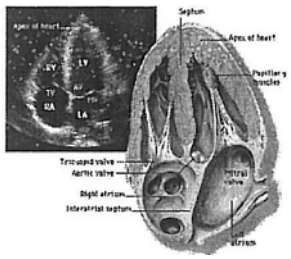

Figure4: 4chamber view

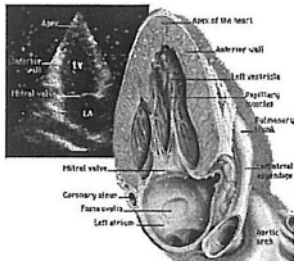

Figure5: 2chamber view

The data studied in this project have been collected according to the Apical method and are from a two dimensional view

3 A Survey on Wavelet Transform

Wavelet analysis does analysis of image low frequency which cause the production of subpass "A" (approximation) by the use of low-pass filter and analysis of image high frequency which cause the production of subband "D" (decomposition) using high-pass filter (figure6). Low frequency content shows the signal identity and is significant in this regard, while, the significance of the image high-frequency content is because of showing details differences. Passing through high-pass and low-pass filters, in the second step A, D coefficients produces two other bands, which finally result in four bands: HH, HL, LH, LL. LL includes image identity with two low-pass frequency filters, three other bands each with details coefficient of horizontal (H), vertical (V) and other direction (D) in which both filters are high-pass frequency. In this step, we have analyzed the image using DWT process and obtained wavelet coefficients. In order to remove noise, these coefficients have been changed using universal threshold technique, then the coefficients which were lower than threshold were removed, finally the image has been recycled from these coefficients using IDWT wavelet reconstruction process (figure 7).

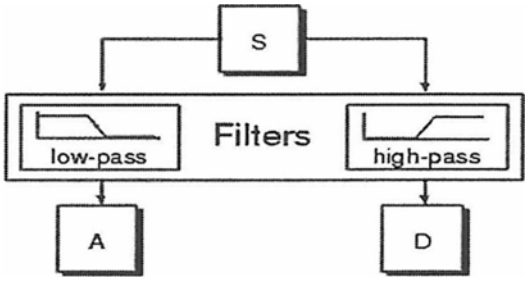

Figure6: production of "A"and "D".

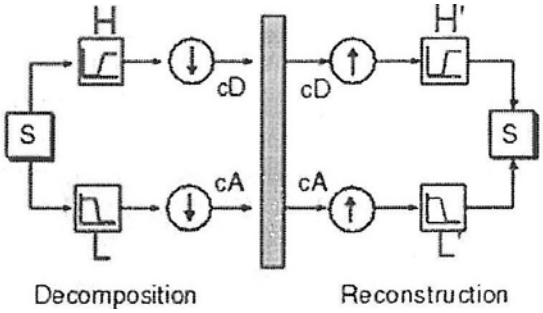

Figure7:Decomposition and Reconstruction.

3.1 The advantage of Wavelet over Short time Fourier Transform(STFT)

Wavelet analysis is one stage newer than short time Fourier transforms. Wavelet analysis provides the possibility of using long windows in low frequencies and short windows in high frequencies. foloowing figures show this advantage : (Figure8,9)

Figure8: Short-time Fourier Transform(STFT)

Figure9:Wavelet Transform

3.2 Wavelet & Wavelet Packets

In each level, in order to change wavelet, just estimation coefficients are analyzed, so that at the end, we would have just one estimation coefficient and details coefficients of each step (figure 10). However, in the analysis of wavelet packets details coefficients are also analyzed in the same way as approximation coefficients (figure 11).

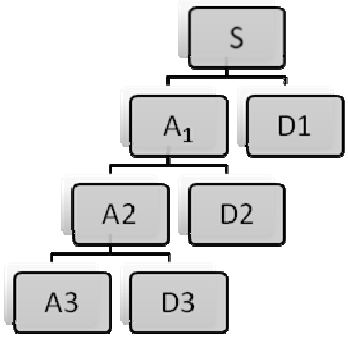

Figure10 :Wavelet analysis..

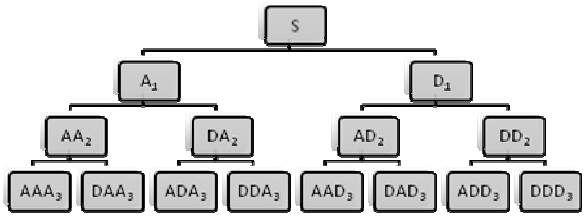

Figure11:Wavelet packet's analysis.

3.3 Universal Threshold Procedures

In universal threshold technique, noise variance is remarkable, and it should be estimated from image. For this purpose, after implementing two-dimensional discrete wavelet (DWT) and computing median wavelet coefficients, these coefficients are computed, then using the following relation, we estimate noise variance (σ).

$$\sigma = \frac{median}{0.6745} \qquad (3)$$

Appropriate threshold for wavelet coefficient has been obtained from the following relation:

$$\lambda = \sigma\sqrt{2\log(n)} \qquad (4)$$

n shows the quantity of wavelet coefficient.

4 A review on other filters used for speckle noise reduction

4.1 Median filter

classifies central pixel and surrounding pixels by determining noise variance. It substitutes pixels mean in the same window for central pixel. It is the simplest technique for removing pixel noise, but it can destroy a quite a few data.

4.2 Wiener Adaptive filter

is a type of linear filter which adapt itself with image local variance, and since small variance do smoothing better, it gives better results as compared with other linear filters. In order to retain edges and other parts, image high frequency is used. One of the disadvantages of Wiener filter is its slowness in computation in comparison with other filters. [2]

4.3 Kaun filter

This filter is the pivot of linear speckle noise model. Minimum mean square error (MMSE) has been designed for obtaining it. This filter identifies area with fixed or very low variance, and introduces them as areas for which denoising process should be taken. When signal is active, it passes signal filter with no change. The case has been introduced by the following equation : [3]

$$\hat{R} = I_{(t)}W_{(t)} + \hat{I}_{(t)}(L - W_{(t)}) \qquad (5)$$

and their weight coefficients is obtained from relation 6:

$$W(t) = \frac{1 - Cu^2 / C_L^2}{1 + Cu^2} \qquad (6)$$

5 results and comparison with PSNR standard

5.1 PSNR (Peak signal to noise ratio)

This parameter is used to measure the difference between two images. Its unit is decibel.

$$PSNR = 10\log_{10}^{\frac{255^2}{MSE}} \qquad (7)$$

$$MSE = \frac{1}{MN}\sum_{i=1}^{M}\sum_{j=1}^{N}(X(i,j) - Y(i,j)) \qquad (8)$$

5.2 We added speckle noise to image noise, performed denoising using different filters and recorded the result in the following table.

Table1: Comparison of PSNRs of different filters for echocardiography image corrupted by speckle noise

Filter type	PSNR noisy image	PSNR denoisy image
Median	19.8886	25.5646
Adaptive wiener	28.9833	30.6211
Kaun	21.2591	17.3363
Wavelet	19.5550	20.4446
Waveletpacket	11.2695	23.0101

Figure12:Noisy image

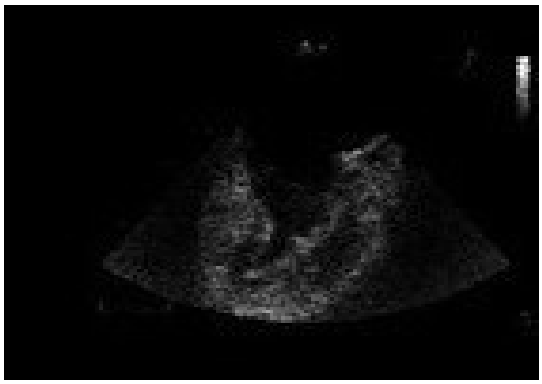

Figure13: Result of Median filter

Figure14: Result of Adaptive Wiener filter

Figure15:Result of Kaun filter

Figure16: Result of Wavelet filter

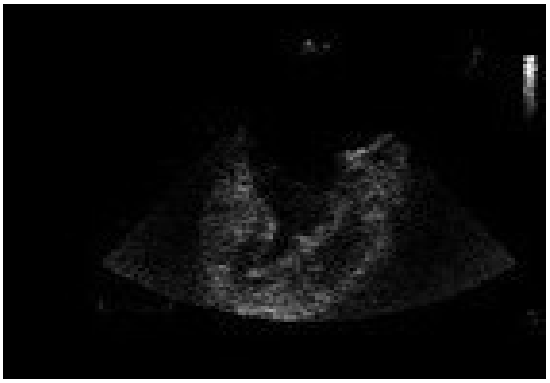

Figure17: Result of Wavelet packet filter

6 Conclusions

As observed in table 1 the results obtained from median and Wiener filters shows the increase of PSNR. These filters perform successfully based on this standard; however as we lose image details and so many other useful image data which help the physician's diagnosis when using these filters, the use of these filters for speckle denoising is not suggested. As observed in table 1 Kaun filter reduces PSNR from 21,2591 to 17,3374 and so it does not perform well for speckle denoising in this regard

Wavelet and Waveletpackets perform well in view of PSNR standard. As observed in table 1, We see PSNR increase from 19,535 to 20,4746. The increase of PSNR when using Wavelet packet is more remarkable and it could be mentioned as the best technique, because it has increased PSNR by about 13.2 units. As you see filtered image with wavelet packets in figure 17, the image details have been mostly retained and image opaque is very less than ordinary wavelet. Finally, in this research wavelet packets are introduced as the appropriate filters and more reliable as compared with older ones. as the results of the table show, mass noise elimination is easier than multiplicative noise elimination and has less error. A proposal for future work is to implement the log function on the database and therefore transform the multiplicative noise into mass noise as much as possible, and then use as the new database.

7 References

[1] S.Sudha[1], GR Suresh[1], R Sukanesh[2] , Noise Reduction in Ultrasound Images Using Context-based Adaptive Wavelet Thresholding, date of publicastion5Aug2009

[2] Amandeep Kaur, Karamjeet , SPECKLE NOISE REDUCTION BY USING WAVELETS, Singh Punjabi University, Patiala, NCCI 2010 -National Conference on Computational Instrumentation CSIO Chandigarh, india, 19-20 March2010 198.

[3] Edmund Hui-On Ng, Speckle Noise Reduction via Homomorphic Elliptical Threshold Rotations in the Complex WaveletDomain, University of Waterloo, inful_lment of the

thesis requirement for the degree of,Master of Applied Science in Electrical and Computer EngineeringWaterloo, Ontario, Canada,2005,c Emund Ng 2005.

[4] Meritz Alfred, Signal Analysis(Wavelet and filter bank),Tehran 1380.

[5] Rafael C. González, Richard Eugene Woods – Digital image processing,Pearson/Prentice Hall (2008).

[6] Rafael C. Gonzalez, Richard E. Woods, Steven L, Digital image processing using MATLAB,2009.

[7] Luc Kluine, Benoit Vbzel, Kuceni Chehdi , Adaptive filtering of multiplicative noise by a new by a new differential method,2005.

[8] Nadia SOUAG ,Images Processing Laboratory, Faculty of Electronics and Computing speckle reduction in echocardiographic images,September4-8,2006.

[9] http://www.cardiophile.com/parasternal-long-axis-view-in-echocardiography.

SESSION

ALGORITHMS AND NOVEL APPLICATIONS

Chair(s)

TBA

CEDE: Collaborative Egocentric Design Environment for CAVE

Sinan Kockara[1], **Tansel Halic**[2]

Computer Science, University of Central Arkansas[1], Rensselaer Polytechnic Institute[2]

Abstract- *The geographical separation of the users and insufficient input from pairs may cause undesired costs in interior/exterior design process. If immersive communication and interaction exist between the pairs, those undesired costs will be minimal. Lack of communication and understanding causes much of the design works to be lost as it is improperly passed on and/or incompletely understood. The combined immersive collaboration can solve these existing problems so that the undesired costs can be eliminated. We present a framework for 3D design of interior/exterior spaces using a CAVE-based immersive virtual environment in that better and intuitive communication among the designers and users would lead to better integration of overall design such that designer would cede some of his/her work to the user. We have developed several user interface and intuitive spatial egocentric/exocentric perception and perceptual constancy techniques to build a fully interactive environment for novice users to help design process of interior or exterior spaces. Efficiencies of these spatial intelligence techniques' are investigated with several experimental cases.*

Keywords: CAVE, immersive environment, interior/exterior design, spatial perception, egocentric, exocentric, perceptual constancy.

1 Introduction

Immersive virtual reality (IVR) is usually a three-dimensional computer generated representation of the real world where user is surrounded by the environment and ideally, can interact with it. This is realized by a viewer centered view by tracking the position of the user. With IVR, complex 3D databases can be rendered and investigated real-time that enables exploration of products. One of the most important uses of virtual environments is that it provides a way where designs can be experimented and tested without actually building them. This would reduce development time, lower total costs of developments and in turn improve efficiency. VR has traditionally been used in planning, design, construction tasks in civil, structural, and mechanical engineering problems. A relatively less explored area is the collaborative design of interior/exterior spaces [28]. This requires an intuitive approach for user interactions as many of the users of the virtual environment will not be expert computer users. Our goal in this project is to provide easy-to-use yet powerful collaborative user interactivity and egocentric/exocentric space perception technique for a CAVE-based [1] virtual environment that will allow users to design interior or exterior spaces effectively and perceive spatial data accurately. Our framework is a tool that overcomes the limitations of communication problems and provides an interactive immersive design environment among the people. Through the methods discussed here, we envision that the users will not only be able to design environments dynamically, but also make distance and size judgments accurately by perceiving spatial data from intuitive egocentric perspective channels.

201 Donaghey Ave Conway, AR 72035
skockara@uca.edu

2 Motivation and Background

The exchange of ideas on a real scene objects rather than relying solely on mutual communications would greatly further the conception of 3D scene between designers and users. If we consider the case of custom designed aircrafts as an example, the necessity of collaborative, immersive, and interactive design environment can be easily understood. Planning, completing complex drawings of aircraft interior furnishings and secondary structural attachments, design analysis, testing of various aircraft interior elements and installations are crucial components of the design process. To ensure responses to customer inquiries are complete and accurate; traditional methods provide immediate technical assistance (on site/phone/fax) and perform routine visits to make customer satisfied. This is tedious, time consuming, and very vulnerable approach to costly errors. To overcome these problems in any design patterns (e.g. architecture design, custom aircraft interior design etc.), we develop egocentric, collaborative, interactive design interface in that customer/user can have hands-on participation on development and installation phases. Working on one-to-one same scale virtual objects corresponding to the real world counterparts would provide real sensation. In addition, user can see his/her interactions through different virtual cameras located into the scene. Cameras' views map to the several view ports as shown in Figure 4. This provides egocentric real sense of size, orientation, and distance perception comparable with user himself/herself since a virtual avatar corresponding to the

user with approximately the same height will be present at the scene.

According to Thurstone [23] spatial aptitude consists of three components: first, capability of distinguishing an object from different perspective views, second, ability to recognize displacements in measure, and third, ability to recognize spatial relations when the body of the observer is an essential part of the scene. Our framework complements all three of these spatial ability components at the same time by displaying different perspective views from virtual cameras, adding reference object with already known distance in the scene, and creating the same height corresponding avatar of the user respectively. CAVE (CAVE Automatic Virtual Environment) is an example system that provides a platform for virtual reality applications. It was first introduced in 1991 by Carolina Cruz-Neira at the University of Illinois at Chicago [1]. The CAVE is composed of three to six projection screens driven by a set of coordinated image-generation systems. It is assisted by a head and hand tracking devices that produces stereo perspective.

Figure 1. Three-wall CAVE used for the development of a design environment

Research in IVR applications has produced control menu techniques that take advantage of the user's inherent knowledge of the natural interactions. These techniques enhance the effectiveness by providing extra interactivity features through various types of menu systems used in such environments [2], [3]. Unfortunately, most of these techniques have not been designed to support full interaction and collaboration among geographically apart pairs as in [4]. Several file formats and Application Program Interfaces (API) or libraries (together or separately) can be used to develop 3D IVR applications. VRML, CAVELib[5], VRJuggler[6], OpenGL Performer[7], OpenGL, CAVERNsoft[8], and Open Inventor are examples to name a few. Germans et al. [9] summarizes some of those IVR libraries and applications which are extensively represented in Table 1 by their features. Among these libraries, we use OpenGL Performer, CAVELib, and OpenGL to implement our framework. OpenGL is used to implement some necessary features which are otherwise nonexistent in OpenGL Performer. CAVELib is used to implement necessary base for collaboration and visualization in CAVE.

Table 1. Some Available libraries and tools

Tools	Interaction	Scene Graph	Data Visualization	VR Hardware Support	Collaboration	Multi Platform
CAVELib	Low-level	No	No	Yes	Low-level	Yes
OpenGL	No	No	No	No	No	Yes
Performer	Low-level	Yes	Yes	Yes	No	Yes
Inventor	Low-level	Yes	No	No	No	Yes
VRML	Low-level	Yes	No	No	No	Yes
VRJuggler	Low-level	no	No	Yes	Low-level	Yes
CAVERNsoft	No	No	No	Yes	Yes	yes

Despite many obvious advantages virtual reality-based 3D space design techniques seem to offer, advanced research in this area is hindered by the lack of effective user interaction. We provide enhanced interactivity features in the immersive environment using our user interface for spatial scene representation, a sample scene of which is shown in Figure 2. In our interactive design environment, users are able to position, select, scale, add, remove, orient the models and change textures. With increased flexibility by our implementation, the users can move and interact in the environment freely. It is possible for the users to change the navigation speed in the 3D scene using user interface, for instance, as shown in Figure 2.

Figure 2. A sample interior scene with menu items (Navigation speed by slider)

3 Collaboration

Presence in the virtual world is generally maintained using avatars, or a computer generated representations of participants such as shown in [16]. Transmitting a sufficient amount of body language, furthermore; seeing real time high quality video of other collaborator can improve negotiation for tele-immersive applications. However, in the situation that users can change environment dynamically, face-to-face communication is not strictly required. Seeing what other participant is manipulating into the scene is a considerable issue rather than what he/she is looking at, pointing at, or what his/her head, hand position and orientations are. The most important advantage of doing design visualization in an immersive and collaborative environment is the ability to have geographically distributed participants sharing virtual scene with each other and the 3D objects into the scene can be manipulated reciprocally. This allows the participants to modify specific objects in the scene or set the parameters of these objects e.g. translation values. Collaboration gives the users a common context for their design.

Collaboration in VR applications is supported through numerous libraries that provide network functionalities [17]-[22]. In our implementation, we use simple network functionalities provided by CAVELib. Our purpose is not to produce a real face-to-face meeting between collaborators during dynamic scene creation, but to provide interface for them to work together in geographically apart virtual environments. By means of our collaboration theme, users immerse into the virtual environments to check on the state of the virtual scene and only one of them (primary user) makes alterations to the scene at the same time. First participant is the initiator of the virtual scene. Only one of the partners playing a leadership role (lead person) can adjust the scene, but by giving permission to other peer makes other participant leading person to make alterations.

3.1 System Architecture

The architecture of the proposed system is a client/server model showed in Figure 3, in which CAVE renders lists of 3D graphics objects created by user in parallel to the other collaboration side from where changes are sent to a server as text. Passing 3D databases to other client when modified by any lead participant in the virtual space requires a fair amount of infrastructure to be established and maintained such as higher network bandwidth even if network connection backbone is internet2. Instead, passing text messages to the other client that includes which part of the scene changed and what changes being done are more appropriate and yet more useful. To accomplish this, each participant should have the same scene with the same 3D databases and texture images initially.

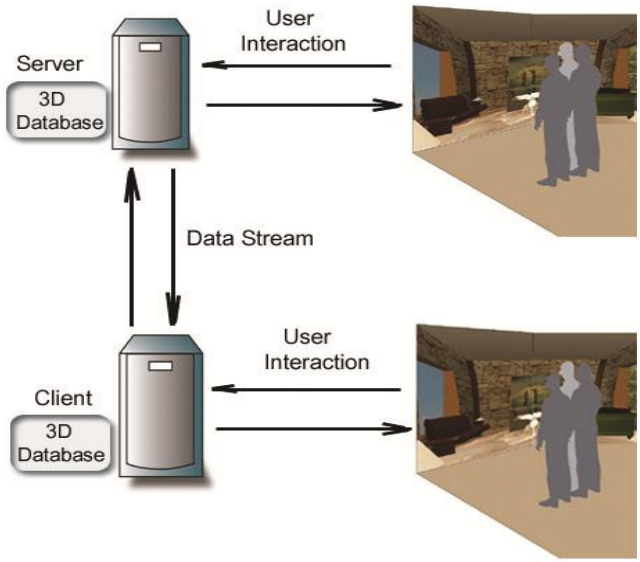

Figure 3 Architecture of the collaborative

We make collaboration synchronous meaning that each participant can see what modifications being done by lead person in the virtual scene. Not to increase network traffic and not to make implementation intricate, we do not provide audio communication between collaborators. Moreover, there is not much advantageous to provide aural communication among users for creating and adjusting virtual scene because every action they can do is implemented in user interface. Still there is no possibility to take user's text input from keyboard like device into the immersive environment except implementing a virtual keyboard. Therefore, we cannot provide users to send each other dynamically created text messages.

Changes made by a lead person in the virtual scene can be recorded as a text message and pass to the other user for informing what modifications being done to prevent confusions. In any case of network connections failure each modification in the 3D world is saved in both sides of the systems. We achieve this by only saving changes into the configuration file that is nothing but text file. This text file consists of all the objects in the scene with their names/IDs, translations, textures, scale factors, color (RGB), navigation speed, and pickable property etc. When collaboration is set up again in both systems, comparison between configuration files is done to detect whether there is any difference between last updated times. If there is difference in time, the most recent one will be transmitted to the other part. This is achieved because each pair has time that last save operation is made into the configuration file.

So far, we have introduced collaborative interactive design environment to found base for egocentric spatial perception framework. Next section introduces human

visual perception metrics and their usage in immersive design environment.

4 Egocentric and Exocentric Judgment by Virtual Channels

In an immersive design environment, human's spatial perception plays a crucial role. Egocentric and exocentric judgments of a space are the most prominent contributors to this perception. Humans can either use egocentric or exocentric distance judgment for determination of absolute scales, positions, and orientations of objects in the environment [10]. Egocentric localization is a process of determination of the objects' spatial positions in the environment relative to one's body. Contrary to egocentric localization, in exocentric localization; instead of using one's body, humans use some objects in the environment as a reference for effectively employing positions, scales, and orientations. Humans usually correlate egocentric or exocentric distance judgments interchangeably and repeatedly to eliminate misperceptions [11], [12]. To circumvent these misperceptions in the virtual domain, we provide both strategies at the same time by tracking the user with virtual cameras so that different view ports from cameras provide exocentric perceived space judgment in egocentric terms [10] (see Figure 4 G). Another factor that contributes to accurate spatial perception is perceptual constancy. Perceptual constancy implies the tendency of humans to see already known objects as having standard shape and size regardless of changes in the viewing perspective, distance, and lighting etc. We take perceptual constancy into consideration in our framework by selecting some objects which have common perception in size for all humans e.g. soccer ball.

4.1 Human Perception Metrics

According to Pelz et. al [13], there are some linear combinations of locations specified by egocentric and exocentric reference frames. In our case, both of those frames are provided to the user via cameras' viewing frustums. To make viewing frustums compatible to human's binocular vision field we select binocular vision field of 200° width and 135° height. User can locate him/herself via his/her corresponding avatar in the virtual scene. Since judgments are made with respect to the position of the eye in the head, we resize and position corresponding avatar to the user's eye position and direction which are taken from the tracking device. This also makes the avatar's height almost equal to observer's height. With this help, insufficient proprioceptive information in the IVR system, which is the reception of information about body position and movement by the sensory systems, is tried to be eliminated as much as possible.

People usually rely on previous visual information for accomplishment of distance and size estimations. Brain compares the sensed size of an object to its known real size. A human's all the vision cues (binocular disparity, convergence etc.) are effective within 2 meters [25]. Arditi in [26] indicates that accommodation is effective within 2 meters. Foley in [27] shows that convergence can be effective for distances as great as 8 meters. Binocular disparity occurs when two eyes look at the same thing at slightly different angles those result in two slightly different images. Eyes convergence is the difference in the direction of the eyes. Eyes convergence is only effective smaller than 10 meters distances.

In our experiments, the soccer balls are viewed stereoscopically so that binocular disparity provides the order of objects in depth. However, it does not provide the exact perceived depth of the objects. For a correct depth perception disparity must be fed with information regarding egocentric distance. Therefore, we provide more visual disparity feedback cues to the user via exocentric cameras in egocentric terms in order to devise as a source of information. Depth perception is most effective on short distances (less than 10 meters). Human depth perception is dependent upon stereoscopic depth cue which consists of relative differences between parts of the images of the two eyes. In normal situations, this depth cueing is effective only the distances less than 25 meters or sometimes up to 30 meters (if we assume human eyes are placed 6.3 centimeters inter pupillary distance).

4.2 Experiments

We investigated the question of whether viewing some common sensed objects in the scene and some virtual cameras' viewing frustum that are continuously tracking the user can provide the information necessary to the user in order to successfully navigate, locate and accurately estimate the distances and the sizes in the virtual environment. To that end, the user is permitted to locate and move the virtual cameras freely (see Figure 4). In addition, experiments are developed in compliance with abovementioned human perceptual specifications. Error rates in predictions of distances and sizes are measured. Observer's estimations in size and distance are compared according to with/without egocentric viewing channels, with/without perceptual constancy objects, with/without corresponding avatar, and interior/exterior designs.

After spatial ability test [24] is applied to the participants, subjects are chosen with the score of 60 or higher. Experimental scenes are shown in Figure 4. Two of

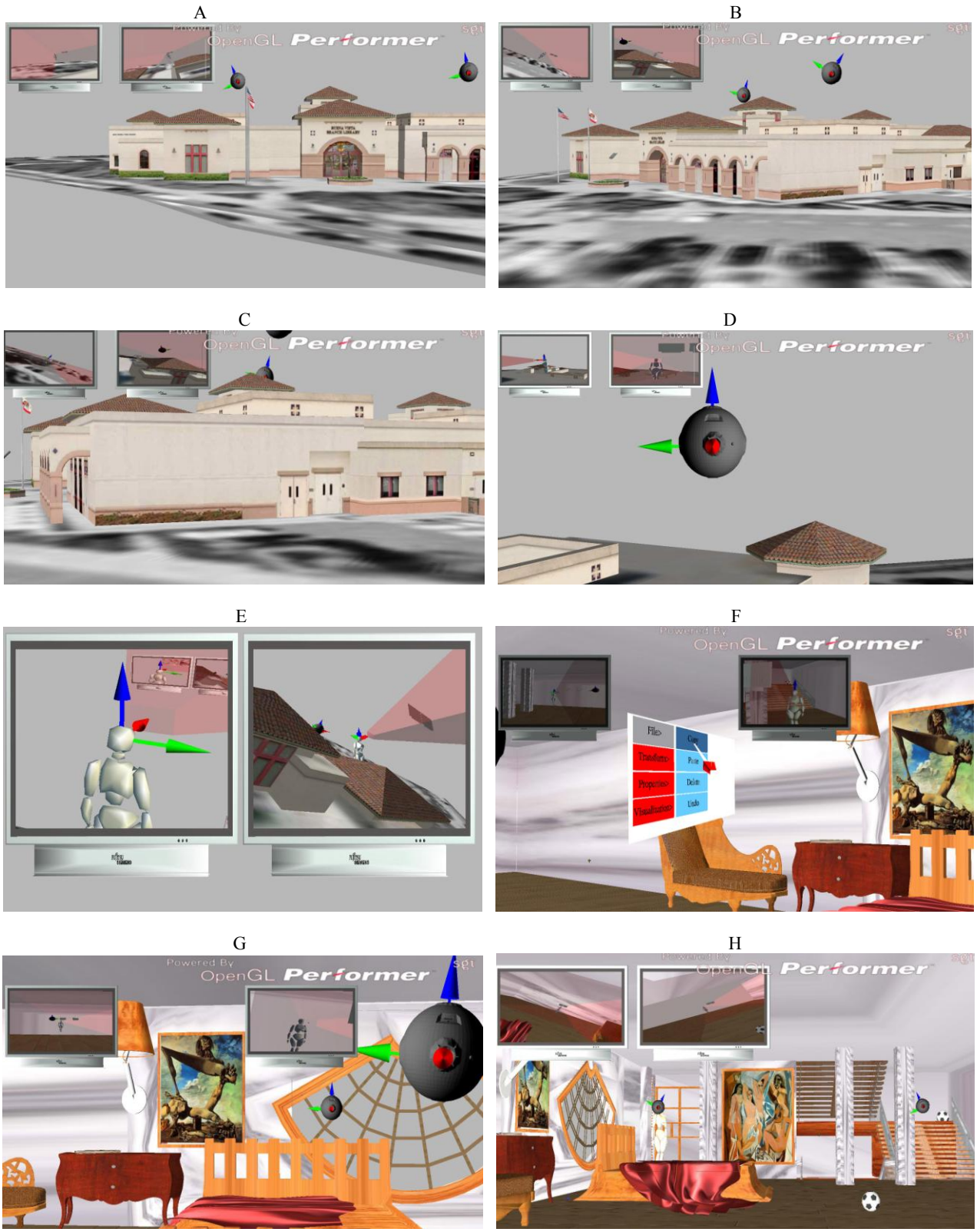

Figure 4. Implementations of spatial intelligence A) B) C) Exterior space with different views and cameras, D) One of the user tracking virtual cameras, E) Virtual cameras' viewing angles on the virtual displays with avatar, F) Object manipulation interface, G)Avatar from two dynamically located virtual cameras and their views on displays, H) Size estimation experiment

the subjects already had very little experience in immersive displays others didn't. Subjects were first guided through a practice session to have little experience and sensation of immersive environment. Interior design scene in Figure 2 is used for this environmental training session. When the subjects verbally declare that they learned how to navigate and interact with the scene, the experiment started.

The 3D interior and exterior scenes are created with exocentric head-up virtual cameras' view ports. Subjects have two different tests; one is depth discrimination, the other one is size discrimination. In the first, subjects are instructed to estimate the distance of a specified object. In the second, subjects are instructed to determine which is the larger of the two soccer balls. Soccer ball is selected because of perceptual constancy. To measure the error rates in depth and size discriminations, soccer balls with different distances (i.e.; 2 Meters, 2.7 meters, 5meters, 10 meters, 20 meters, and 30 meters) are located in front of the user. Extent of the scene is 40 meters in length and 30 meters in width (see Figure 4 H). Verbal indication is taken with questions of how far objects in meters and centimeters are and which one of the objects is larger. Subjects are not informed about their errors or accuracies until finishing all of the experiments. Another experiment was on the number of virtual cameras. We investigated the effect of increased number of virtual cameras would have on the human perception. In addition, shades and shadows are used to resolve some perceptual ambiguities. To that end, user can locate and change the intensity of the light freely.

4.3 Results

Average of all of the subjects' relative erroneous distance estimations with/out virtual cameras and/or the avatar, and the effect of increase on the number of cameras are shown in below graphs.

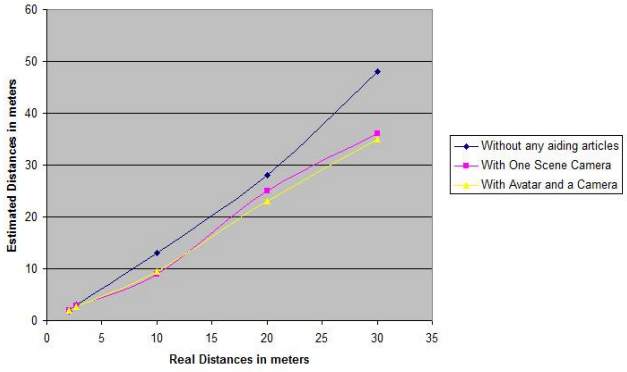

Figure 5. Erroneous Estimations with/out avatar and/or a camera

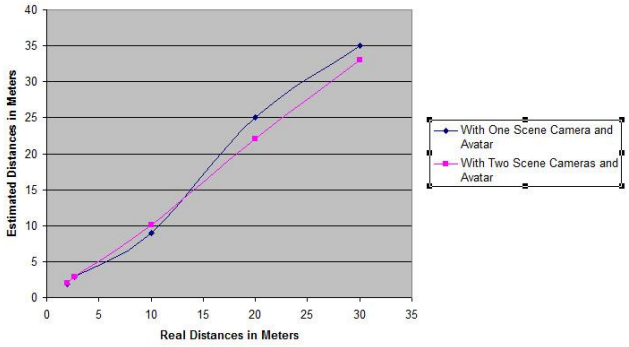

Figure 6. Effects of number of cameras

As seen in the graphs (Figure 5 and Figure 6), including the cameras and the avatar contributes to the spatial intelligence of the human perception and helps to reduce erroneous estimations. This contribution increases with increase in the number of cameras. The experiment showed significant reduction at erroneous distance and size perceptions by combining 3D egocentric view in exocentric virtual displays (which are presenting virtual world representations in an exocentric perspective). We call this intuitive egocentric spatial reading. Without a visual reference (camera's view ports in our case), erroneous judgments of visual directions and spatial perceptions are made by the users. It is also interesting to note that camera's viewpoints' views on the screen are not disorienting the user [13]-[15]. In addition, results showed that perceived size and distance are proportional to perceptual distance and size in immersive displays. Therefore, supporting the proposition of size constancy and distance discrimination is achieved by adding familiar objects to the scene.

5 Conclusion and Future Work

An efficient interactive human centric collaborative design framework is developed. A way of improving human's spatial intelligence in collaborative immersive displays considering human spatial perception metrics is investigated. To that end, egocentric perception from virtual cameras is used as a reference frame. Virtual Cameras with tracking capabilities of the user indeed provide important information for successful navigation and spatial perception through the environment and even affects normal navigational behaviour and perception of the space. Combination of the cameras and the same height avatar with the observer is even further the human perception in space. The results showed that in immersive environments 3D exocentric displays with egocentric frame of reference is far more efficient than only egocentric view.

As a future work we can add some security options to our virtual scene to prevent from fraudulent attacks. In future phase, system can be converted to asynchronous one to make system independent not only from geographical restrictions but also from time zone restrictions. Also, experiments will be pervaded to all subjects including lower scored ones in spatial ability test. Furthermore, gender factors in spatial intelligence for immersive displays will be investigated. Even though effects of increase in the number of cameras are explored, the supportive contributions of more than two cameras on spatial egocentric intelligence are subject to our future study.

7 References

[1] C. Cruz-Neira, D. Sandin, and T. DeFanti. Surround-Screen Projection-Based Virtual Reality: The Design and Implementation of the CAVE. Computer Graphics, pages 135-142. ACM SIGGRAPH, 1993.

[2] S. Kockara, E. Sarioglu, and S. Dagtas. A CAVE-based 3D Interactive System to Design Environments for Performing Arts. ACM SIGGRAPH 2005 Symposium on Interactive 3D Graphics and Games, I3D 05, Washington D. C, April 4–5, 2005.

[3] R.P. McMahan and D.A. Bowman, An Empirical Comparison of Task Sequences for Immersive Virtual Environments. IEEE Symposium on 3D User Interfaces, March 2007.

[4] T. Duval, A. Lecuyer, and S. Thomas. SkeweR: a 3D Interaction Technique for 2-User Collaborative Manipulation of Objects in Virtual Environments. IEEE Symposium on 3D User Interfaces, pages 69-72, March 2006.

[5] http://www.vrco.com, 2007.

[6] C. Just, A. Bierbaum, A. Baker, and C. Cruz-Neira. VR Juggler: A Framework for Virtual Reality Development. In 2nd Immersive Projection Technology Workshop (IPT98), 1998.

[7] J. Rohlf and J. Helman. IRIS performer: A high performance multiprocessing toolkit for real–Time 3D graphics. In Andrew Glassner, editor, SIGGRAPH '94, Computer Graphics Proceedings, Annual Conference Series, pages 381–395. ACM SIGGRAPH, ACM Press, July 1994.

[8] J. Leigh. Issues in the Design of a Flexible Distributed Architecture for Supporting Persistence and Interoperability in Collaborative Virtual Environments. In ACM, editor, SC'97: High Performance Networking and Computing, San Jose (CA) USA, 1997.

[9] D. Germans, H.J.W. Spoelder, L. Renambot, H. E. Bal. VIRPI: A High-Level Toolkit for Interactive Scientific Visualization in Virtual Reality. Proc. Immersive Projection Technology/Eurographics Virtual Environments Workshop, Stuttgart, May 2001.

[10] H. Frenz and M. Lappe. Visual Distance Estimation in Static Compared to Moving Virtual Scenes. The Spanish Journal of Psychology. Volume 9, no 2, pages 321-331, Nov. 2006.

[11] J. M. Foley, N. P. Ribeiro-Filho, and J. A. Da Silva. (2004). Visual perception of extent and the geometry of visual space. Vision Research, volume 44, pages 147-156, 2004.

[12] B. Wu, T. L. Ooi, and Z. J. He. Perceiving distance accurately by a directional process of integrating ground information. Nature, volume 428, pages 73-77, 2004.

[13] J. Pelz and M. Hayhoe. The role of exocentric reference frames in the perception of visual direction. Elsevier Science B.V., Vision Research, volume 35, no 16, pages 2267-2275, Aug. 1995.

[14] L. Matin, E. Picoult, J. K. Stevens, M. W. Jr. Edwards, D. Young, and R. MacArthuer. Oculoparalytic illusion: Visual-field dependent spatial mislocalizations by humans paralyzed with curare. Science, volume 26, pages 198-201, 1982.

[15] L. Stark, and B. Bridgeman. Role of corollary discharge in space constancy. Perception & Psychophysics, volume 34, pages 371-380, 1983.

[16] J. Mortensen, V. Vinayagamoorthy, M. Slater, A. Steed, B. Lok, and M. Whitton. Collaboration in Tele-Immersive Environments. Eurographics Workshop on Virtual Environments, Barcelona, pages 93-101, May 2002.

[17] Christer Carlsson and Olof Hagsand. DIVE — A Platform for Multi-User Virtual Environments. Computers and Graphics, 17(6):663–669, November–December 1993.

[18] Chris Greenhalgh and Steven Benford. MASSIVE: A collaborative virtual environment for teleconferencing. ACM Transactions on Computer-Human Interaction, 2(3):239–261, 1995.

[19] J. Leigh, A.E. Johnson, T.A. DeFanti, and M. Brown. A Review of Tele-Immersive Applications in the CAVE Research Network. In IEEE Virtual Reality'99, pages 180–187, 1999.

[20] M. R. Macedonia, M. J. Zyda, D. R. Pratt, P. T. Barham, and S. Zeswitz. NPSNET: A Network Software Architecture for Large-Scale Virtual Environment. Presence, 3(4):265– 287, 1994.

[21] G. Singh, L. Serra, W. Png, and Hern Ng. BrickNet: A Software Toolkit for Network-Based Virtual Worlds. Presence, volume 3, no. 1, pages 19–34, 1994.

[22] Jason Leigh. Issues in the Design of a Flexible Distributed Architecture for Supporting Persistence and Interoperability in Collaborative Virtual Environments. In ACM, editor, SC'97: High Performance Networking and Computing, San Jose (CA) USA., 1997.

[23] L. L. Thurstone. Primary mental abilities. Psychometric Monographs, 1., 1938.

[24] www.psychometric-success.com/practice-papers/Psychometric%20Success%20Spatial%20Ability%20-%20Practice%20Test%201.pdf, 2007.

[25] L. Kaufman, J. H. Kaufman, R. Noble, S. Edlund, S. Bai, and T. King. Perceptual distance and the constancy of size and stereoscopic depth. Spatial Vision, volume 19, no. 5, pages 439–457, 2006.

[26] A. Arditi. Binocular vision. In: Handbook of Perception and Human Performance, volume 1. Sensory Processes and Perception, Boff, K., Kaufman, L. and Thomas, J. (Eds), pages 23–41.Wiley-Interscience, New York, 1986.

[27] J. M. Foley. Binocular distance perception. Psychol. Rev. 87, pages 411–434, 1980.

[28] Lindsey, P. and McLain-Kark, J., "A Comparison of Real World and Virtual World Interior Environments." Journal of Interior Design, 1998. 24(1): pp. 27-39.

More on Construction of Surfaces

Weihu Hong[1] , Mingshen Wu[2], Nathan Borchelt[3]
[1] Department of Mathematics, Clayton State University, Morrow, GA, 30260
[2]Department of Mathematics, Statistics, and Computer Science, University of Wisconsin-Stout, Menomonie, WI 54751
[3]Department of Mathematics and Computer Science, Western Carolina University, Cullowhee, NC 28723

Abstract - *Surfaces can be constructed by many different methods, such as revolving a planar curve about a line in the same plane or by shifting a planar curve along a given vector (see [3]). This paper presents other means of construction of surfaces: by moving a stick, by remodeling an existing surface, and by inverting an existing surface.*

Keywords: Surface, moving stick, remodeling, and inverting.

1 Introduction

There are many different surfaces that were given in mathematical literatures (see [1], [2], [4]). Two types of surfaces: surface of revolution and surface of cylinder were discussed in [3]. In this paper, we are interested in other means of construction of surfaces: by moving a stick, by remodeling an existing surface, and by inverting an existing surface. All our constructions can be easily implemented via a computer algebra system such as MathCAD [6], Mathematica [7], Maple [8], and MatLab [9]. The images in this paper were created by using MathCAD.

2 Construction by Moving a Stick

Let us begin with $\gamma(t), t \in [a,b]$, which is a smooth curve in space. If α and β are two linearly independent vectors such that the curve does not lie in the space spanned by α and β, then we are going to construct a stick in the plane spanned by the vector α and β as follows. Let v be a unit vector in the space spanned by α and β. There exist two real valued functions $c_1(t)$ and $c_2(t)$ such that

$$v(t) = c_1(t)\alpha + c_2(t)\beta,$$

Define a stick as follows:

$$stick(s,t) = sv(t),\ s \in [-\ell, \ell].$$

Imagine that we are carrying the stick as we walk along the curve. The stick is moving along the curve. The result of doing this will trace out a strip, which can be expressed as follows.

Theorem 1. Let c_1 and c_2 be any real valued functions such that $c_1(t)^2 + c_2(t)^2 = 1, v(t) = c_1(t)\alpha + c_2(t)\beta,$ and $stick(s,t) = s \cdot v(t),\ s \in [-\ell, \ell]$. Then the following will define a strip along the curve $\gamma(t), t \in [a,b]$ with width of 2ℓ.

$$strip(t,s) = \gamma(t) + stick(s,t)$$
$$where\ t \in [a,b], s \in [-\ell, \ell],$$

Proof: For each fixed value of t, the $strip(t,s)$ represents a line segment with length of 2ℓ, which is parallel to the vector v. $\gamma(t)$ is continuous on the interval [a, b], therefore, $strip(t,s)$ is continuous on the $[a,b]\times[-\ell,\ell]$. Thus, it defines a strip. The proof is complete.

Since the curve $\gamma(t), t \in [a,b]$ is smooth, both its tangent and normal vectors are continuous nonzero vectors. Let $\tau(t), \alpha(t), and\ \beta(t)$ be the unit tangent, unit normal, and binormal vectors of $\gamma(t)$, respectively, that is,

$$\tau(t) = \frac{\gamma'(t)}{\|\gamma'(t)\|}, \alpha(t) = \frac{\tau'(t)}{\|\tau'(t)\|},$$
$$\beta(t) = \frac{\tau(t)\times\alpha(t)}{\|\tau(t)\times\alpha(t)\|}.$$

Corollary 1. If the vectors α and β are replaced by the unit normal vector $\alpha(t)$ and the unit binormal vector $\beta(t)$ at the point $\gamma(t)$ for each $t \in [a,b]$ in Theorem 1, then the following defines a strip.

$$strip(t,s) = \gamma(t) + stick(s,t)$$
$$where\ t \in [a,b], s \in [-\ell, \ell],$$

Proof: Since both the unit normal and binormal vectors span a plane that is perpendicular to the tangent vector at each value of t, therefore, the stick will trace out a strip along the curve.

Example 2.1 Consider the famous knot curve (see [1]) :

$$\gamma(t) = \{(8+3\cos(5t))\cos(2t), (8+3\cos(5t))\sin(2t), 5\sin(5t)\}$$
$$where\ t \in [0, 2\pi]$$

If we choose $c_1 = c_2 = \sqrt{2}/2$, and ℓ=2, then we will get the strip as shown in Figure 1. If we choose $c_1 = \cos(t)$, $c_2 = \sin(t)$, and ℓ=2, then we will get the strip as shown in Figure 2.

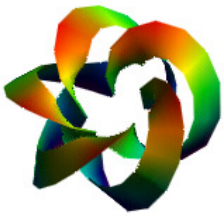

Fig. 1

Fig. 2

Example 2.2 Consider the unit circle on the XY-plane:

$$\gamma(t) = \{\cos(t), \sin(t), 0\},\ \textit{where}\ \ t \in [0, 2\pi]$$

If we choose $c_1 = \cos(t/2), c_2 = \sin(t/2)$, and ℓ=0.3, then we will get the famous Möbius strip (see [5]) as shown in Figure 3 and Figure 4.

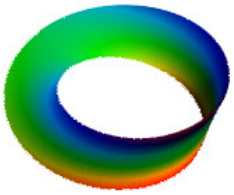

Fig. 3

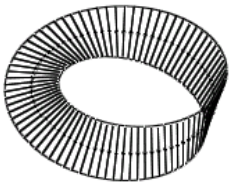

Fig. 4

Example 2.3 Consider the curve in space $\mathbb{R}^3$

$$\gamma(t) = \{\cos(t), \sin(t), \cos(2t)\},\ \textit{where}\ \ t \in [0, 2\pi]$$

If we choose $c_1 = \cos(t/2), c_2 = \sin(t/2)$, and ℓ=0.5, then we will get another Möbius strip as shown in Figure 5 and Figure 6.

Fig. 5

Fig. 6

Example 2.4 Consider the spherical spiral curve (see [1]):

$$\gamma(t) = \{\cos(mt)\cos(nt),\ \ \sin(mt))\cos(nt),\ \ \sin(nt)\}$$

$$t \in [0, 2\pi]$$

If we choose $c_1 = \cos(t/2), c_2 = \sin(t/2)$, and ℓ=0.1, then we will get the strip as shown in Figure 7 and Figure 8.

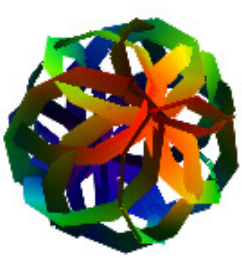

Fig. 7 (m=5, n=7)

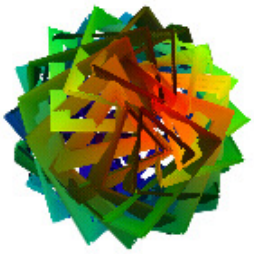

Fig. 8 (m = 17, n =11)

Example 2.5 We are to construct a ribbon as follows:
Start with the node curve $y^2 = x^3 + x^2$ that looks like the Greek character α (see Fig. 9).

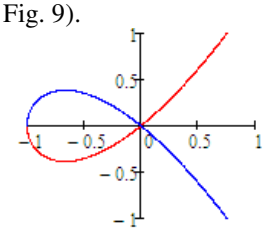

Fig. 9

This has the parametrization

$$h(t) = \begin{cases} -\cos(t)\sqrt{1-\cos(t)} & \textit{if}\ \ -\pi \le t \le 0 \\ \cos(t)\sqrt{1-\cos(t)} & \textit{otherwise} \end{cases}$$

Define its 3D version as follows

$$\gamma(t) = \{\cos(t),\ \ h(t),\ \ 0\}, t \in [-5.6, -0.5]$$

Let $c_1 = \cos(\pi \cdot \cos t/2), c_2 = \sin(\pi \cdot \cos t/2)$,
and ℓ=0.25, define the ribbon as follows

$$Ribbon(t,s) = \gamma(t) + s(c_1 \vec{j} + c_2 \vec{k})$$

then this will generate a ribbon as shown in Figure 10 and Figure 11. Where as usual, $\vec{j} = \{0,1,0\}$ *and* $\vec{k} = \{0,0,1\}$.

Fig. 10

Fig. 11

3 Construction by Remodeling

In this section, we discuss another method of creating surfaces: by remodeling an existing surface. First, we define a remodeling transformation of an existing surface or curve.

Definition 1. For a given surface, and a model, if there exists mapping such that it will map the surface into the region that is bounded by the given model, then it is called a remodeling transformation. The resulting surface is called a remodeling transformation surface of the existing surface.

Theorem 2. If a model is given by a nonnegative function $m(t,s), t \in [a,b], s \in [c,d]$, and $f(t,s), t \in [a,b], s \in [c,d], with \left| f(t,s) \right| \le 1$ is a given surface, then the surface $g(t,s) = m(t,s) f(t,s)$ is a remodeling transformation surface of f.

Proof: It is clear that for each point $f(t,s)$ on the surface f, the point $g(t,s)$ will be bounded by a bumpy sphere of radius $m(t,s)$. Thus, the surface f has been mapped into a region bounded by the bumpy sphere of radius $m(t,s)$. Therefore, the surface $g(t,s) = m(t,s) f(t,s)$ is a remodeling transformation surface of f. The proof is complete.

Example 3.1 We consider the unit sphere

$$f(t,s) = \{\cos(t)\cos(s), \sin(t)\cos(s), \sin(s)\}, t \in [0,2\pi], s \in [0,\pi].$$

We define a function as follows:

$$m(t,s) = \cos(ks)\sin(ks), \text{ for integer } k$$

Then we apply the function to the unit sphere by selecting different values of k, interestingly, we will have new surfaces as shown in Figure 11.

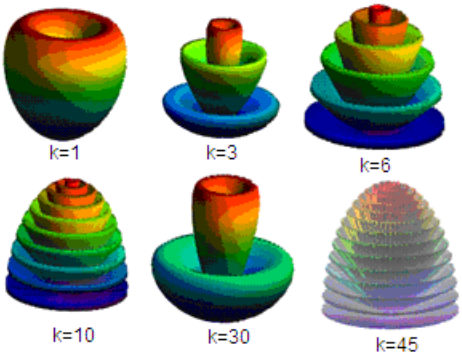

Fig. 11

Example 3.2 We again consider the unit sphere. But we define a different function as follows

$$Set \quad \Delta = \frac{\pi}{8}, \delta = \frac{\pi}{10}.$$

$$m(u,v) = 1 \text{ if } u \in [(2k-1)\Delta, 2k\Delta], v \in [2j\delta, (2j+1)\delta],$$

$$for\ k = 1,2,\cdots,8;\ j = 0,1,\cdots,4;$$

$$m(u,v) = 0.75, otherwise.$$

We then apply the function to the unit sphere, we get new surface as shown in figure 12.

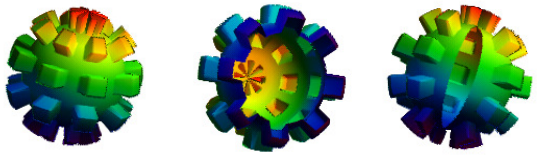

Fig. 12

Example 3.3 We consider the torus:

$$\tau(t,s) = \{\cos(t) - r\cos(t)\cos(s), \sin(t) - r\sin(t)\cos(s), r\sin(s)\}$$

$$where\ r = 0.2$$

which is shown as in figure 13.

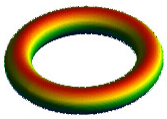

Fig. 13

We define a function as follows

$$m(t) = \begin{cases} 1, if\ t \in \left[\frac{2k\pi}{6}, \frac{(2k+1)\pi}{6}\right) \\ r, if\ t \in \left[\frac{(2k+1)\pi}{6}, \frac{(2k+2)\pi}{6}\right) \end{cases},$$

$$k = 0,1,\cdots,6, r = 0.7$$

If we apply the function to the torus, we will get the following new surface as shown in figure 14.

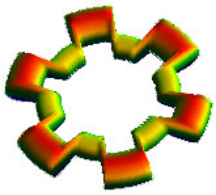

Fig. 14

Now if the function is applied inside the torus as follows, we will have the new surface as shown in figure 15.

$$\xi(t,s) = \{\cos(t) - m(t)\cdot r\cos(t)\cos(s), \sin(t) - m(t)\cdot r\sin(t)\cos(s), m(t)\cdot r\sin(s)\}$$

$$where\ r = 0.2$$

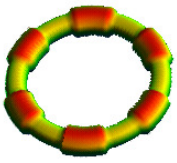

Fig. 15

A remodeling transformation can also be applied to a curve. The following example shows how this can be used to create some special objects.

Example 3.4 We consider the unit circle

$$\gamma(t) = \{\cos(t), \sin(t), 0\}, t \in [0,2\pi]$$

We apply the modeling function m(t) defined in Example 3.3 to the circle, denote the result $f(t) = m(t)\cdot\gamma(t)$, which is shown as in figure 16.

Fig. 16

We are to use this to create a gear as shown in figure 17.

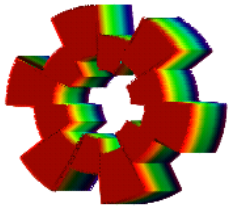

Fig. 17

To do that, we define the top and bottom faces as shown in figure 18 as follows

$$bottom(t,s) := s \cdot f(t), t \in [0,2\pi], s \in [0.5,1],$$

and

$$top(t,s) := bottom(t,s) + \{0,0,1\},$$

$$t \in [0,2\pi], s \in [0.5,1]$$

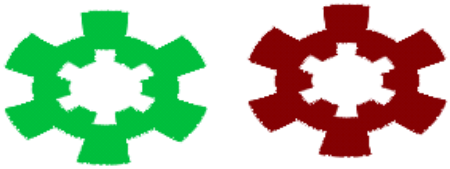

Fig. 18

To make the outside face, we define

$$Outside(t,s) := f(t) + s\{0,0,1\},$$

$$t \in [0,2\pi], s \in [0,1]$$

Likewise, we define the inside face

$$Inside(t,s) := 0.5\, f(t) + s\{0,0,1\},$$

$$t \in [0,2\pi], s \in [0,1]$$

Which are shown as in figure 19

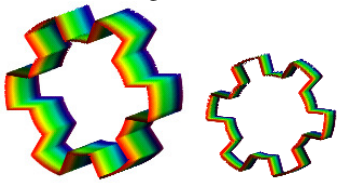

Fig. 19

By assembling these faces together, the gear as shown in figure 17 is obtained.

4 Construction by Inverting

Lastly we discuss creating surfaces by inverting an existing surface.

Inversion in geometry is a transformation. Let P be a given point. Let S be a sphere centered at O and radius r. The inverse of P with respect to S is a point Q on the line $\overleftrightarrow{OP}$ such that $dist(O,P) \cdot dist(O,Q) = r^2$. The result of an inversion of a given closed surface is inside out and outside in.

For a given surface F(x, y, z) = 0, we can find its inversion surface with respect to a sphere centered at the origin with radius of R. To do this, simply let

$$x = r\cos\theta\sin\varphi,\ y = r\sin\theta\sin\varphi,\ z = r\cos\varphi$$

By substitution,

$$F(r\cos\theta\sin\varphi,\ y = r\sin\theta\sin\varphi,\ z = r\cos\varphi) = 0$$

If the above equation is solved for r, then $r = r(\theta,\varphi)$ is obtained.

Theorem 3. The inversion surface of the surface F(x, y, z) = 0 with respect to the sphere centered at the origin with radius of R can be given as follows:

$$InvS(\theta,\varphi) = \{x(\theta,\varphi),\ y(\theta,\varphi), z(\theta,\varphi)\}$$

$$where\ x(\theta,\varphi) = \frac{R^2\cos\theta\sin\varphi}{r(\theta,\varphi)}$$

$$y(\theta,\varphi) = \frac{R^2\sin\theta\sin\varphi}{r(\theta,\varphi)}$$

$$z(\theta,\varphi) = \frac{R^2\cos\varphi}{r(\theta,\varphi)}$$

Proof : Let Q be the point on the inversion surface and P be the corresponding point on the original surface with

$$dist(O,P) = r(\theta,\varphi)$$

It follows from the definition of inversion in geometry that

$$dist(O,Q) = \frac{R^2}{r(\theta,\varphi)}$$

Thus, the point Q has coordinates

$$\{x(\theta,\varphi),\ y(\theta,\varphi), z(\theta,\varphi)\}$$

$$where\ x(\theta,\varphi) = \frac{R^2\cos\theta\sin\varphi}{r(\theta,\varphi)}$$

$$y(\theta,\varphi) = \frac{R^2\sin\theta\sin\varphi}{r(\theta,\varphi)}$$

$$z(\theta,\varphi) = \frac{R^2\cos\varphi}{r(\theta,\varphi)}$$

The proof is complete.

Example 4.1 Given the surface (see [1]) $x^2y^2 + y^2z^2 + z^2x^2 = 1$, find its inversion surface with respect to the sphere centered at the origin with radius of $\sqrt{3}$. It follows from theorem 3 that

$$r(\theta,\varphi) = \frac{1}{\sqrt{\sin(\varphi)}\sqrt[4]{[\cos(\varphi)]^2 + \frac{1}{4}[\sin(2\theta)]^2[\sin(\varphi)]^2}}$$

and the inversion surface can be expressed as follow

$$InvS(\theta,\varphi) = \left\{\frac{3\cos\theta\sin\varphi}{r(\theta,\varphi)},\ \frac{3\sin\theta\sin\varphi}{r(\theta,\varphi)},\ \frac{3\cos\varphi}{r(\theta,\varphi)}\right\}$$

We have both the surface and its inversion surface as shown in figure 20 and figure 21, respectively.

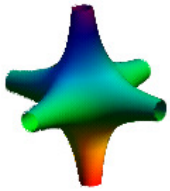

Fig. 20

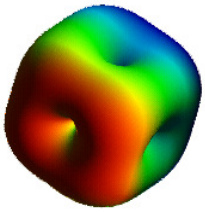

Fig. 21

Example 4.2 Given the surface $\left|x\right|^{\frac{a}{b}}+\left|y\right|^{\frac{a}{b}}+\left|z\right|^{\frac{a}{b}}=1$, find its inversion surface with respect to the unit sphere centered at the origin. It follows from theorem 3 that

$$r(\theta,\varphi)=\frac{1}{\left[\left|\cos\theta\sin\varphi\right|^{\frac{a}{b}}+\left|\sin\theta\sin\varphi\right|^{\frac{a}{b}}+\left|\cos\varphi\right|^{\frac{a}{b}}\right]^{\frac{b}{a}}}$$

and the inversion surface can be expressed as follow

$$InvS(\theta,\varphi)=\left\{\frac{\cos\theta\sin\varphi}{r(\theta,\varphi)},\ \frac{\sin\theta\sin\varphi}{r(\theta,\varphi)},\ \frac{\cos\varphi}{r(\theta,\varphi)}\right\}$$

We have both the surface and its inversion surface as shown in figure 22 (the left graph is for the original surface as while the right graph is for its inversion).

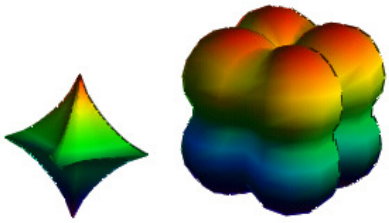

a = 3 b = 4

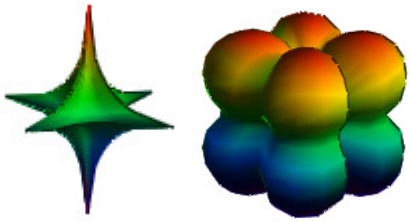

a = 2 b = 4

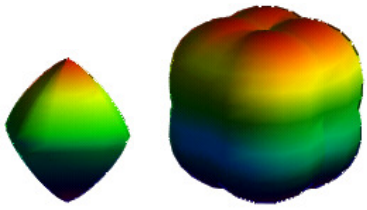

a = 5, b = 4

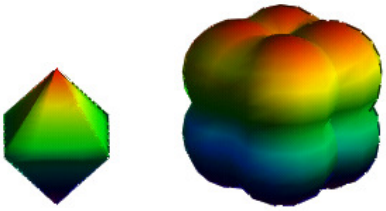

a = 4, b = 4

Fig. 22

5 Conclusions

This paper has presented three different ways to construct a surface: by moving a stick along a curve, by remodeling an existing surface, and by inverting a surface with respect to a sphere centered at the origin. For each method, we have given either a useful formula or a clear demonstration with many examples. These results might be used in surface design for games or other industrial purposes. It is hoped that these methods will inspire inquiry into additional methods of construction of surfaces.

6 References

[1] Alfred Gray, 1993, Modern Differential Geometry of Curves and Surfaces, CRC Press, Inc.

[2] E. Faber and H. Hauser, Today's Menu: Geometry and Resolution of Singular Algebraic Surfaces, Bulletin of the American Mathematical Society, Vol. 47, No. 3, July, 2010

[3] W. Hong, and M. Wu, 2010, Construction of Surfaces, CGVR2010: 22-26

[4] David H. von Seggern, 2007, CRC Standard Curves and Surfaces with Mathematica, 2nd Edition, Chapman & Hall/CRC

[5] J. A. Thorpe, 1979, Elementary Topics in Differential Geometry, Springer-Verlag.

[6] http://www.mathcadsales.com/

[7] http://www.wolfram.com/products/mathematica/index.html

[8] http://www.maplesoft.com/products/maple/

[9] http://www.mathworks.com/

The Forward Problem Algorithm Based on Monte Carlo Method for Diffusion Optical Tomography

Shih-Yang Wu, Shih Kang and Wai-Chi Fang, *Fellow, IEEE*
Department of Electronics Engineering & Institute of Electronics
National Chiao Tung University, 1001 Ta Hsueh Road, Hsinchu, Taiwan (R.O.C.)

Abstract - *In the medical field, abnormal tissues such as tumours or other foreign bodies often affect absorption coefficient in subcutaneous. First, photons are injected into skin, leading to diffusion behaviours, and then diffused light intensity on a specific location is measured. Next, foreign material distribution within the detection region is reconstructed by a specific weighting method for diagnosis. This study proposed a method of simulating photons' behaviours in subcutaneous tissues to obtain the distribution of surface intensity. Also, with assumed source location and detection location, a specific weighting method is used to calculate foreign body distribution.*

Keywords: DOT, diffusion optical tomography, Monte Carlo, simulation, 3D, image reconstruct, medical

1 Introduction

Subcutaneous tissue image reconstruction has been rapidly developed and applied to biomedical research over the past years [1]. As a new optical tissue imaging modality, diffusion optical tomography becomes an effective approach for in vivo imaging because it not only has the benefits of real-time imaging, but also has low-cost production and advantages of portable system [2], [3], [4]. However, simulation of light scattering behavior under highly scattering materials is necessary. The goal of DOT is to reconstruct the internal bioluminescent source with the measured optical signal on the external surface of a human body, which can be used for tumour diagnosis studies, cancer diagnosis, metastasis detection, oxygen concentration detection and development etc. The forward problem of DOT, which describes light transport in tissues, is employed not only to predict the distribution of the bioluminescent light on the object surface, but also to generate a two factor three-dimensional matrix that relates the measurements to internal optical properties and will be used in the inverse problem [5], [9]. Therefore, the accuracy improvement of the numerical solution to the forward problem of DOT is favourable since it enhances the quantification and localization of the reconstructed bioluminescent source.

In bio-photonics, the diffusion equation has been commonly used to model photon propagation in the biological tissue because the radiative transfer equation (RTE) is extremely computationally expensive for its integro-differential nature [3], [5]. And we all know that analytical, statistical and numerical techniques are three kinds of methods to solve the aforementioned diffusion equation [5]. However, data pre-processing and mesh generation for finite element method (FEM) is time-consuming and difficult, especially for three dimensional irregular objects with complex internal structure [5]. In this paper, a modified Monte Carlo method (MMCM) is developed to solve the forward problem of DOT firstly. Because tissues contain various kinds of materials like proteins, carbohydrates, esters, etc. and they are all of highly scattering materials, photons' behaviours in these media are rather complex, making simulation difficult. There are many kinds of simulation methods and an important one among them is the Monte Carlo method [7], which is a numerical calculating method based on statistical probability theories. Probabilities and statistical methods are adopted to simulate photons' paths, intensity changes, and distributions.

The paper is organized as follows. Section II introduces the theory of photon behaviour within a material. In section three, a detailed description of the MMCM algorithm for the forward problem of DOT [6] is presented. In section four, the result of this method is tested using cubic phantoms and applied simulation results on DOT are presented. Finally, the conclusion and future work are presented.

2 Theory of photon behavior in material

Moving electromagnetic waves are affected by all kinds of atomic and molecular. When it is spread out in a material, it interacts with electrons, causing phenomena like absorption, resonating, and sparkling. In the macro view, light absorption coefficient, scattering coefficient, and anisotropy coefficient can then be defined.

In figure 1, the figure of absorption coefficient, the Y axis represents the light intensity while the X axis represents the path length. Light intensity decreases exponentially when distance increases. Therefore, when absorption coefficient increases, average intensity of light reduces at the same time.

$$I = I_0 e^{-\mu_a * t} \quad (1)$$

The definition of anisotropy factor g is g=cos (θ), where θ is the anisotropy angle. In diffused light, the angle between the direction of a moving photon and the direction at the next time point is called the scattering angle. For the anisotropy

scattering phenomenon, different scattering angles leads to different probabilities which are mainly of Gaussian distribution, as shown in figure 2. The definition of anisotropy angle is related to the half-width of the Gaussian distribution. The probabilities of different scattering vectors of the same scattering angle are equal in a three-dimensional space, and the schematic diagram is shown in figure 3.

The Gaussian Probability Density Function is:

$$P_g(\theta) = \frac{1}{\sqrt{\sigma\pi}} e^{\frac{-\theta^2}{\sigma}} \quad (2)$$

In a three-dimensional space, the probabilities of vectors of the same scattering angle, but circling the central axis with different angles are the same. The probability can be written as:

$$P_p(\emptyset) = \frac{1}{2\pi} \quad (3)$$

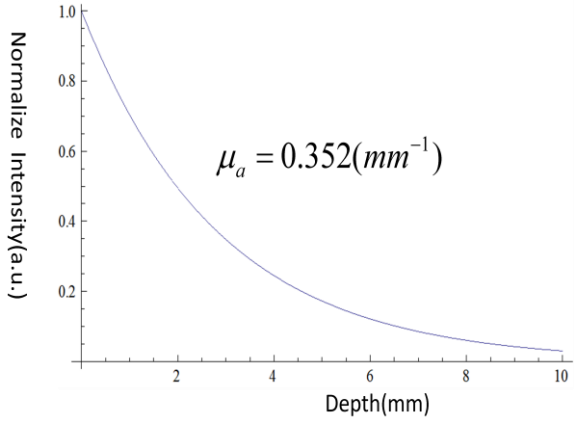

Fig. 1. Given a fixed absorption coefficient, light intensity decreases while depth increases.

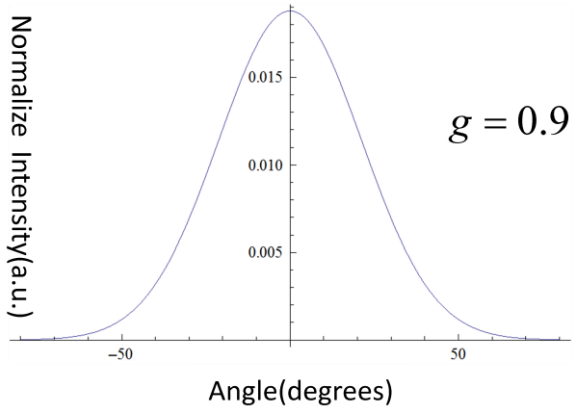

Fig. 2. Given a fixed scattering coefficient, the probability distribution of angles is Gaussian distribution.

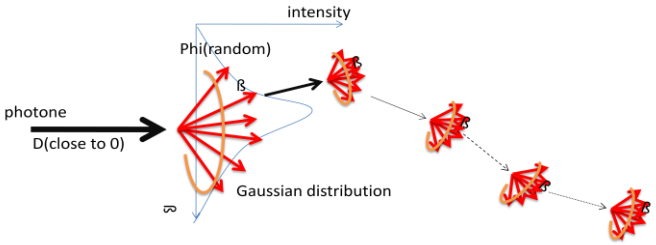

Fig. 3. Schematic diagram of scattering.

3 Approach and methods

3.1 Monte Carlo model

However, the Monte Carlo method can transform the complex function into a probability form, and then use probability to generate the density distribution of the solution. The scattering angle probability function $P_g(\theta)$ can be transformed into a reverse form θ_g which is similar to the Gaussian distribution. It can obtain the angle distribution function at specific standard deviations.

$$\theta_g(\sigma, \text{Rand}) \quad (4)$$

Repeated integration of θ_g results in a Gaussian distribution function. This function describing the angle distribution is the Monte Carlo form.

On the other hand, the probability function $P_p(\emptyset)$ formed by different angles $\emptyset$ encircling the central axis can also be transformed into a Monte Carlo form $\emptyset_p$ from which the angle distribution function can be obtained.

$$\emptyset_p(\text{Rand}) = \text{Rand} * 360 \quad (5)$$

Repeated integration of $\emptyset_p$ also yields back a horizontal line function, indicating that all the angle probabilities in $\emptyset_p$ are equal.

3.2 Algorithm

First, t is defined as time, which is discrete, and then other parameters are defined, including light intensity $I(t)$, position of photon in a space $[L_x(t), L_y(t), L_z(t)]$, and normalizing direction vector of photon in space $\vec{V}(t) = [\vec{V_x}, \vec{V_y}, \vec{V_z}]$. Each parameter represents a state at certain time point.

Assume that the angle between a normalized direction vector and a normalized direction axis $\vec{V_o}$ is θ, and the existing set of $\vec{V_f}$ forms a ring in a space, then the relation between $\vec{V_f}$ and $\vec{V_o}$ is: $\vec{V_o} \cdot \vec{V_f} = \cos(\theta)$. The diagram are shown in figure 4. This ring in the space can be expressed by $\vec{V_f}(\emptyset)$ i, where $\emptyset$ is the angle to circle around the axis $\vec{V_o}$.

Finally, a function TP() can be defined to calculate next state of $\vec{V_f}$.

$$\vec{V_f} = TP(\vec{V_o}, \theta, \emptyset) \tag{6}$$

The angle of incident light is $\vec{V}(0)$ and the position is $[L_x(0) = X_0, L_y(0) = Y_0, L_z(0) = Z_0]$. Then we can use TP() to calculate the light intensity $I(1)$, the position of photon $[L_x(1), L_y(1), L_z(1)]$, and the normalized directional vector of the photon $\vec{V}(1)$ at the next time point:

$$\begin{cases} I(1) = I(0) * e^{-\mu_a} \\ \vec{V}(1) = TP\left(\vec{V}(0), \theta_g(\sigma, Rand), \emptyset_p(Rand)\right) \\ [L_x(1), L_y(1), L_z(1)] \\ = [L_x(0) + \vec{V_x}, L_y(0) + \vec{V_y}, L_z(0) + \vec{V_z}] \end{cases} \tag{7}$$

Therefore, the states can be generally represented by the states of the previous time point as:

$$\begin{cases} I(t) = I(t-1) * e^{-\mu_a} \\ \vec{V}(t) = TP\left(\vec{V}(t-1), \theta_g(\sigma, Rand), \emptyset_p(Rand)\right) \\ \vec{L}(t) = \vec{L}(t-1) + \vec{V}(t-1) \end{cases} \tag{8}$$

Because the recursive function TP() above is too complex, it is not possible to solve the non-recursive function form. The solution has to be obtained step by step. Generally, we can calculate the states of a photon at t+1, by inputting the states at t into the function TP() to obtain the answers. Similarly, by inputting the states at t+1 to function TP(), we can obtain the states at t+2,as shown in figure 4. The shortcoming of this method is the long computation time.

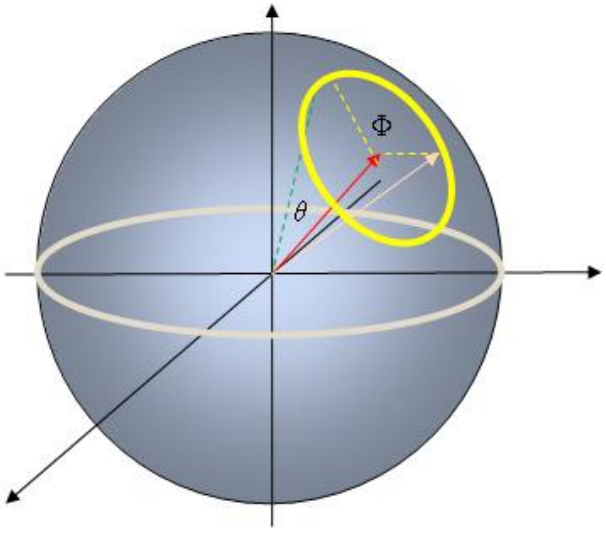

Fig. 4. Red line is the vector $\vec{V_o}$ and the pink is the vector $\vec{V_f}$.

3.3 Simulation

The above calculating method can be implemented using MatLab. First we must define a space that contains the information of absorption coefficient and the anisotropy coefficient to describe a photon's behaviour in the space. Figure 5 is a simulated schematic diagram of a photon's orbit in the space, with the arrow representing the incident light of the direction (0, 0, 1). The light goes upward into medium. The path shows the diffusion state in the space. Given longer transmission time, the probability of the photon deviating from the central axis is bigger. The statistical conclusion is that the trajectory distribution of photons is like a mushroom as shown in figure 5(d).

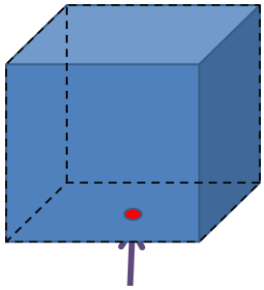

(a) The incidence position and direction in space.

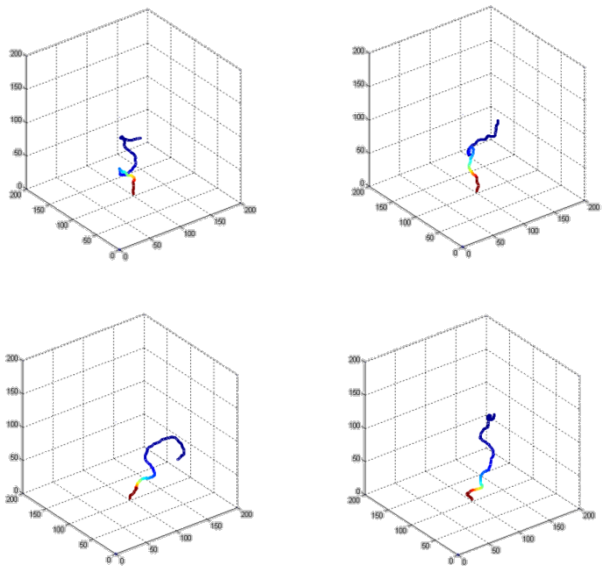

(b) Four examples of the photon's trajectory.

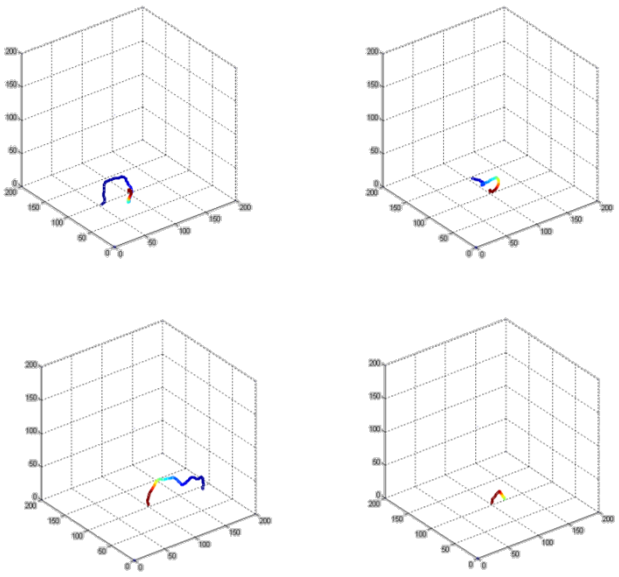

(c) Four examples of diffusion of photons out of the surface.

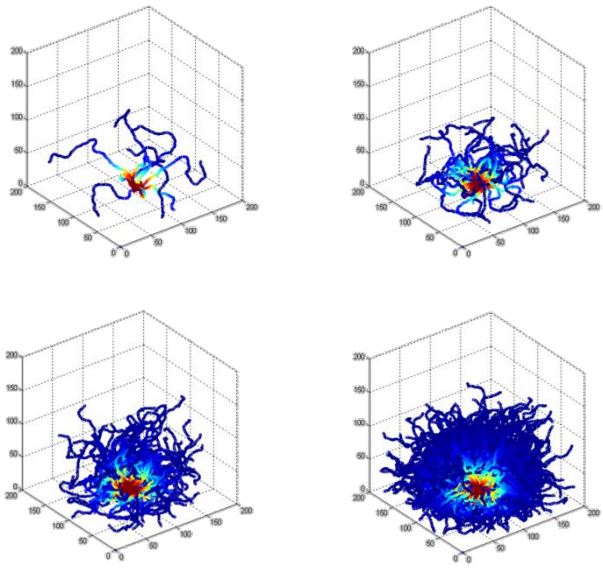

(d) Increasing the number of photons.

Fig. 5. Photon lines in the simulation box.

However, with some angles and some probabilities, there are chances that a photon may turn back. This phenomenon may occur while a photon has not yet been absorbed by the medium. It turns a half-circle and goes out through the incident plane as shown in figure 5(c). The surface intensity is the product of the vector of the photon's direction and the vector perpendicular to the surface.

$$I = I_0 * \left(\overrightarrow{V_i} \cdot \overrightarrow{V_\perp}\right) \quad (9)$$

The surface light intensity signal is detected by a light sensor, although the proportion of detected intensity and input intensity is low, the non-invasion form of the medical imaging is satisfied. The detected intensity on the surface is related to the asymmetrical distribution of absorption coefficient in the medium. Therefore, we adopt a suitable algorithm, with different positions of light sensor and light source, to reconstruct the approximated distribution of the absorption coefficient in the medium.

This study adopts the Monte Carlo method to calculate the probability distribution using photons' appearance probabilities, sending over tens of thousands of photons into the medium and counting all results. Because of the random function, each photon's path is unique. Therefore, the result may be closer to the result under micro view when more photons are simulated, and then the simulation can be close to the actual situation as shown in figure 5(d). Some photons are absorbed by the medium like shown in figure 5(b), and others scatter and go out through the surface before being completely absorbed like shown in figure 5(c). Because only light intensity of surface diffusion light can be detected, we simplify the program so that only surface intensity distribution is recorded, not intensity detected in other depths in medium.

4 Simulation result

First, we explore the influence of absorption coefficient and scattering coefficient before the actual simulation. Figure 6 shows the distributions of light intensity of different depths influenced by different absorption coefficients and scattering coefficients. When absorption coefficient increases, decaying rate of light intensity gets higher, while diffusion length reduces, so that the distribution coverage is rather small. And increasing scattering coefficient means increasing deflection of light path and high diffusion and low anisotropy in this medium. On the other hand, chance of light going back to the surface increases, and the power distribution also changes from fan-shaped to the half-elliptic-shaped. We can predict that if scattering material is perfect, the distribution may be presented in a semicircle shape, meaning that the intensity of light going out the surface must be smaller than half of the intensity of the incident light.

Figure 8 shows the simulation result of surface intensity. This annular structure may suggest that the typical diffusion behaviour in a high scattering medium is banana-shaped. The graphs on the left and the right are of high absorption coefficient and low absorption coefficient, respectively, and we can clearly observe the difference of theirs diffusion radiuses.

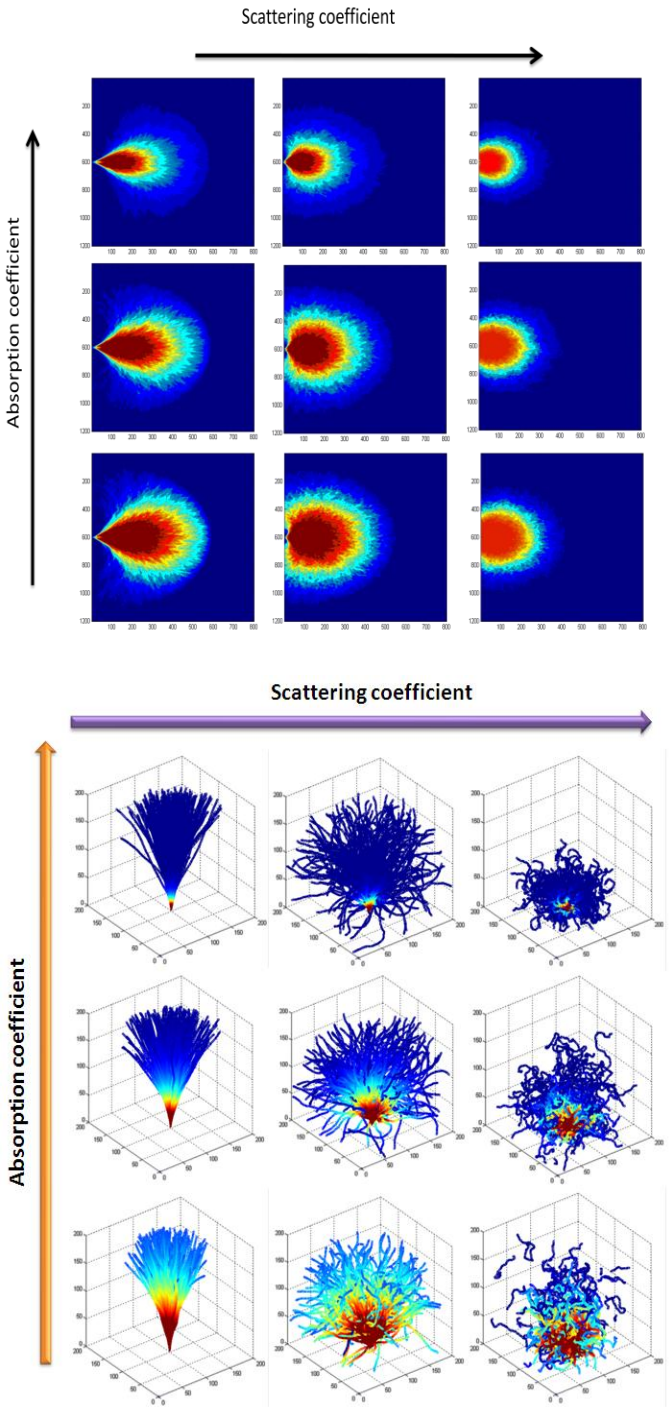

Fig. 6. Sectional drawing and 3D display of different absorption coefficient and scattering coefficient intensity [11].

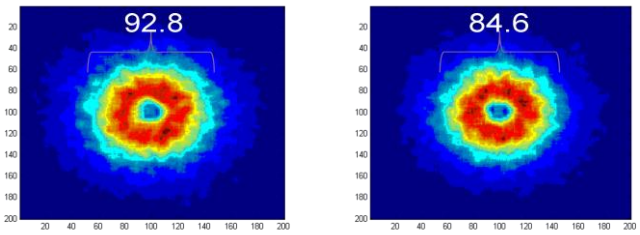

(a) The absorption coefficient is low (b) The absorption coefficient is high

Fig. 7. Surface light intensity

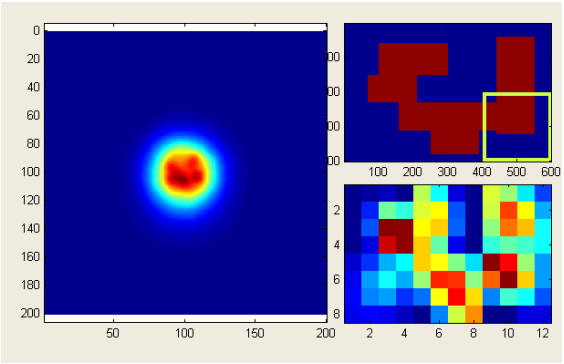

Fig. 8. Result of the complete simulation

5 Conclusion and future work

Based on the optical theory and formula, with the probability distribution of the Monte Carlo method, the parameter change function is constructed for each photon at every unit time. A complete probability path of a photon is then constructed through the iterations of the recursive function. Tens of thousands of photons are simulated in a complete parameter space, so that the simulated situation can be closer to reality. Finally, the sensors and light sources are arranged hypothetically, and then the intensities on the surface are obtained to simulate real hardware equipment, and weights are used to estimate absorption coefficient changes.

Figure 13 is the result of the complete simulation through the GUI. The number of simulated photons per simulation unit is twenty thousands, and a total of 6 units are simulated. The reconstructed result can be used to compare with the distribution of the original absorption coefficient distribution. It is found that the resolution of the reconstruction is quite limited. In the future, the image processing can be improved using techniques like geometric transformation, smoothing, edge detection, nonlinear color mapping, image denoising, etc.

6 Acknowledgment

This work was supported in part by the National Science Council of Taiwan, R.O.C., under grants NSC-99-2220-E-009-028, NSC-99-2220-E-009-030, and NSC-99-2220-E-009-071. This work was also partially supported by the Sophisticated Research and Development Industry Cooperation Project under the contract 99IA04 sponsored by the Hsinchu Science Park. Prof. Wai-Chi Fang is sponsored in part as the TSMC Distinguished Chair Professor by the TSMC Foundation. The authors would also like to express their sincere appreciation to the UMC University Shuttle Program and the National Chip Implementation Center for chip fabrication and testing service.

7 References

[1] V. Ntziachristos, J. Ripoll, L.V. Wang, and R. Weissleder. The QR Transformation I, *Nature Biotechnology*, vol. 23, no. 3, pp. 313-320, March 2005.

[2] C.H. Contag, and M.H. Bachmann. Advances in bioluminescence imaging of gene expression. *Annual Review of Biomedical Engineering*, vol. 4, pp. 235-260, 2002.

[3] W. Cong, G. Wang, D. Kumar, Y. Liu, M. Jiang, L.V. Wang, E.A. Hoffman, G. McLennan, P.B. McCray, J. Zabner, and A. Cong. Practical reconstruction method for bioluminescence tomography. *Optics Express*, vol. 13, no. 18, pp. 6765-6771, August 2005.

[4] Y. Lv, J. Tian, W. Cong, G. Wang, J. Luo, W. Yang, and H. Li. A multilevel adaptive finite element algorithm for bioluminescence tomography. *Optics Express*, vol. 14, no. 18, pp. 8211-8223, September 2006.

[5] A. P. Gibson, J. C. Hebden, S. R. Arridge. Recent advances in diffuse optical imaging. *Physics in Medicine and Biology*, vol. 50, no. 4, pp. 519-561, February 2005.

[6] Yuan-Huang Hsu; Chih-Chung Fu; Wai-Chi Fang; Tzu-Hsien Sang; , "A VLSI-inspired image reconstruction algorithm for continuous-wave diffuse optical tomography systems," *Life Science Systems and Applications Workshop, 2009. LiSSA 2009. IEEE/NIH* , vol., no., pp.88-91, 9-10 April 2009

[7] Tianxin Gao; Jing Bai; , "Finding the Most Probable Diffuse Path of Photons in Tissue by Monte Carlo Method," *Complex Medical Engineering, 2007. CME 2007. IEEE/ICME International Conference on* , vol., no., pp.1124-1128, 23-27 May 2007

[8] T. J. Farrell, M. S. Patterson, and B. Wilson, "A diffusion theory model of spatially resolved, steady-state diffuse reflectance for the noninvasive determination of tissue optical properties in vivo," Medical physics, vol. 19, p. 879, 1992.

[9] S. Arridge, "Optical tomography in medical imaging," Inverse problems, vol. 15, pp. 41-41, 1999.

[10] Qin, Chenghu; Tian, Jie; Liu, Kai; Dai, Yakang; , "The forward problem algorithm based on modified element free Galerkin method for bioluminescence tomography," *Engineering in Medicine and Biology Society, 2008. EMBS 2008. 30th Annual International Conference of the IEEE* , vol., no., pp.3747-3750, 20-25 Aug. 2008

[11] Kurt, B.; Gulsoy, M.; , "Optical and thermal response of laser irradiated tissue," *Biomedical Engineering Meeting, 2009. BIYOMUT 2009. 14th National* , vol., no., pp.1-3, 20-22 May 2009

Adaptive Neuro-Fuzzy Forecasting for Egypt's East Coast Wind-Speed

O. M. Salim
Electrical Engineering Department,
Benha High Institute of Technology,
Benha University, Egypt

M. A. Zohdy
School of Engineering and Computer Science, Oakland University,
Rochester MI 48309, USA

H. T. Dorrah and A.M. Kamel
Electrical Power and Machines
Faculty of Engineering, Cairo University, Egypt

***Abstract*—Wind energy contribution as a source of energy in electric utility systems around the world is on the increase. One of the major challenges of wind energy generation is its natural intermittency; unpredictability, and uncertainty. In this paper, two and three dimensional visualization profiles were presented for the power coefficient. Further, two and three dimensional profiles for the turbine output power as function of rotor-speed and wind-speed were presented. Four different adaptive neuro-fuzzy wind predictors are proposed and compared to forecast the wind speed blowing on the east-coast of Egypt. The proposed wind models are designed using ANFIS toolbox in MATLAB. These models are based on real wind-speed data recordings. Data used in the first model are yearly data for the respective month in which the forecasting is done. Also based on the concept of time series prediction, the other three models are proposed based on one complete month data to forecast daily, half-daily, and quarter-daily of wind-speed.**

Keywords-component; Adaptive Neuro-Fuzzy Inference System, Membership function, Power Coefficient, Tip speed ratio.

I. INTRODUCTION

The wind has served mankind well for many centuries by propelling ships and driving wind turbines to grind grain and pump water [1]. Wind energy is considered one of the very fast growing energy resources all over the world, especially in the Europe, USA, Canada, Middle-East, and Africa [2]. Wind energy offers numerous advantages including clean energy that do not produce atmospheric emissions or cause acidic rain or greenhouse gases [1], [2]. In addition, it cannot be exhausted, and it can be built in farms, benefiting economy, where most of the best wind sites are found. It is one of the lowest-priced renewable energy technologies [2]. Wind energy is increasing its contribution in electric utility systems around the world.

Egypt relies on the burning fossil fuels to satisfy about 85% of its electricity requirements [3]. The National Renewable Energy Authority (NREA) states that Egypt is currently generating 600 MW of power from wind, 2010, with a goal to generate 7,200 MW of wind power by 2020 [3]. Wind atlas of Egypt, 2005, indicated that the coastal plain between Suez and Hurghada (especially Gabal El-Zayt) on Egypt's east coast has sufficient wind resources to generate up to 20,000 MW [4]. According to the annual report of the Egyptian Electricity Holding Company (EEHC) in 2009, Egypt's main wind power generation is achieved by Zafarana wind farm. Zafarana wind farm (425 MWs) contribute to about 2% of total load in Egypt in the year 2009 [5]. Egypt was planning for the wind to be responsible of 5% of electricity capacity by 2010, but Egypt couldn't build up its wind capacity as quickly as it has wished and the latest capacity is approximately 600 MW [6].

One of the major challenges of wind energy generation is its natural intermittency; unpredictability, and uncertainty of wind resources. Due to that irregular nature, and as a result the wind-power production, accurate wind prediction is much needed. Therefore, researchers have focused on deriving accurate stochastic models for wind speed, wind direction, and consequently wind-power prediction. These wind models are based on soft-computing either using probabilistic modeling [7], [8] (using random process estimation theories) or based on approximate reasoning using expert systems [9]—[12] like neural networks, fuzzy logic, and Hybrid systems for random processes estimation.

Wind-power prediction has a great importance for several operations related to power systems. Among these related operations are: the optimal power flow between conventional units and wind farms, the power system generators scheduling, energy reserves and storages planning and scheduling, and the electricity marketing bidding. Forecasting the output power of a wind energy conversion system (WECS) is based mainly on accurate forecasting of the incident wind-speed at the unit site [7]. Wind prediction is a complex task due to the wind's high degree of volatility and deviation. *Very short-term forecasting* is defined as look ahead periods from a few minutes up to an hour, while *short-term forecasting*, which is proposed in this paper, will indicate hours out to a few days ahead. This difference between the two forecasting time periods is important when trying to create a prediction system [11]. In [10], [11] Three main classes of techniques have been identified for wind forecasting. These are numeric weather prediction (NWP) methods, statistical methods, and methods based upon artificial neural networks (ANNs).

NWP methods are mathematical fluid mechanics model-based. NWP methods are the fairly accurate which were developed by meteorologists and are well researched. NWP is achieved by solving conservation equations (mass, momentum, heat, water, etc.) numerically at given locations on a spatial grid in 3D: latitude, longitude, and elevation. This is considered across the fourth dimension of time as well. Predictions using NWP model have some limitations: data variability; digital elevation models' resolution; grid spacing; computation time and also suffers from inaccurate input data [11].

Omar M. Salim is with Electrical Engineering Department, Benha High Institute of Technology, Benha University, Egypt. (E-mail: omar.salem@bhit.bu.edu.eg).
M. A. Zohdy is with School of Engineering and Computer Science, Oakland University, Rochester, MI 48309. (E-mail: zohdyma@oakland.edu).
H. T. Dorrah and A.M. Kamel are with Electrical Power and Machines Faculty of Engineering, Cairo University, Egypt. (E-mail: dorrahht@aol.com , amakamel@hotmail.com respectively).

The conventional statistical models are based on time-series models. These models are including auto regressive (AR), and auto regressive integrated moving average (ARIMA) models. Persistence models are considered as the simplest time-series models. These models can surpass many other models in very short-term prediction. The persistence approach has proven to be a useful first approximation for short-term wind power prediction and provides a benchmark against which to compare alternative techniques [9].

In [7], a technique based on Grey predictor model for wind-power forecasting was proposed, while in [8] a wind-speed predictor was proposed. Grey predictors have been widely applied in different fields. The main advantage of the Grey predictor model is that it requires a small number of data points to achieve the predicted series. During the last decades, several time-series based models have been involved in wind-speed forecasting. These models were used for forecasting average values for the incidents' wind-speed for one step ahead, and they are characterized by requiring a large set of historical data [8]—[12]. In [9] hybrid wavelet particle swarm optimization (PSO) along with adaptive neuro-fuzzy inference systems (ANFIS) predictors were suggested as a short-term wind-power forecasting. While in [10], average hourly wind-speed forecasting with grid partitioning ANFIS, the proposed model was based on ten years of wind-speed data recordings. In [11] a very short-term wind-speed prediction of few minutes ahead was proposed using grid partitioning ANFIS. In [12], a long-term wind-speed and power prediction were proposed, based on years of wind-speed data recordings, using artificial neural networks (ANN) with local recurrent-type models.

This paper is organized as follows. Section II presents the significance of wind generation and the power coefficient and tip speed ratio (TSR) profiles, as well as, the turbine output power profiles. Section III describes the proposed approach for short-term wind-speed forecasting. Section IV presents the results obtained for the case studies, as well as, discusses the results before Section V concludes.

II. SIGNIFICANCE OF WIND ENERGY

WECS have quickly evolved over the last decades, therefore, an efficient and reliable exploitation tools are necessary to make these installations more profitable [13, 14]. The main objective of most of the WECS is to extract the maximum power available in the wind stream [15]. WECS transforms the available energy of the wind blowing through its blades into mechanical energy.

$$P_w = \frac{1}{2}\rho A V_w^3 \quad (1)$$

where, P_w is the total power existing in the wind stream in Watts, ρ is the air density in kg/m^3, A is the swept area of the wind turbine blades in m^2, and V_w is the wind-stream speed in m/s. According to so called Betz limit (16/27) which shows that that an actual turbine cannot extract more than 59.3% of the power in an undisturbed tube of air of the same area. In practice, the fraction of power extracted will always be less because of mechanical imperfections [1].

$$P_m = \frac{1}{2}\rho A C_p(\lambda,\beta) V_w^3 \quad (2)$$

$$\lambda = \frac{\omega R}{V_w} \quad (3)$$

where, P_m is the mechanical power that could be captured from the total wind power, C_p is the power coefficient which is a function of the TSR (λ) and the pitch angle of the wind turbine blades (β) in degrees. Equation (3) shows the TSR is the ratio between the linear speed of the rotor and the wind-speed, where ω is the generator speed in rad/s and R is the blade length in meters. The power coefficient $C_p(\lambda, \beta)$ has a common generic form, available in MATLAB/SIMULINK [16], as shown in (4) and (5)

$$C_p(\lambda,\beta) = C_1\left(\frac{C_2}{\lambda_i} - C_3\beta - C_4\right)e^{\frac{-C_5}{\lambda_i}} + C_6\lambda \quad (4)$$

$$\frac{1}{\lambda_i} = \frac{1}{\lambda + 0.08\beta} - \frac{0.035}{\beta^3 + 1} \quad (5)$$

The coefficient C_1 to C_6 are: C_1=0.5176, C_2=116, C_3=0.4, C_4=5, C_5=21 and C_6=0.068. The turbine output power profile illustrates the mechanical power of a wind turbine versus the rotor speed at different wind speeds. Since power curves are obtained by field measurements, where an anemometer is placed on a reasonably close to the wind turbine (not on the turbine itself, due to turbulences created by the wind turbine itself which make wind speed measurement unreliable). In reality, a swarm of points spreads around each power curve [15]. The reason is that in practice the wind speed always fluctuates, and one cannot measure exactly the column of wind that passes through the rotor of the turbine. Moreover, the wind speed has different values at each point of the blade. The uncertainties associated with the power curves is studied below for both power coefficient and turbine output power [15].

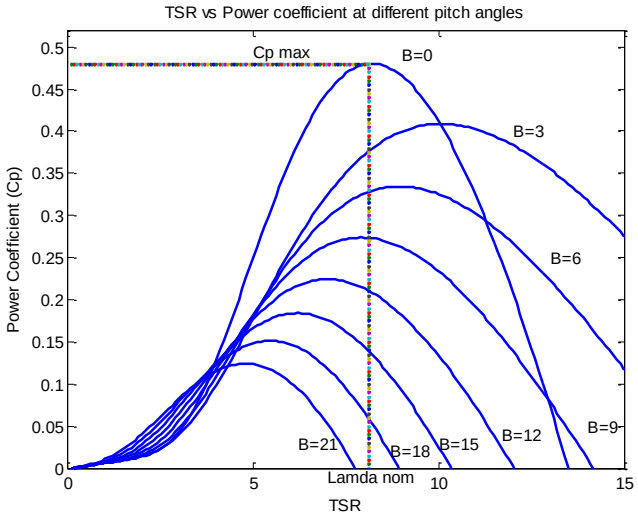

Figure 1. Power effecieny curves in response to changes in TSR and β

A. Power Coeffiecient Profile

The power coefficient curves are illustrated in Fig. 1, which show the relationship between C_p and TSR at different blade's pitch angles. Equations (4) and (5) are used to obtain these curves. Maximum value for C_p (C_{p_max} =0.48) is obtained at the nominal value of TSR (λ=8.1). In Fig. 1 C_{p_max} is obtained at β=0. A three-dimensional surface illustration of C_p(λ, β) is shown in Fig. 2 which illustrate the effect of β as well as the effect of the TSR on the power coefficient (efficiency profile of the wind turbine). As the TSR increase the C_p will increase until it reaches its maximum value at the nominal TSR then in starts to decrease again, while the increase in β decreases the value of C_p.

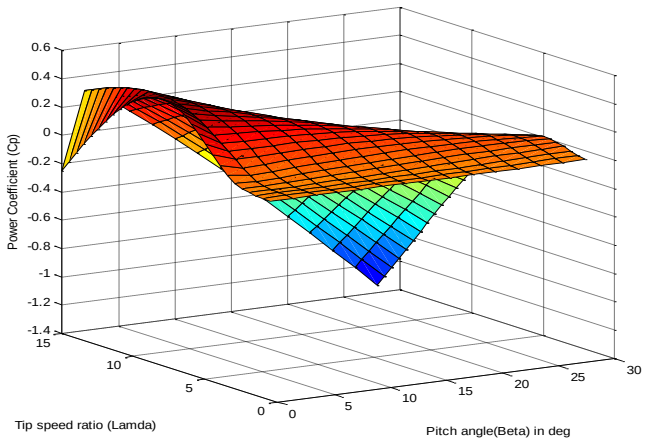

Figure 2. Three-dimensional graph for Cp(λ, β)

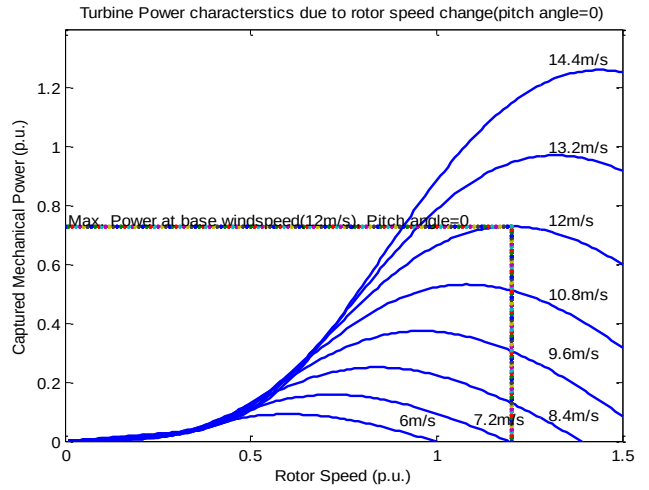

Figure 3. WT output power function of rotor speed at different wind-speed

B. Turbine Output Power Profile

The turbine per unit (p.u.) mechanical output power curves, as p.u. of the nominal mechanical power, are shown in Fig. 3 as a function of the rotor speed at different values of wind-speed. Fig. 3 showed that, at β=0 and wind-speed value equal to the base wind-speed of 12m/s, the maximum power that can be achieved is 0.73p.u. Fig. 4 presents the p.u. output power profile (surface) as a function of both rotor p.u. speed and wind-speed. It illustrates four different surfaces for different values of pitch angle (β =15°, 10°, 5° and 0°) as the fourth dimension of that graph. The lower surface corresponds to the higher pitch angle; on the other hand the higher surface corresponds to zero pitch. The output power curves as well as the surfaces show that as the rotor speed increases, the output power increases, also as the wind-speed increases, the output power increases.

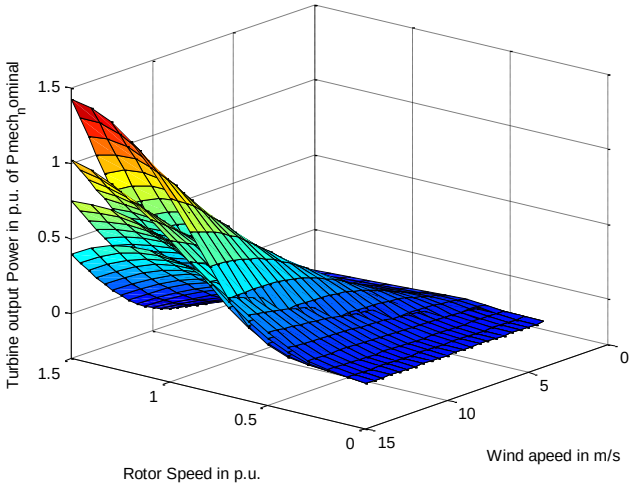

Figure 4. 3-dimensional graph for p.u. output power at different pitch angles (β =15°, 10°, 5° and 0° respectively from the bottom up)

III. WIND-SPEED FORECASTING PROPOSED METHODOLOGY

Integration of accurate wind prediction in the management and control regimes involved in WECS provides a significant tool for optimizing operating costs and improving reliability [12]. However, due to highly complex interactions and the contribution of various meteorological parameters, wind forecasting is a severe task. Stochastic techniques depends on collecting wind-speeds related historical data for the purpose of; wind atlas preparations, wind sites monthly and annual production and wind turbines optimum sites prediction using Weibull statistical model; or predicting the performance of hybrid wind systems and their annual production, consumption of fuel, and costs [8]. Weibull distribution, as the most commonly used probability density function to describe the wind-speed, is shown in (6)

$$f(w) = \frac{k}{c}\left(\frac{w}{c}\right)^{k-1} e^{-(w/c)k} \qquad (6)$$

where k is a shape parameter, c is a scale parameter and w is the wind-speed. If the shape parameter equals 2, the Weibull distribution is known as the Rayleigh distribution. For the Rayleigh distribution the scale factor, c, given the average wind speed ($\bar{w}$) can be found from (k=2, and $c = \frac{2}{\sqrt{\pi}}\bar{w}$) [1].

In Fig. 5, the wind-speed probability density function (pdf) of the Rayleigh distribution is plotted. The average wind-speeds in the figure are 7, 9 and 11 m/s which correspond to Ras-Sedr, Zafarana, and Gulf of El-Zayt some different regions in Egypt [4, 5, 6]. In this paper, four different models for wind-speed prediction were proposed. The differences between these models are in the amount of wind-speed data recordings required and number of hours (Hrs) ahead to be predicted. All

proposed models are short-term models, starting by 24-Hrs ahead down to 6-Hrs ahead of wind-speed forecasting.

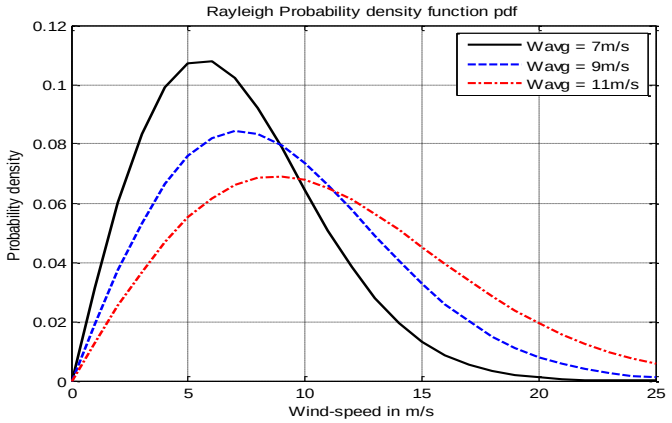

Figure 5. Probability density of the Rayleigh distribution

The proposed approach in this paper is based on an ANFIS as a superior soft-computing technique. It was used as a way to predict many practical time-series data. ANFIS approach is based on using the neural networks training capability to adjust the membership functions' (MF) parameters of the proposed fuzzy inference system (FIS). The real-data sets used to automatically build the proposed models were obtained through huge database for weather recordings website that covers almost all countries around the globe. These recordings are based on real hourly-based measurements for the corresponding sites [17]. The study proposed is done for Hurghada site as one of the candidate sites in Egypt that has sufficient wind resources to generate up to 20,000 MW.

The proposed ANFISs are based on a subtractive clustering technique in which Gaussian MFs are used. Subtractive clustering generates an initial model for ANFIS training. This subtractive clustering method partitions the data into groups called clusters, and generates an FIS with the minimum number of rules required to distinguish the fuzzy qualities associated with each of the clusters [18]. The subtractive clustering avoids the curse of dimensionality of grid partitioning method [18]. Subtractive clustering is a fast, one-pass algorithm for estimating the number of clusters and the cluster centers in a set of data. It is used especially if there is no clear idea about how many clusters there should be for a given set of data.

IV. Results and Discussions

The real-world case study proposed in this paper is divided into four subsections; each subsection has a model to forecast the wind-speed for a certain period of time.

A. Model-I: 24-Hrs Ahead Based on Yearly Data Recordings

Model-I is based on wind-speed data for five months in five consecutive years e.g. the month of December of years 2006, 2007, 2008, 2009 and 2010. In order to train an ANFIS, complete data sets of inputs along with their corresponding desired output data are needed. Thus, wind-speed data from 2006-2009 are used as 4 inputs with data sets of 2010 are used as a corresponding output. Only 30 days data (3600 data points) were used for training, while the 31st whole day is to be predicted using the obtained model. The monthly data selected in the same season to avoid the climate change between seasons.

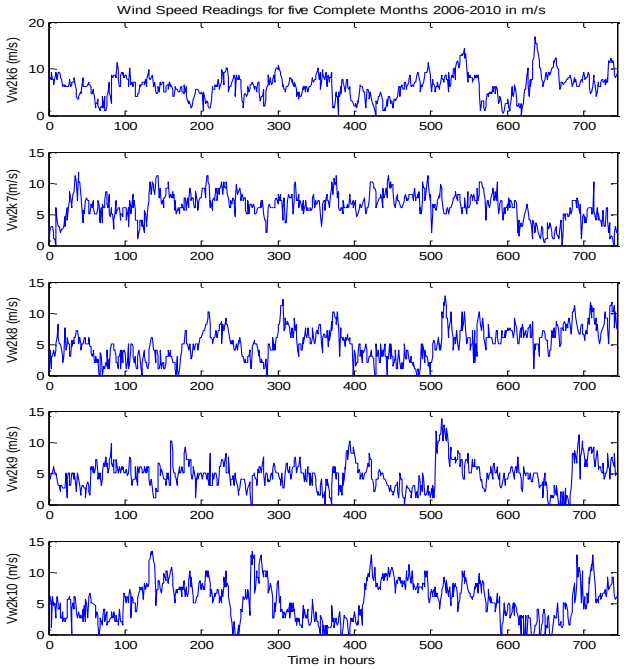

Figure 6. wind-speed recordings for 5 complete months

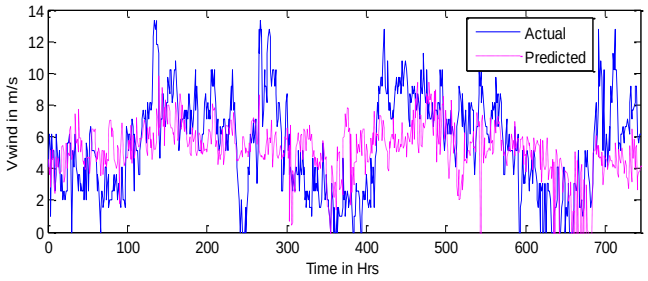

Figure 7. One month wind-speed data for model-I (Actual, Predicted)

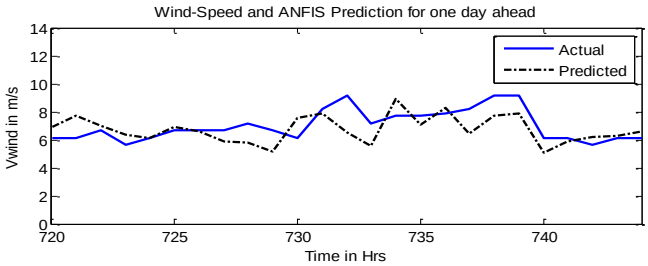

Figure 8. Actual and predicted values for 24-Hrs ahead

Fig. 6 presents the wind-speed data sets in m/s for December 2006 -2010 from upper graph down respectively. The data are hourly recordings, then, for 31 days a total of 744 data point are shown per graph, only 720 points per graph are used for training purposes and the last 24-Hrs are predicted. The generated 4 inputs FIS (using subtractive clustering) provides a single output Takagi-Sugeno-Kang (TSK) type with linear MFs for the output. The root mean square error (RMSE) resulted during training epochs is 2.4 m/s which is considered

as a bias value for the model. This bias value is added to the predicted output as a correction factor. The resulting ANFIS model is used for the purpose of testing and validation to predict the whole month of December 2010 and, hence compared to the real measurement as shown in Fig.7. Fig.8 shows the wind-speed forecasting in m/s for one day ahead for the period starting at hour 720 to hour 744 (24-Hrs) as the 31st day of December. The Mean Error (ME) between actual and predicted wind-speed is found to be around 0.31 m/s with a Mean Absolute Error (MAE) of 0.91 m/s.

B. Model-II: 24-Hrs Ahead Based on one month Data

Model-II is based on wind-speed data for only one month e.g. December 2010. In this model one month of hourly based wind-speed recordings are required. Data are rearranged to create a mapping from 4 sample wind-speed data points, sampled every 24-Hrs, to a predicted future of 24-Hrs.

$$Data(k) = [x(k-3P) \quad x(k-2P) \quad x(k-P) \quad x(k)] \quad (7)$$

The output training data corresponds to the prediction.

$$Target(k) = x(k+P) \quad (8)$$

where, k is the time instant in hours, P is the period to be predicted (in this case P = 24), the training input/output data is a structure whose first component is the four-dimensional input *Data(k)* as in (7), and its second component is the output *Target(k)* as in (8). There are 720 input/output data points. These data points are used for ANFIS training (these became the training data set), while only part of them are used for validating the identified fuzzy model.

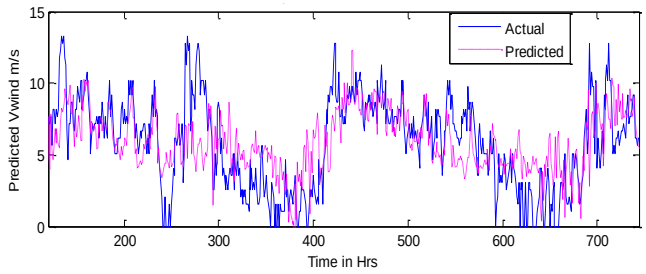

Figure 9. One month wind-speed data for model-II (Actual, Predicted)

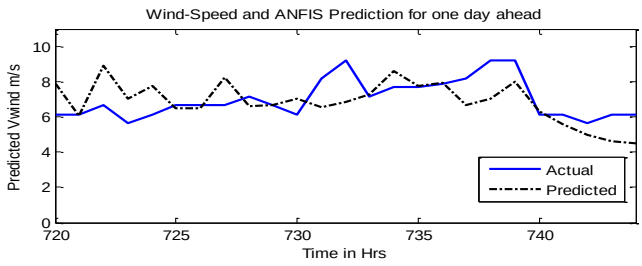

Figure 10. Actual and predicted values for 24-Hrs ahead

Data points are plotted in last graph of Fig. 6. These data points are then rearranged as 5 vectors of shifted wind-speed recordings. Training is done based on the concept of time-series prediction. Then data is used for validating the ANFIS by predicting the whole month and compare it with the actual data as shown in Fig. 9. The prediction of December 31st is shown in Fig. 10, the prediction error is quite similar prediction error for model-II as for model-I. The Mean Error (ME) between actual and predicted wind-speed is found to be around 0.13 m/s with a Mean Absolute Error (MAE) of 1.00 m/s. The results obtained by model-II has a significant advantage over model-I. This advantage is that model-I has much more data points used in the training step (model-II uses only 20% of model-I data points). Thus, model-II is preferred over model-I.

C. Model-III: 12-Hrs Ahead Based on One month Data

Model-III is similar to model-II based on the same date points. Data are rearranged to create a mapping from 4 sample wind-speed data points, sampled every 12 hours (P = 12), to a predicted half-day ahead. There are 732 input/output data points are used for ANFIS training.

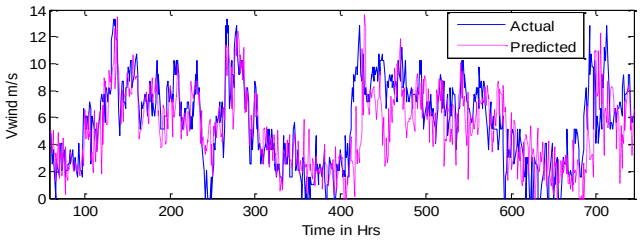

Figure 11. One month wind-speed data (Actual, Predicted)

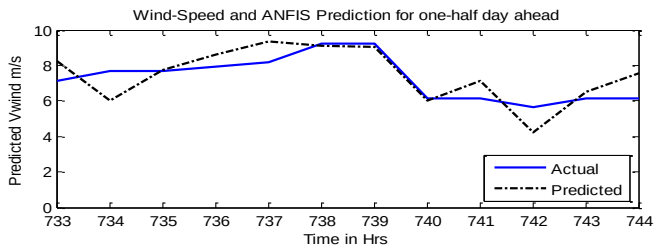

Figure 12. Actual and predicted values for 12-Hrs ahead

Data points (Dec. 2010) are the same used in model-II, which are rearranged as five vectors of 12-Hrs shifted wind-speed recordings. After training, data is then used for validating model-III by predicting the whole month as shown in Fig. 11 as a comparison between actual and predicted model. Prediction of 12-Hrs ahead is shown in Fig. 12. This model shows good prediction performance too with respect to model-I with 20% of real data used in training. The ME between actual and predicted wind-speed is found to be around 0.13 m/s with a MAE of 1.03 m/s.

D. Model-IV: 6-Hrs Ahead Based on One month Data

Model-VI based on the same data, which are sampled every 6-Hrs (P = 6), to a predicted quarter-day ahead. There are 738 input/output data points which are used for ANFIS training. Data points are rearranged as five vectors of 6-Hrs shifted wind-speed recordings. ANFIS training is done based on the concept of time-series prediction. Data is then used for validating the ANFIS by predicting the whole month as shown in Fig. 13 as a comparison between actual and predicted model. The prediction of 6-Hrs ahead is shown in Fig. 14; the ME between actual and predicted wind-speed is found to be around 0.25 m/s with a MAE of 0.97 m/s.

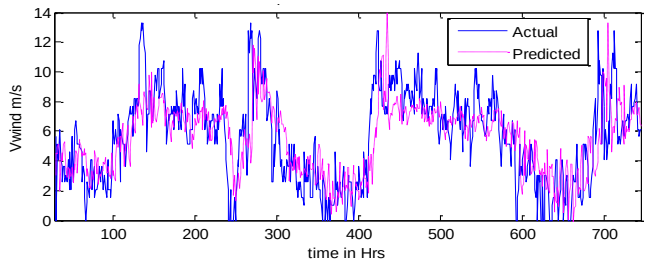

Figure 13. One month wind-speed data (Actual, Predicted)

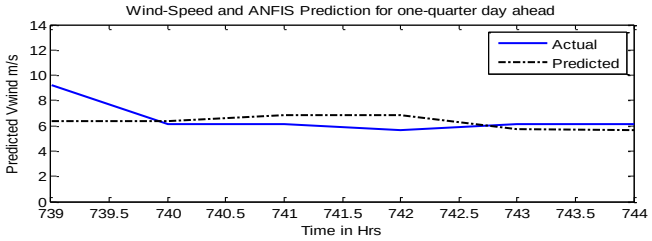

Figure 14. Actual and predicted values for 6-Hrs ahead

TABLE I. ACCURACY STUDY FOR WIND-SPEED FORECASTING.

	Model-I	Model-II	Model-III	Model-IV
Prediction Period	24-Hrs	24-Hrs	12-Hrs	6-Hrs
Data points	3600	720	732	738
RMSE (m/s)	1.13	1.26	1.48	1.31
Mean Error (m/s)	0.31	0.13	0.13	0.25
MAE (m/s)	0.91	1.00	1.03	0.97
MAPE (%)	12.67	14.29	13.98	13.57

Summary for the error and accuracy study, which is summarized in Table I., illustrates that the accuracy of model-I (based on 3600 real data points) showed better than the accuracy of other models in the literature ([7]-[12]), while model II, III and IV have similar accuracy with the advantage of less amount of data are used (20 %).

V. CONCLUSION AND FUTURE WORK

In this paper, two and three dimensional visualization profiles were presented for the power coefficient as function of TSR and pitch angle of the blades. Further, two and three dimensional profiles for the turbine output power as function of rotor-speed and wind-speed were presented. Four effective stochastic wind models were proposed and optimized using ANFIS Toolbox. The model-I was based on yearly wind-speed data sets for the same month from 2006 to 2010; the target was to predict 24-Hrs ahead. The model accuracy was good with a ME of 0.31 m/s. Models II, III and IV, which are proposed to predict 24, 12 and 6 hours ahead respectively, were based on only one month wind-speed data set. Accuracy of model-II, III and IV were similar to model-I with the advantage of using only 20% of wind-speed data sets used in the model-I.

Our future research work is to apply type-2 adaptive neuro-fuzzy inference system to overcome the large uncertainty in wind-speed variation and to rid of data outliers. Also we plan to extend the proposed models to encounter both wind-speed and wind-direction forecasting.

REFERENCES

[1] Gary L. Johnson, 'Wind Energy Systems', Manhattan, Kansas, USA, Electronic Edition, October 2006.

[2] NREL, USA. http://www.nrel.gov/news/press/2010/838.html.

[3] Harry Tournemille Energy Boom Finance, Wind Energy, Sep. 2009. http://www.energyboom.com/wind/egypt-looks-wind-power-solve-dwindling-fossil-fuel-supply.

[4] Wind Atlas of Egypt, http://www.windatlas.dk/Egypt/About.html.

[5] http://www.egelec.com/mysite1/annual%20report/annual%20report.htm

[6] M. Elsobki, P. Wooders, and Y. Sherif, "Clean Energy Investment in Developing Countries: Wind Power in Egypt," International Institute of Sustainable Development IISD, www.iisd.org, October 2009.

[7] T.H.M. El-Fouly, E.F. El-Saadany, and M.M.A. Salama, "Grey Predictor for Wind Energy Conversion Systems Output Power Prediction," IEEE Transactions on Power Systems, vol. 21, no.3, 2006, pp. 1450 - 1452.

[8] T.H.M. El-Fouly, E.F. El-Saadany, and M.M.A. Salama, "One Day Ahead Prediction of Wind Speed and Direction," IEEE Transactions on Energy Conversions,pp. 1-7 , 2006.

[9] J. P. S. Catalão, H. M. I. Pousinho, and V. M. F. Mendes, "Hybrid Wavelet-PSO-ANFIS Approach for Short-Term Wind Power Forecasting in Portugal," IEEE TRANSACTIONS ON SUSTAINABLE ENERGY, vol. 2, no. 1, pp. 50-59, 2011.

[10] F. Castellanos1 and N. James , "Average Hourly Wind Speed Forecasting with ANFIS," ACWE11-2009, 11th Americas Conference on Wind Engineering, San Juan, Puerto Rico, June-2009.

[11] M. Negnevitsky and C. W. Potter, "Very Short-Term Wind Forecasting for Tasmanian Power Generation," IEEE Transactions on Power Systems, vol. 21, no. 2, pp. 965–972, 2006, .

[12] Thanasis G. Barbounis, J. B. Theocharis, M. C. Alexiadis, P. S. Dokopoulos, "Long-TermWind Speed and Power Forecasting Using Local Recurrent Neural Network Models," IEEE TRANSACTIONS ON ENERGY CONVERSION, VOL. 21, NO. 1, pp. 273-284, 2006.

[13] S. Mathew,' Wind Energy Fundamentals, Resource, Analysis and Economics', Springer, Netherlands, pp.1-90, 2006.

[14] J. F. Manwell, J. McGowan, Rogers A. 'Wind energy explained: theory design and applications'. John Wiley & Sons; 2002.

[15] M. Azouz, A. Shaltout, M. A. L. Elshafei, N. Abdel-Rahim, H. Hagras, M. Zaher, M. Ibrahim, "Fuzzy Logic Control of Wind Energy Systems", MEPCON'10 pp. 935-940, 2010.

[16] http://www.mathworks.com/help/toolbox/physmod/powersys/ref/windturbine.html, accessed January 2011.

[17] Weather Underground website, www.wunderground.com.

[18] http://www.mathworks.com/help/toolbox/fuzzy/fp715dup12.html.

Aromaticity and antiaromaticity of Au(III) hexaphyrins: A DFT study

Jesús Muñiz[1], Enrique Sansores[2], V-H Ramos-Sanchez[1], Alfredo Olea[1], Roger Castillo[1]
[1]Cuerpo Académico de Energía y Sustentabilidad, Universidad Politécnica de Chiapas
Calle Eduardo J. Selvas S/N, Col. Magisterial, Tuxtla Gutiérrez,
Chiapas, México. C.P. 29010
[2]Instituto de Investigaciones en Materiales, Universidad Nacional Autónoma de México.
Apartado Postal 70-360, México DF 04510, México.

Abstract - *A theoretical study based on Density Functional Theory at the B3LYP level (DFT/B3LYP), on extended metalated porphyrins: meso-hexakis(pentafluorophenyl)- [26] hexaphyrin (1.1.1.1.1.1), termed hexaphyrins, was carried out. Electronic structure calculations were performed in order to obtain full geometry optimizations of the complexes under study. Such calculations were carried out on a High Performance Computing Cluster. NICS (Nuclear Independent Chemical Shift) calculations are also reported to analyze the aromatic behavior that presents this kind of compounds. The series of complexes under study appear to have aromatic and antiaromatic character, the analogue non-metalated system shows an aromatic character, consistent with the available experimental data.*

Keywords: Hexaphyrin, Density Functional Theory, Excited states, Molecular modeling.

1 Introduction

Porphyrins are aromatic compounds that compose several natural pigments that have been extensively studied. Expanded porphyrins have recently emerged as a new class of conjugated pyrrolic macrocycles. This kind of complexes present optical, electrochemical and coordination properties that are not common in porphyrins. An also interesting property of the expanded porphyrins is the aromaticity of the macrocycles which is determined by the π electrons in the conjugated circuit. The systems under study are the *meso*-hexakis(pentafluorophenyl)-substituted[26] hexaphyrin(1.1.1.1.1.1) and the derivatives obtained by Au(III) metalation of the [26] hexaphyrin (see Fig 1). In particular, complex **1** shows a strong aromaticity with a 26π conjugated circuit [1].

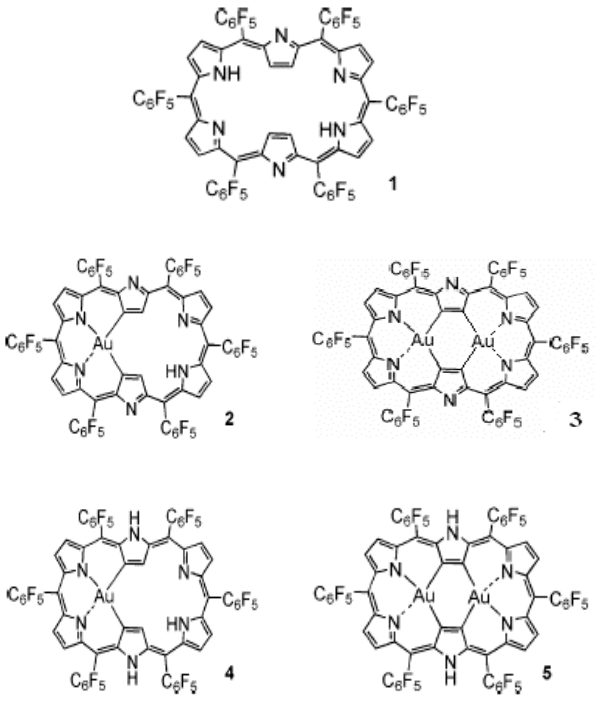

Figure 1. Hexaphyrin structures under study

2 Computational method

The optimized geometries were obtained using Density Functional Theory with the B3LYP [2] functional, which combines the exact Hartree-Fock exchange with the Lee, Yang and Parr correlation functional that includes the most important correlation effects. The pseudopotential LANL2DZ2 with 19 valence electrons was used for the gold atoms to include relativistic effects and the 6-31G++ basis set for the rest of the atoms. All calculations were performed with computational code Gaussian03 [3].

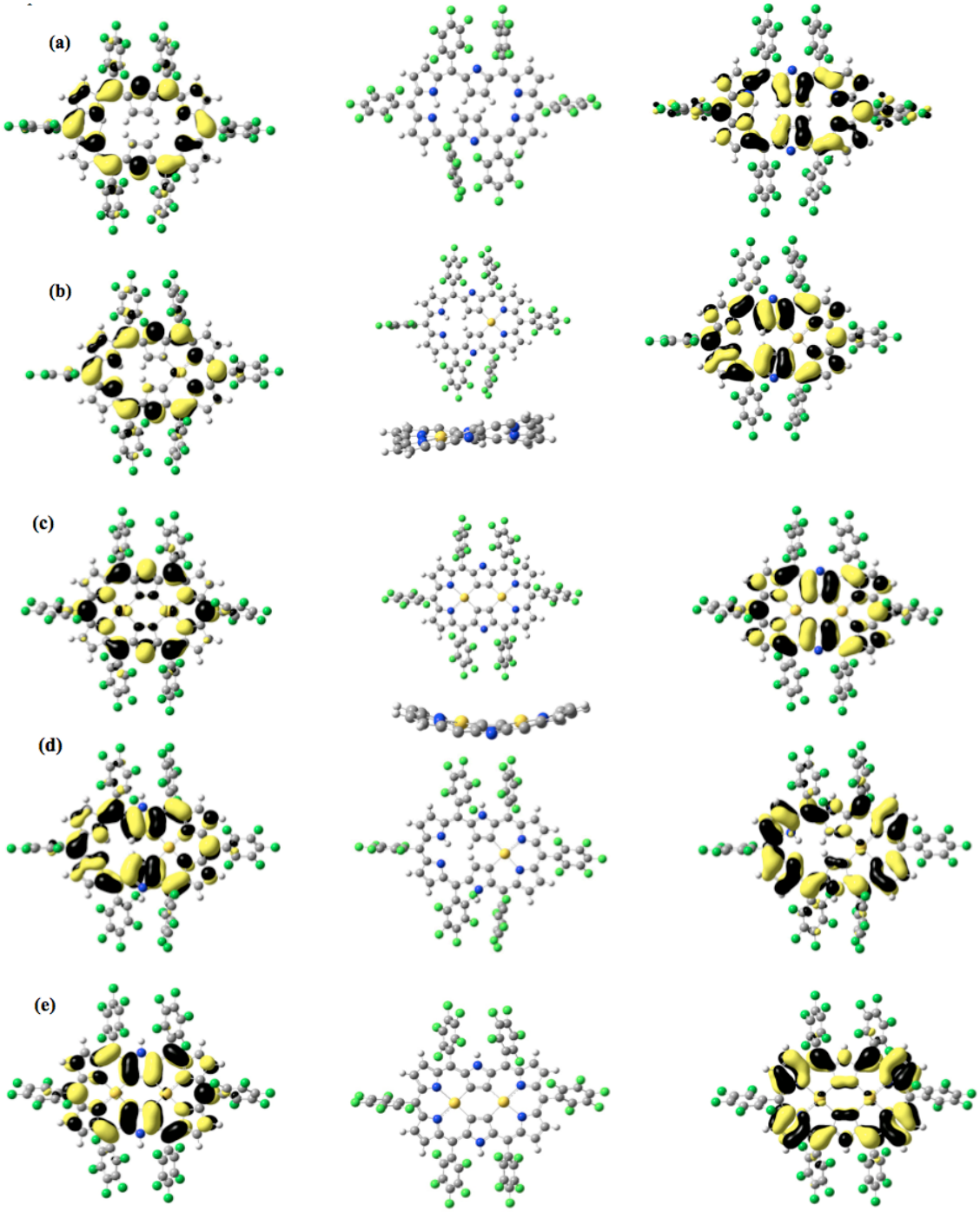

Figure 2. Optimized geometries and spatial representations of the HOMO and LUMO of the compounds under study: (a)compound 1 (Hexakis(pentafluorophenyl)hexaphyrin), (b)compound 2, (c)compound 3, (d)compound 4, (e)compound 5

Aromaticity calculations were performed by the NICS (Nuclear Independent Chemical Shift) methodology, developed by Schleyer *et al* [4].

3 Results and discussion

Complex **1** and its derivatives were fully optimized by the method described above. All optimized structures are shown in Figure 2.

After geometry optimization, complex **1** presents a planar geometry with a slight deviations near the center of the ring. The spatial representation of the frontier molecular orbitals is shown in Figure2(a), the HOMO is composed of π-orbitals located on the C and N atoms of the ring. The LUMO has a contribution of π-orbitals on the center of the ring. Complex **2**, which has a gold atom located close to the center of the molecule presents a twisted structure with a slight deviation from the plane, as can be seen from the view perspective on Figure 2(b) (the pyrrol groups are omitted for clarity).

The HOMO for this complex, has a similar contribution from that of **1** and in this case, a contribution from the p orbitals of gold is also present. The contribution from the LUMO is similar to that of **1**. The presence of a second gold atom in complex **3** changes the geometry of the molecule from a twisted to a bent structure, as can be observed from the lateral view in Figure 2(c), which is in clear agreement with the results found by experiment. In this complex, the gold atoms contribute with p orbitals to the HOMO, while for the LUMO, the contributions are located on the N atoms. A comparison of the structural parameters found experimentally and by the present theoretical method is reported in Table1. It includes bond distances and bond angles. Geometry optimizations of complexes **4** and **5** , which are derivatives of complexes **2** and **3**, were also carried out. The theoretical results for these compounds are in reasonable agreement with those found by experiment, as can be seen from Table1. The HOMO of complex **4** has a contribution on the center of the ring, as can be seen from Figure 2(d) while the contribution to the LUMO is mainly located on the C atoms around the ring. Complex **5** shows a similar pattern on the frontier molecular orbitals to that of **4**, which are presented in Figure 2(e). The characteristic planarity observed on the complexes **2** to **5** is due to the presence of the gold atoms as can be inferred from the optimized geometry for complex **1**, where no gold atoms are present.

3.1 Aromaticity

To understand the aromatic properties of the compounds under study, NICS(Nuclear Independent Chemical Shift) calculations were performed in complexes **1** to **5**. The NICS were calculated following the technique developed by Schleyer [4], a ghost atom is located at the center of the ring and the magnetic susceptibility is calculated at this posotion. These results are summarized in Table2. For complex **1**, the ghost atoms were aligned on the center of the ring. According to the NICS values, complex **1** appears to be strongly aromatic. For complex **2**, the ghost atoms were located at the region far from the gold atoms and an aromatic behavior is also observed. In the case of complex **3**, a ghost atom was located at the center of the ring on the intermediate zone between the gold atoms. As can be seen from Table2, complex **3** reveals a strong aromaticity on this area.

Table 1 Bond lengths and angles for the compounds under study

Bond	Experimental	Theory	Bond angle	Angle (deg.) Experiment	Angle (deg.) Theory
Bond lengths and angles for complex 1					
N1-C5	1.37	1.42	C7-N3-C8	105.23	104.06
N2-C9	1.38	1.42	C9-C15-N6	127.00	130.09
C5-C6	1.41	1.43	C11-N4-C12	107.74	104.19
C9-C10	1.38	1.43	C12-C13-C14	127.46	129.58
N3-C7	1.38	1.40	C13-C14-N5	126.65	130.28
Bond lengths and angles for complex 2					
Au1-C1	1.98	2.03	C1-Au1-C2	91.44	91.82
Au1-C2	2.01	2.03	N1-Au1-N2	88.88	88.67
Au1-N1	2.08	2.13	C5-N1-Au1	126.72	126.11
Au1-N2	2.08	2.13	C7-C2-Au1	124.16	122.82
N1-C5	1.37	1.38	N2-Au1-Cl	90.73	90.37
Bond lengths and angles for complex 3					
Au1-Au2	4.22	4.21	Cl-Au1-C2	88.57	89.74
Au2-C3	2.04	2.03	N1-Au1-N2	86.54	86.30
Au2-C4	2.02	2.03	C3-Au2-C4	88.98	89.74
Au2-N5	2.11	2.14	N6-Au2-N5	87.02	86.30
Au2-N6	2.10	2.14	C5-N1-Au1	126.28	125.58
Bond lengths and angles for complex 4					
Au1-C1	1.98	2.02	Cl-Au1-C2	91.44	91.98
Au1-C2	2.01	2.02	N1-Au1-N2	88.88	89.07
Au1-N1	2.08	2.11	C5-N1-Au1	126.72	125.65
Au1-N2	2.08	2.11	C7-C2-Au1	124.16	122.62
N1-C5	1.37	1.40	N2-Au1-C1	90.73	90.40
Bond lengths and angles for complex 5					
Au1-Au2	4.22	4.26	Cl-Au1-C2	88.57	89.48
Au2-C3	2.04	2.03	N1-Au1-N2	86.54	85.92
Au2-C4	2.02	2.03	C3-Au2-C4	88.98	89.48
Au2-N5	2.11	2.13	N6-Au2-N5	87.02	85.92
Au2-N6	2.10	2.12	C5-N1-Au1	126.28	125.32

region far from the gold atoms and an aromatic behavior is also observed. In the case of complex **3**, a ghost atom was located at the center of the ring on the intermediate zone between the gold atoms. As can be seen from Table2, complex **3** reveals a strong aromaticity on this area.

Complexes **4** and **5**, show a strong antiaromaticity that can be inferred from the hydrogen atoms attached to the N atoms on the upper and lower sides of the molecules. To the best of our knowledge, antiaromatic behavior in porphyrins has been unknown, while for expanded porphyrins this behavior is not common. According to the this study, the presence of the gold atoms on complexes 4 and 5 in the region of the central ring, plays an important role on the antiaromatic properties of these compounds.

Table 2 Calculated NICS

Compound[§]	1	2	3	4	5
NICS1(ppm)	-11.77				
NICS2(ppm)	-14.89	-12.33	-10.16	18.74	34.41
NICS3(ppm)	-11.97	-11.94		21.55	

[§]NICS1 is at the left side of the geometrical center of the ring, NICS2 is at geometrical center of the ring and NICS3 is at the right side of the center of the ring.

4 Conclusions

Full geometry optimizations of the extended porphyrins were carried out, revealing a planar structure with slight deviations for compound **1**, a twisted structure for the complex with one gold atom (**2**) and a bent structure for the compound with two gold atoms(**3**). The optimized geometries of complexes **4** and **5** also reveal a twisted and bent structure, respectively. The planar character of this complexes can be addressed to the presence of the gold atoms. To understand the aromatic behavior of the compounds, NICS calculations were also performed. According to this calculations, complex **1**, **2** and **3** are strongly aromatic. On the other hand, complexes **4** and **5** are antiaromatic. This is caused by the presence of the H atoms attached to the N atoms of the rings.

5 References

[1] Mori S., Osuka A. "Aromatic and antiaromatic Gold(III) Hexaphyrins with multiple Gold-Carbon Bonds"; J. Am. Chem. Soc. (ACS Publications) Vol. 127, (2005) 8030-8031.

[2] Becke, A.D. "Density-functional thermochemistry. III. The role of exact exchange" J. Chem. Phys. (American Institute of Physics) Vol. 98 (1993) 5648-5652.

[3] M.J. Frisch, et al., Gaussian 03, Revision B.05 and D.01, Gaussian, Inc., Pittsburgh PA, 2003.

[4] (a) Schleyer, P. v. R.; Maerker, C.; Dransfield, A.; Jiao, H.; Hommes, N. J. R. E. "Nucleus-Independent Chemical Shifts: A Simple and Efficient Aromaticity Probe" J. Am. Chem. Soc. (ACS Publications) Vol. 118 (1996) 6317-6318.

(b) Tokitoh, N.; Wakita, K.; Okazaki, R.; Nagase, S.; Schleyer, P. v. R.; Jiao, H. "A Stable Neutral Silaaromatic Compound, 2-{2,4,6-Tris[bis(trimethylsily)methyl]phenyl}-2-silanaphthalene" J. Am. Chem. Soc. (ACS Publications) Vol. 119 (1997) 6951-6952.

The "K" Nearest Neighbor (KNN) problem: An "Expanding Boundary" algorithm for Octrees

Robert C. Yoder
Department of Computer Science, Siena College, Loudonville, New York, USA

Abstract - *In this exploratory paper we discuss an algorithm to find a set of the K nearest neighbors of a given point by using a variant of the octree data structure. This algorithm operates by generating a list of boundary nodes that expand from a given query point and placing nearest neighbor data points in a priority queue based on their distance from the query point. The set of boundary nodes are also stored in a priority queue ordered by their centroid distance from the query point. An interesting sub-problem to be solved is determining the neighbor of a node in a given direction that is closest to the query point.*

Keywords: Octree, nearest neighbor

1 Introduction

The nearest-neighbor problem (in both exact and approximate forms) has been studied for its applications for a variety of problems, from image rendering (photon mapping) [4] to the N-body problem for analyzing complex physical systems [5], to data mining in many dimensions and spatial queries in geographic information systems (GIS). One approach employs locality-sensitive hashing to place "close" points in the same "bucket" [1]. Other techniques use spatial decomposition to perform a top-down recursive search, pruning and selecting most likely nodes, backtracking as necessary. This approach can be applied to R-trees [6], k-d trees [3,4] and balanced box decomposition (BBD) trees that store points in axis-aligned (hyper)rectangles with bounds on the ratios of the longest and shortest sides. The BBD algorithm outlined in [2] builds a priority search queue for visiting nodes in increasing distance from the query point. This paper investigates the feasibility of an expanding boundary algorithm for finding nearest neighbors in a variant of an MX (matrix) octree.

Octrees are spatial data structures used for image processing, solid modeling, GIS, and other applications. Octrees can represent 3-D regions, edges, or points by a recursive, cubical decomposition of space in all three dimensions. The path from the root node to other nodes deeper in the tree can be described by a location code that identifies a unique path (sequence of octal digits) from the root of the structure to a specific node. An important problem in many applications is finding adjacent regions within an octree. Given a target location code, how can we determine the properties of neighboring regions?

Our MX-octree variant has the following properties: the maximum depth is defined before creating the octree; and the nodes containing data (x,y,z coordinates) are at the deepest (leaf) level so that the length of their location codes are equal to the maximum depth. When building an MX-octree at a specified maximum level, if a data point is so close to an existing point that it is indistinguishable, we use a Count attribute in leaf nodes, making this an approximate neighbor algorithm.

2 How the Expanding Boundary algorithm operates

Our approach is to build a set of nodes representing the edge of the search space, and incrementally expand the boundary such that nodes containing nearest neighbors are searched first in an MX octree. Geometric adjacency information is encoded in various tables, state machines, and priority queues. Given a query point (QP) to find a set of K neighbors for, we generate an expanding boundary (fringe) from the QP and check for neighbors within the boundary nodes closest to the QP. We implemented this algorithm utilizing two priority queues named KNNQ and FRINGEQ. KNNQ contains the closest neighbors discovered so far (in distance order), and FRINGEQ contains the location codes (LC's) of nodes currently representing the expanding boundary, ordered by the centroid distance to the QP, secondarily ordered by LC. Ordering for the C++ (template library) priority queue data structure was implemented by overriding the OPERATOR< (less than) method. Although some of the issues and implementation aspects of the algorithm are discussed, no claims are made about the efficiency of this algorithm at this stage of the project. The general algorithm is described on the following page (Figure 1), followed by a description of how the nodes representing the boundary are calculated.

After the octree is constructed, prompt the user for the x,y,z coordinates of the QP.
Determine the LC of the QP, then push it onto FRINGEQ since it is our initial boundary.

While the FRINGEQ is NOT EMPTY:
Pop the top node from FRINGEQ into the target node location code called TN.
Pop off and discard all other nodes from FRINGEQ that are duplicates of TN.
(We cannot avoid occasionally placing duplicate LCs in FRINGEQ – discussed later.)
If the TN represents a full node (contains a point), calculate its Euclidean point distance to the QP.
If we already have K points in KNNQ,
replace the topmost (most distant) point with the current point only if it's closer,
otherwise just add the point to KNNQ.
Compute neighbor location codes of TN at the deepest octree level for each of the 6 primary directions:
RIGHT, LEFT, DOWN, UP, BACK, FRONT {R,L,D,U,B,F}.
These neighbor nodes must be the ones closest to the QP.
If the Computed Neighbor (CN) did not go outside the boundaries of the octree:
place it on the FRINGEQ only if it is farther away (using CENTROID distance)
from the QP than the TN.
This way, we expand the fringe while (mostly) avoiding placing duplicate LCs on FRINGEQ.
Once the FRINGEQ is empty, display the contents of the KNNQ listing the closest neighbors.

Figure 1: The Expanding Boundary Algorithm.

3 Computing boundary location codes

Our initial target node (TN) is set to the location code of the Query Point (QP). For a given target octree node TN, we expand the fringe boundary by calculating its neighbor node CN for each primary (octree face) direction, but only use neighbor nodes that are further away from the QP. See Figure 3 (left side) for octree face, edge, and corner direction notations. We start by using a Finite State Machine (FSM) based technique [7] to compute the location code of a SAME-SIZED neighbor node to the target node, as described below. Sometimes we encounter the same neighbor node from more than one direction. For example: in Figure 2 left, assume node 13 is the QP. We find neighbor nodes 11 and 12 farther away from the QP. When processing nodes 11 and 12, both will find node 10. Rather than checking for duplicate nodes when inserting in FRINGEQ, we pop off duplicate nodes when processing the FRINGEQ.

3.1 Step 1: determine the same-sized neighbor of TN

First copy the location code from TN to CN. Using the direction as the row, replace CN's location code digits from *right to left* using the FSM Table until a *halt* is encountered or there are no more digits. The FSM table is shown in Figure 2 (right side). The effect is to ascend the octree from the target node, computing the neighbor node using navigation information encoded in the FSM, until the common ancestor node is reached for the target and its neighbor.

For example, to compute the RIGHT neighbor of node 03 (see Figure 2, left side):

- Lookup the entry in the FSM table for direction R and octant 3. It is 2.
- Replace the 3 with 2. We now have CN=02. No halt was encountered so we continue.
- The next CN digit to the left is 0. The table entry for R and 0 is: 1, halt.
- We replace the 0 in CN with 1. We encountered a halt, so CN=12 is the result.

If no *halt* action is encountered when computing the neighbor, the CN is outside the octree universe and we skip to the next direction.

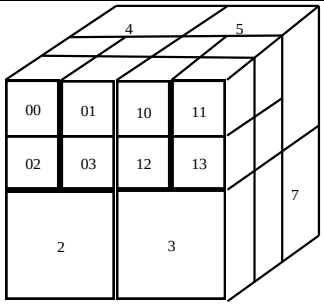

Dir	Octant:0	1	2	3	4	5	6	7
R	1,halt	0	3,halt	2	5,halt	4	7,halt	6
L	1	0,halt	3	2,halt	5	4,halt	7	6,halt
D	2,halt	3,halt	0	1	6,halt	7,halt	4	5
U	2	3	0,halt	1,halt	6	7	4,halt	5,halt
B	4,halt	5,halt	6,halt	7,halt	0	1	2	3
F	4	5	6	7	0,halt	1,halt	2,halt	3,halt

Figure 2: Sample octree decomposition showing nodes 03 and 12 as neighbors, and neighbor FSM.

The complexity of the algorithm comes from the fact that *neighbor nodes must be the ones closest to the QP*. This is because nodes of various sizes can be in the boundary list in FRINGEQ. When computing a neighbor from a non-leaf node, there are potentially many (smaller) neighboring leaf nodes for that direction, since non-leaf nodes have fewer digits in their location codes. We may need to compute the additional LC digits (the *extension*) of the neighbor node that is closest to the QP, so that the expanding boundary grows outward incrementally. This complication could be removed if we simply expanded our boundary by leaf-sized nodes. However, the boundary would grow slowly, and would not exploit the property of non-leaf nodes in the octree representing large regions of empty space. The remainder of this paper explores the details of steps two through five that computes boundary nodes in increasing distance from the QP, taking non-leaf node sizes into account. This process includes determining the direction of the QP in relation to the computed neighbor.

There may be different sized nodes in our FRINGEQ boundary that will become our Target Node. If our TN is not at the deepest level, we will need to calculate the location code of a smaller neighbor node. Which one of the many possible smaller neighboring nodes should we calculate? The one closest to the QP must be calculated to grow the fringe boundary in a monotonically increasing fashion. For example, see Figure 2, left side. Assume the QP is in node 13. If the TN=2, we eventually calculate the Computed Neighbor in the UP direction using the neighbor FSM as CN=0. There are four smaller neighbors in the UP direction {02, 03, 06, 07}, but we need to select 03 since it is closest to the QP=13. Note that nodes 06 and 07 are located behind 02 and 03. Thus, we need to compute extension digits that are appended to the computed neighbor CN when it has fewer location digits than the QP location code at the deepest level in the octree.

Thus, if the length of CN's LC is the same as QP's LC, there is no need to compute the extension, so we can skip to step 5 to probe the octree to determine CN's actual depth. Otherwise, CN's location code represents an interior (larger) node that has child (subtree) nodes in it, so we select the subtree node closest to the query point by computing the extension in step 2. The length of the extension is the difference in length between the target node and the query point LCs. The octree is then probed to find the actual size of the closest neighbor – it will not necessarily be at the deepest level. Details on computing the extension digits follow.

3.2 Step 2: determine the relative direction of the QP and CN

To determine the general direction of the query point with respect to the computed neighbor, scan *left to right* comparing LC digits of CN and QP. Use the first *differing* digits from the computed neighbor (row) and the query point digit (column) to look up the initial relative direction in the Coarse_Direction table (Figure 3, right side). This table describes how the octants are adjacent to each other.

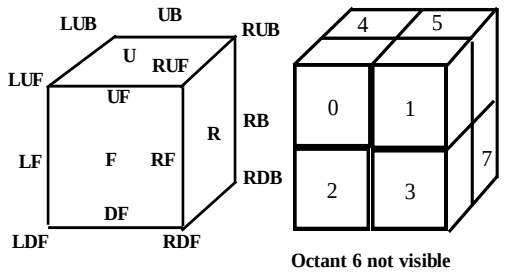

	QP Digit							
CN Digit	0	1	2	3	4	5	6	7
0	-	R	D	RD	B	RB	DB	RDB
1	L	-	LD	D	LB	B	LDB	DB
2	U	RU	-	R	UB	RUB	B	RB
3	LU	U	L	-	LUB	UB	LB	B
4	F	RF	DF	RDF	-	R	D	RD
5	LF	F	LDF	DF	L	-	LD	D
6	UF	RUF	F	RF	U	RU	-	R
7	LUF	UF	LF	F	LU	U	L	-

Figure 3 : Octree directions (Left/Right, Up/Down, Back/Front), Numbering, and Coarse_Direction Table.

If there are no differing digits (e.g., CN=7, QP=74) we have a special case where CN is an ancestor node of QP in the octree, so we return UNKNOWN as the direction and skip to step 4B to resolve the direction from a different perspective.

Otherwise, we use a case statement for each possible direction for possible refinement of the directional relationship between CN and QP. If the coarse direction is a corner {LUF,LUB,LDF,etc}, we proceed to step 3 to fill in CN's extension with a repeating digit from the Corner_Extend table. Otherwise, the direction will be one of 18 non-corner directions {R,L,D,U,B,F,RU,RD,LD,LU,RB,LB,DB,UB,RF,LF,DF,UF} so we use the corresponding secondary 8-by-8 Refined_Direction table (there is one for each non-corner direction) to refine the direction if possible. Rather than list all 18 tables, an example will be given for a single direction case. The R_Refined_Direction table is selected when we have determined the QP is somewhere to the RIGHT of the CN, and is used to refine the relative direction using the remaining CN (row) and QP (column) digits. Secondary tables may reveal edge or corner directions by looking deeper into the tree comparing CN and QP LCs. For example, if CN= 01 and QP = 13, the first differing digits are 0 and 1, so the Coarse_Direction table (Figure 3, right) returns direction R. We use the second digits 1 and 3 in the R_Refined_Direction table to determine that QP octant 3 is to the Right and Down (RD) direction of CN octant 1 (see Figure 4).

If the secondary table returns a corner (e.g., RDB) we can proceed to step 3, otherwise go on to the next CN and QP digits. The secondary tables are used to resolve direction at a deeper level. It is possible for the coarse direction R to further refine to RB or RDB. Note that we only allow transitions that refine the direction from Face to Edge to Corner. Thus, R to [RD or RDF] is allowed but not from RD to [R or RB].

3.3 Step 3: Fill in extension for corner directions

The corner rule: for corner directions, we can use a single repeating digit for the entire extension. For example, in Figure 5, assume the target node TN = 01 and we are computing the neighbor in the D (down) direction. Using the FSM table in Figure 2, we determine that the same-size Computed Neighbor CN = 03. The candidate sub-octants within CN that are adjacent to TN are topmost octants {0,1,4,5}. Assume the QP is anywhere in octant 7 and is 6 digits in length, e.g., 700000. Since the QP is to the RDB (Right, Down, and Back) of CN, we select sub-octant 5 as being closest of the candidate octants to QP and extend CN's LC with 5's until it has the same length of the QP. CN then becomes 035555.

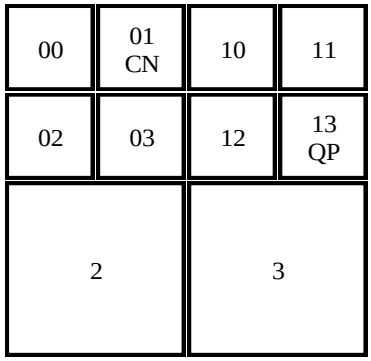

CN	QP digit →							
digit	0	1	2	3	4	5	6	7
0	R	R	RD	RD	RB	RB	RDB	RDB
1	R	R	RD	RD	RB	RB	RDB	RDB
2	RU	RU	R	R	RUB	RUB	RB	RB
3	RU	RU	R	R	RUB	RUB	RB	RB
4	RF	RF	RDF	RDF	R	R	RD	RD
5	RF	RF	RDF	RDF	R	R	RD	RD
6	RUF	RUF	RF	RF	RU	RU	R	R
7	RUF	RUF	RF	RF	RU	RU	R	R

Figure 4: Using the secondary R_Refined_Direction table to determine that QP is to the RD of CN.

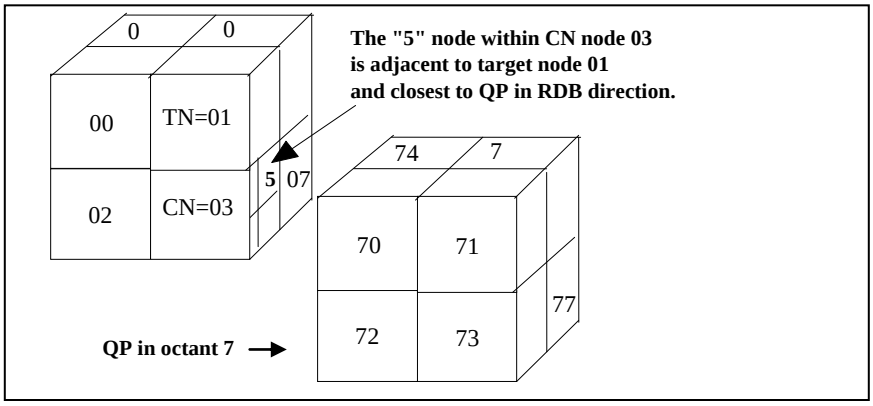

Figure 5: Example of selecting a repeating corner extension octant.

3.3.1 Using the Corner_Extend table

We use a 6-by-26 Corner_Extend lookup table (Figure 6) to determine which digit to fill in for the corner direction, where each row is a primary direction and the columns represent the set of 26 octree face, edge and corner directions. Note that the face directions {R,L,D,U,B,F} never reveal a corner adjacency, they are all set to "-" indicating NULL. Null table entries indicate that the direction is not a corner and to proceed to step 4A.

To use the Corner_Extend table: for a given Target Node (TN), we computed the neighbor node (CN) for each primary direction. Given the current primary direction (ROW), and the refined QP compass direction (COLUMN), the table returns the octree node number of the corner node of the CN that is closest to the QP for that compass direction.

Corner directions can be explicit, where a corner direction such as RDB, RUF, etc is returned by Coarse Direction table, or implicitly where the initial (primary) direction and the refined QP direction together represent a corner adjacency. If it's not a corner, as indicated by "-", continue to step 4A. Otherwise, fill in the extension with the repeating corner digit and proceed to step 5 to add the CN to FRINGEQ.

3.4 Step 4A: If not a corner, project the QP digits to extend the CN

When the refined direction is not a corner, we use a 'projection' table to determine additional CN digits at a finer resolution. The refined direction will be one of 18 possible non-corner directions. We use the remaining (rightmost) QP digits to create corresponding CN extension digits. Imagine two cubes of the same size floating in space, and that we know the relative direction relationship between them. If we bring these cubes together so they touch we can determine which octants in CN become adjacent to (project on) octants in QP for direction determination purposes. Thus, we use the 18-by-8 Closest Neighbor Projection table (Figure 8) to lookup digits for the CN extension, starting with the first QP digit that is longer than the length of the CN LC, and working towards the right. Using the refined non-corner direction of CN as the row and the rightmost QP digits as the column, the intersection yields the next LC digit in CN adjacent to TN that is closest to QP. See Figure 7 and Figure 8 for the following example using TN=00 and QP=113 :

- Given a target node TN=00, compute CN in the D direction.
- Using the FSM table in Figure 2, we determine CN= 02.
- Since the QP (113) has three digits, we need to compute the extension digit for CN.
- Using the Coarse_Direction Table we determine that QP is to the Right (R) of CN.
- Using the R_Refined_Direction table we determine that QP is to the RU (Right and Up) of the CN.
- Using the remaining QP digit of 3 and direction RU in the Closest Neighbor Projection table, we find the extension digit 1.
- Proceed to step 5.

Primary Dir	**Query Point Compass Direction →**																									
	R	**L**	**D**	**U**	**B**	**F**	**RU**	**RD**	**LD**	**LU**	**RB**	**LB**	**DB**	**UB**	**RF**	**LF**	**DF**	**UF**	**RUB**	**RUF**	**RDB**	**RDF**	**LUB**	**LUF**	**LDB**	**LDF**
R	-	-	-	-	-	-	-	-	-	-	-	-	6	4	-	-	2	0	4	0	6	2	4	0	6	2
L	-	-	-	-	-	-	-	-	-	-	-	-	7	5	-	-	3	1	5	1	7	3	5	1	7	3
D	-	-	-	-	-	-	-	-	-	-	5	4	-	-	1	0	-	-	5	1	5	1	4	0	4	0
U	-	-	-	-	-	-	-	-	-	-	7	6	-	-	3	2	-	-	7	3	7	3	6	2	6	2
B	-	-	-	-	-	-	1	3	2	0	-	-	-	-	-	-	-	-	1	1	3	3	0	0	2	2
F	-	-	-	-	-	-	5	7	6	4	-	-	-	-	-	-	-	-	5	5	7	7	4	4	6	6

Figure 6: Corner_Extend table for computing repeating corner LC digits

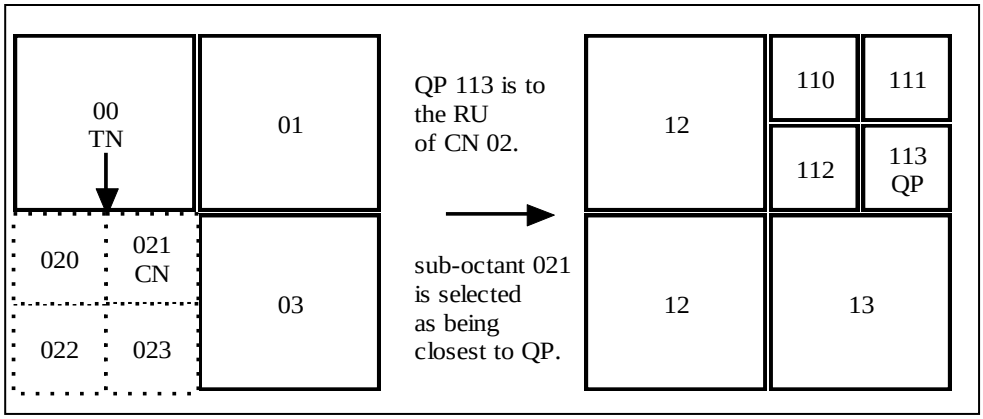

Figure 7: Compute and extend the DOWN neighbor of TN closest to QP at the same level as QP.

Dir	Corresponding QP digit →							
	0	**1**	**2**	**3**	**4**	**5**	**6**	**7**
R	**1**	**1**	**3**	**3**	**5**	**5**	**7**	**7**
L	**0**	**0**	**2**	**2**	**4**	**4**	**6**	**6**
D	**2**	**3**	**2**	**3**	**6**	**7**	**6**	**7**
U	**0**	**1**	**0**	**1**	**4**	**5**	**4**	**5**
B	**4**	**5**	**6**	**7**	**4**	**5**	**6**	**7**
F	**0**	**1**	**2**	**3**	**0**	**1**	**2**	**3**
RU	**1**	**1**	**1**	**1**	**5**	**5**	**5**	**5**
RD	**3**	**3**	**3**	**3**	**7**	**7**	**7**	**7**
LD	**2**	**2**	**2**	**2**	**6**	**6**	**6**	**6**
LU	**0**	**0**	**0**	**0**	**4**	**4**	**4**	**4**
RB	**5**	**5**	**7**	**7**	**5**	**5**	**7**	**7**
LB	**4**	**4**	**6**	**6**	**4**	**4**	**6**	**6**
DB	**6**	**7**	**6**	**7**	**6**	**7**	**6**	**7**
UB	**4**	**5**	**4**	**5**	**4**	**5**	**4**	**5**
RF	**1**	**1**	**3**	**3**	**1**	**1**	**3**	**3**
LF	**0**	**0**	**2**	**2**	**0**	**0**	**2**	**2**
DF	**2**	**3**	**2**	**3**	**2**	**3**	**2**	**3**
UF	**0**	**1**	**0**	**1**	**0**	**1**	**0**	**1**

Figure 8: Closest Neighbor Projection table, selects octant in CN closest to QP.

3.4.1 Step 4B: special case when there are no differing digits in CN and QP, coarse direction unknown

This happens when CN is an ancestor of QP. Re-using Figure 7 (left) for a different example, the DOWN neighbor of TN=00 is CN=02. If the QP=023, we have no relative direction information because QP is contained in CN. The solution is to use additional QP digits (starting at position Length(TN)+1) to select octants in subtree 02 that are adjacent to TN 00 while closest to QP. In this case CN becomes 021. We use the Projection table, but reverse the viewpoint (projection direction) to be from QP and not the usual CN (use L instead of R; U instead of D; F instead of B), thus we use U and octant 3 in the Projection table to find the extension digit (1).

3.5 Step 5: At this point, CN has a location code for a node at the smallest level

Since the actual neighbor in the MX-octree may not be at the deepest level, the octree is probed to find the actual size of CN and its length is updated as needed before adding it to the FRINGEQ.

4 Conclusion

Modifying our algorithm to accommodate a radius cutoff for neighbor finding is simple. We only place data nodes in the KNN queue if they are within the radius. Since the algorithm finds neighboring nodes in distance order (within a constant c), we have found all the neighbors within the radius when a point is encountered at distance greater than radius+c, where c is the diagonal distance within the smallest (leaf) nodes in the octree. Thus we may find a point slightly farther away first, but it will be within a strict bound of distance c.

The main result of this paper is an expanding boundary algorithm for MX-octrees with a procedure to compute location codes for expanding boundary nodes at the deepest level of an octree even when their immediate neighbor is a non-leaf node. These expansion boundary nodes have the property that they are neighbors of a possibly non-leaf sized boundary node that are closest to the query point. Although this algorithm may not be an optimal one, it demonstrates the feasibility of using the MX-octree representation for neighbor finding. This technique may be useful for region-growing applications as well.

5 References

[1] A. Andoni, P. Indyk, Near-Optimal Hashing Algorithms for Approximate Nearest Neighbor in High Dimensions, *Communications of the ACM*, V. 51, No. 1, 2008.

[2] S. Arya, D. Mount, N. Netanyahu, R. Silverman, and A. Wu, "An Optimal Algorithm for Approximate Nearest Neighbor Searching in Fixed Dimensions", *Journal of the ACM*, V. 45, No. 6, 1998.

[3] J. Bentley, Multidimensional Divide-and-Conquer, *Communications of the ACM*, V. 23, No. 4, 1980.

[4] H. Jensen, *Realistic Image Synthesis using Photon Mapping*, AK Peters (publisher), second printing, 2005

[5] M. Warren, J. Salmon, A Parallel Hashed Oct-Tree N-Body Algorithm, *Proceedings of the 1993 ACM/IEEE Conference on Supercomputing*, Portland Oregon, 1993.

[6] N. Roussopoulos, S. Kelley, F. Vincent, "Nearest Neighbor Queries", SIGMOD '95

[7] R. Yoder, "A Practical Algorithm for Computing Neighbors in Quadtrees, Octrees, and Hyperoctrees", *Proceedings of the 2006 International Conference on Modeling, Simulation, and Visualization Methods*, WorldComp 2006, Las Vegas June 26-29, 2006.

A Fuzzy Logic Approach for Optimization of Hardness in Induction Hardening Process

AMIT KOHLI[a] , HARI SINGH[b]
[a] Department of Mechanical Engineering, D.A.V Institute of Engineering & Technology, Jalandhar 144008 , India
[b] Department of Mechanical Engineering, National Institute of Technology, Kurukshetra 136119, India

Abstract

The study finds the effect of different input parameters that are feed rate, dwell time, current and gap between the induction coil & work-piece on the output parameters that are Hardness at rolled {H(R)}, Normalized {H(N)} and Hardened Tempered {H(T)} conditions of the material (AISI 1040 steel). The degree of membership function of an object in a fuzzy set is defined by membership functions (MF). It has been found that after the formulation of rules, the optimum value of hardness at any points (may be in decimal place) in between the low and high limits of the process parameters selected, can be found out. The predicted results are compared with a reliable set of experimental data for the validation of fuzzy model and mathematical model (developed by response surface methodology). It was found that proposed fuzzy model gives the better results than mathematical results and it was well in agreement with experimental results. By Intelligent, model based design and control of induction hardening process parameters in this study will surely help to enables dramatically decreased product and process development cycle times, improved product quality, decreased product cost and maintains the competitive position of steel in applications requiring high strength –to-weight ratio at an affordable cost.

Keywords:

Medium Carbon Steel (EN8D), Induction Hardening, Fuzzy Logic

1.Introduction

Surface hardening is the most important mechanical property for the metals which are worked under friction and treatment condition. Most important characteristic for the material hardening is hardness value [1]. By increasing the surface hardness value through induction hardening, wear resistivity, fatigue life, impact strength, compression strength and resistant of twist force are increased [2]. According to Stickels and Malender [3, 4] induction hardening is one most widely employed to improve component durability. Timothy et. al. [5] took four different input variables feed rate, gap between coil and workpiece , quench distance and part temperature with hardness as output variable and applied design of experiment and neural network approach in case of the induction hardening process. According to Timothy for complex processes with interactions among variables, traditional SPC methods are insufficient. Fuzzy logic is one of the artificial intelligence techniques that have ability to tackle the problem of complex relationships among variables that cannot be accomplished by more traditional methods. This method was discovered by Zadeh in 1965 [6]. It is a mathematical theory of inexact reasoning that allows modeling in linguistic terms of the reasoning process of human [7]. It is widely used for engineering, medical, economical problems and particular applications in very complex industrial systems [8].Fuzzy controllers and fuzzy reasoning are suitable in defining the relationship between system inputs and desired outputs. The Mamdani implication method is employed for fuzzy inference reasoning in this paper. The degree of membership function of an object in a fuzzy set is defined by membership functions which help in determining fuzzy values [9].

2. Induction Hardening Process Parameters

In order to identify the process parameters affecting the output parameter of induction hardened part, an Ishikawa cause and effect diagram was constructed as shown in Figure 1. Kanyan [11] took distance between coil and material, cooling time, applied power and frequency as effecting parameters. Here experimental results and fuzzy results were compared. Y.Tolik.et.al[12] took heating time (feed rate) and temperature as process parameters and concluded that depending upon the process parameters selected the induction hardening treatment helps in improvement of wear characteristics. Material selected by him was AISI 4140 steel. By using the methodology developed in his research, a significant improvement in the process was achieved. The selection of process parameters of interest was based upon the studies of Timothy et al. [5],Kanyan [11] and Tolik.et al[12]. The following parameters were thus selected for the present work that is dwell time, feed rate, gap between coil & work-piece and current at three different conditions of the material that is rolled, normalized and hardened tempered.

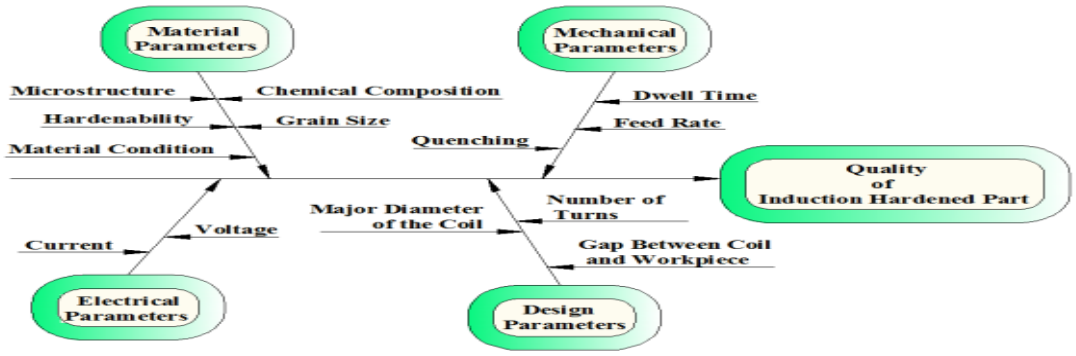

Figure 1: Ishikawa Cause and Effect Diagram of Induction Hardened Part

3. Experimental Details

For performing the experiments, the medium frequency induction hardening machine (10 KHz), Power 120 kW, spindle speed 400 r.p.m, make "Unitherm" is used. Maximum job holding length of the machine is 609.6 mm (distance between two spindles). A source of high frequency electricity is used to drive a large alternating current through a copper coil. The passage of current through this coil generates a very intense and rapidly changing magnetic field in the space within the work coil. The core of the component remains unaffected by this treatment [13]. The material used for induction hardening is AISI 1040 steel bars. Its composition is 0.45%C, 0.65%Mn, 0.21%Si, 0.03%S and 0.025%P. This material is suitable for a wide variety of automotive components like axle and spline shafts [14].

In this investigation four factors are being studied and their low and high levels are shown in the Table 1. The conditions were selected after performing the pilot runs and literature survey. The response variable investigated is hardness at three different conditions of the material as mentioned earlier. The hardness was measured by Rockwell hardness testing machine for C scale at 150 Kg load, having diamond indentor at 120 degree.

Table 1: Factors and Levels for Response Surface Study

Factors	Low level(-1)	High level(+1)
Feed rate (mm/s)	2	4
Dwell time (sec)	5	7
Current (Ampere)	125	135
Gap between work-piece and inductor coil (mm)	5	7

4. Fuzzy Logic Model For Induction Hardening Process (Hardness as Response)

The modeling of induction hardening system has been done using fuzzy inference system (FIS). In this study, three angular membership functions are selected for fuzzy model as shown in the Figure 2.

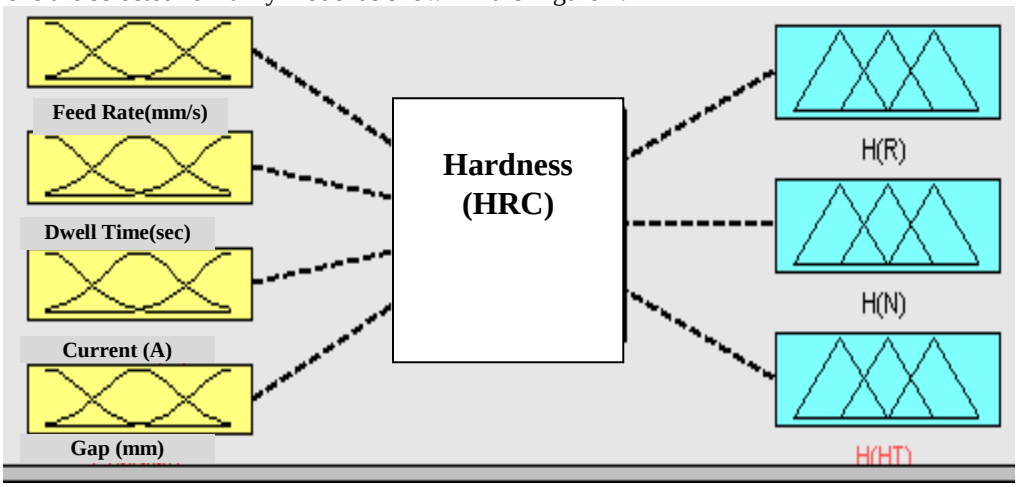

Figure 2: Fuzzy Logic Model of Induction Hardening (Response: Hardness)

4.1 Membership Function for the Input and Output Parameters (Hardness as Response)

This step is to define linguistic values assigned to the variables and that was done via fuzzy subsets and their associated membership functions. A membership function assigns numbers between zero and one, called the grades of membership, to the range of the possible values of the variable. Zero membership value indicates that it is not a member of the fuzzy-set; one represents a complete member. A membership function can have any shape but preferably symmetric. The standard shapes of membership functions include trapezoidal, triangular and bell shaped. Six membership functions were generated for each input variable (feed rate, dwell time, current, and gap between the induction coil and work-piece) as shown in Figure 3 (a, b, c and d).

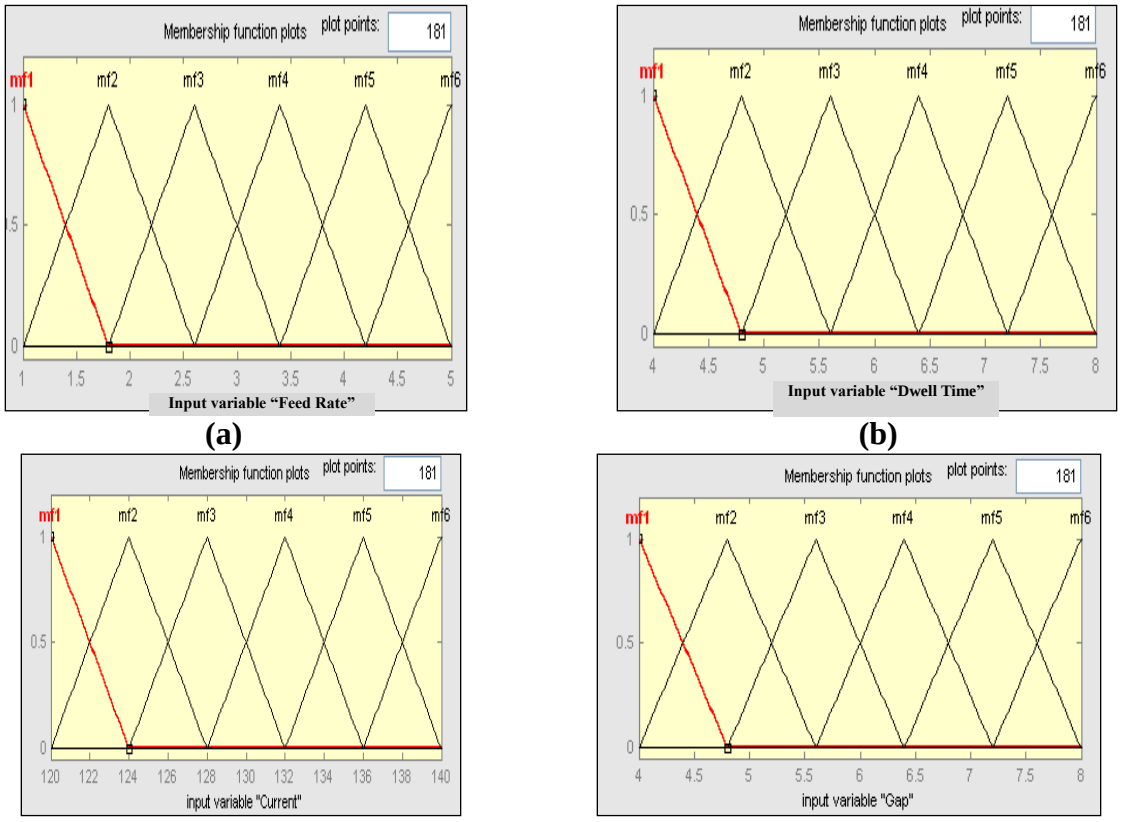

Figure 3: Membership Function Plots for Hardness (a) Current (b) Dwell Time (c) Feed Rate (d) Gap between the Work-Piece and Induction Coil

Membership function for hardness as output variable at three different conditions (as-rolled, normalized, and hardened tempered) of the material are given in Figure 4 (a, b and c).

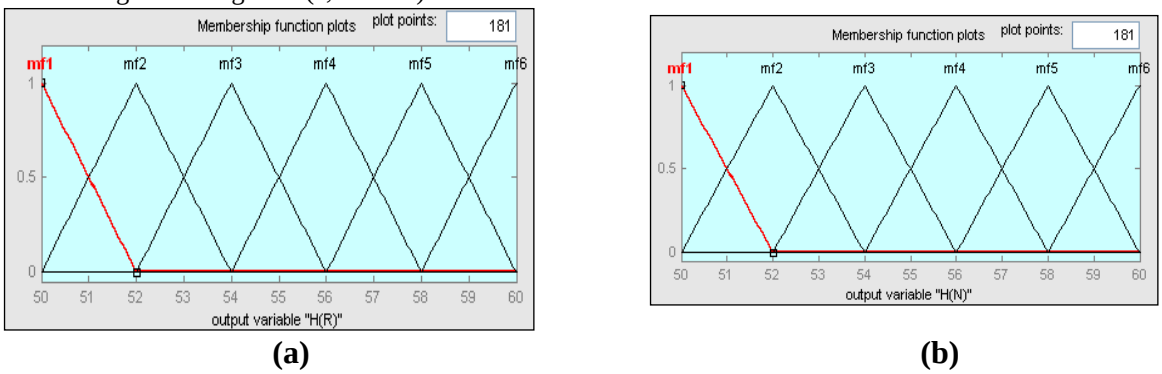

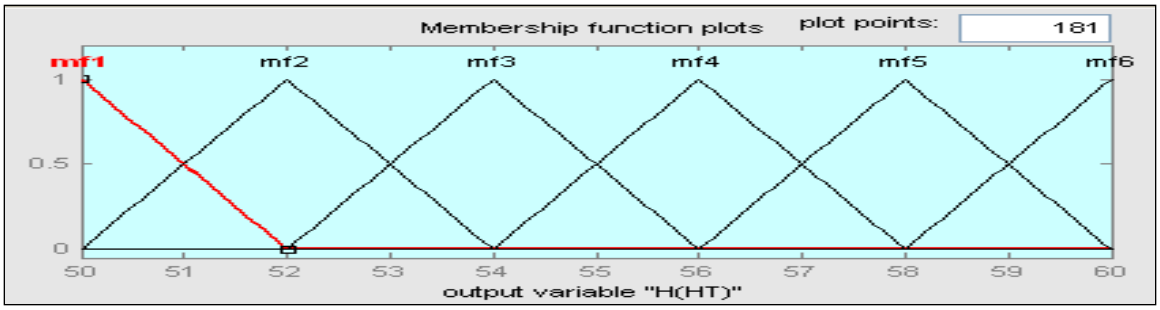

(c)

Figure 4: Membership Functions for Hardness at (a) Rolled (b) Normalized (c) Hardened tempered condition of the material

The location of triangles indicates the determined fuzzy sets for each input /output values.

4.2 FIS Rules Employed in Model (Hardness as Response)

For obtaining optimized solution, the rules at the rule base have been defined correctly and thirty rules have been written based upon the experimental results. While preparing the rules, fuzzy method was used. Some selected rules are reported in Figure 5, using MATLAB 7.0.4 environment using Mamdani-type of fuzzy inference system in fuzzy logic toolbox.

The Figure 5 shows the formulation of rules based upon experiment results of RSM for hardness at three different conditions of the material. Similarly, the formulation of rules was done for other responses.

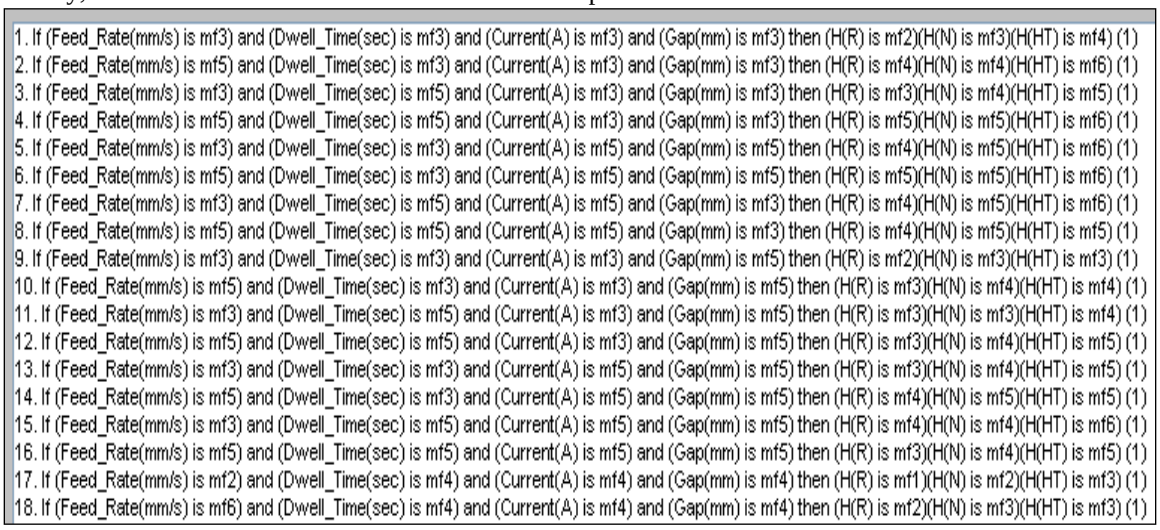

Figure 5: Formulation of Rules (Response: Hardness)

Control surfaces as shown in Figure 6 give the interdependency of input and output parameters guided by the various rules in the given universe of discourse. Control surface given in Figure 6 (a, b and c) shows dependency of hardness at three different conditions (as-rolled, normalized and hardened tempered) on dwell time and feed rate.

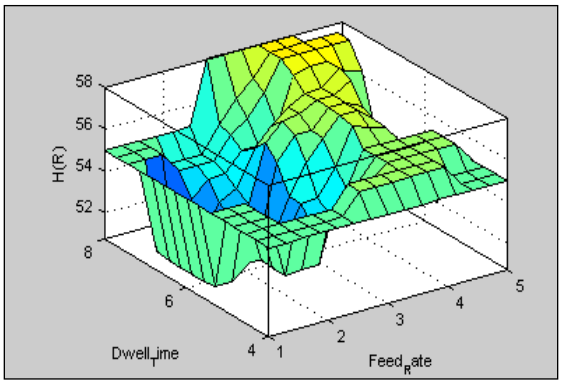

(a)

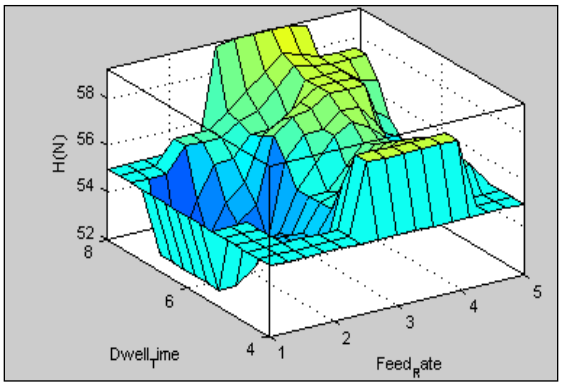

(b)

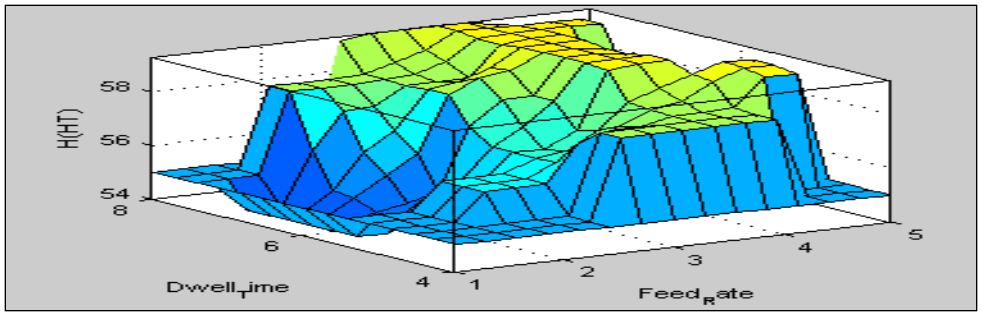

(c)

Figure 6: Control Surfaces of Fuzzy Model Showing Inter–Dependency of Hardness on Dwell Time and Feed Rate a) As-Rolled b) Normalized c) Hardened Tempered Condition

The set of rules along with membership function is shown in rule viewer of fuzzy model (Figure 7). Figure 7.7 reveals that after the formulation of rules, the optimum value of hardness at any setting between the low and high limits of the process parameters can be predicted.

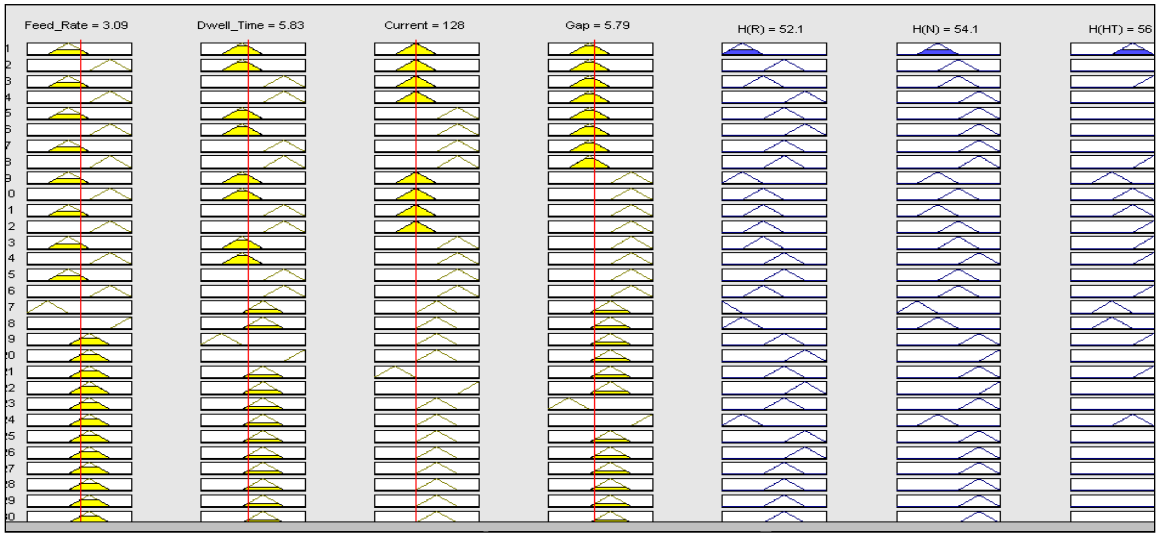

Figure 7: Rule Viewer of Fuzzy Model (Response: Hardness)

The Figure 7 clearly shows that at feed rate 3.09 mm/s, dwell time 5.83 sec, current 128 ampere and gap between the work-piece and induction coil 5.79 mm the predicted optimum values of hardness at rolled, normalized and hardened tempered conditions are HRC 52.1, 54.1 and HRC 56 respectively. Similarly for different sets of data points in the identified universe of discourse of undertaken parameters various other values of hardness in induction hardening process can also be predicted from the fuzzy model. Results predicted from this fuzzy model and mathematical models have been compared with the experimental results for its validation in the following sections given below.

H (R) = [-88.27+23.57 x Feed rate+9.43x Dwell time+0.77 x Current+6.8xGap-0.31 x Feed rate x Dwell time-0.09 x Feed rate x Current-0.31 x Feed ratexGap-0.06 x Dwell time x Current-1.3 x (Feed rate)^2-0.55 x (Gap)^2]

H (N) = [-112.76+25.79x Feed rate+12.68xDwell time+1.01x Current +6.13xGap-0.31xFeed rate x Dwell time-0.11xFeed ratexCurrent-0.09 x Dwell timexCurrent-1.44x (Feed rate)^2-0.57 x (Gap)^2]

H (HT) = [-91.44+30.69xFeed rate+14.71xDwell time+0.88xCurrent-2.19 x Gap -0.37 x Feed rate x Dwell time-0.15xFeed ratexCurrent-0.1xDwell timexCurrent+0.05xCurrentxGap-1.42x (Feed rate) ^{2}-0.42x (Gap) ^{2}]

5. Results and discussion

Table 2 gives the comparison of the predicted responses using developed fuzzy model and reported experimental data.

Table 2: Comparison of fuzzy model and experimental data for various responses

Feed rate	3.23	3.22	2.7	2.52	3.39	3.57	3.83	2.9	2.17	2.4	2.6	2.6
Dwell time	6	5.96	5.7	5.52	5.96	5.96	6.13	6.48	6.57	6.3	6.65	6.65
Current	130	133	131	129	132	134	135	129	134	128	132	126
Gap	6	5.96	5.43	5.7	5.61	5.87	6.74	5.43	5.7	6.3	6.91	6.91
H (R) fuzzy	55.8	57	54.3	52	57.8	57.1	57	56.8	54.8	52	54.3	54.1
Experimental values	55.4	56.4	54.2	53.5	56.63	56.23	55.54	55.67	54	52.3	54	53.4
% variation	0.72	1.06	0.18	2.8	2.06	1.54	2.62	2.02	1.48	0.57	0.55	1.31
H(N) fuzzy	56.7	58	55.4	54	57.9	58	58	57.6	55.7	53.9	54.3	54.2
Experimental values	56	57.6	55	53.8	57.3	58	58.4	57.7	55	53.2	53.9	53.9
% variation	1.25	0.69	0.72	0.37	1.04	0	0.68	0.17	1.27	1.31	0.74	0.55
H(HT) fuzzy	57.6	59.2	56.7	56	59	59.2	58.2	58.7	56.4	55.9	56.1	56.1
Experimental values	57	58.8	55.9	56	58.8	59	57.94	58.7	55.8	55.6	55.9	56

Table 3 gives the comparison of the predicted responses using developed mathematical model and reported experimental data.

Table 3: Comparison of mathematical model and experimental data for various responses

Feed rate	3.23	3.22	2.7	2.52	3.39	3.57	3.83	2.9	2.17	2.4	2.6	2.6
Dwell time	6	5.96	5.7	5.52	5.96	5.96	6.13	6.48	6.57	6.3	6.65	6.65
Current	130	133	131	129	132	134	135	129	134	128	132	126
Gap	6	5.96	5.43	5.7	5.61	5.87	6.74	5.43	5.7	6.3	6.91	6.91
H(R) mathematical	55.37	55.74	55.26	54.3	55.7	55.58	54.07	55.7	55.53	54	54.8	53.99
Experimental values	55.4	56.4	54.2	53.5	56.63	56.2	55.5	55.6	54	52	54	53.4
% variation	0.05	1.17	1.9	1.49	1.64	1.15	2.65	0.05	2.83	3.2	1.4	1.1
H(N) mathematical	56.7	57.1	56	55	57.1	57.1	55.7	56.6	55.8	54	55	54.4
Experimental values	56	57.6	55	53.8	57.3	58	58.4	57.7	55	53.2	53.9	53.9
% variation	1.35	0.79	1.81	2.23	0.35	1.51	4.5	1.83	1.45	1.5	2.04	0.92
H(HT) mathematical	58.1	58.4	58	57	58.4	58.4	57	58.5	58	56	57	56.4
Experimental values	57	58.8	55.9	56	58.8	59	57.9	58.7	55.8	55.6	55.9	56
% variation	1.92	0.64	3.75	1.78	0.68	0.98	1.62	0.29	3.94	0.7	1.96	0.71

Table 4 gives the average percentage error of various responses from fuzzy and mathematical models. In the present study the total data points involved was 12.

Table 4: Average percentage error of various responses from fuzzy and mathematical model

Process Parameters	Fuzzy calculated (% variations)	Mathematical model (% variations)
Hardness(rolled) H(R)	1.41	1.56
Hardness(rolled) H(N)	0.73	1.69
Hardness (hardened tempered) H(HT)	0.53	1.58

Out of various outputs generated by fuzzy models, the total average error is 1.43 % and from mathematical model it is 1.69 % respectively. Thus the system gave overall 98.57% accuracy from fuzzy model and 98.31% from mathematical model. Thus it can be conducted that there is a close relation between the experimental and simulated results for various responses of induction hardening process from fuzzy model in comparison with mathematical model.

Conclusion

1. This paper has set out to apply the fuzzy logic to predict hardness as response at different condition of the material (rolled, normalized and hardened tempered conditions) in induction hardening process. It has been found that results generated by fuzzy model and mathematical model (by response surface methodology) are close to the experimental results with98.57 % and 98.31% accuracy respectively.

2. Fuzzy logic system was found to be more flexible and easy to comprehend than mathematical model and hence can act as an alternative to the conventional modeling techniques. Present study supports that fuzzy logic technique can be introduced as a viable alternative to carry out analysis without conducting actual experiments. Fuzzy logic allowed the modeling and on-line control problem to be treated simultaneously.

References

[1] Bodart, O, Bourean, AV and Touzani, R. (2001). Numerical Investigation of Optimal Control of Induction Heating Process, Applied Mathematical Model; vol 25: pp 697-712.
[2] Kayacan, MC (1991). *Design and construction of a set –up for induction hardening*. M.Sc thesis, University of Gaziante.
[3] Stickels, CA (1984). Steel and its Heat Treatment; Second Edition; 3.
[4] Melander, M. (1984). Theoretical and experimental study of stationary and progressive induction hardening, Journal of Heat Treating,; 2: 145-65.
[5] Timothy James Stich, Julie K Spoerre and Tomas Velasco (2000). 'The Application of Artificial Neural Networks to Monitoring and Control of an Induction Hardening Process' Journal of Industrial Technology, vol16: pp. 1-11.
[6] Zadeh, LA. (1978). Fuzzy Sets as a Basis for a Theory of Possibility, Elsevier, 3-10.
[7] Ross, TJ. (1995). Fuzzy Logic with Engineering Application: McGraw – Hill Inc.
[8] Zadeh, LA. (1978). Fuzzy Sets as a Basis for a Theory of Possibility, Elsevier, 3-10.
[9] Cherkassky and Mulier, F. (1998). Learning from data: Concepts, Theory, and Methods; Wiley, USA.
[10] Hankins, Judy (2001). Infusion Therapy in Clinical Practice: 42.
[11] Kayan, MC. (2004)). A Fuzzy Approach for Induction Hardening Parameter Selection, Journal of Materials and Design, 25: 155-161.
[12] Totik, Y, Sadeler, R, Altun, H and Gavgali, M. (2003). The effects of Induction Hardening on Wear Properties of AISI 4140 Steel in dry sliding conditions, Journal of Materials & Design, 24: 25-30.
[13] Jacobs, JA and Kilduff, TF. (1994). Engineering Materials Technology: Structure, Processing, Properties and Selection, Prentice Hall Career And Technology. 2nd ed. New Jersey.
[14] Oberg, E, Green, RE. (1996). Machinery's Handbook .25th ed, Industrial Press, New York.

The Contributory Effect of Latency on the Quality of Voice Transmitted over the Internet

O. Adegbenro[1], S.N. John[2], B.A. Akinade[3]
[1,3]Department of Electrical and Electronics Engineering, University of Lagos, Lagos State, Nigeria,
[2]Department of Electrical and Information Engineering, Covenant University, Ota, Ogun State, Nigeria.

Abstract: Deployment of Voice over Internet Protocol (VoIP) is rapidly growing worldwide due to the new services it provides and cost savings derived from using a converged IP network. However, voice quality is affected by bandwidth, delay, latency, jitter, packet loss e.t.c. Latency is the dominant factor that degrades quality of voice transfer. There is therefore strong need for a study on the effect of Latency with the view to improving Quality of Voice (QoV) in VoIP network. In this work, Poisson probability theorem, Markov Chain, Probability distribution theorems and Network performance metric were used to study the effect of latency on QoS in VoIP network. This is achieved by considering the effect of latency resulting from several components between two points in multiple networks. The NetQoS Latency Calculator, Net-Cracker Professional® for Modeling and Matlab/Simulink® for simulating network were tools used and the results obtained compare favourably well with theoretical facts.

Keywords: VoIP, Latency, QoV, Network, Modeling

1 Introduction

The use of voice over Internet Protocol (VoIP) is the process of transmitting voice as data over the Internet equipped with coding/decoding devices (CODEC series) that helps in converting sound waves into digital packets so that the packets can be transmitted across a digital line and at the other end decode back to sound. Basically, it involves converting analog voice signals to digital format in form of a data through the Internet Protocol (IP) [1]. The Public Switched Telephone Networks (PSTN
technologies) architecture built primarily for voice is not flexible enough to carry data hence this is largely incompatible with the convergence of data/voice/video. Evolution of audio coding technologies has allowed voice to be transmitted over data links that resulted to emergence of VoIP which has been most sought after device for companies looking to take advantage of IP services. There is a cost benefit to be derived from using this new technology which is also prone to challenges.

The main challenge is improving the Quality of voice (QoV) in VoIP to avoid degradation of the service. The fidelity of Legacy telephone has not been achieved by VoIP yet hence the infrastructure of this new technology must be able to support Latency that degrades voice transmitted over the Internet. Latency stands as the delay that occurs when a packet crosses a network connection, from sender to receiver i.e. end-to-end-delay that occurs in information exchange between two nodes [2], [3]. There are many sources of delay in VoIP systems that add up to the total latency. Among these are the following: Algorithmic delay which is related to the speech codec used; Processing delay which is related to the signal processing performed and depends on the available CPU performance; Hardware delay and network delay caused by physical delay in the transmission lines; buffers in Routers which is time varying delay. Jitter, known as time variable delay as packets streams travel through an IP network in different paths and resulted in varying arrival time. Too much traffic in the network causes packets drop that result in packet loss [4].
It is important to predict expected voice quality under various network conditions and traffic loads so that steps can be taken in advance to prevent potential problems. In this case, the quality of service (QoS) must be capable of prioritizing traffic types; interpreting traffic types (applications running over IP) and then conveying them over the network. Research efforts in the area of studying the effect of Latency on QoS specifically in VoIP network performance were carried out by several researchers which include: Agnihot et al, May et al, Naser et al, S. Sahu et al, Antos et al to mention but a few.
Therefore it becomes necessary to conduct a study on the effect of Latency in VoIP network with the primary objective of improving on Quality of voice transmitted over the Internet toward achieving optimum toll voice quality and high network throughput.

2 Related Works

Research efforts in this area have been reported by several researchers. [5] used time scale modification algorithm, to handle losses that impact quality of voice delivery and jitter but resulting queuing delay from this packet arrival delay variation which cause packet drops after time to live (TTL) must have expired was not considered. [6] used a given buffer size, and two-bit architecture traffic load to estimate the expected delay of packets for constant bit rate and this aim was achieved.
Path Switching carried out by [7] showed that path quality estimator based on International Telecommunication Union (ITU-TE)-model was developed for voice quality assessment and an application driven path switching 'algorithm' 'that' applied the time scales over which path switching decisions are made to voice quality. Though, network emulation and

experiments over a wide area indicated that with sufficient path diversity, path switching can yield noticeable improvement in voice quality by utilizing the inherent path diversity of the internet. The limitation of path switching is that it can also introduce performance degradations through transient disruptions that may results due to switching from one path to another, particularly when the network path differs significantly in their propagation delay and topology.
Integrated Service/ RSVP architecture was influenced by the work of [8] as a signaling protocol for application to reserve resources for aggregation of flows to set up explicit routes (ERs) with QoS requirements. However the requirement on routers is high. All routers must have RSVP, packet scheduling and admission control. This is tasking to the internet core. Despite all these research works the problems of call quality in VoIP remains apparent and the need for further research on effect of latency with the view to minimize the voice degradation in VoIP.

3 Methodology

In this work Poisson probability theorem, Markov Chain and Probability distribution theorems were used to study the effect of latency on QoS in VoIP. This was achieved from the concept of the effect of delay components between end-to-end networks in a multiple networks environment. NetQoS Latency Calculator [9], NetCracker Professional, Matlab/Simulink and NS-2 were tools used in performing the network validation experiment.
In order to achieve accurate results, the conventional legacy data network was first examined to determine the characteristics of the network. The network monitoring tool used for the parameter measurement was the Solar wind Simulation Software® [10] capable of given detail result of the network performance.
The software were modified to measure the latency, throughput, retransmission time (RTT), and packet loss for a single user, then to 30 users along the link between Lagos and the Abuja contact centre in Nigeria, with the results taken at the Cisco® 7201 border router of the Lagos contact centre. The codec for compression used were the uncompressed 64Kbps G.711 protocol, while the compression on the WAN link was G.729 protocol with 8Kbps of bandwidth.

4 Delay Components

The time it takes for a voice to be digitized, packetized transmitted, routed and buffered over the internet is known as delay. It poses one of the major threats to QoS mechanisms. Propagation and processing delay are directly responsible for the major factors that affect quality of service in VoIP. There are several types of delays in an IP network which differ from each other as to where they are created. The delay components are classified based on the place of their creation, mechanism or some other attributes [11] as shown in Figure 1. The VoIP delay components are coder and packetization delay originated from the end-to-end transmission through the communication channel, thus their components affect the result of voice packets in the network.

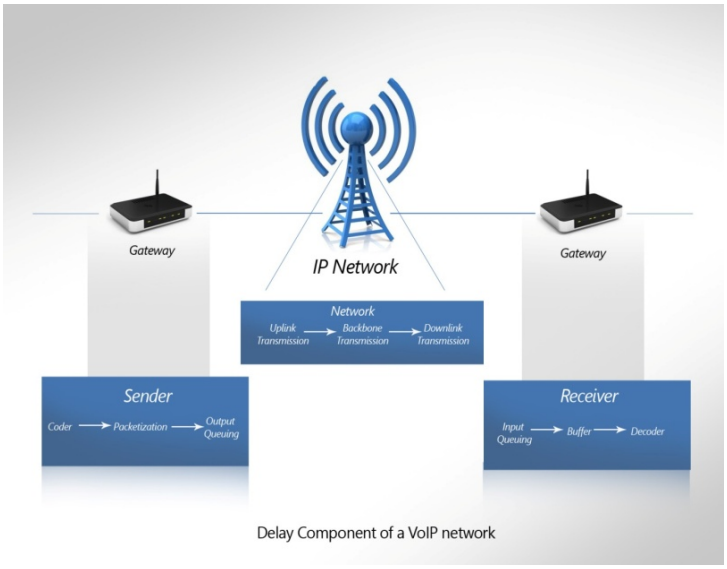

Figure 1. Delay Components in VoIP Network of a Communication Channel.

The detailed description of individual delay components as it goes with the VoIP network are as follows: Queuing delay, serialization delay, propagation delay in transmission network, access / codec delay and packetization delay.

5 Modeling Network Infrastructure of Voice over IP

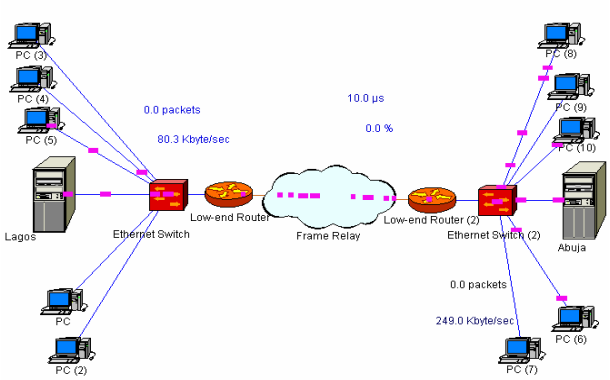

Figure 2. Communication Network of Multiple Nodes.

Communication network of multiple nodes shown in Figure 2, illustrates the developed mathematical model of the research work. The communication network channel is established between two Local Area networks with multiple nodes transferring voice packets along the network media. The transmitting end and the receiving end are depicted in the model and the scenario presents real life network environment as a test-bed for the research using Net-Cracker Professional simulation software®.

6 Mathematical Model

We consider a large network with many stations able to communicate using CSMA/CD protocol. Assume infinite number of host with packet arrival in Poisson stream rate, $\sigma <$ 1,for time, t, in an ascending order t = 1, 2 … We applied

traditional Poisson model, with the assumption that a large number of packets can arrive at a buffer with a Poisson distribution. The probability Pn (t) of exactly n packets arriving during a time interval of length t is given by

$$P_n(t) = \frac{(\sigma t)^n e^{-\sigma t}}{ni} \quad where \quad n = 0,\ 1,\ 2,$$

σ is the average packet arrival rate [12].

This shows that the probability that for a Poisson data flow stream in a given small network area with change in time (ΔT) an event will occur. i.e. the amount of packets which are necessary to be sent at an interval of time, ΔT will be a Poisson data flow. Each station transmits one packet only. It is considered that the time slot for successful transmission of a packet is given as: *(t, t + 1)*.

With the above mathematical expression we come into conclusion that the total delay which comes from the backlog of the systems during data/voice performance within the channel can be considered as the net delay and expressed as follows:

Net delay = Propagation delay (T_p) + Serialization Delay (T_s) + Queue Delay (T_q)

Thus, the total delay on the network can well be represented as:

$T_{total} = T_A + T_D \epsilon (T_p + T_s + T_q)$, where T_A = Encoding time, T_D = Delay,

The derived model for the net latency in the n^{th} network is given as [13]:

$$Latency\_n = \frac{\sum x_n}{0.667c} + \frac{\sum N_n \mu}{(\mu - \lambda_n)B} + \frac{\sum \lambda_n^2}{(\mu - \lambda_n)B\mu}$$

6.1 Results and Analysis of the Network Mathematical Model

From the mathematical model, the net delay was obtained by considering the total delay experienced by the network i.e. *propagation delay, serialization delay, and queue delay* [13]. Data generated from the mathematical model and real world network setup were analyzed with the corresponding result obtained. In the relationship between responses of packet sizes against the throughput of the network, Figure 3, it was observed that the increment noted was on a gradual increase which suggests that the network has not reached a congested state.

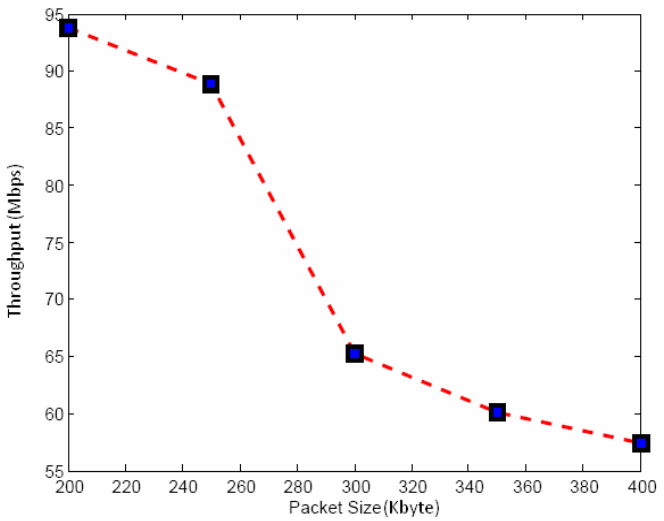

Figure 3. Graph of response of packet sizes against the network throughput

An increase in packet sizes result into the reduction in throughput, A sharp change was observed in the throughput when the packet size was increased to 300Kbytes, having a reduction in value from 89Mbps to 65Mbps.With the utilization value of ρ=0.4 in Figure 4, the packet loss shows a steady increment, though mostly negligible, however it is of considerable value when compared in respect of the packet size between 200 and 400Kbytes. A similar situation is recorded when the utilization factor becomes ρ=0.9 with the Bandwidth Capacity of 100Mbps.

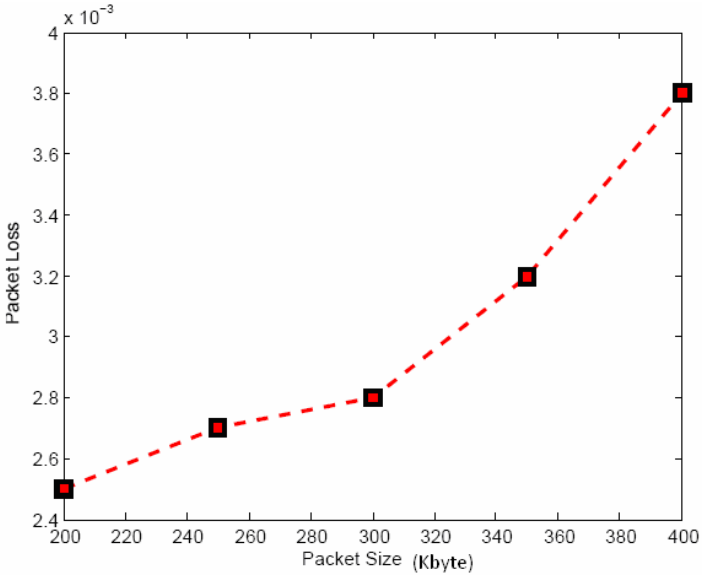

Figure 4. Graph of packet size against packet loss with utilization factor of 0.4 with 100Mbps bandwidth.

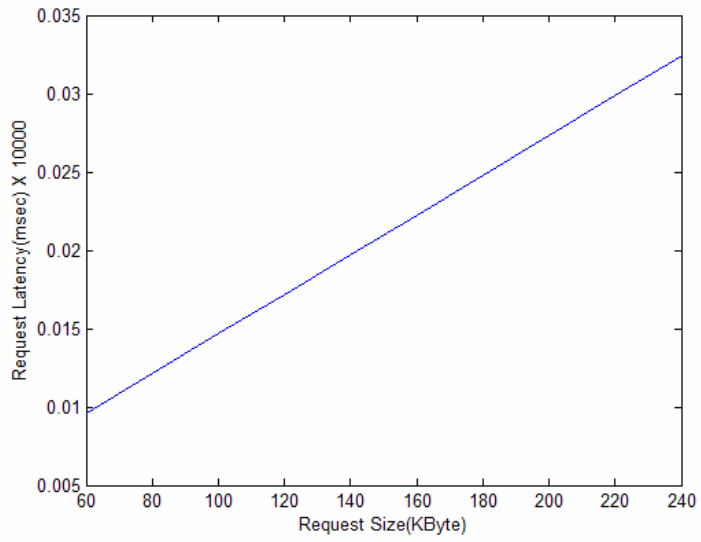

Figure 5. The graph of packet request size against Latency

The Figure 5 shows the graph of request size against overall request latency. As the packet size transmitted increases, so does the latency accordingly hence, the linear relationship. However it is obvious that as packet size increases latency increases such that above 200msec voice becomes impaired degraded. The optimum was attained with packet size of 190Kbyte and request latency of 0.025 x 10^4msec. Beyond this point, toll call quality starts experiencing degradation well notice in Figure 6 graph of packet request size against request Latency indication of decline in network performance.

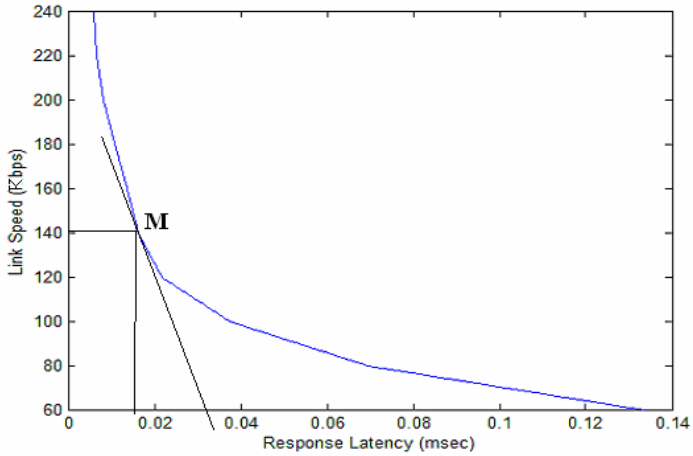

Figure 6. The graph of response Latency against Link Speed

Considering the result in Figure6, as the link-speed drops, latency increases gradually until latency get to the threshold [14] of the throughput on the point M of the tangent (142Kbps and 0.18 x 10^3msec). At this point, latency increases exponentially to approach its peak of (180msec.) for the workload. From the result as the link-speed drops further irrespective of the codec used, prioritization method deployed; with a lot of packet drops at this region, latency tends to a high value that degraded the voice quality. At this point, no amount of bandwidth will minimize the latency for toll call quality to be achieved. Also, we observed that the packet loss becomes so much that throughput has no effect on the degraded voice quality hence the asymptotic increase of latency which results into voice impairment. This follows that at about 142 Kbps no amount of throughput of the network can impact latency positively.

7 Conclusion

Use of developed mathematical model (Poisson probability theorem and Probability distribution theorems) in analyzing and studying the contributory effect of latency on the quality of voice transmitted over the internet. Improved QoS was achieved from the research result:
Toll quality of 5.0 (MOS) => 0 ≤ Latency ≤ 182kbps. By controlling the workload and bandwidth, the efficiency of the network was achieved with minimum latency on the network.
Experimental results obtained correspond to the simulated modeling. Provide fundamental insight to the contributory effect of latency on the amount of bandwidth can change the network performance when the system gets to the threshold point "0 ≤ Latency ≤ 182kbps" as obtained in our result.

8 References

[1] Bur Goode, Senior member IEEE; "Voice over Internet Protocol (VoIP)", Proceeding of the IEEE Vol.90, No. 9, pp 1495-1497, Sept. 2002.

[2] J. Skoglund, E. Kozica, J. Linden, R. Hagen, W. B. Kleijn, " Voice over IP: Speech Transmission over Packet Networks" ; Springer Handbook of Speech Processing; Benesty, Sondhi, Huang (Eds) springer, 2008

[3] Ixia, "Assessing VoIP call quality using the E-Model". URLL: tp://www.ixiacom.com/library/white_papers/display?skey=voip_quality

[4] Juniper Networks, Inc. Voice over IP 101, (White Paper) "Understanding the basic functions, components, and signaling Protocols in VoIP Networks".pp.1-14; URLL: http://www.juniper.net/solutions/literature/white - papers/20087.pdf

[5] Samar Agnihotri, K. Aravindhan, H. S. Jamadagni, B. I. Pawate "A New Technique for Improving Quality of Speech in Voice over IP using Time-Scale Modification"

[6] H. Naser, and O. Aboul-Magd, "Voice over Differentiated Services," IETF Internet Draft <draft Naser-voice-difference-eval-00.txt., 1999.

[7] Shu Tao et al, **"**Improving VoIP Quality Through Path Switching" ; University of Pennsylvania Kuai Xu, University of Minnesota Antonio Estepa, University of Sevilla **...** *works.bepress.com/lixin_gao/75/; 2005.*

[8] A. Jain, et-al, "Resource reservation protocol (RSVP)" – version I Functional specification, RFC 2205; Sept. 1997).

[9] NetQoS Network Estimation Tools. http://ciscoccvp.files.wordpress.com/2009/01/netqos-ss.jpg, 2010.

[10.] Orion Network Performance Monitor (NPM). http://www.**solarwinds**.com, 2011,

[11] Miroslav Voznak, Frantisek Hromek; "Analytic Model of Delay Variation valid for RTP"; CESNET Technical report number16/2007 pp 1-6.

[12] Gerd Keiser, "Local Area Networks" ; PhotonicsComm Solutions, Inc. Second Edition, Mc GrawHill 2002.

[13] S. N. John, R. E. Okonigene, A. Adelakun: Impact of Latency on Throughput of a Corporate Computer Network, Proceedings: The 2010 World Congress in Computer Science, Computer Engineering, and Applied Computing (WORLDCOMP'10), Annual Summer Conference on Modeling Simulation & Visualization Methods (MSV'10), Las Vegas, Nevada, USA, July 12-15, 2010, pp.282-287.

[14] John S. N. "Increasing the efficiency of data exchange in a computer networks based on the protocol of TCP/IP suite" Ph.D. Dissertation, Donetsk National Technical University, Donetsk, Ukraine, Oct. 2005. Thesis in search for Ph.D degree on speciality 05.13.13 – computer, computing systems & networks. Donetsk National Technical University, Donetsk, Ukraine, Oct. 2005; Vol. 93, pp. 256-264, URL: www.lib.uaru.net/diss/cont/258169.

MOBILE ROBOT NAVIGATION USING MONTE CARLO LOCALIZATION

Amina Waqar
NUCES-FAST Lahore
Aminawaqar007@gmail.com

ABSTRACT

This paper presents an algorithm for the mobile navigation of a robot using Monte Carlo. Previously, people did a lot of work for the tracking of mobile robot. Previously people used grid-based approach that used high resolution 3D grids to represent the state space. Whereas, this method is computationally quite efficient. Using Monte Carlo Localization we apply the sampling approach to divide the state space into samples. We can increase the number of samples where required. Monte Carlo Localization is easy to implement. Several results proved that Monte Carlo yields more accurate results. And also, it is computationally very efficient**.**

Keywords: Kalman Filter, Markov Localization, Monte Carlo Localization.

1 INTRODUCTION

Throughout the last decade, sensor-based localization has been recognized as a key problem in mobile robotics. In Localization, a mobile robot estimates its position in a global co-ordinate frame. There are two types of localizations: Global Localization and position tracking. In global localization, a robot does not know its original position whereas in position tracking the robot knows its original position.Global Localization is also known as "hijacked robot problem" (Engelson 1994)in which the robot has to determine its position from scratch.Many of the previous researches were on tracking but now many people are working on both types of localizations.In this paper we shall represent the robot's belief by probability density over the region in its range. The range is determined by the range in which the sensors will be able to work effectively.[1]

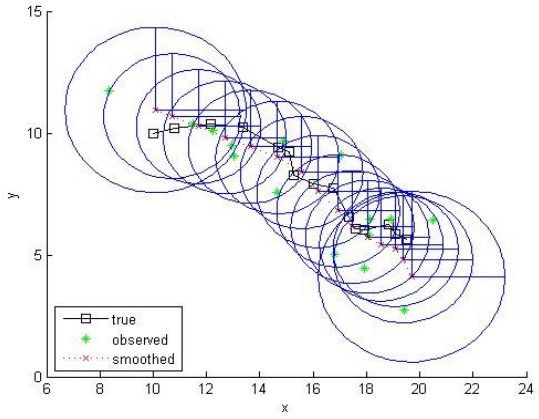

Figure 1 .Tracking using Kalman Filter

2 PREVIOUS WORK

Previously people have done a lot of work on tracking using Kalman filter which is a form of Phase Locked Loop (PLL) and is less efficient , because of it , it can be used as tracking.

Fig.1 shows working of Kalman filter. The black boxes show the original position , green stars

show the estimated position and red crosses show the modified position by taking averages of both.

3 MARKOV LOCALIZATION

Markov localization caters the problem of state estimation from sensor values. Markov localization is a probabilistic algorithm: Instead of maintaining a single hypothesis as to where in the world a robot might be, Markov localization maintains a probability distribution over the space of all such hypotheses. The probabilistic representation allows it to weigh these different hypotheses in a mathematically sound way.

Before we delve into mathematical detail, let us illustrate the basic concepts with a simple example. Consider the environment depicted in Fig 2. For the sake of simplicity, let us assume that the space of robot positions is one-dimensional, that is, the robot can only move horizontally (it may not rotate). Now suppose the robot is placed somewhere in this environment, but it is not told its location. Markov localization represents this state of uncertainty by a uniform distribution over all positions, as shown by the graph in the first diagram in Fig 2. Now let us assume the robot queries its sensors and finds out that it is next to a door.

Markov localization modifies the belief by raising the probability for locates next to doors, and lowering it anywhere else. Consider that the resulting belief is multi-modal, reflecting the fact that the available information is insufficient for global localization. Notice also that places not next to a door still possess non-zero probability. This is because sensor readings have noise, and a single sight of a door is typically insufficient to exclude the possibility of not being next to a door.

Now let us assume the robot moves a meter forward. Markov localization incorporates this information by shifting the belief distribution accordingly, as visualized in the third diagram in Fig 2.

To account for the inherent noise in robot motion, which inevitably leads to a loss of information, the new belief is smoother (and less certain) than the previous one. Finally, let us assume the robot senses a second time, and again it finds itself next to a door.

Now this observation is multiplied into the current (non-uniform) belief, which leads to the final belief shown at the last diagram in Fig 2. At this point in time, most of the probability is centered around a single location. The robot is now quite certain about its position.[6]

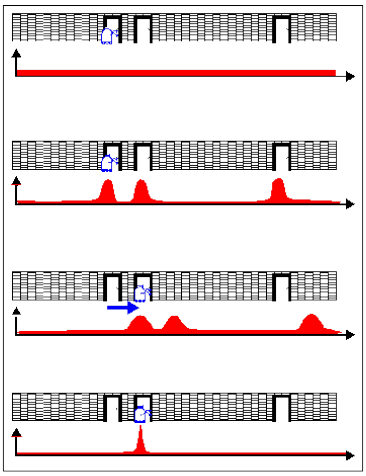

Fig. 2. The basic idea of Markov localization: A mobile robot during global localization.

$$Bel(l)=\int P(l|l',a)Bel(l')dl' \quad (1)$$

[3]

Bel is the belief of the robot that was uniform distribution initially. To update a belief there must an action 'a' done by the robot. The belief at position l, Bel(l) is updated using the previous belief at position l', Bel(l').Then we convolve the both the beliefs to get the new belief which guides the robot where to go.

4 MONTE CARLO LOCALIZATION

In the Monte Carlo localization we discretize the space into random samples. Since it is using global localization, it can represent into multimodal distributions .Due to this reason, less memory is required and is computationally efficient. Grid-based approaches were also used but they were computationally cumbersome. Grid-based approaches required more memory also because they were using 3-D figures.[4]

In our experiment we have modelled the robot with four sensors on each side. Each of it emits a signal which is reflected back as 1 if there is a wall and 0 if there is door or any empty space. The range in our cases is five units (0-4).As it moves along the path from door to wall the signals will convert from 0's to 1's.Fig.3 explains the above simulation. Fig.3(a) represents first belief of the robot after an action. Fig.3(b) is an updated PDF based the previous PDF. Fig3.(c) shows the convolution of both the PDF's where the door actually is and that way the robot should move.[5]

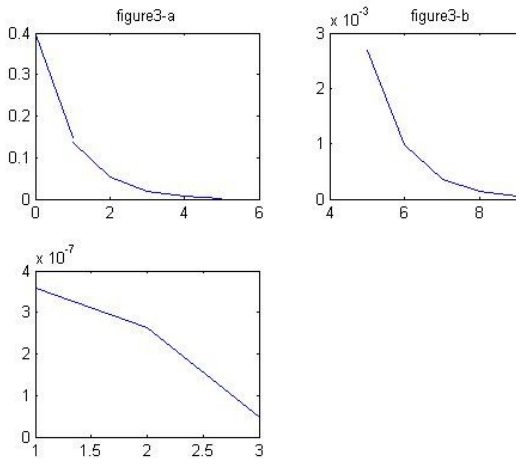

Figure 3 : Monte Carlo Simulation

5 CONCLUSION

In this paper we have concluded that Monte Carlo Localization is an easy to implement and requires less memory and is computationally efficient. Less memory is attributed to the fact that belief is updated in the memory location rather than occupying more and more memory locations.This recursive algorithm is far more effective than Kalman filter which was a form of Phase Locked Loop (PLL) and was less efficient computationally and was not as precise. Hence Kalman filter was only used for tracking purposes.

REFERENCES

[1] Burgard, W.; Cremers, A.; Fox, D.; H ¨ahnel, D.; Lakemeyer, G.;

[2] Schulz, D.; Steiner, W.; and Thrun, S. 1998a. The Interactive

[3] Carpenter, J.; Clifford, P.; and Fernhead, P. 1997.

[4] An improved particle filter for non-linear problems. TR, Dept. of Statistics, Univ. of Oxford.

[5] Chung, K. 1960. *Markov chains with stationary transition prob- abilities*. Springer.

[6] Cox, I. 1991. Blanche—an experiment in guidance and navigation of an autonomous robot vehicle. *IEEE Transactions on Robotics and Automation* 7(2).

[7] Dean, T. L., and Boddy, M. 1988. An analysis of time-dependent planning. Proc. of AAAI-92.

[8] Dellaert, F.; Burgard, W.; Fox, D.; and Thrun, S. 1999a. Using the condensation algorithm for robust, vision-based mobile robot localization. Proc. of CVPR-99.

[9] Dellaert, F.; Fox, D.; Burgard, W.; and Thrun, S. 1999b. Monte Carlo localization for mobile robots. Proc. of ICRA-99.

[10] Doucet, A. 1998. On sequential simulation-based methods for Bayesian filtering. TR CUED/F-INFENG/TR.310, Dept. of Engineering, Univ. of Cambridge.

[11] Endres, H.; Feiten, W.; and Lawitzky, G. 1998. Field test of a navigation system: Autonomous cleaning in supermarkets. Proc. of ICRA-98.

[12] Engelson, S. 1994. *Passive Map Learning and Visual Place Recognition*. Ph.D. Diss., Dept. of Computer Science, Yale University.

[13] Fox, D.; Burgard, W.; Thrun, S.; and Cremers, A. 1998. Position estimation for mobile robots in dynamic environments. Proc. of AAAI-98.

[14] Fox, D.; Burgard, W.; Kruppa, H.; and Thrun, S. 1999. A monte carlo algorithm for multi-robot localization. TR CMU-CS-99-120, Carnegie Mellon University.

[15] Fox, D.; Burgard, W.; and Thrun, S. 1998. Active markov localization for mobile robots. *Robotics and Autonomous Systems* 25:3-4.

[16] uncertainty: Discrete bayesian models for mobile-robot naviga-tion. Proc. of IROS-96.

[17] Kalman, R. 1960. A new approach to linear filtering and prediction problems. *Tansaction of the ASME–Journal of basic engineering* 35–45.

[18] Kanazawa, K.; Koller, D.; and Russell, S. 1995. Stochastic simulation algorithms for dynamic probabilistic networks. Proc. of UAI-95.

[19] Kitagawa, G. 1996. Monte carlo filter and smoother for nongaussian nonlinear state space models. *Journal of Computational and Graphical Statistics* 5(1).

[20] Koller, D., and Fratkina, R. 1998. Using learning for approximation in stochastic processes. Proc. of ICML-98.

[21] Kortenkamp, D.; Bonasso, R.; and Murphy, R., eds. 1997. *AIbased Mobile Robots: Case studies of successful robot systems*. MIT Press.

[22] Leonard, J., and Durrant-Whyte, H. 1992. *Directed Sonar Sensing for Mobile Robot Navigation*. Kluwer Academic.

[23] Maybeck, P. 1979. *Stochastic Models, Estimation and Control*, Vol. 1. Academic Press.

[24] Nourbakhsh, I.; Powers, R.; and Birchfield, S. 1995. DERVISH an office-navigating robot. *AI Magazine* 16(2).

[25] Rubin, D. 1988. Using the SIR algorithm to simulate posterior distributions. *Bayesian Statistics 3*. Oxford University Press.

[26] Schiele, B., and Crowley, J. 1994. A

comparison of position estimation techniques using occupancy grids. Proc. of ICRA-94.

[27] Simmons, R., and Koenig, S. 1995. Probabilistic robot navigation in partially observable environments. Proc. of ICML-95.

[28] Smith, R.; Self, M.; and Cheeseman, P. 1990. Estimating uncertain spatial relationships in robotics. Cox, I., and Wilfong, G.,eds., *Autonomous Robot Vehicles*. Springer.

[29] Tanner, M. 1993. *Tools for Statistical Inference*. Springer.

[30] Thrun, S.; Bennewitz, M.; Burgard, W.; Cremers, A.; Dellaert, F.; Fox, D.; H¨ahnel, D.; Rosenberg, C.; Roy, N.; Schulte, J.; and Schulz, D. 1999. MINERVA: A second generation mobile tour guide robot. Proc. of ICRA-99.

[

SESSION

GEOGRAPHIC INFORMATION SYSTEM BASED DECISION SUPPORT SYSTEMS

Chair(s)

Dr. Omer M. Soysal

The Preparation of An Interactive Lecture – Course on The Density Concept in Urban Planning -

Berna Dikçınar Sel[1], **B. Olcay Çetiner Özdemir**[2]
[1]Department of Urban and City Planning, Yildiz Technical University, Beşiktaş, Istanbul, Turkey
[2]Department of Architecture, Yildiz Technical University, Beşiktaş, Istanbul, Turkey

Abstract: *The "population density" concept in city and regional planning is the basic means of the planning implementation process.*

The determination and calculation of densities differs on different scaled plans. Due to the necessity of this kind of Standard using the city and regional planning and its education, lecture, which is interactive on the computer environment, prepared with this Project. Thus, it can be visually and interactively taught to the users of this system to calculate the necessary building areas and the public activity areas. The developing technology brings novelties for the field of training, as it does in several other sectors.
In the study, a model for the practical courses to take place in remote access training is transferred. In this model, the framework and operation of the course 'Density in City planning' is developed within the rules of the distant access lecture framework.

Keywords: Density in City planning, interactive lecture, remote access training

1 Introduction

By simplifying the spatial structure of a city, it is possible to say that two interdependent processes form this structure. The first one is man-made objects, whereas the second is actions that are spread to certain areas. In urban function areas created as a result of the fact that actions appear by forming groups in a location as a result of their functional relationships, different types and densities of land use patterns (forms) emerge depending on type of action. These land use rates or criteria generally defined as density in conceptual index of urbanology are used as an important tool in the distribution of the scarce resources in urban planning studies [1]. Definition of the density is, in widest sense, the number of person, family or house unit per a certain size area.

Urban planning in general has a hierarchical structure, and density is expressed with different criteria in different planning stages in this hierarchical structure. For example, while the density is defined as "population density" (generally number of people per hectare) in plans defining principles about the city's development and its function areas, it is defined as "building density" (building zoning order, floor number etc) in application oriented plans defining physical spaces. Population density and building density are the criteria that are not independent of each other and can be convertible to each other. The conversion from population density to building density or from building density to population density is made by mathematical calculations. Making these conversions correctly and setting the relationship between two density criteria accurately increase the applicability of the plan and its power in orientability of the city development. Especially in developing countries like our country (Turkey), one of the most important tools of orienting urban developments properly is density criteria in general and the relationship between density criteria and of course planning hierarchy in particular.

This study, supported by Yıldız Technical University research fund, aims to focus on two key areas**.** The first is

- to examine the concept of "density", one of the most important parameters of urban planning, in terms of its derivatives and its application methods and to create the course frame about this subject.

And the second one is

- advancing technology has led to the opening of new horizons also in the field of education as in many areas. The "remote-access course" on internet environment is a new dimension in education. The frame and the teaching of the course of "density in urban planning" have been formed in the framework of the rules of remote-access course.

The education process of Yıldız Technical University, Department of City and Regional Planning has content for construction methods and tools of upper scale principle plan and application plan of the planning process of the applied courses of "Planning 5 and Planning 6". Within the scope of these courses, the concept of density and density conversions should be conveyed to students. In addition, Department of Architecture of our faculty also offers its students an information process related to the concept of density and its criteria within the scope of applied courses.
The aim of the study is to prepare a course supporting not only education of city and regional planning students but also

education of architecture students in terms of the concept of density, its criteria and calculation methods and to simplify it with the help of information technologies. The course is designed as remote accessible. We can list the reasons for the preparation of the course as follows:

- To visually support the concept of density, which is important in terms of planning and architecture professions, with the help of information technologies.
- To convey the calculations of building zoning order in density conversions (population-construction right) and the densities' reflection to space to students with examples.
- To overcome the time problem brought by conveying the concept of density, which is important in city planning and architecture projects, within the scope of applied courses.
- To make the course space and time independent owing to its characteristic of being remote accessible for the purpose of overcoming the space inconveniences existing in our faculty.

Instructions for authors

An electronic copy of your *full camera-ready paper* must be uploaded (in PDF format) to Publication Web site before the announced deadline. Please follow the submission instructions shown on the web site. The URL to the website is included in the notification of acceptance that has been emailed to you by Prof. Arabnia.

2 Preparing an Interactive Course for the Concept of Density in Urban Planing

Within the scope of the course of "density in urban planning", it is necessary to transfer mutual communication with students intensively and various density calculation methods practically. In this direction, the present study aims to present a model in order for especially applied courses to take place in remote-access education.
What have been realized within the scope of the project in the direction of these determined aims are as described below.

2.1 The course of density in urban planning

In preparing the content of the course, the project coordinator Prof. Dr. Emre Aysu's book with the same name was determined as the primary resource, and the course frame was developed in accordance with this book.
It is possible to present the course frame under three main headings: theoretical section, applied section and examples.
Theoretical section: this section introduces with the definition of the concept of density and includes the main topics of density staging, types of density, density-space relationship, relationship between density-physical space components, relationship between density and house types, theories about land use, density as a measure of land use and relationship between land use measures and planning.
Applied section: taking the relationship between density-house types within the scope of construction development scheme applied in our country and calculating various settlement conditions and densities a computer program was created in this section. This program is an original program written using the visual basic programming language by the research project team and is included in the scope of the course such that it is open to students' use in an interactive way.
Section of examples: the actual area examples of the density values calculated in the applied section take place in the section of examples.

2.2 Remote Access Course Model

Remote-access courses are the ones, during which teacher and students share information not directly but through computer networks thanks to a virtual environment.

In the model that this study reveals, the students will follow the course in line with the determined weekly course schedule.

In this course program, there are

- Lecture notes by weeks
- Course works by weeks
- Applications by weeks
- Supplementary resources by weeks

In accordance with the plan, students send their questions and issues about the course to the lecturer and their virtual classmates via e-mail. Besides, on certain days to be specified weekly in accordance with the predetermined requirements, the live-chat environment serves for this purpose.

The course works are also be done in the virtual environment and sent to the teacher via e-mail. As for the midterms and final exams of the course, questions are randomly selected from question bank through the prepared exam program and then these online exams are automatically conducted via a computer.

The lecturer monitors the attendance of the students automatically as the students log in the system in each week. Moreover, the students have capability to follow their own attendance and grades on the same screen. While selecting the courses, students can learn the objective of the course and necessary requirements from prerequisites part on the site. It is possible to access to the course plan belonging to the whole term as well as weekly program about the course from the "this week" part step by step.

3 Studies Developed in Computer Environment For Remote Access Courses

Studies developed in computer environment are conducted under the following titles:

- Texts for conceptual definitions
- Density calculation program
- Exam program
- 2 and 3 dimensional data
- Interactive environment documents
- Preparing the CD-ROM of the course

The texts for conceptual definitions were updated within the scope of the interactive course for the concept of density in urban planning and they were transferred to computer environment. The figures in the book on conceptual lecture were created as 2 and 3 dimensionally and in motion pictures on computer environment using the Autodesk programs. The density calculation methods and variables, which form the concept of density and are used both abroad and in our country, and calculations about 2 and 3 dimensional images and models were transformed to an interactive program on computer environment (Picture 1, 2, 3, 4, 6).

Both visual (aerial photographs, texts, graphics, etc.) and written documents were transferred to computer environment using a scanner.

In an effort to conduct the exam of the course on the network in the week determined in the course program, the exam software and the software that operate the interactive lecture notes were programmed using the visual basic 6.0 software language. The course exam was provided to be active only in the determined week (Picture 5).

When preparing the interactive environment documents, programs used to make the software and the documents interactive in the network are the Director 8.0 and the Flash 5.0 programs. Thanks to the Director 8.0 software, the related documents and software were associated with each other and arranged in line with the weekly program of the course (Figure 1). Since some problems were experienced in making the course materials accessible in the network with the Director 8.0 program, the Dreamweaver 4.0 software was applied.

The Dreamweaver 4.0 and the Flash 5.0 software were utilized in transferring the course to the CD-ROM environment, as well. Except for the live-chat environment and the exam software, all of the visual data, the 2 and 3 dimensional data and the density calculation program were transferred to the CD-ROM environment.

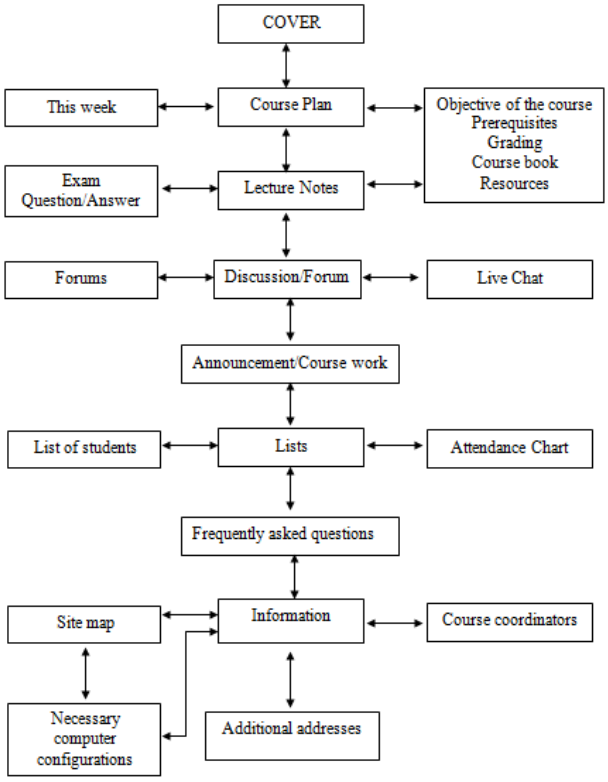

Figure 1. Interactive environment algorithm scheme

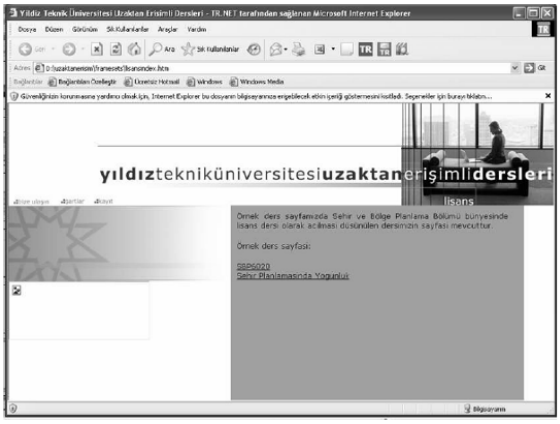

Picture 1.Image from entering of interactive course

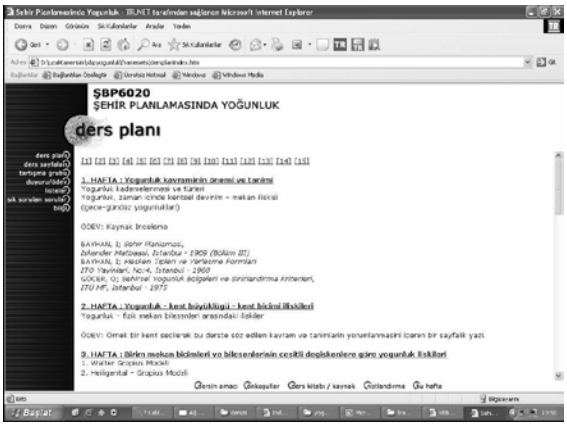

Picture 2. Image from courses program of interactive course

Picture 3. Image from course work of interactive course

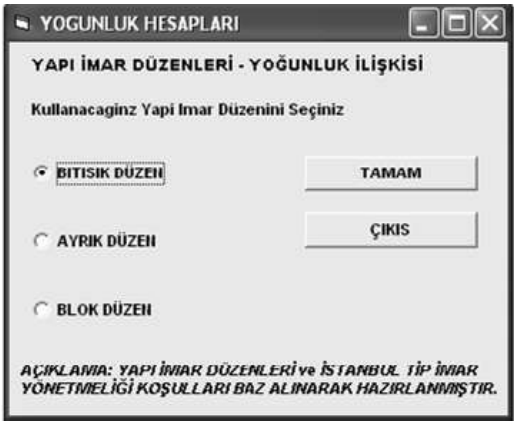

Picture 4. Density calculation program

Picture 5. Exam program

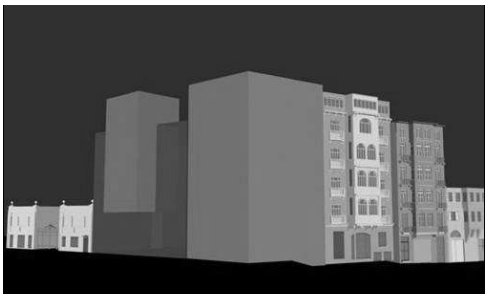
Picture 6. A proposal of with density calculation from Beyoğlu-Galatasaray

4 Conclusions

Preparing an interactive course for the concept of density in urban planning provides contributions to present a different example for urban planning in terms of not only clarifying the standards of the concept of density in project planning but also using computer technology in education and planning.

The course was included in the 2nd term of the academic calendar in the 2003-2004 academic year. The students, all of whom were the students of the department of city and regional planning and who were at different stages of the education process, selected the course in this term. After a half-term trial training, we can classify the impressions about remote access course on density as follows:

- About the hardware: since some of the students have computers at home, the rest ones used the faculty laboratory. This situation prevented fully realization of the objective of being independent of time and space.
- About the software: since a help and tutorial could not be created about using the course program, the problems experienced by the students could only be overcome by one-to-one interviews.
- Evaluations of the students: The students stated that;
  - although a 100 % lesson did not take place as expected, it was a different and productive experience to take a course independent of time and space
  - the fact that the course was supported by information technologies as well as its being remote accessible and that the examples and the calculations were followed easily had a high contribution to their learning the subject
  - the fact that the lecture was enriched with information technologies increased their interest in such a complex subject and it facilitated learning
  - they spent less time for this course, but they learnt more in this course compared to the other courses.

As a conclusion; being the first example of the remote access course trials in our department, the 'density' titled course can be regarded succesful in terms of conveying the subject, bringing a different approach to the problem of space, and using information technologies in solving the complexity of the subject. The course has planned to be scheduled again in the second term of the 2011/2012 academic year after the related updates of the technological and content are made to this course.

The confusion about the concept of density and its calculation was overcome. Moreover, the easiest and the most convenient method was studied in order to set an example about developing courses providing contributions to application and education in computer environment in our

university and to make the subject widespread so that the future courses could be prepared accordingly.

5 References

[1] Aysu, E., "Şehir Planlamasında Yoğunluk", Yıldız Technical University YTU, İstanbul, 1990a.

[2] Aysu, E., 'İstanbul Anakent Alanında Kent İçi Devingenlik Örüntüsü' , YTU Mimarlık Fakültesi, Üniversite Yayın no: 215, Fakülte Yayın no:MF-SBP 90.012, 1990b.

[3] Aysu, E., 'Mekan Biçimlenmesinde Yapı İmar Düzenleri Toprak Kullanma İlişkileri', YTU Mimarlık Fakültesi, Üniversite Yayın no: 231, Fakülte Yayın no:MF-SBP 92.014, 1992.

[4] Aysu, E., Dikçınar, B., Çetiner, O., etc., "The Reparation of An Intecrative Lecture- Course on The Density Concept in Urban Planning", Yıldız Technical University Project of Research Fund, İstanbul, 2002.

[5] Kloesterman, R. E., Community Analysis and Planning Techniques, Rowman & littlefield Publishers, Inc., ISBN 0-8476-3951-7, 1990.

THE EMPIRICAL METHOD FOR URBAN PLANNING PROCESS

B. Dikcinar Sel[1]
[1]Urban and Regional Planning, Yildiz Technical University, İstanbul, Turkey

Abstract *Understanding urban development and defining the problems are essential in urban planning process. Collection and analysis of data are methods that are used to define urban space and its problems. Information systems and computer models are significant tools for applying these methods. Use of information technologies are key components to urban planning education.*
The syllabus for the fourth semester in Yıldız Technical University Department of City and Regional Planning includes lectures related to planning and data collection processes, which are taught at both theoretical and practical levels. For this aim the course "Planning IV" focuses on an existing settlement as its case study, which is used for teaching processes that contribute to urban planning through hands-on exercises, such as analyzing the current condition of the settlement and defining its problems. This text discusses a new method which uses information technologies more intensively and its effects on the course.

Keywords: *Urban planning instructions, geographical information systems, data collection.*

1 Introduction

Planning is a product of enlightenment. Enlightenment has established the belief that reason can grasp regular processes of nature and society, and renders them comprehensible and transferrable. This meant establishment of an objective social science that would guide actions of human beings. If this sort of social science discipline exists, such information would be used for purposes of social engineering. This, therefore, implies the deployment of technical reasoning in leading society. In other words, it means the birth of the idea of modern planning [1].
Planning can be defined in multiple ways. (One) technical definition of planning hints about key words and concepts that planning is interested in. According to this definition, "planning is choosing among alternative future options, and implementation of these options by distributing existing resources accordingly." According to another definition planning is "complementary processes of taking a decision on the basis of determining productive resources among potential options, and calculating the feasibility of selected options." As such, planning is "the act of maintaining the order of actions in order to reach the aimed target(s)." [2].
Planning is based on three theoretical frameworks first of which concerns the process (decision and selection). The second of these concerns the content (choice of place and form) whereby the third one is game theory (realization and implementation). These theoretical frameworks are fundamentally based on the definitions that Geddes developed for planning process about the triad of fieldwork, analysis and plan. This three layered structure is valid even after the inclusion of stages such as determination of targets and aims, formation of planning options, and determination of the most effective implementation. In this context, every planner should be equipped with the knowledge of design, matrix, algorithm; with the ability to develop relational tables; and the ability to observe and analyze while developing qualitative and quantitative models [2]. In other words, planning education should be designed in ways to provide students with these abilities.
Urban and Regional Planning Department at Yildiz Technical University has been offering a four-years undergraduate degree in Urban Planning since 1982. Applied courses offered throughout these four years were designed in ways to incorporate the above-mentioned stages of the planning process. The course titled as Planning IV is the applied course offered to students during their fourth semesters. The purpose of this course is to provide students with the methods and techniques that are necessary for fieldwork and analysis of planning process. As such, it aims to equip students with an analytical perspective. "Information technologies," in general, and "geographical information systems," in particular, have also been used in the course since 1990s.
"Planning IV" course which the author of this paper was one of the instructors of in the spring term of 2006/2007 academic year was designed to use and widely benefit from information technologies and geographical information systems. It also worked as a testing ground of a new method in the implementation of this applied course.
This study critically analyzes how and to which extent geographical information systems in addition to other technologies should be deployed in fieldwork (data collection, observation, survey, etc.) and analysis of the planning process during planning education. The method will be taught in three stages. First the content of the course will be discussed

and then the methods will be taught. At the last stage, general information about the sample field and applications related to this sample will be discussed. In the conclusion section a critique of the method and the results of application will be presented.

2. Analysis Stage and Its Relation to Geographical Information Systems During Planning Education

Urban and Regional Planning Department at Yildiz Technical University has been offering undergraduate and graduate degrees in planning since 1982. "Comprehensive planning" approach that was developed in Turkey during 1960s is the foundation of education principles of the Department.

Hegemonic paradigm in geography around the time when comprehensive-rational planning was developed was regional and idiographic approach. This approach aims to understand the visions and principles that enable conceptual reestablishment of a region that is unique and formed upon the synthesis of information gathered about various topics that might influence the characteristics of this region [3]. The curriculum of Urban and Regional Planning Department was also designed according to this approach. Nevertheless, globalization processes in Turkey and around the world give rise to new political agendas and mobilization forms in spatial planning. Increasing importance of participatory methods due to post-modernist thinking alongside with the deployment of positivist methods in obtaining information transform planning process into a communicative space where different parties form horizontal relations. As an approach that is capable of dealing with the influences of globalization on cities as well as that takes post-modernist emphasis on the need of communication/interaction among different parties into account, strategic spatial planning is under scrutiny in Turkey as well. In this context, planning education should incorporate both comprehensive planning and strategic spatial planning methods. Deployment of these two methods in applied courses implies extending the contents of these courses. Both approaches require comprehensive data collection and analysis of this data by using different methods. Even only when considered from this perspective, deployment of information technologies appears vital in systematization of the data collected, its management, and analysis.

The city of Midyat was chosen as the case study of Planning IV course in the spring term of 2006/2007 academic year. Midyat is a city in Southeastern Anatolia and lies within the boundaries of the least developed region in the country. Its undevelopment negatively affects collection of data concerning planning and the analysis of this data especially in terms of the availability of contemporary data. This required incorporation to the course content of an additional stage of updating the data. A total of four months including the entire spring term and an additional one month in the following summer that was used to conclude the study was spent. A careful consideration of the content, tasks to be completed and the time at hand requires incorporation of information technologies into the process more.

To sum up, following reasons make it necessary to incorporate more information technologies, in general, and geographical information systems, in particular, to the content of the course compared to previous terms:

- The necessity to simultaneously use different planning approaches,
- The obstacles faced in data collection, especially contemporary data, about case study.

2.1. Aims and content of the course

Department's curriculum plan defines Planning IV course as follows:

The content of the course includes data and material collection in a selected area (by making use of information gathered at the scale of the region) through participatory observation, evaluation, interviews; analysis at the office space by deploying analysis tools and methods; teaching students to work in teams and interpreting collected as well as sorted information

The aim of the course is to comprehend economic, social and physical aspects of the area selected for planning; to teach data collection and analysis through team-work discipline; to understand the roles of actors in planning system.

The course would provide students with the capability of accessing institutional and fieldwork-related information at the scale of the selected area and its surroundings; of learning from previous planning process; and of developing planning ethics.

The course is based on two type of studies:

1. Fieldwork,
   - An investigation of physical space
   - Developing surveys about social and economic structure,
2. Office work,
   - Preparation of a database from the data collected through investigation of physical space,
   - Preparation of a database from the data collected through surveys,
   - Analysis of these databases.

3. Methods

Methods are determined by the aim and the content of the course. But the method that is discussed here especially focuses on how and at which stages of GIS studies can be used. The method will be discussed in three stages. Details of the method will also be provided through the sample field.

3.1. Pre-Fieldwork

This stage can be defined as an overview of the field through data collection from the chosen settlement and a preparation period for the fieldwork. It can be examined in three steps.

a) Review of the literature about the settlement and its vicinity to collect numeric data about the socio-economic structure, to explore the demographic features and to make detailed analysis of other topics that are related to the fieldwork. Maps showing the physical, geographical, topographical and other features of the field will be papered at different scales.

b) Collected data are systemized and a database is constructed to digitalize the analogue maps.

c) Preliminary preparations are done such as development of questionnaires related to the fieldwork, preparation of flyers to be used in determination of physical spaces, choice of sub-regions where those physical spaces are determined and choice of students that will work in these sub-regions.

3.2. Fieldwork

Fieldwork is done in two stages:

a) Determination of the physical space: Aims at providing students with the ability of relating maps to the physical space and collecting data through observations. Should there be any differences between the maps and the physical space, determination of these differences and update of maps occur at this stage. Students are paired to process the determination of physical space within the predetermined sub-regions.

b) Questionnaires: Information about the demographic, economic, social and cultural features of the population, economic structure of the city and the development levels were gathered through survey data from households, businesses, state offices, healthcare centers, educational centers and lodging places. Household surveys are done by the same working groups in the sub-regions where determination of physical space is completed.

3.3. Post-Fieldwork

This stage includes the organization of the data collected through the fieldwork and production of refined information about the settlements. At this stage data from surveys and the results of determinations of physical spaces will be analyzed. Preparation of thematic maps and concluding reports are also at this stage.

4. Case Study

4.1. Midyat

Midyat lies in the northeastern part of Mardin in an area that lies in the north of Mesopotamia region that hosted eldest civilizations in history' and where very important cultures, languages and religions met. Midyat lies in the northern borders of Mesopotamia region that is known as Tur-Abdin. Tur-Abdin carries an historically important value for Syriacs[1] as Jerusalem does for Jews. Syriacs in Midyat can be traced back to Assyrians living in Midyat during the period B.C (1367-800). Midyat has a multi-cultural, multi-religious and multi-ethnic culture that hosts Armenians, Yezidis and Muslims in addition to Syriacs.

An analysis of the demographic structure of Midyat in the 16th century when it became an Ottoman territory shows that Christians (Syriac, Armenian and Protestant) constituted at the time 62 per cent, Muslims constituted 27 per cent, and Jews constituted 5 per cent of the population. Multi-ethnic and multi-religious character of Midyat still continues today. According to the results of 3 per cent sample survey[2] done in 2007, 40.6 per cent of the population living in Midyat identify themselves as Arab, 50.9 per cent as Kurdish, 3.8 per cent as Syriac and 4.7 per cent as Turk [4].

Midyat municipality was founded in 1890, and it was included within the administrative boundaries of Mardin in 1927. Midyat which is a Syriac settlement was unified in 1930 under one municipality with Etsal which was an Arab settlement. Midyat's population today that is included in the administrative boundaries of the city of Mardin is 56,666, whereby its total population is 128,085. Its economy is mainly based on agriculture and services sector whereas historically important sectors of masonry and filigreed also appear as significant although not as much as they used to be [5].

4.2. Application of Methods

4.2.1. Pre-fieldwork preparations, decisions

Preliminary data collection for informative purposes about the case study was done at this stage. These preliminary studies can be summarized as literature review about Midyat and its surroundings; and collection of statistics from Turkish Statistical Institution about the economic structure of the region, its demographics and social structure, agricultural statistics, and etc. In addition, maps of different scales were obtained for Southeastern Anatolia that includes Midyat, the

[1] Syriac is mostly used in Christianity to refer to the population living in upper-Mesopotamia. This population is known as "Assyrians" in Iraq and Iran whereas they are known as "Syriac" in Turkey and Syria. Syriac population and culture was very influential in the establishment of Midyat, and its social and physical development [4].

[2] Surveys conducted in the course that is central to this paper.

Table 1: Data and methods of analysis

Data collected	Tasks to be completed	
Analogue maps (Of different scales)	Transformed into raster format through scanning.	Maps in *raster* format were turned into numerical format through the computer, and then, transformed into vectoral data.
Other data	Systematized through tables	Tables were matched with maps in vectoral format.

entire city of Mardin which administratively includes Midyat, and central Midyat and the surrounding villages. All of these maps are analogue maps. Electronic table program and geographical information systems that uses relational database are decided to be used in order to form a database by systematizing the data collected.

Maps of 1/1000 scale for the city of Midyat that were obtained during pre-fieldwork preparations and would be used to establish the relationship between map and real physical space are analogue maps. They need to be transformed into numerical format. However, these maps were drawn in 1997. In other words, these maps that could be defined as graphical data do not reflect the current situation of the city.

Students need to match the current observed physical space with two-dimensional physical space by using these maps. Nevertheless, it is not possible to pursue this aim with maps that do not reflect well the current situation. To avoid this problem, it was decided to use maps that are produced by Turkish Telecommunications Corporation (Türk Telekom) and that have information about subscribers. However, these maps only include information about buildings, blocks and streets. They do not include graphical data that usually exists in maps already at hand such as ownership information and topographic data. For this reason, maps obtained from Turkish Telecommunications were merged with the maps already at hand that include ownership as well as topographic data.

Subareas that would be evaluated on the maps of Turkish Telecommunications were determined during pre-fieldwork studies. Each subarea was given an ID number (subarea ID). The same coding was done for maps at hand as well. Students who were responsible from conducting the fieldwork were divided into groups that consist of two individuals. These groups were allocated subareas on the maps of 1/1000 scale and given related documents. Each group coded blocks, parcels and buildings on the maps of the subareas they were responsible from. These codings will be discussed later in detail.

4.2.2. Fieldwork

Fieldwork conducted in Midyat was done in two stages:

a. Evaluation of physical space ; Paired students collect data for the predetermined sub-regions through observation by using the physical space and map matching technique. Datum that need to be observed for this purpose can be summarized as follows (table 2):

Table 2 :Data Collected trough detemination of physical space and related definitions.

Geographical Unit	Observed characteristics	Geographical Unit ID
Ward	Determination of ward boundaries	1001 (Area no+BlockNo) (Block ID)
Parcel	Determination of parcel boundaries Determination of land cover of the parcel	100101 (Area no+BlockNo+Parcel no) (ParcelID)
Building	Determination of building boundaries Usage type of the building, Number of floors, Characteristics of the building, Building construction material, The year of construction, Total number of units in the building	10010101 (Areano+BlockNo+Parcelno+Building no) (Building ID)
Street	Street name Street quality Street width	Number defined for each street name (Street ID)

Definitions in the first column of Table 2 under the title "geographical unit" also represent the data layers that are used in the construction of the geographical information system. Data collected through observations are presented in the second column of the table as "boundaries", which represent mapping or graph data. Other values are presented through tables and they represent the attributes of the data from a given boundary.

Table 3: Anketler ve örnekleme sistematiği

Area of data collection	Methodology	Form of Implementation	Identification code
Characteristics of the population	Household Surveys	Sampling method	Building ID
Characteristics of commercial sector	Commercial Office Surveys	One-to-one	Building ID
Public services	Public Office Surveys Health Institution Surveys Education Institutions Surveys	One-to-one	Building ID
Characteristics of tourism sector	Tourism survey	One-to-one	Building ID

b. Survey Studies ; Methods for survey preparation to analyze the social, economic and cultural structure of Midyat are presented in Table 3.

Household surveys were prepared according to the sub-regions that were chosen during the determination of the physical space and they were conducted by the same groups that ran the determination process. Household surveys were computerized by using building IDs and they were related with the geographical information system that was constructed for the determination process. This has made spatial analysis of the data collected through surveys possible. The same procedure was applied for other surveys aside the household surveys by taking the building IDs as the primary key. The aim is to make spatial features questionable in social and economic analyses.

Table 4 : Data processing and analysing

	Methodology	Systematization of the data
Transforming map of 1/1000 scale into updated numerical format	1. Hand-drawing data taken from telecommunication maps and data collected through observation on analogue maps of 1/1000 scale 2. Scanning the map on which data was merged and its digitalization in raster data format 3. Transformation of raster data into vectoral maps by using numerization tool of Geographical Information Systems Package programme	Numerization was done in layers, 1. Building (poligon data) 2. Parcel (poligon data) 3. Block (poligon data) 4. Street (Line data) 5. Slope lines (line data) 6. Boundaries (poligon data) Layers were formed separately for each diestock since Working Area consisted of 40 diestocks each of which was of the size of (50cmx70cm).
Survey casting	1. Survey casts at the scale of sub-areas 2. Survey tables at the scale of neighborhoods	Survey charts for each sub-area together with building IDs Statistical tables and necessary graphics that systematize data related to each neighborhood
Matching related graphical and qualitative data	Building, parcel, block, street, and slope layers and data related to characteristics in these layers were matched by using GIS.	Tabled data obtained through surveys and observations that were matched with IDs of each layer that were of building, parcel, block, and slope layers.
Analysis	Implementation of various investigations through GIS and using diestocks; chartization of tables that were not able to be matched with graphic data; drawing charts, etc.	Tables were not only constructed at the neighborhood scale but also at the scale of ethnic groups during analysis.
Creation of synthesis diestocks at individual scale	Interpretation of the entire data according to the primary ideas they raised for planning purposes	

4.2.2. Post Fieldwork

The class was divided into two groups one of which to analyze the graphical data and the other of which to analyze qualitative data. These groups were formed by selecting one

member from each group previously formed to conduct the fieldwork.
Data collected in the pre-fieldwork and fieldwork stages were digitalized before the related analysis. Data collected through determination process, which were also used to update the maps, were manually digitalized in ArcGIS after scanning. That is all the maps were digitalized through a redrawing process. Attributes of the geographical features were also manually transformed into ArcGIS tables.
Data collected through surveys were transformed into tables through MS Excel. These tables were related to the maps again by using ArcGIS.
Data transferred to ArcGIS and MS Excel were also analyzed through these programs and the related reports were prepared presenting these analysis.

5. Conclusion and critiques

This study spanned over an entire period of four months that included one spring semester and one additional month in the following summer. Critiques can be summarized as follows considering the problems and obstacles faced during the study:

- The size of the selected case and its various characteristics increased the variety of data to be collected, and thus, the duration of data collection extended,
- Aim of the applied course went beyond teaching data collection and analysis methods to include actualization of updating maps among other possibilities,
- Although the study was done by using information technologies and computer systems it was a time and effort intensive study due to the amateur character of the method used,
- Despite formation of data lists and standardization of the drawing technique, problems occurred during entering the data and digitalization of maps caused further problems that affect the progress of the study.

- Problems that had occurred during the computerization of data reduced the time that were planned to be allocated for the preparation of reports and the final analyses of the study.

- Planning exercises about the settlement, which was the case study for the data collection, data analysis and synthesis in Planning 4, will be covered in Planning 5. The shortage of time that was allocated for analysis and synthesis stages in Planning 4 affected the syllabus of Planning 5. Therefore, synthesis studies that were partially covered in planning 4 have to be rehashed in planning 5.

- Problems occurred during the entering of data can be overcame through improvements in the hardware by the use of better technologies.

- However, the intensity and uniqueness of the student works in Planning 4 created a positive motivation for further studies in Planning 5. It has also helped students establish ties with their fieldwork, which has paved the way of their success and increased the quality of their work.

- Lastly, a time and labor intensive study has been accomplished. This study brought significant achievements both to the students and to their professors. It is an important experience for professors to see the contributions of technology into the learning process, especially in terms of its positive effects on the quality of works. Besides, the research, updated maps and the result analyses grabbed the attention of the local governments as well. A copy of the final products of this study were shared with the local government as a significant example for the future Planning 4 courses.

References

[1]Tekeli, İlhan; "Bir Modernite Projesi Olarak Türkiye'de Kent Planlaması", Modernite Aşılırken Kent Planlaması, p:9-35, İmge Kitabevi Yayınları, 2000, ISBN 975-533-161-1

[2]Günay,Baykan, "Planlama Kuramı ve Kentsel Planlama Eğitimi", Kentsel Planlama Kuramları, ed.:Melih Ersoy, p:307-340, İmge Kitabevi yayınları, 2007, ISBN 978

[3] Tekeli, İlhan; "Kent plancıları Disiplinlerarası Olmayı Yeniden Tartışmaya Açmalıdır", Modernite Aşılırken Kent Planlaması, p:187-194, İmge Kitabevi Yayınları, 2000, ISBN 975-533-161-1

[4] Ersoy, M., Şengül, T. (ed.), "Kente Göç ve Yoksulluk Diyarbakır Örneği", ODTÜ Kentsel Politika Planlaması ve Yerel Yönetimler Anabilim Dalı 2001 Yılı Stüdyo Çalışması, Ankara: Kasım 2002, yayın No:6

[5]Dikçınar Sel B, Yazgan Gül A, Kentsel Mekanların Aynılaşması: Midyat Örneği, MEGARON 2009;4(2):79-89

[6]Brail, R.K, Klosterman; R.E, Planning Support Systems, ESRI press, 2001, ISBN I-58948-OII-2

[7] Gül Y.A., Sel D.B., Sönmez Ö., Özbakır A., Seçilmişler T., Kurtarır E., are the team of the 2007/2008-2 Planning IV Course.

SESSION

SIMULATION AND MODELING + APPLICATIONS

Chair(s)

Prof. Hamid R. Arabnia

Computation of the expected value and variance of the average annual yield for a stochastic simulation of rainwater tank clusters

John Mashford, Shiroma Maheepala, Luis Neumann and Esther Coultas
Commonwealth Scientific and Industrial Research Organization (CSIRO), Australia
PO Box 56, Highett, Vic. 3190, Australia

Abstract *- The problem of obtaining a detailed understanding of the behavior of a cluster (or a collection) of rainwater tanks is complex and can only be solved by simulation. If the collection of houses is very large, a tractable solution can only be obtained by stochastic simulation in which the parameters defining the houses and tanks are sampled from probability distributions. An important output from the rainwater tank simulation is the average annual yield of the cluster and it is of interest to know its expected value and variance for planning of urban water systems. This paper carries out a theoretical calculation of the expected value and variance of the average annual yield as functions of cluster size and presents an experimental confirmation of these results.*

Keywords: rainwater tank, stochastic simulation, yield, expected value, variance

1 Introduction

The amount of water that can be supplied from a rainwater tank (i.e. yield of a rainwater tank) depends on a number of properties of the house, the tank and the climate [1, 2, 3]. The relevant properties of the house can be modeled as the roof area connected to the rainwater tank, the depression storage (i.e. retention storage of the roof which depends on the type of roof material and shape of the roof), the roof area loss factor (i.e. losses from the roof, which depends on roof material) and the way in which water stored in the rainwater tank is used by occupants of the house (i.e. demand time series). The demand time series is a function of the occupancy status of the house and the type of end uses for which rainwater is used. For example, rainwater can be used for garden use, toilet use, laundry use and hot water use. The principal relevant property of the rainwater tank is its volumetric capacity while the properties of the environment relevant to the rainwater tank's evolution are the rainfall time series and the potential evapotranspiration (PET) time series as the evaporation from the roof of the house and the tank depend on the temperature, wind, humidity and so on. A quantity of considerable interest to urban water management planners is the yield of a collection of tanks over a period of time [4]. The behavior of a tank can be represented by time series $\{V_t\}$ and $\{Y_t\}$ where:

V_t = the volume of water in the tank at the end of time period t; and

Y_t = the yield from the tank during time period t.

It has been shown that a daily time step is sufficient to accurately model a rainwater tank if there is no trickle supply to the tank from mains supply [3]. This study assumes that each rainwater tank is fitted with an appropriate valve which allows end uses of the tank to switch to mains supply when the tank has run out of water (i.e. there is no trickle supply from the mains). The behavior of the tank can be simulated by recursively solving the storage behavior equations for V_t and Y_t, t = 1, …, P where P is the number of time periods in the simulation [3]. In our simulation, the demand pattern is taken from a finite number, N_ds, of demand scenarios.

The yield obtained in this way is a time series which is a function of the rainwater tank capacity C, the roof area A, the depression storage δ, the roof area loss factor L and the demand scenario number d. Thus:

$$Y_t = Y_t(C,A,\delta,L,d). \quad (1)$$

It is also implicitly a function of the rainfall time series and the PET time series which we consider to be the same for all houses. It can be shown using induction that Y_t is a nonlinear continuous function of its continuous parameters for all t = 1, …, P. Let N_years be the number of years over which the simulation is taken. The average annual yield for a house defined by parameters C, A, δ, L and d is:

$$Y = Y(C,A,\delta,L,d) = \frac{1}{N\_years} \sum_{t=1}^{P} Y_t(C,A,\delta,L,d). \quad (2)$$

We will consider the problem of simulating a cluster of houses with rainwater tanks, where the parameters defining each house are chosen randomly according to probability distributions and the demand scenario for a house is chosen randomly from a number of possibilities associated with its occupancy status. In this paper, we will show that the expected value of the average annual yield is independent of the cluster size, while the variance of the average annual yield depends on the cluster size according to a hyperbolic function. This theoretical result will be confirmed by experimental computation.

In Section 2, two deterministic examples motivating the development of the general formulation of the first result are presented. In section 3, the first result of the paper concerning the expected value of the average annual yield is proved. In Section 4, the second result, concerning the variance of the average annual yield, is proved. In Section 5, the experimental confirmation of these results is presented, while Section 6 provides a conclusion to the paper.

2 Two motivating examples

Consider a cluster made up of N identical copies of a house with parameters C, A, δ, L and d. The total yield of the cluster is:

$$\sum_{t=1}^{P} \sum_{i=1}^{N} Y_t(C,A,\delta,L,d) = \sum_{t=1}^{P} N\, Y_t(C,A,\delta,L,d). \quad (3)$$

Therefore the average annual yield (per house) is:

$$Y = \frac{1}{N\_years\, N} \sum_{t=1}^{P} N\, Y_t(C,A,\delta,L,d)$$

$$= \frac{1}{N\_years} \sum_{t=1}^{P} Y_t(C,A,\delta,L,d), \quad (4)$$

which is independent of the number of houses in the cluster.

Averaging is being taken in two ways. Firstly, the annual yield is being averaged over all houses in the cluster. Secondly, the average annual value is being computed by summing over all time periods in the simulation and then dividing by the number of years in the simulation.

Now, consider a slightly more complicated example. Suppose that we have a cluster made up of N different houses defined by parameters C_i, A_i, δ_i, L_i, d_i; i = 1, …, N. Now, scale up the cluster M times to form a cluster of MN houses in which each house in the original cluster is duplicated M times. The total yield of the cluster is:

$$\text{Total yield} = \sum_{t=1}^{P} \sum_{i=1}^{N} MY_t(C_i,A_i,\delta_i,L_i,d_i). \quad (5)$$

Therefore the average annual yield is:

$$Y = \frac{1}{N\_years\, N\, M} \sum_{t=1}^{P} \sum_{i=1}^{N} MY_t(C_i,A_i,\delta_i,L_i,d_i)$$

$$= \frac{1}{N\_years\, N} \sum_{t=1}^{P} \sum_{i=1}^{N} Y_t(C_i,A_i,\delta_i,L_i,d_i), \quad (6)$$

which is the same as the average annual yield of the original cluster.

Thus, scaling up a cluster has no effect on the average annual yield. This is true no matter how small the cluster is.

3 The expected value of the yield as a function of cluster size

We now want to consider the case in which a cluster is generated by sampling the parameters from probability distributions. The yield for a house during any time period is a function of the parameters for the house. We want to work out the average value of the average annual yield over a number of runs in which the probability distributions are sampled.

We will first consider the case of one variable. Let v be a real non-negative random variable distributed according to a probability distribution $\rho : [0,\infty) \to [0,\infty)$. Then:

$$\Pr(v \in [a,b]) = \int_a^b \rho(x)dx, \quad (7)$$

for $0 \le a < b$. Let $f : [0,\infty) \to \mathbf{R}$ be a continuous function. Define, as usual [5], the expectation value of f to be:

$$\langle f \rangle = \int_0^\infty f(x)\rho(x)dx. \quad (8)$$

A quick argument can be used to show that the mean of f(v) over a large number of trials is given by the expectation value of f. Suppose that we carry out n trials resulting in values v_i of v. Then:

$$\text{mean} = \frac{1}{n} \sum_{i=1}^{n} f(v_i)$$

$$= \frac{1}{n} \sum_{j=0}^{\infty} \sum \{f(v_i) : v_i \in I_j\}$$

$$\approx \frac{1}{n} \sum_{j=0}^{\infty} f(a\_j)n \int_{a\_j}^{b\_j} \rho(x)\, dx$$

$$= \sum_{j=0}^{\infty} \; f(a\_j) \int_{a\_j}^{b\_j} \; \rho(x)\, dx$$

$$\approx \sum_{j=0}^{\infty} \; \int_{a\_j}^{b\_j} \; f(x)\rho(x)\, dx$$

$$= \int_{0}^{\infty} \; f(x)\rho(x)\, dx$$

$$= <f>.$$

In the above computation, $\{I_j = [a\_j,b\_j]\}$ is a fine partition of the interval $[0,\infty)$. The approximations become exact in the limit as the partition becomes sufficiently fine and the number of trials becomes infinite.

If one has suitable closed form representations of the functions f and ρ, then it may be possible to evaluate the integral expression for <f> analytically. In other cases, it may be necessary to evaluate the integral numerically which may be as computationally expensive as evaluating the mean value by simulation [6, 7].

A similar argument holds for computing the long run mean value of a continuous function of more than one random variable. Consider a housing cluster of size N generated by random parameters C_i, A_i, δ_i, L_i, d_i; i = 1, …, N which are sampled from distributions $\rho_1 : [0,\infty) \to [0,\infty)$, $\rho_2 : [0,\infty) \to [0,\infty)$, $\rho_3 : [0,\infty) \to [0,\infty)$, $\rho_4 : [0,\infty) \to [0,\infty)$ and $\rho_5 : \{1, \ldots, N\_ds\} \to [0,1]$ with:

$$\int_{0}^{\infty} \; \rho_j(x)\, dx = 1, \; \forall \; j = 1, \ldots, 4, \qquad (9)$$

and:

$$\sum_{k=1}^{N\_ds} \; \rho_5(k) = 1. \qquad (10)$$

The average annual yield for one run or trial is :

$$Y = Y(C_1, \ldots, C_N, A_1, \ldots, A_N, \delta_1, \ldots, \delta_N, L_1, \ldots, L_N, d_1, \ldots, d_N)$$

$$= \frac{1}{N\_years\, N} \sum_{t=1}^{P} \; \sum_{i=1}^{N} \; Y_t(C_i,A_i,\delta_i,L_i,d_i). \qquad (11)$$

The expected or most probable annual average annual yield is given by :

$$<Y> = \sum_{d\_1=1}^{N\_ds} \; \ldots \; \sum_{d\_N=1}^{N\_ds} \; \rho_5(d_1) \ldots \rho_5(d_N) \int_{0}^{\infty} \; \ldots$$

$$\int_{0}^{\infty} \; Y(C_1, \ldots, C_N, A_1, \ldots, A_N, \delta_1, \ldots, \delta_N, L_1, \ldots, L_N, d_1, \ldots, d_N)\, \rho_1(C_1) \ldots \rho_1(C_N)\, \rho_2(A_1) \ldots \rho_2(A_N)\, \rho_3(\delta_1) \ldots \rho_3(\delta_N)\, \rho_4(L_1) \ldots \rho_4(L_N)\, dC_1 \ldots dC_N\, dA_1 \ldots dA_N\, d\delta_1 \ldots d\delta_N\, dL_1 \ldots dL_N$$

$$= \frac{1}{N\_years\, N} \sum_{t=1}^{P} \; \sum_{i=1}^{N} \; \sum_{d\_i=1}^{N\_ds} \; \rho_5(d_i) \int_{0}^{\infty} \; \ldots$$

$$\int_{0}^{\infty} \; Y_t(C_i,A_i,\delta_i,L_i,d_i)\, \rho_1(C_i)\, \rho_2(A_i)\, \rho_3(\delta_i)\, \rho_4(L_i)\, dC_i dA_i d\delta_i dL_i$$

$$= \frac{1}{N\_years\, N} \sum_{t=1}^{P} \; \sum_{i=1}^{N} \; \sum_{d=1}^{N\_ds} \; \rho_5(d) \int_{0}^{\infty} \; \ldots$$

$$\int_{0}^{\infty} \; Y_t(C,A,\delta,L,d)\, \rho_1(C)\, \rho_2(A)\, \rho_3(\delta)\, \rho_4(L)\, dC dA d\delta dL$$

$$= \frac{1}{N\_years} \sum_{t=1}^{P} \; \sum_{d=1}^{N\_ds} \; \rho_5(d) \int_{0}^{\infty} \; \ldots$$

$$\int_{0}^{\infty} \; Y_t(C,A,\delta,L,d)\, \rho_1(C)\, \rho_2(A)\, \rho_3(\delta)\, \rho_4(L)\, dC dA d\delta dL.$$

This is independent of the number of houses in the cluster. The same average annual yield is obtained by doing many runs with one house as by doing fewer runs with many houses as long as the house and tank parameters are sampled from the same probability distributions. This implies that if the cluster size is varied with the same number of runs, the average annual yield will vary depending on the cluster size. As the cluster size increases (with the same number of runs) the average annual yield will become less variable and will begin to approach more closely the expected average annual yield. We will show evidence for this deduction in Section 5.

It is difficult to evaluate the integrals representing the expected average annual yield <Y> because the yield functions Y_t are not given in closed form but can only be obtained by simulation. Thus, in practice <Y> must be obtained by simulation. The number of trials required for the accurate simulation of <Y> can vary depending on the nature of the probability distributions of tank and house related variables and the nature of the yield functions Y_t.

4 Variance of the yield as a function of cluster size

While the expected (average annual) yield is independent of the cluster size, the variance of the yield is dependent on the cluster size. The standard deviation σ of the yield is the square root of the variance σ^2 where σ^2 is the long run average of the square of the difference between the yield and the average yield. By the argument given above, this is given by:

$$\sigma^2 = \langle (Y-\langle Y\rangle)^2\rangle. \quad (12)$$

Now :

$$\begin{aligned}\langle (Y-\langle Y\rangle)^2\rangle &= \langle Y^2+\langle Y\rangle^2-2Y\langle Y\rangle\rangle \\ &= \langle Y^2\rangle+\langle Y\rangle^2-2\langle Y\rangle\langle Y\rangle \\ &= \langle Y^2\rangle-\langle Y\rangle^2. \quad (13)\end{aligned}$$

Using Equation 11 we have:

$$\langle Y^2\rangle = \sum_{d\_1=1}^{N\_ds} \cdots \sum_{d\_N=1}^{N\_ds} \rho_5(d_1) \cdots \rho_5(d_N)$$

$$\int_0^\infty \cdots \int_0^\infty \left(\frac{1}{N\_years\, N}\sum_{t=1}^{P}\sum_{i=1}^{N} Y_t(C_i,A_i,\delta_i,L_i,d_i)\right)^2 \rho_1(C_1) \cdots \rho_1(C_N)\, \rho_2(A_1) \cdots \rho_2(A_N)\, \rho_3(\delta_1) \cdots \rho_3(\delta_N)\, \rho_4(L_1) \cdots \rho_4(L_N)\, dC_1 \cdots dC_N\, dA_1 \cdots dA_N\, d\delta_1 \cdots d\delta_N\, dL_1 \cdots dL_N$$

$$= \left(\frac{1}{N\_years\, N}\right)^2 \sum_{d\_1=1}^{N\_ds} \cdots \sum_{d\_N=1}^{N\_ds} \rho_5(d_1) \cdots \rho_5(d_N) \int_0^\infty \cdots \int_0^\infty \sum_{t,s=1}^{P}\sum_{i,j=1}^{N} Y_t(C_i,A_i,\delta_i,L_i,d_i)\, Y_s(C_j,A_j,\delta_j,L_j,d_j)\, \rho_1(C_1) \cdots \rho_1(C_N)\, \rho_2(A_1) \cdots \rho_2(A_N)\, \rho_3(\delta_1) \cdots \rho_3(\delta_N)\, \rho_4(L_1) \cdots \rho_4(L_N)\, dC_1 \cdots dC_N\, dA_1 \cdots dA_N\, d\delta_1 \cdots d\delta_N\, dL_1 \cdots dL_N$$

$$= \left(\frac{1}{N\_years\, N}\right)^2 \sum_{t,s=1}^{P} \left(\sum_{i=1}^{N} \sum_{d\_i=1}^{N\_ds} \rho_5(d_i) \int_0^\infty \cdots \int_0^\infty Y_t(C_i,A_i,\delta_i,L_i,d_i) Y_s(C_i,A_i,\delta_i,L_i,d_i)\, \rho_1(C_i)\, \rho_2(A_i)\, \rho_3(\delta_i)\, \rho_4(L_i)\, dC_i dA_i d\delta_i dL_i + \sum \left\{ \sum_{d\_i=1}^{N\_ds} \sum_{d\_j=1}^{N\_ds} \rho_5(d_i)\, \rho_5(d_j) \int_0^\infty \cdots \int_0^\infty Y_t(C_i,A_i,\delta_i,L_i,d_i)\, Y_s(C_j,A_j,\delta_j,L_j,d_j)\, \rho_1(C_i)\rho_1(C_j)\, \rho_2(A_i)\rho_2(A_j)\, \rho_3(\delta_i)\rho_3(\delta_j)\rho_4(L_i)\rho_4(L_j)\, dC_i\, dC_j\, dA_i dA_j\, d\delta_i d\delta_j\, dL_i dL_j : i, j = 1, \ldots, N;\ i \neq j \right\}\right)$$

$$= \left(\frac{1}{N\_years\, N}\right)^2 \sum_{t,s=1}^{P} \left(N \sum_{d=1}^{N\_ds} \rho_5(d) \int_0^\infty \cdots \int_0^\infty Y_t(C,A,\delta,L,d) Y_s(C,A,\delta,L,d) \rho_1(C)\, \rho_2(A)\, \rho_3(\delta)\, \rho_4(L)\, dC dA d\delta dL + (N^2-N) \sum_{d=1}^{N\_ds} \rho_5(d) \int_0^\infty \cdots \int_0^\infty Y_t(C,A,\delta,L,d) \rho_1(C) \rho_2(A)\, \rho_3(\delta) \rho_4(L)\, dC dA d\delta dL \sum_{d=1}^{N\_ds} \rho_5(d) \int_0^\infty \cdots \int_0^\infty Y_s(C,A,\delta,L,d)\, \rho_1(C)\, \rho_2(A)\, \rho_3(\delta)\, \rho_4(L)\, dC dA d\delta dL\right)$$

Thus the variance is given by :

$$\sigma^2 = \left(\frac{1}{N\_years\, N}\right)^2 \sum_{t,s=1}^{P} \left(N\gamma_1(t,s) + (N^2-N)\gamma_2(t)\gamma_2(s)\right) - \langle Y\rangle^2,$$

$$= \left(\frac{1}{N\_years}\right)^2 \frac{1}{N} \left(\sum_{t,s=1}^{P} \gamma_1(t,s) - \left(\sum_{t=1}^{P} \gamma_2(t)\right)^2\right), \quad (14)$$

where :

$$\gamma_1(t,s) = \sum_{d=1}^{N\_ds} \rho_5(d) \int_0^\infty \cdots \int_0^\infty Y_t(C,A,\delta,L,d)\, Y_s(C,A,\delta,L,d)\, \rho_1(C)\rho_2(A)\rho_3(\delta)\rho_4(L)\, dC dA d\delta dL, \quad (15)$$

and :

$$\gamma_2(t) = \sum_{d=1}^{N\_ds} \rho_5(d) \int_0^\infty \dots \int_0^\infty Y_t(C,A,\delta,L,d)\, \rho_1(C)$$

$$\rho_2(A)\, \rho_3(\delta)\rho_4(L)\, dCdAd\delta dL. \quad (16)$$

If $f : [0,\infty)^4 \times \{1, \dots, N\_ds\} \rightarrow \mathbf{R}$ is a function define $\langle f \rangle_1$ by :

$$\langle f \rangle_1 = \sum_{d=1}^{N\_ds} \rho_5(d) \int_0^\infty \dots \int_0^\infty f(C,A,\delta,L,d)\, \rho_1(C)$$

$$\rho_2(A)\, \rho_3(\delta)\rho_4(L)\, dCdAd\delta dL. \quad (17)$$

Then:

$$\gamma_1(t,s) = \langle Y_t Y_s \rangle_1 \quad (18)$$

and:

$$\gamma_2(t) = \langle Y_t \rangle_1. \quad (19)$$

The variance is a hyperbolic function of N and:

$$\text{limit as } N \rightarrow \infty \text{ of } \sigma^2 = 0. \quad (20)$$

5 Experimental confirmation

The yield Y_t is a nonlinear function of t and the system parameters which can only be computed by simulation. The results of computing the total yield over the period of simulation projected onto the parameters of tank size and roof area is shown in Figure 1.

Simulation was carried out where the continuous system parameters were sampled from truncated normal distributions as described in [8]. In order to confirm the calculations of Section 3 and Section 4 in numerical detail it would be necessary to numerically compute multiple integrals such as those of Equations 15 and 16. However, the essential correctness of the results can be seen by examination of Figure 2 which shows the result of carrying out 50 runs for a variety of values for the cluster size. The curve labeled "Variable" shows the average over the 50 runs of the average annual yield and it is seen that this is approximately independent of the cluster size. The approximation becomes more accurate as the cluster size increases. This is because the number of houses sampled in the simulation is RN where R is the number of runs and N is the cluster size and as this number increases the average of the average annual yields tends more closely to the expected value, as described in Section 3.

The curves labeled "Variable-1SD" and "Variable+1SD" which show the standard deviation of the average annual yield over the 50 runs have the rational function form of the variance given by Equation 14. The curve labeled "Average" shows the result of computing the average annual yield for a house with parameters equal to the expected value of their respective probability distributions, which, since the yield function is nonlinear, is not equal to the expected value of the average annual yield ("Variable") [9, 8].

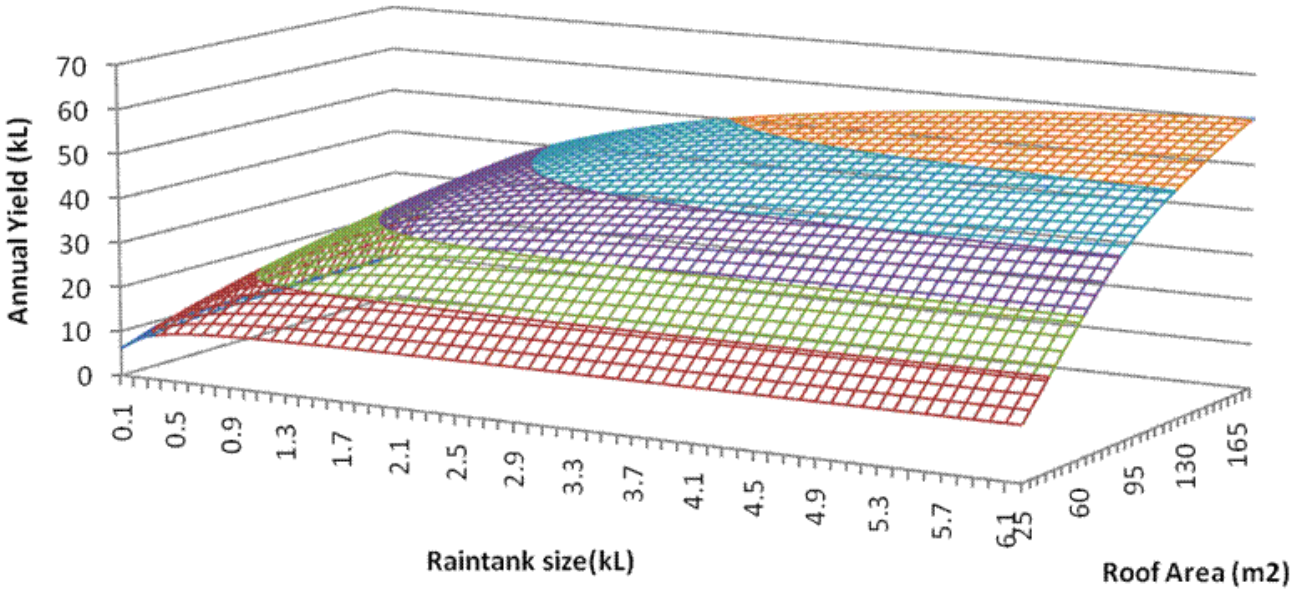

Figure 1: Annual yield as a function of tank size and roof area (source: Neumann et al. [9]).

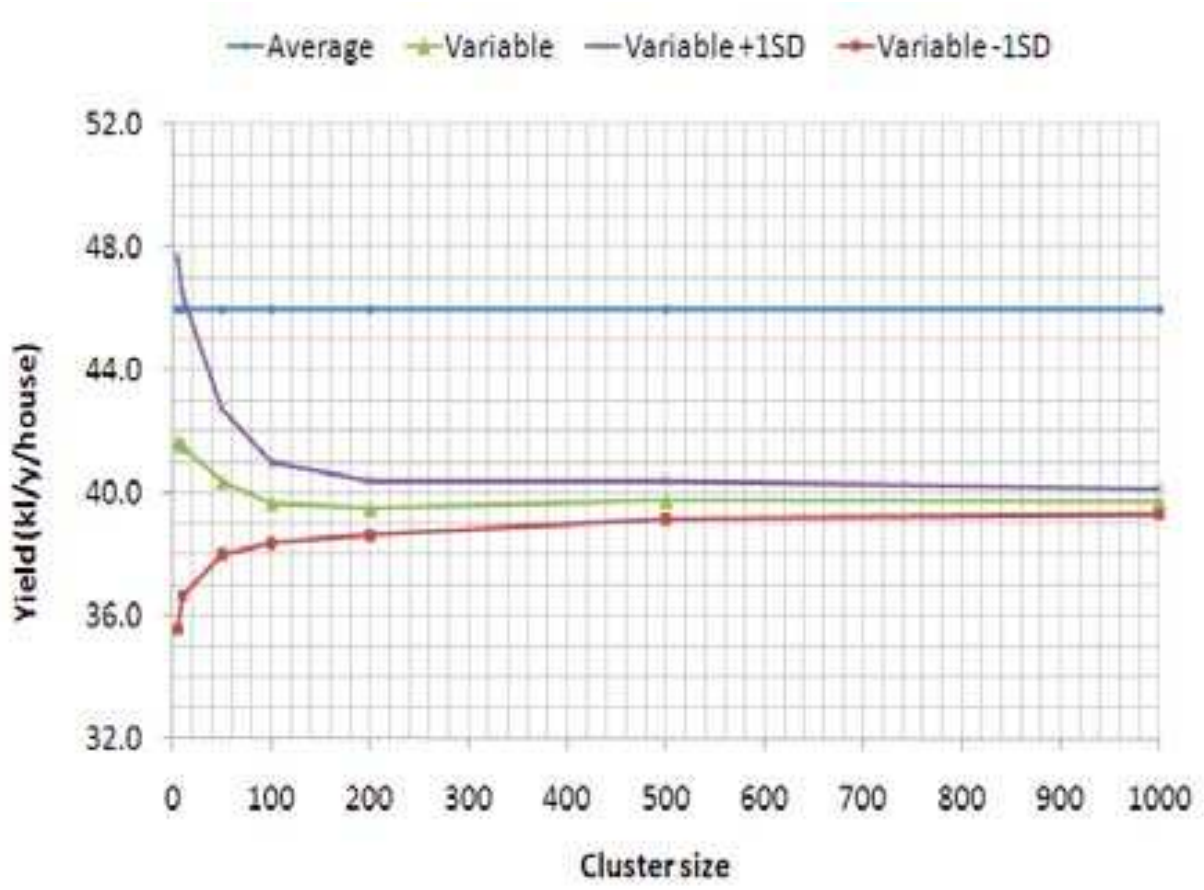

Figure 2: Average value and standard deviation of average annual yield as a function of cluster size for Melbourne based data (source: Maheepala et al. [4]). Each cluster of household rainwater tanks was run 50 times.

6 Conclusion

The determination of the evolution of the state of a cluster of household rainwater tanks given the relevant properties of the houses, the tanks and the climate is too complex to solve analytically (i.e. mathematically). Stochastic simulation seems to be an attractive method to compute the expected value and variance of the average annual yield of a cluster of household rainwater tanks. This paper presents proof that these quantities have certain properties, such as: the expected value of the average annual yield does not vary with the cluster size; and a particular shape of the variance of the average annual yield as a function of cluster size, together with the presentation of experimental results of stochastic simulation which confirm these theoretical derivations.

In addition the theoretical derivation reported in this paper provides a sound basis for the results reported in [4] using stochastic simulation. The practical application of the theoretical derivation is that it shows how the variability of average annual yield of a cluster of household rainwater tanks varies with the cluster size. The acceptable variance can be defined by practitioners. The acceptable variance will define the acceptable cluster size for linear scaling up of the average annual yield of a large number of household rainwater tanks spread across a city of which there could be millions.

Acknowledgements

This research was funded by the Urban Water Security Research Alliance (http://www.urbanwateralliance.org.au/) which is a partnership between the Queensland State Government, Griffith University, the University of Queensland and CSIRO (Commonwealth Scientific and Industrial Research Organization)'s Water for a Healthy Country Research Flagship.

References

[1] Fewkes, A. "Modelling the performance of rainwater collection systems: towards a generalised approach"; Urban Water 1, 323-333, 1999.

[2] Fewkes, A and Butler, D. "Simulating the performance of rainwater collection and reuse systems using behavioural models"; Build, Serv. Eng. Res. & Tech., 21, 99-106, 2000.

[3] Mitchell V.G., Siriwardene N., Duncan H. and Rahilly M. "Impact of temporal and spatial lumping on rainwater tank system modelling"; Conf. Proc. of Wat. Down Under 2008, 15-17 April 2008, Adelaide, South Australia, 2008.

[4] Maheepala, S., Loonat, N., Mirza, F. and Coultas, E. "Quantifying potable water savings of rainwater tanks at a city scale by considering the effect of spatial lumping"; OZWater 2011, 09-11 May 2011, Adelaide, Australia, 2011.

[5] Kallenberg, O. "Foundations of Modern Probability"; Springer, 1997.

[6] Givens, G. H. and Hoeting, J. A. "Computational Statistics"; Wiley, 2005.

[7] Ripley, B. D. "Stochastic Simulation", Wiley, 1987.

[8] Xu, H., Rahilly, M. and Maheepala, S. "Assessing the impact of spatial lumping on rainwater tank performance using daily modelling"; Submitted to the 9th International Conference on Hydro-informatics, September 7-11, 2010, Chinese Academy of Sciences, China, 2010.

[9] Neumann L., Coultas E., Moglia M., and Mashford J. "Errors in yield and overflow estimation in rainwater tank cluster modelling"; to appear in the Proc. of the 12th International Conference on Urban Drainage, September 11 to 16, 2011, Porto Alegre, Brazil, 2011.

Teaching Undergraduate Computational Modeling Courses: Topics & Tools

Shin S. Jou
Department of Computer Science, Winston-Salem State University, Winston-Salem, NC, USA

Abstract - *In this paper, we try to find good ways to teach undergraduate courses in computational science which are taught and used in many different areas of research with diverse different tools of sophistications. We explore core contents of the computational science courses that can satisfy the need of students from different areas of studies and applications.*

Keywords: Computational Science, Simulations & Modeling

1 Introduction

Computational science is fast growing, and combines many interesting aspects such as computer simulation, scientific visualization, mathematical modeling, computer programming, networking, numerical analysis, symbolic computation, and high performance computing, etc. Scientists are able to perform new experiments that they couldn't perform prior to computational science. It involves in constructing mathematical models and solving the model in simulation using computers. Finally adaptations of the models and solutions are through precise verifications and validations. Depending on the nature of the models, some computations are numerically intensive, and need to be computed using supercomputers or distributed computer systems.

Computational science is excellent for performing numerical simulations. Numerical simulations can provide very useful information about many natural phenomena. Numerical simulation help scientists and researchers reconstruct and understand events, like weather, astrophysics & cosmology, computational geometry [9] [10], genetics & genomics, etc. Computational science seeks to gain an understanding of science through the use of mathematical models simulated on computers.

CSC4383 (Introductions to Computational Modeling), CSC4385 (Simulations and Modeling) and CST5333 (Scientific Visualization and Digital Image Processing), are among others courses that I have normally taught in the Computer Science Department of WSSU. In this paper, I will discuss some of the topics and tools used for our Computational Modeling Course and also some related topics of Simulations & Modeling course.

2 Some Methods and Topics to consider

Computational modeling courses are taught in different areas of sciences and also engineering disciplines. The focus of this course is mainly for our computer science junior or senior levels with possibility of serving the students from Biology, Chemistry, Physics, and Engineering. The main challenges are to spend just enough time in mathematics for students to understand and use the mathematical models effectively. Since most students do not have numerical analysis course, selections of mathematics models are important for students to work on their projects successfully. Many students have knowledge of programming in Java. Textbooks that meet the interests of students and cover fundamental core concepts of computational science are important. The book [1] covers sufficient topics for many models and examples from many areas of sciences not too complicated but interesting enough for students to learn. I cover in my syllabus the topics such as, overview, fundamental concepts (mathematics preparations), System Dynamics Problems, Simulation Techniques, System Dynamics Models with interactions and more advanced System Dynamics, Monte Carlo Simulations, Random Walks, data models, and High Performance Computing, etc.

The software tools used for projects are programming languages like Microsoft Visual C++, Java, VENSIM package, and MATLAB. MATLAB is a useful tool for doing numerical computations. MATLAB facilitates for working on Numerical Linear Algebra, and visualizations of graphs. Students work on linear algebra and visualizations using MATLAB in the lab rather working on the hard theory like LU factorizations through Gaussian eliminations, or Linear Algebra algorithms, etc.

3. Mathematics, Algorithms, and Some Sample Class Projects

3.1 The Initial-Value Problems

Consider the first order differential equation [1], [5]:

dy/dt = f(t, y), t0<= t<=T, may have an unique solution

if f satisfies certain conditions.

Euler's Algorithm [1], [5]:

$dP/dt = f(t, P)$, $t_0 <= t <= T$

- $t \leftarrow t_0$
- $P(t_0) \leftarrow P_0$
  Initialize NumberOfIterations //Δt the interval size
- for n going from 1 to NumberOfIterations do the following:
  - $t_n = t_0 + n\,\Delta t$
  - $P_n = P_{n-1} + f(t_{n-1}, P_{n-1})\,\Delta t$

Modified Euler Method [1], [5]:

1 Initialize t_0 and P_0

2 Initialize N, number of iterations

3 for *n* going from 1 to N do:

3.1 $t_n = t_0 + n\,\Delta t$

3.2 $P_n = P_{n-1} + f(t_{n-1}, P_{n-1})\Delta t$, **which is Euler's Method estimate.**

3.3 $P_n = P_{n-1} + ((f(t_{n-1}, P_{n-1}) + f(t_n, P_n))/2.0)\Delta t$

3.4 $P' = f(t, P)$ **with initial condition** $P(t_0) = P_0$. **Suppose that** P_n **is the value of the variable at time** t_n. **The method takes** P_n **and** t_n **and calculates an approximation for** P_{n+1} **at a brief time later,** $t_n+\Delta t$. **It uses a weighted average of approximated values of f (t, x) at several times in the interval** $(t_n, t_n+\Delta t)$.

Runge-Kutta(of order 4) takes more refinements [5] with:

$P' = f(t, P)$
$P(x_o) = P_0$, $h=\Delta t$

$t_{n+1} = t_n + h$
$P_{n+1} = P_n + (1/6)(k_1 + 2k_2 + 2k_3 + k_4)$, where

$k_1 = h\, f(t_n, P_n)$
$k_2 = h\, f(t_n + h/2, P_n + k_1/2)$
$k_3 = h\, f(t_n + h/2, P_n + k_2/2)$
$k_4 = h\, f(t_n + h, P_n + k_3)$

3.2 VEMSIM

VENSIM is a dynamic system modeling package which can deal nicely with the first order initial-value ordinary differential equations. The following model was assigned to students as a project.

Consider an idealized Population Model

$dP/dt = growth\_rate(t)P(t)$, where P(t) the population, and the growth_rate(t) function.

The initial population of P(0) = 100,
growth_rate(t) = 0.05*(2- 1/(1+t)), with 0 <= t<= 40

Simulation settings are as below:

(1) FINAL TIME = 40 Units: Month The final time for the simulation.

(2) growth=
growth rate*population Units: Bacterias/Month

(3) growth rate= 0.05*(2 - 1/(1+Time)) Units: 1/Month

(4) INITIAL TIME = 0

(5) population= INTEG (growth, 100)

(6) TIME STEP = 0.25
Units: Month [0,?]
The time step for the simulation.

The solution in VENSIM look like the following:

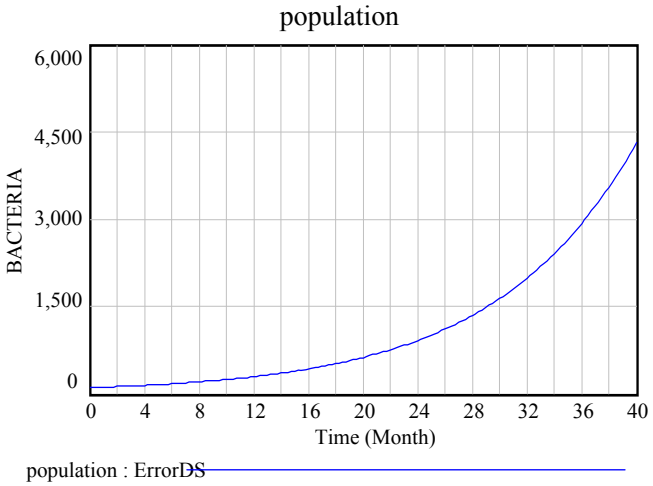

The graph of the Population function P(t)

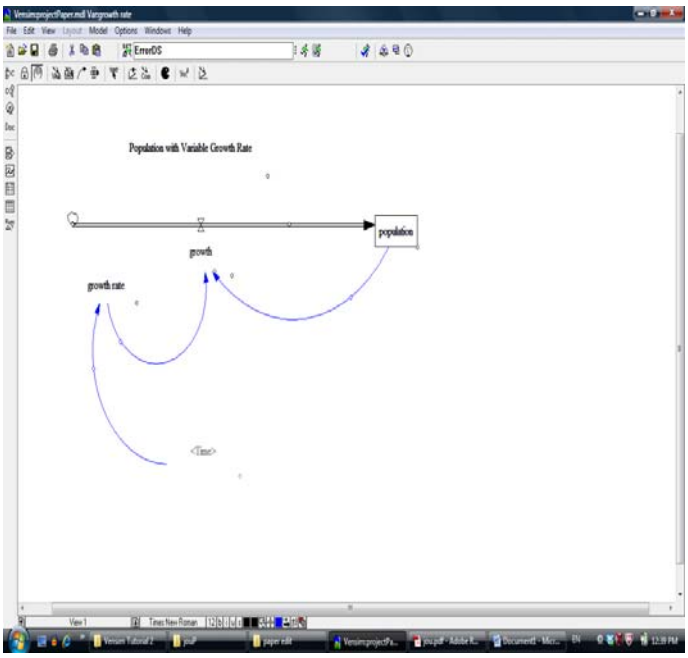

Pictorial Form in VENSIM

3.3 MonteCarlo Simulation

Buffon's Needle ([11], [12]) is one of the oldest problems in the field of geometrical probability. It was first stated in 1777. It involves dropping a needle on a lined sheet of paper and determining the probability of the needle crossing one of the lines on the page. The remarkable result is that the probability is directly related to the value of **π**.

Monte Carlo methods are a class of computational algorithms that rely on repeated random sampling to compute their results.

A project of the following was assigned to students. Students are required to solve this problem using Monte Carlo simulation, and implement the solutions in C++ or Java.

Problem:

y=f(x)= 3 * x^2, for 1<=x <=2.

(A) Find : $Area = \int_1^2 (3x\hat{}2)dx$

(B) Afterward, the function is changed to f(x) = exp(- x ^{2}), and integrated over the interval, -1.0 <= x <= 1.0.

3.4 Using MATLAB

MATLAB is a useful compuational language expecially good for computing big volume of data with clean and clear program codes. Students are asked to implement the same problems in **3.3** using MATLAB. A quick review of basic MATLAB features needs to be done in the class. Although, the basic algorithms are the same, programming code can be reduced as shown below ([1], [16]).

```
  f = @(x) exp(- x.^2);
 smallest_x= -1.0;
 largest_x= 1.0;
 high=1.0;
 NumberOfPoints=50000;
 NumberUnder=0;
 for i=1:NumberOfPoints
   x1 =(largest_x-smallest_x)*rand+smallest_x;
   y1=high*rand;
   if(y1<f(x1))
      NumberUnder=NumberUnder+1;
   end;
end;
Area=(largest_x-smallest_x)*high ;
Area=Area*(NumberUnder/NumberOfPoints);
```

If the MATLAB comes with the symbolic math Toolbox, you can compute the area by two instructions.

```
syms x;
int(exp(-x.^2), -1, 1)
```

3.5 Random Walk (RW)

Random walk (**RW**) is one of the applications of Monte Carlo simulations. A random walk**,** sometimes denoted **RW**, is a mathematical formalization of a trajectory that consists of taking successive random steps. For example, the path traced by a molecule as it travels in a liquid or a gas, the search path of a foraging animal, the price of a fluctuating stock and the financial status of a gambler can all be modeled as random walks (RW) [15].

Using one of the MATLAB program from [1], we can see a simple Random Walk diagram as shown below. General RW programs depending on different stochastic processes can be designed according to the natures of the problems.

```
function [xLst, yLst, dist]=RandomWalk(n)
% RANDOMWALK  Function to generate lists
% of x and y
% coordinates of n steps for a random
% walk of n steps
% along with distance between first and
% last point
% rand('state', sum(100*clock))
x0 = 0;
y0 = 0;
x = x0;
y = y0;
xLst = zeros(1, n + 1);
yLst = zeros(1, n + 1);
xLst(1, 1) = x0;
yLst(1, 1) = y0;
for i = 1:n
    if rand < 0.5
        x = x + 1;
    else
        x = x - 1;
    end;
    if rand < 0.5
        y = y + 1;
    else
        y = y - 1;
    end;
    xLst(1, i + 1) = x;
    yLst(1, i + 1) = y;
end;
dist = sqrt((x - x0)^2 + (y - y0)^2);
```

Suppose that, [x y distance] = RandomWalk(10) generates the following points list.

x = [0 -1 0 -1 -2 -3 -4 -5 -6 -7 -8]

y = [0 1 2 1 0 -1 -2 -3 -4 -3 -4],

p0=(0 0), p1=(-1 1), p2=(0 2), p3=(-1 1), p4=(-2 0), p5=(-3 -1), p6=(-4 -2), p7=(-5 -3), p8=(-6 -4), p9=(-7 -3), p10=(-8 -4).

Diagram of this RW

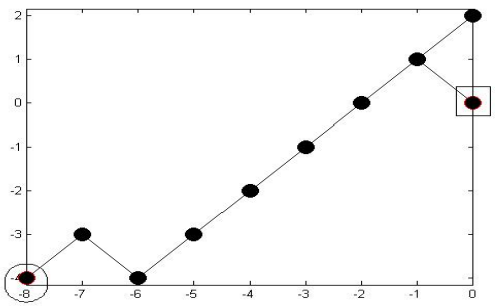

This random walk is based on the uniform random number generator function rand. Hence if we make a different call with the same number of steps of random walk, we may get a different random walk diagram. Some applications of random walk can be found in many literatures. Random walks may follow different probability distributions in deciding the directions of walks. The nature problems will be how to generate the random numbers for different distributions. We turn our attentions to the issues of designing random numbers generators for different random variables, besides using only the standard uniform random number generator.

4. Random Number Generations

4.1. Negative Exponential Distribution functions

$$f(t) = \begin{cases} r\,e^{-rt} & \text{for } t > 0 \\ 0 & \text{for } t <= 0, \end{cases}$$

r a positive constant

The random numbers generator is computed as below:

Compute: - ln(*unif()*)/*r*, with unif() a uniform random number in [0.0, 1.0), and ln(x) a logarithm function.

4.2. Box-Muller-Gauss Method

For a normal distribution with mean μ and standard deviation σ

Random numbers are generated as follow:

Compute:

***b* sin(*a*) + μ and *b* cos(*a*) + μ, where**

a) ***a* = uniform random number in [0, 2π)**
b) ***unif()*, a uniform random number in [0, 1)**
c) ***b* = σ sqrt(-ln(unif()), here sqrt a square root function**

4.3. Discrete Distribution Algorithm

To generate random numbers for a discrete random variable X with probabilities p_1, p_2, …, p_n for

events e_1, e_2, …, e_n, respectively, with $p_1 + p_2 + \ldots + p_n = 1$. Let $S_k = p_1 + p_2 + \ldots + p_k$, $1 <= k <= n$

1. **Generate *rand*, a uniform random number in [0, 1).**
2. **If *rand* < S_1, then return e_1**
   ….
   ….
   else if *rand* < S_{n-1}, then return e_{n-1}
   else return e_n

Some time Rejection Methods may be needed for generating random numbers.

Students also work on random numbers generators for different types of discrete and continuous random variables. A harder one is the Triangular Distributions.

5. Visualization, High Performance Computing (HPC)

MATLAB is a good tool for plotting graphs. Many experimental works are done in the labs. HPC is most commonly associated with computing used for scientific research or computational science. HPC, Parallel Programming, Concurrent Programming concepts/models are briefly covered. There is a separate parallel computing course in our department to work more on these topics. Many visualization works are done in the lab. Parts of the visualizations topics are also covered in my other course CST5333 (Scientific Visualization and Digital Image Processing).

6. Conclusions

In three times of my Introduction to Computational Modeling classes, I had engineering students from overseas, students from computer science, chemistry and biology departments. Engineering students tend to have better preparations for mathematics. Engineering and computer science students have better algorithmic and programming abilities. I try to place students to work in a group of two or three persons. Chemistry students are able to come up with good modeling using some packages for drawing molecular bonding diagram with chemical elements. The instructors often need to find a balanced ways for students to learn more from their prospective needs and preparations. Students actually did more projects than what I mentioned above. Students also like MATLAB, needing helps at the beginning, and explore the easier ways plotting graphics for visualizations. Engineering and computer science students find MATLAB good for working on the linear algebra problems and numerical computations. General concepts and models of HPC, Concurrent & Parallel computing are briefly covered in the course. Separate courses are needed for more theories and actual programming using different software and hardware platforms for solving their specific types of problems.

7 References

[1] Angela Shiflet & George Shiflet, Introduction to Computational Science: Modeling and simulation for the sciences. New Jersey: Princeton University Press, 2006.

[2] Laurence M. Leemis & Stephen K. Park, Discrete Event Simulation, Prentice Hall, 2006.

[3] Banks, J. Carson, B. Nelson, Discrete-Event Simulation, Prentice Hall, 2002.

[4] S. Ross, Simulation, Academic Press, 2006.

[5] Kincaid & Cheney, "Numerical Analysis: Mathematics of Scientific Computing", Brooks/Cole, 1991.

[6] Golub & Ortega, Scientific Computing: An Introduction with Parallel Computing, Academic Press, 1993.

[7] R. Gonzalez, R. Wood & S. Eddin, Digital Image Processing Using MATLAB , Gatesmark, LLC, 2009.

[8] F. Lee & S. Jou, "Efficient Parallel Algorithms on A Mesh of Trees", the Proceedings of the 33rd ACM Southeast Conference, p 213-218, March 1995.

[9] F. Lee & S. Jou, "Constructing The Three-Dimensional Voronoi Diagrams on A Mesh Of Trees", the Proceedings of the 1995 Simulation Multi-Conference, High Performance Computing Symposium, p374-379, April, 1995.

[10] Berg, Cheong, & Krevel, Computational Geometry**:** Algorithms and Applications System, Springer 2008.

[11] Schroeder, L. (1974). Buffon's needle problem: An exciting application of many mathematical concepts. Mathematics Teacher, 67 (2), 183-186.

[12] Cay Hostman, Big Java, 4th edition, 2009.

[13] Ventana Systems, www.vensim.com

[14] System Dynamics, http://www.systemdynamics.org/

[15] RW http://en.wikipedia.org/wiki/Random_walk

[16] Math Works, http://www.mathworks.com/

On Performance of Hybrid Vehicles

Gautham Thyagarajan[1] Opinder Sharma[2] Akhil Kansal [2]
[1]Department of Mechanical Engineering, Wayne State University, Detroit, MI 48202 USA
[2]Department of Electrical and Computer Engineering, Wayne State University, Detroit, MI 48202 USA

Abstract: *Automotive industries always aim to produce high performance vehicles. Developing hybrid vehicles that are better in performance when compared to the competitors in the market is of vital importance for every manufacturer. The research work in this paper is aimed at proposing a method for improving the performance in Hybrid vehicle by data acquisition from ECU. The data taken is that of RPM, Speed, Fuel Pressure, Load, Timing advance, etc, from the OBD port of the vehicles. Emphasis on taking data from engine is the unique feature of this research. The tests were conducted on different models from different manufacturers like Toyota PRIUS Toyota HIGHLANDER, and Ford ESCAPE hybrid vehicles. Dewetron Data analyzer was used to capture the data, and analyze it with precision. The data was exported to Mat lab software. Using fuzzy logic if then conditional rules, the data was processed to graphically to find the regions where the vehicle was operated by the driver beyond optimal limits A procedure for improving the performance of hybrid electric vehicle is suggested.*

Keywords: Online Data Analysis, Fuzzy logic, Matlab, Dewesoft, Offline data processing

Introduction

The automotive manufacturers are expanding their hybrid vehicle segment elaborately. Each manufacturer has their own specific functional hybrid vehicle. For an example, The Toyota Prius and the Highlander have an entirely different mode of operation when compared to the Honda Insight and CRZ. The Toyota segment of vehicles have a strategy that enables vehicles to run on battery till the vehicle achieves a 20mph and above speed for the engine to take the load and charge. This again is dependent upon the passenger load in the vehicle. Unlike this the Honda segment of vehicles have the engine programmed to start first and take up the initial load, and after a certain speed have the motors assist the engine and subsequently cut off until further power is in demand. In either of these ways there is a strategy and computer program behind to govern the working. These complex computer programs can be simplified and made to work using fuzzy logic rules after the ECU data has been captured and analyzed.

The fuzzy logic rules set in this work are based upon certain specifications that manufacturers have set in the vehicle. Previous research in this topic does not get in to details of ECU data acquisition. In this research work, more number of input parameters are considered. They are Fuel pressure, intake air temperature, load, RPM, Speed, Exhaust gas temperature, oxygen sensor reading, absolute throttle position, short and long term fuel trim, manifold absolute pressure, and coolant temperature. To give a precise feedback of the performance to the driver, based on the way the driver, & also, the IF operate the vehicle THEN conditional rules, is where the use of fuzzy logic is justified. In the work done in "Use of Fuzzy Logic in Hybrid Vehicles for Improving Fuel Efficiency by Individual Component Control" [1]. Gautham Thyagarajan utilizes fuzzy logic to improve the fuel efficiency by taking single output from various components. In this paper, apart from component output data, the engine data is also captured analyzed and then control strategy is implemented using Fuzzy logic. Previous work was curtailed only along with lesser input parameters for monitoring efficiency. Work in upbringing complex algorithms for providing feedbacks to the driver was also conducted. Analyzing the data from the ECU of the engine with specific functional parameters which can further enhance the control strategy of the hybrid vehicle has been the key area of research work. The experimental setup and execution of work in stages, its need and justification, and the outcome of the experiment, are described in detail in the following sections of this paper.

2. Experimental Setup

2.1 Calibration and Setup of DEWE 43V data analyzer

The DEWETRON DEWE43V data analyzer is an instrument which is capable of capturing data from different sensors. The core working system of this instrument is software called DEWESOFT. The software is capable of data capturing, formatting and analysis by itself. Data in the form of electrical signals from the sensors are acquired in to the DEWE 43V and stored in to the hard disk of the computer. The experiment is conducted in 3 stages.

The first one is to check the self capability of the DEWETRON and DEWESOFT. The second stage is to check the readability of the acquired data in to MATLAB and imply fuzzy logic rules in the offline mode. The third phase is to do the second phase of the experiment on the data which is coming out live from the ECU of the vehicle, which is called online data analysis.

In the first stage, the data inputs that were available were stored in the form of channels. Each channel gives an output of a certain voltage range from each sensor on the engine, and this is converted in to graphical data for better visualization.

In the first stage, the DEWE 43V was calibrated to the requirements of this experiment. The key requirements which were needed are that it should provide us with values of specific parameters like Manifold Absolute pressure, Absolute Throttle Position, Intake air flow Temperature, Exhaust gas temperature, Coolant temperature, Timing advance, Short and long term Fuel Trim, Engine RPM, and Vehicle speed.

The numerical values of these parameters were obtained in the maximum and minimum ranges. The CAN (control area network port) was connected to the OBD (out bound data) port of the vehicle. After the channels were assigned their titles the hybrid vehicle was turned on. The turn on mode is the point where the data from the ECU Starts flowing in through the CAN port.

2.2 Evaluation and Basic Formulation

Dewesoft has an option called offline math, which actually helps us in setting up rules. The logic rules are assigned based on the recorded input values, and numerical limitations are provided. The maximum limit to which the incurred value can elevate is shown here. Based on this value we can assign a control rule which will give is a triggered signal when the sensors obtain a signal that is outside the limit of our boundary. The logic rule assigned to govern the vehicle speed v/s the Engine RPM are

IF " ENG RPM" = 0 AND "VEHICLE SPEED">0,1,0 (1)

The rule here triggers a linear function in the Graphic screen of dewesoft when the vehicle is in motion and is being propelled in BATTERY alone mode. The 0 and 1 are set trigger values which can be manually adjusted. Similarly the fuzzy rule implemented to indicate the point where the engine takes over is represented with

IF " ENG RPM" >0 AND "VEHICLE SPEED">20,1,0 (2)

This rule triggers a linear function on the graphic screen of dewesoft that will show the ENGINE taking over mode. Here again the trigger values are set between 0 and 1.

The Figure below shows the graphic display scene monitoring the vehicle in the static and moving conditions. Rule1 is shoed when triggered by the solid Green trigger line and Rule 2 is shown by the solid orange line respectively as indicated in Fig.1.

Fig.1.Dewesoft screen shot of rules triggered.

2.3 Advanced formulation & Experimentation in Offline mode

Once the work foundation is set up to trigger the basic modes of operation of the hybrid vehicle, the advanced data is programmed in the Dewesoft for evaluation. Here the parameters are set to obtain triggered functions which exceed the set values at different point of time during vehicle runtime.

To achieve this, the vehicle was operated in Driver alone mode, driver and single passenger, driver and two passengers, driver and three passengers, and driver and four passengers respectively.[6] This was done so as to obtain the various load governed conditions for the engine take over time. The rules assigned for other conditions are

If TA <1deg AND ENGINE RPM < 1500,0,1 (3)

Engine Power (IHP) = (2 π*N*τ) / 60 Nm (4)

Rule (3) and Formula (4) are assigned to calculate the spark timing, as all vehicles Gasoline (or) hybrid, are equipped with a mechanism which will automatically advance the current excitation given by the distributor to the spark plug of the engine, so as to reduce the phenomenon of knock. All manufacturers have their own specific timing advance and retard mechanism according to the road and load conditions of the vehicle. Also the driver behavior is an important aspect.

Torque output from the engine is available from the engine CAN data, but then in general the formula for calculating the torsion force is explained by Formula (4), Where π = 3.14 which is a constant, N= Engine RPM, T = torque in NM and IHP = indicated horse power. The indicated horse power is a form of Brake horse power and the deductible frictional horse power.. Brake Horse power is the Power available at the flywheel of the engine. Frictional horse power is always a negative value. The peak values of various sensor readings which are preset by the manufacturers are shown in Table 1.

The minimum value and maximum values are indicated. This is a further justification for the rules assigned hereafter. Rules assigned are within the boundaries of maximum and minimum values. Any numerical value which exceeds these rule boundaries at any point of operation of the vehicle, due to any circumstances shall trigger a linear graph on the display which is an error indication or a warning.

TABLE1. PARAMETERS WITH MIN AND MAX READINGS

Parameter With Units	Minimum Value	Maximum Value
Engine RPM	0	7500
Vehicle Speed MPH	0	150
Intake Air Temperature Deg C	-40	115
Coolant Temperature Deg c	-40	115
Manifold Air Flow gm/sec	-50	655.35
Load value %	00	100
Fuel trim %	-5	99.21
Timing Advance Deg	-64	63.50
Absolute Throttle Position %	-15	100.00
Oxygen Sensor voltage V	-5	1.275

Further the rules including other parameters are

IF RPM>3000AND Speed<40 and MAF<-50, 0,1 (5)

IF Load>100AND fuel trim< >-1 and ATP>100 , 0,1 (6)

IF OSV>= -1 AND ATP> <25 0, 1 (7)

Rule (5) justifies for defects occurring at the time of lower air intake or a faulty air intake system. Rule (6) is used to detect the point where the engine delays to start up at maximum load condition. This may result in over discharge of battery current and thereby this rule helps in avoiding the same. Rule (7) maps the oxygen sensor voltage. This is needed for detecting the exhaust levels from the Engine and also helps in detecting if the oxygen sensor has failed. At this time the ECU shall not allow the engine to start and thus the battery will have to take the entire load and it may discharge at a very short running period. The limitation of Dewesoft is that on the application of logic rules, it can only trigger a linear function which can make the operator understand that at this point the distortion or deviation from the usual running cycle of the Internal combustion Engine is taking place, and further it cannot directly communicate with the ECU of the engine to readjust parameters at the point of defect. Taking this in to consideration, we now incorporate the same data obtained from Dewesoft and import it in to MATLAB. The fuzzy logic toolbox is used to further enhance the efficiency of the research work, which is covered in the following section.

3. FUZZY LOGIC AND MATLAB

In the second stage of the research, as mentioned above, the data acquired from Dewesoft was imported to Matlab. Using the fuzzy logic toolbox, and Mamdani method, logic rules were assigned to the input parameters retaining their values exactly the same as that acquired. A mat lab program was written to call the function from Dewesoft. From dewesoft the files are exported to matlab by the "export" function which makes the file readable by mat lab. [8] The program would then execute the fuzzy logic rules on the input parameters. Two output parameters are assigned to the function which are, Control, and Execute Respectively. Gaussian membership function was assigned to all the input as well as output parameters. The ranges of each function in the input variables are as provided by the manufacturers, but the output parameters are ranged between 0 and 1. The control [3] and execute mode has three respective membership functions which are NIL LOWER AND ACCELERATE, and NIL, CONTROL, AND STOP. These MF's are assigned for the ease of program to take a logic decision at the time of error and is set to give a feedback as well as execute the function in the simulation mode.

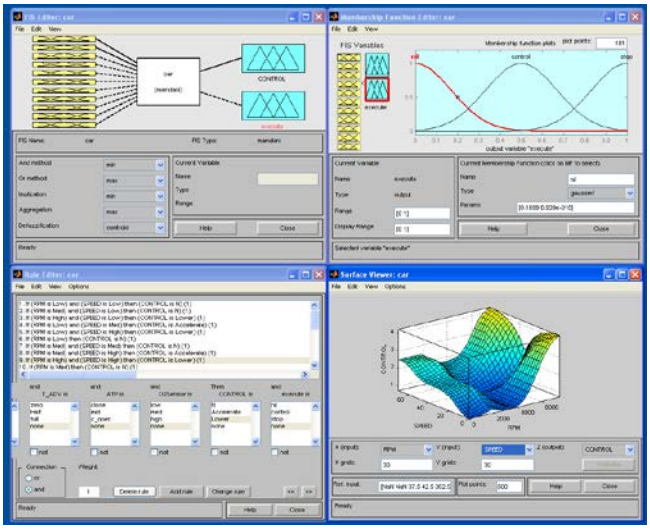

Fig.2 Fuzzy logic interface and surface view.

Fig.2 shows the results of fuzzification of the input parameters in MATLAB[8] and the surface diagram for the same. The defuzzified results are in the output parameters which are control and Execute. The program is capable of reading the specific file which has the stored data in the offline mode. The tests were conducted within the range starting at 20mph speed to 80mph speed and the readings of all parameters that changed or showed a warning signal as mentioned earlier were noted graphically. To test the efficiency of the warning function, the vehicle was accelerated to speeds of 80mph for a small interval of time. The function, as desired showed warning signals triggered on the graphic screen of dewesoft, as well as a written prompt shown on the Fuzzy logic screen. The factor which prompts the use of logic rules integrated with the acquired data from dewesoft is the view interface which is not an added feature in dewesoft. This again justifies the use of Matlab.

The Fuzzy logic rules that were assigned on MATLAB are shown in Fig.3 Here all the input parameters assigned are shown in the form of yellow columns and the defuzzified result is shown with a blue marking intend at the right corner of the Figure. The Red colored indent is the display parameter which shows output respectively. Thus the offline data processing using dewesoft (independently), and matlab integrated data processing was achieved.

Fig.3 Fuzzy logic rules with limits and output.

Therefore the experiment has so far proven success in capturing the offline data and processing it. Further as mentioned is the Third and final stage of the experiment which is designed to import the exported data live into matlab and perform the tests on the hybrid vehicle at various speed and load conditions. Apart from this, the test has been carried out on different models like the sports utility hybrid vehicle FORD ESCAPE Hybrid, and also the Toyota HIGHLANDER hybrid respectively. For the same set of rules mentioned earlier, and on the same test conditions.

4. Processing Online Data

In the third stage of the experiment, as data keeps flowing in to the dewetron data analyzer, it is simultaneously exported to matlab. This data is then linked to the matlab program as a live streaming file. This is then delivered to the set of fuzzy logic rules assigned to each input parameter. All this is very similar to the work done in previous stages, but for data being readily captured from the OBD2 port of the hybrid vehicle to the CAN port of the data analyzer and exported to Matlab. During this test phase the same set of experimental runs are conducted on the vehicle starting from a running speed of 20Mph to 70 Mph. This covers the vehicle starting from the parking space to driving in the street conditions, and then entering the highway. This is done to successively increase the speed of the vehicle. The vehicle was intensely tested on the highway where the merging speed was 45mph and the minimum speed was 55Mph. the maximum limit allowed on highway conditions is 70Mph.Here when the vehicle is subjected to sudden acceleration to take the required speed from 55Mph to 70Mph hard acceleration is required and in this speed the hybrid vehicle is designed to operate in dual mode, where in the electric motor powered by the battery provides extra torsion force to the wheels along with the torsion force of the engine. When the live data is captured, the rules assigned here would assist the system to adapt the throttle level to lower itself according to the assigned rules.[7]. Fig.5 shows the online data that is flowing along with the rules assigned to reduce the engine effort for propelling the vehicle with respect to various driver behaviors. These include normal low and hard acceleration patterns.

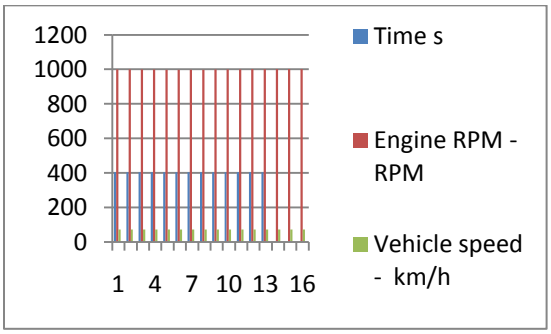

Fig.4. Eng rpm, and speed for 15sec runtime

Fig.4. shows the first 400 sec run time of the vehicle where in after implication of fuzzy rules, the rpm v/s speed was non fluctuation. This is in the simulated mode where the fuzzy rule would automatically adjust the RPM if the driver over accelerates the vehicle. [2] In the case of over acceleration, more fuel flow to the engine is obvious. Reducing the same is the prime motive.

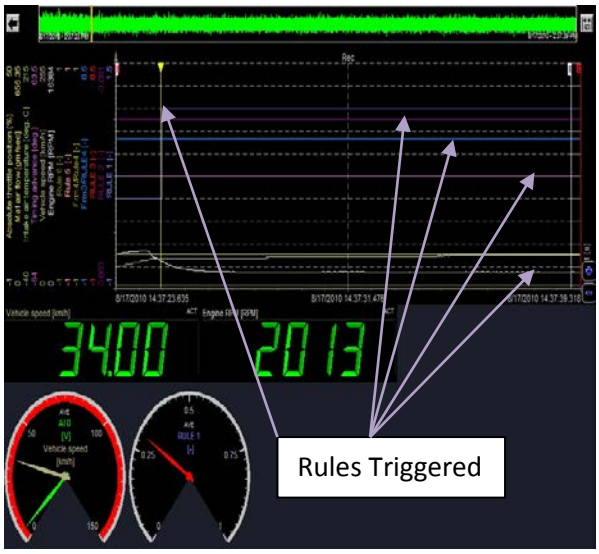

Fig.5 Online Data processed with rules triggered

Along with implying formulae and rules for the Engine, for calculating values on both offline as well as online modes, formulae to calculate the torque of the electric motor was used in order to balance the control strategy on motor and battery current operated propulsion side, as well as the engine propelled side respectively. The torque of the electric motor is calculated by using the relation [6]

$$\tau=(5252*HP)/N \qquad (8)$$

Where τ = torque, 5252 is a numerical constant, HP = power of the motor in Horsepower, N= revolutions per minute of the motor. Also the torque is calculated using another relation [6]

$$\tau=(120*F)/P \qquad (9)$$

Where τ = torque, F = supply frequency in cycles/sec, P = number of motor winding poles. Different formulas are used because some manufacturers will have different data output, and using different formulae eliminates the factor of error in calculations.

5. Result and Discussion

The experimental setup was also simulated using LABVIEW software where manually adjustable parameters were set to simulate the real time situation of passengers occupying the vehicle. This was done to view the change in load conditions and study the effect of increased load over performance of the vehicle under various road conditions and speeds respectively. Variables were also assigned on the LABVIEW deck to validate the driver behavior inputs like over acceleration, under acceleration, hard braking, and reverse motion. Boolean function was used to indicate the error if shown in the simulation mode. Fig.6. shows the screenshot in LabView, where in all controls and variables were assigned to simulate the situation. The Dials shown in the deck are similar to those in the real automobile.[3] Additional dials are assigned to monitor the motor torque and load conditions which are not available as standard equipments in the instrument panel of vehicles.

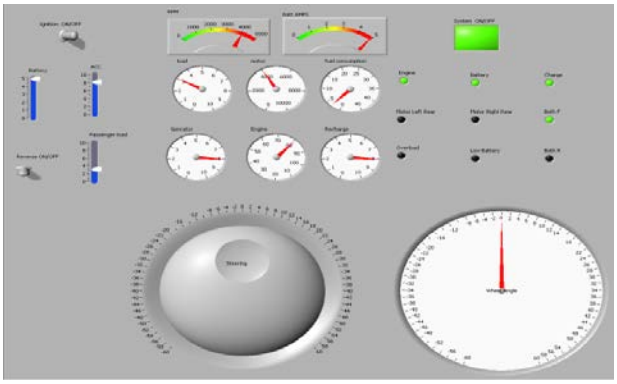

Fig.6 Lab view screenshot.

Fig.7.shows the DEWESOFT deck where in at time intervals the rules implemented on the online data takes place and the graphical output display is obtained. Here the experimental test run on FORD ESCAPE HYBRID is recorded for various runs starting from 20mph and successively increasing the speed in 10 MPH increments. The maximum speed travelled was 75mph on the FORD vehicle.

It is not a safe practice even for the purpose of testing to accelerate the hybrid vehicle above the speed limits because it may cause unwanted damage to the motor control[7]. and propulsion system. Hence the 75mph was maintained as the peak limit of acceleration during the entire range of experiments conducted on each class of vehicle respectively.

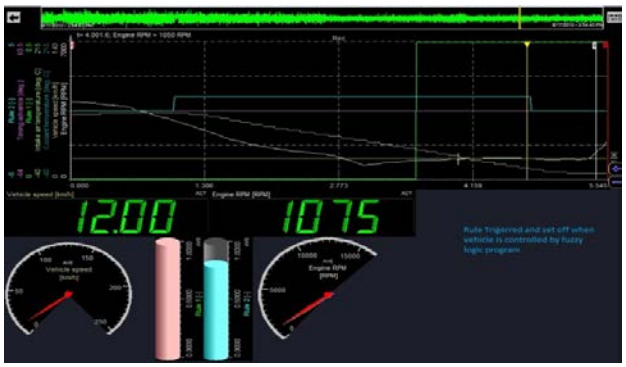

Fig.7. Fuzzy rules implemented on live data obtained from Ford Escape.

Fig.8.shows the same experiment with same set of procedures and same set of logic rules applied for the Toyota Prius [5] which belongs to the Economy segment. Here the blue lines depict the error trigger and the red is the automatic correction in the simulation mode. This is further for communication with the driver to have a check on his mode of operation as well as to auto correct the system to stabilize the values obtained.

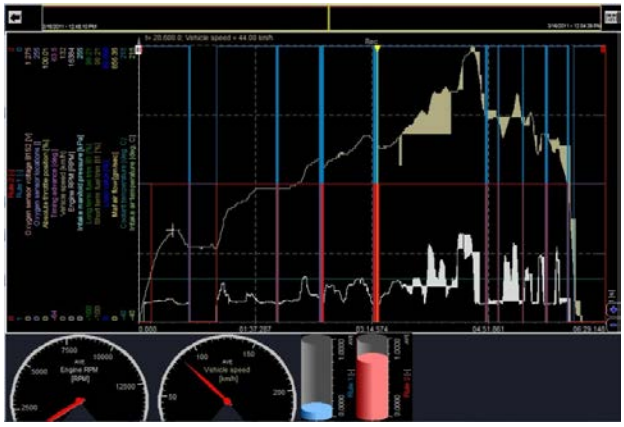

Fig.8. Trigger and correction graphs for Toyota Prius.

In the final step of the research conducted the same set of procedures were repeated on the Toyota HIGHLANDER. The results obtained after the tests on SUV's and Economy size cars of different manufacturers are discussed in detail in the following section.

Fig.9.shows the Trigger mode and correction graphs which are for the rests conducted on the Toyota Highlander. Being a mid size SUV [4] in it s segment, the Toyota Highlander hybrid has potentially lesser use of battery propulsion and the motor has lesser torque output compared to the small segment and the ford segment of vehicles. This is done by the manufacturers, for keeping the vehicle performance curves to the maximum. Yet use

of the electric motor propulsion system in the HIGHLANDER does help in reducing the fuel consumption especially during the cruise mode where the operation is carried out on a large scale in the dual operating mode which lowers the propulsion load to the engine.

Fig.9. Trigger and correction graphs for Toyota Highlander.

Here the white lines represent use of engine propulsion. It is visible that at lower instances in comparison to the Prius, and Ford escape, the engine has to take command of propelling the vehicle.[5]. The blue lines are trigger for the system to identify over acceleration, and the green trigger lines depict the control. Control is triggered during the beginning and at the end of the test run of the vehicle respectively. The yellow and pink bars are excitation current triggers that are shown when the vehicle is overloaded and the LED display at the bottom of the screen shows a warning of damage to the system if operated above these rule ranges. This is done to provide a feedback to the operator and caution the control system simultaneously. The response time of the vehicle in simulated mode with rules applied, is much larger when compared to the normal operation. Thus it justifies the use of fuzzy logic rules in the governing of fuel economy, and energy conservation.

Table.1. shows the fuel consumption in percentage of the three test vehicles at various speeds.TP represents Toyota Prius, HL represents Toyota highlander, and, FE represents Ford Escape respectively. The fuel consumption at various speeds ranging from 20 to 70mph is recorded.

TABLE.1. FUEL CONSUMPTION OF TEST MODELS WITHOUT RULES IMPLEMENTED

S.no	Speed.Mph	RpM	TP	HL	FE
1	20	000	0.0	0.0	0.0
2	25	000	0.0	0.05	0.02
3	30	000	0.0	0.05	0.02
4	40	1500	0.15	0.25	0.30
5	45	2500	0.30	0.42	0.36
6	50	2650	0.32	0.47	0.41
7	55	2800	0.56	0.56	0.48
8	60	2000	0.28	0.36	0.32
9	70	1200	0.13	0.23	0.20

Fig.10. shows the plot of Horse power, torque and Bmep at various RPM of engine during the test where in the rules were not triggered.

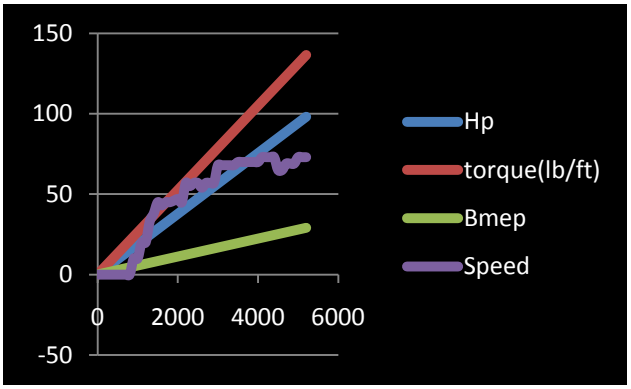

Fig.10. Hp, torque, and bmep at various speeds without rules triggered

Fig.11.Shows the plot where the rules were triggered and the data was recorded. There is a significant drop in theRpm, torque, bmep ,and hp which are key contributors in determining the performance. The figures are the summed values of data that was obtained from the three test vehicles respectively. The plot values in the triggered mode are obtained in the simulated version of data, which was acquired from dewetron data analyzer, and exported to matlab, where the IF-Then conditional rules were implemented.

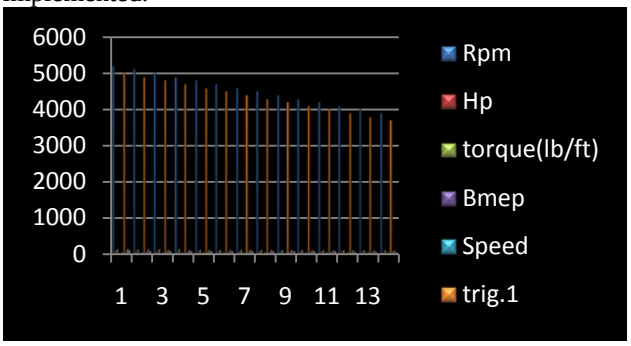

Fig.11. Hp, torque, and bmep at various speeds with rules triggered

7. Acknowledgement

The authors are very grateful to Ms.Maureen Kelley, service advisor, and, Mr. John Monteleone, General manager, Victory Honda, MI, Mr. Scott Schindler,Victory Toyota, MI, Mr.Dean Short, Tom Holzer Ford, and Mr. Matt Baker, support tech, Dewetron,for all their support.

8. Conclusion

By using the data acquisition system and implementing the Fuzzy rules the vehicle performance can be analyzed. The battery propulsion time can be maximized. Small segment vehicles have lesser errors triggered when compared to the SUV range of vehicles. The load value plays a very vital role in determining the take over time for engine in propelling the vehicle. Simulated results show when compared to the standard mode of operation of hybrid vehicles under various driver and load conditions are discussed. The data can be processed as and when it is acquired and corrective rules can be applied for simulation instantaneously. The work carried out here is in a simulated mode, which limits direct communication with the ECU of the vehicle. Further work can be done to enhance the performance of Hybrid electric vehicle. Further work is being done to develop electronic chips for controllers of Hybrid electric vehicles.

9 . References

[1] Gautham Thyagarajan, Opinder Sharma, Paramjit Kaur: "Use of Fuzzy Logic in Hybrid Vehicles for Improving the Fuel Efficiency by Individual Component Control", MSV 2010: pp337-341Jun 2010

[2]Milton Martinez: "Fuzzy Logic Controller for Two mode Parallel Hybrid Electric Vehicle", http://faculty.utep.edu/Portals/1255/Milton.pdf

[3]Fazal U Syed, Dimitar Filev, Hao Ying, "Adaptive Real-Time Advisory System for Fuel Economy Improvement in a Hybrid Electric Vehicle", The 28th North American Fuzzy Information Processing Society Annual Conference (NAFIPS2009), pp 1-7, June 2009

[4]Fazal Syed, John Czubay, "Improving the Efficiency of Production Level Algorithm Development for an SUV HEV Powertrain," SAE 2004 , Power train and Fluid Systems Conference and Exhibition, paper no 2004-01-3039, Oct 2004.

[5] Toyota Prius, & Highlander service manual

[6] John.Bird Mechanical Engineering principles pp109-116,Oxford 2002
http://www.engineeringtoolbox.com/electrical-motors-hp-torque-rpm-d_1503.html

[7] *DEWESoft* 7.0 data acquisition, processing, analyzing and storage software tutorial.

[8]http://www.mathworks.com/help/pdf_doc/fuzzy/fuzzy.pdf

Mathematical Modeling of Automatic Voltage Regulators and Power System Stabilizers for a Hydroelectric Generating Unit of CFE-México

G. Villa-Carapia[1], O. Mora-Hoppe[1], F. Sánchez-Tello[1], G. Carreón-Navarro[1], R. García-Kasusky[1], A. Guzmán-Terrones[1], and E. Espinosa-Juárez[2]
[1]National Energy Control Center, Comisión Federal de Electricidad, México, México
[2]Electrical Engineering Faculty, Universidad Michoacana de San Nicolás de Hidalgo
Morelia, Michoacán, México

Abstract - *On July 31, 2008, undamped power oscillations of low frequency were registered in the Mexican National Electric System in which the 600 MW Hydroelectric Generating Station "El Caracol" oscillates in respect to the national network. The event was recorded by phasor measurement units making possible the identification of an unstable electromechanical mode and the dominant modes of the oscillation. From the developed analysis, an unstable electromechanical mode was found which is associated whit the generating units of "El Caracol".*
In this paper, the performance tests of Excitation Systems and Power System Stabilizers of the "El Caracol" generating units are presented, as well as the developed analysis for mathematical modeling and validation of these control systems.

Keywords: mathematical modeling, excitation systems, power system stabilizers, automatic voltage restorers.

1 Introduction

The analysis of power systems and operating and planning decisions are mainly based on the results of studies and simulations carried out by using mathematical models of electronic devices and electrical components in the electrical system. Therefore, modeling and validating the components of the analyzed system properly is of the greatest interest in order to have confidence in the obtained results [I].

Damping problems in power systems are generally associated with the interaction of the control system of generating units, the power demand condition and the electrical network topology. In modern interconnected power systems, the power system stabilizer (PSS) is widely utilized to damp low frequency power oscillations [2][3].

In this paper, the main interest is in the Automatic Voltage Regulators (AVR) of the generating units and in the PSS, which mathematical models representing properly their performance and their corresponding validation by means of field testing and computer simulations constitute a fundamental part in determining the factors of greatest impact on the damping problem and its solution [2][4].

The events reproduction and the solution of the oscillations problems in power systems is difficult because of the high level of modeling required for such studies, due to the detail needed to represent each generator and its control systems, which requires considerable work in identification, mathematical modeling, validation and testing of control systems of the generating units. In most cases field tests must be conducted, which implies the need for highly trained human capital, test equipment and the availability of generating units.

In this paper the methodology for modeling and validating a real AVR and PSS installed in the Hydroelectric Generating Units (HGU) "El Caracol" of the Federal Electricity Commission (CFE) is presented. This is a 600 MW generating station which is part of the Mexican National Electric Power System.

The particular interest in obtaining an appropriate representation of the AVR and PSS that allows a detailed analysis exists because the "El Caracol" generating station has contributed whit the greater participation in the undamped low frequency power oscillations, recorded on July 31, 2008, in the Mexican National Electric Power System. The focus for the solution of the oscillations problem was directed toward adjustments of the PSS of this generating unit.

2 Methodology for the mathematical modeling of the AVR and PSS

In order to obtain a model for the AVR and PSS control devices of the mentioned generating unit, the next procedure is carried out:

1) To check the AVR, PSS and generators parameters.
2) To verify in field data of manufacturer and adjust of the control system.
3) To test the performance of the AVR and PSS.
4) To develop and to validate the mathematical models.
5) To constitute a data base about the dynamic performance.

For constructing a data base which properly describes the dynamic performance of the power system, each of the sources of damping in the system must be represented, such as excitation systems, PSS and speed governor. Thus, the load characteristics that will allow the model to truly represent the system can be found.

It is important to mention that, under the coordination of the Operation Management of the National Energy Control Centre (CENACE) of CFE, a group of engineers was formed to analyze and to solve the undamped oscillations of power recorded on July 31, 2008. The analysis group included the CFE specialists of the sub-management of CENACE, the Specialized Engineering Unit, sub-management of Programming, Generation and Transmission, and The Equipment and Materials Test Laboratory.

3 Performance test of the excitation systems and Power System Stabilizers

The main objective of testing the control systems of the HGU "El Caracol" is to verify and to validate the electrical parameters of their excitation systems and PSS through controlled testing by applying voltage steps and steps of positive and reactive power, with and without the PSS [5][6].

The parameters of the excitation system to verify are the time constant of the transducer (TR), the gain in transitory state and the time constants of the advance-delay networks.

The parameters of the power system stabilizer to verify are the gain of the power loop and constants of delay time.

3.1 No-load tests for dynamic regime

No-load tests are carried out to evaluate the performance of the excitation control system with typical test signal (voltage step) and verify that the characteristic response parameters meet the correspondent CFE norm in [4].

The characteristic parameters are response time, overpass time, stabilization time, damping constant, overpass and maximum and minimum limits of the excitation.

Tests are developed by modifying the AVR reference value in order to vary the generator voltage by 5%, 10% and 20% of its rated voltage.

3.2 Load tests for dynamic regime

Load tests are carried out to evaluate the performance of the excitation control system with typical test signal (voltage step) and verify that the characteristic response parameters meet the correspondent CFE norm in [7].

Load tests evaluate the damped characteristics and the response time of excitation control system when there are sudden changes of reactive power in the system [7].

Tests are developed by modifying the AVR reference value in order to vary the generator voltage, which is equivalent to an increase of reactive power (% of nominal MVAr).

4 Development of mathematical models for control systems and PSS

Because studies to solve the power oscillations of low frequency registered on July 31, 2008 will be developed in the DSATools digital simulator [8], mathematical models of control systems and the PSS for the HGS "El Caracol" are required in the format of this simulator.

4.1 Excitation system

The block diagram of AVR provided by the manufacturer of the HGU 'El Caracol" is shown in Fig. 1. The generating station consist on three generating units which have the same type of AVR.

The DSATools power system simulator has an available library of standard IEEE models for control systems; however, as can be observed in the block diagram of Fig. 1, this excitation system does not correspond to a standard model. Therefore, building a "user-defined model" is necessary; this is a particular model to adequately represent the dynamic behavior of the excitation system.

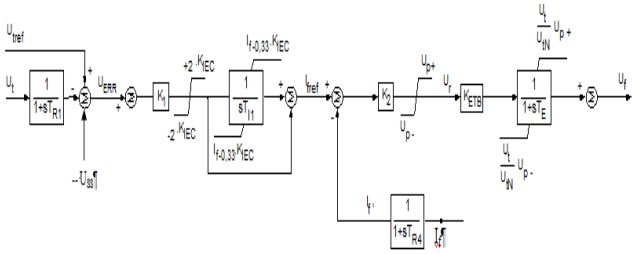

Fig. 1 Block diagram of the excitation system for the HGU "El Caracol"

In the AVR scheme a proportional-integral (PI) type controller with variable limits is observed (see Fig 1). To develop the mathematical model using DSATools a block of dynamic limits and an artifice to represent the proportional action of the controller must be created.

A series of analyses were carried out with the information provided by the manufacturer (block diagram and description of variables, short circuit and saturation curves, firing angles of the thyristors converter, etc.) for calculating the parameters values of the mathematical model describing the dynamic behavior of AVR [2].

Fig. 2 shows the block diagram in DSATools format of the mathematical model developed for studies of AVR in the time domain. Fig. 3 shows the detailed block of the integrator with variable limits.

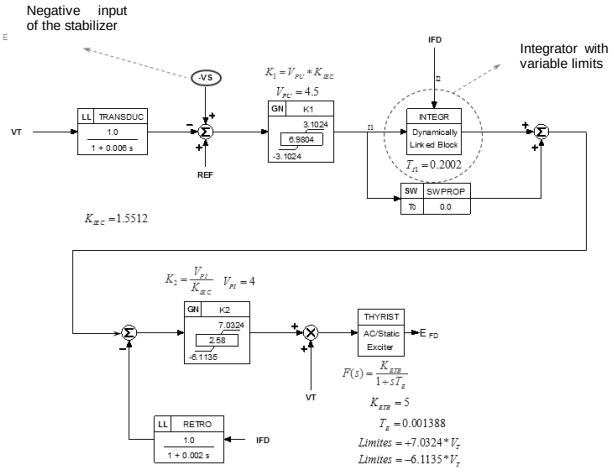

Fig. 2 Mathematical model of the excitation system for the HGU "El Caracol" in DSATools format

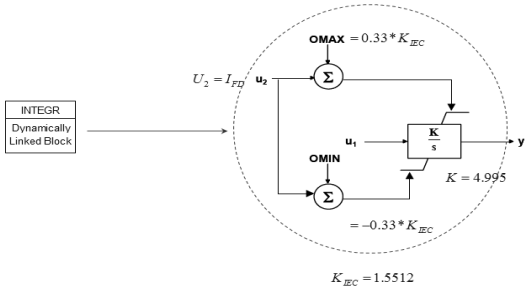

Fig. 3 Mathematical model of the integrator with variable limits in DSATools format

4.2 Power System Stabilizer

The block diagram of the PSS provided by the manufacturer of the HGU "El Caracol" is shown in Fig. 4. The PSS model is the same for all three units.

The diagram shown in Fig. 4 does not correspond to a standard model. Therefore, a "user-defined model" to adequately represent the dynamic behavior of the PSS must be constructed.

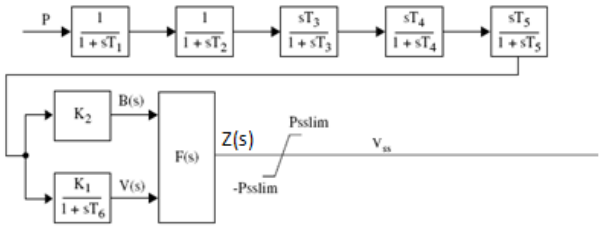

Fig. 4 Block diagram of the Power System Stabilizer

Fig. 5 shows the block diagram in DSATools format of the mathematical model developed for studies of the PSS in the time domain.

5 Validation of mathematical models

With the developed mathematical models of AVR and PSS, a dynamic database was created, and digital simulations were conducted of the tests of voltage steps at no-load and reactive steps, with two settings of the phase shift angle of the signal of stabilization (0 and 0.25 p.u., equivalent to 0º and 22.5 º, according to the model of the PSS) [6].

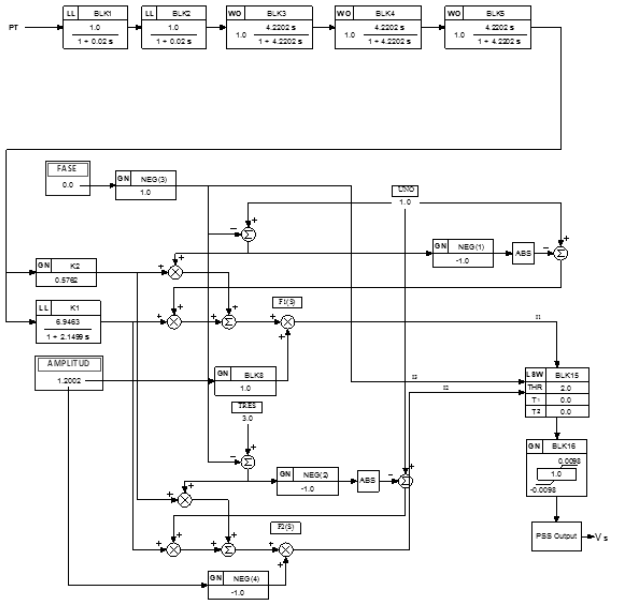

Fig. 5 Mathematical model of the PSS for "El Caracol" generating units in DSATools format.

The mathematical model validation is carried out by comparing computer simulations with the results of the performance tests. Since the AVR and PSS for the three "El Caracol" generating units are equal, in this paper only comparative results of one unit are shown, the HGU-U2 unit.

Before the testing of voltage steps at no-load, the machine must be carried at nominal voltage; values of field current and field voltage must be monitored, since these data will be considered as basic values referred to rotor, and will be required to standardize the signals of field voltage and field current from the numerical simulation, which will be compared with developed tests.

5.1 Tests of voltage step at no-load

This test consists of increasing by 10% the specified generator terminal voltage for the HGU-U2 (from 0.9 p.u. to 1 p.u.), when the generator is rotating at synchronous speed and is disconnected from the power system. For digital simulation, conditions of the test were considered, and a voltage step of 10% was applied in the reference signal of the mathematical model. Fig. 6 shows the HGU-U2 voltage at terminals obtained from the test and the results obtained by means of digital simulation.

As seen in Fig. 6 the results obtained by means of digital simulation are very close to those obtained from the applied test. Then, it can be concluded that the mathematical model adequately reproduced the performance of the excitation system.

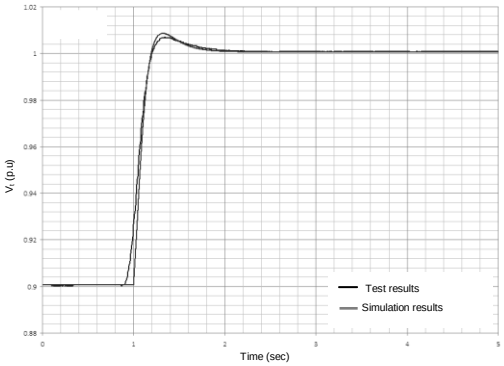

Fig. 6 Voltage at terminals of the HGU-U2 unit for the test of voltage step at no-load: test and simulation results

5.2 Tests of reactive step without PSS

For this test the generator must be connected to the power system and voltage regulator in automatic mode, with the PSS disabled.

For the digital reproduction of the test, an increase at terminal voltage of 0.0381 p.u. was considered, which is equivalent to an increase of 42 MVAr in reactive power.

In Fig. 7-Fig. 11test results and simulation results of active power, reactive power, voltage at terminals, field voltage and field current are shown.

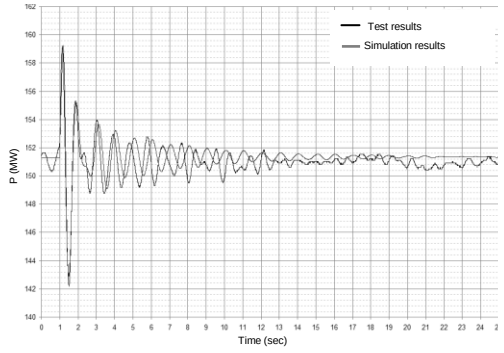

Fig. 7 Active power of the HGU-U2 unit for the test of reactive step without PSS: test and simulation results

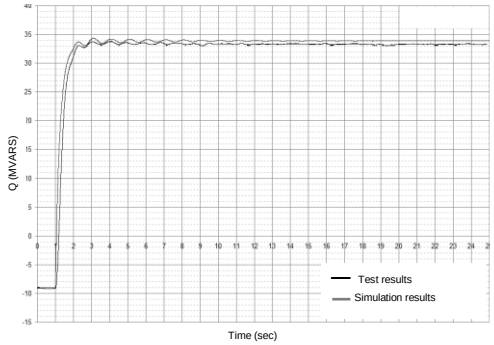

Fig. 8 Reactive power of the HGU-U2 unit for the test of reactive step without PSS: test and simulation results

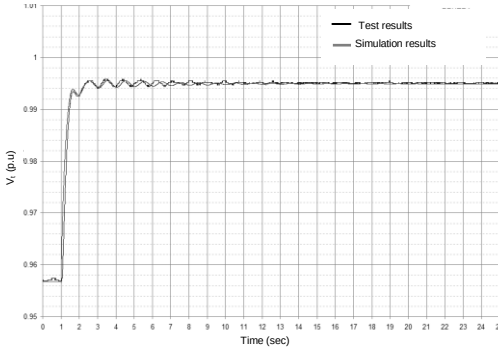

Fig. 9 Voltage at terminals of HGU-U2 unit for the test of reactive step without PSS: test and simulation results

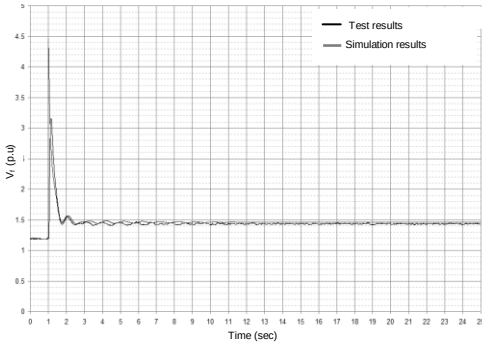

Fig. 10 Field voltage of the HGU-U2 unit for the test of reactive step without PSS: test and simulation results

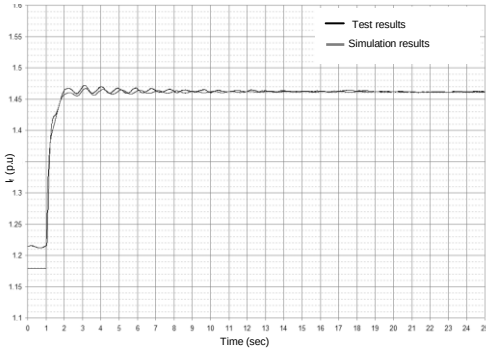

Fig. 11 Field current of the HGU-U2 unit for the test of reactive step without PSS: test and simulation results

PSS has no effect for this test, as this is developed with the PSS disabled. From the graphs in Fig. 7-Fig. 11 a good approximation of the monitored signals is observed; therefore, the mathematical model of the AVR is considered to successfully reproduce its dynamic performance.

5.3 Tests of reactive step with PSS and 0^o phase shift angle

In this test, the generator must be connected to the power system and voltage regulator in automatic mode with the PSS enabled. A 0° phase shift angle setting of the PSS stabilization signal and 1.2002 p.u. gain of this signal have been considered.

The AVR and PSS settings used for the simulation were obtained from the manufacturers information, which were verified in the field.

In the digital simulation for the reproduction of the test, an increase in the voltage at terminals of 0.0381 p.u. was considered, which is equivalent to an increase of 42 MVAr in reactive power. In Fig. 12-Fig. 16 active power, reactive power, voltage at terminals, field voltage and, field current are compared.

From the graphs in Fig. 12-Fig. 16 a good approximation in magnitude and phase of the shown signals can be observed. Thus the mathematical model of the PSS is validated; the developed model satisfactorily reproduces the dynamic performance of the PSS.

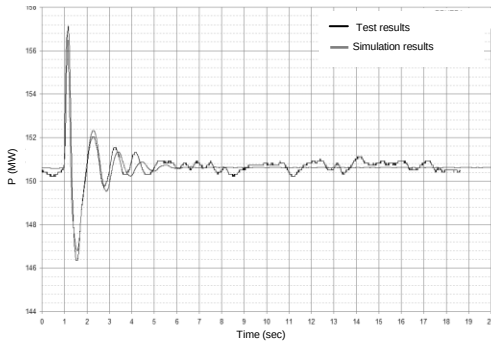

Fig. 12 Active power of the HGU-U2 unit for the test of reactive step with PSS: test and simulation results

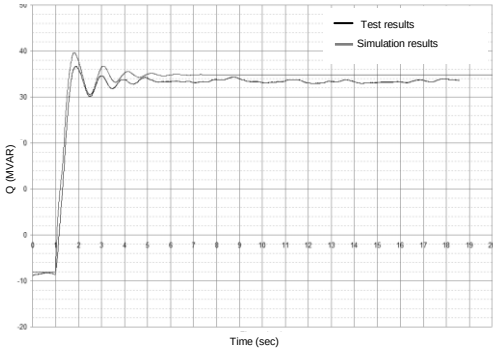

Fig. 13 Reactive power of the HGU-U2 unit for the test of reactive step with PSS: test and simulation results

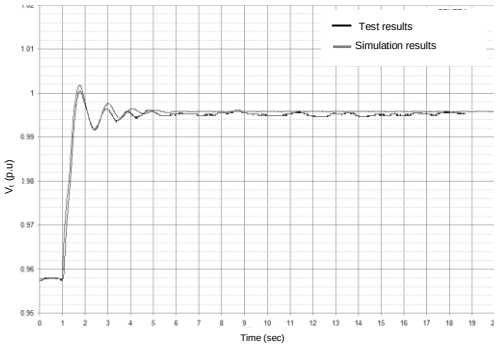

Fig. 14 Voltage at terminals of the HGU-U2 unit for the test of reactive step with PSS: test and simulation results

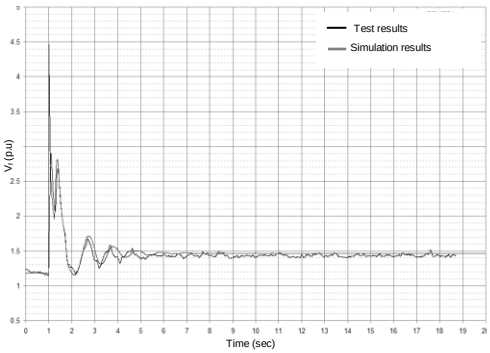

Fig. 15 Field voltage of the HGU-U2 unit for the test of reactive step with PSS: test and simulation results

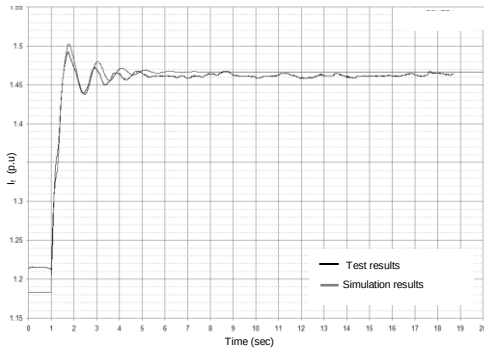

Fig. 16 Field current of the HGU-U2 unit for the test of reactive step with PSS: test and simulation results

6 Conclusions

In this paper the methodology for the mathematical modeling and validation of AVR and PSS for real generating units has been presented.

Mathematical models of AVR and PSS developed in the DSATools simulator permit to analyze the dynamic performance of these devices with an acceptable accuracy.

It is essential to have all the information provided by the manufacturer about the generators and their controls, otherwise, field tests must be performed for estimating parameters of generators and their control systems, in such a way that the identification and validation of math models to be successful.

Equally crucial is the highly qualified human capital to develop the identification, mathematical modeling, performance tests and validation of mathematical models to ensure success in solving problems of low frequency oscillations.

7 References

[1] E. Allen, D. Kosterev, P. Pourbeik, "Validation of power system models", IEEE Power and Energy Society General Meeting, 2010, Minneapolis, MN, USA.

[2] P. Kundur, "Power system stability and control", EPRI Power System Engineering Series, McGraw Hill, 1994.

[3] H. G. Far, H. Banakar, P. Li, C. Luo, B. T. Ooi, "Damping interarea oscillations by multiple modal selectivity method", IEEE Trans. Power Delivery, vol. 24, no. 2, pp. 766-775, May. 2009.

[4] A. Dysko, W. E. Leithead, J. O'Reilly, "Enhanced power system stability by coordinated PSS design", IEEE Trans. Power Systems, vol. 25, no. 1, pp. 413-422, Feb. 2010.

[5] IEEE 421.2-1990, "IEEE Guide for identification, testing and evaluation of dynamic performance of excitation control systems", 1990.

[6] IEEE 421.5-1992, "IEEE Recommended practice for excitation system models for power system stability studies", 1992.

[7] NMX-J-501-1994-ANCE, "Productos eléctricos-reguladores automáticos de tensión (RAT) para sistemas de excitación para generadores síncronos de centrales de generación. –especificaciones y métodos de prueba", 1994.

[8] Power Systems Technologies, Powertech, "Dynamic security assessment software", DSAToolsTM", 2008.

[9] R. T. Byerly, E. W. Kimbark, "Stability of large electric power systems", IEEE Press, 1974.

Biographies

Gustavo Villa-Carapia was born in Morelia, Mich. México. He received the Electrical Engineer degree from the Instituto Tecnológico Regional de Morelia, the M.Sc. degree in Electrical Engineering from the Instituto Tecnológico de Estudios Superiores de Monterrey, in 1979. From 1988 to 1989 he completed specialization studies in electrical engineering in General & Electric, Schenectady, N.Y. He was a university professor in the Instituto Tecnológico de San Luis Potosí from 1975 to 1978 and in the Universidad Panamericana in 1988. Since 1980 he is with the Comisión Federal de Electricidad, México. Currently, he is the Operation Manager of the National Electric System in México.

Olga Mora-Hoppe received the Industrial Engineer degree from the Instituto Tecnológico Regional de Pachuca in 1986. She studied for a M.Sc. in power systems in the Instituto Politécnico Nacional, México D.F., México (1991). Since 1994 she is with the Comisión Federal de Electricidad, México.

Fernando Sánchez-Tello received the Industrial Engineer degree from the Instituto Tecnológico Regional de Morelia in 1981. He studied a M.Sc. in power systems in the Universidad Autónoma de México (1986) and received the Ph. D. degree in Electrical Engineering from the Universidad Autónoma de Nuevo León, México, in 1997. Since 1982, he is with the Comisión Federal de Electricidad, México.

Gilberto Carreón-Navarro received the Industrial Engineer degree from the Instituto Politécnico Nacional, México (1979). He studied for a M.Sc. in power systems in the Instituto Politécnico Nacional (1982). Since 1983, he is with the Comisión Federal de Electricidad, México.

Elisa Espinosa-Juárez received the Electrical Engineer degree from the Universidad Michoacana de San Nicolás de Hidalgo (UMSNH), México, in 1986, the M.Sc. degree in Electrical Engineering from the Instituto Politécnico Nacional, México D.F., México, in 2001, and the Ph. D. degree in Electrical Engineering from the Universidad Politécnica de Madrid, Madrid, Spain, in 2006.

Currently, she is a university professor with the UMSNH, Morelia, México. Her research interests include power systems and power quality.

From M/G/1 and M/G/infinity to Simulation: Staged Service Performance Design

W. Mitchell
Computer Science, California State U., Sacramento, Sacramento, CA, USA

Abstract *- There are various techniques for dealing with server saturation. Under duress, some variation of admission control is usually applied, including possibly refusing (aka "throttling") all arrivals. As parallelism, threading, etc. become commonplace, alternative approaches to servicing heavy workloads are feasible. For a given stream of arriving requests, classical M/G/1 and M/G/infinity queuing models can establish initial estimates for both serial and parallelized service requirements. As analysis and design proceed, request streams that are not necessarily exponential are understood more fully. Verified simulation can subsequently translate queuing model predictions to more refined workload service allocations. Such staged modeling is also extendable to capacity planning for arbitrary service workloads.*

Keywords: queuing models, system performance evaluation, simulation

1 Introduction

Computer system capacity planning has survived the test of time as an essential (rather than optional) component of IT operations [5]. Significant analytical research along with pragmatic advances continues. However, as many studies have noted, systems are often analyzed and designed with insufficient consideration for the disruptive nature of service overloading. Until recently, the literature focused on a fixed single-server paradigm and various sophisticated ways to operate during heavy utilization. Some form of admission control was applied, by which some subset of service requests are simply dropped. And, when admission control failed to resolve server duress, the server is suspended (often referred to as "throttling") [4].

The service models proposed are based on the classical Kendall notation A/B/c/K/N for queuing models. Recall that A and B are the inter-arrival and service distributions, c is the number of (parallel identically distributed) servers, K is the system capacity (maximum number in the system), and N is the size of the request stream. Kendall system service is non-pre-emptive, whereby each service executes without interruption. Also, service queuing is FIFO, and there are no dependencies concerning order of requests. We use Kendall configurations M/G/1, M/G/c and M/G/infinity, where M stands for exponential distribution of arriving requests and G is an arbitrary service distribution with known mean and standard deviation. K and N are omitted when they are both unbounded (that is, infinite).

This paper is organized as follows. The first section shows that although delaying requests might be feasible in a network of interconnected services, it is not useful in a single service center. The second section considers queuing models for a single service center in which service is parallelized for dealing with heavy request rates. The third section maps these parallel queuing models to simulation models that can compare the merits of different service configurations. The fourth section outlines a probability-based cost estimate for dynamically allocated service threads. The concluding section summarizes the applicability of queuing and simulation staging from initial analysis through finalized service design.

1.1 RRQ – An Alternative to Admission Control in M/G/1

An This section describes an approach (referred to as "request re-queuing", abbreviate "RRQ") to heavy server utilization. RRQ is based on delaying arriving service requests (aka requests) for a distribution-specified amount of model time whenever the current service queue length exceeds a parameter value. Conceptually, this attempts to smooth out short timeframes having bursty requests compared with recent request rates. For example, exponentially-distributed arrivals having arrival rate λ, could experience small time windows having service queue length much larger than the steady-state (abbreviate SS) average queue length. Rather than dropping arriving requests, as with admission control, some arrivals are delayed. Specifically, a queue length threshold called qlen is specified such that whenever the service queue length exceeds qlen, each arriving request is delayed. The delay time is specified by a distribution that has the effect of advancing some of the current arrivals to a time t_f in the near future. Assuming request bursts are relatively short duration, server utilization U_{tf} at time t_f is hopefully less than current utilization U.

A discrete-event simulation, called M_RRQ implements the above RRQ rationale. M_RRQ results such as Figure 1 show that 1) SS request average response times and 2) SS average service queue lengths increase by 20-25% even for quite low qlen values (such as 2, 5, and 10) relative to average queue length. Note that the legend for Figure 1 defines the labels for the columns of Figures 1-3 inclusive. Figure 2 shows that the general conclusions drawn from Figure 1 also apply to many other arrival and service distributions.

Figure 1 – An M_RRQ model run group, 3 replications per row.
Figure 1 Legend – ia,λ: inter-arrival distribution, and mean = $1/\lambda$; svce,μ: service distribution, and rate (uniform with mean = $1/\mu$; qlen: qlen value for all replications; ρ: server utilization; msql: max service queue length during run; mrd: maximum number of requests in service enqueue delay state during run; reqtot: total number of arrivals during the run; totreqd: total number

of request delayed during run; rm,rsd: mean response time and response time standard deviation; dm, dsd: mean enqueue delay and enqueue delay standard deviation; run_el: elapsed model run time (clock ticks) ;
table column headers are bold, and split tables/boxes have italic header lines

ia, λ	*svce, μ*	*qlen*	*ρ*	*msql*	*mrd*	*reqtot*
exp,5	unif(2.5,2)	2	0.499	8	12	10**6
exp,5	unif(2.5,2)	5	0.499	9	10	10**6
exp,5	unif(2.5,2)	10	0.499	11	5	10**6

totreqd	*rm, rsd*	*dm, dsd*	*run_el*
43150	4.820,6.713	3.636,2.009	5002405
1477	4.029,2.853	3.988,2.568	5005138
9	4.014,2.654	4.014,2.652	5005291

Figure 2 – M_RRQ model run groups ranging over moderate server utilizations

ia, λ	*svce, μ*	*qlen*	*ρ*	*msql*	*mrd*
exp,5	unif(4,2)	2	0.799	28	17
exp,5	unif(4,2)	5	0.799	30	16
exp,5	unif(4,2)	10	0.799	29	14
exp,5	unif(3.5,2)	2	0.7	16	16
exp,5	unif(3.5,2)	5	0.7	13	13
exp,5	unif(3.5,2)	10	0.7	14	9
exp,5	unif(2.5,2)	2	0.499	8	12
exp,5	unif(2.5,2)	5	0.499	9	10
exp,5	unif(2.5,2)	10	0.499	11	5
ia, λ	svce, μ	qlen	ρ	msql	mrd
exp,5	unif(4.5,2.25)	2	0.9	47	19

reqtot	*totreqd*	*rm, rsd*	*dm, dsd*	*run_el*
10**6	236729	14.854,15.925	8.352,4.909	5008509
10**6	60049	12.688,11.754	11.040,6.967	500xxxx
10**6	8668	12.630,10.473	12.389,9.330	5004821
10**6	129979	9.693,11.553	6.118,3.044	5001831
10**6	16186	8.016,6.632	7.570,4.783	5000357
10**6	802	7.972,5.847	7.950,5.698	5000439
10**6	43150	4.820,6.713	3.636,2.009	5002405
10**6	1477	4.029,2.853	3.988,2.568	5005138
10**6	9	4.014,2.654	4.014,2.652	5005291
reqtot	totreqd	rm, rsd	dm, dsd	run_el
10**6	475027	29.164,27.270	16.109,15.87	5000922

1.2 M_RRQ – A discrete-event simulation model for RRQ

This section implements RRQ behavior by means of a discrete-event simulation called M_RRQ. Although RRQ is shown to be an unsuitable technique for dealing with single-point service saturation, we illustrate how M_RRQ results are validated against the SS results for an M/G/1 queuing model.

M_RRQ simulates RRQ behavior for various Kendall A parameter ranges. The simulator used is GPSS World, a dialect of the well-known GPSS discrete-event simulation language [3]. An M_RRQ execution/run has input parameters specifying request, service, and request delay distributions along with the qlen value. Run results include distributions for service, service queuing, re-queue delay, and request response times. In discrete-event simulators, events occur at discrete instants of model time. The model clock tick or time unit is an abstract value. Simulation values such as the inter-arrival distribution mean □=5 are based on the abstract clock tick. The clock tick value for a given simulation is interpreted by the simulation model developer. A clock tick value 1 millisecond might be suitable for simulating packet processing in a network simulation, as most actions involve timing in this scale. GPSS also represents fractions of a clock tick as appropriate.

Each arriving request r either has its service enqueued or not, depending on the current model state and the model input parameter qlen. Whether delayed (exactly once) or not, r is enqueued to the FIFO service queue. The model response time for r is (enqueue delay duration, else 0) + (service queue duration) + (service duration). For simplicity, we are not modeling enqueue/dequeue, service startup and other such processing.

1.3 M_RRQ model verification

In this section, selected M_RRQ results are shown to agree with SS statistics for the Kendall M/G/1 model. Each row of Figures 1-3 represents results averaged over a "replication" of 3 model runs. The only model input differences per replication run are the seeds for simulation random number streams, and each set of 3 replications differs only in qlen value. A qlen maximum models the case where no arriving requests delay their service enqueue, whereas a qlen minimum value models the largest percentage of arrivals that delay their service enqueue. Collectively, Figure 1 runs indicate model results for moderate server utilization of 50%. Aggressive arrival delay rate (qlen=2) does not strongly affect the maximum server queue length or the average residence duration of requests. Figure 2 indicates that total model run elapsed time (run_el) is essentially constant within each run group, and across run groups, and does not depend significantly on the distributions involved. By contrast, Figure 3 shows high utilization and its excessive response time.

Figure 3 – An M_RRQ model run for high utilization ($\rho = 0.9$)

ia, λ	*svce, μ*	*qlen*	*msql*	*mrd*	*reqtot*	*totreqd*
exp,5	unif(4.5,2.25)	2	47	19	10**6	475027

rm, rsd	*dm, dsd*	*run_el*
29.164,27.270	16.109,15.874	5000922

Kendall models M/M/1 and M/G/1 have SS formulas for server utilization, average number of resident requests, etc. By definition, model verification is established when a queuing model's SS results agree with corresponding simulation model results. The M_RRQ model that generated the data in Figures 1 to 3 simulated M/G/1. SS average residence time (time between arrival into the system and service completion) in M/G/1 is $w = (1/\mu) + \lambda * ((1/\mu)^2 + \sigma^2) / (2 * (1-\rho))$
where λ and μ are the request inter-arrival and service duration means respectively, $\rho = \lambda/\mu$ is the server utilization, and σ^2 is the square of the standard deviation of

service durations. For $\lambda = 1/5$, $\mu = 1/2.5$, server utilization ρ is thus 0.5. σ^2 was specified in the service distribution as $(1.44)^2 = (b-a)^2/12$, where b=5 and a=0 in the expression for σ^2. Then, the expression for w is 4.166. The simulator M_RRQ gives average(w) = 4.164 (the AVE.TIME value) in Figure 4. This result closely agrees with the corresponding queuing theory SS formula, validating that aspect of M_RRQ.

Figure 4 – Simulation results for M_RRQ validation (ρ = 0.5, μ = 1/2.5; 1 million requests)

QUEUE	*MAX*	*CONT.*	*ENTRY*	*ENTRY(0)*	*AVE.CONT.*	*AVE.TIME*	*AVE.(-0)*	*RETRY*
Q_SVR	14	1	1000001	0	0.833	4.164	4.164	0

Finally, it is instructive to understand M_RRQ model's inability to reduce single-server utilization during local demand peaks. Exponentially distributed requests occasionally exhibit bursts of arrivals in short time periods relative to inter-arrival mean $1/\lambda$. For $\rho = \lambda/\mu$ in M/G/1, we see that temporarily reducing λ would also temporarily reduce ρ. Therefore, the average enqueue delay should be $n*(1/\lambda)$ time units, for some modest-sized integer n such as 10 or greater. However, when the (once-only) delayed requests are enqueued for service, they generate their own increase in the current value of ρ. Figure 5 illustrates a more active than normal section of a queue length graph. Intuitively, the smoothing attempts from delayed enqueue do not involve large enough request rate changes per time unit.

Figure 5 – Exponential and uniform inter-arrival and service distributions: (queue length) vs. time

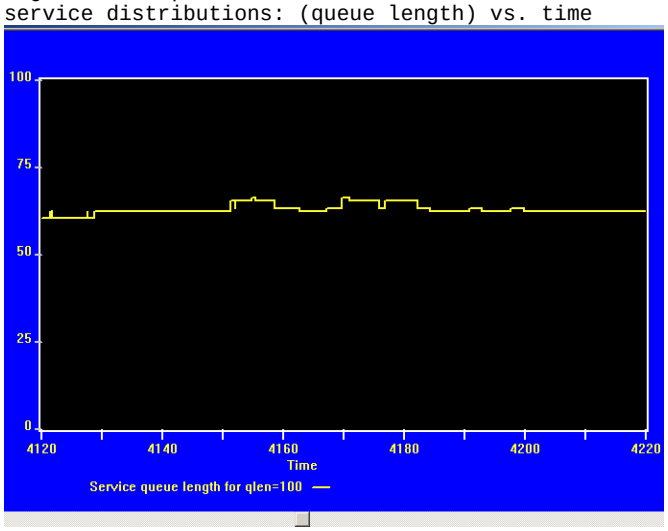

It should be noted that techniques such as "Adaptive Overload Control (AOC)" can successfully deal with request saturation of Internet traffic [6]. AOC is basically a variation of our delayed enqueuing. However, AOC is applied in a network of service centers by simply delaying slightly the service enqueue at various service points. Such delayed queuing is a distributed and controlled degradation that can be masked (hidden from the user) and statistically tolerable (from an operations viewpoint) for many kinds of network requests.

2 MG1c - M/G/1 for light load and (M/G/c + M/G/infinity) for heavy load

This section describes a service we refer to as MG1c that behaves like M/G/1 during light to moderate request loads. In addition, MG1c adds identical parallel service clones ("threads") to the M/G/1 component for heavy loads. The parallel component behaves almost always like M/G/c, but will be referred to as MGc since it is a variation of Kendall's M/G/c. Implementing MG1c could utilize the now commonplace multi-threading paradigm. The parallel component consists of 1) an M/G/c, the fixed thread pool, and 2) dynamically created and destroyed service clones for processing requests when there are more that (c+1) requests currently being served in parallel. As such, MG1c is an alternative to admission control that potentially reduces request dropping. When there are currently (c+1) busy servers, threads are dynamically created to process arriving requests. In practice, dynamic thread processing can be very costly and is, at best, a crude approximation to M/G/infinity.

2.1 Description of the model for MG1c service

The notation and simulation environment described in previous sections will also be used here. In the MG1c system, an arriving request enqueues for service whenever the M/G/1 component has current queue length less than parameter-specified value qlen; otherwise, when current queue length exceeds qlen, an arriving request r is queued with 50% probability to M/G/1 or to the MGc component Other service balancing algorithms are of course possible.

It is straightforward to simulate MG1c behavior by using a GPSS World model (refer to such a simulation as M_MG1c). M_MG1c models the MGc component as a Kendall M/G/c with a service queue. Fortunately, there are known SS approximation formulas for M/G/c, for fixed c >1 [1].

The MG1c processing for an arriving request r dynamically determines whether MG1c is and will remain a single-component M/G/1 service. When the qlen threshold is exceeded, r is queued with probability 0.5 to the M/G/1 and M/G/infinity components. This simple load balancer biases traffic to the M/G/1 component, in effect making it a "primary" server (referred to as svr1). Thus, the hybrid parallelized request processing (referred to as p_svr) is active during intense workload intervals. By default, the GPSS models p_svr as a variable number of servers, each allocated and de-allocated from the fixed pool size c, per service request. Note that the queue content for the M/G/c component is not explicitly serviced in MG1c by an M/G/infinity model. This is because we are confining our study in this paper to determining the distribution of such queued requests. In addition, MG1c does not model service-specific overhead

associated with processing such as service startup, service finish, and service queue dispatch.

2.2 Section Analytics of MG1c during peaks in arrival request rate

System saturation for a single server consists of a time interval with $\lambda >= \mu$. This is an unstable operating scenario. We now generalize our earlier 50/50 load-balancing method as follows. M/G/1 component arrivals are limited to rate $\lambda 1$ (using a qlen setting) so that utilization never exceeds a prescribed level. The p_svr component sees "effective" arrival rate = $(\lambda - \lambda 1)$. Since p_svr behaves almost always like M/G/c, the SS expression for the number of requests in p_svr (often denoted as "L" in the literature) can be derived from the approximation formula for P_0 = the probability that there are no requests currently in p_svr1. Recall that in M/M/c, P_0 is given by

$$1 \; / \; \{ \; \Sigma_{0 \text{ to } (c-1)} \; ((c\rho)^j/j!) \; + \; [(c\rho)^c \; (1/c!) \; (1/(1-\rho)) \;] \; \} \qquad (1)$$

where $\rho = \lambda/c\mu$ is the p_svr component utilization, λ, the effective arrival rate, is a simplified re-representation of the above effective arrival rate, and μ is the service rate. It is also known that the probability that there are at least c requests currently in p_svr can be approximated by

$$(c\rho)^c \; P_0/(c!(1-\rho)). \qquad (2)$$

3 M_MG1c – Simulation alternatives or for queuing models

This section describes two different simulation models for the queuing models of the previous section. Simulations contribute another representation layer useful for service performance modeling [2]. One example of system saturation is simulated in M_MG1c by setting qlen = 0 and setting $\lambda = \mu$. A range of scenarios is summarized in Figure 6.

Figure 6 – M_MG1c simulator runs for qlen range and arrival intensity, per qlen; 1 million requests processed, per run

Inter-arrival distr & mean	*Service distr & mean*	*ρ svr1*	*avg(Response) mean & std*
exp,5	unif(4,3)	0.703	6.496,3.434
exp,5	unif(4.5,3.375)	0.758	7.532,3.969
exp,5	unif(4.75,3.56)	0.783	8.041,4.232
R1 exp,5	unif(4.9,3.675)	0.796	8.356,4.399
exp,5	unif(4,3)	0.774	9.85,6.15
exp,5	unif(4.5,3.375)	0.848	12.781,7.677
exp,5	unif(4.75,3.56)	0.878	14.277,8.370
exp,5	unif(4.9,3.675)	0.893	15.151,8.785
exp,5	unif(4,3)	0.796	12.531,9.289
exp,5	unif(4.5,3.375)	0.884	19.407,13.158
exp,5	unif(4.75,3.56)	0.919	23.568,14.902
exp,5	unif(4.9,3.675)	0.937	26.359,15.880
R2 tria(0,1,9,6)	unif(4.9,3.675)	0.917	8.521,4.133

Number of p_svr used	*qlen*	*Number of requests that used p_svr*
7	2	121149
7	2	157684
7	2	176723
8	2	188324
4	5	290
7	5	59026
7	5	77654
7	5	90223
6	10	4266
7	10	18827
7	10	33379
7	10	44887
4	2	64025

In this version of M_MG1c, p_svr is simulated as M/G/infinity. First, under increasing values of ρ, svr1 utilization, ρ_{svr1}, lies between 70% and 93%, and the maximum number of parallel requests serviced does not exceed 10. This has the practical implication that our abstract thread pool is utilized to a modest extent. Second, Figures 7 and 8 depict p_svr during saturation. The value for AVE.C in Figure 7 validates the average number of requests being

Figure 7 – Steady-state p_svr statistics during saturated MG1c operation; 1 million requests processed

STORAGE	*CAP.*	*REM.*	*MIN.*	*MAX*	
ENTRIES	*AVL.*	*AVE.C.*	*UTIL.*	*RETRY*	*DELAY*
P_SVR	1000	999	0	8	
499545	1	0.499	0.000	0	0

Figure 8 – MG1c saturated operation: 1) Distribution of number of p_svr servers used (Chart P_SVR_NUM_USED), and 2) Request residence time (Chart W_HISTO)

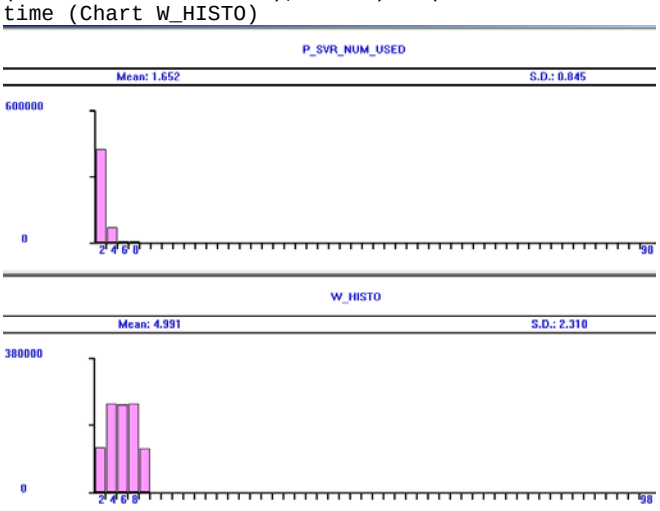

processed in p_svr (that is, L = λ/μ) as 0.5. Figure 8 histogram W_HISTO charts service duration distribution. In M/G/infinity, the SS average w value is $(1/\mu) = 5$ = average service duration. The M_MG1c value 4.991 validates the M/G/infinity prediction. Third, Figure 9 shows that under

modest system load, say $\rho = 0.33$, p_svr is never deployed. M_MG1c can easily assess the effect of distributions and other inputs. For example Figure 6 rows "R1 exp,5" and "R2 tria(0,0,9,6)" show that triangular request distributions have quite different p_svr statistics.

Figure 9 – MG1c statistics under moderate load

FACILITY	ENTRIES	UTIL.	AVE. TIME	AVAIL.	OWNER	PEND	INTER	RETRY	DELAY
SVR1	1000000	0.334	1.670	1	0	0	0	0	0

QUEUE	MAX	CONT.	ENTRY	ENTRY(0)	AVE.CONT.	AVE.TIME	AVE.(-0)	RETRY
Q_SVR1	9	0	1000000	0	0.428	2.139	2.139	0

STORAGE	CAP.	REM.	MIN.	MAX.	ENTRIES	AVL.	AVE.C.	UTIL.	RETRY	DELAY
P_SVR	1000	1000	0	0	0	1	0.000	0.000	0	0

A second form of M_MG1c represents p_svr as an M/G/c. The c servers (p_svr) implement a fixed allocation of servers for use during heavy loads. Also, requests arriving when all p_svr servers are busy are simply queued to this parallel server. Our cost estimates in the next section are such that the simulator does not need model the service for queued requests.

4 Cost estimates for the M/G/c form of p_svr

Consider the p_svr component of an M_GC1c model for which p_svr is represented by M/G/c service and service queue. In this section we focus on the cost Cv of the transient part of p_svr. For given c, λ, and μ, equation (2) expresses the SS probability that all servers in p_svr (when p_svr is modeled as M/M/c) are busy. For example, setting c=2, $\lambda = 2$, and $\mu = 3/2$ gives the value of (2) as 0.533. Over a total of 1 million requests to p_svr, the number of requests that did not wait for service is 466,482 (the GPSS ENTRY(0) value for row "R", Figure 10). Thus, 533,518 requests were queued, or 53.4%. This agrees with the queuing theory prediction above. Conversion of M/M/c values to M/G/c can be done by adjusting SS formulas based on the coefficient of variation of the service distribution. For most service distributions, the M/G/c value for equation (2) is less compared with M/M/c. We have omitted this corrective factor. Figure 10 displays p_svr behavior for a range of c values. Note the rapid convergence to 0 of the average queue length (value of AVE.CONT.).

We see that simulation-based decision support is more flexible than deriving a c value for "optimum thread pool size" [7]. Finally, Cv could subsequently be converted to an estimate of "system" cost (for platform-specific OS service calls, library calls, etc.) for dynamically processing x threads for each y million service requests.

Figure 10 – M_MC1c results for p_svr service queue; 1 million requests; range of c; same $\lambda = 2$ and $\mu = 3/2$ in all runs

QUEUE	MAX	CONT.	ENTRY	ENTRY(0)	AVE.CONT.	AVE.TIME	AVE.(-0)	RETRY	c
Q_P_SVR	27	0	1000001	466482	1.058	0.529	0.992	0	2
Q_P_SVR	10	0	1000000	947654	0.026	0.013	0.252	0	4
Q_P_SVR	3	0	1000000	999920	0.000	0.000	0.096	0	8

5 Conclusions

At a single service node, service requirements can be estimated using queuing theory predictions of service throughput. Focused simulations can then refine the queuing theory predictions, thereby enumerating service alternatives such as degree of parallelism, server speed, etc. Such staged modeling facilitates drill-down estimates from system analysis through design. Future work examines extensions of service modeling to concurrent service workloads.

6 References

[1] Banks, Carson, Nelson, and Nicol, *Discrete-Event System Simulation, 4th edition*, Prentice Hall, 2005

[2] Kobayashi H., *Modeling and Analysis: An Introduction to System Performance Evaluation Methodology*, Addison Wesley, 1978

[3] Minuteman Software, GPSS WORLD Student Version 5.5.5 http://www.minutemansoftware.com, 2007

[4] Peha, J. and Tobagi, F, "Cost-Based Scheduling and Dropping Algorithms to Support Integrated Services" IEEE Transactions on Communications, Vol 44, NO 2, February 1996

[5] Menasce D. A. and Almeida V.A. F., *Scaling for E-Business,* Prentice Hall, 2000

[6] Welsh M. and Culler D., "Overload Management as a fundamental service design primitive", Proceeding of the Tenth ACM SIGOPS European Workshop, Saint-Emilion, France, 2002

[7] Ling Y., Mullen T., and Lin X., "Analysis of Optimal Thread Pool Size", Operating Systems Review, 34(2), pp. 42-55, 2000

Modeling and optimizing the temperature distribution around cancerous tissues during magnetic hyperthermia treatment

Mehdi Kohani, Masoud Talebi, Mohammad Behshad Shafii

Department of Mechanical Engineering, Sharif University of Technology, Tehran Iran

Abstract - *In magnetic nanoparticle hyperthermia treatment, the ideal objective is to destroy all tumor cells without any damage to neighboring normal tissues. Thus, the temperature distribution in cancerous tissue and also surrounding healthy tissues should become closer to the desired distribution. In this paper, the temperature distribution is estimated by using a numerical scheme to solve the Penne's bioheat transfer equation in a bi-layered spherical tissue with blood perfusion and metabolism. The accuracy of the present model was justified by comparing with an experimental data and similar analytical schemes. Changing the parameters of cancerous tissue showed that the most effective parameter, to optimize the treatment, is the tissue conductivity. Subsequently, we demonstrated that among different factors influencing the tissue conductivity, the mass fraction of water in the tissue is the main factor. According to mass fraction of water in cancerous tissue, two methods of magnetic nanoparticle hyperthermia treatment was suggested.*

Keywords: Penne's Bioheat transfer equation, Magnetic Nanoparticle Hyperthermia, Bi-layered solid sphere

1. Introduction

Magnetic fluid hyperthermia is a new method of cancer treatment. In the realm of oncology therapeutics, hyperthermia is a general term for increasing the temperature of tissue above the physiologic level (40°C to 45°C) within a targeted tumor without damaging the surrounding healthy tissue. [1]

During magnetic hyperthermia treatment, the drug which contains magnetic nanoparticles is injected into the patient's body. Thus, by using an alternating magnetic field near the tumor site, not only does drug absorption increase near cancerous cells, but also heat is produced and adjacent cells are ablated because of hysteresis effects. The underlying mechanism that dominates this type of heating results from the production of (electric) eddy currents. These currents produce heat that scales as:

$$SAR_{EC} \propto f^2.H^2.r^2$$

Where SAR is the tissue-specific absorption rate, measured as W/g tissue, r is the radius of exposed region, and f and H are the AMF frequency and amplitude, respectively. [2]

Andrä et al. [3] modeled small breast carcinomas surrounded by extended healthy tissue as a solid sphere with constant heat generation caused by FePt magnetic nanoparticles (MNPs), and measured the temperature distribution.

Maenosono and Saita [6] and Lin & Liu [5] used FePt magnetic nanoparticles (MNPs) for magnetic hyperthermia and estimate the temperature distribution by using numerical approaches to solve Penne's bio-heat equation.

As one of the current obstacles in using this method is that surrounding tissue is also affected or ablated by heat, this method will be optimized when the heat produced by metallic compounds only affects tumor tissue. Therefore, a mechanism must be introduced to minimize the susceptibility of surrounding tissue to heat. This will be possible when the temperature distribution in tumor tissue is ideal. In order to do this, a model is needed to approximate the temperature distribution in tumor and surrounding normal tissues. Because of the sensitivity of healthy cells to temperature fluctuation, the accuracy of this model is critical to obtain reliable results.

In this paper we introduce a modified model that uses a new numerical approach to obtain the inverse Laplace transform of Penne's bio-heat equation. The estimated results are compared with those in the literature [3, 5, 6]. These comparisons show that the present model has a better accuracy than other numerical approaches. Base on this model, we compare the effect of changing three main parameters to determine the most critical one which is conductivity. Subsequently, we found that the most important parameter in conductivity is the mass fraction of water in the tissue. Finally with respect to our results some suggestions were made to optimize the temperature distribution by changing effective parameters.

2. Material and methods

To simplify the problem, we assume the tumor to be a spherical tissue with radius R, and the surrounding normal tissue to be a bigger concentric sphere with radius a. We also make the assumption that nanoparticles absorb homogeneously only into the tumor tissue. As the result of homogeneity, all thermodynamic parameters in the tissues are constant. By alternating the magnetic field, a constant power density will be produced in the tumor tissue due to hysteresis losses. This power density is denoted by P which is directly related to the SAR value. This power produces a temperature distribution in both the tumor and normal tissue as a function of time (t) and radius (r). Now, by employing the heat transfer equation the temperature distribution in tissues can be obtained.

Regarding the spherical shape of tumor tissue, a shell spherical control volume can be assumed. By using the heat transfer equation in spherical coordinates, the following equations are obtained:

$$\frac{\partial}{\partial t}(\rho cT) = div\big(k.grad(T)\big) + generation + convection$$

$$\rho c\frac{\partial T}{\partial t} = k\frac{1}{r^2}\frac{\partial}{\partial r}\left(r^2\frac{\partial T}{\partial r}\right) + q_m + p + ? \quad (1)$$

In the equation above, convection heat transfer is unknown. This quantity can be approximated by assuming quasi-steady state conditions and applying the first law of thermodynamics:

$$\dot{m}(h_i - h_e) + \dot{Q}_c - \dot{W} = \frac{\partial E}{\partial t} \quad (2)$$

$$\dot{Q}_c = \dot{m}(h_i - h_e) = \dot{m}c(T_i - T_e) = \rho_b c_b w_b (T_i - T_e) \quad (3)$$

Equations 1 and 3 lead to Penne's bioheat equation, formulated in equations 4 and 5 below:

$$\rho_1 c_1\frac{\partial T_1}{\partial r} = k_1\frac{1}{r^2}\frac{\partial}{\partial r}\left(r^2\frac{\partial T_1}{\partial r}\right) + \rho_b c_b w_{b1}(T_b - T_1) + q_{m1} + p \;\; for \;\; r \le R \quad (4)$$

$$\rho_2 c_2\frac{\partial T_2}{\partial r} = k_2\frac{1}{r^2}\frac{\partial}{\partial r}\left(r^2\frac{\partial T_2}{\partial r}\right) + \rho_b c_b w_{b2}(T_b - T_2) + q_{m2} \;\; for \; R \le r \le a \quad (5)$$

The various parameters in these equations are defined as follows:

(The subscript "1" refers to tumor tissue, while the subscript "2" refers to normal tissue)

T represents the temperature.

ρ is the density.

c is the specific heat capacity.

k is the thermal conductivity.

T_b represents the blood temperature far from cancerous tissue.

q is the metabolic heat generation rate.

P is the heat generated by magnetic nanoparticles at the tumor site.

w_b is the blood perfusion rate.

Following equations are applied for initial and boundary conditions [5]:

Spherical symmetry:

$$T_1(0,t) \; is \; finite \quad (6)$$

Continuity of temperature at the interface:

$$T_1(R,t) = T_2(R,t) \quad (7)$$

Thermal energy conservation:

$$K_1\frac{\partial T_1(R,t)}{\partial r} = K_2\frac{\partial T_2(R,t)}{\partial r} \quad (8)$$

Heat flux rate at the edge of surrounding normal tissues

$$\frac{\partial T_2(a,t)}{\partial r} = 0 \quad (9)$$

The initial conditions become (j= 1, 2):

$$T_j(r,0) = T_0 \quad (10)$$

$$\frac{\partial T_j(r,0)}{\partial t} = 0 \quad (11)$$

$$q_j(r,0) = 0 \quad (12)$$

A new dependent variable, H, is defined as:

$$H = r(T - T_0) \quad (13)$$

Therefore the initial and boundary conditions are rewritten as:

$$H_1(0,t) = 0 \quad (14)$$

$$H_1(R,t) = H_2(R,t) \quad (15)$$

$$K_1\left[\frac{\partial H_1(R,t)}{\partial r} - \frac{H_1}{R}\right] = K_2\left[\frac{\partial H_2(R,t)}{\partial r} - \frac{H_2}{R}\right] \quad (16)$$

$$\frac{\partial H_2(a,t)}{\partial r} - \frac{H_2}{a} = 0 \quad (17)$$

$$\frac{\partial H_j(r,0)}{\partial t} = 0 \quad (18)$$

$$q_j(r,0) = 0 \quad (19)$$

Applying the Laplace transform to the equations above with respect to time (t), the initial and boundary conditions can be rewritten as:

$$\frac{d^2\widetilde{H_j}}{dr^2} - \gamma^2{}_j\widetilde{H_j} = -f_j r \quad (20)$$

$$\widetilde{H_1}(0,s) = 0 \quad (21)$$

$$\widetilde{H_1}(R,s) = \widetilde{H_2}(R,s) \tag{22}$$

$$K_1\left[\frac{\partial \widetilde{H_1}(R,s)}{\partial r} - \frac{\widetilde{H_1}}{R}\right] = K_2\left[\frac{\partial \widetilde{H_2}(R,s)}{\partial r} - \frac{\widetilde{H_2}}{R}\right] \tag{23}$$

$$\frac{\partial \widetilde{H_2}(a,s)}{\partial r} - \frac{\widetilde{H_2}}{a} = 0 \tag{24}$$

$$\gamma_j^2 = \frac{1}{K_j}\left(\rho_j c_j s + \rho_b c_b w_b\right) \tag{25}$$

$$f_1 = \frac{q_{m1} + p}{k_1 s} \tag{26}$$

$$f_2 = \frac{q_{m2}}{k_2 s} \tag{27}$$

The initial and boundary conditions used in the equations above give the following solution:

$$\widetilde{H_1} = C_1(e^{\gamma_1 r} - e^{-\gamma_1 r}) + r\frac{f_1}{\gamma_1^2} \tag{28}$$

$$\widetilde{H_2} = C_2\left(\frac{(a\gamma_2 + 1)}{(a\gamma_2 - 1)}e^{\gamma_2(r-2a)} - e^{-\gamma_2 r}\right) + r\frac{f_2}{\gamma_2^2} \tag{29}$$

Where constants are as:

$$N_0 = \frac{(a\gamma_1 + 1)}{(a\gamma_1 - 1)}e^{\gamma_1(R-2a)} - e^{-\gamma_1 R} \tag{30}$$

$$N_1 = \frac{(e^{\gamma_1 R} - e^{-\gamma_1 R})}{N_0} \tag{31}$$

$$N_2 = \frac{\left(\frac{f_1}{\gamma_1^2} - \frac{f_2}{\gamma_2^2}\right)R}{N_0} \tag{32}$$

$$N_3 = \frac{(a\gamma_2 + 1)}{(a\gamma_2 - 1)}e^{\gamma_2(R-2a)} - e^{-\gamma_2 R} \tag{33}$$

$$N_4 = K_1\gamma_1(e^{\gamma_1 R} - e^{-\gamma_1 R}) + \frac{K_2 - K_1}{R}(e^{\gamma_1 R} + e^{-\gamma_1 R}) + K_2\gamma_2 N_1 N_3 \tag{34}$$

$$N_5 = K_2\gamma_2 N_2 N_3 - K_2\left(\frac{f_1}{\gamma_1^2} - \frac{f_2}{\gamma_2^2}\right) \tag{35}$$

$$C_1 = \frac{N_5}{N_4} \tag{36}$$

$$C_2 = N_1 C_1 + N_2 \tag{37}$$

Therefore, the inverse Laplace transform yields the temperature distribution function H, which cannot be obtained analytically. Thus, the numerical solution presented by J. Abate and P. P. Valko [7] is applied to this problem, which gives an approximate result for the function H.

The accuracy of this method can be determined as [7]:

$$\left|\frac{f(t) - f(t,M)}{f(t)}\right| \approx 10^{-0.6M} \tag{38}$$

M is the number of precision decimal digits which is assumed to be three in this article.

Using above method, the function H can be approximated as:

$$H(t,M) = \frac{r}{M}\left\{\frac{1}{2}\widetilde{H}(r)e^{rt} + \sum_{K=1}^{M-1} Re\left[e^{ts(\theta_k)}\widetilde{H}\left(s(\theta_k)\right)\left(+i\sigma(\theta_k)\right)\right]\right\} \tag{39}$$

$$s(\theta) = r\theta(\cot\theta + i) \qquad -\pi < \theta < \pi \tag{40}$$

$$\sigma(\theta) = \theta + (\theta\cot\theta - 1)\cot\theta \tag{41}$$

$$r = \frac{2M}{5t} \tag{42}$$

By calculating H from equation (40) and using equation (13), the temperature in the tumor will be obtained, at every radius r and at every time t.

3. Results and discussion

The thermal effects of nanoparticle-injected (FePt) tissues, was demonstrated by Maenosono & Saita [6].
In this research work, parameters of the table 3.1 and table 3.2 were used.

Table3.1. Dimensions of tissues and properties of magnetic field used by Maenosono & Saita [6]

Radius of tumor tissue	R=5mm
Radius of normal tissue	a=15mm
The magnetic field's amplitude	5mT
The magnetic field's frequency	300kHz

Table3.2. Heat produced by magnetic nanoparticles [6]

Type of magnetic nanoparticles	9-nm FCC FePt	19-nm magnetite
Heat Generation	$P_1=3.97\times10^5 \frac{W}{m^3}$	$P_2=1.95\times10^5 \frac{W}{m^3}$

Figure (1) shows the temperature distribution at t=600s for P_1 and P_2 as a function of distance from the center of the tumor.

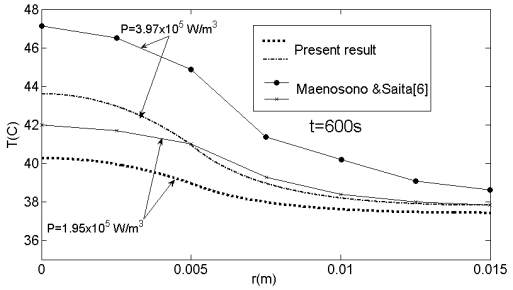

Figure 1. *Temperature distributions in the finite tissue at t=600s, for P_1=3.97×10^5 W/m^3 (9-nm fcc FePt MNP s) and P_2=1.95×10^5 W/m^3 (19-nm magnetite MNPs)*

Here the diagram is compared with the results of Maenosono & Saita [6]. Obviously, since Maenosono & Saita [6] used far less data points, we can conclude that our results have improved accuracy. Moreover, it is demonstrated in figure (1) that the temperature distribution in the tumor tissue (r < 0.005m) is approximately linear. This is in complete contradiction with the nature of heat transfer in that region. Due to heat generation in tumor tissue by the nanoparticles, the temperature distribution must be parabolic which agrees with present results.

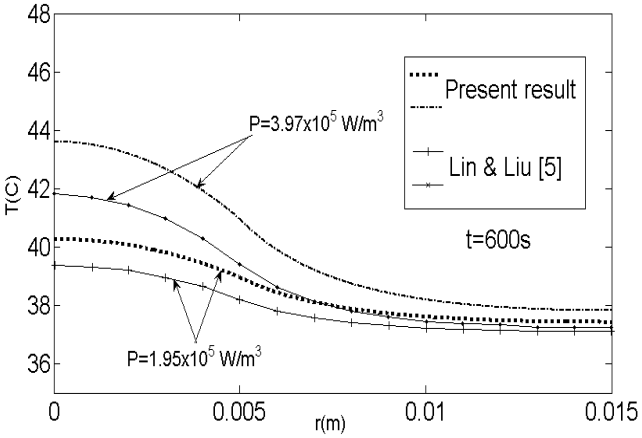

Figure 2. *Temperature distributions in the finite tissue at t=600 s for P_1=3.97×10^5 W/m^3 (9-nm fcc FePt MNPs) and P_2=1.95×10^5 W/m^3 (19-nm magnetite MNPs)*

Figure (2) show that the present results are in better agreement with the curves presented by Lin & Liu [5].

In order to confirm the accuracy of the present approach, it is necessary to compare the present results of temperature distribution with experimental results. The temperature distribution of the tumor and neighboring normal tissue is calculated using parameter values given by Andra et al. [3], and it is compared with experimental results in figure (3). It should be mentioned that although Andra et al. [3] and Lin & Liu [5] used the same parameters, they differ in value.

According to figure (3), the analytical results are in good agreement with the experimental results obtained by Andra et al. [3]. Therefore, the method presented in our work is a reliable means of modeling the temperature distribution in cancerous and normal tissue.

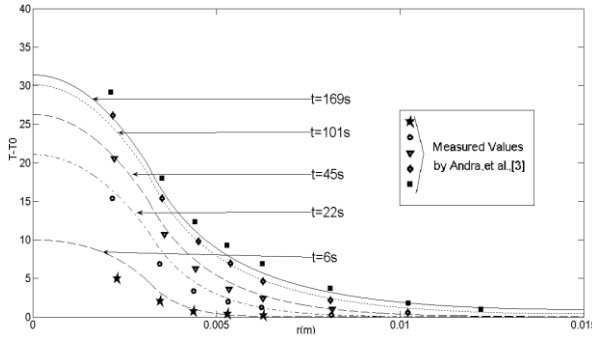

Figure 3. *Temperature distribution as a function of the distance from the center of the tumor for different exposure times, using the parameters given in [3]. Measured values for the same parameters are plotted with symbols.*

The present distribution curve can be converged to that of the ideal condition by changing the effective parameters

of normal and cancerous tissue. This necessitates the knowledge of the effect that each of these parameters has on the temperature distribution.

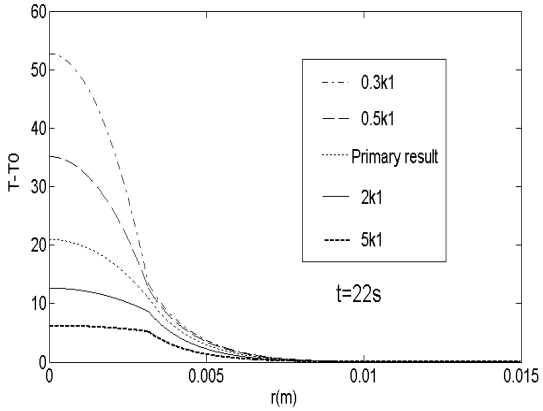

Figure 4. *Temperature distribution variation for different values of k1 (heat conductivity of tumor tissue) calculated at t=22s.*

Different curves of temperature distribution with different values of parameters (k_1, c_1, wb_1) are compared in figures (4), (5), (6) (all calculated at t=22s). It should be noted that c_2 and k_2 are the normal tissue parameters and it is obvious that changing these parameters is not as easy as changing the tumor tissue parameters.

In figure (4), the temperature distribution converges to the ideal condition as k_1 is reduced.

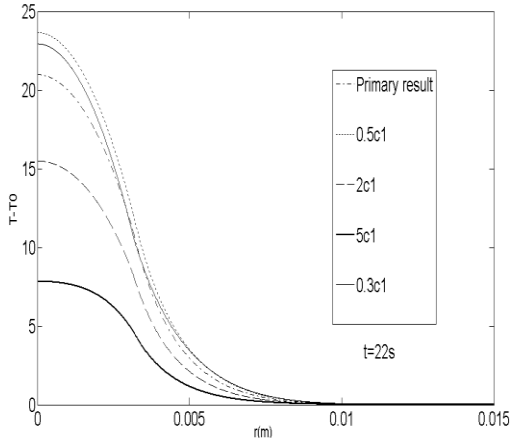

Figure 5. *Temperature distribution variation for different values of c1 (specific heat capacity of tumor tissue) calculated at t=22s.*

Figure (5) shows that the temperature of the center of tumor decreases with increasing c_1.

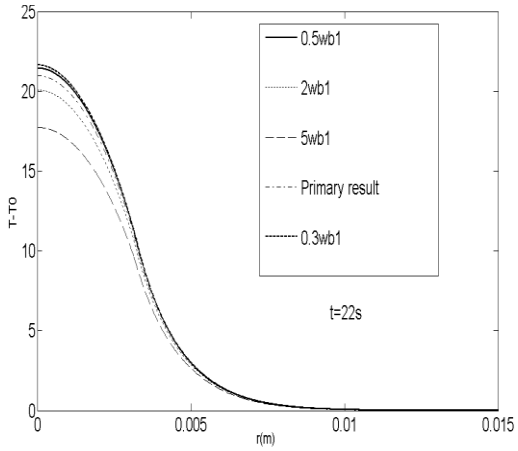

Figure 6. *Temperature distribution variation for different values of wb1 (blood flow rate in tumor tissue), calculated at t=22s.*

Figure (6) shows that temperature distribution is less sensitive to w_{b1} variation as compared to c_1 & k_1. It seems that decreasing human activity, resulting in less blood flow rate, can enhance this therapy. The reason is that decreasing blood flow rate leads to less convection heat transfer, and so heat generated by nanoparticles would not be transferred through the bloodstream.

Summarizing the results of figures (4), (5) and (6), it can be concluded that the temperature distribution at the tumor site is mostly affected by the heat conductivity of the tumor tissue, among other factors. This can also be inferred from boundary condition (9). Therefore to achieve ideal temperature distribution, the most effective way is to reduce k_1.

From the knowledge of heat transfer principles, it is obvious that large values of conductivity make the temperature distribution uniform and small values make a large temperature gradient. Therefore it could be concluded that, there are two methods in magnetic nanoparticle hyperthermia. The first is to destroy all tumor tissue, while also destroying nearby normal tissue cells, by increasing conductivity of the tumor tissue. The second is to completely destroy the center of the tumor with incurring less damage to normal tissues by decreasing conductivity of the tumor tissue. The best treatment is a choice that would have to be made by the physician.

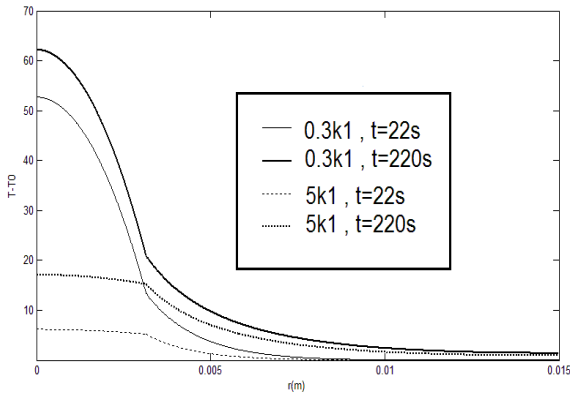

Figure 7. *Temperature distribution for conductivity value equal to 0.3k1 and 5k1 at t=22s and t=220s, where k1 is the conductivity of the cancerous tissues given by Andra et al. [3].*

Fig (7) shows the temperature distribution for conductivity value equal to 0.3k1 and 5k1 at t=22s and t=220s. This figure illustrates the two suggested method of magnetic hyperthermia treatment therapy.

Conductivity of biological tissues (k) depends on various parameters such as water content percentage, the amount of fat and protein [8], and temperature [9].

Noting the first assumption in solving Penne's equation which states that conductivity is independent of temperature, variation of K should be measured based on changing water and fat and protein content, only.

According to Cooper and Trezck [9], the following relation holds between these parameters:

$$k(mW/cm-℃) = \rho \sum_{n} \frac{k_n m_n}{\rho_n} = \rho\left(6.28 m_{water} + 1.17 m_{protein} + 2.3 m_{fat}\right) \qquad (43)$$

Based on equation (43), it seems that changing the water content of a tissue is more effective than changing fat or protein content because its coefficient is greater than others. Thus it is possible to obtain different temperature distributions based on different water contents in order to draw closer to our ideal temperature distribution.

4. Conclusion

A numerical solution has been introduced in this paper in order to obtain temperature distribution in tumor tissue treated with magnetic nanoparticle hyperthermia. Based on the proposed method of calculation, the results were very close to experimental curves. These results are reliable as they are close to other numerical results in literature [5, 6], as well as experimental measurements [3]. Some factors that affect thermodynamic parameters of the tissue are presented in this article and their relative effects are shown in various figures. According to these figures, the best way to obtain optimal distribution is to reduce conductivity of the tumor tissue by increasing its water content. Also, two methods of magnetic nanoparticle hyperthermia treatment based on conductivity value were suggested.

5. References

[1] G.F. Goya, V. Grazu and M.R. Ibarra: Current Nanosci. 4 (2008) 1.

[2] Ivkov R., DeNardo S., et al. Application of High Amplitude Alternating Magnetic Fields for Heat Induction of Nanoparticles Localized in Cancer. Clin Cancer Res 2005; 11 (19 Supply): 7093s.

[3] Andra W, d'Ambly C G, Hergt R, Hilger I and Kaiser W A 1999 Temperature
distribution as function of time around a small spherical heat source of local magnetic
hyperthermia Journal of Magnetism and Magnetic Materials 194 197-203.

[4] N. Tsuda, K. Kuroda, Y. Suzuki, An inverse method to optimize heating conditions in RF-capacitive hyperthermia, IEEE Trans. Biomed. Eng. 43 (1996) 1029–1037.

[5] Chin-Tse Lin, Kuo-Chi Liu, Estimation for the heating effect of magnetic nanoparticles in perfused tissues, International Communications in Heat and Mass Transfer 36 (2009) 241–244.

[6] S. Maenosono, S. Saita, Theoretical assessment of FePt nanoparticles as heating elements for magnetic hyperthermia, IEEE Trans. Magn. 42 (2006) 1638–1642.

[7] Abate J. and P. P. Valko. 2004. Multi-precision Laplace inversion. Int. J. Numer. Meth.
Engng. 60, 979-993.

[8] Valvano, J.W., Badeau, A.F., and Pearce, J.A., 1987, "Simultaneous Measurement of Intrinsic and Effective Thermal Conductivity", Heat Transfer in Bioengineering and Medicine, ASME Winter Annual Mtg., Boston, HTD Vol. 95, BED
Vol. 7, ed. Chato, Diller, Diller, Roemer, pp. 31-36.

[9] Cooper, T.E., and Trezck, G.J. Correlation of thermal properties of some human tissues with water content, Aerospace. Med., 42, 24–27, 1971.

Numerically Estimating Derivatives During Simulations

Respectfully submitted to Modeling, Simulation and Visualization Methods (MSV'11),
a conference of (WORLDCOMP'11)—the 2011 World Congress
in Computer Science, Computer Engineering, and Applied Computing

Gregory V. Bard
Dept. of Mathematics, Statistics and Computer Science
University of Wisconsin—Stout
Menomonie, WI, 54751-0790
Email: gregory.bard@ieee.org
http://www.math.umd.edu/∼bardg/

***Abstract*—When a function's value is known at several distinct points, there exist "numerical differentiation" formulas which provide estimates for the first derivative, and with various error bounds. In fact, many times the numerical differentiation formula chosen must be complex to avoid intolerable error as shown below. However, in computer simulations, as well as in real-time programming, while several past data points might be known, as well as the present data, the future is not yet known or computed!**

This renders those formulas, at least as classically presented, useless for both real-time computing and for simulations. This research began as an inquiry to discover similar formulas usable when only the past and present, but not the future, are known. The author uncovered an extremely obscure corner of numerical analysis, where solutions to these dilemmas are feasible. An extremely simple algorithm can produce suitable formulas, for any number of data points, not only for the first derivative but also higher-order derivatives. Moreover, the data points can be irregularly spaced, and it is straight-forward to calculate the appropriate error terms, and the impact of noisy data.

The standard presentation of these methods would require *Multivariate Calculus*, one or two semesters of *Real Analysis*, and one semester of *Numerical Analysis*. However, many computer science graduate students have only *Calculus I* and *Calculus II*. This is a novel presentation of this extremely obscure topic, meant not only to publicize it among simluation-oriented computer scientists and those working in real-time computing, but also to be comprehensible to someone who has 2–3 semesters of calculus and nothing more. A rigorous proof of correctness is provided in the appendix, as well as sample code for the algorithm in SAGE—the open source competitor to Maple, Mathematica, Matlab and Magma.

***Index Terms*—Simulations, Numerical Differentiation, Discretization Error.**

I. INTRODUCTION

When one has some data, perhaps about the position of an aircraft, at times one wants to calculate the first derivative. Perhaps the aircraft is being modeled by a simulation, and one has position data at discrete time slices separated by h seconds. Obviously, one can estimate the derivative by

$$\frac{f(t)-f(t-h)}{h} \approx f'(t)$$

but because h is an actual length of time, and not infinitesimal, this produces some error, usually called discretization error. In numerical analysis, this is called the "backward difference" formula. In Section V, we will show that its error is $(h/2)f''(t)+\mathcal{O}\left(h^2f'''(t)\right)$, which is well known.

Many people working in the overlap of computer science and mathematics know that the "center difference" formula

$$\frac{f(t+h)-f(t-h)}{2h} \approx f'(t)$$

produces slightly less error and the much less well-known "four point" formula is

$$\left(\frac{-1}{3}\right)\left[\frac{f(t+2h)-f(t-2h)}{4h}\right]+\left(\frac{4}{3}\right)\left[\frac{f(t+h)-f(t-h)}{2h}\right] \approx f'(t)$$

which is better still. Nonetheless, both of these numerical differentiation formulas are not useful in simulations, because if $f(t)$ represents the present moment, then $f(t+h)$ and $f(t+2h)$ represent the future, which has not been calculated yet, (or is not yet known.)

Accordingly, many simulation experts go with the "backward difference formula" given above, which is wasteful. Instead, we will show that one can use

$$\frac{1}{h}\left[\frac{1}{4}f(t-4h)-\frac{4}{3}f(t-3h)+3f(t-2h)-4f(t-h)+\frac{25}{12}f(t)\right]$$

which while it look strange, requires no knowledge of the future, and produces

$$f'(t)-\frac{h^4}{5}f^{(5)}(t)+\mathcal{O}\left(h^5f^{(6)}(t)\right)$$

and since $h \approx 10^{-4}$ or 10^{-3} in many applications, there is virtually no discretization error. We will use this example as the "main example" of the paper, and derive it, as well as derive its error terms. Other sample formulas that the algorithm can produce are given in Figure 1.

Such formulas look miraculous but they have an algorithmic derivation. In this paper, we will explore how to construct such formulas that do not require knowledge of the future, for any number of data points, as well as how they can be adapted to irregular spacings, how the error terms can be simply and exactly derived, and how similar formulas can be derived for higher-order derivatives.

Before we describe the algorithm, we will examine the numerical motivation for finding them in Section II and briefly examine some hypothetical applications in Section III. The algorithm itself is given in Figure 2 and is discussed in Section IV, followed by two warm-up calculations given in Section V. Then the technique for calculating the error (and verifying the correctness of the output) is described in Section VI. Next we discuss the impact of noise in Section VII. We give a survey of the classic expositions on numerical differentiation in Section IX, to demonstrate that these techniques are extremely rare inside the numerical analysis community, and so therefore it is unsurprising that they are essentially unknown outside of it.

A rigorous proof of the correctness of the method, along with the error terms, is given in the appendices, but most readers will not necessarily have the background for what is presented there. Instead, the techniques of Section VI allow the reader to verify the formula outputted by the algorithm for any particular inputs, and an example of this is found in Figure 3. It is hoped that the paper, without appendices, is comprehensible to anyone with a full year of calculus, though this is false for the appendix. The appendices can be found in the full version of the paper on the author's webpage, at the URL given at the top of the front page.

A. Notation

As is customary, the second and third derivatives are written $f''(t)$ and $f'''(t)$ while the fourth and fifth are written $f^{(4)}(t)$ and $f^{(5)}(t)$. Furthermore, $f^{(k)}(t)$ means the kth derivative for any $k \geq 1$. Mathematicians, and this paper, denote the upper-left-hand entry of a matrix A as A_{11}, not A_{00}, as would be required by some programming languages. The basic time slice of a simulation will be denoted h. That is to say, the data points available are assumed to be $f(0)$, $f(h)$, $f(2h)$, $f(3h)$, ...

II. Numerical Motivation

If one is using a simulation to compute something, usually it is because no mathematical function to compute it is known. Otherwise, one would not bother with a simulation, except perhaps for pedagogical purposes. Nonetheless, it is useful to explore some explicit example functions to see the discretization error. Here we take two functions which could come up in the analysis of a physical system, in a first-semester course of *Differential Equations*.

We consider the functions

$$\phi(t) = e^{-4t} \qquad \text{and} \qquad \psi(t) = e^{-4t}(\sin 10t)$$

at $t = 1$, and time slice of 10 msec (i.e. $h = 10^{-2}$.) We compare the performance of the backward-difference formula (denoted BDF) and main example (denoted ME). The data is given in Table I.

While 2.03% error could be perhaps overlooked in the case of $\phi(t)$, the 9.12% error perhaps cannot, in the case of $\psi(t)$. Of course, $h = 0.01$ is a bit large, and more typical values would be $h = 0.001$ or $h = 0.0001$. Yet, that means that the computation would have to run $10\times$ or $100\times$ as long.

TABLE I
A Numerical Example

	phi(t)	psi(t)
Actual	-0.073262555555	-0.113824934424
Predicted by ME	-0.073262515448	-0.113828751659
Absolute Error, ME	0.000000040107	-0.000003817234
Relative Error, ME	-0.000054743602%	0.003353601199%
Predicted by BDF	-0.074747540288	-0.124203517934
Absolute Error, BDF	-0.001484984733	-0.010378583510
Relative Error, BDF	2.026935480971%	9.118022832760%

The greater accuracy can then be realized as a tradeoff against running time. Suppose the tolerable error is some fixed amount. If the h required to achieve that amount is much less with a more complex numerical differentiation formula, than another, surely the ratios of the hs is the factor of the speed-up. However, this is overly simplistic, as a researcher can choose the granularity of the simulation for many reasons, not just the discretization error of some rate that is being calculated.

Also, we will explore in Section VII how making h too small can cause both rounding error and instrumentation error to become large.

III. Potential Applications

There are too many uses of calculating derivatives to even be summarized here. However, in this section we present five hypothetical applications which demonstrate the potential uses of being able to handle irregular spacings, being able to achieve high accuracy, or being able to take higher-order derivatives.

First, in guided missile tests, an altimeter is a simple and off-the-shelf component, but taking the derivative accurately would convert this into a *vertical* velocity measurement. Note, this is not the same as airspeed, which while easily measured with a Pitot tube, and includes the *horizontal* component of velocity. In fact, in this case, second, third and fourth derivatives would be useful, as acceleration, jerk, and jostle are important parameters for any guided missile.

Second, in modeling a biological system of three or more competing components (e.g. viruses, red cells, and white cells) the microscope might be connected to a camera, and either an automated system, or more realistically, a graduate student, would count the number of such visible inside a given grid square. These population counts could not be taken too close together in time, otherwise there would be too many photographs to analyze during the length of the experiment. Nonetheless, it might be useful to discover the rates of growth, to a high level of accuracy. This is particularly important if the rates of growth are actually similar, yet it is pivotal to know which is growing faster than which.

Third, from the purchasing records of medieval colleges (e.g. New College, Oxford, established in 1379), it has become fashionable to reverse engineer the prices of commodities [10] [8]. This enables price data to become known where it

$$\frac{1}{h}\left[\frac{-1}{1}f(t-h)+\frac{1}{1}f(t)\right]=f'(t)+\frac{-1}{2}hf^{(2)}(t)+\mathcal{O}\left(t^2f^{(3)}(t)\right)$$
$$\frac{1}{h}\left[\frac{1}{2}f(t-2h)+\frac{-2}{1}f(t-h)+\frac{3}{2}f(t)\right]=f'(t)+\frac{-1}{3}h^2f^{(3)}(t)+\mathcal{O}\left(t^3f^{(4)}(t)\right)$$
$$\frac{1}{h}\left[\frac{-1}{3}f(t-3h)+\frac{3}{2}f(t-2h)+\frac{-3}{1}f(t-h)+\frac{11}{6}f(t)\right]=f'(t)+\frac{-1}{4}h^3f^{(4)}(t)+\mathcal{O}\left(t^4f^{(5)}(t)\right)$$
$$\frac{1}{h}\left[\frac{1}{4}f(t-4h)+\frac{-4}{3}f(t-3h)+\frac{3}{1}f(t-2h)+\frac{-4}{1}f(t-h)+\frac{25}{12}f(t)\right]=f'(t)+\frac{-1}{5}h^4f^{(5)}(t)+\mathcal{O}\left(t^5f^{(6)}(t)\right)$$
$$\frac{1}{h}\left[\frac{-1}{5}f(t-5h)+\frac{5}{4}f(t-4h)+\frac{-10}{3}f(t-3h)+\frac{5}{1}f(t-2h)+\frac{-5}{1}f(t-h)+\frac{137}{60}f(t)\right]=f'(t)+\frac{-1}{6}h^5f^{(6)}(t)+\mathcal{O}\left(t^6f^{(7)}(t)\right)$$
$$\frac{1}{h}\left[\frac{1}{6}f(t-6h)+\frac{-6}{5}f(t-5h)+\frac{15}{4}f(t-4h)+\frac{-20}{3}f(t-3h)+\frac{15}{2}f(t-2h)+\frac{-6}{1}f(t-h)+\frac{49}{20}f(t)\right]=$$
$$f'(t)+\frac{-1}{7}h^6f^{(7)}(t)+\mathcal{O}\left(t^7f^{(8)}(t)\right)$$

Fig. 1. Numerical Differentiation Formulas that use Past and Present but not Future, as were found by the algorithm in Figure 2.

would otherwise be unavailable. But because such 600-year-old purchasing records have missing "bits", where a record or entry is missing or has been destroyed, techniques are needed which can deal with "lacunae," which are gaps in the data. When the data is sequential, formulas like those given in Figure 1 can be used, but when the data has lacunae, then the algorithm can be called to generate a custom formula that does not involve the missing data point.

Fourth, many financial instruments are traded around the clock, "24-7," but the trading is divided into Monday through Friday periods during normal hours, when the market is open, as well as trading that occurs while the market is closed in the evening and night or weekends. The trading while the market is open results in data that is freely available through web-based tools such as "Yahoo! Finance," whereas the after-hours data is not as easily available in some cases. Let $f(t)$ be the closing price of a financial security on a given day. On a Wednesday, the 5 most-recent data points would represent $f(t)$, $f(t-h)$, $f(t-2h)$, $f(t-5h)$ and $f(t-6h)$, being namely the present day, last Tuesday, last Monday, last Friday, and last Thursday, if h is one day. Thus one needs to be able to take the derivatives when the samples are irregularly spaced.

Fifth, the problem of a rocket taking off is a classic in any *Differential Equations* course. When the instructor includes one feature of realism, such as a rocket meeting with air-resistance, the reduction in mass because of the burnt fuel, or the declining strength of gravity at very high altitudes, then the problem becomes somewhat challenging. But when two or three of these phenomena are included, then the problem is analytically intractable, but can be addressed via a simulation. Such a simulation, at each time slice, would calculate several forces, divide by the instantaneous mass, and then get the acceleration. Then numerical differentiation could be used to calculate the jerk and jostle.

IV. The Algorithm

The algorithm below is more general, as it can find second, third, or arbitrarily higher derivatives. For the kth derivative, at least $k+1$ data points are needed. The spacing of the data points can be highly irregular. The notation used is $f(t+\delta_i h)$, and in a simulation the $\delta_i \leq 0$, because the future is not yet known. For example, the formula presented in Section 2 used the present moment and four previous time slices, as data points. This would be

$$\delta_1=-4,\quad \delta_2=-3,\quad \delta_3=-2,\quad \delta_4=-1,\quad \delta_5=0$$

in this notation. Note, that each δ must be distinct, i.e. no two δs can be equal.

The algorithm, given in Figure 2, is nothing more than a matrix problem of the form $A\vec{c}=\vec{b}$ and in fact, it is a "Vandermonde" matrix [11] named for Alexandre-Théophile Vandermonde. This matrix is shown in Figure 4 of the appendices, and will appear in the proof of correctness of the algorithm. The algorithm, while simple, is probably difficult to understand without reading the proof, but we can verify the validity of its output easily for any particular inputs. In fact, we will do so, in Figure 3, for the "main example" of the paper. For any other inputs, the verification would proceed extremely similarly. Most readers will want to skip the proof.

As stated earlier, only exceptionally pathological functions will fail to be "amenable of type (h,n)", a term defined in Appendix A, and dealt with in Lemma 1. Such functions are very unlikely to arise in applications. This is an obscure technical requirement to remove pathological cases.

A. Numerical Warning on Reducing A:

The bad news is that Vandermonde matrices are known to have extraordinarily high condition number for their size [11], so much so that they are used to "stress test" computer algebra systems before shipment. However, since n is the number of data points used by the formula, and in any practical applied scenario, $n < 11$, this will not be a problem. Computer algebra packages like Maple [1] or SAGE [2] can solve these matrix problems exactly, and not using floating-point notation at all, thus avoiding rounding error entirely. To be precise, the entries of the matrix and both vectors will be rational numbers

Input: A spacing of samples, δ_1, δ_2, δ_3, ..., δ_n, all distinct, and some integer k such that $1 \leq k < n$.
Output: A vector $\vec{c}$ such that

$$\frac{1}{h^k}\sum_{j=1}^{j=n} c_j f(t+\delta_j h) = f^{(k)}(t) + \mathcal{O}\left(h^{n-k} f^{(n)}(t)\right)$$

for any function $f(t)$, that is "amenable of type (h, n)."

1) Define a $n \times n$ matrix A such that $A_{ij} = (\delta_j)^{i-1}$.
2) Define an n-dimensional vector $\vec{b}$, and let $\vec{b} = \vec{0}$, except that $b_{k+1} = k!$.
3) Via Gaussian Elimination or some other means, find $\vec{c}$ such that $A\vec{c} = \vec{b}$.
   Note: Such a $\vec{c}$ always exists and is unique.
4) Return $\vec{c}$.

Fig. 2. The algorithm that produced the formulas in Figure 1.

represented exactly, as the ratio of two explicit integers which are themselves stored as binary strings. For even medium-sized problems, this is normally infeasible, but these A will not have more than a hundred entries or so, and therefore there is no difficulty in using this exact representation.

V. Two Simple Examples

We start with Taylor's Theorem from calculus, an important infinite sum:

$$f(t+h) = f(t) + \sum_{i=1}^{i=\infty} \frac{h^i}{i!} f^{(i)}(t)$$

which can be truncated early for $h \ll 1$, to produce a finite sum, using big-Oh notation

$$f(t+h) = f(t) + \left(\sum_{i=1}^{i=n} \frac{h^i}{i!} f^{(i)}(t)\right) + \mathcal{O}\left(h^{n+1} f^{(n+1)}(t)\right)$$

and note that this is the same big-Oh used when explaining to students that sorting is $\mathcal{O}(n \log n)$ time. It is justified because every term after the nth will be a multiple of h^{n+1}, and since $h \ll 1$ then the h^{n+1} term will dominate the sum. We will clarify precisely when this use of big-Oh notation is correct in the formal proof given in Appendix A. For now, we point out that the big-Oh, instead of being as the data-input length goes to infinity, represents the granularity of the calculation (here h) going to zero.

For the backward-difference we select $n = 2$ and then have

$$f(t+h) = f(t) + hf'(t) + \frac{h^2}{2} f''(t) + \mathcal{O}\left(h^3 f'''(t)\right)$$

and so

$$\frac{f(t+h) - f(t)}{h} = f'(t) + \frac{h}{2} f''(t) + \mathcal{O}\left(h^2 f'''(t)\right)$$

therefore the error is $(h/2)f''(t) + \mathcal{O}\left(h^2 f'''(t)\right)$.

Meanwhile, for the "main example," we offer two roads to proof. The main example is, of course, a special case of the more general theorem. However, a direct proof is provided in Figure 3, for two reasons. First, the rigorous proof of the theorem is relatively arcane and might be easier to understand after looking over the more calculation-oriented proof in Figure 3. Second, if an undergraduate must read this paper, note that the formal proof requires some facts learnt during *Real Analysis* and *Linear Algebra*, where as the simpler proof in the figure requires only Taylor's Theorem, which is usually taught in *Calculus II* or sometimes *Calculus III* or even *Calculus I*.

A. Note on the Error Terms:

Typically, the error term of Taylor's Theorem, for an nth-degree Taylor polynomial approximating $f(t+h)$ by expansion around $f(t)$ is stated via

$$f(t) + \sum_{i=1}^{i=n} \frac{h^i}{i!} f^{(i)}(t) = f(t+h) - \frac{h^n}{n!} f^{(n+1)}(\xi)$$

where ξ is some number between t and $t+h$.

However, this is non-descriptive for us for several reasons. First, the computer science audience is already extremely familiar with Big-Oh notation. Second, we wish to model derivatives of $f(t)$ and so our error bounds really should be in terms of those derivatives, and not f itself, otherwise one is comparing apples and oranges. Third, a happy and very unexpected coincidence is that the proof works out to be much simpler in Big-Oh notation. Naturally, this is not the first use of Big-Oh notation in real analysis, as Landau is known to have used Big-Oh notation between the world wars [12].

VI. Exploring the Discretization Error

It turns out that the error can be explored very precisely, independent of the notions of "amenability" which make the proof of the main theorem a bit complicated. All that is needed is to extend the Taylor polynomial a few extra terms, and calculate a particular double summation. We begin again, with Taylor's Theorem, but now with extra terms:

$$f(t+\delta_1 h) = f(t) + \sum_{i=1}^{i=n+4} \frac{\delta_1^i h^i}{i!} f^{(i)}(t) + \mathcal{O}\left(h^{n+5} f^{(n+5)}(t)\right)$$

and now sum this over all n data points

$$\sum_{j=1}^{j=n} c_j f(t+\delta_j h) = \sum_{j=1}^{j=n} c_j f(t) + \sum_{j=1}^{j=n}\sum_{i=1}^{i=n+4} \frac{c_j \delta_j^i h^i}{i!} f^{(i)}(t) + \mathcal{O}\left(h^{n+5} f^{(n+5)}(t)\right) \quad (1)$$

and from the double summation in Equation (1) you can see that the coefficient of $h^i f^{(i)}(t)$, to be denoted E_i, is given by

$$E_i = \sum_{j=1}^{j=n} \frac{c_j \delta_j^i}{i!}$$

We start with Taylor's Theorem, restricted to seven terms, which is

$$f(t+h) = f(t) + hf'(t) + \frac{h^2}{2}f''(t) + \frac{h^3}{3!}f'''(t) + \frac{h^4}{4!}f^{(4)}(t) + \frac{h^5}{5!}f^{(5)}(t) + \frac{h^6}{6!}f^{(6)}(t) + \mathcal{O}\left(h^7 f^{(7)}(t)\right)$$

and apply this to each of $a \in \{0, -h, -2h, -3h, -4h\}$ and thus obtain

$$\begin{aligned}
f(t-4h) &= f(t) - \frac{4}{1!}hf'(t) + \frac{16}{2!}h^2f''(t) - \frac{64}{3!}h^3f'''(t) + \frac{256}{4!}h^4f^{(4)}(t) - \frac{1024}{5!}h^5f^{(5)}(t) + \frac{4096}{6!}h^6f^{(6)}(t) + \mathcal{O}\left(h^7f^{(7)}(t)\right)\\
f(t-3h) &= f(t) - \frac{3}{1!}hf'(t) + \frac{9}{2!}h^2f''(t) - \frac{27}{3!}h^3f'''(t) + \frac{81}{4!}h^4f^{(4)}(t) - \frac{243}{5!}h^5f^{(5)}(t) + \frac{729}{6!}h^6f^{(6)}(t) + \mathcal{O}\left(h^7f^{(7)}(t)\right)\\
f(t-2h) &= f(t) - \frac{2}{1!}hf'(t) + \frac{4}{2!}h^2f''(t) - \frac{8}{3!}h^3f'''(t) + \frac{16}{4!}h^4f^{(4)}(t) - \frac{32}{5!}h^5f^{(5)}(t) + \frac{64}{6!}h^6f^{(6)}(t) + \mathcal{O}\left(h^7f^{(7)}(t)\right)\\
f(t-1h) &= f(t) - \frac{1}{1!}hf'(t) + \frac{1}{2!}h^2f''(t) - \frac{1}{3!}h^3f'''(t) + \frac{1}{4!}h^4f^{(4)}(t) - \frac{1}{5!}h^5f^{(5)}(t) + \frac{1}{6!}h^6f^{(6)}(t) + \mathcal{O}\left(h^7f^{(7)}(t)\right)\\
f(t-0h) &= f(t)
\end{aligned}$$

and therefore we can, with much effort and patience, substitute those formulae into

$$\begin{aligned}
&\frac{1}{4}f(t-4h) - \frac{4}{3}f(t-3h) + 3f(t-2h) - 4f(t-h) + \frac{25}{12}f(t)\\
&= \left[\left(\frac{1}{4}\right)(1) - \left(\frac{4}{3}\right)(1) + (3)(1) - (4)(1) + \left(\frac{25}{12}\right)(1)\right] f(t)\\
&\quad + \left[\left(\frac{1}{4}\right)\left(\frac{-4}{1!}\right) - \left(\frac{4}{3}\right)\left(\frac{-3}{1!}\right) + (3)\left(\frac{-2}{1!}\right) - (4)\left(\frac{-1}{1!}\right) + \left(\frac{25}{12}\right)\left(\frac{0}{1!}\right)\right] hf'(t)\\
&\quad + \left[\left(\frac{1}{4}\right)\left(\frac{16}{2!}\right) - \left(\frac{4}{3}\right)\left(\frac{9}{2!}\right) + (3)\left(\frac{4}{2!}\right) - (4)\left(\frac{1}{2!}\right) + \left(\frac{25}{12}\right)\left(\frac{0}{2!}\right)\right] h^2f''(t)\\
&\quad + \left[\left(\frac{1}{4}\right)\left(\frac{-64}{3!}\right) - \left(\frac{4}{3}\right)\left(\frac{-27}{3!}\right) + (3)\left(\frac{-8}{3!}\right) - (4)\left(\frac{-1}{3!}\right) + \left(\frac{25}{12}\right)\left(\frac{0}{3!}\right)\right] h^3f'''(t)\\
&\quad + \left[\left(\frac{1}{4}\right)\left(\frac{256}{4!}\right) - \left(\frac{4}{3}\right)\left(\frac{81}{4!}\right) + (3)\left(\frac{16}{4!}\right) - (4)\left(\frac{1}{4!}\right) + \left(\frac{25}{12}\right)\left(\frac{0}{4!}\right)\right] h^4f^{(4)}(t)\\
&\quad + \left[\left(\frac{1}{4}\right)\left(\frac{-1024}{5!}\right) - \left(\frac{4}{3}\right)\left(\frac{-243}{5!}\right) + (3)\left(\frac{-32}{5!}\right) - (4)\left(\frac{-1}{5!}\right) + \left(\frac{25}{12}\right)\left(\frac{0}{5!}\right)\right] h^5f^{(5)}(t)\\
&\quad + \left[\left(\frac{1}{4}\right)\left(\frac{4096}{6!}\right) - \left(\frac{4}{3}\right)\left(\frac{729}{6!}\right) + (3)\left(\frac{64}{6!}\right) - (4)\left(\frac{1}{6!}\right) + \left(\frac{25}{12}\right)\left(\frac{0}{6!}\right)\right] h^6f^{(6)}(t) + \mathcal{O}\left(h^7f^{(7)}(t)\right)\\
&= 0f(t) + 1hf'(t) + 0h^2f''(t) + 0h^3f'''(t) + 0h^4f^{(4)}(t) - \frac{1}{5}h^5f^{(5)}(t) + \frac{1}{3}h^6f^{(6)}(t) + \mathcal{O}\left(h^7f^{(7)}(t)\right)\\
&= hf'(t) - \frac{h^5}{5}f^{(5)}(t) + \mathcal{O}\left(h^6f^{(6)}(t)\right)
\end{aligned}$$

allowing us to finally conclude (by dividing both sides by h) that

$$\frac{1}{h}\left[\frac{1}{4}f(t-4h) - \frac{4}{3}f(t-3h) + 3f(t-2h) - 4f(t-h) + \frac{25}{12}f(t)\right] = f'(t) - \frac{h^4}{5}f^{(5)}(t) + \mathcal{O}\left(h^5f^{(6)}(t)\right)$$

and while this was not the shortest calculation in human history, since $t \approx 10^{-3}$ or 10^{-4} in most cases, then h^4 makes the error *completely* negligible. That is, of course, provided that the fifth derivative of $f(t)$ is not huge, which is why $f(t) = \sin\left(10^6 t\right)$ cannot be used here. This will be sorted out in the appendices via Lemma 1.

Fig. 3. An Elementary Approach to Proving the "main example," suitable for an undergraduate who has taken one year of calculus.

which is a sum that can be computed, either with a pencil or a computer algebra package. In fact, if one adopts the syntax convention that the 0th derivative of $f(t)$ is $f(t)$ itself, and that 0!=1, then this remains true for the first sum to the right of the equal sign as well, in Equation (1).

Using this, we can compute the following for the "main example" of the paper:

$$\begin{aligned}\frac{1}{h}&\left[\frac{1}{4}f(t-4h)-\frac{4}{3}f(t-3h)+3f(t-2h)-4f(t-h)+\frac{25}{12}f(t)\right]\\ &= 0f(t)+1tf'(t)+0h^2f''(t)+0h^3f'''(t)+0h^4f^{(4)}(t)\\ &\quad -\frac{1}{5}h^5f^{(5)}(t)+\frac{1}{3}h^6f^{(6)}(t)-\frac{13}{42}h^7f^{(7)}(t)+\frac{5}{24}h^8f^{(8)}(t)\\ &\quad -\frac{9}{80}h^9f^{(9)}(t)+\mathcal{O}\left(h^{10}f^{(10)}(t)\right)\end{aligned}$$

and the SAGE code that did this is given in the next section. Keep in mind that $h = 10^{-4}$ is a common value, so the h^6th and higher terms are *completely* negligible.

VII. Exploring the Impact of Noise

The above work is all performed under the assumption that the functions are evaluated without error (e.g. a computer simulation.) Errors in function evaluation can be noise in the data (due to instrumentation issues), or rounding error. This is distinct from the discretization error that the paper principally addresses. However, because both rounding error and instrumentation error are inescapable to some degree, we will now explore their impact on the accuracy of these methods.

Suppose a particular evaluation of f is off by a relative error of ϵ. Then we can replace $f(t)$ with $(1+\epsilon)f(t)$. To be general, we can select any of the $f(t+h\delta_i)$. Then we have

$$\frac{1}{h^k}\left[\sum_{i=1}^{i=n}c_if\left(t+h\delta_i\right)\right]$$

...becomes...

$$\begin{aligned}&\frac{1}{h^k}\left[c_j(1+\epsilon)f(t+h\delta_j)+\sum_{i=1,i\neq j}^{i=n}c_if\left(t+h\delta_i\right)\right]\\ &= \frac{1}{h^k}\left[c_jf(t+h\delta_j)+c_j\epsilon f(t+h\delta_j)+\sum_{i=1,i\neq j}^{i=n}c_if\left(t+h\delta_i\right)\right]\\ &= \frac{c_j\epsilon}{h^k}f(t+h\delta_j)+\frac{1}{h^k}\sum_{i=1}^{i=n}c_if\left(t+h\delta_i\right)\end{aligned}$$

And so the absolute induced error is

$$\text{absolute error} = \frac{c_j\epsilon f(t+h\delta_j)}{h^k}$$

and under the quite reasonable assumption that all the f's are of approximately the same magnitude, then the relative error is

$$\text{relative error} = \left(\frac{\epsilon}{h^k}\right)\left(\frac{c_j}{\sum_{i=1}^{i=n}c_i}\right)$$

As you can see from that formula, the dominant effect will be that the relative instrumentation or rounding error is magnified by a multiplicative factor proportional to h^{-k}. Since $k > 1$, then using too small h will make any errors of these kinds catastrophic.

In Section V, we calculated that the error for the backward-difference formula was proportional to $(h/2)f''(t)$, and for the "main example" it was proportional to $(h^4/5)f^{(5)}(t)$. This means a user of the main example who uses $h = 0.001$ can, under the assumption that $f''(t) \approx f^{(5)}(t)$ have the same discretization error as a user of the backward difference formula and $h = 4 \times 10^{-13}$. Likewise, for $h = 0.01$ in the main example, it is equivalent to using $h = 4 \times 10^{-9}$.

But, the consequences of this would be that instead of an instrumentation error being multiplied by a factor of 1000, it would be multiplied by trillions or billions.

Rounding error in computer systems using only `double` floating-point numbers, to say nothing of `long double`, are on the order of 2^{-53} or $10^{-15.9545\cdots}$ and so a magnification of $1000\times$ is acceptable, while a magnification of several trillion is not.

On the other hand, most scientific instruments are not capable of more than 4 significant digits, and so very large h, e.g. $h \approx 0.1$ should be chosen, to keep instrumentation error low.

VIII. Sample SAGE Code

The following SAGE code will execute the algorithm given in Figure 2 as well as the error modeling as described in Section VI. As you can see, the former is just a matrix computation, though A has a very special form, and the latter is just a double summation. The proof of correctness is in the appendices. This SAGE code was used to produce the formulas found in Figure 1.

More information about SAGE can be found at [2].

```
n=5
k=1
d=[-4,-3,-2, -1,  0];
debug=false

# don't modify what comes below this point.

A=matrix(QQ, n,n);
b=matrix(QQ, n,1);
for i in range(0, n):
    b[i]=0
    for j in range(0, n):
        A[i, j] = d[j]^(i)
b[k]=factorial(k)
c=A.inverse()*b

if (debug==true):
    print "The Matrix A:"
    print A
    print "The Vector b:"
    print b
    print "The Vector c:"
    print c

for i in range(0, n):
    print "f(t + (",
    print d[i],
    print ")h) is multiplied by ",
    print c[i]
```

```
print "To yield:"

for i in range(0,n+5):
    answer=0;
    for j in range(0,n):
        answer += c[j-1] * (d[j-1]^i) / factorial(i)
    if (i>0):
        print "For t^%d times %dth derivative:" % \
                                ((i-k),i),
    else:
        print "For t^%d times the function: " % \
                               (i-k),
    print answer
```

Note that the `c[j-1]` has a $j-1$ because the computer language "Python," upon which SAGE is built, numbers its array entries with the first component being 0 and not 1, likewise `d[j-1]`.

IX. Prior and Related Work

In order to demonstrate the obscurity of these methods, as well as to give the reader further reading, a survey now follows which covers the most famous textbooks that would be used in a first-year graduate course in *Numerical Analysis* or a senior-year course for undergraduates at a highly-ranked university.

In [14, Ch. 5.7], usually the surest refuge of interesting and rarely known algorithms, there is a discussion of numerical derivatives, but there is no mention whatsoever of formulas which avoid data points in the future, or even derivatives taken with more than 3 evaluations of $f(t)$, nor methods for second derivatives.

On the other hand, in [3, Ch. 5.4] the general technique of this paper is almost, but not quite, discussed under the title "method of undetermined coefficients," a name which numerous mathematical techniques share. That book does not cover the case of irregularly spacings, and only considers first and second derivatives. It makes no allowance for formulas which avoid data points in the future. They include formulas with 5 evaluations of $f(t)$, but none with more than 5 evaluations. The solving for the coefficients is not treated as a matrix problem, and so it is unsurprising that they miss the connection with Vandermonde matrices.

The text [9, Ch. 4.9] does provide formulas for numerical differentiation, including formulas with 5 evaluations to $f(t)$ but none with more. They do consider formulas which only refer to data points on one side of t—the only book the author found to have done so. They only consider the first and second derivative, and sadly, the formulas are not derived at all, to say nothing of rigor. This is perhaps understandable, as this text was written to be the "soft core" version of the following book, by the same authors.

Meanwhile, [6, Ch. 4.1] is the "hard core" version of the book in the previous paragraph, by the same authors. The formulas are derived, but much differently (using Lagrange Polynomials), and the authors restrict to the case of f' and f'' only. They do consider formulas with 5 points, but none larger, and they say nothing about formulas using only past and present but not future points.

While all the books previously mentioned ignore derivatives above the second, the text [7, Ch. 4.3] does go higher, and does do non-symmetric spacings of the data. The derivation there is from the Taylor Series, but that book does not consider formulas using only past and present but not future points.

Last but not least, the classic [13, Ch. 7] has a section on numerical differentiation, but no mention of formulas with irregular spacing, nor those that do not require knowledge of the future. It also does not consider those formulas that utilize more than 3 points.

The approach to handling noisy data was taken from [4].

Acknowledgments

The author would like to thank the National Science Foundation, Division of Mathematical Sciences, for Grant Number # `DMS-0821725`, awarded to Prof. William Stein and the SAGE community, as SAGE played a pivotal role in this research. This includes certain computational resources at the University of Washington in Seattle which Prof. Stein permitted the author to use, including for simulations.

The author would also like to thank Prof. Peter Wolfe, of the University of Maryland Department of Mathematics, who taught him *Numerical Analysis*, and whose perspective on the subject in general has guided this researcher's work on several topics.

Appendix

The appendices do not fit within the 7-page requirement of the conference, but can be found in the full version of the paper, available on the author's webpage. The URL is found on the front page of this paper.

References

[1] Maple. Software Package. Available at http://www.maplesoft.com/
[2] SAGE. Software Package. Available at http://www.sagemath.org/
[3] Kendall Atkinson and Weimin Han. "Ch. 5.4.2: Numerical Differentiation via The Method of Undetermined Coefficients." *Elementary Numerical Analysis*, 3rd ed. John Wiley and Sons. 2004.
[4] as above, but "Ch. 5.4.3: Effects of Error in Function Values."
[5] R. Creighton Buck. "Ch 3.5: Taylor's Theorem." *Advanced Calculus.* McGraw-Hill Book Company. 1978.
[6] Richard Burden and J. Douglas Faires. "Ch 4.1: Numerical Differentiation." *Numerical Analysis*. 8th ed. Thomson, Brooks and Cole. 2005.
[7] Ward Cheney and David Kincaid. "Ch. 4.3: Estimating Derivatives and Richardson Extrapolation." *Numerical Mathematics and Computing*. 6th ed. Thomson, Brooks and Cole. 2008.
[8] Christopher Dyer. *Standards of Living in the Later Middle Ages*. Cambridge University Press, 1989.
[9] J. Douglas Faires and Richard Burden. "Ch. 4.9: Numerical Differentiation." *Numerical Methods*. 3rd ed. Thomson, Brooks and Cole. 2003.
[10] Elizabeth Gemmill and Nicholas Mayhew. *Changing Values in Medieval Scotland: A Study of Prices, Money, and Weights and Measures*. Cambridge University Press. 1995.
[11] Gene Golub and Charles van Loan. "Ch. 4.6: Vandermonde Systems and the FFT." *Matrix Computations.* 3rd ed. Johns Hopkins University Press. 1996.
[12] Edmund Landau. *Foundations of Analysis.* 1930.
[13] Francis Scheid. "Ch. 7. Numerical Differentiation." *2000 Solved Problems in Numerical Analysis (Schaum's Solved Problem Series)*. McGraw-Hill. 1990.
[14] William Press, Saul Teukolsky, William Vetterling, and Brian Flannery. "Ch 5.7: Numerical Derivatives." *Numerical Recipes in C*. 2nd ed. Cambridge University Press. 1992.

Electrification of Chassis using Motor Assisted Differential and Reverse Motion System

[1]Gautham Thyagarajan
Dept. Of Mechanical Engineering, Wayne State University, Detroit, MI 48202

Abstract— *There has been increasing interest for manufacturers to produce hybrid vehicles. This is due to high pollution levels, increasing fuel prices, and customer demands of fuel efficient vehicles. Similarly there is interest in use of electrical components instead of mechanically operated ones in automobiles. Mechanical differential is used in automobiles for providing torque transmission through 90 degrees from the engine drive shaft to the road wheels. The objective of this paper is to propose the use of electric motors instead of the differential mechanism. The motors are controlled by fuzzy logic rules, and help in electric current generation when the vehicle travels on highways. The objective of elimination of the mechanical differential unit has been fulfilled by simulation in Lab view software, and the results have been discussed in detail. The proposed model helps in weight reduction, ride quality enhancement, part reduction, engine load reduction and decreasing the number of mechanical parts, lowering the manufacturing costs, and decreasing atmospheric pollution.*

Keywords- Fuzzy Logic ,Reduction of mechanical parts, Ease of maintenance, Motor assisted driveline

1. Introduction

In the present world of automotive technology, alternative techniques to conserve energy and save fuel have been of key importance. This has led to the reduction of mechanically driven components. This has helped to reduce the curb weight of the vehicle. The reduced load on the engine gives better fuel economy. In this paper, a model of a vehicle is proposed where electric motors are used to drive the rear set of wheels. This eliminates the use of differential mechanism. The components of an all wheel drive vehicle chassis are shown in Fig.1.

1. **Chassis frame**: This supports all the components of the vehicle and also holds the body shell.
2. **Steering mechanism**: This is used to steer the vehicle in any desired direction. Left or right.
3. **Axles**: These components hold the wheels to the chassis
4. **I.C.engine**: converts chemical energy of the combustible fuel in to mechanical energy in the form of torque.
5. **Clutch:** This component engages and disengages the engine torque from the gear box. This can be manual foot operated or hydraulic in the form of a torque converter.
6. **Gear box**: This component which provides variable torque to the road wheels and also facilitates the reverse motion of the vehicle through the reverse idle shaft.
7. **Drive/propeller shafts**: These components transmit the torque to the road wheels. These are dependent on the kind of drive, either front wheel drive or rear wheel drive, or all wheel drive.

Using Electric motors instead of the differential may increase the fuel efficiency of the vehicle. Using fuzzy logic, a control strategy has been developed for assisting the vehicle in various drive modes such as turning, forward motion or backward motion, by providing required torque through drive motors. Steering angle sensors are used to monitor the various driving modes, which triggers signal to the motor to provide the required torque.

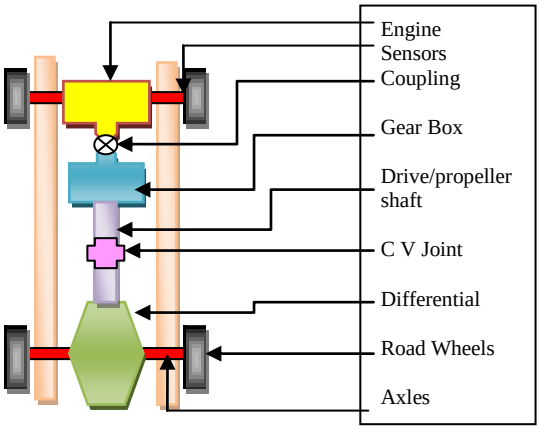

Fig.1. Driveline layout for an all wheel drive automobile.

2. Comparison/ case study

2.1 Proposed model

In this section the comparison of the proposed model and its benefits over the Hybrid vehicles of various manufacturers is done. Some of the popular models of hybrid vehicles in the current market include the Toyota Highlander, Toyota Prius, Ford Escape Hybrid, and Chevrolet Volt, etc. The primary intend of this proposed model is to reduce the use of engine power and increase the role of motors. In the proposed model, electric motors fitted to the rear wheels of the vehicle, spin the wheels in the reverse direction. This eliminates use of reverse gear and thus engine power. This

model has not been brought in to production by any of the manufacturers. The results of simulation show that at optimal load conditions (250Lbs of passenger weight) the vehicle can travel up to a 36Mph speed without the assistance of the internal combustion engine. Even for vehicles with large curb weight, when the proposed model is incorporated, reduces the use of internal combustion engine. There is an automatic control for switch over between battery and engine takeover. The various modes of operation are described as follows.

2.1.1 Motor powered propulsion

Here the batteries alone are in charge of driving the vehicle in forward direction through the electric motor. **2.1.2 Engine powered propulsion**

Here the engine alone is responsible for propelling the vehicle. This stage is only for the forward motion.

2.1.3 Motor assisted turning

In this mode, the proposed model will assist the engine by spinning the rear outer wheel at a speed (in RPM) greater than that of the inner wheel.

2.1.4 Motor assisted reverse motion

In this mode the batteries through electric motors shall propel the vehicle in the reverse direction. Here again, the engine does not have any role in propulsion. This is a unique feature of the proposed model as compared to other vehicles in the market.

2.1.5 Combined propulsion

In this mode the motors assist the engine in propulsion. This reduces the load on the engine. This mode is usually activated when the vehicle is cruising on the highways.

2.2 Toyota highlander.

In these vehicles, the gearboxes have a reverse idler shaft. This shaft engages to the drive shaft and spins in a parallel axis. This reverses the direction of spin of the gearbox output shaft. Toyota Highlander, being a SUV, has a higher curb weight as compared to other vehicles listed in Table.1.

And engine modes. There cannot be a constant monitor for limiting the use of engine, unless conservatively used.

2.3 Ford escape hybrid

The Ford Escape Hybrid is a smaller SUV as compared to the Highlander and has lesser fuel consumption. It has a reverse gear mechanism in the gear box. It also has a rear wheel drive mechanism. Table.1.shows the comparison of various features of the proposed model with other leading brands. In this paper, Toyota Highlander and Ford Escape Hybrid are taken as the Baseline models. Improvement is proposed with respect to the current vehicles. Both of these vehicles use a differential mechanism.

TABLE.1.
COMPARISON WITH MANUFACTURERS

MAKE	**PROP MDL**	**T.P**	**F.E.H**	**T.HL**	**CH.V**
DRIVE	F+/ALL	F	ALL	ALL	F
CTRL (control)	EM+ ENG	EM+ ENG	EM+ ENG	EM+ ENG	EM / ENG
FWD (forward)	EM/ ENG	EM	EM	EM	EM/ ENG
REV (reverse)	EM	EM / ENG	EM / ENG	EM / ENG	EM / ENG
Change Over (mph)	36	25	21	20	28
Gearbox	5F/1R	5F/1R	5F/1R	5F/1R	1F 1R
Default Drive	4WD	2WD	4WD	4WD	2WD
Charging. (MPH)	40	45	30	55	Engine Drive Mode

3. Proposed electrical assisted mechanism:

This proposed technology as shown in Figs.2, 3 and 4, helps to run the vehicle with an internal combustion engine transmitting the primary drive to the front wheels. With the assistance of two motors, the rear wheels are powered. This is controlled by a computer controlled chip. These motors are powered by a battery. The motors also work as generators in charging the battery once the vehicle attains a set speed of 50Mph. Steering angle sensors are located on the front wheels as shown in Fig.1.They determine the steering angle or angle of rotation of the front wheels. The sensors give continuous feedback to the chip controlling the motors. When the vehicle is steered to more than a preset angle of+/- 25 degrees with respect to the axis of the wheel, normal to the axle, the diagonally opposite motor is activated to drive the rear wheel. If the front left side road wheel is turning at an angle more than +/-25 degrees with respect to the wheel axis, the rear right side motor drives the wheel at a speed faster than the front left wheel. This makes the turn more efficient and decreases the load on the engine.

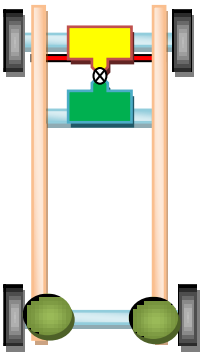
Fig.2.Normal motion.

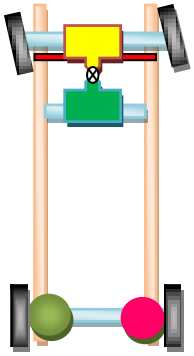
Fig.3. Left turn.

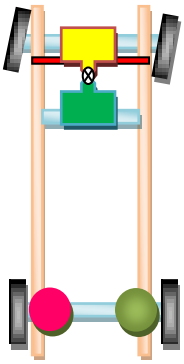
Fig.4. Right turn

As the vehicle is accelerated, both motors in the rear assist the engine by supplying additional torque to the rear wheels. If the vehicle is trapped in snow or sand, and is being unable to be pulled out, the motors also assist by supplying additional torque "pull out". The simulation of the pull out is done using Lab View software.

4. Implementation of fuzzy logic:

Fuzzy logic is a thought process [1]. The implementation of fuzzy logic is carried out by assigning with IF –Then conditional rules.

4.1 Setting input and output parameters

The battery current "I", engine power "W", speed of the vehicle in Mph known as "S", Speed of the engine in RPM known as "N" (in this paper), steering angle with respect to the wheel axis, normal to the axle of the vehicle denoted by "A", are the input parameters. Battery charging "C" motor speeds "M1&M2", and control "Y" are the output parameters.

4.2 Role of driver behavior

Driver behavior plays a very important role in deciding upon the ride condition, engine load and fuel consumption. Each person has a different driving pattern. Some drivers accelerate the engine suddenly while others accelerate slowly. The driving pattern affects the fuel economy of a vehicle as well.

4.3 Logic involved.

The chip controlling the vehicle has been programmed to respond to driver inputs. It provides the required acceleration according to that situation. The implementation of fuzzy logic is carried out in three stages.

4.4 Stage1.

In the first stage, the control strategy is implemented with the engine power "W" and Battery current "I" as input parameters. The primary source of power of the vehicle is the engine. As the engine runs, the battery is charged through the generator. If-Then conditional rules in Fuzzy Logic are implemented for "I" and "W". Mamdani method [4] is used to implement the conditional rules. Engine power and generator current are considered as the input parameters. Battery current "charging" is the output parameter. Membership functions are Null, Initializing, and Charging. These are related to the generator speed. Charging is again dependent on the Engine RPM. Battery state of charge and electrical output are very important for determining the switch over between motor and engine to propel the vehicle. Battery is responsible to power the motors which assist the engine. Having this in consideration, the rules are assigned using fuzzy logic. This is shown in Fig.5. If – Then conditional rules [4] are assigned to the membership functions.

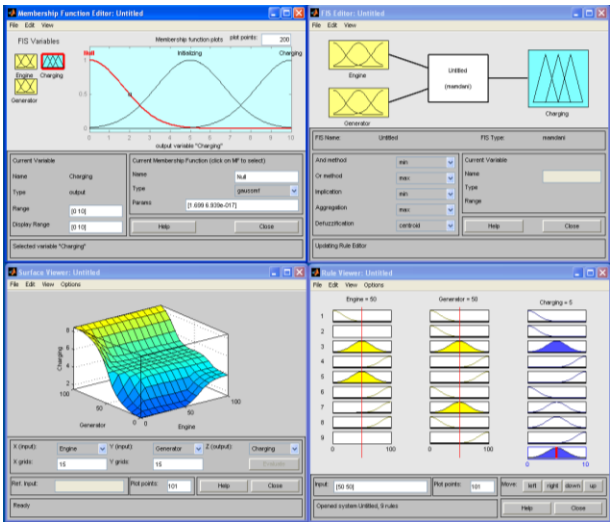
Fig.5. Implementation of fuzzy logic on engine and generator.

4.5 Stage 2.

The second stage of the work focuses on acceleration and power as parameters for the chip to control. The acceleration is assigned with three membership functions, according to driver behavior. They are low medium and high (or) hard acceleration. The fuzzy logic set of rules is applied to provide a steady response from the chip. This is shown in Fig.6. The control is featured on sustaining, acceleration and deceleration of the vehicle.

4.5.1 Engine power calculation

Brake horse power, Indicated horse power and Frictional horse power are the primary measures of engine power. The Brake horse power for any vehicle can be calculated by the relation [7]

$$P = \frac{\tau\,(\text{ft.lbf}) * \text{RPM}}{5252}. \qquad (1)$$

Where P is power in HP, τ is torque, and RPM is rotations/ minute.

The constant 5252 is taken from (33,000 ft-lb/min)/ (2π rad. /rev.).The standard equation relating torque {in-lbf}, speed in RPM and horsepower is [7]

$$P = \frac{\tau\ (\text{in.lbf})^* \text{RPM}}{63025} \quad . \qquad (2)$$

4.6 Stage 3.

Coming to the third stage of the work, we consider the steering angle which is the angle of rotation of the wheel with respect to its axis. Here the measurement is taken in angles between 0 to 180 degrees. When the driver executes a turn, the motor of the diagonally opposite wheel has to spin faster.

Input parameter is the Steering angle. The output parameters are the rear left and right side motors. Apart from assisting the engine by spinning the rear outer wheels faster during turning, these motors provide high torque for the vehicle in forward and reverse motion. It relieves the engine from taking additional load.

The gearbox of this model proposed, is lighter in weight than those used in other models. It does not use reverse mechanism.

The motors can also provide assistance to the engine when power demand is high. Once the vehicle attains a speed of 50Mph, the battery recharging begins. This helps save a significant amount of energy. Fig.6. shows the implementation of fuzzy logic over the steering angle, acceleration, and gear. Steering angle is a vital indicator for determining the activation of motors fixed to the rear wheels of the automobile. Depending on the angle of turn the respective outer wheels turn faster.

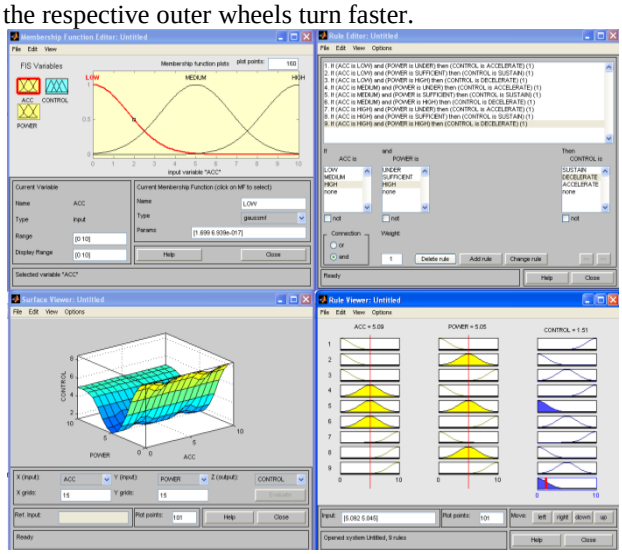

Fig.6. Acceleration and power to set control over vehicle drive.

The gear is selected for assigning the If-Then conditional rules. The conventional automatic transmission has 6 preset modes, called the P, R, N, D 2, & 1 respectively. On selecting the appropriate gear the rules are assigned for the motors in the rear of the vehicle.

The proposed model implemented for the prototype vehicle is shown in the Figs.2, 3, and 4 respectively. The figures depict the presence of motors attached to the rear wheels, and the turn mechanism.

In case of the left /right turn, the associated motor (indicated in red) drives the outer wheel faster.

Moreover, this eliminates the use of differential mechanism and the propeller shafts and universal joints, [5] thus reducing chassis weight.

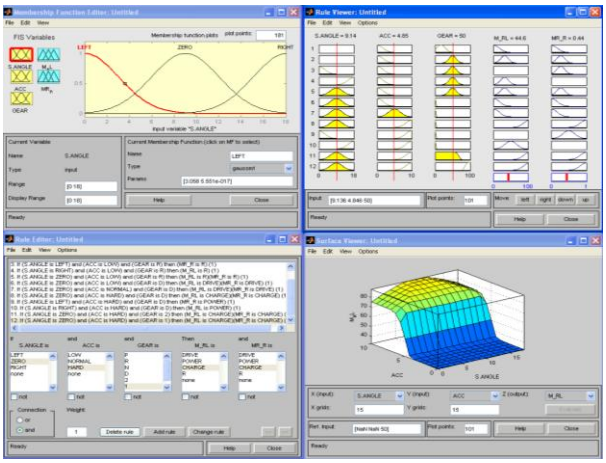

Fig.7. Steering angle, acceleration, & gear v/s rear drive motors.

Fig.2shows the normal motion which is either the engine, shown by the yellow block, and (or) driven by the motors shown in light green oval shape near the rear wheels of the vehicle. Fig.6. and Fig.7 are the two stages where the differential action is carried out by the electric motors when the vehicle negotiates a left and a right turn respectively. The motor is responsible for providing additional torque to the outer road wheel to spin faster from the inner wheel. This is indicated by the red oval shape depicting an electric motor.

Simulation of the above is carried out in LABVIEW software. The screen is prepared for various controls and dials, and indicators showing the exact function like in a real automobile.

5. Lab view implementation

The proposed model is now simulated in Lab view. Each and every stage is run to simulate the working. The ignition switch is turned on at the beginning. This activates the entire system. Further the steering is set to rotate in angles of 2 degrees increment on either side, within a range of -60 to +60 degrees as shown in Fig.8. Boolean function is assigned to the LED indicators showing the state of battery charge, motor rotation in forward and reverse directions, for front and rear and also for overload and low battery conditions. [3]

5.1 Screen layout.

State of charge of battery is indicated and with a low passenger load and low acceleration set, the simulation is thus recorded. Slider function in Lab view software is used. The need to vary the load and battery state parameters had to be visualized. As proposed in the paper, as the prototype vehicle attains speed, the system begins to charge up the battery. It is seen that both the motors propel the vehicle. The engine is relieved of rendering more power for propelling the vehicle.

5.2 Simulation of turns

For turning left, the driver steers the wheel to the left side, for more than an angle of 20degrees.The motor in the right rear side begins to propel the right rear wheel faster. If the steering is turned to the right and the 20 degree angle barrier is exceeded. Thereby the rear left side motor will spin faster. This is shown in Fig.10.

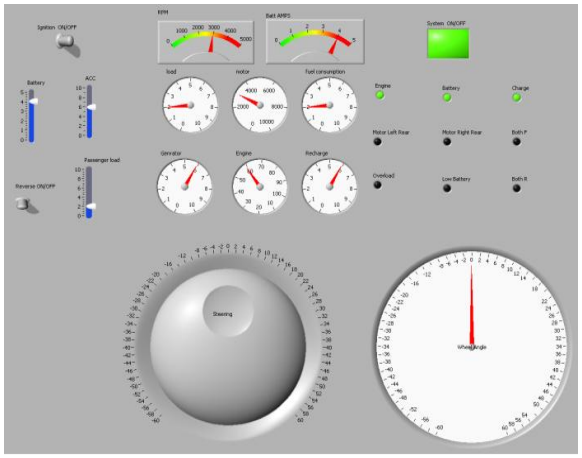

Fig.8.Labview screenshot of systems switched on.

5.3 Quality demand

When a vehicle is set to be in the mass production line, it needs to render a good durability. In other words the performance of the vehicle must not be unsatisfactory to the operator. This is even after various loading conditions, and driving through tough terrains. Structural reinforcement of the chassis needs to be done so that the durability increases. [6]

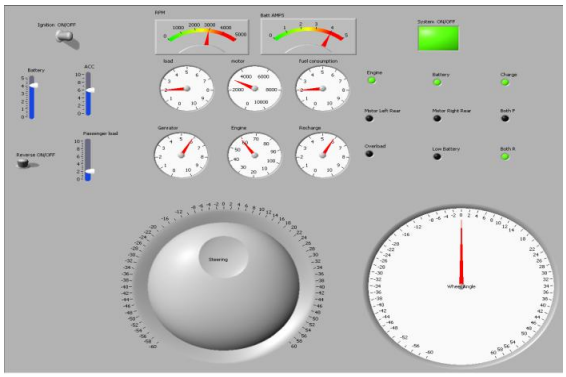

Fig.9.Labview screenshot of reverse motion engaged.

5.4 Simulation of Reverse motion

As shown in Fig.9 when the simulation is set to engage in reverse mode. The engine automatically cuts off. During this time, the electrical energy in the battery is provided to the motor. The Fuzzy logic rules make the motor spin in the opposite direction. Battery current is alone responsible for propelling the vehicle in this mode. The advantage of this system is that a great amount of fuel is conserved. Usually when the reverse gear is engaged the drive shaft of the gear box in any automobile has to transfer torque to the reverse idler shaft to achieve reverse motion. Mechanical power is lost in this action. Reverse gear requires more torque. Implying, more power has to be generated.

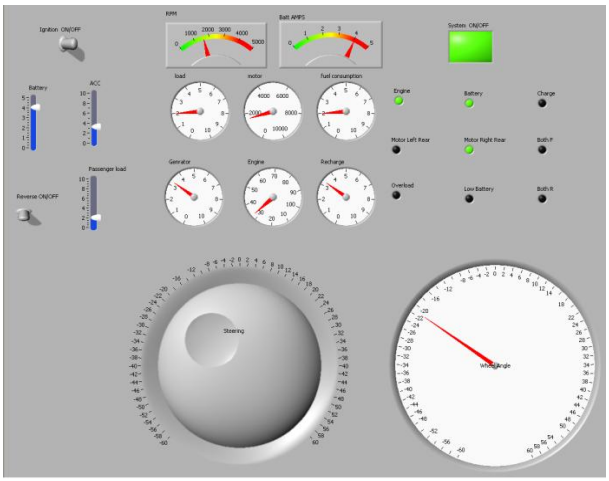

Fig.10. Lab view screenshot of turn

6. Mathematical evaluation

In vehicles using differential mechanism, the torque reduction starts right from the gearbox. Compound gear system is used here. This is similar to the gearboxes used in Ford Escape Hybrid, and Toyota Highlander Hybrid. Fig.11.shows the front view of a gear box.

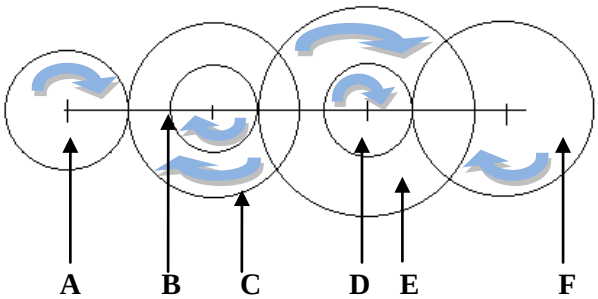

Fig.11. Front cross section of a gear box

A, B, C, D, E, and F are the gear wheels for providing various torque. Each of these will be having a number of gear teeth. A is the gear wheel connected to the input shaft of the gear box. F is the output shaft connected to the same. Gear wheel F is attached to the input shaft of the Gear box.

The speed ratio of gear wheel A to Gear wheel F is calculated by using the relation

In our case A is the first driver gear, C, and E, are following driver gears, B,D,F are driven gears respectively. Let N be the engine Speed in RPM, which will be transmitted to gear wheel A. Let T be the number of teeth on each gear wheel respectively. Therefore mathematically,

(3)

Let us assume that Na is 1500 Rpm, and the teeth in each gear Ta=20, Tb=50, Tc=25, Td=75, Te=65 respectively. This is similar to the gear teeth count in Ford Escape hybrid and Toyota Highlander Hybrid.

Then using Eqn. (3)

18.75

Therefore Nf = 80 Rpm.

At 1500 Rpm on a test data taken in Toyota Highlander Hybrid, the power available at the flywheel is 55KW. So the power available at the output shaft of the gearbox at 80 rpm is

= 3.4KW power loss at idling.

.

Fig.12.Shows the rear wheel differential mechanism.

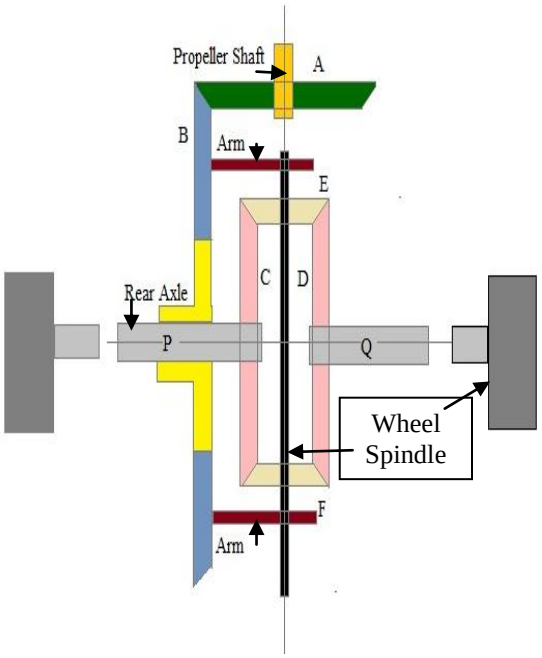

Fig.12. The rear wheel differential in an automobile.

The front Wheels are mounted on separate axles. They are used for steering the vehicle. Therefore the independent wheel speed control is easily achieved. A is the gear wheel attached to propeller shaft of the automobile. Gear B is driven by A, and is called the crown gear. It is free to rotate on the axle P. Gear C is fixed on the end of axle P. Gear D is fixed on axle Q. Gear B has an arm which connects Gears E and F through the spindle. Gears C, D, E, and F are meshed together. Axles P and Q are split by the meshed gears C,D,E ,and F which allows them to rotate at different speeds respectively. Axles P and Q are connected to the rear wheels of the automobile.

Table 2 shows a typical differential table of motion. Calculations are made with revolutions made by sun gear and planet pinions. This is shown for various situations of revolution. For calculating the speed of a road wheel as shown inFig.12, attached to axle P and axle Q, we follow the method mentioned below.

Firstly we have to know the speed of the propeller shaft, in RPM. This is the speed of Gear A. We then have to know the number of teeth on Pinion gears A, B, C, and E respectively.

The number of teeth on gear C is same as that on D. Likewise, Gear E and F have the same number of teeth. Speed of gear C will be Speed of Left Wheel. Speed of Gear D Will is the Speed of Right wheel.

TABLE.2.
DIFFERENTIAL TABLE OF MOTIONS.

S. No	Conditions of Motion	Gear B	Gear C	Gear E	Gear D
1	Gear B fixed, Gear C rotated through +1rotation(anti clockwise)	0	+1	—	-1(-Tc/Te)*Te/Td) and Tc=Td
2	Gear B fixed and Gear C rotated through +x revolutions	0	X	X*(Tc/Te)	-x
3	Adding +y revolutions to all elements	Y	Y	+y	+y
4	Total motion	Y	X+Y	Y+x*(Tc/Te)	y-x

7. Derivation of gear speeds.

As mentioned previously, let N be the speed of each gear wheel.T is the number of teeth on each wheel.
From Eqn. (3) as A is the driver gear and B is the driven gear

— — (4)

Which means that Nb = ——— (5)

This helps in calculating the speed of Gear B when Speed of A is known. Further, to calculate the speed of Gear C

(Nb/Nc) = (Tc/Tb) (6)

Which means that Nc = ——— (7)

Nc is the speed of the road wheel P. During normal forward motion of the vehicle Np = Nq. But when the vehicle negotiates a turn, the outer wheel speed has to be greater than that of the inner wheel. In this case, it is necessary to calculate the speed of gear wheel D.

Tc = Td, and Te = Tf (8)

Gear E drives gear C, and therefore the speed of Gear E can be calculated as

(Ne/Nc) = (Tc/Te) (9)

Which means that Ne = ——— (10)

Gear C also drives gear F. Therefore the speed of gear F can be calculated as

(Nc/Nf) = (Tf/Tc) (11)

Which means that Nf = ——— (12)

Gear F drives Gear D. Therefore the speed of gear D which is the speed of right side wheel can be calculated as

(Nf/Nd) = (Td/Tf) (13)

Which means that Nd = ——— {From Eqn. (8)} (14)

As Tc = Td and Te = Tf
But while turning Nd is not Equal to Nc.
Considering a case of a differential mechanism where the number of teeth in Gears A to F is tabulated in Table 3.The engine is presumed to run at 1000 Rpm.

TABLE.3
GEAR TEETH COUNT IN A GEAR BOX

Gear →	A	B	C	D	E	F
No. Of → Teeth	20	60	75	75	25	25

Therefore using Eqn. (5) the speed of Gear B Nb is calculated as

Nb = ——— = (20* 1000) / 60 = 333.33Rpm

From Eqn. (1) the power is a function of torque and Engine speed in RPM.

This explains that when there is a reduction in the RPM, there is a significant decrease in Power. In this case, the Rpm is reduced to 33% when transferred to the differential mechanism.

Now using Eqn. (7) when we calculate the speed of Gear C which is the speed of the rear wheels during forward linear motion of the vehicle, Nc= Nd (in this case)

Nc = ——— = (333.33* 60) / 75 = 266.67 RPM.

Here we can see that only 26.66% of RPM is transferred to the road wheels from the engine. So it is proven that there is a significant amount of speed that is lost in the transmission.

Considering the same case, using Table 2. Which is the table of motions, of a differential gear mechanism, knowing that Ta = 20, Tb = 60, Na = 1000 Rpm, and we assume from above that Nd = 266.67Rpm, and the vehicle is taking a turn.

We know Nb= 333.33Rpm as we have calculated above.
Considering the total motion of Gear B (row 4 in table 2)
We know that Y = 333.33
Axle Q is fixed to road wheel through a shaft which has gear D. And we know that speed of Gear D is 266.67Rpm from above. Therefore from Table 2.Row 4 the total motion of gear D = (Y)-(X)
Therefore Y – X = 333.33 Rpm
Or X = Y – 333.33 Rpm = 266.67 – 333.33
= (- 66.66Rpm).
So Speed of the wheel attached to Axle P is calculated by calculating the speed of Gear C which is taken from the table of motions Table.2. The total motion of Gear C is calculated as X+Y

= -66.67+ 266.67 = 200 Rpm.

Thus it is proved that on taking a turn only 20% of the Rpm is transferred to the inner wheel and 26.67% is transferred to the outer wheel.

Eliminating the use of differential and providing motors that provide additional RPM, at the rear outer wheels of the vehicle is explained as follows.
In the case considered above, at engine speed of 1000Rpm if the Front wheels are spinning at 200 Rpm, and there is NO differential unit, and Let Nf_i and Nf_o = Speed of front inner and outer Wheels Nr_i and Nr_o = speed of Rear inner and outer wheels .80% of Rpm is lost. During Normal motion,

$$Nf_i = Nf_o = Nr_i = Nr_o \quad (16)$$

During taking turns , with the differential unit
In terms of a left turn the rear outer wheel will spin faster

So speed of front inner wheel in total = Nfi + (0.26*Nro)
Where 74% of power is lost due to differential mechanism
Total Speed at 200 rpm of front wheel is 200+ (0.26*200)
= 252Rpm(74.8% of rpm is lost.)
In case of electric motor assisted system, as mentioned earlier, The electric motor assists the engine by providing same Rpm as front inner wheel to the rear outer wheel.

That is, 200+200 = 400 Rpm. In this case at 1000 Rpm of Engine Speed, 60% of Rpm is lost. This accounts for 14.8% of save in Engine speed, which in effect reduces the torque load on the engine and increases power.

8. Conclusion

In this paper, electrification of chassis has been done by elimination of differential mechanism replacing the same with electric motors, which drive the rear wheels of the vehicle.
By implementing a system to eliminate the use of engine and mechanical power and by incorporation of electric machinery to the chassis of the vehicle, a great deal of engine load can be reduced. This improves the ride quality. This also helps in reducing the curb weight of the vehicle. Maintenance is also made easier.

The electrical energy is a renewable source. When used for simulation in the proposed model, a great deal of engine power and fuel usage was reduced. The simulation of the proposed technology has been done in Lab view

act like generators to recharge the battery. This helps in reducing the charging load on the engine. The main purpose of this research work is to reduce the load on the engine. All concepts are proposed in interest of load reduction.

9. References

[1] Milton Martinez: "Fuzzy Logic Controller for TwoMode Parallel Hybrid Electric Vehicle", http://faculty.utep.edu/Portals/1255/Milton.pdf

[2] Fazal U Syed, Dimitar Filev, Hao Ying, "Adaptive Real-Time Advisory System for Fuel Economy Improvement in a Hybrid Electric Vehicle", The 28th North American Fuzzy Information Processing Society Annual Conference (NAFIPS2009), pp 1-7, June 2009

[3] Gary.W.Johnson *Lab VIEW Graphical Programming: Practical Applications in Instrumentation and Control*, pp31-42,55-70,178-214,California, 1997

[4] R.K.Bansal,A.K.Goel,M.K.Sharma *Matlab and its Applications in Engineeering*,pp392-402 Delhi 2009

[5] Nammalwar Purushothaman, James Critchley, Jessica Hulings, Amarendra Joshi : "Durability Analysis for Off Road Vehicle Systems Engineering and Technology Symposium, Modeling and Simulation Testing and Validation (MSTV) Mini Symposium pp 135-137, August 17-19, Dearborn, Michigan 2010

[6] Shaleel .N . Avadhani, Zack M.Anderson, David Diamond, Ross Wendell : " Regenerative Semi Active Shock Absorber Technology for Improved Ride Handling and Fuel Economy on Combat and Tactical Vehicles" NDIA Ground Vehicle Systems Engineering and Technology Symposium, Power and Energy (P&E) Mini Symposium, August 17-19, Dearborn Michigan 2010

[7] John.Bird *Mechanical Engineering Principles* pp109-116, Oxford 2002, http://www.engineeringtoolbox.com/electrical-motors-hp-torque-rpm-d_1503.html

[8] R.S.Khurmi, J.K.Gupta *Theory of Machines* pp428-461Eurasia Publishing House Pvt.Ltd, New Delhi 2005

Economy
on
Combat
and
Tactical
Vehicles"
NDIA
Ground
Vehicle
Systems

IPPD AND LEAN SIMULATION USING VIRTUAL REALITY

Pinkeshkumar Attarwala[1],Sumant Kulkarni[2] ,Suren N. Dwivedi[2]

Department of Mechanical Engineering

University of Louisiana at Lafayette
Louisiana, LA

[1]Pja7518@louisiana.edu

[2]ssk7136@louisiana.edu

[3]snd7483@louisiana.edu

Abstract— **Product development in every industry is the pioneer base to the future. Development of any industry is depending upon several factors, one of the summit and powerful base and factor is product development cycle and implementation. New generation and era demands firm foundation of product development to sustain position in competitive market. Competition forcing companies to maintain their life cycle of product in different stages of growth. Our society expects engineers to develop products that are affordable, functional and sustainable. Effective product realization methods and tools are the answers to these societal expectations**

In this paper, a classical approach to Integrated Product and Process Design and Development and new approach to Integrated Product and Process Design and Development using powerful software packages CAE, CAD and CAME will be discussed. Results reveal that approach to IPPD using VR is more powerful and develop competitively-priced quality products. Last but not the list the end of the paper will cover lean simulation activity using Virtual Reality.

Keywords— **IIPD, VR**

I. INTRODUCTION

The process of creating and making statues has been around since the starting age of humankind. It was implemented first for survival: weapons, shelters, clothing and farming. These implements were improved upon with the appearance of such invention as fire, the wheel, and steel and as time went on they became more substantial and more suave. As evolution of mankind and societies happed from being local one to regional ones, parallel transforming their local economies in to regional ones. In the starting, these transformations took hundreds to thousands of years. Since the start of industrial revolution about 300 years ago, the lopes of development and improvement of devices and artefacts has increased all of the sudden[3].

Thus transformation from primarily local societies to once that must now complete globally has had a very solid influence on the product realization process. It is an environment in which one must compete on cost, quality, performance and time-to-market on a worldwide basis. This requires individuals and companies to examine back how they go about creating product and services and how these products and services can be brought to marketplace. During the last 40 years it has become clear that the way to do this is through an integrated approach to the product realization process. This approach tends to do the following: "plane" organizational structures; involve many more constituencies in the process at the very beginning; place greater emphasis on the customer, product quality, customer and time-to –market; use a large amount of simultaneity in the product realization process; and require organizations to be creative and innovative[3].

In the era of product proliferation there was no international competition involved in product manufacturing. Inventors invented and manufactured their products. In the era of mass production, end customers demanded more functionality in to the products the mass production came in to picture. In the era of mechanization, industries moved to more intricate products. It gained its popularity in taking place of human and animal power. In the era of departmentalization, people used to divide their work and hence barriers developed and productivity decreased. In the era of realization analysing of situation by organizations and close interaction between various group of departments. In the era of global manufacturing companies started customers driven and became more competitive.

These new approaches have been developed to eliminate situations and conditions that resulted in poor corporate performance and poor customer satisfaction. Examples of such conditions like inconsistent product quality; slow response to the marketplace; lack of innovative, competitive service; and inefficient resource allocation. In its place, these new approaches have transformed many companies in to entities that are able to

1) Responding to the customer quick by new innovative ideas and technology into products.
2) Developing and produce product that satisfy customers' requirements.
3) Accustomed to competitive environ.
4) Generate new ideas and combine existing elements to create new sources of value.

At different stages in the evolution of product development in the last decades, various descriptors have been used to indicate that an improved method was being implemented to design and manufacture products. The descriptor that will be used here is the integrated product and process design and development team method.

The classical approach to development of product leads to the many intricacy like involvement of human being in each phase of the creation of the steps while product development.

The starting of product development at adolesce to the mature phase product needs to emphasise on design but, in real sense and practical life is very encumber to emphasize and become unrealistic. Decade later it was found that development of product incurred cost which includes primary design cost and then labour cost which is most unaffordable to bear by any company. Moving from *age of control* to *age of flexibility*, later possible by concurrent engineering (CE) and Continuous Acquisition and Life cycle Support.

The new approach to development of product comes which is superior in all aspect. CAE software being used to development product realization phases.

II. CONVENTIONAL IPPD

Conventional IPPD contain several steps for new product development. The approach is generally involve concurrent engineering.

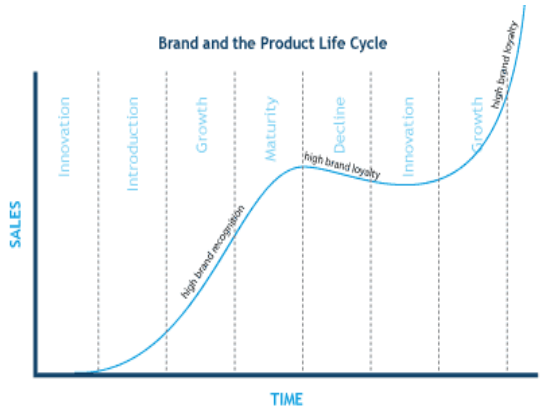

Fig: (A) [2] Product Life Cycle Management by IPPD and various approaches.

Few stages of product life cycle development involves

A) Conceive: Imagine ,innovate
This is first stage of the Product development and it comes through customer i.e. it is customer driven phase.

B) Design: Drawing release, specification, develop
This is major part of any product development and takes huge cost involvement followed by number of design engineers. This phase taking approximate cost of 70% of over all product development.

C) Realize: Manufacturing, physical approach
This phase is basically containing the actual parameter to build any product i.e. physical approach to any product.

D) Service: Manage, support
This phase is also called after sales and support. Generally to maintain good image of any company this phase is useful. This is basically driven by the customers. To maintain life of any product after sales support is needed. This is also called maintenance phase for any product.

In above figure (A), shows how number of changes increased or decreased with different approach to product development in different phases of product development.

i) IPPD approach:

Number of design changes in different phase of product life cycle is decreases exponentially when we use IPPD approach to any product development. This reveals important result if we use IPPD approach one can save 30% [5] of production cost.

ii) Serial Approach:

This approach will show less involvement while initial phase of design but, eventually it hikes to the maximum in number of design changes while we move ahead in various stages of product development. This kind approach is not good for any product development. Design changes in any product incurred huge cost. Repairing or design change cost is approximate one third of the total design cost.

iii) Cost of change graph:

This graph shows the change in the cost while in serial approach and IPPD approach. Cost incurred increasing exponentially.

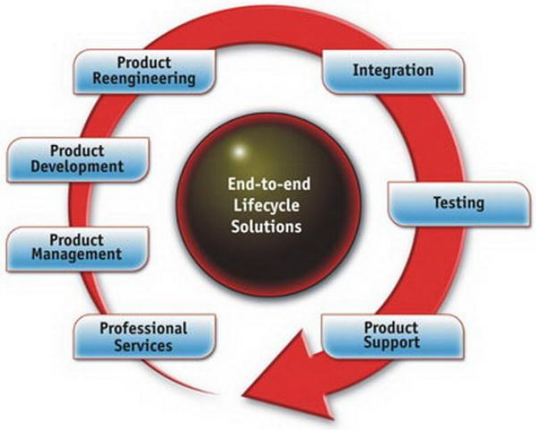

Fig: (B) [2] Product development cyclic process

Above figure (B) indicates, development of any product is not a one time process. This involves cyclic processes from various departments to the resources.

Any process is starts from raw material and eventually ends with the new product development. There is not yet end the process. This is continuous cycle which encircles both customers and company. Company includes all departments in the loop for product development process with embodiment of customers.

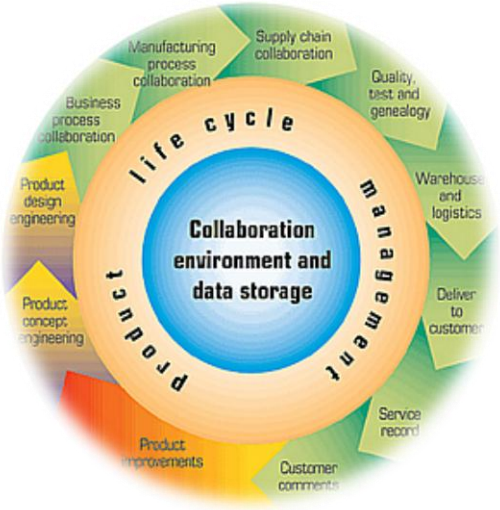

Fig (C) [2]:Generic product life cycle management with various components involve in product development.

Above figure (C) explaining approaches and resources needed in product development cycle.

a) Management :
This is commonly known as organization hierarchy specially developed for any product develop. This layer of IPPD integrates people like manufacturing, Supply chain, suppliers, customers, service, marketing, marketing, and engineering. For better clarity

b) Lifecycle :
This layer of product development is embodying by management at top and product at bottom. This is basically the life of any product with entry and death of particular product in the market. This layer integrate all attributes of product development like conceive of product, development of product, process of any product, realization and eventually use of product.

c) Product:
This is basically developed product that is covered with previous two layers i.e management and lifecycle of product development. This layer basically contain i i) tools for product development like Computer added manufacturing, computer added drawing, computer added engineering, MRO, PPM, CAQ, CAPP, AEC etc. ii) methods to develop flawless product which contain methods like Design failure mode and defect analysis also known as DFMA , Concurrent, DFSS, ETO, NPDI etc.iii)Technology that used to develop product like MPM, CAx, PDM, CPD etc..iv)data those are used for development of product like geometry which says physical dimensions also known as specification at initial, structure which shows how this product has organised specially used by customers and indicate to designers, metadata these data are provided by customers for any product to develop and basically it is customer driven parameter.

III Concurrent Engineering

Concurrent engineering is powerful tool in IIPD which integrate different discipline in company in to one, for successful development of any product. It is proposed as a means to minimize product development time also systematic approach to the integrate, concurrent design of products and their related processes. Concurrent engineering emphasizes the response to customer expectations.

There are seven influencing agents which effect Concurrent engineering and eventually product development

1) Time: this is followed by different factors which includes process time and total lifecycle time till product development.

2) Tools: this is basically tools those are used to develop product and which has major roll at conceptual design stage.

3) Talents: this is deal with workforce, integration and utilization of skill in to development of product.

4)Tasks; this is basically generated for initialization of ideas for product development here more important is to assign tasks to talented pool of people to get better result in the product.

5)Teamwork : followed by tasks and talents .Team work is the base of concurrent engineering .To get better out put in terms of product quality and better product organization should promote team work. Concurrent engineering use team work as a tool to optimize product lifecycle time with idea generation and brain storming.

6) Techniques: followed by teamwork, basically this is result of ideas which will reduce development time for the product. Ides are actually implemented while approaching manufacturing of product. Techniques will decide what will be the output with what cost incurred on the product. Techniques can be generated with brain storm or team work.

III. IPPD APPROACH USING VIRTUAL REALITY

Virtual reality (VR) is a term that applies to computer-simulated environments that can simulate places in the real world, as well as in imaginary worlds. Most current virtual reality environments are primarily visual experiences, displayed either on a computer screen or through special stereoscopic displays, but some simulations include additional sensory information, such as sound through speakers or headphones. Some advanced, haptic systems now include tactile information, generally known as force feedback, in medical and gaming applications.
Furthermore, virtual reality covers remote communication environments which provide virtual presence of users with the concepts of telepresence and telexistence.

In recent era of industrialism customers demands increasing day by day which leads companies to respond very quick and should be agile. This is only possible when companies will use sort of tool which can give the idea of product .They can realize it before it got manufactured.

They can feel its quality and its appearance. Companies can make their effort without investing huge amount of money in manufacturing of particular product which if eventually not worth while. Any product manufacturing is followed by huge amount of money and other resources including machine and man. Product examination throughout various stages of a design process is crucial to the final product's success, and this may be a costly, time consuming and logistically complex process there must be a tool to answer all of these questions.

VR(Virtual Reality) is the solution of all of the answers. This is state of art in which generally companies can realize their product before it got manufactured. All phases of IPPD can be demonstrated by using Virtual Reality which inturn savings in money, time and other great valuable resources.

IV Virtual Reality

VR is basically computer generated environment which makes user to feel as if it is in real sense. Virtual reality can be generated using different hardwares and software.

i) Hardware part includes:

a) Over head mountain display, this is basically 3-D image analyser which will generate images about the focal length of the lenses with respect to the user. This hardware comes in variety of lenses. This hardware comes in different designs like i-Trek 3D PC,i-glasses VR, VR vision, I-Port, V-real viewer,i-Trek, Sunvisor,Jordy etc.

b) Data Gloves , this hardware is basically to feel the motion in 3-D virtual environment. Data Glove has direct connection with the computer. It comes in verity of sizes and in accordance with data transfer like P5 glove ,5DT glove, SDT glove 14,Pinch glove,cyber force, midi glove, cyber touch ,shadow hand, shape hand etc [1].

Fig (D): VR hardware Glove [1]

c) Motion trackers, it is basically to track different motion on the screen. In any case user must be the centre of attraction .Motion tracker does so.These are also coming in various shapes according their principle of use virtual cube, inertia cube2 , inertia cube3, Hy-BIRD ,3D-BIRD all these are inertia motion tracker. Minuteman, colibri, patriot, fasttrak[1], liberty, micro BIRD[1], pci BIRD[1] etc are magnetic motion trackers[1].

d) Force feedback, this device also known as haptic device. This is generally output device which will show the force feedback. In any stage of product realization this device is very useful while to have feel of product physical features like size, shape and most important is weight. This device is also vey useful to design any product with force and load characteristic. This device available in different sizes according to the amount of force exertion like Panthom, VR cushion etc [1].

Fig (E) Haptic force feedback device [1]

e) 3-D controllers, this device is very useful to control exact motion of user in to space. While talking about product realization it is very useful when we approach huge products like boogies, aircraft etc. we have to control exact user motion. These controllers are available in different shapes according to the sensitivity offered like 3D mouse, X-Gun, cyberstik, space explorer, space traveller, space mouse, space ball, space pilot, impulse stick, 6D mouse, wanda , soft mouse, space grips etc [1].

Fig (F) 3-D mouse [1]

ii) Software part includes :

Basic environment includes simulation software like Eon professional, Eon studio, 3-D CAD softwares, CAM softwares etc. These softwares

provide environment between input (User input data) to the output (User feeling) [1].

V IPPD SIMULATION USING VR

As explained in above consecutive paragraphs steps for IPPD starts from initial conceive of design to the end of the customer though this process is cyclic and never end.

We can simulate those steps of IPPD using Virtual reality tool and can reduce all resources those are used to manufacture any product.

CAD/CAM tools are the most powerful tool to simulate real part in virtual window of computer. CAM softwares like GIBS cam is nowadays gained popularity to simulate virtual manufacturing and virtual product development.

A) Conceptual design :
VR is very good tool for conceptual design. Design generated using Virtual Reality application has minimum number of engineering changes because of its robustness of repeatability. Engineering changes incurred more cost than designing new concept. In above 3-D graphic shows conceptual design with solidworks and I-DEAS.

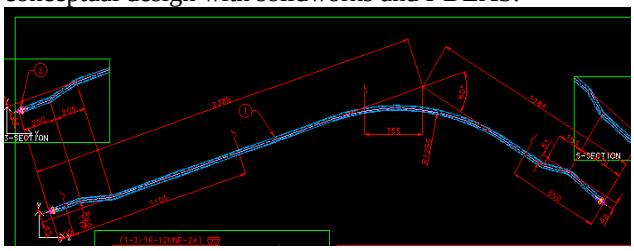

Fig(G): Conceptual design with virtual software I-DEAS

B) Styling design :
Styling in any product is important feature to attract customers .In conventional IPPD process this feature generally neglected and taken care at last, even to change at the time of production is very difficult. Using virtual reality one can change stying as many time as customer wants as well as in accordance with customers. Styling feature developed using virtual software solidworks. One can use surfacing and styling feature to develop product .This is parametric hence can be used and modify as many times as user wants.

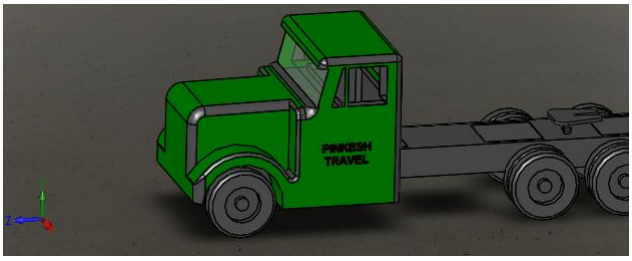

Fig (H): Styling with solidworks Virtual product development tool

C) Ergonomics design:
This is one of the other features which products like cabin in automobiles, excavators and other earth moving equipment. In conventional IPPD it is very difficult to maintain.

D) Design Review:
When it comes to design review conventional IPPD has sluggish response. If we use same with VR approach then it is very easy and effective to visualise every condition in the product. It becomes panoramic.

E) Virtual Manufacturing :
Developing any product and prototype costs very huge. Virtual manufacturing is the tool which will show product specification and aesthetic before it got manufactured physically. Computer Added Manufacture is the great example of virtual manufacturing.

F) Virtual Assembly and Production:
When it comes on part of virtual assembly and force feedback, VR is the tool without wasting money in to assembly manpower cost, time and analysing problems deal with assembly.

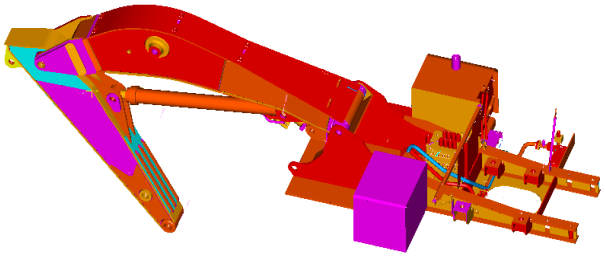

Fig(H): Virtual Assembly using solidworks

G) Virtual Training :
In conventional IPPD , recruit and train workforce if very difficult. VR training in this sense is very effective.

H) Virtual Planning :
This is PPC(Production Planning and Control) part where processes are designed to optimize over all operation time on particular product.

I) Rapid Virtual Prototype:
"Smart Assembly" refers to a next generation capability in assembly systems and technologies which integrate "virtual" and "real-time" methods in order to achieve dramatic improvements in productivity, lead-time, and agility for the design, engineering, validation, construction, installation, launch and operation of assembly processes and systems

V LEAN SIMULATION USING VR

Lean is the Japanese terminology defining reduction in the waste irrespective of any process. This tool has further broad classification such as different strategies discussed below.

1) Kanban : This is basically deals with the inventory management in the production system .When all raw material will be consumed by process and con verted to finish goods then visual display will be highlighted and shows sign of replenishment.

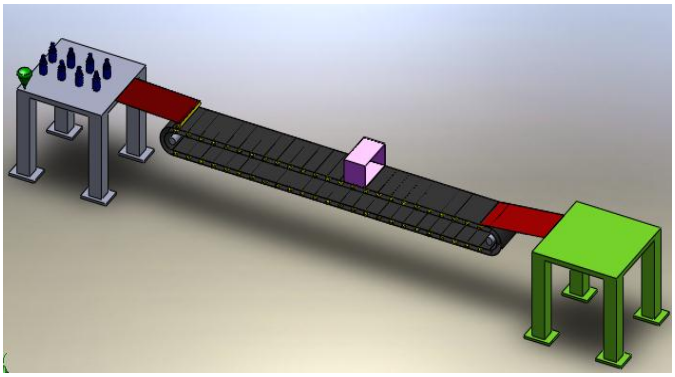

Fig(I) : VR Model for Kanban Simulation

2) Material Handling and Motion: This basically deals with unnecessary movement in the plant. Using VR one can reduce this unnecessary motion in the plant.

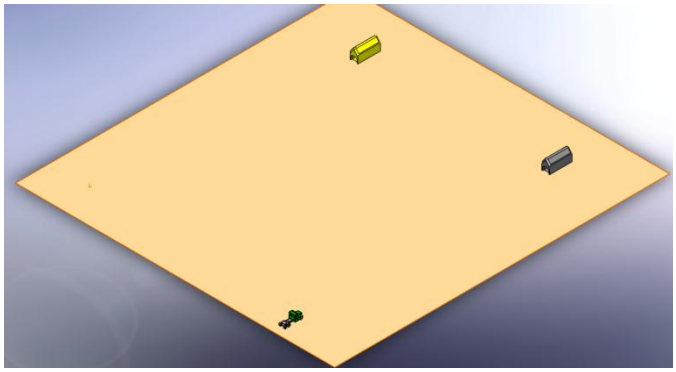

Fig (J): VR model of transportation system within two warehouses

3) Batch and Queue system :This lean tool basically deals with the type of assembly lines. It might be the queue type assembly or might be batch type of assembly. The aim behind is to reduce lead time of particular process.

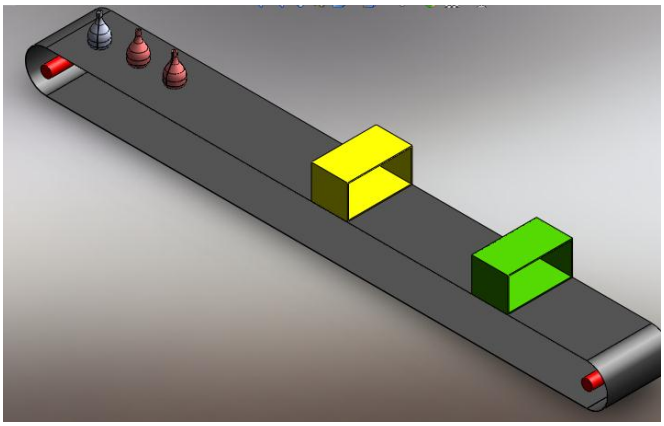

Fig (K) : Batch and Queue type of process

4) TPM : This is also called 5S activities. The abbreviation stands for Total Productive Maintenance.

VI RESULT

It is explored that IPPD using conventional approach it have all cost, money, man and other resources incurred substantially. Time taken by conventional IPPD is much more than that of time taken by Virtual reality IPPD approach. Virtual reality approach is very sophisticated and optimized approach in industries.

In the ear of competition and industrialization customers become more and more aware of quality product with relative cheaper cost, to survive in this global market only tool for survival VR can be helpful.

Lean simulation using VR will reduce total cost of the assembly as well as will increase sustainable profit in the organization.

REFERENCES

[1] http://www.vrealities.com/company.html (2009)
[2] http://en.wikipedia.org/wiki/Product_lifecycle_management (2010)
[3] Integrated Product and Process Design and Development
[4] The Product Realization Process(2009) Edward B. Magrab,Satyandra K. Gupta, F. Patrick McCluskey ,Peter A. Sandborn
[5] Analysis of cost estimating processes used within a concurrent engineering environment throughout a product life cycle by Christopher Rush, Dr. Rajkumar Roy
VIRTUAL AND AUGMENTED REALITY TECHNOLOGIES
FOR PRODUCT REALIZATION by S. C-Y. Lu (2), The IMPACT Laboratory, University of Southern California, USA
M. Shpitalni (1), R. Bar-Or, CAD Laboratory, Mechanical Engineering, TECHNION, ISRAEL
Rajit Gadh, The I-CARVE Laboratory, University of Wisconsin-Madison, USA
Virtual Prototyping for Customized Product Development
Mitchell M. Tseng, Jianxin Jiao, Chuan-Jun Su
Department of Industrial Engineering & Engineering Management
The Hong Kong University of Science & Technology
Clear Water Bay, Kowloon, Hong Kong

Modeling, Simulation and Optimization Analysis on Steering Knuckle Component For Purpose of Weight Reduction

W. M. Wan Muhamad[1], E. Sujatmika[1], Hisham Hamid[1] and Faris Tarlochan[2]
[1]UniKL Malaysia France Institute, Universiti Kuala Lumpur, Bandar Baru Bangi, Selangor, Malaysia
[2]Mechanical Engineering Department, Universiti Tenaga Nasional, Kajang, Selangor, Malaysia

Abstract - *Reducing weight of vehicle components will contribute towards overall weight reduction of a vehicle, lower its energy consumption demand, therefore, will improve its fuel efficiency. Material resources will be saved too. The objective of this research is reduce weight of an existing steering knuckle component of a local car model by applying shape optimization technique. A finite element modeling and analysis software, HyperWorks which contains several modules, is used to achieve this objective. HyperMesh was used to prepare the finite element model while HyperMorph was utilized for defining shape variables. For optimization purpose, OptiStruct was used. The improved design achieves 8.4% reduction of weight while meeting the strength requirement. This result can be considered satisfactory in view of using optimization in shape only, with limited design space given and no change in material properties.*

Keywords: Simulation, Optimization, CAD/CAE, Vehicle Component, Weight Reduction

1 Introduction

In this investigation, steering knuckle was used as component for study. Suspension system in any vehicle uses different types of links, arms, and joints to let the wheels move freely; front suspensions also have to allow the front wheels to turn. Steering knuckle/spindle assembly, which might be two separate parts attached together or one complete part, is one of these links [1].

Weight reduction is becoming important issue in car manufacturing industry. Weight reduction will give substantial impact to fuel efficiency, efforts to reduce emissions and therefore, save environment. Weight can be reduced through several types of technological improvements, such as advances in materials, design and analysis methods, fabrication processes and optimization techniques, etc.

Another tool had been developed beside the CAD software which is CAE. The needs of the CAE in industrial field are reported by Yoshio Kojima [1]. Car's components are subjected to many types of loadings; those components are designed and manufactured to meet the requirements for strength and safety.

Optimization methods were developed to have lighter, less cost and may have better strength too. Many optimization types, methods and tools are available nowadays due to the revolution of the high speed computing and software development. There are four disciplines for optimization process [2]:

a. Topology optimization: it is an optimization process which gives the optimum material layout according to the design space and loading case.

b. Shape optimization: this optimization gives the optimum fillets and the optimum outer dimensions.

c. Size optimization: the aim of applying this optimization process is to obtain the optimum thickness of the component.

d. Topography: it is an advanced form of shape optimization, in which a design region is defined and a pattern of shape variable will generate the reinforcements.

Shape optimization was developed using optimization techniques such as Genetic Algorithms (GAs) [3]. Shape optimization is applied to many fields such as Computational Fluid Dynamics (CFD) especially aerodynamics [4,5] and electrical engineering field [6] as well as mechanical engineering, for example : strain gauge load cell [7], a cantilever beam [8] and cam [9].

Finite element method used for many type of analysis, such as linear analysis, nonlinear analysis, fatigue analysis and another types. FE analysis was developed to solve the optimization process such as OptiStruct linear solver [2], TopShape [10].

2 Objective

This research aims to contribute to the development of structural design and weight reduction of vehicle components using shape optimization by the gradient based method.

Optimization process for this work was conducted using OptiStruct solver in order to reduce the weight of the component which will reduce the cost with respect to the weight production process.

3 Methodology

Shape optimization was applied to reduce volume of steering knuckle model. OptiStruct was used to perform the process. The approach is shown in Fig. 1.

All of the optimization processes use some application software that included in the HyperWorks. Using HyperMesh as one of the application, solid model was imported for finite element modeling which is loads and constraints applied. Shape optimization process requires shape definition for design variables and HyperMorph can be used to conduct such purposes.

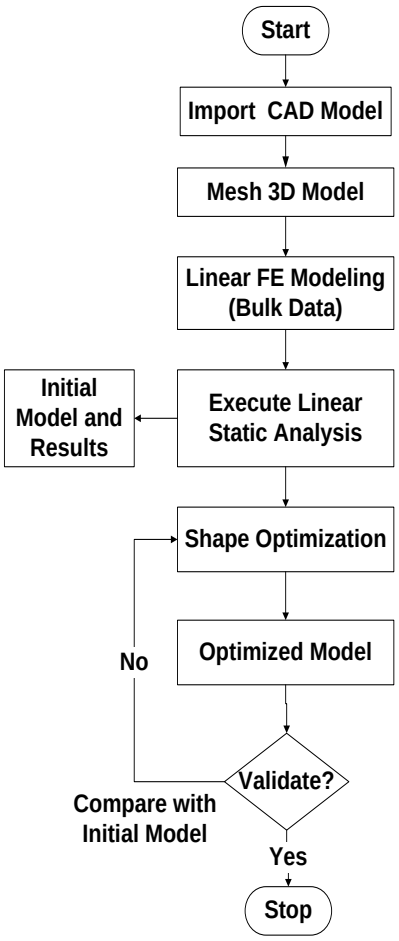

Fig. 1: Design Optimization Flowchart.

Furthermore, Hyperview and Hypergraph were used to display and plot the data for results interpretation.

4 Modeling and Optimization Processes

4.1 Model Boundary Condition

The boundary condition and loading condition were set following conditions for testing purpose in one automotive manufacturing company. The boundary conditions were defined by fixing all the hub bolt holes except the pair of bolt holes A (see Fig. 2). Those holes were released in the horizontal direction and coincided with the plane of moment, while any moving was not allowed for the other bolt holes B, C and D. In the vehicle, pair of holes A are attached to lower control arm, hole B is connected to steering system by a tie rod while holes C and D are connected the strut joints of suspension system (MacPherson-strut front suspension).

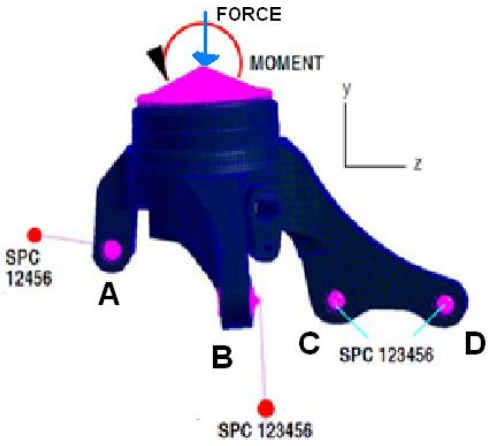

Fig. 2: Free Body Diagram of the model

Force and moment were applied through the holder that was attached to top of the model. Load of 2.8 G were charged continuously in the other end of the holder. That load was represented by a force and moment that worked on top of the model.

4.2 Finite Element Model

Finite element model for the knuckle is shown in Fig. 3 below.

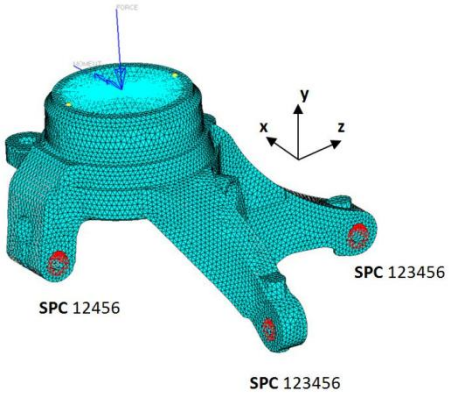

Fig. 3: Finite Element Model of Knuckle

Material properties and loading conditions are shown in Table 1 and Table 2 respectively.

Table 1: Material Properties

Young modulus	207000 Mpa
Poisson ratio	0.29
Density	7.85 E-09 tone/mm^3
Ultimate Tensile Stress	522 Mpa
Yield Stress	391.5 Mpa

Table 2: Loads Conditions

Description	Magnitude
Force	12375.44 (2.8G)
Moment	4950176 N.mm
Total number of nodes	15294
Total number of elements (Tetra)	56496

There are two type loads that applied to knuckle, those are force and moment. The knuckle has two constraints that restraint them on all direction (x, y, z translation and xx, yy and zz rotation) and one constraint that allow it translate to z direction.

4.3 Design Variables for Shape Optimization

The vector of nodal coordinates (x) is used to define the shape of steering knuckle structure in finite elements model. Changes of the boundary in model structure will translate to interior of mesh to avoid distortion of the elements when shapes change. During shape optimization, there are two approaches that can be used to account for mesh changes; those are the basis vector approach and the perturbation approach. Those approaches refer to the definition of the structural shape as a linear combination of vectors.

Using the basis vector approach, the structural shape is defined as a linear combination of basis vectors. The basis vectors define nodal locations.

$$x = \sum DV_i \,.\, BV_i \qquad (1)$$

Where x is the vector of nodal coordinates, BV_i is the basis vector associated to the design variable DV_i.

Using the perturbation vector approach, the structural shape change is defined as a linear combination of perturbation vectors. The perturbation vectors define changes of nodal locations with respect to the original finite element mesh.

$$x = x_o + \sum DV_i \,.\, PV_i \qquad (2)$$

Where x is the vector of nodal coordinates, x_o is the vector of nodal coordinates of the initial design, PV_i is the perturbation vector associated to the design variable DV_i.

4.4 Shape Optimization Parameters

An general optimization or a mathematical programming problem can be stated as follows [11].

$$\text{Find (X)} = \begin{Bmatrix} x_1 \\ x_2 \\ \vdots \\ x_n \end{Bmatrix} \text{ which minimize } f(X)$$

subject to the constraints

$$g_j(X) \le 0,\ j = 1, 2, \ldots, m$$

$$l_j(X) = 0,\ j = 1, 2, \ldots, p$$

where X is an n-dimensional vector called the *design vector*, f (X) is termed the *objective function*, and g_j (X) and l_j (X) are known as *inequality* and *equality* constraints, respectively.

In this paper, the objective function of shape optimization problem is as implicit function that is to minimize volume and subject to maximum stress of the elements as constraint. Design variables were determined using Hypermorph. There are 8 shapes were defined (shape 1, shape 2, shape 3, shape 4, shape 5, shape 6, shape 7 and shape 8) as design variables.

5 Simulation Results and Discussions

For the optimization process, eight shape variables were defined and optimized considering stress constraint. Figures 4 (a), (b), (c) and (d) show the shape optimization results that obtained using OptiStruct solver.

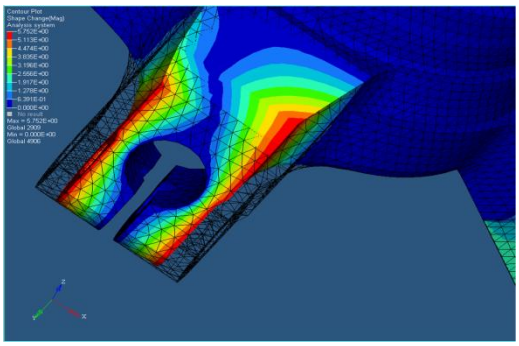

(a)

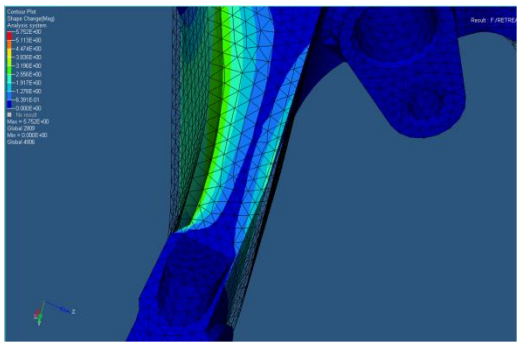

(b)

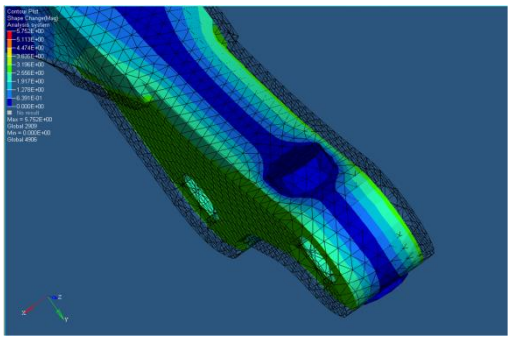

(c)

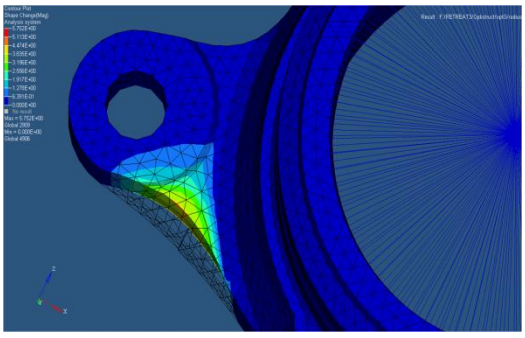

(d)

Fig. 4: (a) Shape 1, Shape 2 and Shape 3, (b) Shape 4 and Shape 5, (c) Shape 6 and Shape 7, (b) Shape 8

The design region that was defined to have three shapes changing (1, 2 and 3) had the most reduction among all shapes as shown in Fig. 4(a).

Second design region is shown in Fig. 4(b), and it was defined to have the (4th, 5th) shape variables and it has less changing than that in Fig. 4(a). Fig. 4(c) and 4(d) show the optimization of shapes (6, 7 and 8) and all of them have less shape changing than that in Fig. 4(a).

The objective of the research is to reduce the weight (represented by reduction volume) using shape optimization, Fig. 5 shows the graph of volume minimization versus the iteration of the shape optimization process. The weight reduction for the front knuckle was 8.37%.

The weight reduction was not too much because of the original design already sufficient. Nevertheless, more reduction is possible to be achieved if there is more design space through redesigning of assembly layout.

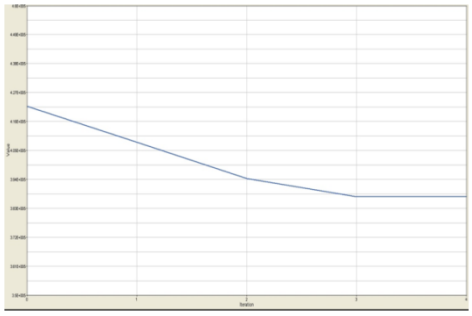

Fig. 5: Objective vs. Iteration

Summary of the results is shown in table 3.

Table 3: Results Summary

	Initial Design	Node #	Optimized Design	% reduction
Displacement	0.142 mm	5070	0.151 mm	
Stress	341 MPa	6016	342 MPa	
Volume	421746 mm^3		386559 mm^3	
Mass	3.3318 kg		3.0530 kg	**8.37%**

6 Conclusions

Optimization method used in this study succeeded in reducing the weight of existing knuckle component to 8.4% while meeting the strength requirement. This result is satisfactory considering using optimization in shape only, with limited design space given and no change in material properties. Other vehicle components, similarly, have the potential to be reduced with respect to weight using shape

optimization. Therefore, the overall weight of the vehicle can be reduced to achieve savings in costs and materials, as well as, improve fuel efficiency and reduce carbon emissions to sustain the environment.

7 References

[1] Zurofi M. "Manufacturing Process Effects on Fatigue Design and Optimization of Automotive Components– An Analytical and Experimental Study", The University of Toledo, Ph.D. thesis, 2004.

[2] Kojima,Y. "Mechanical CAE In Automotive Design", R & D review of Toyota CRLD, Vol 35, No. 4, 2000.

[3] "Altair Hyperworks 9". Altair Engineering Inc., India, 2009.

[4] Goldberg DE. "Genetic Algorithms In Search, Optimization And Machine Learning". Addison-Wesley, Reading, MA, 1989.

[5] Obayashi S. Pareto. "Genetic algorithm for aerodynamic design using the Navier-Stokes equations". In: Genetic Algorithms And Evolution Strategies In Engineering And Computer Science, Wiley, Chichester, England, 1997.

[6] Obayashi S, Tsukahara T. "Comparison Of Optimization Algorithms For Aerodynamic Shape Design". AIAA Journal, Vol. 35, No. 8, pp.1413–5. 1997.

[7] Pe´riaux J, Sefrioui M, Mantel P. "GA Multiple Objective Optimization Strategies For Electromagnetic Backscattering". In: Quagliarella D, Pe´riaux J, Poloni C, Winter G, editors. Genetic Algorithms And Evolution Strategies In Engineering And Computer Science, 1997.

[8] Robinson GM. "Genetic Algorithm Optimisation Of Load Cell Geometry By Finite Element Analysis". PhD Thesis. City University, Measurement and Instrumentation Centre, Department of Electrical, Electronic and Information Engineering, School of Engineering. London, 1995.

[9] Richards RA. "Zeroth-Order Shape Optimization Utilizing A Learning Classifier System". PhD Dissertation, Mechanical Engineering Department, Stanford University, 1995.

[10] Lampinen J. "Cam Shape Optimisation By Genetic Algorithm", Journal of Computer-Aided Design, Vol. 35, pp. 727–737, 2003.

[11] Harzheim L., Graf G., "Topshape: An Attempt To Create Design Proposals Including Manufacturing Constraints", International Journal of Vehicle Design, Vol. 28, No. 4, pp. 389-409, 2002.

[12] Rao S.S., "Engineering Optimization Theory and Practice", John Wiley & Sons, Inc.,(2009), 4th edition.

IPPD USING VIRTUAL REALITY

Pinkeshkumar Attarwala[1],Sumant Kulkarni[2], Suren N. Dwivedi[3]

Department of Mechanical Engineering

University of Louisiana at Lafayette
Louisiana, LA

[1]Pja7518@louisiana.edu

[2]ssk7136@louisiana.edu

3snd7483@louisiana.edu

Abstract— **Product development in every industry is the pioneer base to the future. Development of any industry is depending upon several factors, one of the summit and powerful base and factor is product development cycle and implementation. New generation and era demands firm foundation of product development to sustain position in competitive market. Competition forcing companies to maintain their life cycle of product in different stages of growth. Our society expects engineers to develop products that are affordable, functional and sustainable. Effective product realization methods and tools are the answers to these societal expectations**

In this paper, a classical approach to Integrated Product and Process Design and Development and new approach to Integrated Product and Process Design and Development using powerful software packages CAE, CAD and CAME will be discussed. Results reveal that approach to IPPD using VR is more powerful and develop competitively-priced quality products. ,

***Keywords*— IIPD, VR**

I. INTRODUCTION

The process of creating and making statues has been around since the starting age of humankind. It was implemented first for survival: weapons, shelters, clothing and farming. These implements were improved upon with the appearance of such invention as fire, the wheel, and steel and as time went on they became more substantial and more suave. As evolution of mankind and societies happed from being local one to regional ones, parallel transforming their local economies in to regional ones. In the starting, these transformations took hundreds to thousands of years. Since the start of industrial revolution about 300 years ago, the lopes of development and improvement of devices and artefacts has increased all of the sudden [3].

Thus transformation from primarily local societies to once that must now complete globally has had a very solid influence on the product realization process. It is an environment in which one must compete on cost, quality, performance and time-to-market on a worldwide basis. This requires individuals and companies to examine back how they go about creating product and services and how these products and services can be brought to marketplace. During the last 40 years it has become clear that the way to do this is through an integrated approach to the product realization process. This approach tends to do the following: "plane" organizational structures; involve many more constituencies in the process at the very beginning; place greater emphasis on the customer, product quality, customer and time-to –market; use a large amount of simultaneity in the product realization process; and require organizations to be creative and innovative[3].

In the era of product proliferation there was no international competition involved in product manufacturing. Inventors invented and manufactured their products. In the era of mass production, end customers demanded more functionality in to the products the mass production came in to picture. In the era of mechanization, industries moved to more intricate products. It gained its popularity in taking place of human and animal power. In the era of departmentalization, people used to divide their work and hence barriers developed and productivity decreased. In the era of realization analysing of situation by organizations and close interaction between various group of departments. In the era of global manufacturing companies started customers driven and became more competitive.

These new approaches have been developed to eliminate situations and conditions that resulted in poor corporate performance and poor customer satisfaction. Examples of such conditions like

inconsistent product quality; slow response to the marketplace; lack of innovative, competitive service; and inefficient resource allocation. In its place, these new approaches have transformed many companies in to entities that are able to

1) Responding to the customer quick by new innovative ideas and technology into products.
2) Developing and produce product that satisfy customers' requirements.
3) Accustomed to competitive environ.
4) Generate new ideas and combine existing elements to create new sources of value.

At different stages in the evolution of product development in the last decades, various descriptors have been used to indicate that an improved method was being implemented to design and manufacture products. The descriptor that will be used here is the integrated product and process design and development team method.

The classical approach to development of product leads to the many intricacy like involvement of human being in each phase of the creation of the steps while product development. The starting of product development at adolesce to the mature phase product needs to emphasise on design but, in real sense and practical life is very encumber to emphasize and become unrealistic. Decade later it was found that development of product incurred cost which includes primary design cost and then labour cost which is most unaffordable to bear by any company. Moving from *age of control* to *age of flexibility,* later possible by concurrent engineering (CE) and Continuous Acquisition and Life cycle Support.

The new approach to development of product comes which is superior in all aspect. CAE software being used to development product realization phases.

II. CONVENTIONAL IPPD

Conventional IPPD contain several steps for new product development. The approach is generally involve concurrent engineering.

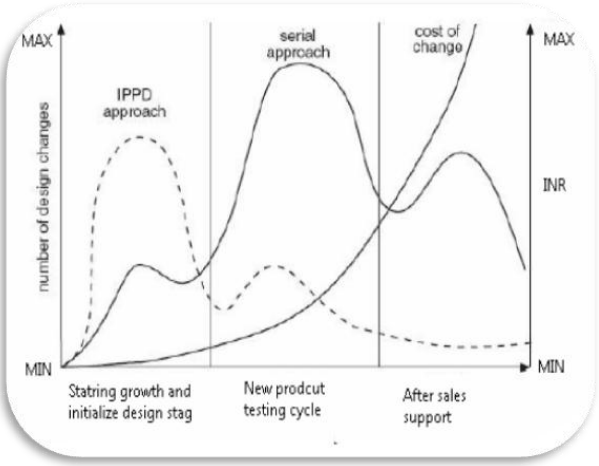

Fig: (A) [2] Product Life Cycle Management by IPPD and various approaches.

Few stages of product life cycle development involves

A) Conceive: Imagine ,innovate
This is first stage of the Product development and it comes through customer i.e. it is customer driven phase.

B) Design: Drawing release, specification, develop
This is major part of any product development and takes huge cost involvement followed by number of design engineers. This phase taking approximate cost of 70% of over all product development.

C) Realize: Manufacturing, physical approach
This phase is basically containing the actual parameter to build any product i.e. physical approach to any product.

D) Service: Manage, support
This phase is also called after sales and support. Generally to maintain good image of any company this phase is useful. This is basically driven by the customers. To maintain life of any product after sales support is needed. This is also called maintenance phase for any product.

In above figure (A), shows how number of changes increased or decreased with different approach to product development in different phases of product development.

i) IPPD approach:

Number of design changes in different phase of product life cycle is decreases

exponentially when we use IPPD approach to any product development. This reveals important result if we use IPPD approach one can save 30% [5] of production cost.

ii) Serial Approach:

This approach will show less involvement while initial phase of design but, eventually it hikes to the maximum in number of design changes while we move ahead in various stages of product development. This kind approach is not good for any product development. Design changes in any product incurred huge cost. Repairing or design change cost is approximate one third of the total design cost.

iii) Cost of change graph:

This graph shows the change in the cost while in serial approach and IPPD approach. Cost incurred increasing exponentially.

Fig: (B) [2] Product development cyclic process

Above figure (B) indicates, development of any product is not a one time process. This involves cyclic processes from various departments to the resources.

Any process is starts from raw material and eventually ends with the new product development. There is not yet end the process. This is continuous cycle which encircles both customers and company. Company includes all departments in the loop for product development process with embodiment of customers.

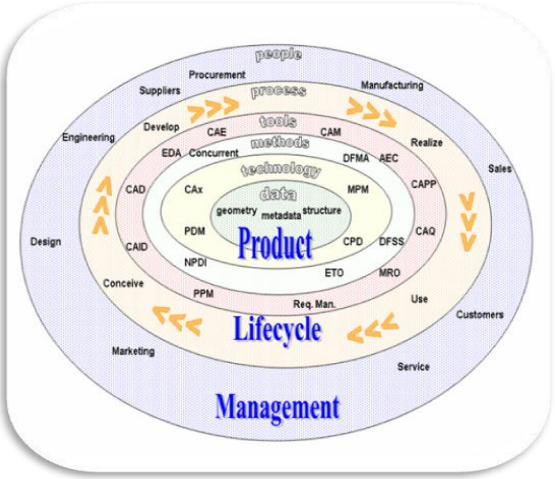

Fig (C) [2]: Generic product life cycle management with various components involve in product development.

Above figure (C) explaining approaches and resources needed in product development cycle.

a) Management :
This is commonly known as organization hierarchy specially developed for any product develop. This layer of IPPD integrates people like manufacturing, Supply chain, suppliers, customers, service, marketing, marketing, and engineering. For better clarity

b) Lifecycle :
This layer of product development is embodying by management at top and product at bottom. This is basically the life of any product with entry and death of particular product in the market. This layer integrate all attributes of product development like conceive of product, development of product, process of any product, realization and eventually use of product.

c) Product:
This is basically developed product that is covered with previous two layers i.e management and lifecycle of product development. This layer basically contain i i) tools for product development like Computer added manufacturing, computer added drawing, computer added engineering, MRO, PPM, CAQ, CAPP, AEC etc.

ii) methods to develop flawless product which contain methods like Design failure mode and defect analysis also known as DFMA , Concurrent, DFSS, ETO, NPDI etc.iii)Technology that used to develop product like MPM, CAx, PDM, CPD etc..iv)data those are used for development of product like geometry which says physical dimensions also known as specification at initial, structure which shows how this product has organised specially used by customers and indicate to designers, metadata these data are provided by customers for any product to develop and basically it is customer driven parameter.

III Concurrent Engineering

Concurrent engineering is powerful tool in IIPD which integrate different discipline in company in to one, for successful development of any product. It is proposed as a means to minimize product development time also systematic approach to the integrate, concurrent design of products and their related processes. Concurrent engineering emphasizes the response to customer expectations.

There are seven influencing agents which effect Concurrent engineering and eventually product development

1) Time: this is followed by different factors which includes process time and total lifecycle time till product development.

2) Tools: this is basically tools those are used to develop product and which has major roll at conceptual design stage.

3) Talents: this is deal with workforce, integration and utilization of skill in to development of product.

4)Tasks; this is basically generated for initialization of ideas for product development here more important is to assign tasks to talented pool of people to get better result in the product.

5)Teamwork : followed by tasks and talents .Team work is the base of concurrent engineering .To get better out put in terms of product quality and better product organization should promote team work. Concurrent engineering use team work as a tool to optimize product lifecycle time with idea generation and brain storming.

6) Techniques: followed by teamwork, basically this is result of ideas which will reduce development time for the product. Ides are actually implemented while approaching manufacturing of product. Techniques will decide what will be the output with what cost incurred on the product. Techniques can be generated with brain storm or team work.

IV.IPPD approach using virtual reality

Virtual reality (VR) is a term that applies to computer-simulated environments that can simulate places in the real world, as well as in imaginary worlds. Most current virtual reality environments are primarily visual experiences, displayed either on a computer screen or through special stereoscopic displays, but some simulations include additional sensory information, such as sound through speakers or headphones. Some advanced, haptic systems now include tactile information, generally known as force feedback, in medical and gaming applications. Furthermore, virtual reality covers remote communication environments which provide virtual presence of users with the concepts of telepresence and telexistence.

In recent era of industrialism customers demands increasing day by day which leads companies to respond very quick and should be agile. This is only possible when companies will use sort of tool which can give the idea of product .They can realize it before it got manufactured. They can feel its quality and its appearance. Companies can make their effort without investing huge amount of money in manufacturing of particular product which if eventually not worth while. Any product manufacturing is followed by huge amount of money and other resources including machine and man. Product examination throughout various stages of a design process is crucial to the final product's success, and this may be a costly, time consuming and logistically complex

process there must be a tool to answer all of these questions.

VR(Virtual Reality) is the solution of all of the answers. This is state of art in which generally companies can realize their product before it got manufactured. All phases of IPPD can be demonstrated by using Virtual Reality which inturn savings in money, time and other great valuable resources.

V Virtual Reality

VR is basically computer generated environment which makes user to feel as if it is in real sense. Virtual reality can be generated using different hardwares and software.

i) Hardware part includes:

a) Over head mountain display, this is basically 3-D image analyser which will generate images about the focal length of the lenses with respect to the user. This hardware comes in variety of lenses. This hardware comes in different designs like i-Trek 3D PC,i-glasses VR, VR vision, I-Port, V-real viewer,i-Trek, Sunvisor,Jordy etc.

b) Data Gloves , this hardware is basically to feel the motion in 3-D virtual environment. Data Glove has direct connection with the computer. It comes in verity of sizes and in accordance with data transfer like P5 glove ,5DT glove, SDT glove 14,Pinch glove, cyber force, midi glove, cyber touch ,shadow hand, shape hand etc [1].

Fig(D): VR hardware Glove[1]

c) Motion trackers, it is basically to track different motion on the screen. In any case user must be the centre of attraction .Motion tracker does so.These are also coming in various shapes according their principle of use virtual cube, inertia cube2 , inertia cube3, Hy-BIRD ,3D-BIRD all these are inertia motion tracker. Minuteman, colibri, patriot, fasttrak[1], liberty, micro BIRD[1], pci BIRD[1] etc are magnetic motion trackers[1].

d) Force feedback, this device also known as haptic device. This is generally output device which will show the force feedback. In any stage of product realization this device is very useful while to have feel of product physical features like size, shape and most important is weight. This device is also vey useful to design any product with force and load characteristic. This device available in different sizes according to the amount of force exertion like Panthom, VR cushion etc [1].

Fig (E) Haptic force feedback device [1]

e) 3-D controllers, this device is very useful to control exact motion of user in to space. While talking about product realization it is very useful when we approach huge products like boogies, aircraft etc. we have to control exact user motion. These controllers are available in different shapes according to the sensitivity offered like 3D mouse, X-Gun, cyberstik, space explorer, space traveller, space mouse, space ball, space pilot, impulse stick, 6D mouse, wanda , soft mouse, space grips etc [1].

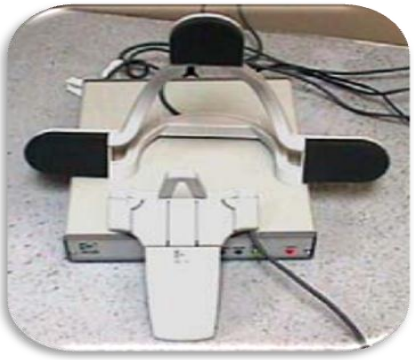

Fig (F) 3-D mouse [1]

ii) Software part includes :

Basic environment includes simulation software like Eon professional, Eon studio, 3-D CAD softwares, CAM softwares etc. These softwares provide environment between input (User input data) to the output (User feeling) [1].

V IPPD SIMULATION USING VR

As explained in above consecutive paragraphs steps for IPPD starts from initial conceive of design to the end of the customer though this process is cyclic and never end.

We can simulate those steps of IPPD using Virtual reality tool and can reduce all resources those are used to manufacture any product.

CAD/CAM tools are the most powerful tool to simulate real part in virtual window of computer. CAM softwares like GIBS cam is nowadays gained popularity to simulate virtual manufacturing and virtual product development.

A) Conceptual design :

VR is very good tool for conceptual design. Design generated using Virtual Reality application has minimum number of engineering changes because of its robustness of repeatability. Engineering changes incurred more cost than designing new concept. In above 3-D graphic shows conceptual design with solidworks and I-DEAS.

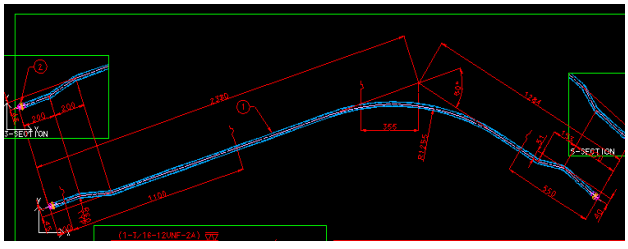

Fig(G): Conceptual design with virtual software I-DEAS

B) Styling design :

Styling in any product is important feature to attract customers. In conventional IPPD process this feature generally neglected and taken care at last, even to change at the time of production is very difficult. Using virtual reality one can change stying as many time as customer wants as well as in accordance with customers. Styling feature developed using virtual software solidworks. One can use surfacing and styling feature to develop product .This is parametric hence can be used and modify as many times as user wants.

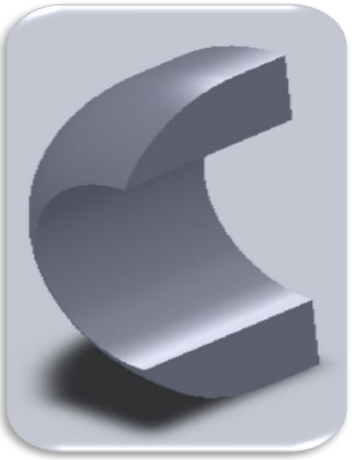

Fig (H): Styling with solidworks Virtual product development tool

C) Ergonomics design:

This is one of the other features which products like cabin in automobiles, excavators and other earth moving equipment. In conventional IPPD it is very difficult to maintain.

D) Design Review:

When it comes to design review conventional IPPD has sluggish response. If we use same with VR approach then it is very easy and effective to visualise every condition in the product. It becomes panoramic.

E) Virtual Manufacturing :

Developing any product and prototype costs very huge. Virtual manufacturing is the tool which will show product specification and aesthetic before it got manufactured physically. Computer Added Manufacture is the great example of virtual manufacturing.

F) Virtual Assembly and Production:

When it comes on part of virtual assembly and force feedback, VR is the tool without wasting money in to assembly manpower cost, time and analysing problems deal with assembly.

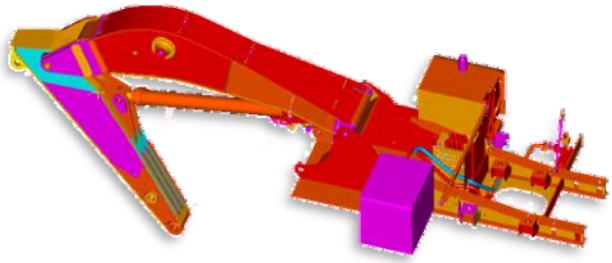

Fig(H): Virtual Assembly of Excavator using solidworks

G) Virtual Training :

In conventional IPPD , recruit and train workforce if very difficult. VR training in this sense is very effective.

H) Virtual Planning :

This is PPC(Production Planning and Control) part where processes are designed to optimize over all operation time on particular product.

I) Rapid Virtual Prototype:

"Smart Assembly" refers to a next generation capability in assembly systems and technologies which integrate "virtual" and "real-time" methods in order to achieve dramatic improvements in productivity, lead-time, and agility for the design, engineering, validation, construction, installation, launch and operation of assembly processes and systems

VI RESULT

It is explored that IPPD using conventional approach it have all cost, money, man and other resources incurred substantially. Time taken by conventional IPPD is much more than that of time taken by Virtual reality IPPD approach. Virtual reality approach is very sophisticated and optimized approach in industries.

In the ear of competition and industrialization customers become more and more aware of quality product with relative cheaper cost, to survive in this global market only tool for survival VR can be helpful.

REFERENCES

[1] http://www.vrealities.com/company.html (2009)

[2] http://en.wikipedia.org/wiki/Product_lifecycle_management (2010)

[3] Integrated Product and Process Design and Development, Second Edition" by JEdward B. Magrab Publisher:CRC | ISBN: 1420070606 | 2009The Product Realization Process(2009) Edward B. Magrab,Satyandra K. Gupta, F. Patrick McCluskey ,Peter A. Sandborn

[4] Analysis of cost estimating processes used within a concurrent engineering environment throughout a product life cycle by Christopher Rush, Dr. Rajkumar Roy

VIRTUAL AND AUGMENTED REALITY TECHNOLOGIES

FOR PRODUCT REALIZATION by S. C-Y. Lu (2), The IMPACT Laboratory, University of Southern California, USA

M. Shpitalni (1), R. Bar-Or, CAD Laboratory, Mechanical Engineering, TECHNION, ISRAEL

Rajit Gadh, The I-CARVE Laboratory, University of Wisconsin-Madison, USA

Virtual Prototyping for Customized Product Development

Mitchell M. Tseng, Jianxin Jiao, Chuan-Jun Su

Department of Industrial Engineering & Engineering Management

The Hong Kong University of Science & Technology

Clear Water Bay, Kowloon, Hong Kong

EFFECT OF UNCERTAINTIES ON DEMAND FORECASTING

Ari Hämäläinen
EThekwini Electricity
Durban, South Africa
hamalainenap@elec.durban.gov.za

Abstract – The electricity planning department of eThekwini Municipality performs a power system load forecast based on individual substation forecasts. The individual substation forecasts have uncertainty. It is desired to understand the effect of these uncertainties on the accuracy of the total system forecast. A Monte Carlo simulation of the forecasted system loadflow was performed. By means of this application of Monte Carlo, the planners can observe and visualize the extent to which uncertainties can affect the city's total forecast. What is presented is not new theory but rather the application of well-known MC simulation method in the context of this developing nation municipal power transmission and distribution system.

Keywords: uncertainty, load forecast, Monte Carlo

1 INTRODUCTION

The high voltage electricity network of the city of Durban, South Africa, is operated by the eThekwini Municipality's Electricity Service Unit. This system consists of 275 kV, 132 kV and 33 kV voltage levels. Medium voltage distribution is provided by 11 kV networks originating at 132/11 kV and 132/33 kV substations. The area of supply is approximately 2000 km² servicing more than 600 000 customers with a total demand of almost 2GW.

EThekwini Electricity compiles a 5-year load forecast for network planning and loadflow studies. This is based on forecasts of individual substation loads. A system base model is created using present scada load measurements of individual substations. From this basis a 5-year loadflow model is created by forecasting the individual loads of the base model.

The 5-year forecast of each individual substation is subject to uncertainties due to errors in the scada data and errors introduced by forecasting assumptions and uncertainties. These uncertainties at substation level will affect the total system demand forecast. In other words, the total system demand forecast has uncertainty due to the uncertainties of the individual substation forecasts which collectively constitute the total system demand.

Planners desire to understand to what extent the individual substation uncertainties are reflected in the variableness of the total system demand forecast.

An application of the Monte Carlo [1] method was adopted to visualize and demonstrate the effects of random uncertainties upon total demand.

2 SIMULATION APPROACH

2.1 Uncertainties modeled as random errors

The true value of the future total system demand is always unknown. For the purpose of this simulation, the 5-year forecast loadflow model was used as a reference i.e. this case was assumed to represent the true value. Thus a solution of this case yields the true value of the future total system demand and computes to 2193 MW. Errors were then introduced to simulate a real forecast. The first step was to assume a reasonable value of uncertainty for an individual substation's forecast. An uncertainty of ± 20 % was considered reasonable. This uncertainty was modeled by random errors within the bounds of ± 20 % which were applied to each substation load in the 5-year loadflow model. A pseudo-random number generator was used to generate a random multiplier in the range {-1.2; +1.2} for each substation which was then multiplied with that substation's load in the 5-year loadflow reference case. This resulted in a new set of substation loads. A modified substation load may be represented as equation (1),

$$y_{ki} = x_i + e_{ki} \tag{1}$$

where,
x_i is the reference load of bus i
e_{ki} is the load error for bus i on iteration k
y_{ki} is the modified load on bus i on iteration k

or as Nx1 matrices for iteration k,

$$[Y_k] = [X] + [E_k] \tag{2}$$

The set of loads $[Y_k]$ is used as input to the loadflow solution on iteration k.

2.2 Effect on total system demand

The process of modifying all substation loads resulted in a new powerflow case which was solved using commercial power system analysis software. This solution produced a new value for the total system demand and

constitutes one iteration. This iteration was repeated 10000 times. At each iteration the reference case was opened and random errors applied to all substation loads. The computed total system demand for each iteration was plotted in a spreadsheet. Calculated powerflows on two important transmission circuits were also plotted to observe the variability of powerflows in these circuits. The size of the modeled system is approximately 300 busses and 130 loads.

2.3 Procedure automation

This procedure was automated in the power system analysis software. The flowchart is depicted in Figure 9. The actual distribution of errors in reality is unknown.

3 RESULTS

As expected the computed values for total system demand are distributed about the reference value. Figure 1 depicts a histogram of the computed values.

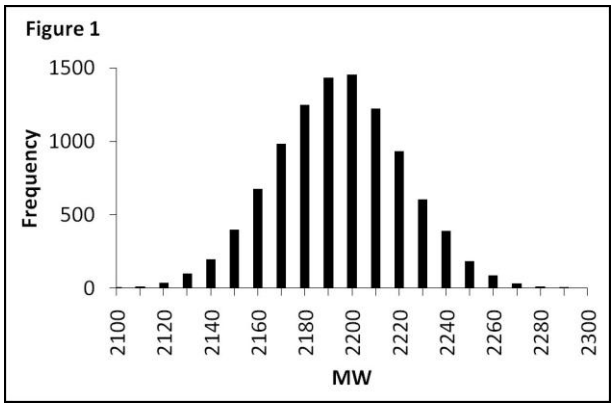

Figure 1: Histogram of computed total demand values

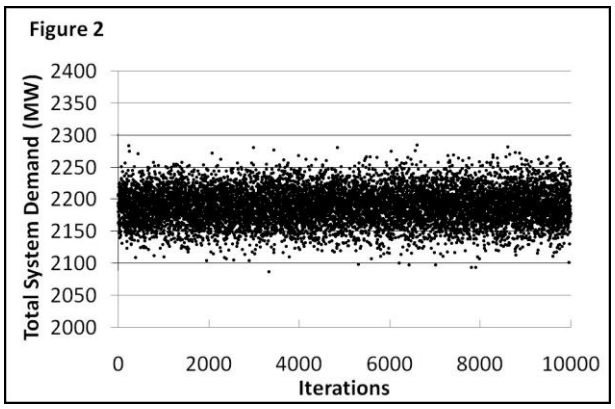

Figure 2: Computed total demand values for all iterations

Figure 2 shows the computed values of total demand plotted for each iteration. The values vary by up to ± 100 MW or ± 5 % of the reference value of 2193 MW. Most of the values are in the range ± 50 MW.

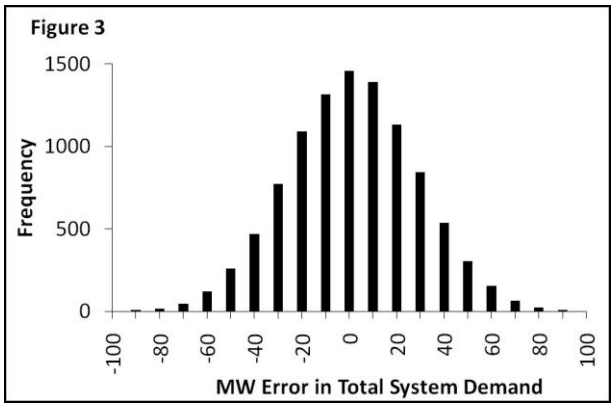

Figure 3: Computed total demand values for all iterations

The mean value of the computed total demand values is 2189 MW which is quite close to the reference value. Figure 3 shows the convergence of the computed total demand values towards the mean value.

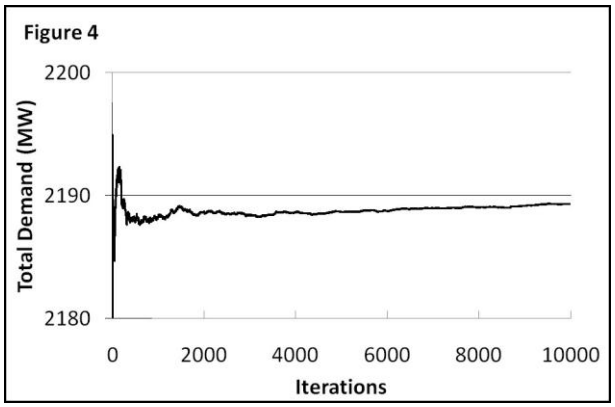

Figure 4: Convergence of total system demand

The powerflows on two important 132 kV lines were plotted for each iteration as computed by the power system analysis software. These lines are in different locations within the network and have different loadings. Thus it was expected that the random errors should have a different impact on the forecasted powerflows through each line. The KLA-UMG circuit is a 132kV interconnector and showed a variation of ± 7 % in forecasted powerflow. The DAL-CAT circuit is a 132kV interconnector in the inner-city and showed a variation of ± 16 % in forecasted powerflow. The absolute range of variation is almost identical for both lines at approximately 20 MW. These are depicted in Figure 5 and 6 below. The length of each vertical scale is approximately half the circuit capacity allowing one to see the variation of forecasted powerflow in relation to the circuit capacity.

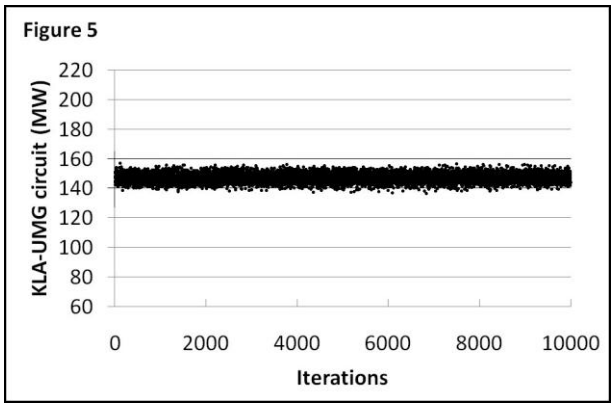

Figure 5: Powerflow through KLA-UMG circuit

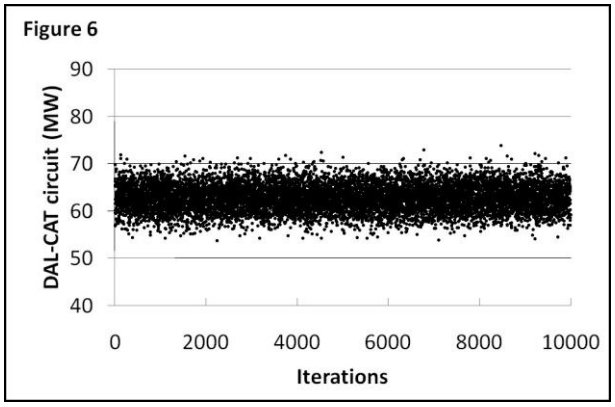

Figure 6: Powerflow through DAL-CAT circuit

A supplementary set of 10000 iterations was performed to test the repeatability of this simulation approach. The mean value was 2190 MW. Figure 7 shows this histogram, while Figure 8 shows the convergence.

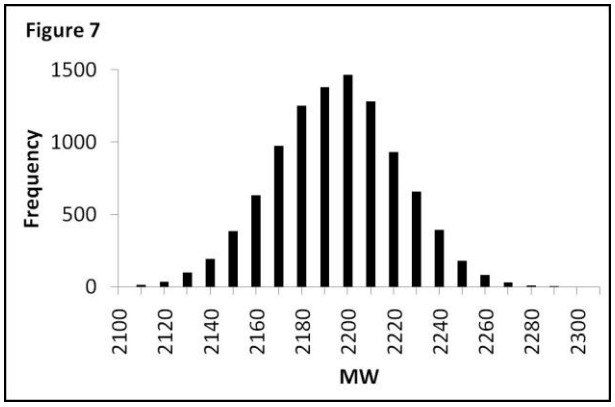

Figure 7: Histogram of total demand (supplementary)

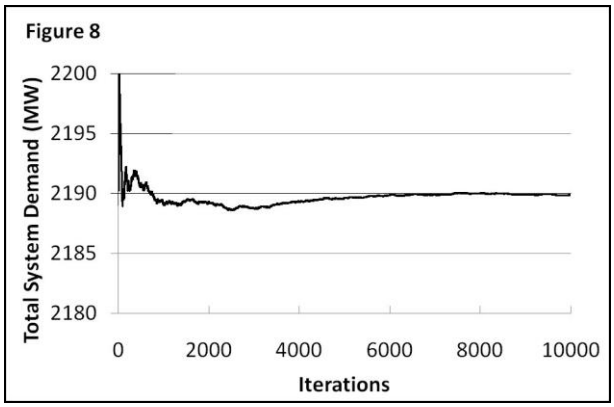

Figure 8: Convergence of total demand (supplementary)

4 SIMULATION FLOWCHART

The flowchart in Figure 9 below essentially consists of two nested loops. The inner loop modifies each load in the reference case by applying the random error. Once this inner loop is complete and all the loads have been modified, the power system analysis software solves the case. The outer loop repeats the entire iteration starting with re-opening the reference case.

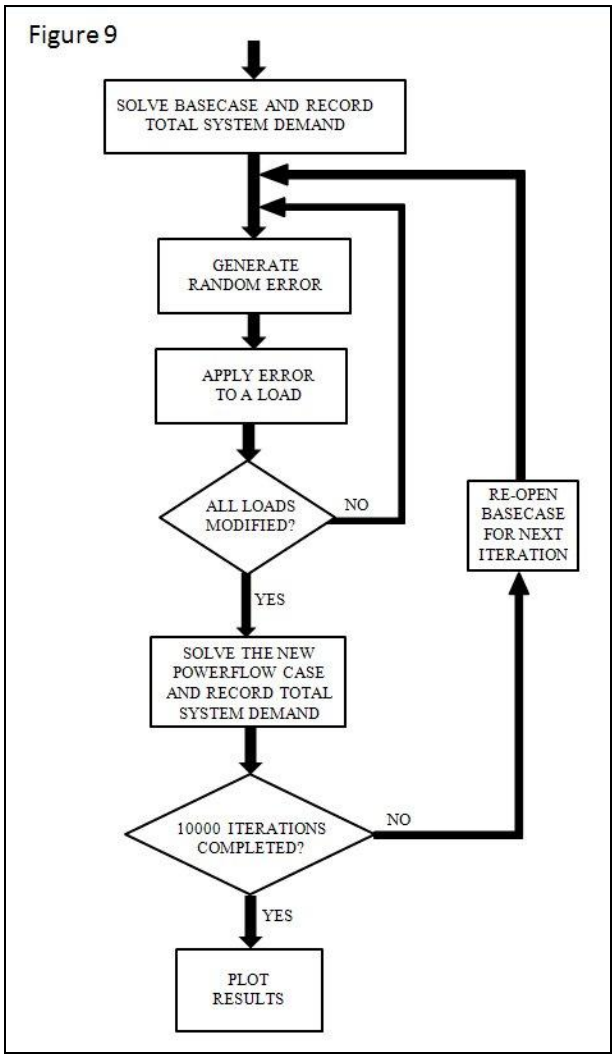

5 CONCLUSION

An appreciation of the magnitude of uncertainty in forecasted total system demand is useful and important for system planning purposes. This study shows a demonstration of Monte Carlo simulation to observe the extent to which uncertainty in substation forecasted loads affects the total system demand forecast. The variation in total system demand in response to random variations in all the input loads is observed.

This study uses the same error bounds for all individual substation loads. Possible enhancements include use of varying types and magnitudes of errors to model varying levels of uncertainty (eg if different substation supply areas are characterized by different degrees of uncertainty). This could be useful in spatial load forecasting where quality of data (and hence uncertainties) may vary geographically. Also, the probability distributions of the errors can be specified if they are known.

This type of application contributes towards answering the question: "How accurate is the system forecast?". Instead of a single value, the system demand forecast is interpreted as a range of possible values which reflects the uncertainties of the input loads.

6 REFERENCES

[1] R. Billinton, R. N. Allan, Reliability Evaluation of Engineering Systems – Concepts and Techniques, Plenum Press, New York, 1983

On the Effect of Mutually Coupled Autonomous Chaotic Third-Order Phase-Locked Loop

Ahmad Harb[*], Qasem Qananwah[*] and Bassam Harb[**]
Electrical Engineering Department
Jordan University of Science and Technology
Irbid, Jordan
E-mail:aharb@just.edu.jo

Abstract

A third order Phase locked loop, PLL, is widely used in communication systems. Lately, researcher had found that under certain conditions, such as gain, PLL is experiencing chaotic oscillations. For a single PLL, studies have shown that when the gain of PLL increases, it will encounter a chaotic behavior. To see the mutual effect of two coupled PLL, this paper will derive the mathematical dynamical model and use the modern nonlinear theory to investigate the chaotic oscillations. Chaotic signal could be generated from mutually coupled PLL the coupling gives a wide chaotic region and a robust one if intended to be use for chaos generation, also the coupling value vary the region of stability, here in this paper we demonstrate this by computer simulation.

Introduction

Since the chaos phenomena has been discovered, the researchers pay their attention to the methods of avoiding it; due to the worse effect it produce in power and control systems. But recently the situation is changed due to the advantageous applications for it in the area of communication; the chaos signal has desirable features that make it very useful as a carrier in communication. Using chaotic signal for data communication is attractive for several reasons. It allows for the application of traditional methods of processing noise like signals such as, match filters and correlation methods. Or one can apply a nontraditional methods "Nonlinear Dynamic". So far Chaos gain recently a wide interest in the area of communication and since the active researches in this area which was initiated by Pecora and Carrol [1], and the increasingly interesting in it comes from the features obtained from the use of it in communication such that Chaotic signals are no periodic, wide-band, and more difficult to predict, reconstruct, and characterize than periodic carriers.

The PLL is a versatile function device which is widely used in many electronic systems due to accuracy, controllability, capability to provide high power and frequency. PLL can become chaotic under certain conditions for wide range of systems parameter values. Many paper published investigating the chaotic behavior of single PLL [2]-[5], a PLL offers a very simple circuits configurations, and because its VCO output is a band-pass it gain its popularity to be used in chaotic communication systems since the communication Band-pass chaotic signals are needed ,

To generate chaotic signal one could use single third-order PLL which recognized by the accuracy, controllability, capability to provide high power and frequency. In this paper the PLL model was put in [2] and it is suitable as chaos generator for chaos based communication systems. Namely this PLL has a chaotic attractor whose power spectrum distribution can be changed arbitrarily in its RF range by varying the time constants of the loop filter. Since the order of the loop filter is two, then can be represented as a third order autonomous system the nonlinearity of the PLL comes from the Phase detector which is seen here as a sinusoidal periodic function which is highly nonlinear.

In this paper we explore the effect of mutual coupling on the bifurcation between two coupled PLL, since mutually coupled Phase-Locked Loop give more advantage than the single due to the wide range of chaotic region if intended to used in communications.

Mathematical Model

The considered model here consist of two identical PLL's that incorporate a voltage control oscillator (VCO), a phase detector (PD) having a sinusoidal characteristics and a two cascade lag-lead filters Fig 1 shows a block diagram of the system. The mathematical model representing the coupled PLL could be derived based on the model above, where we use two cascade lag-lead filters, $F_1(s) = (1+\tau_{z1}s)/(1+\tau_{p1}s)$ and $F_2(s) = (1+\tau_{z2}s)/(1+\tau_{p2}s)$, so we can directly obtain the following set of state-space equations representing the dynamics of the output of the corresponding VCO's:

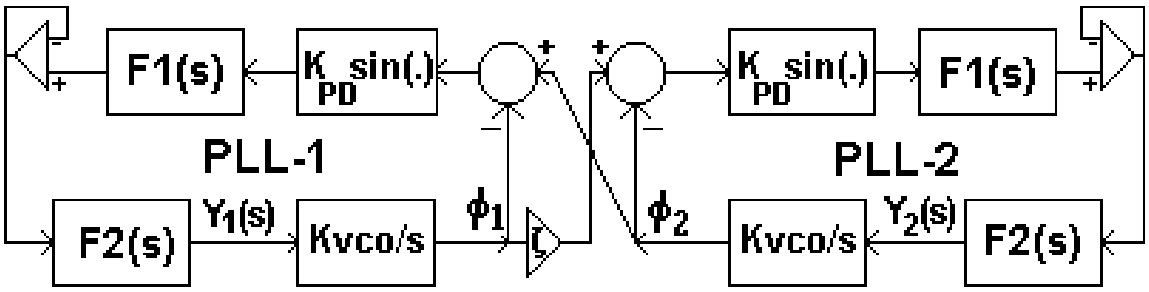

Figure 1: A Block Diagram of considered mutually coupled PLL's.

To reduce Equation.(1) and Equation.(2) to this simplest equivalent **ODE** we have normalized them by changing the time variable $t' = (k_o / \tau_{P!}\tau_{P2})^{1/3} t$

State space representation

$$\dot{x}_1 = x_2$$

$$\dot{x}_2 = x_3$$

$$\dot{x}_3 = \delta_1 - ax_3 - cx_2 + b\cos(x_4 - x_1)(x_6 - x_3) - b\sin(x_4 - x_1)(x_5 - x_2)^2 + d\cos(x_4 - x_1)$$
$$(x_5 - x_2) + \sin(x_4 - x_1)$$

$$\dot{x}_4 = x_5$$

$$\dot{x}_5 = x_6 \qquad (4)$$

$$\dot{x}_6 = \delta_2 - ax_6 - cx_5 + b\cos(\zeta x_1 - x_4 + x_7 \frac{\omega}{W}[\zeta - 1])(\zeta x_3 - x_6) - b\sin(\zeta x_1 - x_4$$
$$+ x_7 \frac{\omega}{W}[\zeta - 1])(\zeta x_2 - x_5 + \frac{\omega}{W}[\zeta - 1])^2 + d\cos(\zeta x_1 - x_4 + x_7 \frac{\omega}{W}[\zeta - 1])$$
$$(\zeta x_2 - x_5 + \frac{\omega}{W}[\zeta - 1]) + \sin(\zeta x_1 - x_4 + x_7 \frac{\omega}{W}[\zeta - 1])$$

$$\dot{x}_7 = 1$$

Numerical Simulation

Computer simulation holds for single PLL shows that chaos occur by the following scenario so if we take only PLL-1 or PLL-2, we find that at K_o=7292.3 a Hopf bifurcation occur (Limit cycle) and increasing the control parameter lead to deformation of the periodic solution until it reach chaos at K_o =79885 rad/s. In the contrary at the coupled PLL's and numerically tracking the eigen values of the system we find that it bifurcate at multiple points depending on the coupling factor(so the bifurcation point vary with the coupling factor) as seen in **Table 1** below.

Table 1: Hopf Bifurcation as Coupling Factor Vary

Coupling Factor ζ	K_o[rad/s] where the Hopf bifurcation points occur
0	**100**
0.5	**1500**
0.8	**2310**
1	**3665.4**

Equilibrium and Dynamical Solutions

The two PLL's are identical and have the same parameters used for single stage PLL. Again, by evaluating the Jacobean matrix for different values of the control parameter K_o, the stability of the eigenvalues of the Jacobean matrix have been changed.

The simulation results showed that for ζ=1, the system become periodic (Out-of-Lock), i.e, their is a Hopf bifurcation point at K_o=3665.4 rad/s as shown in Fig 2. By increasing the control parameter K_o, the system begin to deform. Further increase in K_o drive both states to the chaotic region at K_o=82160.5 rad/s as shown in Fig. 3. Then, the two states go back to period one for K_o=105726 rad/s as shown in Fig. 4. At this coupling factor (where all the output of VCO-1 is fed to PLL-2), the two states behave identically at all stages and the whole system behavior is very close to the single PLL including the chaotic region and the value of control parameter at which chaos occurs.

When the output of VCO-1 is disconnected from PLL-2 or ζ=0, then the system is connected in a cascade manner. Simulation results indicate that by increasing the control parameter K_o up to K_o=100 rad/s the whole system becomes periodic as shown in Fig. 5. Further increasing in the control parameter, the system becomes chaotic at K_o=67 Krad/s as shown in Fig. 6 and remain chaotic for very large variation of control parameter.

Conclusion

The Coupling between two coupled Phase-Locked Loop Has been investigated and influence of it in the chaotic behavior of the system is studied to find that the coupled PLL's coupled be used as chaos generator with robustness more than the single one, investigating the coupling factor reveal that the stability region increase through increasing the coupling factor. For the coupling factor ζ=0.5, we noticed that the chaotic region is wide and very robust in a wide variation control parameter, so it is recommended to use it as a chaos generator since it could be generated at low dc gain (K_o).

References

[1] Hisa-Aki Tanaka,Shini'ichi Oishi, and Kazuo Horiuchi, "Geometric Structure of Mutually Coupled Phase-Locked Loops, "IEEE Trans. on circuits and syst.-I, vol.43,No.6,June 1996,PP.438-443.

[2] Tetsuro Endo,and Leon O.Chua,"Chaos from Two-Coupled Phase-Locked Loops, "IEEE Trans. on circuits and syst., vol.37,No.9,Sep. 1990,PP.1183-1187.

[3] Akio Hasegawa,Motomasa Komuro,Tetsuro Endo,and Ryo Igarashi, "A New Type of Intermittency from a Ring of Four Coupled Phase-Locked Loops,"IEEE Trans. on circuits and syst.-I, vol.45,No.6,June 1998,PP.623-633.

[4] Marina V.Korzinova, Valery V.Matrosov and Vladimir D. Shalfeev, "Communications Using Cascade Coupled Phase-Locked Loop Chaos, "Int. Journal of Bifurcation and Chaos, vol.9,No.5,1999,PP.963-973.

[5] Khaled Dessouky and William Lindsey, "Phase and Frequency Transfer Between Mutually Synchronized Oscillators, "IEEE Transaction on Communications, Vol. COM-32, No.2, Feb. 1984,PP.110-117.

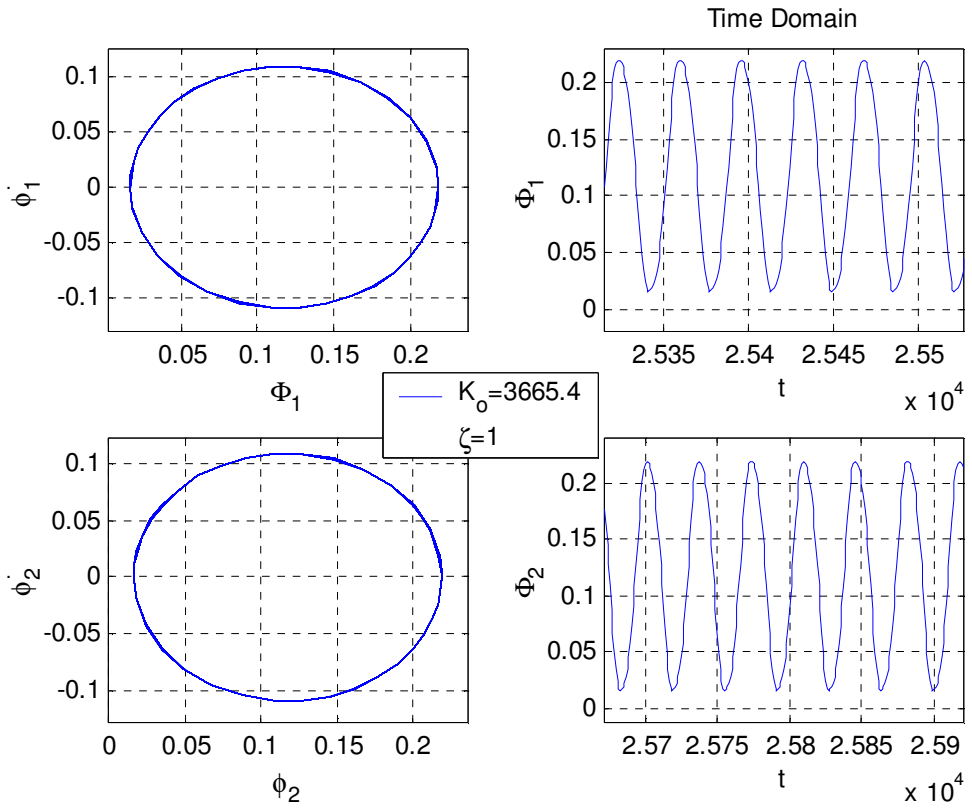

Figure 2: Periodic Solution for Both Φ_1 and Φ_2 , at ζ=1, K_o=3665.4 rad/s.

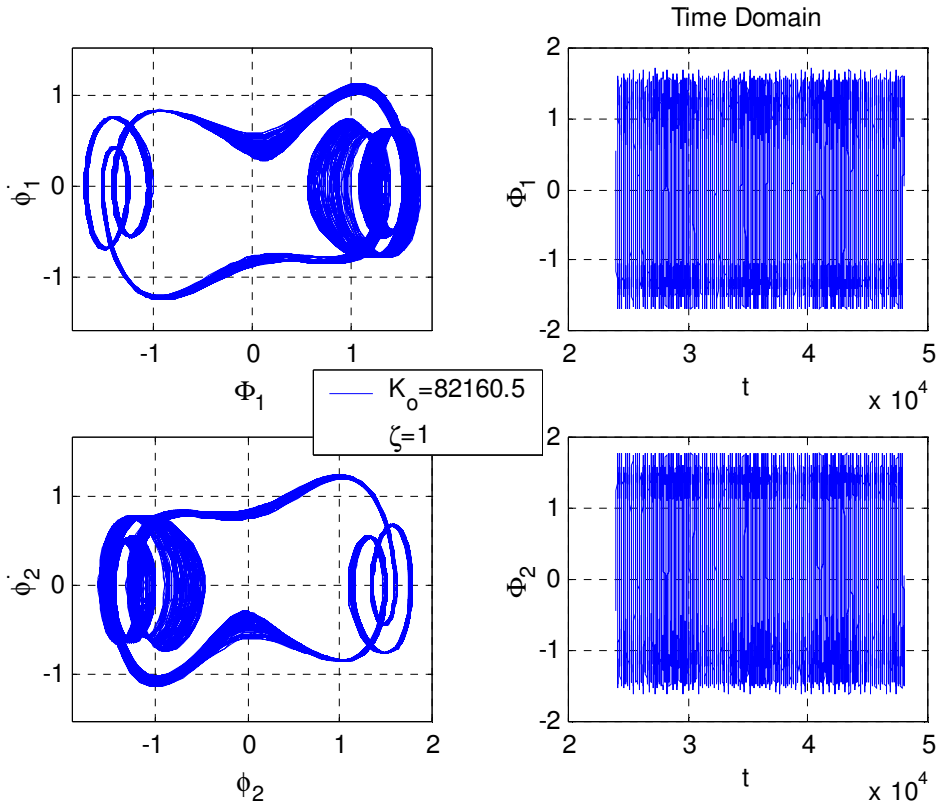

Figure 3: Chaos for Both Φ_1 and Φ_2, at ζ=1, K_o =82160.5 rad/s.

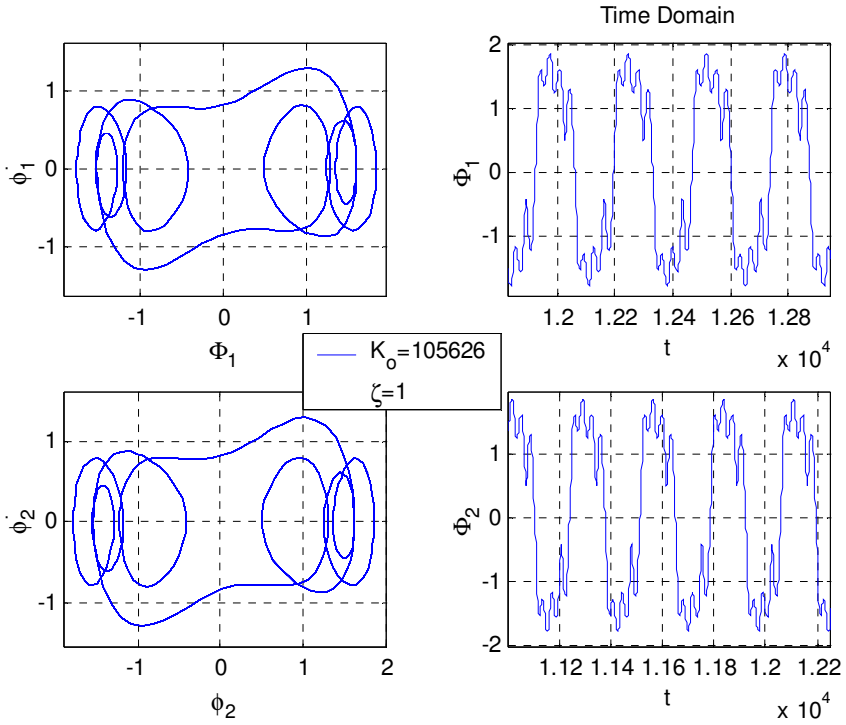

Figure 4: Periodic Solution for Both Φ_1 and Φ_2, at ζ=1, K_o =105726 rad/s.

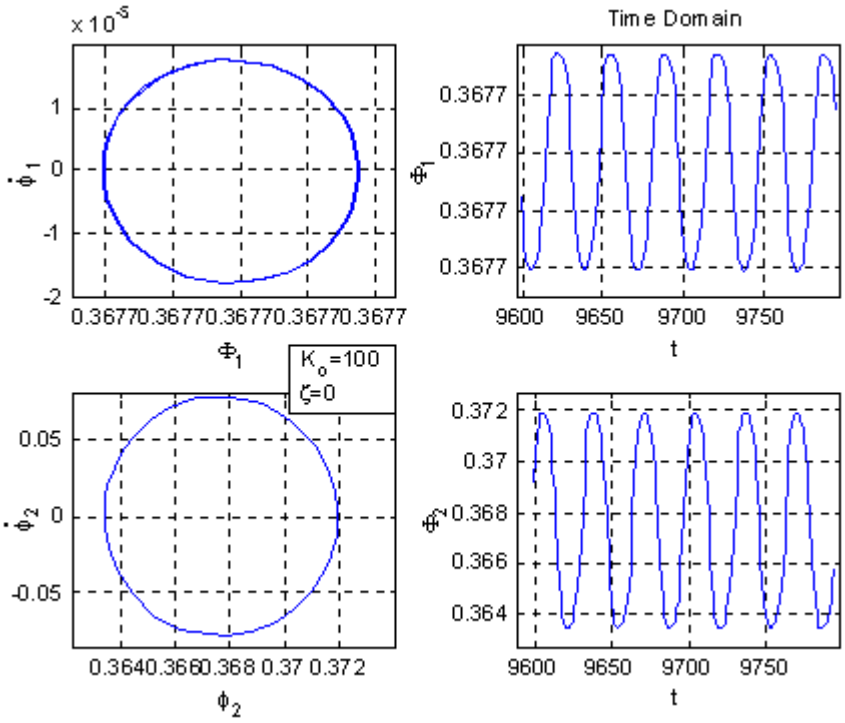

Figure 5: Periodic Solution for Both Φ_1 and Φ_2, at ζ=0, K_o =100 rad/s.

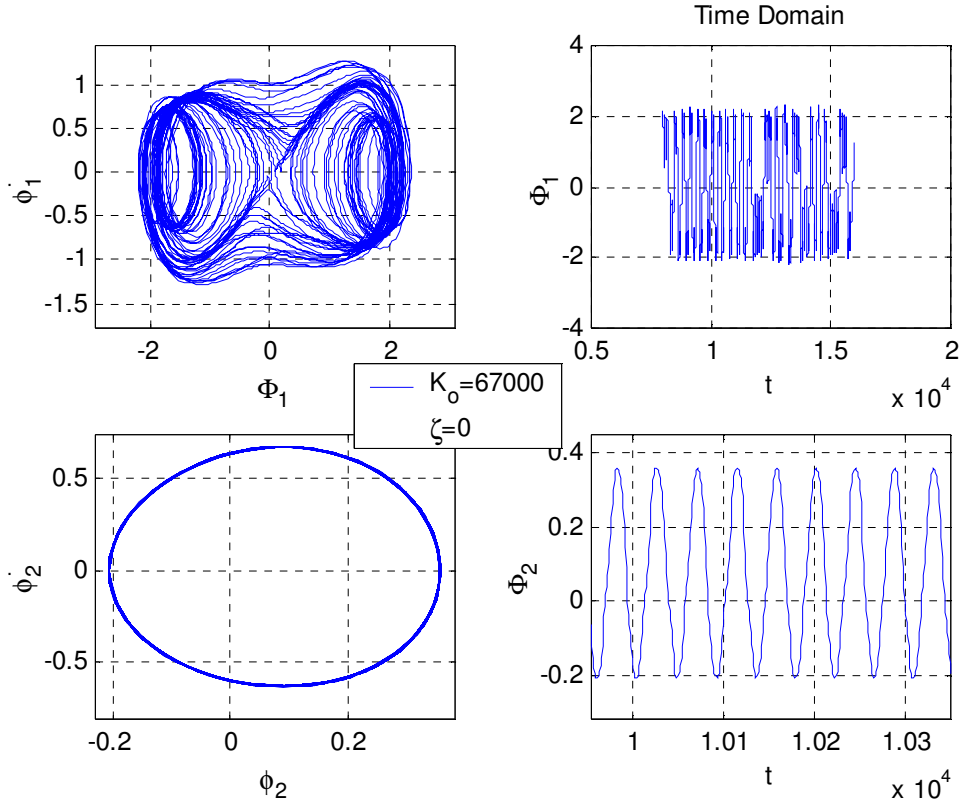

Figure 3: Chaos recoginzed for state Φ_1 while Φ_2 remain in it's state, at ζ=0, K_o =67 Krad/s.

Time-domain Nonlinear Restoring Force Modeling for a MDOF Structure with MR Damper

Bin Xu[1,2, b], Jia He[1, a], S.F. Masri[3, c]

[1]College of Civil Engineering, Hunan University, Changsha, 410082, Hunan, P.R. China

[2] Key Laboratory of Building Safety and Energy Efficiency (Hunan University), Ministry of Education, Changsha, 410082, Hunan, P.R. China

[3]Department of Civil Engineering, University of Southern California, Los Angeles, CA90089, USA

[a]binxu@hnu.edu.cn, [b]hj19830507@126.com, [c] masri@usc.edu

Keywords: power series polynomial model; nonlinear restoring force; system identification; least-square techniques; incomplete excitations.

Abstract. The modeling and identification of nonlinear system is a problem widely encountered in the area of structure dynamical analysis. Based on the the applied excitations and the corresponding response time series under incomplete excitations, a power series polynomial model was utilized to represent the nonlinear restoring force (NRF) of the system in this paper, and each coefficient of the polynomial was identified by means of least-square techniques. No information about the system was needed. The feasibility and robustness of the proposed approach was validated via numerical simulation with a 2-DOF frame structure model incorporating a nonlinear member which was used to simulate nonlinear hysteretic performance. The results show that the proposed approach is capable of identifying NRF in engineering structures, and provides a promising way for damage detection where structural nonlinearity needs to be considered.

Introduction

The modeling and identification of nonlinear system is a problem widely encountered in the area of structure dynamical analysis. Much efforts have been made by numerous investigators to develop modellin and identification approaches for hysteretic restoring forces [1]. Using information about the state variables of nonlinear systems, Masri and Caughey [2] proposed a fruitful approach, named the restoring force surface (RFS) method, to identify and express the nonlinear system characteristics in terms of orthogonal functions, e.g. Chebyshev polynomial. Wen [3] proposed a method for modeling the hysteretic restoring force by a nonlinear differential equation. Based on the modified least-squares adaptive law with forgetting factor and Bouc-Wen model [3], Smyth et al. [4] proposed a method for the on-line identification of hysteretic system under arbitrary dynamic environments. Yang et al. proposed an on-line adaptive tracking technique to identify the system parameters and their changes of non-linear hysteretic structures by means of least-square estimation (LSE) [5]. Masri et al. [6] presented a general data-based approach by using power series fitting techniques for developing reduced-order, non-parametric models in nonlinear MDOF systems.

In most of the approaches above, all excitations (inputs) applied to the nonlinear structural system should be known and available for the nonlinearity identification. However, in practical situation it is either too difficult to excite all of the DOFs of a structure for identification, or some external excitations are unmeasurable. Mohammad et al. [7] proposed a direct parameter estimation method for identifying the physical parameters of linear and nonlinear MDOF structures with only one input excitation. Using a recursive least-square estimation with unknown inputs (RLSE-UI) approach, Yang et al. [8] identified the parameters of a nonlinear structure as well as the unmeasured excitations. Based on the basic idea of equivalent linearization and the symmetry of the identified stiffness matrix, A non-classical approach based on genetic algorithms (GAs) was adopted to identify unknown stiffness and damping parameters solely using output information of the structure [9]. Xu et

al. [10] proposed a data-based model-free hysteresis identification approach for nonlinear systems under incomplete excitations.

Based on the applied excitations and the corresponding response time series under incomplete excitations, a power series polynomial model was utilized to represent the nonlinear restoring force (NRF) of the system in this paper, and each coefficient of the polynomial was identified by means of least-square techniques. No information about the system was needed. The feasibility and robustness of the proposed approach was validated via numerical simulation.

Formulation and identification approach under incomplete excitation

Consider a discrete *n*-DOF lumped mass chain-like structural system incorporating nonlinear non-conservative dissipative members. The motion of this nonlinear system can be governed by the following equation of motion:

$$M\ddot{x}(t) + R(x, \dot{x}, p) = F(t) \tag{1}$$

where *x(t)* = the displacement vector of order *n*, *M* = the constant matrix that characterizes the inertia forces, $R(x, \dot{x}, p)$ = the nonlinear non-conservative restoring force vector, p = the vector of system-specific parameters, and *F(t)* = the directly external forces, respectively.

In this study, the NRF of the system is assumed to be represented in the form of power series polynomial as shown in the following equation,

$$R_{i,i-1}(x, \dot{x}, p) \approx R_{i,i-1}(V, S) \approx \sum_{h=0}^{k} \sum_{j=0}^{q} c_{i,i-1,h,j}^{non} V_{i,i-1}^{h} S_{i,i-1}^{j} \quad (h \text{ and } j \text{ are not equal to 0 simultaneously}) \tag{2}$$

where $R_{i,i-1}(x, \dot{x}, p)$ is the NRF between the i^{th} DOF and the i-1^{th} DOF, $V_{i,i-1}$ and $S_{i,i-1}$ are relative velocity and relative displacement vectors, $c_{i,i-1,j,h}^{non}$ is the coefficient of the polynomial, and k and q are integers which depend on the nature and extent of the nonlinearity of the system, respectively. Consequently, the equation of motion of the i^{th} DOF can be rearranged as follows,

$$m_i \ddot{x}_i(t) + \sum_{h=0}^{k} \sum_{j=0}^{q} c_{i,i-1,h,j}^{non} V_{i,i-1}^{h} S_{i,i-1}^{j} + \sum_{h=0}^{k} \sum_{j=0}^{q} c_{i,i+1,j,h}^{non} V_{i,i+1}^{h} S_{i,i+1}^{j} = F_i(t) \tag{3}$$

Based on the acceleration, relative velocity, relative displacement, and external forces time series, the algebraic coefficients used to represent the restoring force, as well as the mass distribution (m_i), can be identified by means of least-square techniques. Subsequently, the NRF between the i^{th} DOF and the i-1^{th} DOF can be directly obtained according to Eq. (2).

Consider the nonlinear system mentioned above under arbitrary incomplete excitations (assume the force applied on the i^{th} DOF), the rank of force matrix *F(t)* defined in Eq. (1) will be less than the order of *n*. Consequently, the unknown coefficients including the mass distribution cannot be uniquely determined. Assuming the force is only applied on the i^{th} DOF, the corresponding coefficients of the i^{th} DOF can be identified from Eq. (3). However, due to no excitations being applied on the remaining DOFs, the coefficients of these DOFs cannot be uniquely determined by LSE because the right-hand-side (RHS) of the motion equation is zero. Here, the Newton's third law is employed. According to the relationship between the action force and the reaction force, such an equation exists:

$$\sum_{h=0}^{k} \sum_{j=0}^{q} c_{i,i-1,h,j}^{non} V_{i,i-1}^{h} S_{i,i-1}^{j} = -\sum_{h=0}^{k} \sum_{j=0}^{q} c_{i-1,i,h,j}^{non} V_{i-1,i}^{h} S_{i-1,i}^{j} \tag{4}$$

Utilizing the relationship between the action force and the reaction force now provides the basis of using the identified NRF in the previous step as an input to the following identification. According to this idea, the equation of motion of the i-1th DOF can be rearranged as follows,

$$m_{i-1}\ddot{x}_{i-1}(t)+\sum_{h=0}^{k}\sum_{j=0}^{q}c_{i-1,i-2,h,j}^{non}V_{i-1,i-2}^{h}S_{i-1,i-2}^{j}=-\sum_{h=0}^{k}\sum_{j=0}^{q}c_{i-1,i,j,h}^{non}V_{i-1,i}^{h}S_{i-1,i}^{j}=\sum_{h=0}^{k}\sum_{j=0}^{q}c_{i,i-1,j,h}^{non}V_{i,i-1}^{h}S_{i,i-1}^{j} \quad (5)$$

Since the NRF of the i^{th} DOF was previously obtained from Eq. (3), the RHS of Eq. (5) can be considered as known, and the unknown coefficient of the left-hand-side (LHS) can be identified by using least-square techniques. From this point of view, the NRFs of the remaining DOF, on which no external forces are applied, can be identified in sequence.

Numerical study with 2-DOF nonlinear numerical model

To illustrate the accuracy of the method under discussion, a 2-DOF nonlinear lumped mass structure is considered as an example as shown in Fig. 1. Each story of the model is associated with one horizontal DOF. The properties of the structure are m_i=10Kg, k_i=1×10^5N/m, and c_i=100N·s/m, (i=1, 2). In order to mimic the nonlinearity, an MR damper, which is a widely used as typical energy dissipation device, is introduced on the 1st floor as shown in Fig. 1.

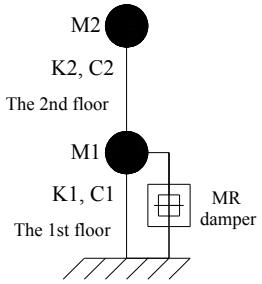

Fig. 1. 2-DOF nonlinear numerical model with MR damper

In this study a modified Dahl model given by the following equations is employed[11]:

$$F_n = K_0 y + C_0 \dot{y} + F_d Z + f_0, \quad (6)$$

$$\dot{Z} = \sigma \dot{y}(1 - Z\,\mathrm{sgn}(\dot{y})) \quad (7)$$

where K_0=the stiffness coefficient, C_0=the viscous damping coefficient, F_d=the adjustable coulomb friction, f_0=the initial force, σ =the coefficient used to control the shape of the hysteretic curve, y=the displacement of the damper, and Z=a dimensionless of hysteretic parameter which describes the coulomb friction. In this example, the following numerical values for the MR damper model are used: K_0=50N/m, C_0=399N·s/m, F_d=34.85N, f_0=0N, and σ =50000s/m.

Here, only the 2nd floor of the nonlinear numerical model shown in Fig. 1 is assumed to be excited by a set of random excitations. The corresponding responses are also determined by the Newmark-β method. Selecting values for the order k+q=3 of the basis functions in Eq. (2) results in the following basis including 9 power series:

$$\text{Basis} = \{v,\ s,\ v^2,\ vs,\ s^2,\ v^3,\ v^2s,\ vs^2,\ s^3\} \quad (8)$$

In this example, the NRF of the 2nd floor should be previously obtained due to the excitation being applied on this floor. Based on the time series measurements of the excitation and the responses of the 2nd floor, the coefficients shown in Eq. (3) can be identified by means of least-square techniques and the expression of the external excitation applied on the 2nd floor is given as follows,

$$F_2 = 10.00\times a_2+1.00\times10^5\times s_2+100.01\times v_2-0.07\times s_2^2+0.01\times s_2v_2-7.86\times10^{-6}\times v_2^2+56.68\times s_2^3$$

$$+0.42\times s_2^2 v_2 - 0.01\times s_2 v_2^2 - 2.34\times 10^{-5}\times v_2^3 \quad (9)$$

From Eq. (9), it's easy to obtain m_2=10.00 which means the identified mass has good agreement with the actual one. Moreover, the NRF on the 2nd floor can be determined and shown below,

$$R_{2,1}^{non}(s_2,v_2) = 1.00\times 10^5\times s_2 + 100.01\times v_2 - 0.07\times s_2^2 + 0.01\times s_2 v_2 - 7.86\times 10^{-6}\times v_2^2 + 56.68\times s_2^3 + 0.42\times s_2^2 v_2 - 0.01\times s_2 v_2^2 - 2.34\times 10^{-5}\times v_2^3 \quad (10)$$

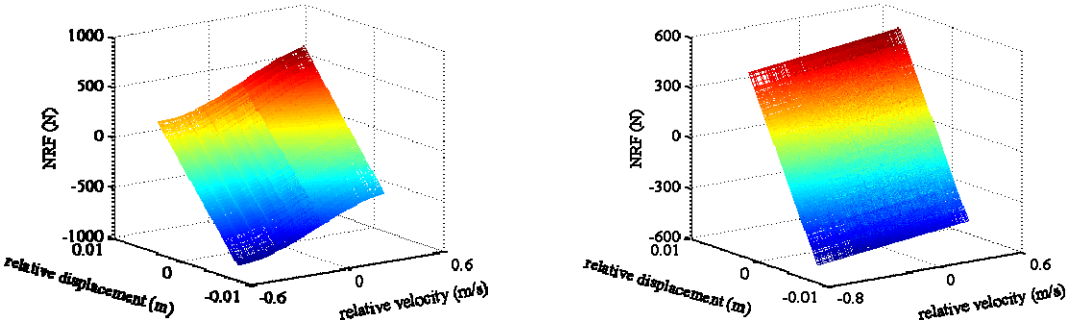

(a) (b)

Fig. 2. The identified NRFs: (a) on the 1st floor, (b) on the 2nd floor

Since $R_{2,1}^{non}(s_2,v_2)$ is determined, the motion of equation of the 1st DOF can be rearranged according to Equations (4-5),

$$m_1 a_1 + \sum_{h=0}^{k}\sum_{j=0}^{q} c_{1,0,h,j}^{non} v_1^h s_1^j = R_{2,1}^{non}(s_2, v_2) \quad (11)$$

Based on the responses of the system and the identified $R_{2,1}^{non}(s_2,v_2)$, the unknown coefficients in the LHS of Eq. (11) can be identified. Consequently, the lumped mass can be found as m_1 = 9.85. Also, the NRF on the 1st floor is given by

$$R_{1,0}^{non}(s_1,v_1) = 0.98\times 10^5\times s_1 + 749.74\times v_1 + 1.60\times 10^5\times s_1^2 + 5.02\times 10^3\times s_1 v_1 - 68.26\times v_1^2 + 1.71\times 10^7\times s_1^3 + 1.27\times 10^5\times s_1^2 v_1 + 9.52\times 10^3\times s_1 v_1^2 - 1.04\times 10^3\times v_1^3 \quad (12)$$

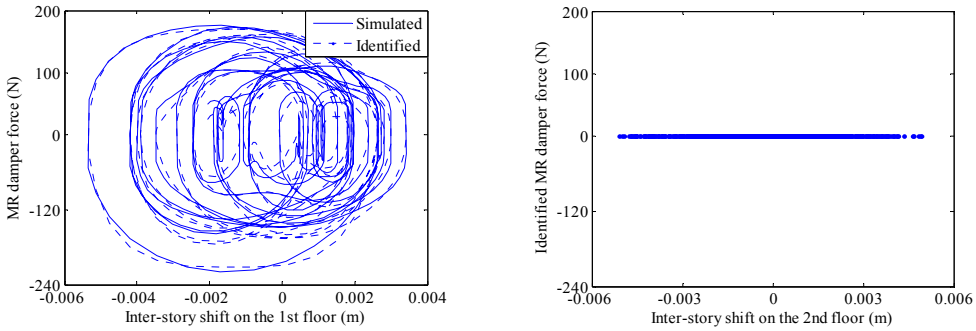

(a) (b)

Fig. 3. The MR damper force: (a) on the 1st floor; (b) on the 2nd floor

The three-dimensional graph in the form of the identified NRF plotted against the relative displacement and relative velocity is shown in Fig. 2, and clearly represents the nonlinearity of the system in this case. The similar conclusion that the MR damper is located on the 1st floor can be obtained by comparing these NRF surfaces. Since the NRF is determined, the MR damper force can be obtained. The identified MR forces as well as the simulated forces are displayed in Fig. 3. From Fig. 3, it can again be concluded that the MR damper is located on the 1st floor. Moreover, it is clear from the results displayed in Fig. (3a) that the modeling approach under discussion yields reasonably accurate fidelity in the identification of the NRF even under incomplete excitations.

Conclusions

A power series polynomial modeling technique is presented for the identification of NRF while the system is under complete and incomplete excitations. A distinguishing feature of the proposed modeling approach is that it does not need information about the structure, and only the applied excitations and corresponding responses are required. The feasibility and robustness of the proposed method is validated via numerical simulation with a 2-DOF system incorporating a parametric MR model. Results show that the identified polynomial models can capture the dominant features of the nonlinear system and the proposed method can be suitable for linear and nonlinear systems.

Acknowledgements

The authors gratefully acknowledge the support provided through the National Natural Science Foundation of China (NSFC) under grant No. 50978092, the Fok Ying Tung Education Foundation (111078) and the Program for New Century Excellent Talents in University (NCET-08-0178).

References

[1] G. Kerschen, K. Worden, A.F. Vakakis, and J.C. Golinval. Past, present and future of nonlinear system identification in structural dynamics, *Mechanical System and Signal Processing*, 20:505-592, 2006.

[2] S.F. Masri and T.K. Caughey. A nonparametric identification technique for nonlinear dynamic problems, *Journal of Applied Mechanics*, 46: 433-447, 1979.

[3] T.K. Wen. Equivalent linearization for hysteretic systems under random excitations, *Journal of Applied Mechanics*, 47(1): 150-154, 1980.

[4] A.W. Smyth, S.F. Masri, A.G. Chassiakos, and T.K. Caughey. On-line Parametric Identification of MDOF Nonlinear Hysteretic System, *Journal of Engineering Mechanics*, 125(2): 133-142, 1999.

[5] J.N. Yang, and S. Lin. On-line identification of non-linear hysteretic structures using an adaptive tracking technique, *International Journal of Non-linear Mechanics*, 39: 1481-1491, 2004.

[6] S.F. Masri, J.P. Caffery, T.K. Caughey, A.W. Smyth, and A.G. Chassiakos. A general data-based approach for developing reduced-order models of non-linear MDOF systems, *Nonlinear Dynamics*, 39: 95-112, 2005.

[7] K.S. Mohammad, K. Worden, and G.R. Tomlinson. Direct parameter estimation for linear and nonlinear structures, *Journal of Sound and Vibration*, 152(3): 471-499, 1992.

[8] J.N. Yang, and H.W. Huang. Sequential non-linear least-square estimation for damage identification of structures with unknown input and unknown output, *International Journal of Non-Linear Mechanics*, 41: 789-801, 2007.

[9] M.J. Perry and C.G. Koh. Output-only structural identification in time domain: Numerical and experimental studies, *Earthquake Engineering and Structural Dynamics*, 37: 517-533, 2008.

[10] B. Xu, J. He, R. Zhou, and S.F. Masri. Data-based model free hysteresis identification for nonlinear structures, *Engineering Science*, 8(2): 12-19, 2010.

[11] Q. Zhou and W.L. Qu. Two mechanic models for magneto-rheological damper and corresponding test verification, *Earthquake Engineering and Engineering Vibration*, 22(4):144-150, 2002.